



Bundesamt für  
Kartographie und Geodäsie



# Proceedings

## 16<sup>th</sup> Working Meeting on European VLBI for Geodesy and Astrometry

Leipzig, May 9-10, 2003

Edited by  
Wolfgang Schwegmann and Volkmar Thorandt



Bundesamt für Kartographie und Geodäsie  
Leipzig/Frankfurt am Main



## Preface

The 16th Working Meeting on European VLBI for Geodesy and Astronomy has been organized by the Federal Agency for Cartography and Geodesy (Bundesamt für Kartographie und Geodäsie) BKG, Frankfurt. On May 9-10, 2003 the Very Long Baseline Interferometry (VLBI) meeting took place at the BKG branch in Leipzig. 39 participants from Europe and USA contributed to this workshop by oral and poster presentations but also in the discussions. The expertises of radio telescope operators, developers, data analysts, researchers and scientists are reflected in these proceedings.

The papers from 26 oral presentations as well as from the posters are organized in the course of the programme:

- Station Activities
- Technical Developments
- Local Ties
- Astrometric VLBI
- Geodetic Analysis and results
- Combination of VLBI and other Space Geodetic Techniques
- Future Perspectives of VLBI.

The introductory talk about the International VLBI Service (IVS) demonstrated impressively the position and perspectives of VLBI as space technique and backbone for Earth rotation monitoring and reference systems. The detailed statements in the following papers describe the enormous efforts to improve the hardware including the station environments, the data processing, the analysis techniques and the tropospheric modelling.

Besides all technical aspects it is very encouraging to see a large number of young researchers actively contributing to the working meeting. This is the best investment to guarantee the long-term progress in VLBI.

Bernd Richter and Volkmar Thorandt



## Citation Instructions

These proceedings are published in a printed and in an electronic version by the Bundesamt für Kartographie und Geodäsie, Frankfurt, in 2003. The copyrights for the articles in these proceedings are by the authors. Any material used from the printed or the electronic version of the proceedings must be cited in the following manner:

*Name of author: Title of contribution*, In: Proceedings of the 16<sup>th</sup> Working Meeting on European VLBI for Geodesy and Astrometry, held at Leipzig, May 09-10, 2003, edited by W. Schwegmann and V. Thorandt, Bundesamt für Kartographie und Geodäsie, Frankfurt/Leipzig, 2003.

Any article of the proceedings can be printed for personal use only.

## Electronic Version

The full text electronic version of these proceedings is available on the WWW under the address

<http://vlbi.leipzig.ifag.de/mm/proceedings.htm>

The electronic version is identical to the printed version.

# Opening of the „16<sup>th</sup> Working meeting on European VLBI for Geodesy and Astrometry“ 09 / 10. Mai 2003, Leipzig, Germany

D. Grünreich

*Bundesamt für Kartographie und Geodäsie (BKG), Frankfurt am Main, Germany*

Dear Colleagues,

The working meetings on European VLBI for Geodesy and Astrometry exist since the beginning of the eighties. These meetings have the characteristics of an open forum where results can be presented as well as technical problems and developments can be discussed in an informal but scientific atmosphere. Since the end of the eighties the meetings take place every 12 to 18 months.

Meanwhile the most dense VLBI network worldwide has been established in Europe with 10 radio telescopes. In Europe the first stations were Onsala / Sweden and Effelsberg / Germany. A significant step in quality and availability of data took place with the inauguration of the Wettzell telescope in 1984. Today there is a good chance to extend the European network for geodetic VLBI again by two stations, namely Torun / Poland and Dwingeloo / Netherlands. But the prerequisite would be the integration of new hardware at these stations.

After the meeting in Viechtach, 1999, it is a great honour to host the meeting again here in Germany. The 16<sup>th</sup> meeting on European VLBI for Geodesy and Astrometry with its activity reports and sessions in

- (1) station activities
- (2) technical developments
- (3) local ties
- (4) astrometric VLBI
- (5) geodetic VLBI analysis and results
- (6) combination of VLBI and other space geodetic techniques
- (7) future perspectives of VLBI

is organised by the VLBI group of the BKG its branch office in Leipzig. This group is relatively young and was created in 1991 after the reunification of Germany. An IVS analysis centre and one of the 3 IVS data centres were established here in Leipzig. Besides the engagement in the IVS products the group here in Leipzig supports the software development of the NASA CALC-SOLVE program.

The group works in close cooperation with the VLBI groups in Bonn and at Goddard Space Flight Centre (GFSC).

I am pleased to welcome 41 participants from 9 countries (Germany, Norway, Austria, Ukraine, The Netherlands, Italy, Sweden, Russia, USA). Colleagues from US make the meeting more international and demonstrate the broad interest in this meeting.

I welcome you here in Leipzig. In specific let me greet one of the fathers of the European VLBI activities James Campbell. In addition I'm happy to see the chair of the International VLBI Service, Wolfgang Schlüter, in this room.

I wish you pleasant stay here in Leipzig. You will see that Leipzig is a lively city with historic and modern building and the German candidate for the Olympic games in 2012.

Have an efficient and successful working meeting.



# Table of Contents

Preface	iii
Welcome Address	v
Session 1: Station Activities	1
International VLBI Service for Geodesy and Astrometry (IVS) – Status and Perspective – <i>W. Schlüter and N.R. Vandenberg</i>	3
MPIfR-BKG MK IV Correlator Report <i>W. Alef and A. Müskens</i>	15
Geodetic Experiments at the Bonn Correlator <i>I. Rottmann, A. Müskens, A. Höfner, and A. Bertarini</i>	19
The EVN MkIV Data Processor at JIVE <i>R.M. Campbell</i>	23
First Results of the TIGO Borehole Tiltmeters in Concepción <i>H. Hase, A. Böer, S. Riepl, M. Avendaño, S. Sobarzo, R. Aedo, G. Remedi, M. Moreno, and M. Sanchez</i>	33
Effelsberg Station Report: May 2003 <i>R.W. Porcas</i>	39
Activities Around the Radiotelescope Wettzell (RTW) <i>W. Schlüter, R. Kilger, G. Kronschnabl, W. Schwarz, and R. Zernecke</i>	41
Planned Improvements at German Antarctic Receiving Station (GARS) O’Higgins <i>W. Schlüter, C. Plötz, R. Wojdziak, and W. Schwarz</i>	46
Session 2: Technical Developments	51
Tropospheric Delay Measurements at Effelsberg With Water-Vapour Radiometry <i>A.L. Roy, U. Teuber, and R. Keller</i>	53
The Geodetic VLBI Network Station at the Onsala Space Observatory – Activities During 2002 – <i>G. Elgered and R. Haas</i>	61
Residual Plotting and Ambiguity Resolution <i>V. Thorandt and G. Engelhardt</i>	67
Mark 5 VLBI Data System Update <i>A. Withney</i>	73
Session 3: Local Ties	81
Stability of Space Geodetic Reference Points at Ny Ålesund and Their Eccentricity Vectors <i>C. Steinforth, R. Haas, M. Lidberg, and A. Nothnagel</i>	83
2002 Local Geodetic Survey of VLBI and GPS Reference Points and Eccentricity at Medicina (Italy) <i>P. Tomasi, P. Sarti, L. Vittuari, M. Negusini, and P. Sillard</i>	91
Neotectonic Geological Study and Classical Geodesy Methods Applied to Active Fault Monitoring in Ny Ålesund (Western Svalbard) <i>E. Gueguen, P. Sarti, E. Tavarnelli, L. Vittuari, and P. Tomasi</i>	99
The IVS-Reference Point at Onsala – High End Solution for a Real 3D-Determination <i>C. Eschelbach and R. Haas</i>	109

Session 4: Astrometric VLBI	119
Phase-reference Astrometry Investigations Using 86 GHz VLBI <i>R.W. Porcas and M.J. Rioja</i>	121
Session 5: Geodetic VLBI Analysis and Results	129
Vienna Mapping Functions <i>J. Boehm and H. Schuh</i>	131
IVS Analysis and Data Center at BKG – Works in 2002/2003 <i>G. Engelhardt, V. Thorandt, and D. Ulrich</i>	145
Investigations of Atmospheric and Hydrological Loading by VLBI <i>G. Estermann and H. Schuh</i>	151
The K4 Intensive Project 2002 for UT1 Determination <i>D. Fischer, A. Nothnagel, R. Kilger, W. Schlüter, S. Kurihara, and K. Takashima</i>	165
The Role of Parameter Constraints in VLBI Data Analysis <i>H. Kutterer</i>	171
Tropospheric Parameters From Geodetic VLBI Data Analysis <i>M. Negusini and P. Tomasi</i>	181
VTRF2003: A Conventional VLBI Terrestrial Reference Frame <i>A. Nothnagel</i>	195
Refinement of the Stochastic VLBI Model: First Results <i>V. Tesmer</i>	207
Investigations on European Baseline Rates <i>M. Vennebusch</i>	219
Preliminary Analysis of the Free Core Nutation From VLBI Data <i>Z. Malkin and D. Terentev</i>	227
Tropospheric Zenith Delays Determined by VLBI as a Contribution to Climatological Studies <i>J. Boehm, H. Schuh, V. Tesmer, and H. Schmitz-Huebsch</i>	237
Robust Outlier Detection in VLBI Data Analysis <i>H. Kutterer</i>	247
Determination of Tropospheric Parameters Within the new IVS Pilot Project <i>H. Schuh and J. Boehm</i>	257
Session 6: Combination of VLBI and Other Space Geodetic Techniques	265
European Vertical Site Motions by VLBI and GPS – An Update <i>J. Campbell</i>	267
Assessing Long Term Trends in the Atmospheric Water Vapor Content by Combining Data From VLBI, GPS, Radiosondes and Microwave Radiometry <i>R. Haas, G. Elgered, L. Gradinarsky, and J. Johansson</i>	279
Session 7: Future Perspectives of VLBI	289
The Project „VLBIonos” – how VLBI Contributes to Ionospheric Research <i>T. Hobiger, J. Boehm, S. Todorova, and H. Schuh</i>	291
Annex	299
Participants	301
Programme	303

Session 1  
Station Activities



# International VLBI Service for Geodesy and Astrometry (IVS) – Status and Prospectives –

W. Schlüter<sup>1</sup> and N.R. Vandenberg<sup>2</sup>

<sup>1</sup>*Bundesamt für Kartographie und Geodäsie, Fundamentalstation Wettzell, Germany*

<sup>2</sup>*NVI, Inc./NASA Goddard Space Flight Center, Greenbelt, USA*

**Summary:** This report reviews the results and the progress made over time since the establishment of the IVS. It summarizes and qualifies the products generated continuously by VLBI. Prospective developments and wishes for the products and the related observing programs are given. Finally the ambitious goal set by the IAG with its upcoming IGGOS project (International Geodetic Global Observing System) will be realized, which requests a global reference system on the millimeter level consistent over decades. Within IGGOS the VLBI technique will play a key role.

## 1 General remarks and the key role of geodetic VLBI

The Very Long Baseline Interferometry (VLBI) technique has been employed in geodesy for nearly 40 years. Covering intercontinental baselines with highest accuracy, monitoring Earth rotation at the state of the art and providing the quasar positions as the best approach to an inertial reference frame, VLBI significantly contributed to the tremendous progress made in geodesy over the last decades. VLBI was a primary tool for understanding the global phenomena changing the “Solid Earth”. Today VLBI continuously monitors Earth rotation and its variations and also crustal movements in order to maintain global reference frames, coordinated within the International VLBI Service for Geodesy and Astrometry (IVS) – a Service of the IAG and IAU. Science and applications set the requirements for the realization and maintenance of global reference frames at VLBI’s technical limitations. VLBI, as the unique technique for providing a celestial reference frame and for deriving the full set of Earth rotation parameters, plays the fundamental role of generating the basis for many applications and research in the geosciences.

VLBI today is the key technique for monitoring and realizing global reference frames. The importance of global reference frames has increased as space and satellite technologies, e.g. satellite navigations systems, are employed for many applications in research in particular in geosciences and in all kinds of surveying and navigation. For the description of satellite orbits a “quasi” inertial system is required, which does not rotate with the Earth – a celestial reference frame (CRF). Such a system is realized by positions of radio sources and is internationally available as the International Celestial Reference Frame (ICRF). Point positioning on the surface of the earth needs an Earth fixed system – a terrestrial system (TRF). The terrestrial reference frame is realized through stations for which the positions and velocities are determined and known. The most recent realization (the adopted international realization) is the ITRF2000. Both TRF and CRF systems are needed and the relation between both must be known to an accuracy as best we can, in order to meet the broad spectrum of applications. The relation between the CRF and TRF is described by the Earth Orientation Parameters, which fix the Earth rotation axis with respect to the CRF ( $de$ ,  $d\phi$ ) and by the polar motion parameters  $x_p$  and  $y_p$  which fix the Earth’s crust. The rotation is described by the parameter DUT1 as the difference between the time scale provided by the Earth rotation itself (Universal Time UT1) and the time scale generated by atomic clocks (Universal Time Coordinated UTC).

As all the parameters are changing with time and no model is precise enough for prediction, the parameters have to be derived continuously from observations. Among the geodetic space techniques (Satellite/Lunar Laser Ranging and GPS etc.), VLBI plays a unique role, as it is the only technique which is capable of realizing and maintaining the CRF, of providing the complete set of Earth orientation parameters and in particular of observing DUT1. Due to superior accuracy in the determination of long baselines VLBI dominates in the determination of the ITRF scale. Because subdaily variations in Earth rotation occur, it is important to observe regularly with adequate resolution in time and accuracy. Regular and more dense observations will become a demand with the request for mm-precise reference frames, consistent for decades, that will be set by the IAG within its upcoming project International Global Geodetic Observing System (IGGOS).

## 2 International VLBI Service for Geodesy and Astrometry

The International VLBI Service for Geodesy and Astrometry (IVS) is a Service of the International Association of Geodesy (IAG) and of the International Astronomical Union (IAU) and a member of the Federation of Astronomical and Geophysical Data Analysis Services (FAGS). The charter and the basis for international collaboration is given by the Terms of Reference (ToR) accepted by IAG and IAU and by the proposals provided by individual agencies in response to the call for participation.

IVS is an international collaboration of organizations that operate or support Very Long Baseline Interferometry (VLBI) components. The goals are

- to provide a service to support geodetic, geophysical and astrometric research and operational activities,
- to promote research and development activities in all aspects of the geodetic and astrometric VLBI technique,
- to interact with the community of users of VLBI products and to integrate VLBI into a global Earth observing system.

As IVS has no funds of its own, but is tasked by IAG and IAU for the provision of timely, highly accurate products (Earth Orientation Parameters (EOPs), Terrestrial Reference Frame (TRF), Celestial Reference Frame (CRF), etc.), IVS is dependent on the support of individual agencies. Figure 1 shows the global distribution of the IVS components.

In order to maintain the strong requirement for consistency, which is the basis for realizing and maintaining global reference frames such as the CRF and TRF, IVS initially employed and accepted existing infrastructure, observing programs such as the National Earth Orientation Service (NEOS), coordinated by the US Naval Observatory, or the Continuous Observations of the Rotation of the Earth (CORE), initiated by NASA. During its first two years of existence, the efforts of IVS were concentrated on the installation of new components and adoption of new IVS tasks. Coordination of activities within the service took effort, resources and time to mature.

All the activities of the first years are documented in the Annual Reports of the IVS for the years 1999, 2000, 2001 and 2002 [Vandenberg and Bayer, 1999, 2001, 2002, 2003]. The first General Meeting was held in Kötzing/Germany in February 2000, the second General Meeting was held in Tsukuba/Japan in February 2002 and several technical meetings concerning analysis and technology aspects were conducted. Proceedings of the General Meetings are available [Vandenberg and Bayer 2000, 2002b]

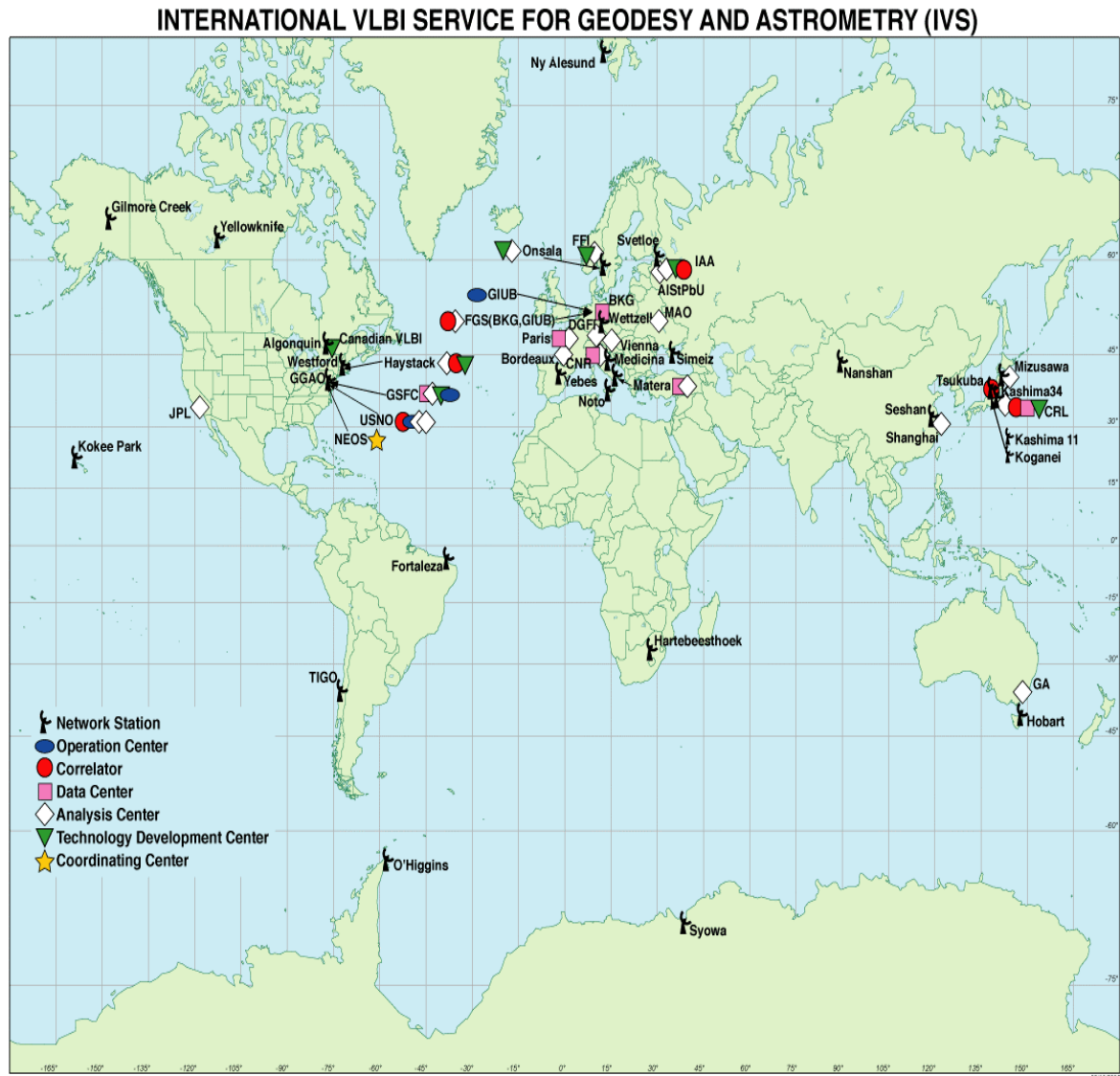


Figure 1: IVS components and their global distribution

Emphasis was placed on data analysis, coordinated by the Analysis Coordinator. Today six Analysis Centers provide a timely, reliable, continuous solution for the entire set of five Earth Orientation Parameters (EOPs) – two polar motion coordinates, Universal Time 1 determined by the rotation of the Earth minus Coordinated Universal Time (UT1-UTC), two celestial pole coordinates. The IVS Analysis Coordinator makes a combined solution – the official IVS product – as timely input for the IERS and its combination with the GPS, SLR/LLR and DORIS solutions. It turns out that the IVS combined solution gains 20% in accuracy over the single VLBI solutions.

After the initial phase of IVS as a service the question “Are the products appropriate to meet the service requirements?” came up and a Working Group was established at the 5<sup>th</sup> Directing Board Meeting in February 2001.

### 3 Review of products and observing programs

At the 4<sup>th</sup> IVS Directing Board meeting held in September 2000 in Paris, the requirement for reviewing the products and the related observing programs was discussed with the view that IVS must meet its service requirements and improve its products. Because such a review requires overall expertise, a broad discussion and acceptance within the entire community, a Working Group (WG2) for Product Specification and Observing Programs was established at the 5<sup>th</sup> Directing Board Meeting in February 2001. (The Minutes of all meetings are published and made available on the IVS web site.) The assignment of WG2 was to

- review the usefulness and appropriateness of the current definition of IVS products and suggest modifications,
- recommend guidelines for accuracy, timeliness, and redundancy of products,
- review the quality and appropriateness of existing observing programs with respect to the desired products,
- suggest a realistic set of observing programs which should result in achieving the desired products, taking into account existing agency programs,
- set goals for improvements in IVS products and suggest how these may possibly be achieved in the future,
- present a written report to the IVS Directing Board at its next meeting.

To establish a broad basis for discussion and to secure acceptance in the community, the members were chosen from among experts in the field of geodetic/astrometric VLBI. Led by Professor Harald Schuh from Technical University of Vienna as chair, the following experts are the members of the Working Group:

- Patrick Charlot, Observatoire Bordeaux/France
- Hayo Hase , Bundesamt für Kartographie und Geodäsie, Concepcion/Chile,
- Ed Himwich, NVI Inc./Goddard Space Flight Center, Greenbelt/USA,
- Kerry Kingham, US Naval Observatory, Washington D.C./USA,
- Calvin Klatt, Geodetic Survey Division of Natural Resources Canada, Ottawa/Canda,
- Chopo Ma, Goddard Space Flight Center, Greenbelt/USA,
- Zinovy Malkin, Institut of Applied Astronomy, St. Petersburg/Russia,
- Arthur Niell, MIT Haystack Observatory, Westford-Haystack/USA,
- Axel Nothnagel, Geodätisches Institut, Universität Bonn /Germany,
- Wolfgang Schlüter, Bundesamt für Kartographie und Geodäsie, Wettzell/Germany,
- Kazuhiro Takashima, Geographical Survey Institute, Tsukuba/Japan,
- Nancy Vandenberg , NVI Inc./Goddard Space Flight Center, Greenbelt/USA

A report of the WG2 was presented in November 2001. The IVS Directing Board reviewed the final version and accepted it for publication ,which is available under <sup>(1)</sup> or in the Annual Report 2001 [Vandenberg and Baver,

<sup>1</sup> <http://ivscc.gsfc.nasa.gov/WG/wg2>

2002]. The report is the basis for continuous improvements and for related research within IVS over the next few years. The results of the report will help IVS meet the objectives and future requirements set up by the IAG and IAU for research in the geosciences and astronomy.

### 3.1 Products and prospective improvements in the next few years

IVS is required to deliver products according to its ToR. Some products are uniquely provided by VLBI such as UT1, CRF, and celestial pole, other products are available from more than one technique: Polar Motion, EOP, TRF, and certain geodynamical and physical parameters. The IVS products can be defined in terms of their accuracy, reliability, frequency of observing sessions, temporal resolution of the estimated parameters, time delay from observing to final product, and frequency of solutions. The current situation with IVS products is described in detailed tables in the WG2 report. The main IVS products, their current accuracies and the goals are summarized in table 1.

Table 1: Summary of IVS main products, status and goal specifications.

Products	Specification	Status	Goal (2002-2005)
Polar Motion $x_p, y_p$	accuracy latency resolution frequency of solution	$x_p \sim 100\mu\text{as}$ , $y_p \sim 200\mu\text{as}$ 1 – 4 weeks ..... 4 months 1 day +3 days/week	$x_p, y_p$ : 50 $\mu\text{as}$ ..... 25 $\mu\text{as}$ 4 – 3 days ..... 1 day 1 day ..... 1 h ..... 10 min ..... 7 days/week
UT1-UTC DUT1	accuracy latency resolution	5 $\mu\text{s}$ .... 20 $\mu\text{s}$ 1 week 1 day	3 $\mu\text{s}$ ..... 2 $\mu\text{s}$ 4 – 3 days ..... 1 day 1 day ..... 10 min
Celestial Pole $de; d\psi$	accuracy latency resolution frequency of solution	100 $\mu\text{as}$ .... 400 $\mu\text{as}$ 1 – 4 weeks ..... 4 months 1 day ~ 3 days/week	50 $\mu\text{as}$ ..... 25 $\mu\text{as}$ 4 – 3 days ..... 1 day 1 day ..... 7days/week
TRF ( $x, y, z$ )	accuracy	5 mm – 20 mm	5mm ..... 2 mm
CRF ( $\alpha; \delta$ )	accuracy frequency of solution latency	0.25 mas – 3 mas 1 year 3 – 6 months	0.25mas (improv. distribution) 1 year 3 months .... 1 month

As of late 2001, IVS products were generated from ~3 days/week observing with 6-station networks. The time delay ranged from several days up to 4 months, with an overall average value of 60 days. Over the next four years, the goals of IVS with respect to its products are the following (specific goals for each product are listed in the WG2 report tables):

- improve the accuracies of all EOP and TRF products by a factor of 2 to 4 and improve the sky distribution of the CRF,
- decrease the average time delay from 60 to 30 days, and designate 2 days per week as rapid turnaround sessions with a maximum delay of 3-4 days,
- increase the frequency of observing sessions from 3 to ~7 days per week,
- deliver all products on a regular, timely schedule.

It is certainly feasible to achieve these challenging goals for IVS products, if the proposed observing programs are carried out and if required improvements are realized. The VLBI technique will allow us to provide additional products and IVS intends to set up the extended products summarized in table 2.

Table 2: Extended products derived by VLBI and intended to be provided by IVS.

Earth Orientation Parameter additions	<ul style="list-style-type: none"> <li>• <math>dUT1/dt</math> (length of day)</li> <li>• <math>dx_p/dt; dy_p/dt</math> (pole rates)</li> </ul>
Terrestrial Reference frame (TRF)	<ul style="list-style-type: none"> <li>• <math>x-, y-, z-</math> time series</li> <li>• Episodic events</li> <li>• Annual solutions</li> <li>• Non linear changes</li> </ul>
Celestial Reference Frame (CRF)	<ul style="list-style-type: none"> <li>• Source structure</li> <li>• Flux density</li> </ul>
Geodynamical Parameter	<ul style="list-style-type: none"> <li>• Solid Earth tides (Love numbers <math>h, l</math>)</li> <li>• Ocean loading (amplitudes and phases <math>A_i, \phi_i</math>)</li> <li>• Atmospheric loading (site-dependent coefficients)</li> </ul>
Physical Parameter	<ul style="list-style-type: none"> <li>• Tropospheric parameters (e.g. 1<sup>st</sup> IVS Pilot Project)</li> <li>• Ionospheric mapping</li> <li>• Light deflection parameter <math>\gamma</math></li> </ul>

### 3.2 Evolving observing programs

To meet its product goals, beginning with the 2002 observing year IVS designed an observing program coordinated with the international community. The 2002 observing program included the following sessions:

- EOP: Two rapid turnaround sessions each week, initially with 6 stations, increasing to 8 as soon as station and recording media resources are available. These networks were designed with the goal of having comparable  $x_p$  and  $y_p$  results. One-baseline 1-hr INTENSIVE sessions four times per week, with at least one parallel session.
- TRF: Monthly TRF sessions with 8 stations including a core network of 4 to 5 stations and using all other stations three to four times per year. The number of stations may be increased if the correlator can support the increase data load.
- CRF: Bi-monthly RDV sessions using the Very Long Baseline Array (VLBA) and 10 geodetic stations, plus quarterly astrometric sessions to observe mostly southern sky sources.
- Monthly R&D sessions to investigate instrumental effects, research the network offset problem, and study ways for technique and product improvement.
- Annual, or semi-annual if resources are available, 14-day continuous sessions to demonstrate the best results that VLBI can offer, aiming for the highest sustained accuracy.

Although certain sessions have primary goals, such as CRF, all sessions are scheduled so that they contribute to all geodetic and astrometric products. Sessions in the observing program that are recorded and correlated using S2 or K4 technology will have the same accuracy and timeliness goals as those using Mark 4/Mark 5.

To support the IVS Coordinating Center in the coordination of the observing program with the international community and to realize the new program, an Observing Program Committee (OPC) has been established. The new IVS observing program began in January 2002.

The observing program and product delivery can only be accomplished by making some changes and improvements in IVS observing program resources (station days, correlator time, and magnetic media), by improving and strengthening analysis procedures, and by pursuing a vigorous technology development program.

## 4 Status and experiences of the new IVS program one year after its implementation

As the official IVS product, a complete set of Earth Orientation Parameter is regularly submitted to the International Earth Rotation Service (IERS). The set is obtained as a combination of the individual solutions of the six IVS Analysis Centers operated at

- Geoscience Australia, Canberra, Australia (AUS)
- Bundesamt für Kartographie und Geodäsie, Leipzig, Germany (BKG)
- NASA's Goddard Space Flight Center, Greenbelt, USA (GSF)
- Institute of Applied Astronomy, St. Petersburg, Russia (IAA)
- Astronomical Institute of St. Petersburg University, St. Petersburg, Russia (SPU)
- US Naval Observatory, Washington, USA (USN).

Figure 2 show the residuals of the individual Analysis Centers with respect to the combined solution as an example for the parameter DUT1 (UT1-UTC). Up to the end of the year 2001, the parameters were derived from the NEOS observations, while since January 2002 the IVS R1 and IVS R4 were used. It should be noted that up to the end of 2001 NEOS was the rapid turn around program which since January 2002 is known as the IVS R4.

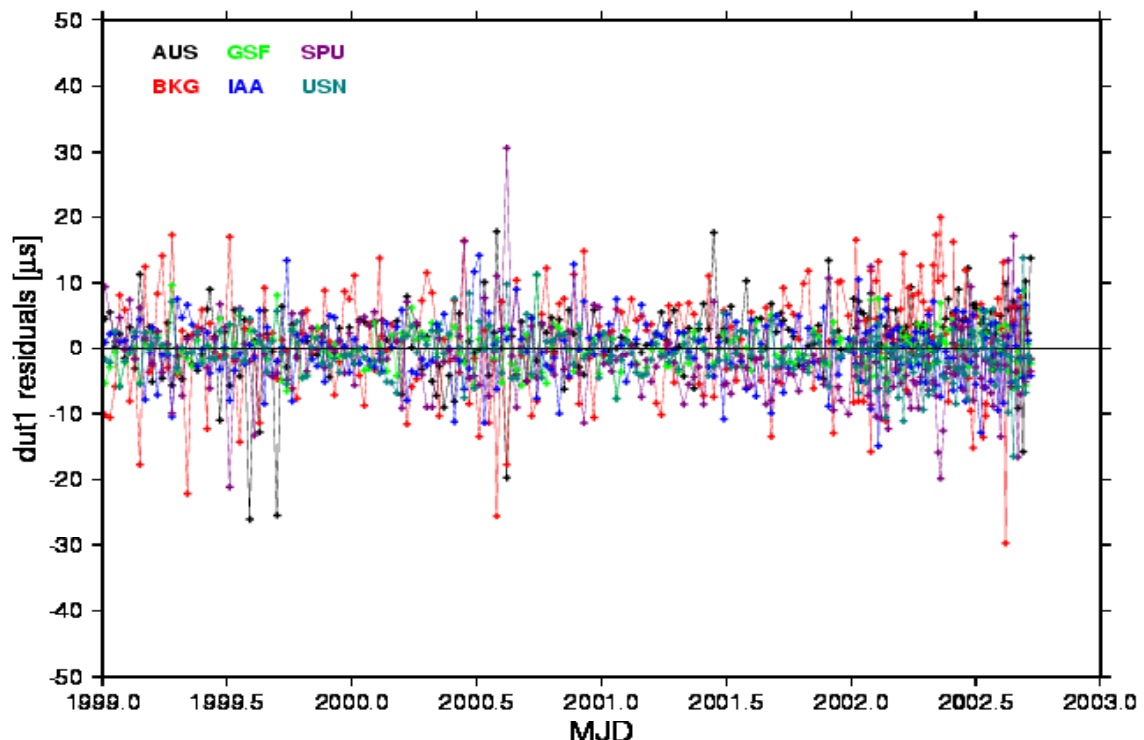


Figure 2: DUT1 residuals of the individual solutions of the 6 Analysis Centers with respect to the combined solutions derived from the NEOS observations and since 2002 from the IVS R1 and IVS R4 observing programs. Note that the NEOS series was continued as the IVS R4.

The objective of the rapid turn around observation sessions is to minimize the delay between the observations and the availability of the results. For the NEOS the delay was approximately 2 weeks, which has not changed by its transition to the IVS R4 as all the routine procedures were already established. For the IVS R4, as new stations were added the data shipping procedures needed to be set up to be routine. Initially this caused unexpected delays, which were overcome with time. For the IVS R1 processing, experience needed to be gained at the correlators at Bonn, Haystack and Washington during the first months. As shown in figure 3 the delay between the observation to the results is approximately two weeks since April 2002. This should be regarded as significant and real progress, even though the WG2 goal of only 4 days has not been achieved. Improvements still are required for data transmission and a higher throughput at the correlator has to be achieved. Both will be improved after the implementation of the newly developed Mark 5 digital data recording system, which has e-VLBI capabilities, allowing data transmission via high speed Internet links. With Mark 5 no time consuming tape positioning will be necessary at the correlator in case of recorrelations, which will obviously save correlator time and will increase the throughput.

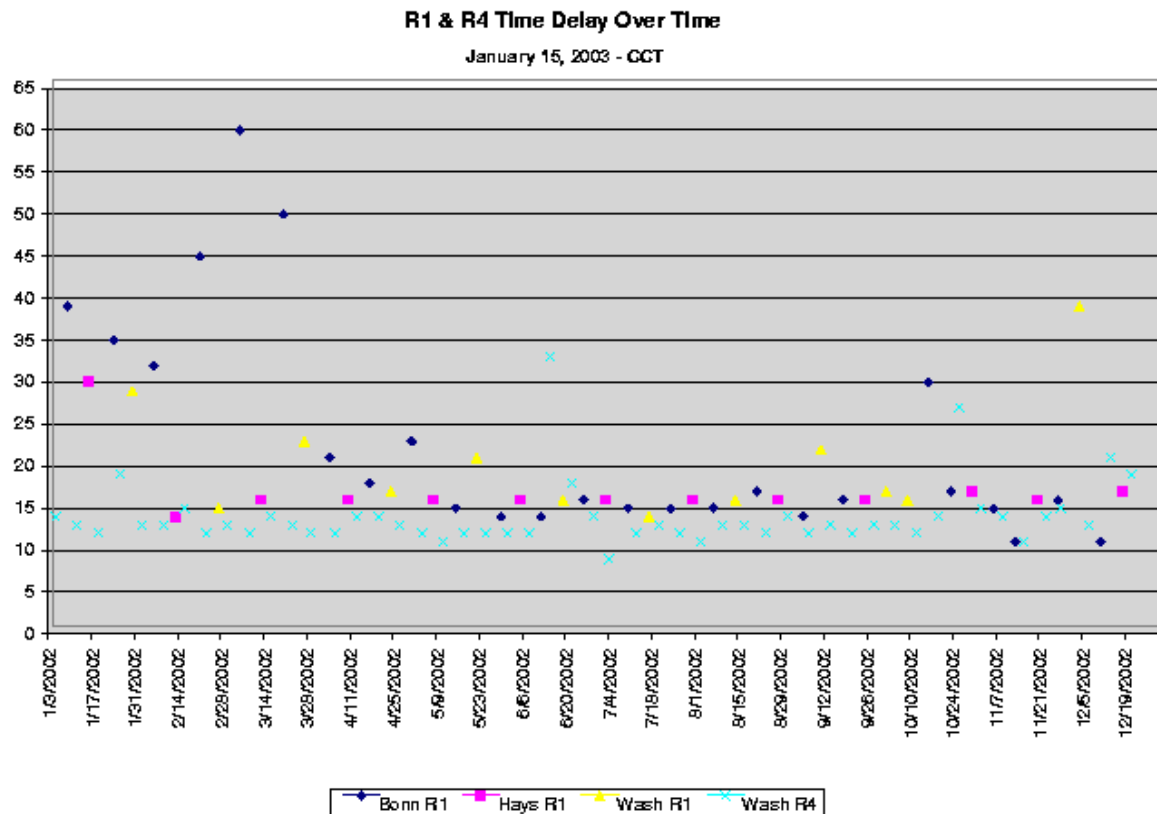


Figure 3: Delay (in days) between the observation and the availability of the results of the IVS R1 and IVS R4 as performed since January 2002.

The determination of DUT1 from the near-daily 1-hour observations known as “Intensives” have been carried out since 1983 via the baseline Wettzell-Westford, since 1994 via the baseline Wettzell-Green Bank and since 2000 via the baseline Wettzell-Kokee Park. These baselines employed Mark III, Mark 4, and now Mark 5 systems. In the year 2002 a time series observed on the baseline Wettzell-Tsukuba/Japan with the Japanese K4 system was set up. The results agree within the error bars with the results of the original Intensive time series. Figure 4 shows the residuals of both series with respect to the C04 solution from the BIPM.

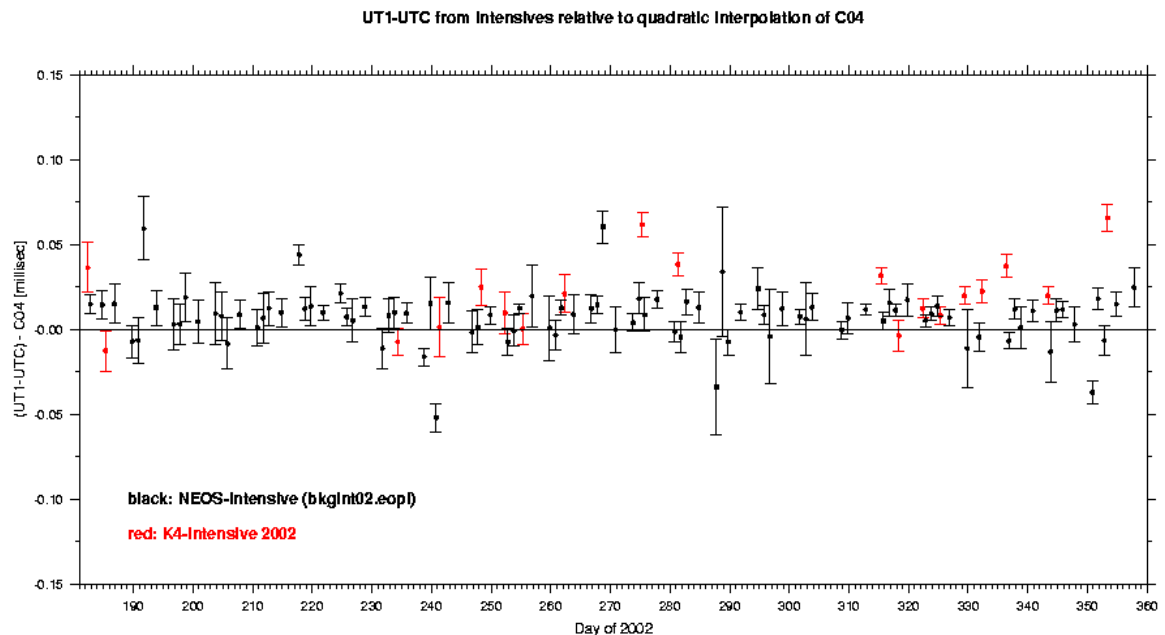


Figure 4: Comparison of the DUT1 (UT1-UTC) results obtained from the MK 4 and K4 Intensives.

The VLBI observations from the rapid turnaround observing sessions R1 and R4 allow determination of tropospheric parameters, in particular the wet zenith path delay. An IVS Pilot Project was established by the IVS Directing Board at its 7<sup>th</sup> Meeting in order to investigate this product and also to set up the capability to provide the zenith wet path delay as an official IVS product. The University of Vienna is combining the solutions of five Analysis Centers. Figure 5 shows the zenith wet delays for an R4 observation in the GPS Week 1180. The results are comparable to those which were provided by the IGS (International GPS Service) or seem to be slightly better. At the 8<sup>th</sup> Directing Board Meeting it was decided to generate the tropospheric parameter as an official IVS product, which will be available as of the beginning of July 2003.

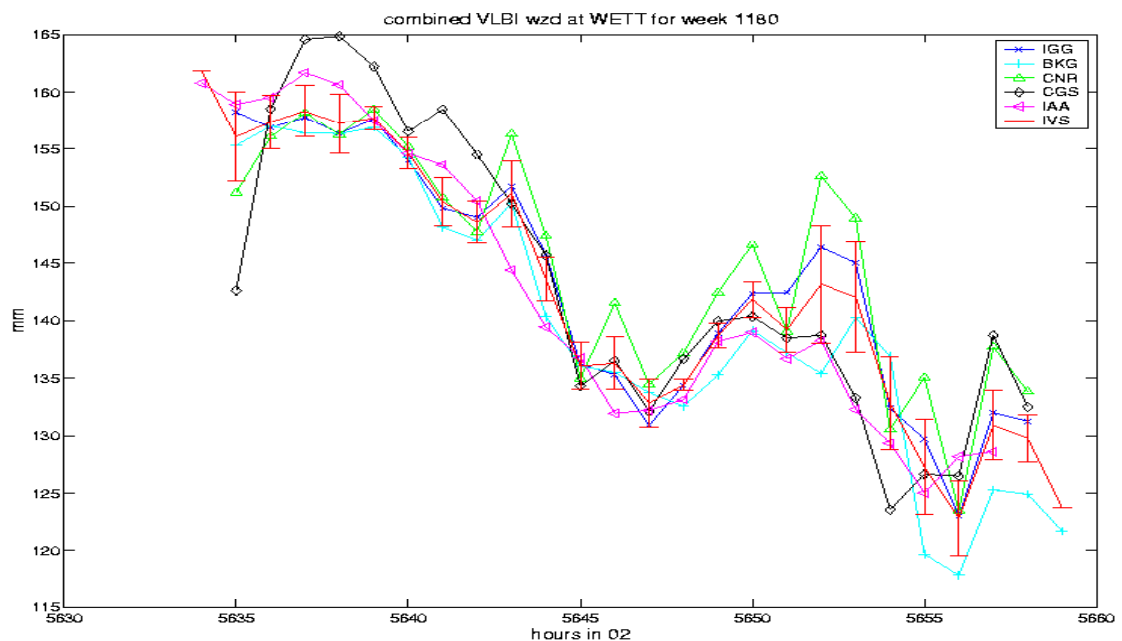


Figure 5: Wet Zenith Delays, derived from R4 observations, taken in GPS week 1180.

## 5 Requirements on IVS components to meet the goals

The WG2 report contains many recommendations for different aspects of IVS, its products, and its programs.

**Program resources:** The number of station observing days increased by about 10% in 2002 compared to 2001, with an additional 12% devoted to the CONT02 campaign. Not counting CONT02, the number of observing days will increase in 2003 by another 12%. The required observing days will continuously increase such that by 2005 the top dozen geodetic stations will need to be observing up to 4 days per week – an ambitious goal. Increased station reliability and unattended operations can improve temporal coverage by VLBI and also allow substantial savings in operating costs. Higher data rate sessions can yield more accurate results, and therefore all geodetic stations must be upgraded to Mark 5 technology involving the digital recording system as soon as possible. More stations need to be equipped with S2 and K4 systems so that global geodetic networks can be designed using these systems. The present level of support at the three Mark 4/Mark 5 correlators must be sustained to meet the IVS product goals, and support is needed from the S2 and K4 correlators. The efficiency of the correlators needs to approach a processing factor of unity, i.e. one day processing for one day observing. All correlators must commit to handling the IVS data with priority processing for meeting timely product delivery requirements. High capacity disks will have to be purchased to replace magnetic tapes and additional recording media capacity, equivalent to ~ 300 disks of 200GB capacity, will be needed to support the higher data rate observing that is necessary for increased accuracy. Alternatively, additional media capacity can be realized by using rapid shipping modes to shorten the cycle time. A deployment plan for the Mark 5 system has been proposed. It is expected that by the end of 2003 the correlator and most of the observing stations will be equipped with Mark 5 digital recording systems.

**Analysis:** More Analysis Centers and those using different software packages should participate in the analysis that is required for robust IVS products. The increased amount of VLBI data to be produced under the new observing program will require Analysis Centers to handle a larger load. Partially automated analysis procedures will help improve the timeliness of product delivery. New IVS products such as EOP rates, a combined TRF solution, tropospheric parameters and geodynamical parameters should be developed because they can contribute to scientific investigations.

**Technology upgrades and improvements:** The Mark 5 system should be deployed at as many stations as possible and the correlators should be outfitted with Mark 5 systems, following the deployment proposal. Not only will Mark 5 technology enable higher data rate recording but it will also improve station and correlator reliability and efficiency. In addition, new methods for data transmission, including electronic media, should be strongly pursued because higher data rates, automated observing and processing methods will lead to increased accuracy, reliability, timeliness, and efficient use of resources. Several tests have been conducted on national, continental and global levels. The progress in communication technologies will support the breakthrough for e-VLBI over the next few years.

A Vision Paper 2010 for VLBI is under development by IVS. Considering our increasing requirements (e.g. the IGGOS project, the increase in radio frequency interference, our aging antennas) general refinements and upgrades of VLBI technology are needed in the future. A Working Group, WG3, is in the process of being established with the objective to develop future visions. Goals include unattended observation, improved global coverage of the net-

work, employment of the new data transmission technologies and provision of near real time correlation and products. In collaboration with radio astronomers some guidelines for future developments will be derived.

## References

- Vandenberg, N.R. (editor): Annual Report 1999, NASA/TP-1999-209243, Greenbelt, MD, August 1999
- Vandenberg, N. R., Baver K.D.(editors): Annual Report 2000, NASA/TP-2001-209979, Greenbelt, MD; February 2001
- Vandenberg, N. R., Baver K.D.(editors): Annual Report 2001, NASA/TP-2002-210001, Greenbelt, MD; February 2002
- Vandenberg, N. R., Baver K.D.(editors): Annual Report 2002, NASA/TP-2003-211619, Greenbelt, MD; May 2003
- Vandenberg, N. R., Baver K.D.(editors): 2000 General Meeting Proceedings, NASA/CP-2000-209893, Greenbelt, MD; June 2000
- Vandenberg, N. R., Baver K.D.(editors): 2002 General Meeting Proceedings, NASA/CP-2002-210002, Greenbelt, MD; June 2002
- Schuh, H. et al.; IVS Working Group 2 for Product Specification and Observing programs, Final Report, Annual Report 2001, page 13 – 45, NASA/TP-2002-210001, Greenbelt, MD; February 2002
- Nothnagel, A.; Ch. Steinforth, IVS Analysis Coordination, IAG CSTG Bulletin no.17, Progress Report 2001, Munich 2002
- Schuh H., Boehm, J.: IVS- Zenith Wet path delay , 2002 General Meeting Proceedings, NASA/CP-2002-210002, Greenbelt, MD; June 2002



# MPIfR-BKG MK IV Correlator Report

W. Alef<sup>1</sup> and A. Müskens<sup>2</sup>

<sup>1</sup>*Max-Planck-Institut für Radioastronomie, Bonn, Germany*

<sup>2</sup>*Geodetic Institute, University of Bonn, Germany*

**Summary:** A report of the present status, capabilities and usage of the MK IV VLBI correlator in Bonn are given. Status and plans for MK5 data acquisition/playback units for Effelsberg and the correlator are discussed in particular with regard to IVS's ambitious MK5 plans.

## 1 Introduction

Geodetic correlation of MK IV data is done at Bonn, Washington, and Haystack (and sometimes at Tsukuba). The MK IV correlator in Bonn is jointly operated by the MPIfR<sup>1</sup> and the BKG<sup>2</sup>. It is a major correlator for MPIfR's astronomical projects, the CMVA<sup>3</sup>, and geodetic observations. The correlator has been operational since early 2000.

The correlator consists of:

- 9 Honeywell/Metrum MK IV playback units each with 1 head and switchable equalisers for 80, 135, and 270 ips playback.
- 9 station units (plus 1 spare) for handling up to 64 tracks from the playback units at a maximum data-rate of 18 Mbps, including phase-cal extraction.
- a standard 2 crate (16 modules) MK IV correlator unit with 2 HP real-time crate computers.
- a correlator control computer (CCC) HP 9000/360 with a Raid 5 disk array for raw correlated data.
- a post-processing computer (HP 9000/B2000) with 240 GB of disk space.

The correlator is controlled with the standard Haystack correlator software, plus some enhancements developed at Bonn. It has an export interface to CALC/SOLVE for data base generation. In addition it has an interface (MK4IN) to the astronomical AIPS software, which can be used for fringe-fitting, calibration, mapping, and also allows data export to CALC/SOLVE via a different route.

MK4IN was written at MPI and Haystack, where Haystack provided a modification to fourfit and the MK IV standard I/O routines. Its features are:

- data selection and first fringe fitting in HOPS (Haystack software)
- export of phase-cal as well as amplitude- and phase-corrections
- export of baseline-based fringe-fit solutions (from which AIPS task BLAPP can calculate antenna-based solutions)
- export of the correlator model to AIPS

The raw data is archived onto DATs. Depending on the size of the datasets DDS2, 3, or DDS4 DATs are used. For reasons of data integrity 2 copies are made. In order to minimise the risk of data loss, daily backups of the correlated data are stored on a PC disk.

For more info see (<sup>4</sup>).

---

<sup>1</sup>Max-Planck-Institut für Radioastronomie, Bonn

<sup>2</sup>Bundesamt für Kartographie und Geodäsie, Frankfurt

<sup>3</sup>Coordinated mm VLBI Array

<sup>4</sup><http://www.mpifr-bonn.mpg.de/EVN/MK4CORstatus>

## 2 Improvements Since The 16th Meeting

### 2.1 Throughput

Since the commissioning of the MK IV correlators it has been obvious that the data throughput had to be increased to reach and eventually surpass that of the old MK III correlators. Therefore software efforts concentrated mostly on that area. With improvements in the tape pass finding algorithms quite an improvement could be achieved.

The amount of re-correlation could significantly be reduced after a long-standing bug in the Track Recovery Modules of the station units (SU) was fixed by Metrum, UK under contract from JIVE. This bug caused loss of fringes in individual channels during the correlation.

Haystack developed a work-around for a problem in the station unit interface module which was responsible for another major part of the re-correlation load. Further improvements in the tape drive electronics led to better playback quality and a software safeguard against playing back with a one-head-pitch offset was introduced at MPI. In total the throughput of the MK IV correlator has now surpassed that of the old MK III correlator.

### 2.2 2-bit sampling

An important step forward for astronomical observations was achieved when the sampler statistics for 2-bit sampled data could be utilized for correcting the amplitude in the fringe-fitting process. In theory all four bit combinations should occur with the same frequency in 2-bit digitized data, but in reality this is not the case due to imperfections in the electronics and bad adjustments of sampler thresholds. In combination with the architecture of the MK IV correlator chip, bad sampler statistics lead to losses in the amplitude of the correlated data. The relative frequency of each sampler state is measured by the station units and is now applied to the data.

### 2.3 Fringe Rotator Model Problems

At the beginning of 2002 several significant errors in the MK IV fringe rotation software were uncovered, investigated, and corrected. Due to the dependence of the problems on baseline length, there are systematic errors in the correlator output. In general they scale with observing frequency. For astronomy programs (mostly at mm-wavelength) the effect is primarily to lower visibility amplitudes for long baselines, leading to over-estimates of source sizes. For geodetic observing, where the frequencies are an order of magnitude lower, the effect is much less. Nevertheless, delays on long baselines have been noted to be systematically affected at a level close to the standard error of the group delay measurement.

The corrected fringe rotation software was introduced at the Bonn correlator in February 2003.

### 2.4 MK 5

BKG and MPI financially supported the MK5 development. As a result two MK5p units were delivered to Bonn in summer 2002. Already at the end of 2002 production correlation with 2 MK5p units was successfully done at the Bonn correlator.

At the end of 2002 100 8-pack kits were purchased from Conduant of which 12 were later sent to Hobart on loan in support of NASA. 266 disks with a capacity of 120 GB and 80 200 GB disks were purchased as

well, so that MPIfR now owns 33 8-packs with 960 GB capacity and 10 with 1600 GB capacity. They are mostly meant for mm-VLBI.

At the beginning of 2003 two additional MK5 A units were acquired and the MK5p units were upgraded. With these units correlation with track data rates of 18 Mbps was tested as well as recording and correlating at bit-rates of 512 and 1024 Mbps.

A first big field test with MK5 A at 512 Mbps was conducted in April 2003 with the four mm-telescopes Pico Veleta, Plateau de Bure, HHT, and Kit Peak. This test was mostly successful even though new, unexpected problems were encountered, like the need for conditioning of new disks. Recordings at 1024 Mbps failed at 2 of the stations because of unconditioned disks other subtle problems, which are now under control. During the test some data was transmitted to Haystack via Internet to verify if fringes could be found. More work has to be done still for a full integration of MK5 into VLBI observing and correlation.

The results of all MK5 tests so far are very promising and indicate that a further increase in throughput and reliability can be achieved when all telescopes have been converted to MK5.

### 3 Problems

The Metrum recorders/playback units are still the most critical component of the MK IV/VLBA VLBI systems. Recordings are sometimes bad, the longitudinal stability of the tracks is occasionally suboptimal, and maintenance is difficult and expensive; spare parts typically cost a significant fraction of a MK5 unit.

The processing factor — the ratio of correlation time over observing time — is still too high in relation to IVS' ambitious plans of how the amount of geodetic observing should grow. For a significant improvement of the processing factor, MK5 recording equipment is needed at all antennas. It would also open the avenue of unattended observing and correlation, by which a significant increase in correlator time could be achieved. But before this goal can be reached the soft- and hardware have to be improved, e.g. in our first tests with MK5 A we observed a few additional problems with the station units which might hinder smooth and unattended operation. The projected increase in the amount of correlated data can be handled by the existing computers.

If we succeed in adding more MK5 playback units (and station units) to the correlator, we might be limited by the fact that the digital signal processors (DSPs) on the correlator boards are still not implemented. Functioning DSPs would also permit shorter averaging periods and thus higher data output rates from the correlator. This would be desirable for instance for VLBI observations above 100 GHz. Another limitation in data output rate is imposed by the slow crate computers of the correlator — a type of computer now no longer in production.

### 4 Correlation

60% of the total time is used for data correlation. This is an increase by about 20% compared to the time of the last meeting. While the agreement between MPIfR and BKG is for a 50/50 usage of the correlator, the demand for geodetic correlation is so high that MPIfR and the geodesists agreed to increase the geodetic usage to 60%. As compensation the geodesists contribute more to the running costs of the correlator, for example by purchasing four MK5 A units.

Both the geodetic and the astronomical backlog are small at present. These total to about 4 to 8 weeks and should be gone by autumn.

## 5 Future Plans

BKG will supplement the four MK5 units which we have at the correlator now, by another four in summer of 2003. Re-building of the correlator room to host all 8 MK5s is underway. It will be possible to simply switch between MK5 and MKIV playback in software. Only for correlation of 1024 Mbps recordings some modest recabling will be needed, as in this mode all 64 track inputs of the station units are needed. We are considering purchasing one or two more units to bring the correlator up to 10 stations total.

To fully exploit the advantages of MK5 we will improve the correlation system towards unattended operation during the night, which will be mostly software changes.

MPIfR is also involved in attempts to develop e-VLBI. For a proof of concept we are investigating 1 Gbps Internet connections to the correlator and Effelsberg. For real e-VLBI operation the costs are currently prohibitive in Germany.

# Geodetic Experiments at the Bonn Correlator

I. Rottmann, A. Müskens, A. Höfner, and A. Bertarini

*Geodetic Institute, University of Bonn, Germany*

**Summary:** We present an overview of the processing stages of geodetic experiments correlated in Bonn during the years 2001 and 2002, showing the efficiency improvements achieved over that period.

## 1 Introduction

The correlator in Bonn is operated jointly by the "Bundesamt für Kartografie und Geodesie" (BKG) and the "Max Planck Institut für Radioastronomie (MPIfR). In 2002 49 geodetic experiments were correlated: IVS-EUROPE (4), IVS-OHIG (6), CONT (2), IVS-R1 (25), IVS-T2 (12), using ~70% of the total correlator time. Since 2001 we analyzed the efficiency of all processes from the tape shipment to the creation of the database. Our goal was to identify the weak points within the processing chain and to develop procedures to further speed up the correlation.

## 2 Geodetic experiments

The processing chain of an experiment can be divided into the following stages:

- Shipment
- Waiting queue
- Correlation
- Post-correlation
- Recorrelation
- Database

For the definitions and the details of the calculations see *Mueskens et al. 2002*. Due to the low number of EUROPE, OHIG and CONT experiments, we have excluded them from our analysis.

The IVS-R1 campaign provides the Earth Orientation Parameters (EOP) once a week and is the continuation of the 2001 CORE-3 campaign. Fig. 1 compares the processing time in the CORE-3 with those in the IVS-R1 experiments, showing that the largest amount of time for both IVS-R1 and CORE-3 campaigns was spent on the shipment of the tapes. In 2002 the shipment time was reduced by a factor of 35% compared to 2001, partly due to correct paperwork filled by the stations and provision of Air Waybill numbers. The queuing time for correlation was reduced by a factor of 30% by streamlining correlator operations. The correlation time was slightly increased due to the "STC" error problem solved in November 2001 thanks to a software upgrade at the correlator. The fringe fitting and analysis time for the correlated data (post-correlation phase) was reduced by a factor of 77% due to increased manpower. The fringe fitting and analysis time for the recorrelated data (database phase) was reduced by a factor of 66% also due to increased manpower.

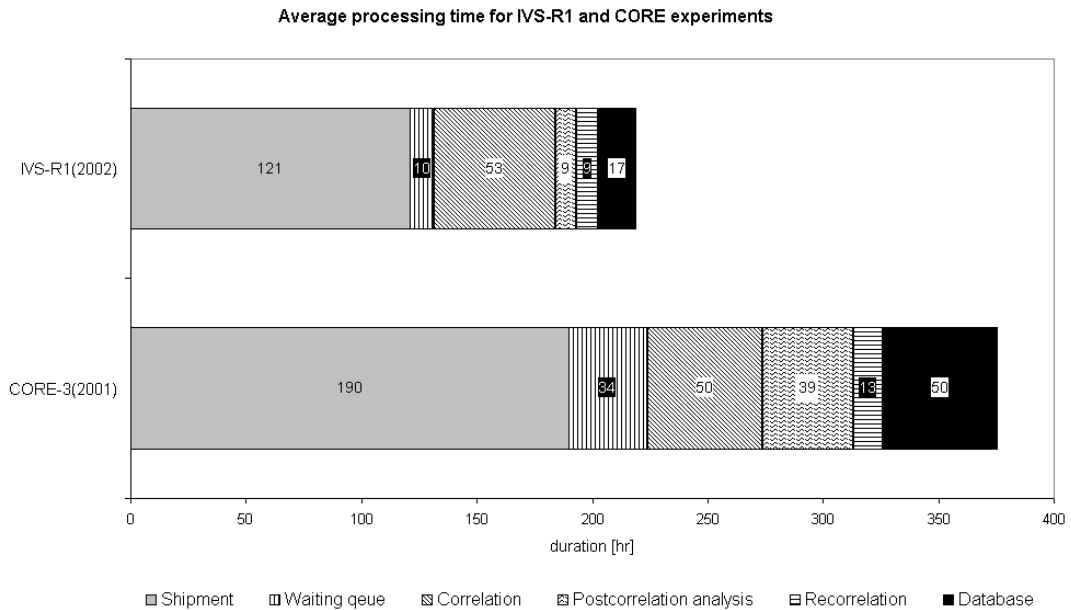


Figure 1: Average processing time [hr] for IVS-R1(2002) and CORE(2001) experiments.

The IVS-T2 campaign monitors the Terrestrial Reference Frame (TRF) and is the continuation of the IRIS-S campaign. Since IVS-T2 has lower correlation priority than IVS-R1, we excluded the queuing time when comparing time delays between the 2001 IRIS-S and the 2002 IVS-T2 campaigns (Fig. 2). In IVS-T2 half of the total processing time was due to the shipment of the tapes, the same as for IRIS-S. In 2002 the shipment time was reduced by a factor of 30% compared with 2001, when shipment of extreme stations such as Crimea and O'Higgins were not included in the statistic. The correlation and recorrelation time was increased by a factor of 45% due to an increase in the number of participating stations. The fringe fitting and analysis time for the correlated data (post-correlation phase) was reduced by a factor of 40% due to increased manpower.

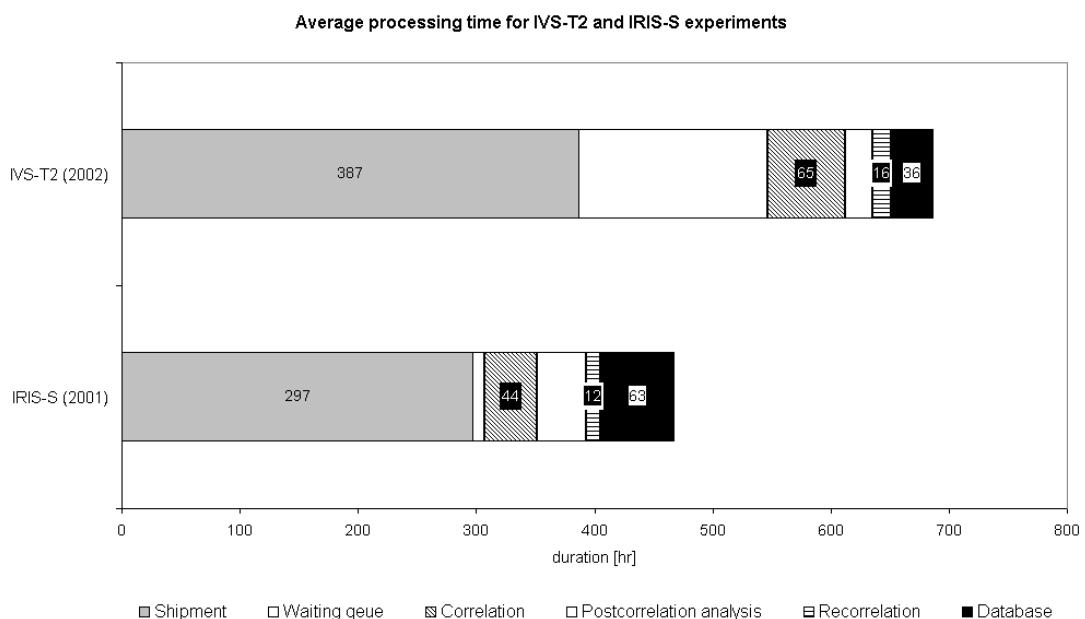


Figure 2: Average processing time [hr] for IVS-T2(2002) and IRIS-S(2001) experiments.

### 3 The “recorrelation question”

The data after correlation must be inspected in detail prior to recorrelation. Preparation for recorrelation requires identification of bad data. Several programs have been written to streamline this process. The scans selected for recorrelation are those with playback problems and those with lengths less than 50% of the scheduled length. In 2002 about 10% of the correlated scans yielded poor quality data that might be recoverable by reprocessing. Recorrelation resulted in the improvement of 60% to 70% of those scans. However the improvement by recorrelation typically consumes about half of the total observing time mostly due to tape positioning and synchronization.

The criteria for recorrelation (the recorrelation question) are somewhat arbitrary. Some scans are much more important than others. We can conclude that recorrelation degrades significantly the data processing efficiency.

### 4 The quality of the data

In 2002 we examined the quality of the final data from IVS-R1 and IVS-T2 campaigns. The data was divided in five categories:

- good quality data with fringe quality (FQ) between 6 and 9
- bad quality data with FQ between 0 and 5
- bad quality data with FQ between A-H
- no valid correlator data (FQ=N)
- scheduled scans which were not observed due to station problems (FQ=not observed)

The proportion of data in each category is shown in Fig.3. About 75% of the final data in 2002 had good quality. Almost 6% of the data had bad quality, for which mostly fringes were not found (FQ=0). The bad data was due either to antenna problems (e.g. slewing) or receiver chain problems (e.g. high system temperature). Radio interference (FQ=G) affected about 2% of the final data. About 14% of the scheduled scans were not observed due to various problems at the observing station, such as observations of other experiment or antenna failure.

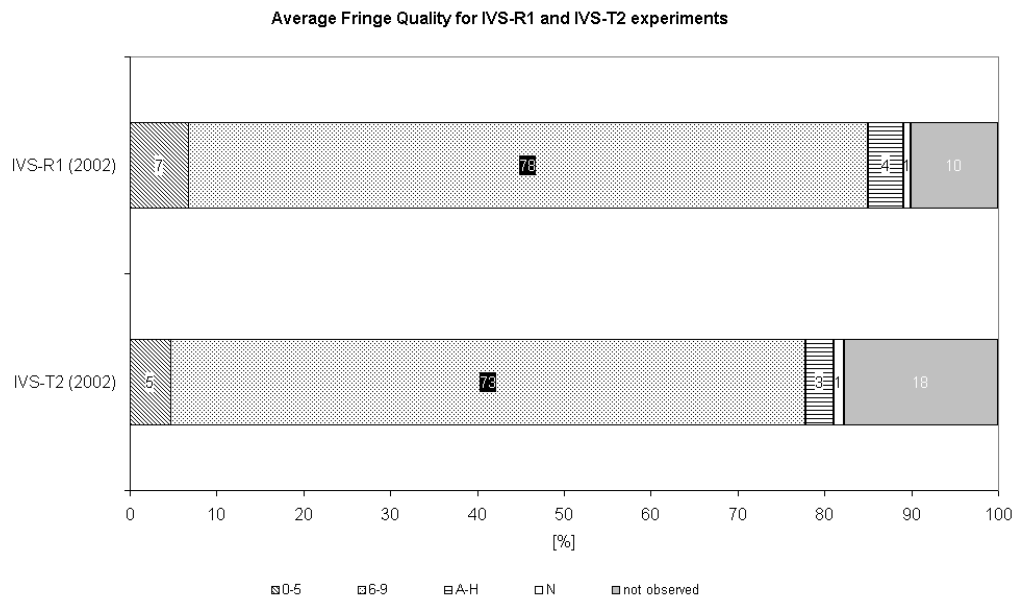


Figure 3: Average fringe quality of the final data for IVS-R1 and –T2 experiments.

## 5 Conclusions

Based on the detailed analysis of the processed experiments at the Bonn Correlator in the years 2001 and 2002 the following conclusions can be made:

- The tape shipment is the bottleneck in the processing chain. This can be optimized by either choosing fast couriers or migrating to e-VLBI.
- The correlation and recorrelation take a factor of 2.5 with respect to the total observing time. This is dominated by 60 seconds scan setup time needed for head-positioning, synchronization and is additional increased by tape changes. An improvement is expected with the usage of Mark5 and/or e-VLBI recording systems.
- Recorrelation is a major source of experiment processing inefficiency. The necessity of the recorrelation is still an individual question of each experiment.
- About 75% of the final data produced in 2002 had good quality, about 24% of them had bad quality due to various problems present at the stations and about 1% of them had bad quality due to playback problems at the correlator.
- The close cooperation between the correlator and the observatories is extremely important and should continue.

## References

- A. Müskens, I. Rottmann, H. Rottmann, A. Höfner, I. Benndorf, General Meeting Proceeding, 2002, eds. N. R. Vandenberg & K.D. Baver, Tsukuba, Japan, p.102

# The EVN MkIV Data Processor at JIVE

R.M. Campbell<sup>1</sup>

*Joint Institute for VLBI in Europe (JIVE), Dwingeloo, the Netherlands*

**Summary:** The vast majority of astronomical EVN experiments, and about half of the global experiments, are now correlated at JIVE. Processing continuum, cross-polarization, phase-reference, or spectral-line experiments is now essentially routine. Since the Barcelona meeting we have significantly increased throughput and efficiency, in terms of boosting physical limits, reducing vulnerability to various bugs, developing new astronomical capabilities, and strengthening liaison procedures with PIs. The move to Mark5 and fiber-linked VLBI (*e*-VLBI) is already underway. Small-scale test observations have been carried out in both areas. In the longer term, we have entered into a proof-of-concept project with a pan-European gigabit research network (GÉANT) and various national research and educational networks to demonstrate the feasibility of real-time correlation among EVN stations.

## 1 Background

A key item in the MkIV upgrade of the EVN was the construction of the EVN MkIV data processor at the Joint Institute for VLBI in Europe (JIVE). JIVE is hosted by ASTRON in Dwingeloo, the Netherlands, and is funded by science councils of a number of European countries. Special projects have been funded directly by the EU. The EVN MkIV data processor (Casse, 1999; Schilizzi *et al.*, 2001) was constructed in the context of the International Advanced Correlator Consortium through which the other MkIV geodetic correlators were also built, with significant contributions, from European members, in hardware from CNR/IRA, control software from Jodrell Bank, and correlator software from ASTRON.

The first fringe on the EVN MkIV data processor was seen on 21 July 1997 (Phillips and van Langevelde, 1999), and its official inauguration took place on 22 October 1998. The “first science” resulting from data correlated on the EVN MkIV data processor detected HI absorption against the counter-jet very close to the nucleus of NGC 4261 (van Langevelde *et al.*, 2000). The first paper to be published in *Nature* based on EVN observations correlated at JIVE has also appeared (Klöckner *et al.*, 2003), which uses OH mega-maser emission to study the kinematics and spatial structure of the circumnuclear torus in Mrk 231.

The EVN MkIV data processor now correlates the vast majority of astronomical EVN experiments, and about half of the global experiments. Here, we will concentrate on areas of interest to the user having data correlated at JIVE: tools for planning observations with regard to the data processor’s increased capabilities, current operational and communication flow between JIVE and the PI, and what we at JIVE do to get your data to you in a usable form. More information about using the EVN and JIVE can be found at the websites <sup>(2)</sup> and <sup>(3)</sup>. We conclude with a look towards the future in terms of disk-based recording (Mk5) and linking the stations to the correlator via fibre (*e*-VLBI).

---

<sup>1</sup>on behalf of the EVN Data Processor Group at JIVE

<sup>2</sup><http://www.evlbi.org>

<sup>3</sup><http://www.jive.nl>

## 2 Capabilities

Basic characteristics of the design of the EVN MkIV data processor include: correlation of up to 16 stations with 16 channels per station, 1 Gb/s recording (via 2 head-stacks  $\times$  32 tracks/head-stack  $\times$  16 Mb/s/track), and use of either MkIV and VLBA format recordings. Figure 1 shows the data playback units, the station units, the data distributor unit, and control computers. The correlator itself is housed in a separate room out of this view.



Figure 1: A view of the data playback units, the station units, the data distributor unit, and control computers of the JIVE MkIV Data Processor.

The principal science drivers behind the development of the data processor and associated software include the ability to handle continuum dual-polarization observations, spectral line experiments (*i.e.*, providing lots of frequency points and narrow bandwidths to provide high spectral resolution), and phase-reference mapping.

### 2.1 Features Snapshot

The EVN MkIV data processor can currently correlate/provide:

- 1- and 2-bit sampling (2-bit observations are by far the more common).
- parallel- and cross-polarization products if desired in dual-polarization observations.
- up to 4096 frequency points per baseline (see the discussion following equation 1 below).
- fan-out modes, where 1 channel is written onto 2 or 4 tracks during recording, increasing bandwidth without using higher tape speeds.
- Mk III, Mk IV, VLBA, and Mk5 recordings.
- sustained 512 Mb/s recordings, a capability that is currently unique to the EVN (full 1 Gb/s awaits deployment of the disk-based Mk5 recorders, owing to cross-talk within the playback heads in the tape-playback units at 320 ips).
- oversampling at 2 or 4 times the Nyquist frequency in order to provide subband bandwidths,  $BW_{sb}$ , down to 500 kHz (the maximum Nyquist-sampled  $BW_{sb}$  is 16 MHz).
- multi-pass correlation (*i.e.*, for observations having  $>16$  stations at any given time).

Capabilities whose development is still underway or not yet fully tested include:

- ⊙ pulsar gating.
- ⊙ multiple field centers (correlation of >1 phase centers in one pass) — most likely to be implemented in the PCI (*cf* §2.3).
- ⊙ playback at a tape speed different than that used in recording.

Capabilities that are yet to come include:

- phase-cal extraction.
- sub-netting.
- recirculation — achieving greater equivalent correlator capacity for observations that don't use the maximum bandwidth per channel (see the discussion following equation 1).
- space VLBI.

## 2.2 Correlator Capacity

There are two equations that are useful when planning observations that will be correlated on the EVN MkIV data processor. The first relates to total correlator capacity:

$$N_{\text{sta}}^2 \cdot N_{\text{sb}} \cdot N_{\text{pol}} \cdot N_{\text{frq}} \leq 131072 \cdot \mathcal{R}. \quad (1)$$

Here, from right to left,  $\mathcal{R}$  is the recirculation factor (see next paragraph).  $N_{\text{pol}}$  is the number of polarization combinations wanted in the correlation (1, 2, or 4).  $N_{\text{sb}}$  represents the number of different frequency subbands, counting lower- and upper-sidebands from the same BBC as distinct subbands, but not multiple polarizations in the same sideband (these enter via  $N_{\text{pol}}$ ). The value to use for  $N_{\text{sta}}$  is “granular” in multiples of 4: *e.g.*, if you have 5–8 stations, use “8”. Independent of this equation, the maximum ( $N_{\text{sb}} \cdot N_{\text{pol}}$ ) is 16 (a station-unit limitation), and the maximum  $N_{\text{frq}}$  is 4096 (a single baseline/SB/pol must fit onto a single correlator board). You should pick the various  $N_x$  parameters in designing your observation such that the equation holds, otherwise you will have to compromise on at least one of them when it's time to correlate. Some examples of configurations that would use the full correlator capacity (without recirculation) include:

8 sta	1 SB	1 Pol	2048 Frq	(EVN spectral-line)
16 sta	8 SB	4 Pol	16 Frq	(global cross-polarization mapping)
12 sta	14 SB	1 Pol	64 Frq	(geodesy)

When recirculation is operational, the constant term 131072 can be multiplied by recirculation factor,  $\mathcal{R}$ , for observations that don't use the full (Nyquist-sampled) 16 MHz bandwidth per SB/polarization channel. In principle,  $\mathcal{R}_{\text{max}}$  would be set by 16 MHz/ $BW_{\text{sb}}$ , but there may be a smaller absolute limit depending on the actual implementation.  $N_{\text{frq}}$  would still be subject to the maximum limit of 4096, as discussed above.

## 2.3 Output Capacity

The second equation relates to output rate,  $\mathcal{U}_{\text{out}}$ , capacity:

$$\left( \frac{N_{\text{sta}}^2 \cdot N_{\text{sb}} \cdot N_{\text{pol}} \cdot N_{\text{frq}}}{4096} \right) \cdot \frac{48}{t_{\text{int}}} \simeq \mathcal{U}_{\text{out}} \quad [\text{kB/s}]. \quad (2)$$

The first term in the left-hand side is the number of boards,  $N_{\text{brd}}$ , required for the correlation (the full correlator comprises 32 boards). Our current peak  $\mathcal{U}_{\text{out}} \simeq 1500$  kB/s. An alternative way to think about the output-rate limit is to remember that the minimum  $t_{\text{int}}$  for a configuration using the whole correlator is now 1 s; configurations that use no more than one-half or one-quarter of the correlator can achieve minimum  $t_{\text{int}}$  of 1/2 s and 1/4 s respectively. In the future, the Post-Correlator Integrator (PCI) will provide  $\mathcal{U}_{\text{out}}$  as high as 96 MB/s, providing minimum  $t_{\text{int}}$  for the whole correlator of 1/64 s. However, if recirculation is being used, the minimum integration time would be  $\mathcal{R}/64$  s. The low integration times, together with the fine spectral resolution afforded by large  $N_{\text{frq}}$ , will provide the possibility to map considerably wider fields of view through reduced bandwidth- and time-smearing effects in the  $u$ - $v$  plane. Furthermore, besides increasing the absolute output data rate, the PCI will also provide additional computational capability prior to sending the correlated data to the receiving workstation, which could be used, among other things, to FFT the data into frequency-space or to apply phase-corrections to obtain multiple field-centers in a single correlation pass. This latter capability would appeal to people interested in specific targets within the primary beams of the participating stations, but who wouldn't necessarily want the volume of data ( $N_{\text{frq}} \cdot N_{\text{int}}$ ) associated with being able to map the entire area on the sky subtended by them.

## 2.4 Recent Improvements

Since the Barcelona meeting, we have continued to improve the throughput, reliability, and astronomical capabilities of the correlator. The following points represent some of the accomplishments within this period:

- A TRM byte slip is an event where one track of data spontaneously shifts by 8 lags with respect to all the other tracks. For our typical 2-bit fan-out data, such an occurrence results in a multi-peaked fringe, and hence ringing in the frequency-space spectrum. Recorrelation of a pass containing a byte slip was the only recourse; ensuring all of them were found significantly lengthened the post-correlation review (*cf* §3.3). We implemented a mechanism to detect and repair TRM byte slips and to flag associated data in the logic of the responsible station-unit boards. We have thus cut down on the number of recorrelations required and streamlined the review process, while ensuring data integrity.
- Observations at  $BW_{\text{sb}} = 16$  MHz could cause read/write pointers of a circular buffer in a board in the station unit to fall on top of each other, resulting in a shift of the data- and model-times of  $\simeq 131$  ms and an associated jump in the residual delays and rates. Use of a servo feature for the buffer pointers overcame this problem.
- We increased correlator output rate by a factor of 8, so that the whole correlator can be read out in 1 s (*cf* §2.3). This improvement came about primarily by incorporating software to read out the four crates in parallel, and also by reducing the size of the auxiliary information output along with the correlated data.
- The van Vleck correction for 2-bit data depends on the fraction of high- and low-magnitude bits within an integration, but this dependence was not being taken into account. If a BBC at a station had such "sampler statistics" different from the expected values, a non-unity autocorrelation peak would result. The amplitudes on baselines containing it would be affected to a lesser degree. If the sampler statistics were especially bad on both stations in a baseline, even the closure amplitudes could be affected at a  $\sim 1\%$  level. We now compensate for the observed sampler statistics per station/BBC in a post-correlation program.

- Positions of EVN stations that don't usually participate in geodetic campaigns have been significantly improved, in some cases with adjustments on the order of 5m (Charlot et al., 2001, Charlot et al., 2002). In addition, a better tie between the Wb single-dish and array positions was determined, and an unrelated effect that introduced discrete phase jumps in  $Wb_{arr}$  (typically once per several hours) was detected and repaired during this process. We contacted PIs of previously correlated experiments to help them incorporate these station-position improvements directly into their AIPS data (Campbell, 2002). The EVN performance in phase reference experiments has significantly improved following these improvements (*i.e.*, more reliable detection/imaging of fainter sources).
- JIVE has begun the process of consolidating experiment information of interest to PIs into a web-accessible archive. This will contain station feedback, a summary of the correlation and post-correlation review, various standard plots, preliminary calibration results, and the FITS data (*cf* §3.3).

### 3 Operational Overview

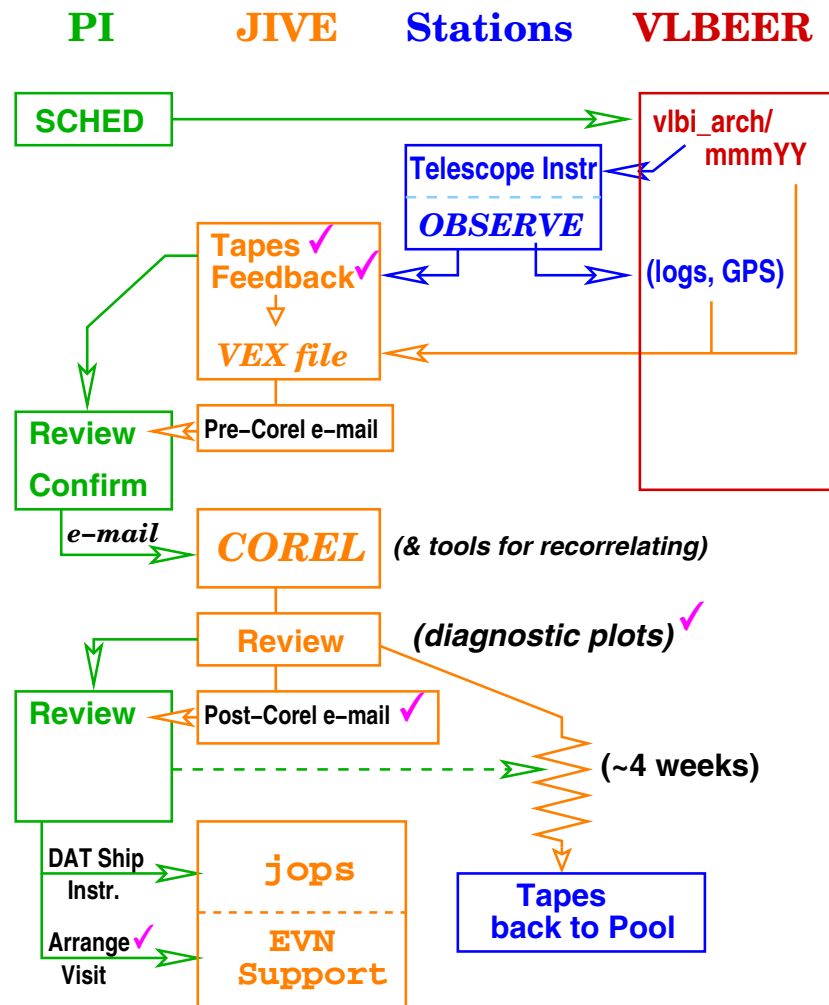


Figure 2: Operational flow for the observation and correlation of an experiment.

### 3.1 Pre-correlation

Figure 2 summarizes operational and communication flow between the PI, JIVE, and various EVN assets during an EVN astronomical experiment. The user deposits SCHED output on VLBEER, from which individual stations draw their observing instructions. Help from JIVE may of course be requested during the scheduling process, especially if any problems are encountered. Following the observations, the stations deposit logs and GPS data on VLBEER, send tapes to JIVE, and post comments to the EVN feedback facility. We pull necessary information off VLBEER and prepare files that will drive the correlation. Our principal control file is in VEX format, and is based on information gathered from the observing schedule, station logs and GPS data, and EOP data from the IERS. We correct scheduled station positions to reflect our best current values, including plate motion computed to the observing epoch. We send e-mail to the PI describing what we envision the correlation of the experiment to entail. The PI has the opportunity to review the correlation parameters (*cf* equation 1) and all other available information (items with a check in Figure 2 are available via the EVN or JIVE web pages) and writes back to pass along any requests for changes (*e.g.*, improved source coordinates, *etc.*) and/or confirm that correlation can go ahead.

### 3.2 Correlation & Logistics

We operate the correlator 80 hours per week, from which time system testing and development must also come. Our basic unit of correlation is usually a tape pass. Our control software is best suited to continuous tape motion; reasonably short gaps in the schedule are “waited out” in real time. Preparation for a pass, assuming the tapes are pre-positioned to approximately the correct footage, is  $\sim 9$  minutes (for thin tape, passes are typically either 22 or 44 minutes). This preparation time includes:

- calculations: parsing the VEX file, selecting stations/scans to include, and computing the *a priori* model.
- tape manipulation: going to *a priori* footage, positioning the heads transversely such that they read tracks with an expected time-on-tape (*i.e.*, one within the bounds of the requested scans), positioning the tape longitudinally such that the time-on-tape corresponds to the initial scan time, and waiting until the slowest tape is ready.

When correlation of the experiment is finished we review the output, looking for any necessary recorrelations that weren’t caught in the course of the original correlation. The shift to thin-tape-only operation has improved playback quality; this together with the excision of TRM byte slips has markedly reduced the amount of passes requiring recorrelation. Once all recorrelations are exhausted, we make a variety of information available to the PI (as described in §3.3), and arrange for shipment of the resulting FITS data. Unless contacted by the PI to the contrary, we aim to release an experiment’s tapes four weeks after the PI is notified of the experiment’s completion, in order to ensure the supply of tapes in the pool remains replenished for future observations — which is of increased importance now that the EVN has moved to thin-tape-only operation. Besides the review products mentioned below, the PI of course may also discuss the experiment/correlation with the responsible JIVE support scientist and/or arrange for visiting JIVE for help in data reduction if desired. Specific programs exist to provide financial support for European PIs from non-EVN institutes and their collaborators to encourage visits to EVN institutes, including JIVE — see the EVN web page under the “[Access to the EVN](#)” menu item.

### 3.3 Post-correlation Data Review

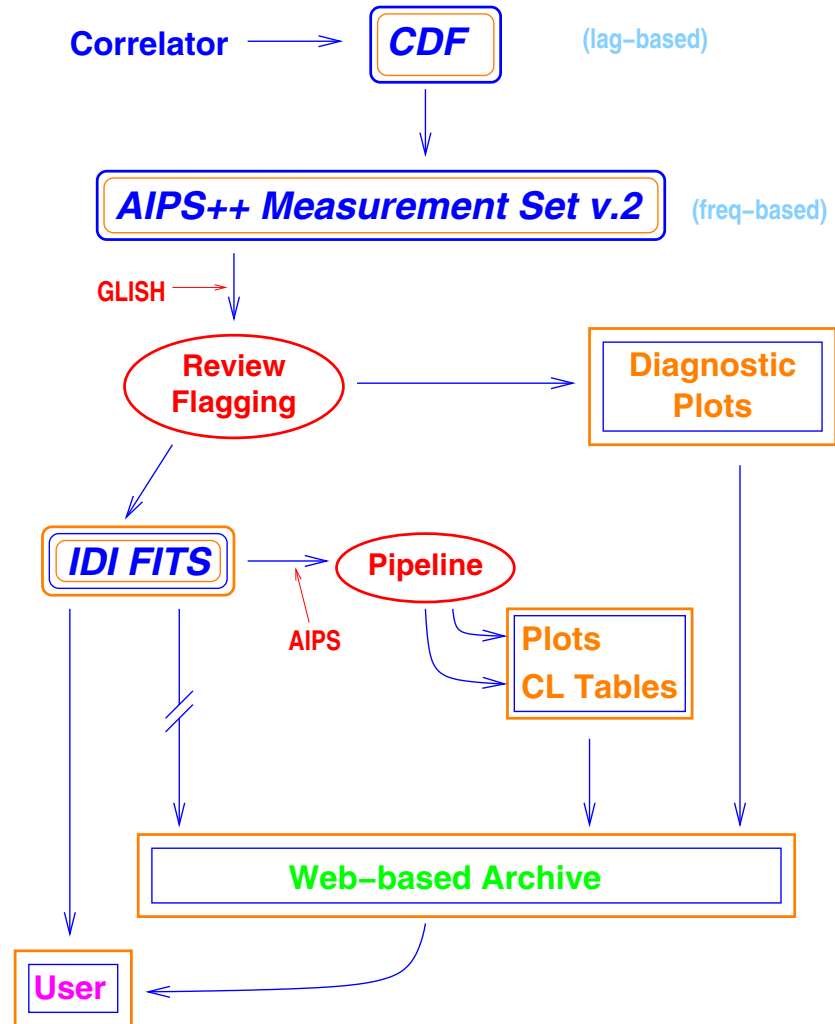


Figure 3: Post-correlation review process for an experiment.

Our main priority is always the quality of the data we provide to the EVN users. Our internal data review process, as shown in Figure 3, begins by transforming the lag-based correlator output into AIPS++ Measurement Sets (MS). This MS contains a data-cube of the real & imaginary components of the correlation-function spanning, for each subband of each baseline/autocorrelation,  $N_{\text{pol}}$ ,  $N_{\text{int}}$ , and  $N_{\text{frq}}$  (or  $N_{\text{lag}}$ , if the need arises). We can then investigate, using the `glish` language, slices of the correlation functions in both time and frequency/lag, allowing us to detect and diagnose various problems with the recorded data or the correlation itself, and to determine any scans for which recorrelation would be profitable. We can also make various plots more suited to providing feedback to the stations rather than to the PI (*e.g.*, parity-error rates, sampler statistics). We apply various corrections to the correlated data at this stage (*e.g.*, the 2-bit van Vleck compensation, *cf* §2.4). We also flag subsets of the data for low weights and other known problems resulting in (uncorrectable) spurious correlation amplitudes and/or phases.

The last step converts the final MS into FITS format, usually written to a DAT tape. We send this to the PI, along with a summary of the correlation itself. The FITS DAT can be read into AIPS directly using

FITLD. We also make various diagnostic plots available to the PI. The EVN pipeline operates on the FITS data to create the first few AIPS CL tables (*e.g.*,  $T_{\text{sys}}$ -based amplitude calibration, off-source flagging, *etc.*), which put the data in a state that the PI can use more easily. Plots, summaries, and pipeline results also go to the EVN archive (accessible via <sup>(4)</sup>). The FITS files themselves, subject to release policies that are still under review, will also be available from this archive.

### 3.4 Statistical Summary

At the time of the Leipzig meeting, we had managed to work through the correlation backlog that had accumulated over the years. Since the beginning, we have now completed correlation and distribution of 129 user and 71 test experiments, with a further user experiment on hold awaiting specific correlator features. A total of 57 different PIs from 18 different countries are represented among the user experiments. The May/June 2003 session will bring 23 user and 5 test experiments into JIVE (boosting the PI total to 64). For the first time, we are correlating user experiments from a given session while the session is still underway.

## 4 Towards the Future

Traditional VLBI recording onto tape has some well-known drawbacks in terms of logistical turn-around, playback reliability, hardware/media cost and availability, *etc.* The shift to disk-based recording (Mk5) and data transmission via fibre (*e*-VLBI) should lead to marked improvements. In this section, we'll briefly discuss recent activity in these areas at JIVE.

### 4.1 Mark 5

Disk-based recordings will provide better and more reliable playback, higher data rates, and increased correlation efficiency (via significantly shorter per-job preparation time — saving  $\sim 6$  min per pass by accomplishing the equivalent of the tape-synchronization tasks mentioned in §3.2 in  $\sim 10$  s). The expected reduction in recorrelations owing to bad playback will further increase the net correlation efficiency.

We have recently performed our first tape-tape/disk-tape/disk-disk comparisons, using data from a network monitoring experiment (NME) in February 2003 in which some stations recorded in parallel on both disk and tape. Separately, 1 Gb/s observations were made in March between Jodrell Bank (Jb<sub>2</sub>) and Metsähovi at K-band with the PC-EVN recording system. The data were transformed into Mk5 format and correlated successfully, leading to our first fringes from 1 Gb/s recordings. More information about these and other disk-recording test observations can be found on the EVN web-page, under the heading “[Latest News on EVN Developments](#)” via the “[EVN TOG](#)” (Technical & Operations Group) menu item.

### 4.2 *e*-VLBI

Transmission of data directly from the stations to the correlator provides potentially much faster turn-arounds, as days-worth of shipping delay can be avoided. This can open the way for target-of-opportunity

---

<sup>4</sup><http://www.jive.nl/archive/scripts/fits/listfits.php>

observations of transient phenomena, without concern for having a pre-deployed supply of recording media in place at all stations outside network sessions. Further, considerably faster feedback can be provided to stations, potentially avoiding problems that may otherwise have remained undetected for some time. During fringe-test observations at the beginning of network sessions, some stations already `ftp` a small amount of data to JIVE, and indeed some problems have been detected in time to repair prior to the session. For future correlators, *e*-VLBI also provides the opportunity for bandwidths exceeding our current 1 Gb/s limit.

JIVE participated in iGrid2002, an international grid application tested event held in Amsterdam in September 2002. Our project demonstrated data rates over existing research networks. Data recorded onto disk at Jodrell Bank were transmitted to Amsterdam, where packet tracing and transit times were checked, and then forwarded up to Dwingeloo. After buffering onto disk, they were correlated against a tape from Wb, and a direct connection back to iGrid2002 allowed simultaneous display of the resulting fringes.

A more ambitious test will be the “EVN-NREN Proof of Concept” project, which aims to provide a real-time connection for five EVN telescopes (outside the Netherlands) to JIVE. These connections will be via individual national research & education networks (NRENs) and GÉANT, a pan-European research network. The status of the “last-mile” problem — connecting the telescopes themselves to the closest NREN node — differs from station to station. An EVN goal for this project would be same-day imaging of sustained 1 Gb/s observations. Considerably more information about the iGrid2002 demonstration and the EVN-NREN PoC can be found on EVN web-page under the “[e-VLBI](#)” menu item.

To help process small amounts of fringe-test observations that have been `ftp`'ed into JIVE, we have entered negotiations with CRL in Kashima to obtain a version of their KSRC/CRL VLBI software correlator. They have already found Wb-Ks fringes using Wb data `ftp`'ed to Kashima and transformed from Mk5 to K5 format (also discussed under the “[EVN TOG](#)” web page, as above in §4.1). Use of such a software correlator would permit rapid investigation of smaller amounts of data without impacting the operations of the main correlator.

The week after the Leipzig meeting, JIVE hosted the 2<sup>nd</sup> *e*-VLBI Workshop. Abstracts and most presentations can be downloaded from the workshop web-page, which is linked from the main JIVE web-page.

## References

- Casse, J.L., “The European VLBI Network MkIV Data Processor,” in *Proceedings of the 4<sup>th</sup> EVN/JIVE Symposium*, eds. M.A. Garrett, R.M. Campbell, & L.I. Gurvits, *New Astron. Rev.*, **43**, 503–508, 1999.
- Schilizzi, R.T., Aldrich, W., Anderson, B., *et al.* “The EVN-MarkIV VLBI Data Processor,” *Exper. Astron.*, **12**, 49–67, 2001.
- Phillips, C.J. & van Langevelde, H.J., “Fringes on the EVN MkIV Data Processor at JIVE,” in *Proceedings of the 4<sup>th</sup> EVN/JIVE Symposium*, eds. M.A. Garrett, R.M. Campbell, & L.I. Gurvits, *New Astron. Rev.*, **43**, 609–612, 1999.
- Van Langevelde, H.J., Pihlström, Y.M., Conway, J.E., *et al.* “A Thin HI Circumnuclear Disk in NGC4261,” *Astron. & Ap.* **454**, L45–48, 2000.
- Klöckner, H.-R., Baan, W.A., & Garrett, M.A., “Investigation of the Obscuring Circumnuclear Torus in the Active Galaxy Mrk 231,” *Nature*, **421**, 821–823, 2003.

- Charlot, P., Campbell, R., Alef, W., *et al.* "ITRF2000 Positions of Non-geodetic Telescopes in the EVN," in *Proceedings of the 15th Working Meeting on European VLBI for Geodesy and Astrometry*, eds. D. Behrend & A. Rius, (IEEC/CSIC: Barcelona), 194–200, 2001, <sup>(5)</sup>.
- Charlot, P., Campbell, R.M., Alef, W., *et al.* "Improved Positions of Non-geodetic EVN Telescopes," in *Proceedings of the 6th EVN Symposium*, eds. E. Ros, R.W. Porcas, A.P. Lobanov, & J.A. Zensus, (MPIfR: Bonn), 9–12, 2002, <sup>(6)</sup>.
- Campbell, R.M. "Operational Issues of the Improved EVN Station Positions," in *Proceedings of the 6th EVN Symposium*, eds. E. Ros, R.W. Porcas, A.P. Lobanov, & J.A. Zensus, (MPIfR: Bonn), 37–40, 2002, <sup>(7)</sup>.

---

<sup>5</sup><http://www.ieec.fcr.es/hosted/15wmevga/proceedings/charlot>

<sup>6</sup><http://www.mpifr-bonn.mpg.de/div/vlbi/evn2002/book/PCharlot.pdf> or \*.ps.gz

<sup>7</sup><http://www.mpifr-bonn.mpg.de/div/vlbi/evn2002/book/RCampbell.pdf> or \*.ps.gz

# First Results of the TIGO Borehole Tiltmeters in Concepción

H. Hase, A. Böer, S. Riepl, M. Avendaño, S. Sobarzo, R. Aedo,  
G. Remedi, M. Moreno, M. Sanchez, G. Hermosilla

*Observatorio Geodésico TIGO, Universidad de Concepción, Chile*

**Summary:** The Transportable Integrated Geodetic Observatory (TIGO) is the only fundamental station for geodesy in Latin-America. TIGO was designed and constructed by the German Federal Agency for Cartography and Geodesy (BKG) and it is now installed at Concepción, Chile since 2002. The data production for international services as such as IVS, IIRS, IGS, BIPM began in 2002. In 2003 a set of 3 borehole tiltmeters has been installed. First results are presented here, focussing on the stability of the largest monument for the radiotelescope.

## 1 Achievements of TIGO in 2002

The Transportable Integrated Geodetic Observatory (TIGO) was designed as a fundamental station for geodesy. Hence it is equipped with all relevant sensors and instruments like radiotelescope for VLBI, a satellite laser ranging system, GPS/GLONASS permanent receiver, superconducting gravity meter, seismometer, meteorological sensors, water vapour radiometer and an atomic clock ensemble. The instrumentation of TIGO allows significant contributions to the realization of global reference systems (*Hase, 1999*). Within its first year of operation in Concepción, Chile, TIGO fulfilled the expectations with its recognition by four international services: IVS, IIRS, IGS and the UT-Service of BIPM.

In 2003 the installation and operation of secondary devices which are helpful to measure local and regional position changes has to be realized. In March 2003 a local survey was performed to determine the space vector between the VLBI-, SLR- and GPS/GLONASS reference point. The analysis of the local survey is pending.

For monitoring the local movements 3 borehole tiltmeter had been installed at the monuments for VLBI, SLR and GPS/GLONASS operation and are working since April 2003. The regional control network with GPS-permanent stations and the installation of a tide gauge for vertical datum are pending and will be realized in the second half of 2003.

## 2 Borehole tiltmeter at TIGO

The monument for the radiotelescope consists of a block of concrete with the dimensions  $10 \times 10 \times 1.5m^3$ . During the construction an empty PVC-tube was put vertically at the edge of the block (see fig. 2) to host later the borehole tiltmeter. Whatever inclination will happen to the block of concrete, it also will move the radiotelescope with the reference point, the tube and hence the tiltmeter as sensor of for the inclination.

As for the radiotelescope monument, a similar construction was realized by the SLR monument and the GPS-pillar. During April 2003 the tiltmeter had been installed and since then data are archived.

The borehole tiltmeters Model 722-B were produced by the company Applied Geomechanics Incorporated. The resolution is according to its specification in order of  $1\mu rad$  (*Manual, 1999*). The borehole tiltmeter is about 1.2m long (s. fig. 1). This type of tiltmeter measures inclinations with two perpendicular channels ( $X, Y$ ) and the device's temperature

(Avendaño, 2003). A measured inclination of about  $1\text{mrad}$  corresponds therefore to a relative horizontal movement of about  $1\text{mm}$  between both ends of the tiltmeter ( $b/r = \alpha/\rho$ ). With the borehole tiltmeter it is possible to determine the local stability of the monumentation and find out about periodically variations which might have an effect to the geodetic measurements.

The resolution of the borehole tiltmeter is not sensitive enough to monitor the Earth tides which usually show inclinations below  $1\mu\text{rad}$ . TIGO records the Earth tides with its superconducting gravity meter.



Figure 1: One of the three TIGO borehole tiltmeter before its vertical installation in the TIGO monuments for radiotelescope, lasertelescope and GPS/GLONASS-pillar.

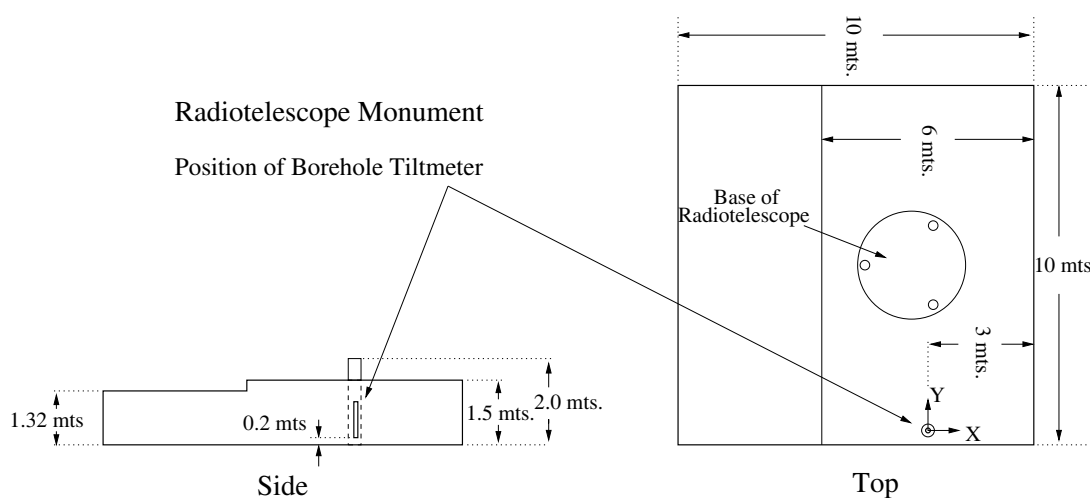


Figure 2: Location of the tiltmeter within the block of concrete serving as monumentation for the radiotelescope. The top view shows also the orientation of the axis of the tiltmeter, which are in parallel to the physical limits of the monument.



Figure 3: Foto of the TIGO radiotelescope monument. The location of the tiltmeter is inside the black PVC-tube with the small grey switch box next to the white cable channel box.

## 2.1 First results of TIGO's tiltmeters

The installation of the tiltmeters was realized during April 2003. The data sets are recorded in a database of TIGO (Avendaño, 2003).

Fig. 4 and 5 show the measured signals of the first three weeks of data. A strong daily signal can be detected. The daily periodicity can be very well explained with temperature variations due to the illumination of the monument by the sun during the day. The daily warming and cooling cycle of the monument results in thermal expansions at the upper part of the platform. Hence the expansion is larger on the top than inside the ground soil resulting in a daily tilt is caused by air temperature variation. E.g. April 21 was a rainy day where clouds covered the entire day the sky, while the days before and after the monument was exposed to the strong sun illumination. In Y-direction the sensor is sensitive to the effective thermal expansion of almost 10m of platform. In X-direction the sensor is less sensitive because of its location (fig. 2) and therefore the amplitude is lower (fig. 4, 5).

The measured tilts are decoupled from the instrumental temperature as it is shown in the instrument temperature (fig. 6), but coupled to the ambient temperature as it is measured by the TIGO meteorological station (fig. 7).

The proportionality in the amplitudes of the X, Y-tiltchannels compared with the amplitude of the ambient temperature (fig. 7) confirms the interpretation that the tilts are induced by thermal expansion of the monument due to solar illumination.

The thermal expansion of the monument is at maximum at the physical limit of the monument (Y-direction). Assuming a homogeneous expansion of the monument, the center which is near the mount of the radiotelescope will very likely not move significantly. The measured tilt at the edge of the monument corresponds to a horizontal movement of

about  $0.2\text{mm}$ . This value is not critical for the analysis of VLBI-data, since the bearings of the radiotelescope also allow  $0.2\text{mm}$  of game for turning the axis. However a shadding construction for the concrete monument will decrease the max. amplitudes during sunny and hot days to about less than a third part (as shown on the rainy day April 21).

Equivalent data sets are available for the SLR and GPS/GLONASS installation. The amplitudes due to daily thermal expansions are significant, but much lower compared with the radiotelescope monument. This behaviour is explained with the much smaller dimension of the SLR-monument ( $3 \times 3 \times 1.5\text{m}^3$ ) and the deeper installation of the tiltmeter in the GPS/GLONASS pillar at  $-5\text{m}$  which is less exposed to the daily temperature variations.

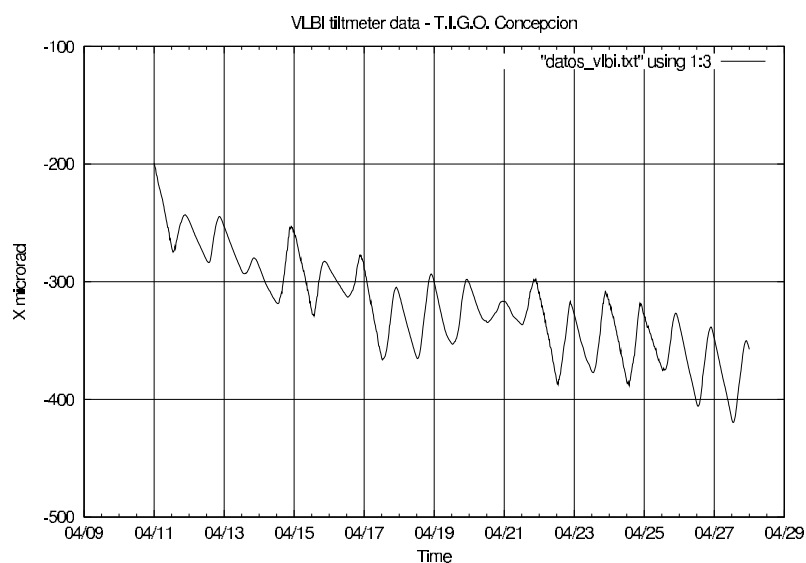


Figure 4: Tiltmeter channel X at radiotelescope monument.

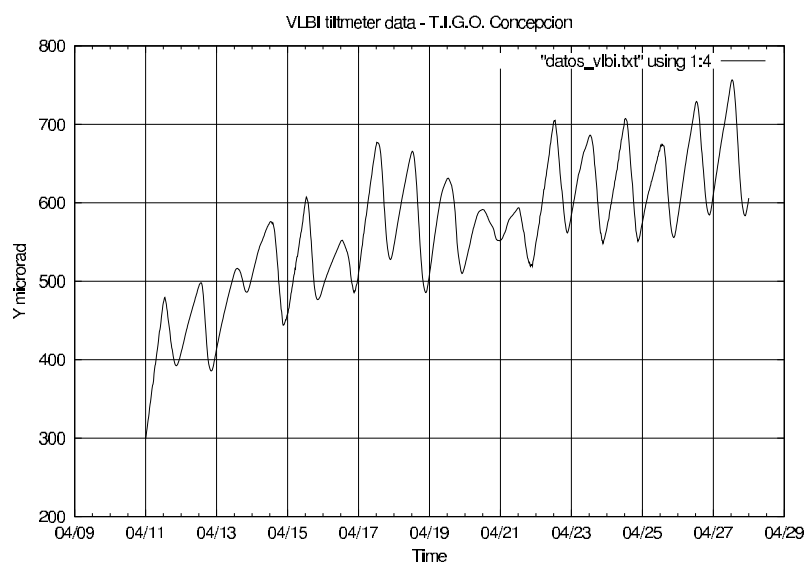


Figure 5: Tiltmeter channel Y at radiotelescope monument shows the largest amplitudes.

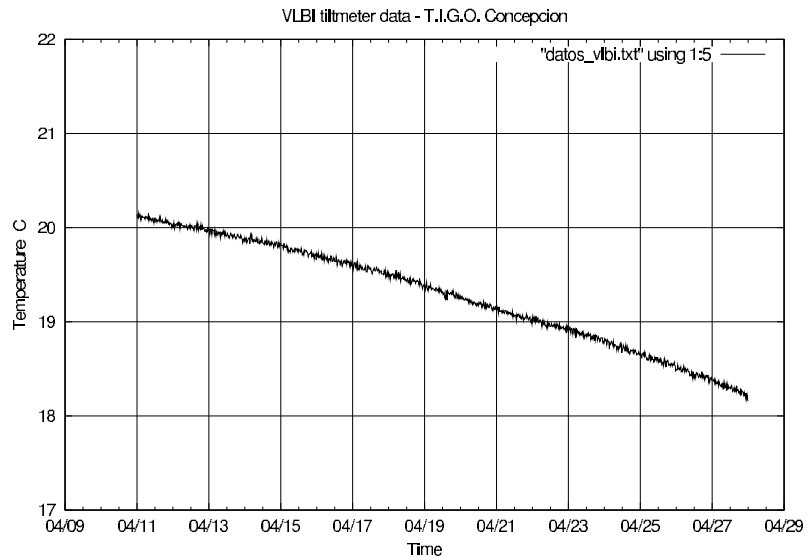


Figure 6: Tiltmeter channel temperature at radiotelescope monument confirms that the X, Y periodicity are real tilts. The negative gradient of the instrumental temperature is a seasonal effect due to autumn in the southern hemisphere.

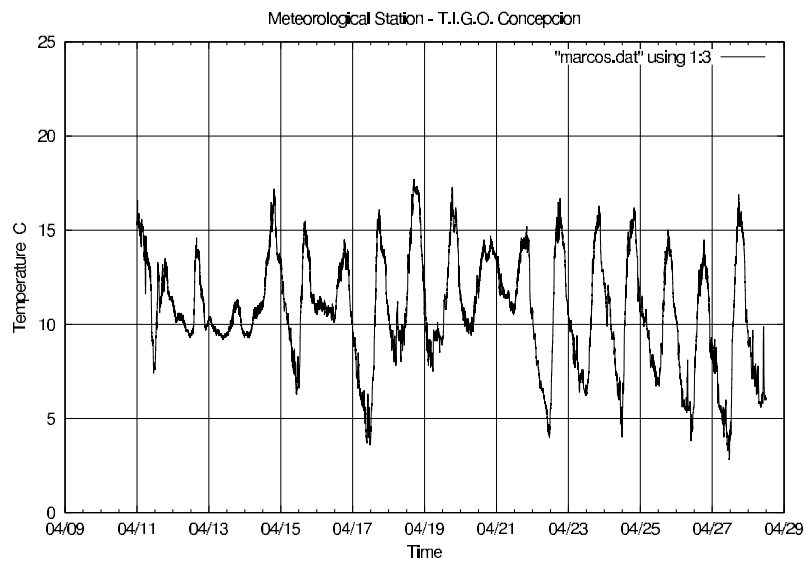


Figure 7: Ambient air temperature at TIGO. April 21 was a covered day with rain. Hence the temperature variations were much smaller than on sunny days before and after.

### 3 Outlook

The installation of the borehole tiltmeter at the TIGO monuments will accompany the ongoing measurements for the international services and allow to know the local behaviour. The tiltmeter recordings require complementation by levelling and local survey as well in order to determine vertical or horizontal movements. They are performed in yearly intervals.

The regional control network with four GPS-permanent stations in the surrounding area of the TIGO-platform in about 40km distance is in the planning phase and should be realized during 2003.

While the local and regional sensors are being installed the VLBI experiments for the International VLBI Service continue in the two rapid series R10xx and R40xx. Other VLBI experiment series such as E30xx, RDV and OHIG are part of observation program at TIGO.

## References

- Avendaño, M.: Los Inclínometros de TIGO, unpublished thesis, Universidad del Bío Bío, 2003.
- Hase, H.: Theorie und Praxis globaler Bezugssysteme, Mitteilungen des BKG, Band 13, Frankfurt a.M., 1999
- Applied Geomechanics Incorporated: User's Manual: Modell 722 Borehole Tiltmeter, Santa Cruz, CA 95062, U.S.A., 1999

# Effelsberg Station Report: May 2003

R.W. Porcas

*Max-Planck-Institut für Radioastronomie, Bonn, Germany*

**Summary:** This is a brief station report for the Effelsberg 100 m radio telescope for the period since the last Working Group Meeting.

## 1 Developments: October 2001 - May 2003

- **Replacement of worn gears in the azimuth drive.** This was completed by the end of 2001. During 2002 the “official” azimuth drive speed remained at 20° per minute, but tests of higher drive speeds are being made.
- **Adjustment of surface panels.** During summer 2002 holography measurements were made which confirm the improvement brought about by the adjustment, and revealed a discontinuity at “ring 14” (which is the boundary between the old solid surface panels and the outer, perforated aluminium panels).
- **Crack in the azimuth track.** This was discovered in January 2003 and fixed by the end of March. The telescope is now back in full operation.
- **MK5A: A unit has been ordered for Effelsberg.**
- **Dual-frequency GPS receiver.** This is used for making tropospheric delay measurements. Results are uploaded daily to BKG Wettzell. It is hoped to include these later as part of the MK4 correlator model.
- **Water Vapour Radiometer.** This has now been installed on the main building in Effelsberg. First attempts are being made to correct the atmospheric phase contribution for 3 mm VLBI data (see report by Alan Roy in these proceedings).



# Activities Around the Radiotelescope Wettzell (RTW)

W. Schlüter<sup>1</sup>, R. Kilger<sup>2</sup>, G. Kronschnabl<sup>1</sup>, W. Schwarz<sup>1</sup>, and R. Zerneck<sup>2</sup>

<sup>1</sup>*Fundamentalstation Wettzell, Bundesamt für Kartographie und Geodäsie, Kötzing, Germany*

<sup>2</sup>*Forschungseinrichtung Satellitengeodäsie, Technische Universität München, Germany*

**Summary:** The RTW is strongly involved in the IVS observing program. It contributes to the rapid turn around observing series as well as to the regular time series. In particular Wettzell and Kokee Park carry out the observations for the INTENSIVE-Program, which is a real candidate for the application of e-VLBI. Since 2002 in addition observations of INTENSIVE-type were carried out with the Tsukuba Telescope in Japan employing the Japanese K4-recording technology.

This paper documents the activities required to perform the observations, to maintain and improve the RTW and to meet the increasing expectations. As the RTW is in collocation with different space techniques and different local sensors a short summary of the major activities at the Fundamental Station are given.

## 1 Observations with RTW

RTW is designed for geodetic VLBI, which means that the intersection point of the azimuth and the elevation axis is clearly defined, that the telescope stability is given to parts of Millimeter even under the condition of strong wind loads and that the velocity in azimuth and elevation is fast compared to other telescopes of this size.

RTW contributes strongly to the IVS observing program. It could be pointed out that in the last years Kokee Park and Wettzell have been employed more than 100 days per year. In particular RTW participates in the observing programs as

- IVS R1, IVS R2,
- RDV (R&D with VLBA),
- IVS INT1, IVS INT2,
- EUROPE,
- O'Higgins,
- IVS-CRF,
- IVS R&D,
- IVS-T2.

Further more, during a few days per year some observations for Radio-astronomy were carried out.

RTW contributes since 1983 to the geodetic observing programs. A summary is given in table 1.

RTW is equipped with the Data Recording Systems as

- MK 4
- MK 5P
- MK 5A and
- K4

The MK 5P/A is employed for the IVS INT1 time series Wettzell-Kokee Park, the K4 is used for the IVS INT2 time series Wettzell-Tsukuba.

The MK 5 is the basis for e-VLBI tests, which are of importance for the data transfer of the INTENSIVE observations. The amount of data will be transferable via a high speed data link.

Table 1: RTW observations since 1983.

**BEOBACHTUNGEN AM RADIOTELESKOP IN WETTZELL VON 1983 - 2002**

BEOBACHTUNGEN	1983	1984	1985	1986	1987	1988	1989	1990	1991	1992	1993	1994	1995	1996	1997	1998	1999	2000	2001	2002	Σ2002
POLARIS-A/IRIS-A/ NEOS-A+B/CORE	3	67	72	72	72	73	73	73	59	48	60	62	52	53	52	45	51	58	90	106	1241
INT [A(UT1)]	0	73	211	276	281	282	287	287	292	236	281	225	287	200	277	248	278	235	200	202	4658
IRIS-S	0	0	0	4	5	3	3	12	12	12	12	12	12	12	12	10	12	12	12	0	157
EUROPE	0	0	0	0	0	5	2	4	3	5	4	6	6	6	6	5	6	7	3	4	72
NASA-Geod./CORE	0	2	12	12	12	5	1	0	21	22	15	23	15	33	5	6	7	6	6	13	216
NASA-Planet-Astr.	0	0	0	0	2	2	0	0	0	0	0	0	2	0	8	3	0	0	0	3	20
USNO	0	0	0	0	0	0	0	0	1	11	6	14	4	4	0	0	2	0	0	0	42
UNI/MPI/R/Inst.	0	0	0	0	0	0	0	3	5	0	2	2	3	5	2	4	2	3	1	3	35
Mobile Kampagne	0	0	0	0	0	0	10	0	4	21	4	4	-	0	0	0	0	0	0	0	43
Sonst. 1bis8h(K4)	0	16	13	25	27	1	19	23	22	1	1	2	6	10	1	0	1	0	0	21	189
Sonst. 24h/Mk-II	-	-	1 0	0 0	1 0	7 3	18 3	3 4	9 1	13 0	0 0	2 0	0 0	2 0	-	-	1 16	-	-	-	57 27
Anlagen.LaufZeit[h]	78	2061	2856	3191	3290	3137	2972	3322	3568	3259	3420	3775	3323	3568	3044	2642	2917	2941	3512	4023	60899
Wettzell-Team [h]	344	2640	3688	3908	4032	3976	3408	3976	3842	2921	2703	3468	2957	3140	2701	2428	2828	2548	2919	3620	62047
Studenten [h]	-	-	-	192	224	56	1140	256	443	1690	1365	808	390	504	214	201	286	383	676	383,5	9212
Σ Beob.zeit [h]	344	2640	3688	4100	4256	4032	4548	4232	4285	4611	4068	4276	3347	3644	2915	2629	3114	2931	3595	4004	71259

## 2 e VLBI activities at Wettzell

The IVS INTENSIVES are ideal candidates for data transfer via Internet (eVLBI), since the delay between recording of the data and getting the result for UT1 should be as short as possible. Wettzell will observe in 2003:

- 202 IVS INT1 (Baseline Wettzell-KokeePark) in Mk5 mode,
- 22 IVS INT2 (Baseline Wettzell-Tsukuba) in K-4 mode.

Employing a courier the transportation of the data to the correlator in Washington takes 2-4 days, the transportation to the correlator in Tsukuba takes 5-6 days. The transportation delay could be reduced to 4-8 hours for each INTENSIVE with a 34Mbps Internet link, which will be available for a reasonable price including the required support.

First Internet link tests were performed with servers in Germany, the Netherlands and the USA. Data-rates up to 40Mbps to USA were achieved with well configured standard equipment, employing i. e. a PC or Mk5 System with a 100Mbps/s Ethernet card.

## 3 Measuring the height variations

An invar wire system is installed in the RTW in order to measure the height variations, which usually result from thermal expansions. The seasonal temperature of the concrete wall of the basement, which is relevant for the expansion, varies between  $-10$  and  $+20^{\circ}\text{C}$ . This results in a height variation of 2-3mm over a period of one year. At the RTW continuous time series of height variations are recorded for some years for introduction of the measured correction in the analysis. Figure 1 shows the principal and the installation of the invar wire, Figure 2 show the time series of the measured expansion and the corresponding wall temperature of the telescope basement.

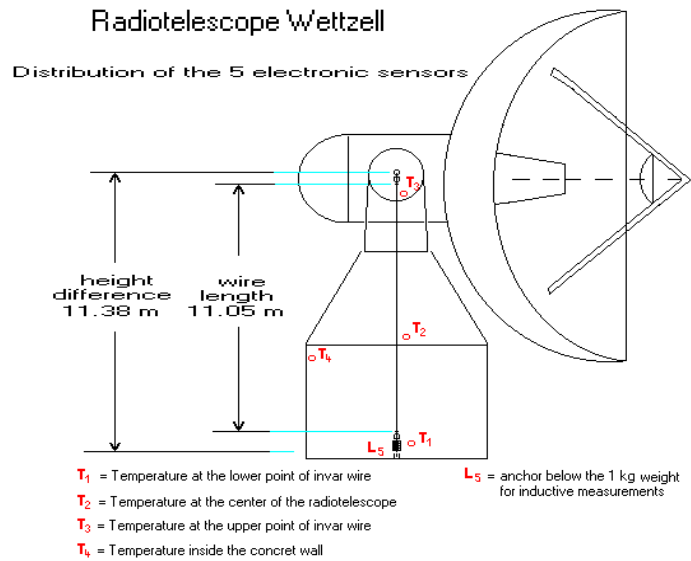


Figure 1: Measuring the height variations with an Invar Wire System.

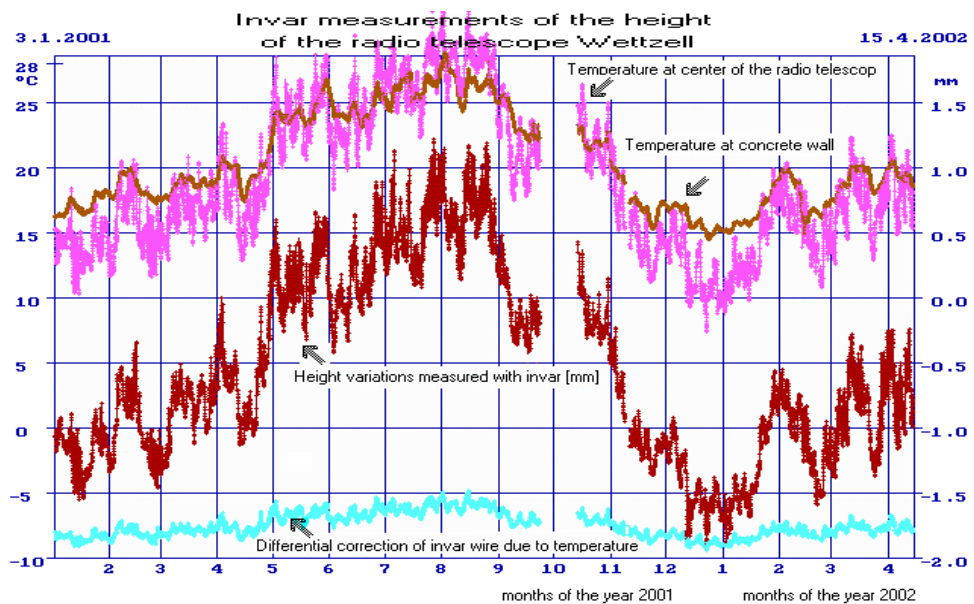


Figure 2: Measured height variations and wall temperature since January 2001.

#### 4 Collocation with other techniques at FSW

At the Fundamental Station in Wettzell (FSW) various systems are installed as:

- WLRS: Wettzell Laser Ranging System
  - New system in planning (SOS-W)
- permanent GPS/GLONASS receivers
  - Turbo Rogue (ACT),
  - Trimble SSI4000,
  - ASHTECH Z12, Z18
- DORIS in preparation (May 2003)
- Local Rotation Sensor: Ringlaser „G“

- Local Sensors as
  - Time & Frequency System (UTC-Wetzell),
  - Meteorological Recording Systems,
  - Water Vapour Radiometer, temperature-, pressure-, humidity-sensors,
  - Superconducting Gravity Meter,
  - Seismometer,
  - Tiltmeters.

In the period from July to September 2002 various water vapour radiometers have been collocated in order to investigate their precision and the systematic behaviour. The campaign was called RadCalWet.

5 water vapour radiometers were collocated at FSW

- 2 Radimetrix Systems from
  - Universität der Bundeswehr, Neubiberg
  - Technische Universität Dresden
- 3 ETH-Zürich type radiometers from
  - Bundesamt für Kartographie und Geodäsie
  - Royal Observatory Belgium
  - Eidgen. Technische Hochschule Zürich (ETH)

First comparisons of the time series have been made, the results will be soon available.

During the CONT 02 campaign the Radiometrix System of the Universität der Bundeswehr was sent to Kokee Park, while the ETH-System of BKG was sent to Westford for monitoring the profiles of the water vapour close to the radiotelescopes.

The local survey network at the FSW has been re-observed by students of the Fachhochschule Würzburg, in order to determine the eccentricity vectors between all network points, respectively the reference points of the geodetic systems and to investigate local instabilities. Moreover the Footprint Network has been re-observed, employing GPS receivers, during a short campaign in September 2002. The campaign was organized to combine the old Footprint Network to the newly established permanent GPS Network consisting of 5 GPS points, which are continuously monitoring GPS data for analysing local movements.



Figure 3: Water Vapour Radiometer (ETH-type) in front of RTW.

# Planned Improvements at German Antarctic Receiving Station (GARS) O'Higgins

W. Schlüter<sup>1</sup>, C. Plötz<sup>2</sup>, R. Wojdziak<sup>3</sup>, and W. Schwarz<sup>1</sup>

<sup>1</sup>*Bundesamt für Kartographie und Geodäsie, Fundamentalstation Wettzell, Germany*

<sup>2</sup>*Forschungseinrichtung Satellitengeodäsie, Technische Universität München, Germany*

<sup>3</sup>*Bundesamt für Kartographie und Geodäsie, Außenstelle Leipzig, Germany*

**Summary:** Since 10 years the German Antarctic Receiving Station (GARS) O'Higgins contributes to the VLBI observing program. During the Antarctic spring-summer period regular campaigns were organized to perform the observations, to maintain the system, to improve and upgrade the station. The radio telescope is used for geodetic VLBI by the BKG and for receiving remote sensing data from ERS1 respectively ERS2 by the DRL (German Space Agency).

Some plans are under development by upgrading the station towards remote control, to extend the access of the 9m-radiotelescope for observations when the station is unmanned. In particular the MK5 system allow the improvement of such a remote station for unattended operations.

This paper review the O'Higgins activities and the collocation with the techniques employed at O'Higgins and it will present the plans for upgrading GARS O'Higgins in the next years.

## 1 Objectives of GARS O'Higgins

The German Antarctic Receiving Station (GARS) O'Higgins (Figure 1) is operated since more than 10 years as a joint effort by

- BKG: Federal Office of Cartography and Geodesy
- DLR: German Aerospace Center
- INACH: Instituto Antartico Chileno

in order to receive

Remote Sensing Data from ERS (mainly ERS2), LANDSAT and JERS

as well as to obtain

Geodetic Data such as VLBI -, GPS/GLONASS- and PRARE-data

for the support of research in the field of space geodesy, in particular geokinematics and geodynamics as well as for the maintenance of the global reference frame. In addition tide gauge data for monitoring sea level changes and meteorological data were observed.

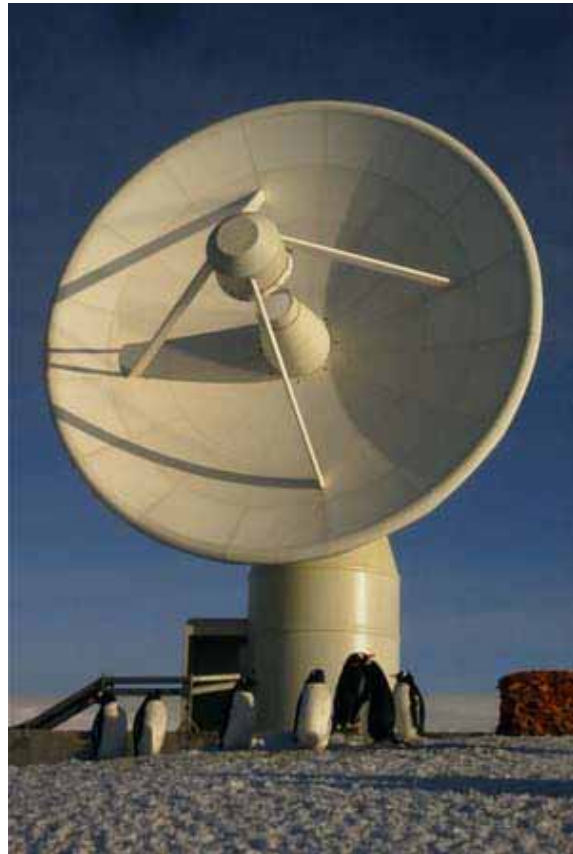


Figure 1: GARS O'Higgins 9m Radiotelescope.

## 2 Observations at O'Higgins

Due to the very remote location and due to the strong climate conditions the O'Higgins station could only be operated campaign wise during the Antarctic spring-summer period, when operators can have access to the location. Since 1992 periodically a team consisting of four to six engineers from BKG and from DLR visit the station in general from October to February with a break during Christmas and New Year.



Figure 2: Two Engineers are removing the shield in front of the feed.

Before the observations can be started several components have to be initialized for operation, e.g. the H-Maser has to be activated after the break and a shield plate in front of the feed has to be taken off, which protects the feed during the non active period, when no observer is in place. Figure 2 shows two engineers taking off the plate. In total the station participated in 61 VLBI observing sessions. In the 2001/2002 campaign the MkIII Data Recording System was upgraded to MKIV. In collaboration with Michael Wunderlich from Max Planck Institute for Radioastronomy the thintape drive could be upgraded in place.

Permanent GPS Observations were carried out since 1995. Since end of 2000 also the GLONASS Satellites can be observed. Two systems were installed and are operating

- Turbo Rogue ATC since 1995 (figure 3)
- Ashtech Z18 (GPS and GLONASS) since end of 2000

Transmission of GPS data was carried out via INMARSAT at the beginning. Today an INTERNET access is available and the transmission could be done hourly via the GPS operations center Wettzell to the European data base in Frankfurt at BKG.

PRARE (figure 4) observations are carried out since 1996.



Figure 3: TUBO Rogue antenna.

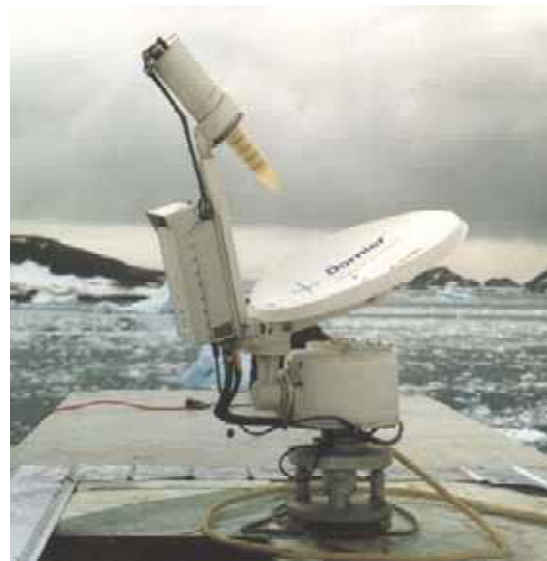


Figure 4: PRARE System.

A Tide Gauge Measuring System was installed in 1995 for permanent registrations. Due to damages of the cable from the sensor to the registration system by the ice of the frozen sea during the Antarctic winter the time series was interrupted from spring 1997 to 1999. Today the tide gauge is included in the TIGA project - the international GPS-Tide Gauge Benchmark Monitoring project. Figure 5 show the installation of the tide gauge sensor , Figure 6 show the system itself.



Figure 5: Installation of the Tide Gauge Sensor.



Figure 6: Tide Gauge Sensor.

### 3 Future plans

The existence of an observatory in Antarctica will become of importance for some future applications e.g.

- for the upcoming satellite missions for remote sensing (TerraSAR X),
- for GALILEO as a candidate for a reference and monitoring station,
- or for the IVS observing program to provide more and regular observations.

DLR and BKG jointly plan to extend the station operations in collaboration with the Chilean partner INACH. It is dependent on the access during the year, which has to be supported by the partners for the logistics (mainly via INACH by Chilean Military). Nevertheless the control of the VLBI Antenna requires high automation and robustness of the technique. It is planned to improve the antenna control system, to implement a MK V VLBI data acquisition system and to improve the infrastructure, in particular to improve the power generation and the access to Internet. Remote control routines will have to be established for the operation of GARS more or less unmanned or with reduced staff.

The diagram (figure 7) shows the flow chart for the remote control part for the geodetic instruments at O'Higgins..

The Chilean Military Base at O'Higgins has been extended by a new building which will allow to house scientists and operators from Chilean Partners who will collaborate at GARS.

Figure 8 show the new building viewed from GARS.

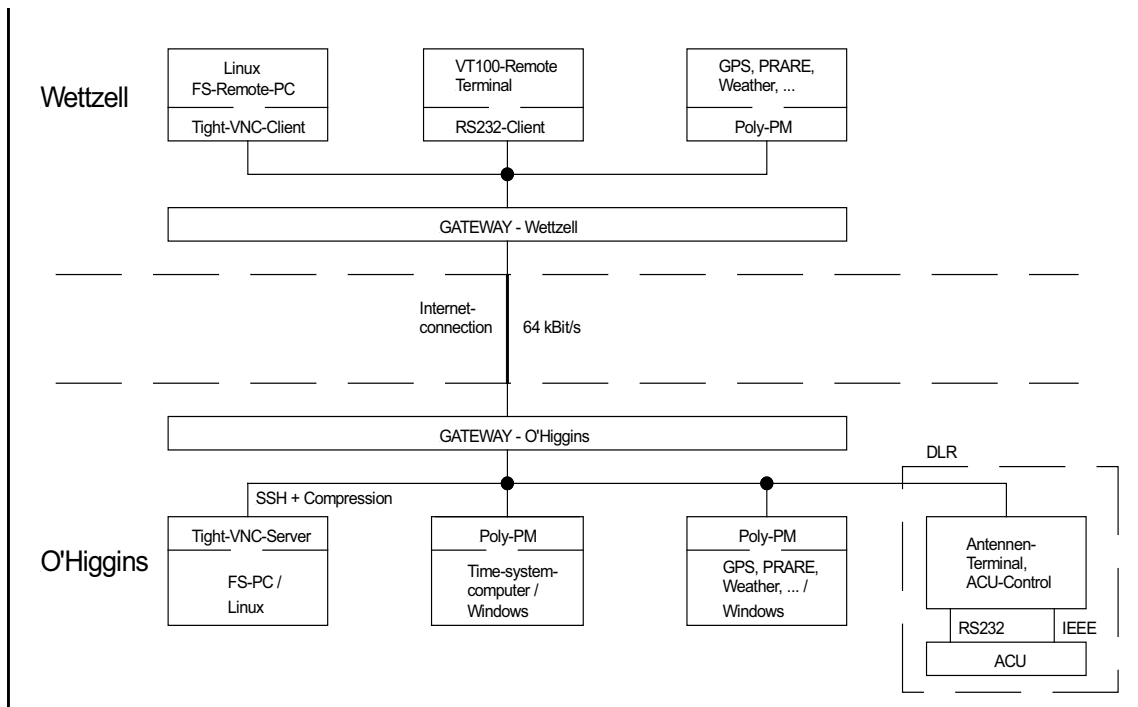


Figure 7: Planned Remote Control Access from the Fundamental Station Wettzell.



Figure 8: New building of the Military Base O'Higgins, viewed from GARS.



Session 2

# Technical Developments



# Tropospheric Delay Measurements at Effelsberg With Water-Vapour Radiometry

A.L. Roy, U. Teuber, and R. Keller

*Max-Planck Insitut für Radioastronomie, Bonn, Germany*

Summary: We have installed a scanning 18 GHz to 26 GHz water-vapour radiometer during March 2003 at the Effelsberg 100 m telescope for tropospheric delay and phase and opacity correction during high-frequency VLBI observations. It is based on the design by Tahmouh & Rogers (2000) but with noise injection for calibration, weather-proof housing, and temperature stabilization. The radiometer observed in parallel with astronomical VLBI experiments at 86 and 22 GHz during April and June 2003 and those measurements will be compared to VLBI data when correlation is complete. The radiometer will deliver data into a public archive where it will be available for download. This paper describes the radiometer and shows some early results and performance measurements.

## 1 The Effelsberg WVR

Some views of the radiometer are shown in Fig. 1. The radiometer is presently located on the control building roof, 125 m distant from the axis intersection of the 100 m telescope, but should be moved by late 2003 to the top of the prime focus cabin looking skyward along the optical axis. The basic parameters are given in Table 1. The project status is maintained at <sup>(1)</sup>.

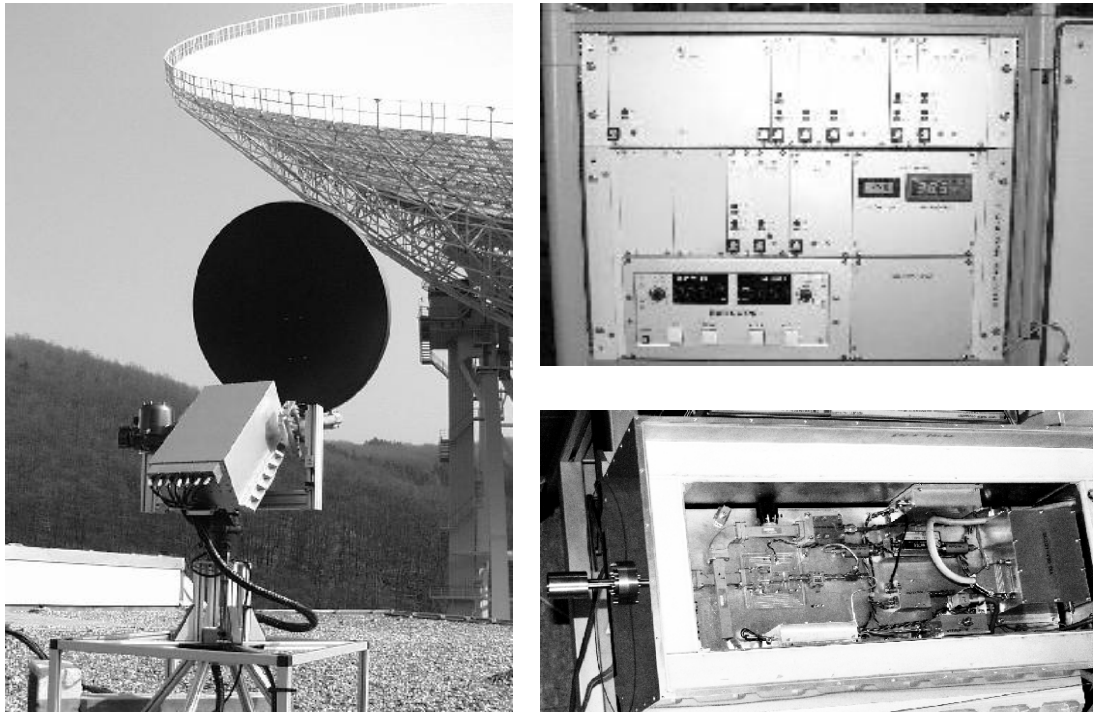


Figure 1: *Left*: View of the radiometer at Effelsberg. *Top right*: Front panel of the control rack. *Bottom right*: Front end opened.

<sup>1</sup> <http://www.mpifr-bonn.mpg.de/staff/aroy/wvr.html>

Table 1. Basic parameters of the Effelsberg WVR

Frequency	18.3 GHz to 26.0 GHz	25 channels
Bandwidth	900 MHz	double sideband
$T_{\text{receiver}}$	200 K	
Physical temperature	25 °C	stabilized by a Peltier cooler
Thermal noise	61 mK	for 0.025 s total integration time in a 25 channel sweep (= 0.27 mm path length noise, assuming 4.5 mm K <sup>-1</sup> )
Absolute accuracy	~ 1 % of $T_{\text{sys}}$ (= 9 mm path length systematic offset assuming 4.5 mm K <sup>-1</sup> )	
Gain stability	$2.7 \times 10^{-4}$ over 400 s	after calibration with box temperature
Desired Sweep Time	3 s	set by atmospheric coherence time
Beamwidth	1.3°	for best overlap with main beam
Gain calibration	uses noise injection or temperature coefficient of system.	
Monitor and control	ethernet on optical fibre	
IWV retrieval	by fitting theoretical line profile to measured spectrum and frequency-squared term for cloud component and a constant term for calibration errors. Upgrade to ATM is pending.	

## 2 How it works

The block schematic of the front end is shown in Fig. 2. The LNA covers the 18 GHz to 26 GHz band with a receiver temperature of 200 K to 230 K. A YIG local oscillator is steered between 18.8 GHz and 25.7 GHz and mixes the RF signal to baseband using a double-sideband conversion. The signal is filtered to 450 MHz bandwidth (equivalent to 900 MHz at RF) and is detected by a square-law detector, and is sampled by a commercial ethernet data acquisition system (EDAS). All RF components are mounted on a temperature-stabilized plate in an insulated weather-proof enclosure. The user can open a socket connection to the EDAS unit over the intranet and issue commands to read back the detector output level, steer the local oscillator, fire the noise diode, point the radiometer, and read back monitor points.

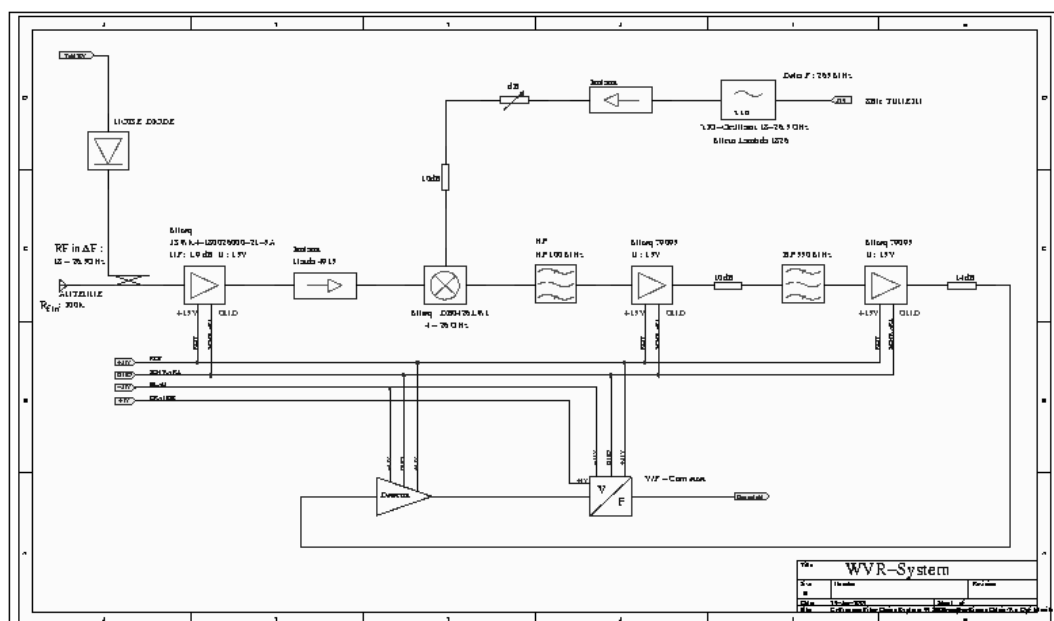


Figure 2: Block schematic of the front end.

Each spectrum acquired is calibrated immediately by the online software by dividing by the gain (measured previously against a hot load and the cold sky, using a skydip to measure the sky temperature) and by subtracting the frequency-dependent receiver and spillover temperatures. The spectrum is then fit by a three-component model consisting of a frequency-squared term which models black-body emission from the ground and from liquid water in clouds, a Van Vleck-Weisskopf line profile which models the water vapour emission, and a constant term which models residual calibration errors. The brightness temperature of the water vapour line is related to excess path length due to refractivity of the atmosphere by a scale factor, which, for surface air temperature of 273 K and surface air pressure of 900 hPa is  $\sim 4.5 \text{ mm K}^{-1}$ . This approach was developed by Tahmouh & Rogers (2000). The extraction of path length from radiometer measurements has recently been incorporated into the ATM software package by J. Pardo (2003, private communication), which we aim to use. The atmospheric path lengths are written to a log file along with a time-stamp for use after correlation to correct the VLBI data before fringe-fitting.

### 3 Performance requirements

#### 3.1 Tropospheric phase fluctuation correction

Coherence on a baseline after atmospheric phase correction should be (somewhat arbitrarily) at least 0.9. When observing at 3.4 mm, this requires an rms path length noise after atmospheric phase correction of 0.18 mm. The noise comes from four sources (thermal noise, gain fluctuations, beam mismatch and calibration noise) at each end of the baseline, so each noise source should contribute at most  $1/\sqrt{8}$  of that, or 0.062 mm, corresponding to 14 mK using a nominal scale of  $4.5 \text{ mm K}^{-1}$ . This stability should be achieved on the time-scale of a single VLBI scan which is conventionally 400 s at present. This can be translated into a requirement for the gain stability as follows. Gain fluctuations multiply the typical water-line brightness of 116 K, (derived from the median atmospheric conditions measured by radiosonde at Essen, Germany, for an elevation of  $30^\circ$ ) and the resulting error should not exceed 14 mK, so the gain stability should be  $14 \text{ mK} / 116 \text{ K} = 1.2 \times 10^{-4}$ . The Allan variance and structure function of the radiometer were measured on an ambient absorber and showed noise of 135 mK at 400 s for  $T_{\text{sys}}$  of 480 K, corresponding to stability of  $2.7 \times 10^{-4}$  on a 400 s time-scale (Fig. 3 a/b).

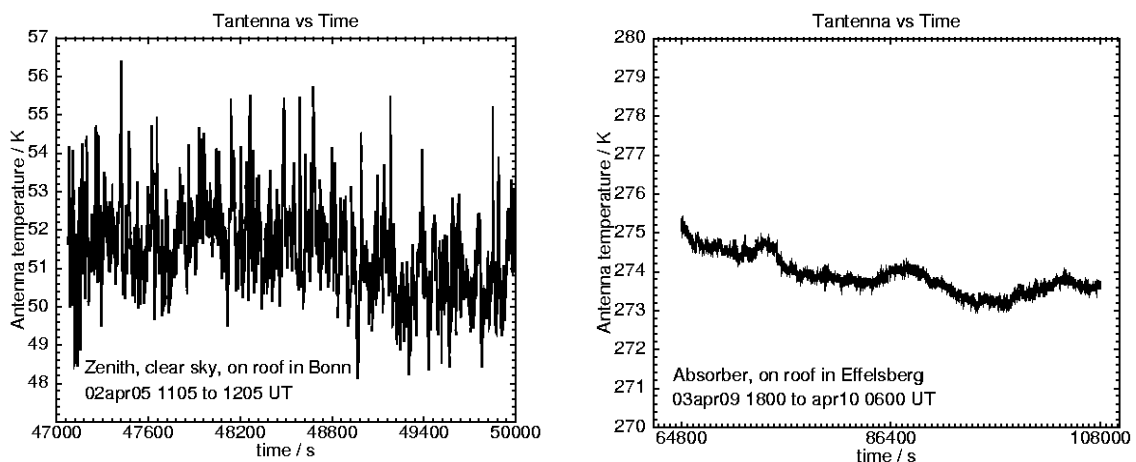


Figure 3a: *Left*: time series of  $T_{\text{antenna}}$  at zenith on clear blue sky for 1 h shows fluctuations mostly due to atmospheric water vapour. Integration time was 0.3 s per point. *Right*: Time series of  $T_{\text{antenna}}$  on an ambient-temperature absorber for 12 h shows much smaller fluctuations, due to gain and absorber temperature changes. Integration time was 0.025 s per point.

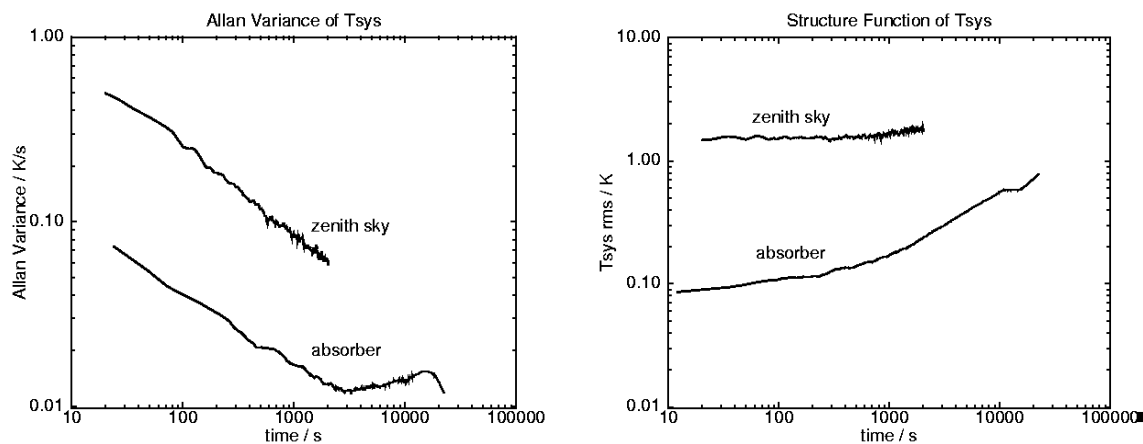


Figure 3b: *Left*: Allan variance of the two time series. *Right*: Structure functions of the two time series.

### 3.2 Tropospheric delay measurement

Tropospheric delay measurement with WVRs could in principle reduce noise in geodetic baseline length determination by reducing the atmospheric contamination to the vertical station position. Comparisons of delay measurement with WVRs, GPS and VLBI have shown some systematic biases in the WVR estimates and so the standard practice during geodetic VLBI data reduction is to estimate the troposphere from the VLBI data themselves.

A systematic offset in the tropospheric delay measured by a WVR could arise from error in the absolute measurement of radiometer gain or receiver temperature. Such absolute calibration is normally carried out against hot and cold loads, for which the uncertainty is typically 1 % due to uncertainty in the absorber temperature and efficiency of coupling radiation into the radiometer. A 1 % error in the gain measurement would introduce a 1 % error in the line-height measurement. For a typical total wet path of 100 mm, this would be 1 mm, which is small.

An error in the receiver-temperature measurement would produce an effect that depends on the frequency structure of the error. Were a constant offset added to the receiver temperature at all frequencies, this offset would be removed when differencing the on-line and off-line channels to measure the line height and would have no effect. Were a 1 % error added to the on-line channels only, this would change the line brightness systematically by 1 % of the receiver temperature, or 2.0 K for the Effelsberg radiometer. Assuming a scaling factor of  $4.5 \text{ mm K}^{-1}$  this corresponds to a systematic 9 mm error, which would be significant. A similar frequency-dependent gain error would produce a path-length error of 5 mm.

Thus, if a significant bias in the measurement of tropospheric delay comes from calibration errors, one should look for a source of frequency-dependent errors.

A detailed error analysis of the calibration of the Effelsberg radiometer has yet to be done, and comparison of the WVR measurements to VLBI determinations of tropospheric delay need to be made during a suitable geodetic VLBI campaign.

## 4 Sky survey

All-sky panoramas in Effelsberg and Bonn (Fig. 4) were made to determine the horizon limits and to survey the RFI environment. They were made in  $1^\circ$  steps, by scanning in elevation at each azimuth and measuring a 30-point spectrum at each position. One frequency channel was selected from which to render the images (22.2 GHz at Effelsberg and 20.5 GHz in Bonn). The sky in Effelsberg showed streaks due to changing atmospheric water vapour column caused by weather changes during the four-day measurement period. The Effelsberg 100 m telescope appeared streaked because the telescope moved during the measurement. The panorama in Bonn is dominated by streaks caused by transmitters around the city. A gradient in the sky brightness is visible nevertheless, due to the longer path length through the atmosphere at low elevation. The white dot above the building near the left edge of the image is the sun and that near the right hand edge of the image is a geostationary satellite.



Figure 4: 360° panoramas in Effelsberg (*top pair*) and in Bonn (*bottom pair*) made by the water-vapour radiometer and the optical view for comparison.

## 5 The line profile

Three examples are shown in Fig. 5 of line profiles and sky conditions during the 3 mm VLBI experiment 2003 April 27-30. The left frame shows a spectrum measured by the radiometer, the middle frame shows the simultaneous view from a camera looking along the axis of the radiometer. The water line is prominent and, as the cloud thickened, both the line and the baseline levels rose, until under the heaviest storm conditions the baseline swamped the line. The right frame shows path-length time series derived from a succession of spectra, beginning with the spectra shown in the left frames. In the first, the series of steps from 100 to 200 mm was due to a tipping scan. In the second, a path-length change of 50 mm over 25 min was produced by a passing storm cell. In the third, the line is saturated due to an intense storm and rain and the baseline is raised, and the measurements were then not reliable.

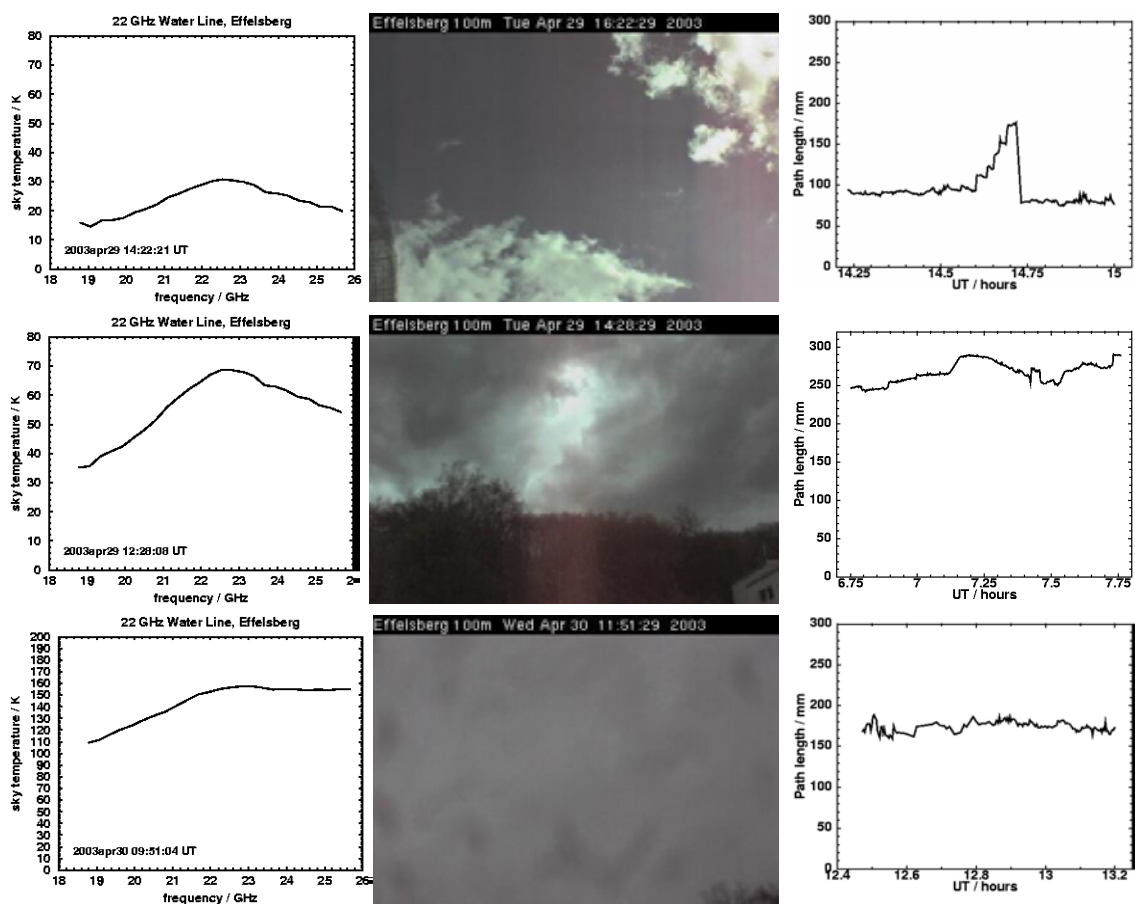


Figure 5: Examples of water line spectra (left) and the corresponding sky conditions (centre) measured during 2003 April 29-30. Right: tropospheric path length time series, beginning at the time of the spectra shown at left.

## 6 Conclusion

A new water-vapour radiometer has been installed at Effelsberg. Line profiles look good under clear skies and under heavy cloud and rain. The line is saturated only by the most intense storms. The radiometer measured in parallel with 86 GHz VLBI in April 2003 and comparison between the WVR data and the VLBI phases is awaiting correlation of the VLBI data. The radiometer is available to observe in parallel with geodetic and astronomical VLBI experiments to deliver measurements of the tropospheric delay.

## **Acknowledgements**

We thank Alessandra Bertarini for providing her expertise with IDL, without which the sky survey images would not have been made.

## **References**

Tahmoush, D.A. & Rogers, A.E.E. 2000, *Radio Science*, 35 (5), 1241



# The Geodetic VLBI Network Station at the Onsala Space Observatory – Activities During 2002 –

G. Elgered and R. Haas

*Onsala Space Observatory, Chalmers University of Technology, Sweden*

**Summary:** We summarise the geodetic VLBI experiments performed at Onsala during 2002. An update of the measurements for continuous monitoring of the stability of the 20 m telescope using classical geodetic methods and GPS is reported as well as an overview of calibration activities related to the ground-pressure observations. The research using microwave radiometry to investigate the spatial and temporal variations in the wet delay has continued. During the CONT02 experiment two radiometers were acquiring data simultaneously following two different observing strategies. The microwave radiometer ASTRID was upgraded in terms of a LabView-based software and hardware for instrument control and data acquisition at the end of the year 2002.

## 1 Introduction

This report presents several different aspects of the research around the geodetic VLBI observations at the Onsala Space Observatory during 2002:

- First, in Section 2 we summarise the performed geodetic VLBI experiments during 2002. We also put these activities in a long term perspective by presenting long term statistics of geodetic VLBI experiments using the Onsala telescope.
- The monitoring of the local geodetic tie has continued. A tie between the space geodetic techniques is maintained by using a GPS antenna mounted on the backside of the subreflector of the VLBI telescope. The most recent summary has been presented on the IVS General Meeting 2002 (Lidberg et al., 2002). Also the monitoring of the concrete foundation of the VLBI telescope continues and the results are consistent with the earlier findings. The very strong correlation between measured height and the temperature of the concrete telescope tower is manifested (Lidberg et al., 2002). For the CONT02 campaign we also developed a model to express the vertical height variations, acquired with the invar measurement system, as a function of the outside temperature at the station (Haas and Scherneck, 2002). Furthermore, in 2002 the telescope's reference point was determined by classical geodetic measurements performed for the realisation of a new local tie and the question about a possible azimuth and elevation axes offset of the telescope was assessed (Eschelbach, 2002). The measurements and the results are presented by Eschelbach and Haas (2003, this volume) and will not be further discussed in this report.
- Accurate observations of the total pressure at ground are important for assessing the atmospheric influence in geodetic VLBI. The VLBI data analysis (as well as that of GPS data) can provide estimates of the equivalent zenith total delay (ZTD). In order to validate these estimates one method is to subtract the zenith hydrostatic delay (ZHD) from the ZTD and obtain a zenith wet delay (ZWD). This ZTW can be compared to independent data acquired by microwave radiometers or radiosondes. Especially for the application of climate monitoring based on long time series of the ZWD stable ground pressure measurements are of funda-

mental importance. At Onsala we now have more than 20 years of geodetic VLBI data and in Section 3 we review the history of pressure calibration.

- During the the CONT02 campaign in October 2002 we operated two different microwave radiometers. ASTRID is the old instrument originating from 1980 and KONRAD was developed and built during 2000-2001. The radiometer data from CONT02 have been processed and in Section 4 we present and compare the time series of ZWDs to estimates from both the VLBI and the GPS data.
- A new interface for the old WVR ASTRID was developed (Elgered and Stoew, 2002) and installed at the end of 2002. The old system was not user friendly by today's standards. Another aspect of the upgrade was to copy the main part of the data acquisition system recently developed for our second radiometer KONRAD so that the operation will be experienced as identical from the operator's point of view, even though the hardware of the two radiometers is slightly different. In Section 5 we summarise the main features now available when operating this instrument.

## 2 Geodetic VLBI observations at the Onsala Space Observatory 2002

During 2002 the observatory has been involved in four regular VLBI-experiment series EUROPE, IVS-R1, IVS-T2, and RDV, and in the special series CONT-02. In total Onsala was scheduled to participate in 31 geodetic VLBI experiments as follows: 5 RDV, 4 IVS-R, 3 IVS-T, 4 EURO, 15 CONT02. Two experiments were lost, IVS-R001 due to a formatter failure and IVS-T2007 due to a problem with the hydrogen maser. In a long term perspective the year 2002 was rather busy (see Figure 1). The main reason for this is of course the fifteen day long CONT02 campaign.

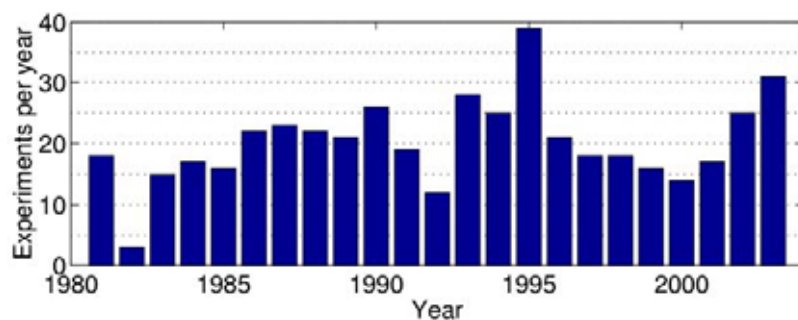


Figure 1: VLBI observations at the Onsala Space Observatory including the years 1980 to 2002.

## 3 Ground-pressure calibration history

The ground pressure sensor used at the Onsala site today is the standard unit developed by NASA and was installed for the six day long geodetic VLBI experiment in June 1982. The ground pressure data acquired before June 1982 are inaccurate and shall be replaced by nearby pressure observations, e.g. from the site Nidingen, operated by the Swedish Meteorological and Hydrological Institute (SMHI).

Since the installation in June 1982 the ground pressure sensor has been calibrated at five occasions. First in June 1982 a mercury barometer was borrowed from SMHI at Gothenburg-Landvetter Airport. A bias of 2 hPa was

observed. However, this result is questionable since it is based on manual readings and 2 hPa is approximately 1 mm of mercury.

The next calibration was in 1989 when a specially developed system was shipped around between the different VLBI stations. We then observed a bias within  $\pm 0.1$  hPa over the range 950–1050 hPa. This type of calibration was repeated in 1993, when a bias within  $\pm 0.4$  hPa was seen over the same range, and in 1994 with a bias within  $\pm 0.3$  hPa over the range 960–1080 hPa.

Motivated by the applications of long-term monitoring of water vapour using the space geodetic techniques of VLBI and GPS we arranged for a long term loan of a calibrated barometer from SMHI starting in September 2002. The results obtained so far are shown in Figure 2. The resolution of both barometers is 0.1 hPa. The SMHI barometer was temporarily brought back to SMHI in Norrköping in June 2003 and its accuracy was checked. The results indicate that a seasonal variation is present in the uncertainty of one or both of the barometers. The simultaneous measurements will continue although the differences seen so far are at an acceptable level from the water vapour monitoring point of view. The largest observed difference, 0.5 hPa, corresponds to a zenith hydrostatic delay of 1 mm.

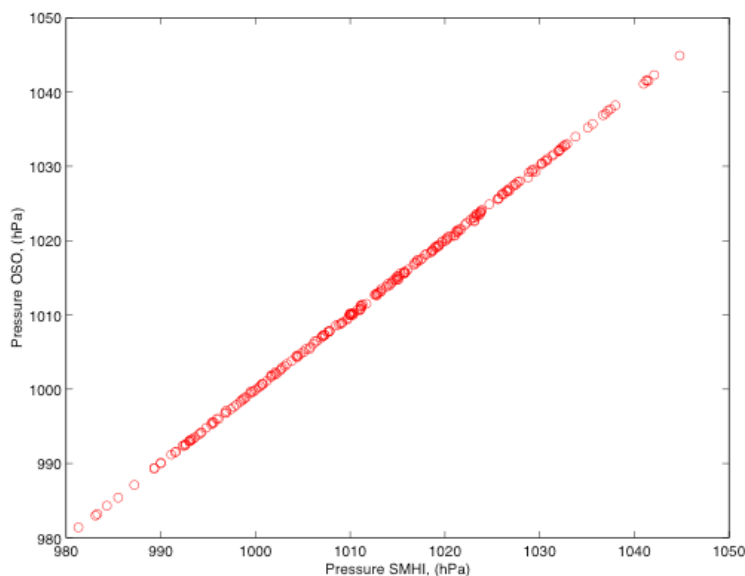


Figure 2a: Results from the ongoing pressure calibration: Ground-pressure readings of the Onsala barometer vs. the SMHI instrument.

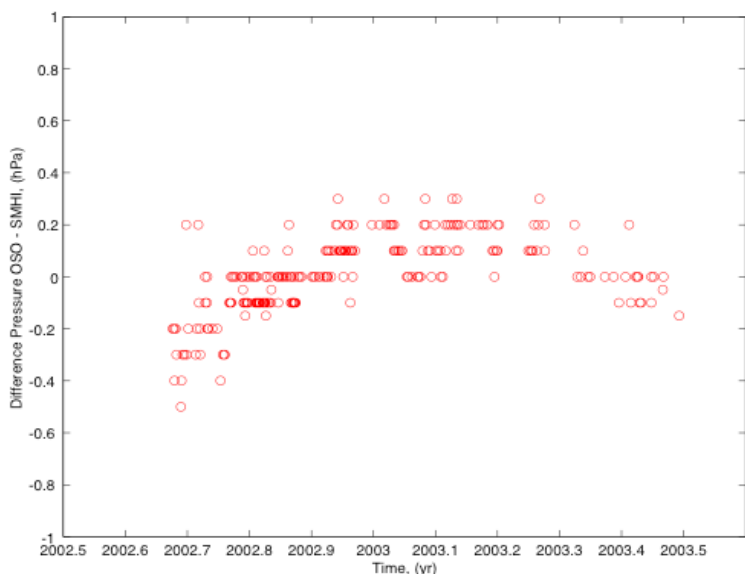


Figure 2b: Results from the ongoing pressure calibration: Time series of the differences between the two instruments.

## 4 Atmospheric measurements during the CONT02 experiment

A special focus was made towards atmospheric measurements during the CONT02 experiment. Both the older ASTRID and the newer KONRAD microwave radiometers were operated during the experiment but with slightly different approaches. ASTRID having beam widths of six degrees was mapping the entire sky above elevation angles of roughly 23 degrees independent of the VLBI observing schedule. KONRAD with antenna beam widths of three degrees was slaved to the VLBI schedule and observed towards the VLBI sources during each scan. In the time between the scans so called tip curves were acquired for calibration purposes.

This means that in total we have four different instruments or techniques to estimate the water-vapour content in the atmosphere. The time series are shown in Figure 3 where we have also included the measured rain rate at the ground obtained from a micro rain radar (Gradinasky et al., 2000). It is worth noting that, as expected, the estimates from VLBI and GPS are not affected by rain. The data from the two radiometers have been edited and observations suggesting a liquid water content larger than 0.7 mm have been removed. We also see that the scatter in the KONRAD data is larger compared to the ASTRID data. We interpret that as a consequence of the smaller antenna beam width since it seems to occur mainly before or after precipitation. For example, on October 18 there was a major event of wet snow falling on the site. The Konrad data (red circles) show a significant scatter during this event. Preliminary results for the Zenith Wet Delay (ZWD) are that the space geodetic techniques (GPS, VLBI) agree within  $1.0 \pm 0.5$  mm. ZWD from GPS are above ZWDs from VLBI. The two radiometers also agree within  $1.0 \pm 0.5$  mm. ZWDs from ASTRID are above ZWDs from KONRAD. The ZWDs observed with the space geodetic techniques are  $5.3 \pm 1.0$  mm larger than the ZWDs observed with the radiometers. The analysis of this data set will continue and will also compare estimated horizontal gradients from the different techniques.

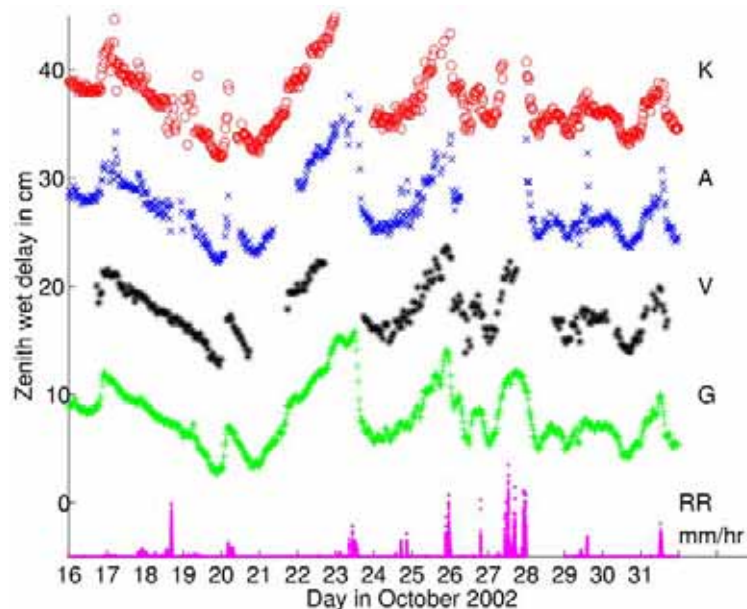


Figure 3: Time series of the ZWD measured during the CONT02 campaign. The data from the Konrad radiometer (red circles) have an added offset of 30 cm (for an improved visibility). The result from the Astrid radiometer (blue crosses) has an added offset of 20 cm. The VLBI time series (black stars) has an added offset of 10 cm. The GPS data (green pluses) are plotted with the correct y-scale. Also shown is the rain rate (bias  $-5$  mm/hr) observed using a micro rain radar.

## 5 A new interface for the ASTRID microwave radiometer

Directly after the CONT02 experiment the ASTRID radiometer was taken out of operation. Its present control and data acquisition system had been running since February 1992 and spare (computer) components were becoming difficult to find.

A new system using the commercial software LabView and its hardware FieldPoint from National Instruments was developed during 2002 as a masters thesis project (Strömbäck and Backman, 2003). The microwave parts of the radiometer are, however, not changed at all. The user interface and the FieldPoint hardware are shown in Figure 4. The new system has been operating since February 2003 and after corrections of some unwanted features in both the hardware and the software ASTRID seems to produce data of good quality since February 2003.

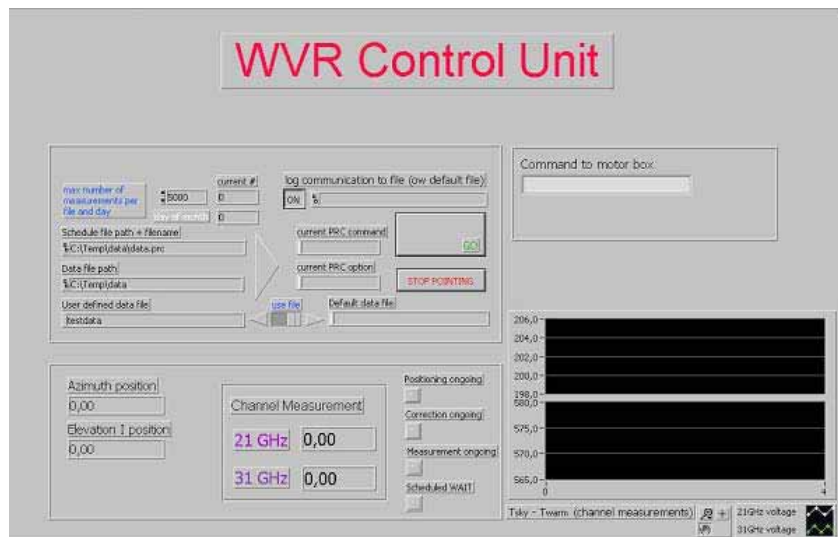


Figure 4a: Examples of new features of the ASTRID microwave radiometer: the computer screen from which commands are entered and the acquired data are plotted in real time.

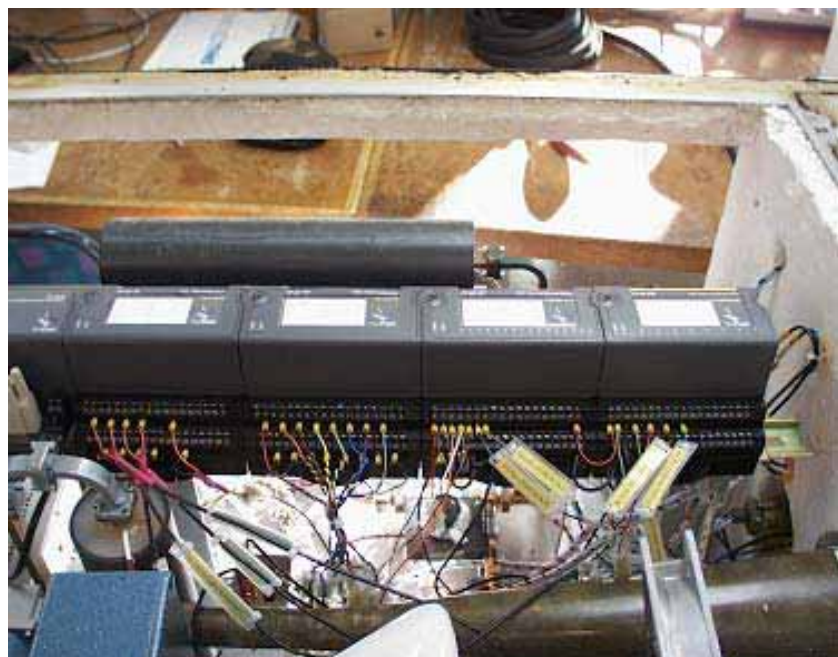


Figure 4b: Examples of new features of the ASTRID microwave radiometer: the FieldPoint hardware mounted in the microwave radiometer module. The hardware includes A/D converters, digital control and status signals to and from the radiometer.

## References

- Elgered, G., and P.O.J. Jarlemark, Ground-based microwave radiometry and long-term observations of atmospheric water vapor. *Radio Science*, **33(3)**, 707-717, 1998.
- Elgered, G., and B. Stoew, The IVS Technical Development Center at The Onsala Space Observatory. In: N. R. Vandenberg and K. D. Baver (eds.): IVS 2002 Annual Report, NASA/TP-2003-211619, 311-313, 2003.
- Eschelbach, C., Determination of the IVS-reference point at the Onsala Space Observatory in a local reference frame. Diploma thesis, Geodetic Institute of the University of Karlsruhe, 2002.
- Eschelbach, C., and R. Haas, The IVS-Reference Point at Onsala – High End Solution for a Real 3D-Determination, In: Proceedings of the 16<sup>th</sup> Working Meeting on European VLBI for Geodesy and Astrometry, held at Leipzig, 9-10 May, 2003, edited by W. Schwegmann and V. Thorandt, Bundesamt für Kartographie und Geodäsie, 109-118, (this volume), Frankfurt/Leipzig, 2003.
- Gradinarsky, L., G. Elgered, and Y. Xue, Using a micro-rain radar to assess the editing of ground-based microwave radiometer data, in P. Pampaloni and S. Paloscia (eds.), *Microwave Radiometry and Remote Sensing of the Earth's Surface and Atmosphere*, pp. 183-191, Proceedings of the 6-th Specialist Meeting on Microwave Radiometry and Remote Sensing of the Environment, 16-18 March 1999, Firenze, Italy, Publisher VSP, Netherlands, February, 2000.
- Haas, R., and H.-G. Scherneck, The IVS Analysis Center at the Onsala Space Observatory. In: N. R. Vandenberg and K. D. Baver (eds.): IVS 2002 Annual Report, NASA/TP-2003-211619, 277-280, 2003.
- Lidberg, M., R. Haas, S. Bergstrand, J. Johansson, and G. Elgered, Local Ties Between the Space Geodetic Techniques at the Onsala Space Observatory. In: N. R. Vandenberg and K. D. Baver (eds.): IVS 2002 General Meeting Proceedings, NASA/CP-2002-210002, 91-95, 2002. (<http://ivscc.gsfc.nasa.gov/publications/gm2002/lidberg>)
- Strömbäck, M., and D. Backman, Construction of a data acquisition and pointing control interface for a microwave radiometer, Master of Science Thesis, Dept. Radio and Space Science, Chalmers University of Technology, Göteborg, Sweden, 2003.

# Residual Plotting and Ambiguity Resolution (REPA)

V. Thorandt and G. Engelhardt

*Bundesamt für Kartographie und Geodäsie (BKG), Außenstelle Leipzig, Germany*

**Summary:** Some elements of the Calc/Solve software have been identified which badly needed re-programming for migration of the package to LINUX operating system. One of this elements is the interactive graphics tool CNPLT. The program REPA is a new interactive graphics tool which replaces CNPLT and can be used for visualization of observations and residuals, manual ambiguity resolution, and other interactions for a given VLBI experiment. As of now program versions on the basis of FORTRAN77 respectively FORTRAN90 are running on HP workstations.

## 1 General idea

REPA is based on the open PGPLOT software and on the DiaGI/MultiDiaGI layer which is a comprehensive set of graphic tools basing on PGPLOT (Petrov (2002)). REPA is a module of the Calc/Solve analysis software package and can be used either in standalone mode or it can be started from interactive Solve. The main idea is a four level structure as shown in figure 1.

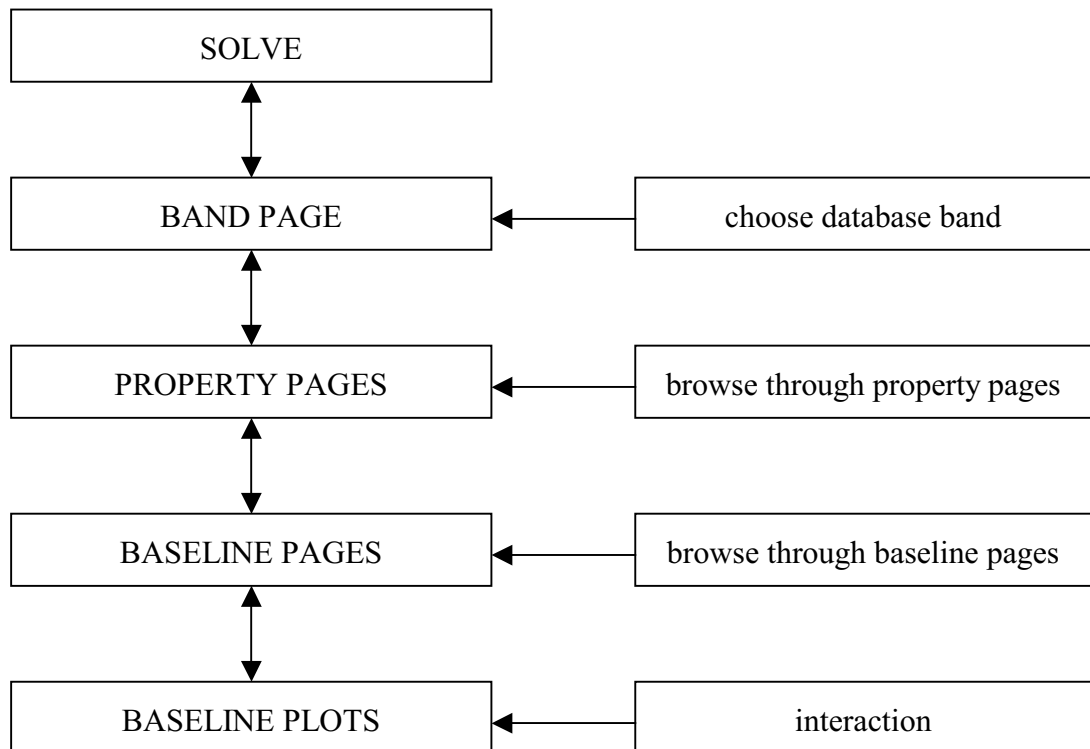


Figure 1: Four level structure of REPA.

## 2 1<sup>st</sup> level (Band Page)

At the 1<sup>st</sup> level the user can choose one of the available experiment bands (figure 2).

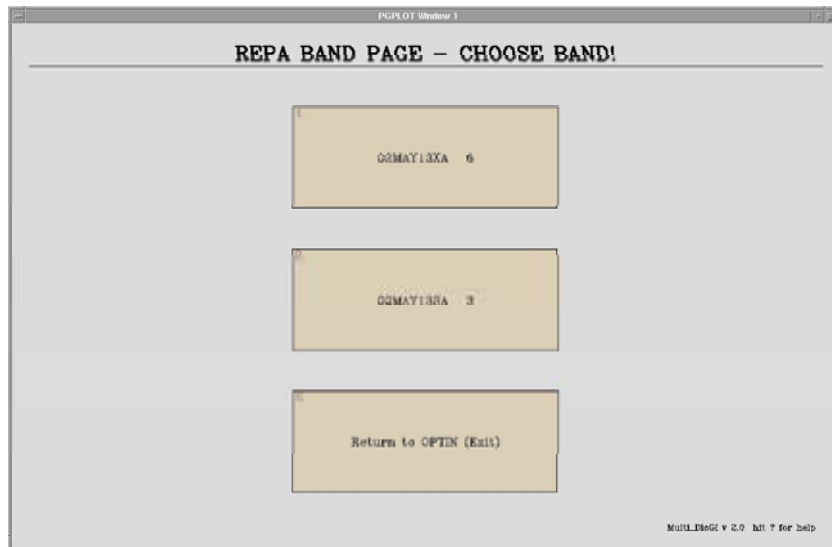


Figure 2: REPA – 1<sup>st</sup> level: Band Page.

## 3 2<sup>nd</sup> level (Property Pages)

Here the analyst can choose one of the available so-called “properties”. Properties are different kinds of observations and residuals which can be displayed and changed interactively, depending on the kind of data. In the current version of REPA there are three Property Pages with the following “properties” (cf. figure 3):

- group delay residuals with full sigmas vs. time
- rate residuals with full sigmas vs. time
- group delay residuals (full sigmas) vs. elevations - station 1
- group delay residuals (full sigmas) vs. elevations - station 2
- group delay residuals (full sigmas) vs. azimuths - station 1
- group delay residuals (full sigmas) vs. azimuths - station 2
- group delay residuals with correlator sigmas vs. time
- rate residuals with correlator sigmas vs. time
- signal to noise ratios vs. elevations - station 1
- signal to noise ratios vs. elevations - station 2
- phase delays
- temperatures on both stations of a baseline
- pressures on both stations of a baseline
- humidities on both stations of a baseline
- cable calibrations
- group ionosphere corrections

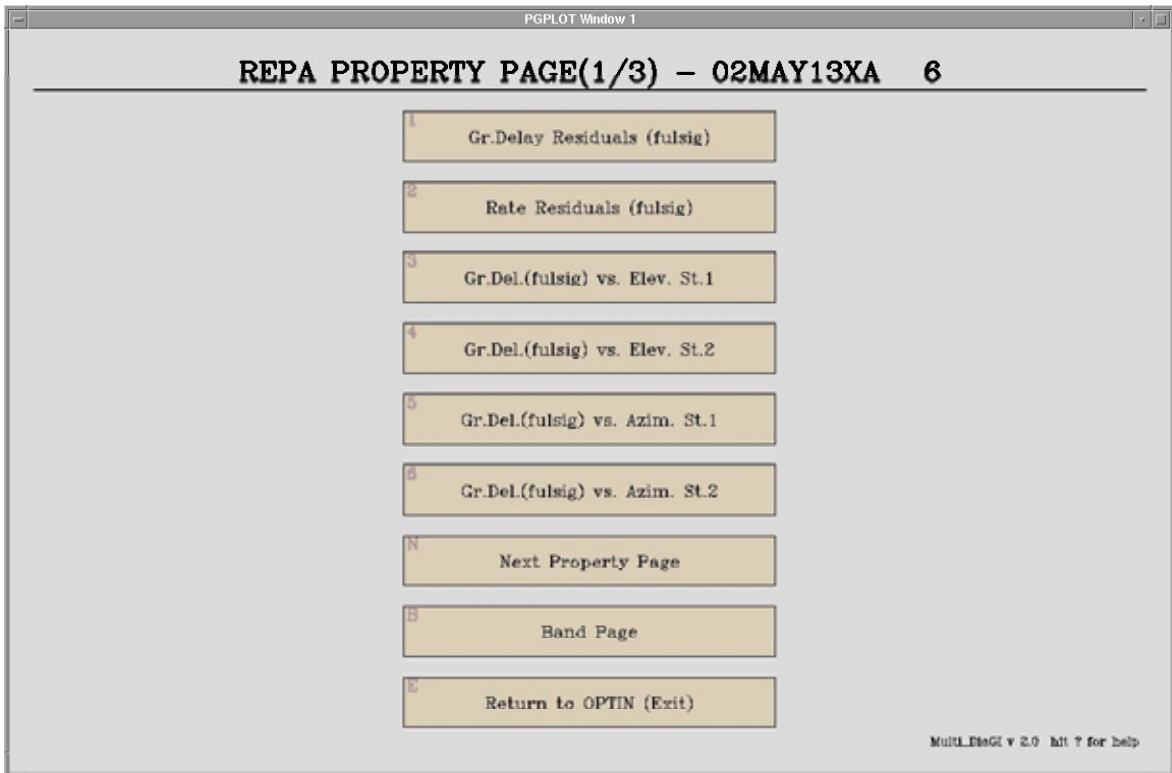


Figure 3: REPA – 2<sup>nd</sup> level: Property Pages.

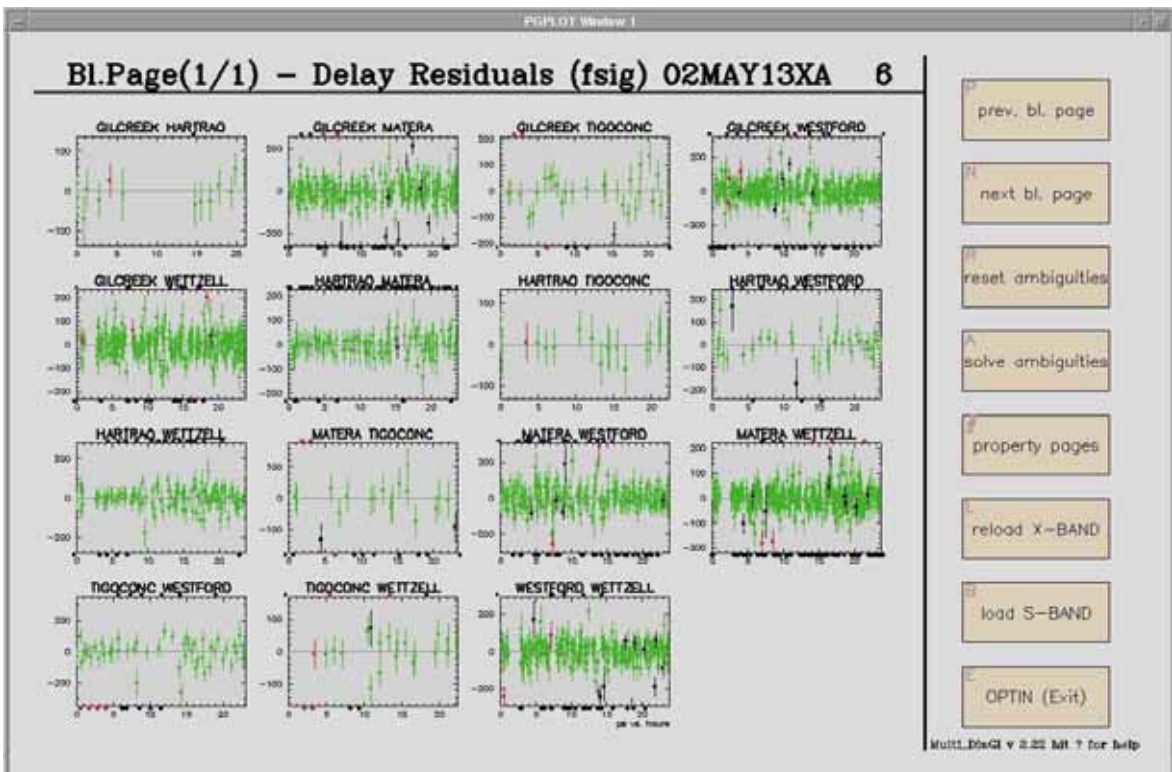


Figure 4: REPA – 3<sup>rd</sup> level: Baseline Pages.

## 4 3<sup>rd</sup> level (Baseline Pages)

Small plots of all baselines are displayed in MultiDiaGI plots (figure 4). The user can browse through all baseline pages to find the baseline which she/he likes to treat. A set of different buttons is located on the right hand side of the Baseline Pages. Here it is possible to browse through the Baseline Pages (if there are more than one), to change or to reload the experiment band, and to work on the ambiguities. By pressing the “reset ambiguities” button all ambiguities can be set back to the original state.

The “solve ambiguities” button causes the ambiguity resolution for all baselines of the loaded experiment. To make it easier to evaluate the result of this action the program writes some information about it onto the terminal similar to the example below.

Weighted Mean Residuals (WM) in nanoseconds

BASELINE		CALCULATED	THEORETICALLY	
----- IDP: independent baselines -----				
GILCREEK	HARTRAO	37	46	IDP
GILCREEK	MATERA	-15	-19	IDP
GILCREEK	TIGOCONC	-61	-61	IDP
GILCREEK	WESTFORD	-52	-46	IDP
GILCREEK	WETTZELL	63	56	IDP
HARTRAO	MATERA	-45	-65	
HARTRAO	TIGOCONC	-109	-107	
HARTRAO	WESTFORD	-86	-93	
HARTRAO	WETTZELL	33	10	
MATERA	TIGOCONC	-48	-42	
MATERA	WESTFORD	-37	-28	
MATERA	WETTZELL	77	74	
TIGOCONC	WESTFORD	22	15	
TIGOCONC	WETTZELL	137	117	
WESTFORD	WETTZELL	115	102	

## 5 4<sup>th</sup> level (Baseline Plots)

All observations of the chosen baseline are displayed in the Baseline Plot as shown in figure 5.

The plot consists of:

- observation plot area with axes and inscriptions
- the user function line
- the headline
- the bottom line(s)
- one or two (if more than 50) source name columns
- status labels

Depending on the chosen property there are different sets of user functions available which are displayed in the user function line and can be chosen by a left mouse click onto the buttons. This action causes the binding of the chosen user function(s) to the mouse button(s).

The analyst has the following user functions at her/his disposal:

- information on single observation
- ambiguity shift (down) of single observation
- suppress/recover single observation
- ambiguity shift (up) of single observation
- suppress observation groups
- recover observation groups
- ambiguity resolution of observation groups
- reset ambiguities to original status
- connect observations with the same source
- user input of source name for connection
- jump to next baseline
- jump to previous baseline
- shrink plot area to "good" observations

(the last four functions can be used only by keyboard keys)

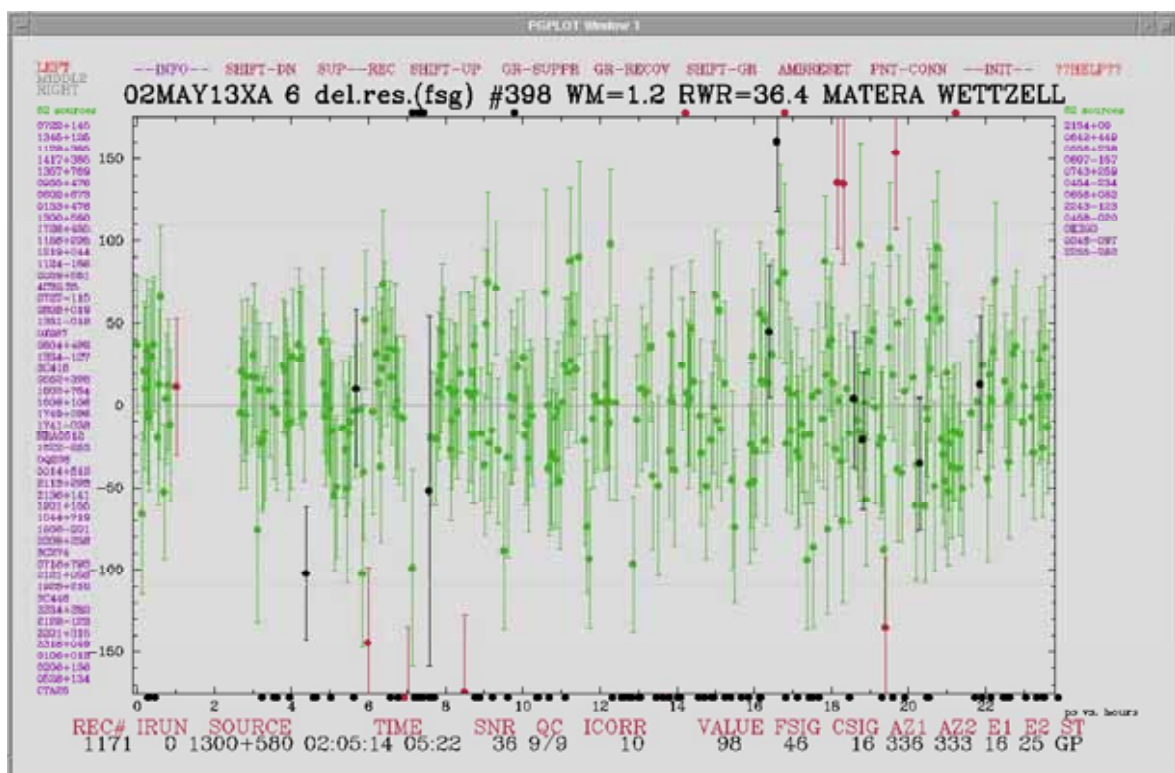


Figure 5: REPA – 4<sup>th</sup> level: Baseline Plots.

## 6 Future plans

Together with the whole Calc/Solve package the program REPA will be ported to the LINUX operating system.

## References

- [1] Leonid Petrov (2002), Release of Mark-4 VLBI Analysis Software CALC/SOLVE from December 27, 2002 ([http://gemini.gsfc.nasa.gov/solve\\_root/release](http://gemini.gsfc.nasa.gov/solve_root/release)).
- [2] Gerald Engelhardt, Volkmar Thorandt, Dieter Ullrich (2003), IVS Analysis and Data Center at BKG - Works in 2002/2003, this volume.

# Mark 5 VLBI Data System Update

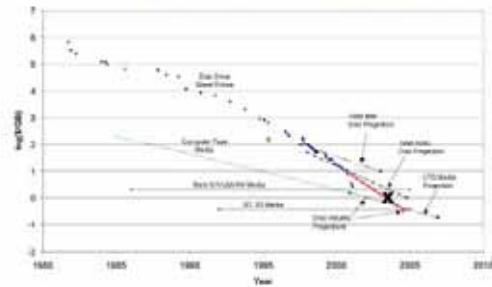
A. Whitney

MIT Haystack Observatory, USA

## Goals of a New VLBI Data System

- Low cost
- Based primarily on unmodified COTS components
- Modular, easily upgradeable
- Robust operation, low maintenance cost
- Easy transportability
- Conformance to VLBI Standard Interface specification (VSI)
- Compatibility with existing VLBI systems
- Flexibility to support e-VLBI
- Minimum of 1 Gbps data rate
- 24-hour unattended operation at 1 Gbps

## Tape vs. Disc Price Comparison



## Current Mark 5 Status

- ~35 Mark 5 systems deployed
- ~200 Mark 5A '8-pack' disk modules now in use
- Daily Intensive UT1 observations Wettzell-Hawaii have been exclusively Mark 5 for ~10 months with almost no problems
- Westford recorded 15-day CONT02 experiment entirely on Mark 5
- Several astronomy experiments have now successfully used Mark 5A at rates to 1 Gbps, including a recent very successful mm-wavelength experiment
- A number of e-VLBI experiments have been conducted with Mark 5A
- Current Mark 5A price ~\$16K from Conduant Corp
- Mark 5B (VSI-compatible) system under development
  - VLBA DAS with VSI interface → 1 Gbps
  - Mark 4 DAS with VSI interface → 2 Gbps

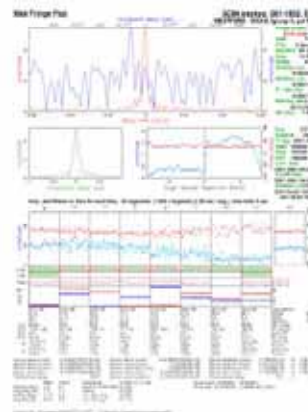
## Mark 5A Data System

- Direct plug-compatible replacement for 64-track Mark4 or VLBA tape drives
- Will record 8, 16, 32 or 64 tracks from Mark4 formatter (1024 Mbps max) or VLBA formatter (512 Mbps max)
- Parity bits are stripped before recording; re-inserted on playback
- Arbitrary mixing of modes (#tracks, data rate, bits/sample) is allowed, always using 100% of installed disk capacity
- Playback at any rate up to 1024 Mbps
- Reliability features
  - All channels are always distributed over all recorded disks; no need for barrel-roll
  - Recording: loss or substandard performance of a disk on record is compensated for automatically (in progress)
  - Playback: loss of a disk will lose only fractional data equally over all 'tracks'
  - Individual disk-performance statistics are kept to weed out marginal or failing disks

## Mark 5 VLBI Demonstration System – March 2001

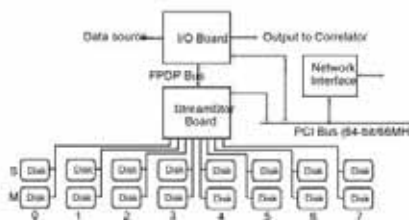


3 months start to finish!



**Mark 5P Data System – mid 2002**

- Direct replacement for 32-track Mark4 or VLBA tape drive
- Records 32 tracks from Mark4 formatter (1024 Mbps max) or VLBA formatter (512 Mbps max)
- Playback at any rate up to 1024 Mbps
- Can use 1 to 16 disks depending on data rate & capacity needs

**Mark 5A '8-pack' chassis****Mark 5A Block Diagram****Mark 5 '8-pack' disk module**

- Drastically simplifies disk-handling logistics by keeping all disks together as a single unit
- Each module can be managed just like a reel of Mark4/VLBA tape, using nearly identical management and tracking software
- Shipping covers completely enclose disks and connector

**Mark 5A I/O Panel****Mark 5 Software Status**

- 'Bank mode' now supported
- Bank switching can be done either with keyswitches or under software control
- Automatic bank switching is in development
- 'Write-protect' has been implemented
- 'Permanent' VSN's can be written to the module
- Automatic playback recovery from bad disk in module will be available soon
- Still some problems to be solved, but being addressed
- All software available on-line
- Field System support software is still somewhat rudimentary

### Documentation

- On-line documentation at [www.haystack.edu/mark5](http://www.haystack.edu/mark5)
- Mark 5A Users Manual
- Mark 5A Test Procedures
- Assembly and Test of Modules
- Disk-module management and handling
- Mark 5A command set

### Mark 5 Implementation Plans

By end 2003, expect:

- Haystack, MPL, USNO, JIVE correlators outfitted --40 units
- EVN -- 10 additional units
- Other geodetic stations --15
- JPL --8
- Others
  - NRAO - 3
  - KVN - 3

Total --75-80

VLBA implementation -- at least partially dependent on pending proposal to NASA for deep-spacecraft tracking

### Disk-Media Status

- Hard disk price vs capacity/performance will continue to drop rapidly
  - Now ~\$1.00/GB, expected to drop to ~\$0.50/GB by ~2005 (Mark 4/VLBA tape is ~\$2.00/GB)
- 200 GB disks now available -- 27 hours @ 256 Mbps unattended (comparable to ~5 VLBA/Mark 4 tapes)
- 320 GB disks expected soon -- 22 hours @ 512 Mbps unattended (comparable to ~9 VLBA/Mark 4 tapes)
- 700 GB disks expected ~2005 -- 24 hours @ 1 Gbps unattended (comparable to ~19 VLBA/Mark 4 tapes)

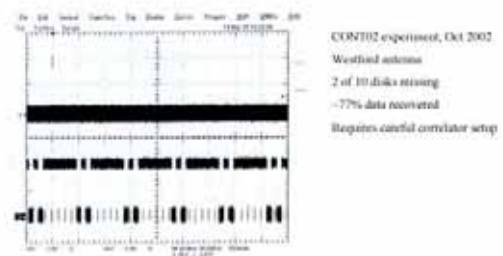
### Disk Conditioning

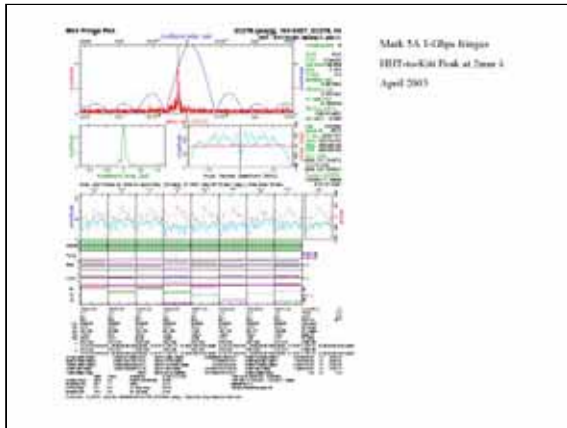
- Disk modules should be 'conditioned' before field usage; special software utility 'SSERase' is available for this purpose
- We feel some of the disk problems encountered during April 03 mm VLBI experiment were due to unconditioned disks (but we didn't know any better at the time)
- Modern commodity disk drives do not have surfaces fully checked
  - First write is done with no checks
  - First read marks bad sectors
  - Next write spares bad sectors, but slow process
- Conduant is writing special software to condition with just two passes (read/write) at full data transfer rate (~1600 Mbps) to maximize efficiency

### Western Digital vs. IBM

- WD disks have generally been recommended due to large capacity, low price and general high reliability
- However, more WD failures of shipped disks have been observed than expected
- We have recently learned a significant difference between WD and IBM disks
  - o Powered-down 3.5" WD disks leave head in contact with surface (at either innermost or outermost diameter)
  - o Powered-down 3.5" IBM disks move heads off surface onto a 'ramp', offering better protection to the heads and the surface.
- Apparently, 2.5" disk drives used in notebook computers use a similar 'ramp' parking scheme for ruggedization
- Though IBM disks are currently not available with the same capacities as WD disks, the price is about the same per GB
- We recommend purchasing IBM disks for the near future.
- Careful statistics must be kept to determine which is better
- Head-parking schemes used by other manufacturers is not known

### Mark 5 Data-recovery Example





### Plans for Serial-ATA Support

- PATA and SATA disk modules will be interchangeable in Mark 5 chassis
- How this will be done:
  - New SATA disk module with connector on R side of module (connector on PATA module is on L)
  - Ejector lever moved to R (on L on PATA module)
  - New chassis backplane
  - New sheet metal piece to accept module with ejector lever on R or L
  - No other changes
- Expected upgrade price ~\$1000
- Module price ~\$260 (same as PATA module)
- ~\$35K development cost; hope to complete by end 2003

### Other Problems and Issues

- Cabling: We suspect that failures to properly record at 1 Gbps at Pico Veleta and HHT in April 03 are due to inadequate cabling between formatter and Mark 5
- Disk modules should not be handled on hard surfaces
  - Very easy to subject disk to quite high shocks
- For shipping: Shipping covers should be installed to protect disks from debris and, perhaps, prying eyes
- Use special shipping boxes:
  - Boxes may not yet be adequate
  - Plan to instrument some shipments with accelerometers



### Mark 5B Data System

- Full VSI (VLBI Standard Interface) capability
- Up to 1024 Mbps
- Requires new Mark 5B I/O card
- Eliminates need for Mark 4 or VLBA formatter
- Same chassis as Mark 5A
- Will also provide adapter for Mark 4/VLBA DASS to provide VSI-compatible output
- Expect Mark 5B to be ready early 2004

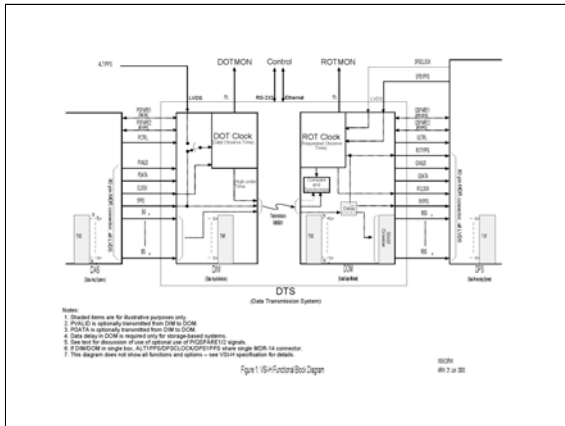
### Mark 5B Compatibility Matrix

Record	System	From	To	Platform			
				Mark 5A	Mark 5B	Mark 5C	Mark 5D
Mark 5A	Mark 5A	Mark 5A	✓	✓	✓	✓	
Mark 5A	Mark 5B	Mark 5B	✓	✓	✓	✓	
Mark 5B	Mark 5B	Mark 5B	✓	✓	✓	✓	

- In summary:
- Mark 5D can play only Mark 5B recordings (VSI format in/out)
  - Mark 5A can play
    - All Mark 5A recordings
    - Mark 5B recordings will playback in VLBA-track-format (requires upgrade to current Mark 5A)

### VLBI Standard Interface (VSI)

- Joint effort by astronomy (GVWVG) and geodetic (IVS) communities
- **The purpose of VSI is to define a standard interface to and from a VLBI Data Transmission System (DTS) that allows heterogeneous DTS's to be interfaced to both data-acquisition and correlator systems with a minimum of effort.**
- Focuses on those functions independent of DTS technology
- VSI-H – complete
  - Data and control interfaces for recording and playback, including connectors and pinouts
  - Electrical and timing specs
- VSI-S – complete
  - Communications model
  - Application Protocols
  - Command/Response Syntax
  - Suggested basic command set
- VSI-E – new, in progress!
  - Will define e-VLBI standards
- VSI-H and VSI-S specs available at <http://www.luytstack.edu/vsi>



- ### VSI Committee
- Wayne Cannon York University Canada
  - Brent Carlson DRAO Canada
  - Dick Ferris ATNF Australia
  - Dave Graham MPI Germany
  - Ed Himwich NASA U.S.
  - Richard Hughes-Jones U. of Manchester England
  - Nori Kawaguchi NAO Japan
  - Tetsuro Kondo CRL Japan
  - Ari Majunen Metsahovi Finland
  - Sergei Pogrebenko JIVE Netherlands
  - Sergey Likhachev ASC Russia
  - Jon Romney NRAO U.S.
  - Ralph Spencer Jodrell England
  - Harro Verkonter JIVE Netherlands
  - Alan Whimpey Haystack U.S.

- ### Scientific Advantages of e-VLBI
- **Bandwidth growth potential for higher sensitivity**
    - VLBI sensitivity (SNR) proportional to square root of bandwidth resulting in a large increase in number of observable objects (only alternative is bigger antennas - hugely expensive)
    - e-VLBI bandwidth growth far exceeds recording capability (practical recordable data rate limited to ~1 Gbps)
  - **Rapid processing turnaround**
    - Astronomy
      - Ability to study transient phenomena with feedback to steer observations
    - Geodesy
      - Higher-precision measurements for geophysical investigations
      - Better Earth-orientation predictions, particularly UT1, important for military and civilian navigation

- ### Practical Advantages of 'e-VLBI'
- **Increased Reliability**
    - remove recording equipment out of field
    - remote performance monitor & control capability in near real-time
  - **Lower Cost**
    - Automated Operation Possible
      - eliminates manual handling and shipping of storage media
    - Real-time or near-real-time Processing
      - forestalls growth of storage-capacity requirements with bandwidth growth
      - Elimination of recording-media pool (millions of \$'s)
  - **Avoid unexpected media-shipping interruptions and losses**

- ### e-VLBI Development at Haystack Observatory
- **Phase 1** Develop eVLBI-compatible data system
    - Mark 5 system
  - **Phase 2** Demonstrate 1 Gbps e-VLBI using Bossnet (w/ DARPA and NASA support)
    - ~700km link between Haystack Observatory and NASA/GSFC
    - First e-VLBI experiment achieved ~700Mbps transfer rate
  - **Phase 3** Develop adaptive network protocol (newly awarded NSF grant to Haystack Observatory; collaboration with MIT Lab for Computer Science and MIT Lincoln Laboratory)
    - New IP-based protocol tailored to operate in shared-network 'background' to efficiently using available bandwidth
    - Demonstrate on national and international networks
  - **Phase 4** Extend e-VLBI to national and global VLBI community
    - 'Last mile' problem remains a serious challenge



### Mark 5 e-VLBI Connectivity

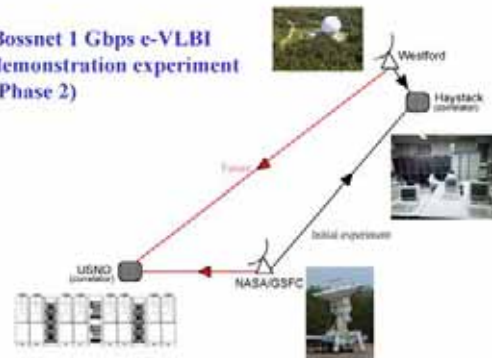
- Mark 5 supports a triangle of connectivity for e-VLBI requirements



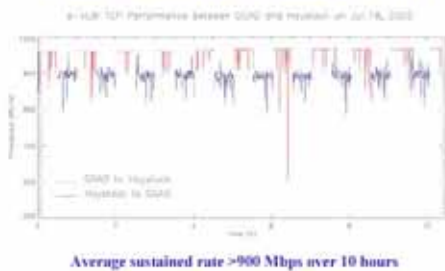
Mark 5 can support several possible e-VLBI modes:

- e-VLBI data buffer (first to Disc Array, then to Network); vice versa
- Direct e-VLBI (Data Port directly to Network); vice versa

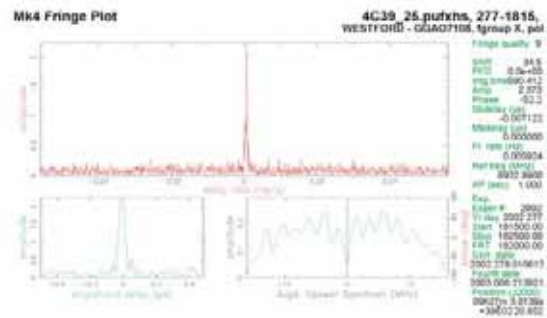
### Bossnet 1 Gbps e-VLBI demonstration experiment (Phase 2)



### Performance test results – Haystack/GGAO



### Correlation results of e-VLBI test observation



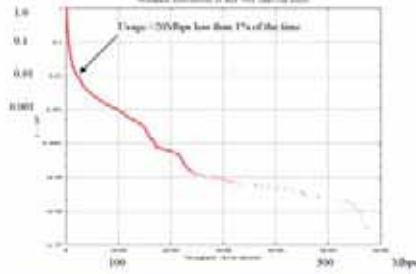
### International e-VLBI experiments

- Westford, MA to Kashima, Japan - experiments in Oct 02 and Mar 03
  - Files exchanged over Abilene/GEMnet networks
    - Nominal speed expected to be ~20 Mbps, best achieved so far ~11 Mbps
  - Correlation on Mark 4 correlator at Haystack and PC Software correlator at Kashima, nominal fringes obtained
  - Further experiments are scheduled, network tuning is in progress
  - Expect >100 Mbps in near future
- Kauai, Hawaii to Wettzell, Germany (in progress)
  - Daily experiments of ~100GB are ideal candidate for early e-VLBI
  - Data will be transferred to Haystack Observatory for processing (DS-3 speeds are possible in short term)
  - Network links are now being brought up

### New IP Protocols for e-VLBI (Phase 3)

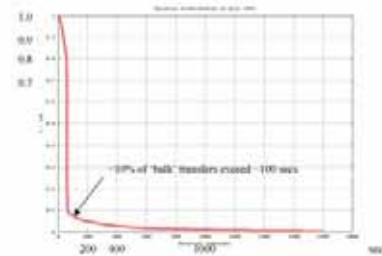
- Based on observed usage statistics of networks such as Abilene, it is clear there is much unused capacity
- New protocols are being developed to utilize networks in "background" mode for applications such as e-VLBI
  - Will "scavenge" and use "secondary" bandwidth
  - Will give priority to "normal" users
  - Requires a new "end-point adaptive strategy"
- Work being carried out under NSF sponsorship by MIT Haystack Observatory in collaboration with MIT Laboratory for Computer Science and MIT Lincoln Laboratory
  - 3-year program, will demonstrate e-VLBI connections both nationally and internationally

**Typical bit-rate statistics on Abilene network**



Conclusion: Average network usage is only a few % of capacity

**Typical distribution of heavy traffic on Abilene**

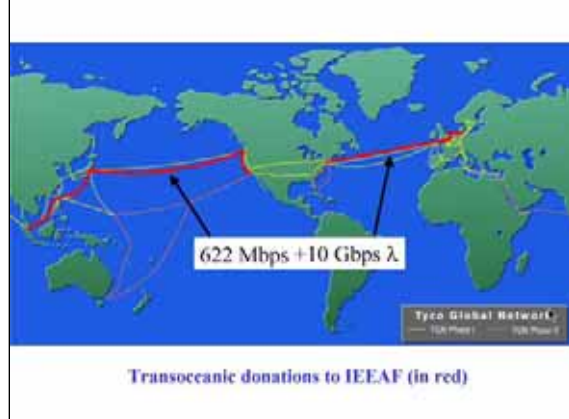
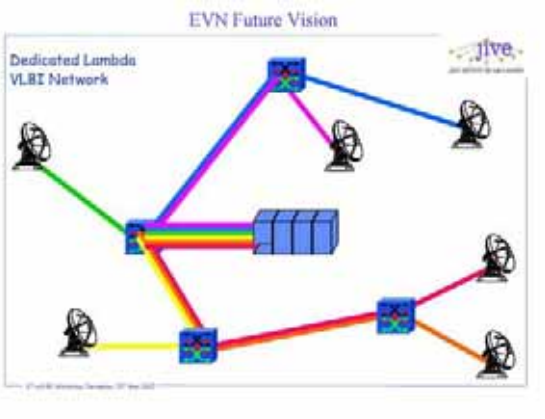


Conclusion: Heavy usage of network tends to occur in bursts of ~2 minutes

**Extend to national and global community (Phase 4)**

- Many possibilities for international connections
  - Surfnet - U.S. to Europe at 2.5 Gbps
  - IEEAF - U.S. to Europe at 10 Gbps
  - TransPAC - U.S. to Japan at 655 Mbps (upgrade to 1.2 Gbps planned)
  - GEMnet - currently ~150 Mbps
  - Super-Sinet - 2.5 Gbps Japan-to-U.S.
  - AMPATH - possible connections to telescopes in Chile and Brazil
- Not well covered
  - Australia
  - Africa
  - China
  - Large parts of South America

**Abilene Network Backbone - February 2002**  
10 Gbps



**But there is a significant problem -- 'Last-mile' costs**

- Most of the world's telescopes are not well connected
- Electronic and electro-optic costs are dropping rapidly
  - GigE switch: 2001 - \$15K, 2003 - \$1.2K
  - GigE transceivers: 2001 - \$750, 2003 - \$180
  - CWDM transceivers: \$400-800 for 50-100km reach!
- Direct fiber cost is relatively low-- \$60/fiber-km in 80-fiber bundle
- If you can buy or lease existing fiber, there is no better time!
- But - fiber installation cost is still tall pole
  - Europe: >\$20m (or any populous wide-area)
  - U.S.: >\$10m (in simplest desert environment)
- The upside: there is developing a lot of momentum and support from the greater networking community to get the job done!

**Also desperately needed:**

- Modern digital filter banks to replace aging and obsolete analog BBC's!

**....and a longer term e-VLBI issue as well**

- Can e-VLBI survive the long-term networking costs?

**...and some hope!**

- There is momentum gathering in the networking community to provide national and international ultra-high-speed networking as a critical 'enabling infrastructure' for international science; in U.S., NSF 'Atkin's Report' recommends spending \$1B/yr for next 5 years to improve national 'cyberinfrastructure'!
- the VLBI community needs to make its voice heard loud and clear!

**Conclusions**

- Transition to all disks will be rapid due to technical, economic and practical advantages
- e-VLBI is riding an unprecedented wave of global network connectivity and networking community enthusiasm
- There is no better time to lease or buy installed fiber than now!
- Gradual transition from disks to disk/e-VLBI to all e-VLBI is likely
- 10-100 Gbps/antenna is technically possible with e-VLBI (can VLBI correlators keep up?!)
- The VLBI community should move aggressively to exploit these new technologies

Session 3  
Local Ties



# Stability of Space Geodetic Reference Points at Ny-Ålesund and Their Excentricity Vectors

C. Steinforth<sup>1</sup>, R. Haas<sup>2</sup>, M. Lidberg<sup>2</sup>, and A. Nothnagel<sup>1</sup>

<sup>1</sup>*Geodetic Institute, University of Bonn, Germany*

<sup>2</sup>*Onsala Space Observatory, Chalmers University of Technology, Sweden*

**Summary:** The Ny-Ålesund Geodetic Observatory is equipped with two permanent GPS units which are part of the IGS network and the VLBI telescope close by. A DORIS beacon is operated in the vicinity. This paper gives an overview about measurements that have been carried out at Ny-Ålesund in two local survey campaigns in August 2000 and August 2002 and the corresponding results.

## 1 Introduction

Due to its extreme northern location the co-location site Ny-Ålesund plays an important role in global geodetic and geodynamic studies. In close vicinity to each other a VLBI telescope (Fig. 1) and two GPS units (Fig. 2) are operated routinely in global monitoring programs by the Norwegian Mapping Authority (NMA). A DORIS beacon (Fig. 3) is located on top of the French polar research station in about 1.5 km distance from the VLBI telescope and the GPS units. The data collected with these space geodetic observing platforms are used for example for investigations into Earth rotation (VLBI and GPS) or precise orbit determination (DORIS and GPS). All platforms also provide crucial data for the establishment and maintenance of the International Terrestrial Reference Frame (ITRF) (*Altamimi et al., 2001*).



Figure 1: The Ny-Ålesund VLBI telescope.



Figure 2: The GPS units NYAL (left) and NYA1 (right).



Figure 3: The DORIS beacon.

Two general requirements have to be fulfilled for successful investigations of the areas mentioned above. For global geodynamic studies the *stability* of the reference points has to be monitored regularly with high accuracy in order to separate local effects from global phenomena like plate tectonics or crustal deformation. At sites with multiple observing platforms the *excentricities*, i.e. the 3D vectors between the observing instruments, have to be determined and kept up-to-date for the maintenance of the

terrestrial reference frame. Both aims can only be reached by repeated precise local surveying. Therefore, two surveying campaigns have been carried out in August 2000 and in August 2002.

The main focus of this paper is on the comparison of the results derived in the two surveying campaigns and, as a result of the comparison, on the stability of the space geodetic reference points. Most methods and observing principles used in the campaigns were already described extensively in recent publications (e.g. *Lidberg et al., 2002; Nothnagel et al., 2001; Nothnagel et al., 2002* or *Steinforth et al., 2002*).

## 2 Space Geodetic Reference Points at Ny-Ålesund

In geodetic VLBI all parameters estimated in the data adjustment are referred to the so-called VLBI reference point. In the case of an azimuth-elevation mount the reference point is either the point where both axis intersect or, if they do not intersect as in the case of the Ny-Ålesund telescope, it is the point of the azimuth axis where the distance to the elevation axis is minimal (Fig. 4) (e.g. *Ma, 1978; Nothnagel et al., 1995*). This point should be invariant to any antenna movements necessary for the VLBI observations.

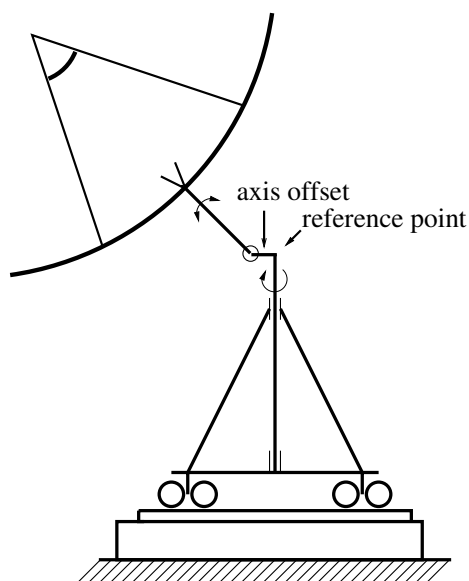


Figure 4: Axis geometry of the Ny-Ålesund VLBI telescope.



Figure 5: Target materialized by a pop rivet at the end point of the elevation axis.

The reference point of the Ny-Ålesund telescope is not directly accessible and cannot be materialized, either. In order to determine the reference point, the end points of the elevation axis have been materialized by small pop rivets which were placed in the centric bores of the elevation bearings (Fig. 5). When rotating in azimuth each end point of the elevation axis ideally describes a circle about the VLBI reference point. Determining the 3D positions of the markers at different azimuths subsequently permits the computation of the VLBI reference point as the center of the circles. The average height of the two end points represents the height of the reference point. For full visibility coverage of the targets at the elevation axis end points, three auxiliary survey points on tripods were established augmenting the existing network of concrete surveying pillars (Fig. 6).

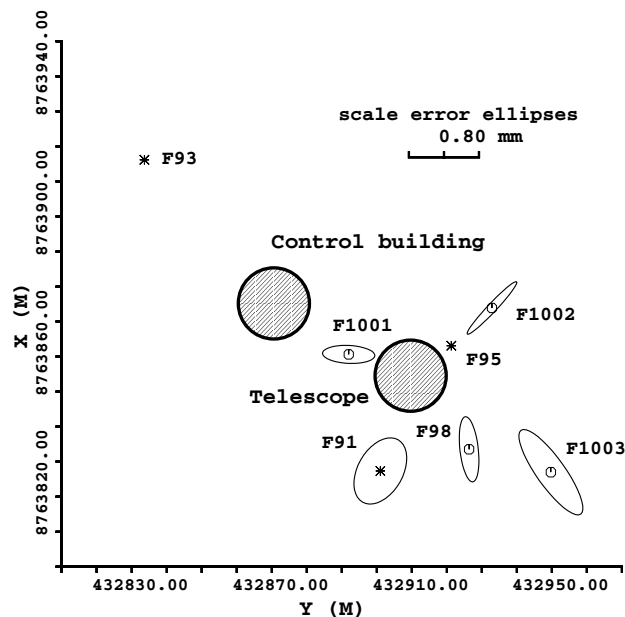


Figure 6: Layout of the Ny-Ålesund control network; F91, F93, F95, F98 = pillars; F1001, F1002, F1003 = tripods.

The GPS antenna reference point (ARP) is, in contrast to the somehow virtual reference point of a VLBI antenna, physically defined. Its height is related to the bottom of the pre-amplifier (BPA) of the GPS antenna. The position of the ARP can be represented by the center of the ground plane. The height components of the ARP and the center of the ground plane differ by 35 mm according to the IGS database (antenna type AOAD/M.T) (Fig. 7).

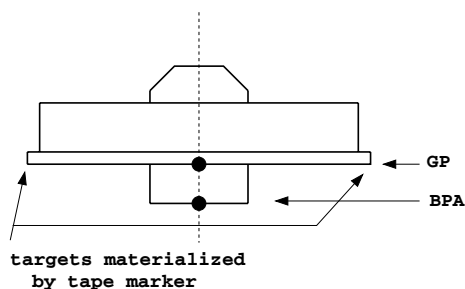


Figure 7: Cross-section of the NYA1 GPS antenna, BPA = bottom of pre-amplifier, GP = ground plane,  $\Delta h_{GP-BPA} = 35 \text{ mm}$ .



Figure 8: NYA1 with tape markers.

Since the GPS antenna could not be removed and there was no direct line of sight to the BPA the reference point had to be determined indirectly. In order to determine the reference point four tape markers were used which were affixed to the ground plane at four directions (North, South, East, West, Fig. 8). These tape markers materialize the lower edge of the circular ground plane (Fig. 7). After measuring the 3D positions of the tape markers relative to a control network of tripods through forward intersects it is possible to estimate the position of the ARP as the center of a circle.

The reference point of the DORIS beacon (Starec type) is normally the 400 MHz phase center of the antenna (Fig. 10). If the 400 MHz and 2 GHz phase centers are not on the same vertical line (tilt of antenna) the height reference of the antenna is the 400 MHz phase center, but the horizontal position is referred to the 2 GHz phase center (H. Fagard, personal communication).

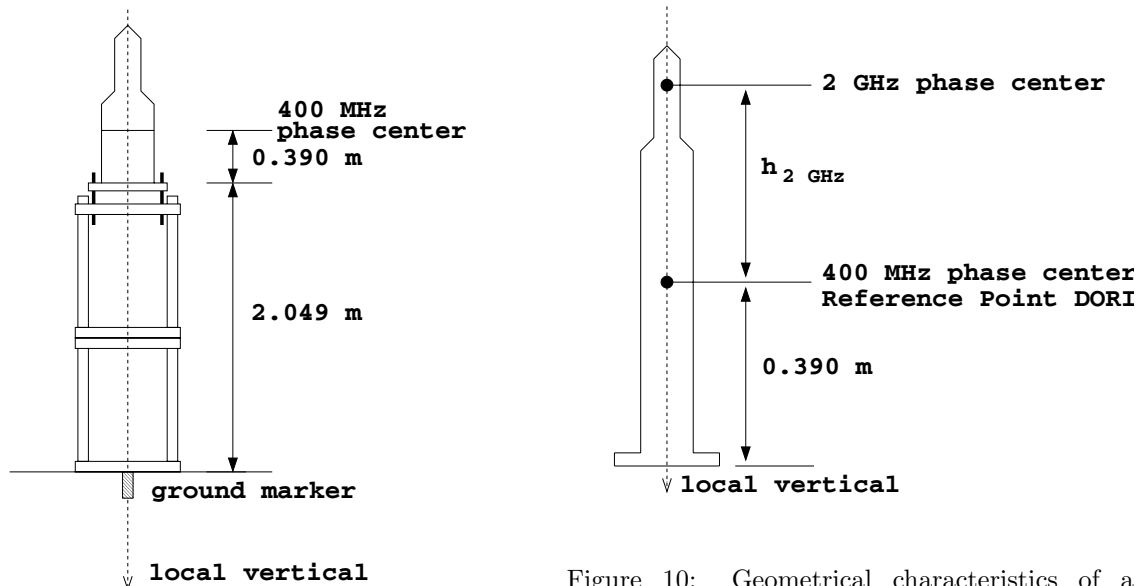


Figure 9: DORIS steel monument with ground marker.

Figure 10: Geometrical characteristics of a DORIS antenna (Starec type);  $h_{2\text{ GHz}} = 487\text{ mm}$ .

The DORIS beacon is located on a balcony at the building of the French polar research station in Ny-Ålesund village (cf. Fig. 3; Fagard, 1990). The local tie between the DORIS antenna and the other techniques was observed by GPS since the distance is too long for a position transfer by terrestrial surveying methods (adverse error propagation).

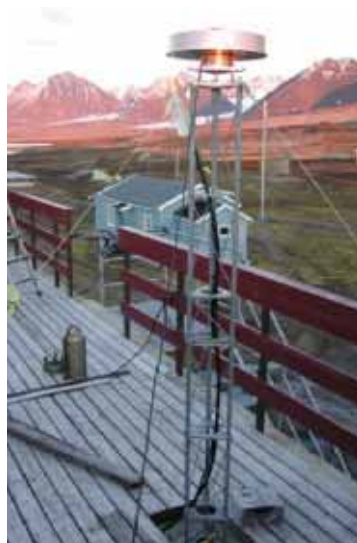


Figure 11: The GPS antenna mounted on the DORIS monument.

In a first step, the centering of the DORIS beacon with respect to its nominal position marked by a brass bolt was checked in order to remount the beacon in its proper position (cf. Fig. 9). Then the beacon was dismantled and replaced by a GPS antenna for a 5-day continuous GPS measurement (Fig. 11). At the end of the GPS measurements the DORIS antenna was replaced and the centering was checked again.

### 3 Results

The analysis of the trigonometric measurements was carried out with the least squares adjustment program PANDA (*GeoTec, 1998*). After some testing the topocentric coordinates of point F93, the East and North component of F95 and the Up component of F91 were fixed in the least squares adjustment to the coordinates used in the 2000 campaign (e.g. *Nothnagel et al., 2002*). The topocentric coordinates for the VLBI and the GPS reference point were then estimated in this local frame (Tab. 1).

Table 1: Topocentric coordinates of the VLBI and GPS reference points

	East [m]	$\sigma$ [mm]	North [m]	$\sigma$ [mm]	Up [m]	$\sigma$ [mm]
VLBI	432927.7704	0.8	8763860.7518	0.1	87.2926	0.2
GPS	432836.5156	0.1	8763915.2683	0.1	84.1872	0.5

In the next step the stability of the VLBI reference point was checked by comparing the results of the two epochs (Tab. 2). It can be stated that there is no obvious displacement of the VLBI reference point.

Table 2: VLBI reference point determined in the two campaigns

Year	East [m]	$\sigma$ [mm]	North [m]	$\sigma$ [mm]	Up [m]	$\sigma$ [mm]
2000	432927.7704	0.2	8763860.7526	0.2	87.2929	0.4
2002	432927.7704	0.8	8763860.7518	0.1	87.2926	0.2
$\Delta_{2002-2000}$ [mm]	<b>0.0</b>	–	<b>-0.8</b>	–	<b>-0.3</b>	–

The survey setup chosen here also offers a good opportunity to check the antenna axis offset. The results of the two campaigns agree quite well (difference 0.6 mm, Tab. 3) again confirming the significant discrepancy of the value provided by the manufacturer from the value determined on site. One of the reasons for such a big discrepancy may be the fact that the VLBI reference point cannot be materialized and that the manufacturer determined this value just by trying to measure it with the help of a CAD software. In addition, the actual telescope construction at Ny-Ålesund is not necessarily the same as it was projected (H. Digre, personal communication).

Table 3: Axis offset

Year	Offset [m]	$\sigma$ [mm]
manufacturer	0.5080	–
2000	0.5245	0.3
2002	0.5239	0.3
<b>mean</b>	<b>0.5242</b>	<b>0.2</b>

Excentricity vectors between different observing techniques to be used in the computations of the ITRF are normally given in geocentric X,Y,Z coordinate differences. Since the coordinates of the surveying pillars have

been computed in both systems, i.e. in global X,Y,Z and in topocentric North,East,Up coordinates, it is possible to transform one system into another by a simple 7-parameter Helmert transformation (Tab. 1 and 4).

Table 4: Geocentric Coordinates of the VLBI and GPS reference points after transformation

	X [m]	$\sigma$ [mm]	Y [m]	$\sigma$ [mm]	Z [m]	$\sigma$ [mm]
VLBI	1202462.7055	0.7	252734.4291	0.8	6237766.0458	0.3
GPS	1202433.9070	0.2	252632.2608	0.1	6237772.5076	0.5

Table 5: Geocentric Coordinate Differences relative to NYA1 (VLBI – NYA1 and DORIS – NYA1 resp.)

to point	Year	$\Delta X$ [m]	$\sigma$ [mm]	$\Delta Y$ [m]	$\sigma$ [mm]	$\Delta Z$ [m]	$\sigma$ [mm]	Distance [m]	$\sigma$ [mm]
VLBI	2002	28.798	1.0	102.168	1.0	-6.462	1.0	106.344	1.0
	2000	28.794	2.0	102.162	2.0	-6.470	2.0	106.339	2.0
	<b>mean</b>	<b>28.797</b>	<b>1.0</b>	<b>102.167</b>	<b>1.0</b>	<b>-6.464</b>	<b>1.0</b>	–	–
DORIS	2002	360.061	1.7	1530.850	1.5	-162.944	5.7	1581.043	–

Table 5 summarizes the geocentric excentricity vectors between the NYA1 GPS reference point and the VLBI and DORIS reference points. The standard deviations of the values derived in the 2000 campaign are mainly influenced by the determination of the NYA1 reference point. This was measured by GPS only in the precise point positioning mode (NMA, personal communication). In order to calculate a reasonable weighted mean and to mitigate a disproportion of the two campaigns the standard deviations of the 2002 excentricities were fixed to 1.0 mm giving the NYA1 reference point measured by terrestrial methods a stronger weight. In addition, the standard deviations of the mean values (cf. Tab. 5) were also fixed to 1.0 mm which corresponds approximately to the accuracy of the terrestrial measurements. The resulting mean values are intended as updates to the previous figures originating from the 2000 campaign and will be published in the SINEX format.

It should be mentioned here that the vectors as computed from the ITRF2000 coordinates of these reference points (VLBI–NYA1  $\Delta X = 28.794$  m,  $\Delta Y = 102.166$  m,  $\Delta Z = -6.475$  m; DORIS–NYA1  $\Delta X = 360.060$  m,  $\Delta Y = 1530.851$  m,  $\Delta Z = -162.949$  m, Distance = 1581.044 m) show a good agreement with the vectors determined in this study.

## Acknowledgements

The research carried out at the Ny-Ålesund Geodetic Observatory was funded by the European Community (EC) – Access to Research Infrastructure – Improving Human Potential Programme and the Large Scale Facility Programme (LSF) under grants NMA-22/2000 and NMA-76/2001. We are particularly thankful to Helge Digre, Tom Pettersen, David Holland and Sune Elshaug of the Norwegian Mapping Authority (Statens Kartverk) and to the staff of Kings Bay AS who supported us in every aspect creating the basis for the success of this project.

## References

- Altamimi, Z. et. al., EOS Transactions, AGU, Vol. 82, No. 25, 2001, 278-279
- Fagard, H., Remplacement de la station DORIS de Ny-Ålesund (Spitsberg, Norvège), Comptes Rendus CR/G 108, Institut Géographique National, Paris, France, 1999
- Panda für Windows, Version 2.12, Systemhandbuch, GeoTec GmbH, 1998, Laatzen
- Lidberg, M., C. Steinforth, R. Haas, A. Nothnagel, Local tie measurements at Ny-Ålesund - a status report; in: Proceedings of the 14th General Meeting of the Nordic Geodetic Commission, Espoo, Finland, 1.-5.10.2002, ed. M. Poutanen and H. Suurmäki, Kirkkonummi 2002, 94-98
- Ma, C., Very Long Baseline Interferometry Applied To Polar Motion, Relativity and Geodesy, NASA Technical Memorandum 19582, 1978, Greenbelt MD
- Nothnagel, A., M. Pilhatsch, R. Haas, Investigations of thermal height changes of geodetic VLBI telescope, Proceedings of the 10th Working Meeting on European VLBI for Geodesy and Astrometry, ed. R. Lanotte and G. Bianco, Matera, 1995, 121-133
- Nothnagel, A., C. Steinforth, B. Binnenbruck, L. Bockmann, L. Grimstveit, Results of the 2000 Ny-Ålesund Local Survey; in: A. Rius and D. Behrend (Eds.): Proceedings of the 15th Working Meeting on European VLBI for Geodesy and Astrometry, Institut d'Estudis Espacials de Catalunya, Consejo Superior de Investigaciones Cientificas, Barcelona, Spain, Sep. 07-08, 2001, 168-176
- Nothnagel, A., D. Behrend, S. Bergstrand, B. Binnenbruck, R. Haas, C. Steinforth, Local Survey Ties at VLBI Observatories, In: Measurement of Vertical Crustal Motion in Europe, ed. J. Campbell, R. Haas, A. Nothnagel, TMR Network FMRX-CT96-0071 Scientific Report 1996-2001, Bonn, 2002, 63-97
- Steinforth, C., A. Nothnagel, R. Haas, M. Lidberg, Stability of VLBI and GPS reference points at Ny-Ålesund, In: The Changing Physical Environment, Proceedings from the 6th Ny-Ålesund International Scientific Seminar, Tromsø, Norway, 8.-10.10.2002, ed. J.B. Ørbæk, K. Holmén, R. Neuber, H.P. Plag, B. Lefauconnier, G. de Prisco and Hajime Ito, 185-188



# 2002 Local Geodetic Survey of VLBI and GPS Reference Points and Eccentricity at Medicina (Italy)

P. Tomasi<sup>1</sup>, P. Sarti<sup>1</sup>, L. Vittuari<sup>2</sup>, M. Negusini<sup>1</sup>, and P. Sillard<sup>3,4</sup>

<sup>1</sup>*Istituto di Radioastronomia – CNR, Bologna, Italy*

<sup>2</sup>*DISTART, Università di Bologna, Italy*

<sup>3</sup>*Institut National de la Statistique et des Etudes Economiques, Paris, France*

<sup>4</sup>*Institut Géographique National, Marne la Vallée, France*

**Summary:** The geodetic activity at Medicina radio-astronomical observatory (Italy) has been continued in 2002 with the third survey of the local network. Previous surveys had been carried out in 2000 and 2001. Our main purpose was to monitor the stability of the VLBI reference point after two major interventions on the VLBI antenna: in August 2002 there has been a substitution of the track while in 2001 the concrete under the track has been completely replaced. It has also been the second year in which we have surveyed co-located VLBI and GPS antennas thus estimating a new value for the eccentricity vector connecting the Reference Point of each technique.

The importance of co-locations and local ties in different aspects of space geodesy and especially in ITRF computation is well known. We concentrate here on the surveying aspects and on the local ground control network presenting the results of the most recent campaign performed in September 2002 in Medicina (Italy). 2002 local survey data analysis (terrestrial and GPS data) and eccentricity estimate are presented and compared to 2001 results. Eccentricities are estimated using a new and comprehensive methodology that has been presented at the EGS 2003 and is extensively described in a paper by Sarti et al. recently submitted to Journal of Geodesy.

## 1 Introduction

During the last few years, there has been a constant increase in the interest for the information that is provided by local surveys. They are extremely important for the applications of Integrated Global Geodetic Observing System (IGGOS) and for reaching the highest accuracy in multi-technique geodetic products. The establishment of a Working Group for local ties within the International Earth Rotation and Reference Systems Service (IERS) clearly demonstrates the increasing attention that is given to this kind of activities. At present spatial geodetic techniques are able to determine the position of the reference point of the observing instrument with a precision of few millimetres. The rate of the same point can be determined with sub-millimetres precision. That means that the local possible motion of the reference point must be monitored with at least the same precision or better.

Local ground control networks must therefore be regularly maintained and surveyed in order to obtain the larger amount of geodetic information. Particular care must be paid when locating the reference point of those techniques, such as VLBI and SLR that do not have a clearly materialised reference marker. In order to compute eccentricity vectors it is necessary to develop a geometrical model for locating the reference points and a rigorous statistical approach for estimating their positions. Using terrestrial geodesy (e.g.: triangulation and trilateration) it is possible to estimate, with very high precision, the position of the reference points along with the positions of the pillars of the local network. These latter positions are strictly related to the geodetic and geological features that characterize the observatory and can provide remarkable additional information. Site surveying, adjustment of local networks, SINEX generation with full variance-covariance information and other co-location issues (e.g. environmental parameters) are different phases of the same activity and are strictly connected. We concentrate here on the first two aspects of the local tie: site surveying and data processing.

## 2 Local survey

We give some details on the surveying strategy used in the terrestrial measurements (see 2.1) and in GPS measurements (see 2.2) for recovering the 2002 eccentricity vector. We also compare the results obtained for September 2002 survey with the results of the previous survey performed in June 2001 and during 2000. In the last case we have determined only the VLBI reference point in the local reference frame.

### 2.1 Terrestrial measurements

Triangulation and trilateration of the local network has to be performed measuring angles and distances with very high precision. It is therefore very important to use special care in performing the measurements and use high precision instrumentation. In particular:

- 3-D forced centring markers allow stable stationing and reliable reoccupations,
- modern instruments of high technical quality are fundamental for a quick and precise survey
- retro reflecting prisms are widely used for distance measurements.

Practical aspects, directly connected to network surveying strategy, are very important too: the geometry of the network, being directly connected to the design matrix of the adjustment, has a remarkable impact on the correlations between estimated positions.

A critical aspect in the local ground control network at Medicina is related to the lack of concrete pillars on the East side of the VLBI antenna (points with T-code in the upper part of Figs. 1 and 2 ). For more details on the site a map is presented on Figure 3. VLBI and GPS antennas, permanent and not permanent reference marker of the local network are visible in the map.

The experience that we have developed during the previous terrestrial surveys (Sarti et al., 2000; Tomasi et al., 2001; Vittuari et al., 2001; Vittuari et al., 2002) has been of great advantage in optimising the survey activities and connect the different phases of the local tie.

In order to perform measurements that are homogeneously distributed in space, it is necessary to daily install tripods: their position changes each day and must be recovered using backwards intersection on known points. As can be seen in table 1, where some information on the surveys of 2001 and 2002 are given, this increases considerably the number of unknowns. A large redundancy of observations is therefore fundamental to reach accurate results.

Table 1: Observations and unknowns of the local ties used as datasets.

Local tie	June 2001	September 2002
Number of stations	110	105
azimuth angles	297	308
Zenith angles	289	339
distances	272	327
unknowns	324	312

Figure 1: Local ground control network and cluster of targets' positions observed on the VLBI antenna in 2002.

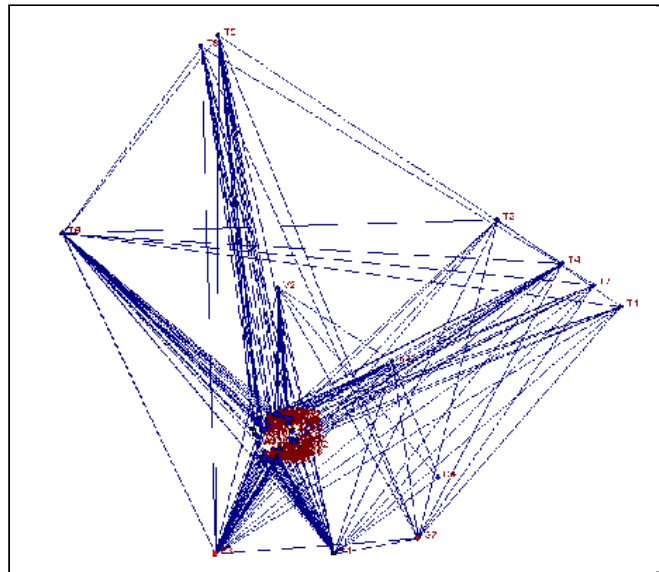


Figure 2: Local ground control network and cluster of targets' positions observed on the VLBI antenna in 2001.

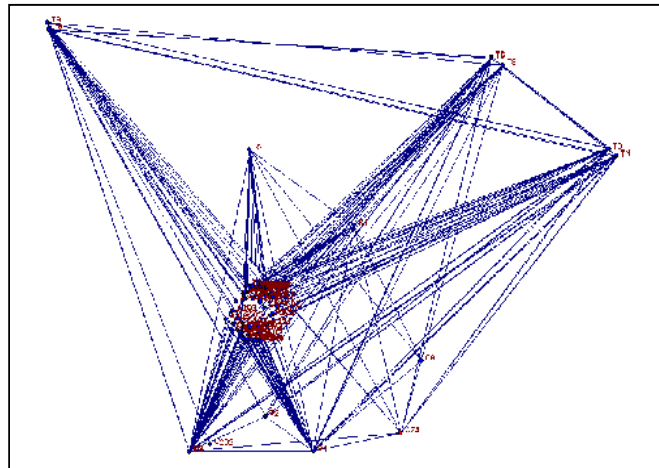
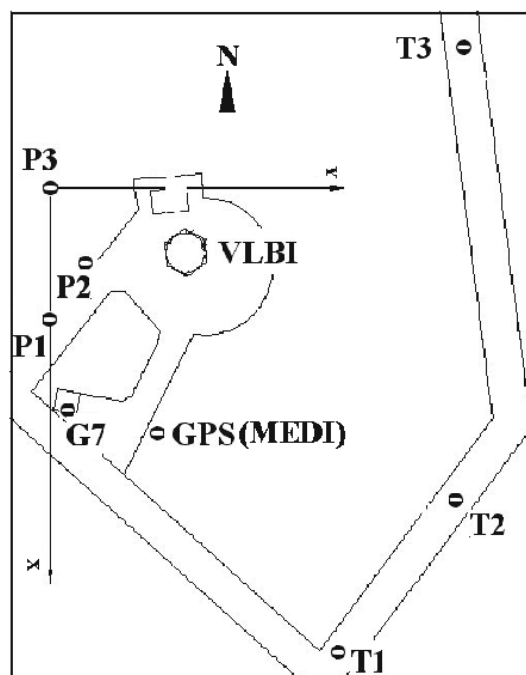


Figure 3: Map of the Medicina site and the local reference system. P are permanent concrete pillars, G7 is height reference point (on a pillar of the mobile laser pad), T are the point materialized with tripods.



Data acquired in the two surveys have been processed using STAR\*NET of Starplus software Inc. and have been post-processed using a rigorous statistical approach that has been especially developed for estimating eccentricities between any Space Geodesy technique (Sarti et al., 2003 submitted). Results, obtained in the local frame for the eccentricity vector  $(X_V, Y_V, Z_V, X_G, Y_G, Z_G)$  between the VLBI and the GPS reference points, are shown in table 2. For both surveys the precision of position estimates is very high, with a slight improvement (about 20 %) for 2002 survey. There is no evidence of motion of the VLBI reference point between 2000 and 2001 survey. The position of the VLBI reference point has changed between the two 2001 and 2002 surveys. This is not very surprising, though: the antenna has been up-lifted and the track has been changed in August 2001.

Table 2: VLBI-GPS eccentricity vector estimates in the local frame for the 2001 and 2002 local tie, and VLBI reference point for 2000.

Local tie Eccentricity	Local tie		
	May 2000	June 2001	September 2002
$X_V$ (m)	$21.581 \pm 0.001$	$21.5805 \pm 0.0004$	$21.5825 \pm 0.0003$
$Y_V$ (m)	$45.534 \pm 0.001$	$45.5356 \pm 0.0003$	$45.5360 \pm 0.0002$
$Z_V$ (m)	$17.699 \pm 0.001$	$17.6995 \pm 0.0008$	$17.7024 \pm 0.0006$
$X_G$ (m)		$79.9215 \pm 0.0011$	$79.9268 \pm 0.0006$
$Y_G$ (m)		$29.9692 \pm 0.0010$	$29.9692 \pm 0.0008$
$Z_G$ (m)		$0.5699 \pm 0.0008$	$0.5701 \pm 0.0005$

More interesting is the movement, which is associated with the GPS reference point. No interventions have been made on the GPS antenna and the movement we observe with terrestrial measurements is also detected using GPS observations. The movement is most probably associated to instability of the pillar on which the GPS antenna is positioned.

Very important information is contained in the correlation matrices of the two surveys, shown below:

$$\rho_{2001} = \begin{pmatrix} 1 & -0.0126 & 0.0055 & -0.0159 & 0.0331 & -0.0001 \\ & 1 & 0.0187 & -0.0476 & 0.0990 & 0.0041 \\ & & 1 & 0.0561 & 0.0559 & 0.4306 \\ & & & 1 & 0.3453 & -0.0083 \\ & & & & 1 & -0.0125 \\ & & & & & 1 \end{pmatrix}$$

and

$$\rho_{2002} = \begin{pmatrix} 1 & 0.0595 & -0.0004 & 0.0035 & -0.0131 & -0.0005 \\ & 1 & -0.0054 & -0.0149 & 0.1773 & -0.0002 \\ & & 1 & 0.0003 & -0.0009 & 0.3985 \\ & & & 1 & -0.0587 & -0.0169 \\ & & & & 1 & -0.0122 \\ & & & & & 1 \end{pmatrix}$$

We want to outline few important aspects of these matrices. In both cases they are far from being diagonal and the correlation between the heights of the reference points (elements  $\rho_{36}$ ), is remarkable. This is due to an anisotropy in height observations.

The correlations change in the two surveys, as previously stated, is also due to a change in the geometry of the observation (see Figs. 1 and 2).

## 2.2 Local survey: GPS measurements

We have also measured the reference point of the VLBI antenna, using GPS antennas. Three GPS antenna has been installed on ground reference pillars, and to GPS antennas has been installed on the external part of the VLBI antenna dish, like we have done in previous observations (Negusini et al. 2002a, Negusini et al. 2002b, Tomasi et al. 2001, Sarti et al. 2000). The GPS data have been analyzed by means of the Bernese GPS software Version 4.2 (Hugentobler et al., 2001). Together with the data collected during the campaign, the data of the permanent IGS station in Medicina (MEDI) have been analyzed in order to strength the results within ITRF2000 reference frame (Altamimi et al., 2002). In a first step, we analyzed the data collected by the GPS antennas located at the three ground pillars (P1, P3 and G7) (see Figs. 1 and 2) together with MEDI, in order to obtain good coordinates for the pillars. Unfortunately, there was a failure in the power supply and MEDI was not available for part of the campaign. Then, in order to obtain good tropospheric parameters to be used as a priori for all the observation sessions, we made a specific analysis with G7 and 4 IGS stations. We used CODE tropospheric parameters as a priori for the IGS stations and we computed the tropospheric parameters for G7. Then, we used these parameters for all the stations, taking into account the relative height differences. Baselines between mobile and MEDI GPS antennas have been formed, when MEDI was available, and between mobile and G7 stations in the other cases. Different baselines were formed to obtain good solutions whenever problems in ambiguity resolution showed up. The precise IGS orbits, in the given reference system and for the relevant time frame, were used. The CODE pole coordinates have been used together with the IGS phase eccentricity file (elevation-dependent phase center corrections). In the GPS data analysis, an elevation cut-off angle of  $10^\circ$  has been set, an ambiguity-fixed solution has been computed. L1 carrier frequency has been analyzed and, therefore, an ionosphere model had been previously computed using the available data. Since results obtained using terrestrial measurements showed an evident movement of the GPS antenna, we decided to compute MEDI coordinates into ITRF2000 using a network of IGS stations. Geocentric coordinates of mobile antennas have been estimated for each observing session, fixing MEDI coordinates at this latter estimated value.

In order to compute the VLBI reference point, GPS positions have been post-processed using a 3-D least-squares analytical geometry approach. This approach is geometrically identical to the one that has been used in post-processing terrestrial data but is statistically less complete.

VLBI antenna movements in azimuth (at fixed elevations) determine GPS antenna positions that ideally draw a circumference centered on the azimuth axis. In a similar manner, the centers of circumferences described by movements in elevation at fixed azimuth positions, belong to the elevation axis.

Using the approach described above, which has already been successfully applied (Negusini et al., 2002a; Negusini et al., 2002b), it is possible to determine the reference point with a purely analytical computation. Once the centers' coordinates have been estimated, they have been transformed into a

topocentric system, with origin in published ITRF2000 VLBI reference point. Within this system, East and North components of azimuth circles' centers have been used to compute a weighted mean that represent east and North components of the invariant point. Similarly, up component of the different elevation circles' centers have been combined to obtain the weighted mean estimate of the Up component of the reference VLBI point. These components and their wrms have been transformed back into ITRF2000. Table 3 shows the eccentricity vectors obtained using GPS observations. Formal precision associated with positions' estimate is much smaller for 2002 survey where a rapid static approach has been used. In 2001 a kinematic approach had been used instead. Standard deviations for 2002 seem to be too optimistic.

Table 3: VLBI-GPS eccentricity vector and standard deviations (estimated using GPS technique) expressed in ITRF2000 for the 2001 and 2002 local tie.

Eccentricity \ Local tie	Kinematic survey	Rapid static survey
	June 2001 (epoch 10/09/02)	September 2002 (epoch 10/09/02)
$X_V$ (m)	$4461369.885 \pm 0.015$	$4461369.8769 \pm 0.0004$
$Y_V$ (m)	$919596.933 \pm 0.005$	$919596.9313 \pm 0.0010$
$Z_V$ (m)	$4449559.271 \pm 0.001$	$4449559.2532 \pm 0.0010$
$X_G$ (m)	$4461400.7881 \pm 0.003$ (ITRF fixed)	$4461400.7845 \pm 0.0002$
$Y_G$ (m)	$919593.5365 \pm 0.001$ (ITRF fixed)	$919593.5319 \pm 0.0001$
$Z_G$ (m)	$4449504.7305 \pm 0.003$ (ITRF fixed)	$4449504.7331 \pm 0.0002$

W

We will soon apply the analytical methodology used for terrestrial data post-processing to GPS data post-processing (Sarti et al., 2003 submitted). It will permit a rigorous treatment of the GPS observation and will allow the computation of the correlation matrix for GPS estimates too.

The estimated 2002 GPS reference point has been transformed using a 7 parameters transformation into the local frame. Transformation parameters have been estimated using the known positions of four pillars that have been surveyed in the local frame using terrestrial measurements and in the ITRF2000 using static GPS. GPS reference point transformed in the local frame confirms the movement observed with terrestrial measurement in direction and in magnitude.

### 3 Conclusions

Using terrestrial measurements, local ties can be performed efficiently and results are statistically complete and contemporarily show a very high precision. The information that resides in the correlation matrix is fundamental and its computation should be considered a mandatory task when performing local ties. It is possible to see that correlations are far from being equal to zero. Therefore, all local ties should provide complete statistical information to efficiently help Space Geodesy in producing multi-technique products (e.g.: ITRF frame computation) and efficiently realize an IGGOS at its best.

Local ties performed using GPS might also be efficient and with good results. That is particularly true for the rapid static observing method. They are performed much quicker in respect to terrestrial method and with reduced efforts, but results and post processing methodology must still be investigated and tested.

## References

- Altamimi Z., Sillard P., Boucher C. (2002): "ITRF2000: A new release of the International Terrestrial Reference Frame for Earth Science Applications", *J. Geophys. Res.*, vol. 107, No B10, 2214
- Hugentobler U., Schaer S., Fridez P., (Eds.) 2001. *Bernese GPS Software Version 4.2*. Astronomical Institute, University of Berne, pp. 515
- Negusini M., P. Sarti, P. Tomasi, (2002a), "Results from the 2000 GPS campaign for the measurement of the reference point for the VLBI antenna in Ny Ålesund". *Proceedings of the Sixth Ny Ålesund international scientific seminar, The changing Physical Environment, Tromsø, Norway, 8-10 October, 2002*. pp 193-196.
- Negusini M., P. Sarti, P. Tomasi, (2002b), "The measurement of the reference point of the VLBI antenna at Ny Ålesund using GPS". *Extended Abstract. Proceedings of the Eleventh General Assembly of the WEGENER Project, Athens, Greece, June 12-14, 2002*. [http://www.survey.ntua.gr/wegen/files/abstracts/1406\\_s1\\_negusini.pdf](http://www.survey.ntua.gr/wegen/files/abstracts/1406_s1_negusini.pdf)
- Sarti P., Sillard P., Vittuari L., 2003 Submitted, "Surveying co-located Space Geodesy techniques for ITRF computation" Submitted to *Journal of Geodesy*.
- Sarti P., Vittuari L., Tomasi P., (2000), "GPS and classical survey of the VLBI antenna in Medicina: invariant point determination", *Proceedings 14th Working Meeting on European VLBI for Geodesy and Astrometry, Castel San Pietro Terme (Bologna), Italia, 8-9 Settembre*, pp. 67-72
- Tomasi P., Sarti P., Rioja M.J., (2001), "The determination of the invariant point of the VLBI antenna in Ny Ålesund", *Memoirs of National Institute of Polar Research, Special Issue No. 54*, pp. 319-330
- Vittuari L., P. Sarti, P. Tomasi, M. Dubbini, (2002), "Misura del punto invariante dell'antenna VLBI di Medicina rispetto alla stazione GPS permanente", *Atti 6a Conferenza Nazionale ASITA Geomatica per l'Ambiente, il Territorio e il Patrimonio Culturale, Perugia, 5 - 8 novembre 2002*, pp 2027-2032.
- Vittuari L., Sarti P., Tomasi P., (2001), "2001 GPS and classical survey at Medicina observatory: local tie and VLBI antenna's reference point determination" In: D. Behrend and A. Rius (Eds.): *Proceedings 15th Working Meeting on European VLBI for Geodesy and Astrometry, Institut d'Estudis de Catalunya, Consejo Superior de Investigaciones Cientificas, Barcelona, Spain, 2001*, pp. 161-167.



# Neotectonic Geological Study and Classical Geodesy Methods Applied to Active Fault Monitoring in Ny Ålesund (Western Svalbard)

E. Gueguen<sup>1</sup>, P. Sarti<sup>1</sup>, E. Tavarnelli<sup>2</sup>, L. Vittuari<sup>3</sup>, and P. Tomasi<sup>1</sup>

<sup>1</sup>*Istituto di Radioastronomia – CNR, Matera, Italy*

<sup>2</sup>*Department of Earth Sciences, University of Siena, Italy*

<sup>3</sup>*DISTART, University of Bologna, Italy*

**Summary:** The western Svalbard fold-and-thrust belt has a complex tectonic history, that culminated with the opening of the North Atlantic Ocean. The last recognised important tectonic event in this area is dated from the late Tertiary, when sediments of the Ny Ålesund tertiary basin have been overthrust by older, carboniferous rocks. From this late Tertiary event onwards, the area of Ny Ålesund (western Svalbard) is supposed to have mainly been affected by post-glacial rebound processes. By contrast, there is to date little or no information available for recent tectonic deformations. This has led previous workers to neglect or ignore a possible role of recent active tectonics in western Svalbard. However, in more recent times, high heat flow anomalies and a sparse seismic activity have been recorded offshore western Svalbard, suggesting that this province and its adjacent onshore continuation could still be tectonically active domains.

The Ny Ålesund VLBI observatory is located in the Brøgger peninsula, which is affected by several faults and deformation zones of uncertain age that, in places, control the landscape. Thus it represents a unique opportunity to attempt testing a possible activity for these structures, some of which are exposed in a spectacular section just below the antenna. The most recent results obtained by different geodetic techniques (VLBI, GPS) show a motion of the Ny Ålesund station up to 6 mm/yr. in vertical component, that cannot be explained by post-glacial rebound only. We found thus fundamental to investigate the stability of the site combining both structural geological and classical geodetic techniques. For this purpose, an integrated geodetic network (spirit levelling and GPS) was established and measured in July 2002, in order to verify the stability of VLBI antenna site. The preliminary results of our investigation appear broadly consistent with the hypothesis of active, or at least very recent tectonic activity in western Svalbard. If confirmed by further work, this finding may yield relevant constraints to an enhanced understanding of the recent tectonic evolution of the arctic region. Moreover, analogue data from other provinces could be used to test the methodological consistency of our integrated analysis.

## 1 Geological settings

The northern part of the Euro-VLBI network covers the Fennoscandian shield and the Svalbard archipelago (Fig. 1). This region is usually considered as stable from the plate tectonics standpoint. But if this is true for continental Scandinavia the situation of Svalbard is quite different. The western Svalbard fold-and-thrust belt has a complex tectonic history linked to the opening of the Northern Atlantic Ocean. This area is located close to the Hornsund Fault Zone, one of the major active fault zones during the separation of the NE Greenland and Svalbard-Barents shelves. The last recognised important tectonic event in this area is dated from the Tertiary (Blythe and Kleinspehn, 1998), when the Ny Ålesund tertiary basin has been overthrust by carboniferous rocks (Fig. 2, 3). But western Svalbard is located only 150 km far from the Knipovich Ridge, which is considered an active segment of the Mid-Atlantic Ridge system. High heat flow anomalies and considerable seismic activity (Fig. 4) have been recorded offshore western Svalbard (Mitchell et al., 1990; Hoegden, 1999) showing that the area is tectonically active and in the Kings Bay area, minor seismicity may indicate some neotectonic activity.

During Pleistocene time this area was covered by a thick ice sheet. The entire region is now affected by a post-glacial rebound due to isostatic response to the melting of the ice shield about 10,000 years ago. This phenomenon induces an obvious vertical motion but also a tangential deformation with horizontal displacement in particular at the transition between the central dome and the fore-bulge area. Geological data based on raised shore deposit give a 3.3 mm/yr uplift at Kvadehuksletta west of Ny Ålesund (Hjelle, 1993) during the last 9 kyr, and a 2.8 mm/yr uplift at Recherche Fjord (Salvigsen 1976; Salvigsen et al., 1991). Furthermore massive erosion of the Svalbard linked to glacial and post-glacial geomorphological processes, leads to mass redistribution and may increase the post-glacial effects. (Cf Blythe and Kleinspehn, 1998; Hooke and Elverhøi, 1996; Fiedler and Faleide, 1996) Hooke and Elverhøi, 1996:  $\sim 330 \text{ km}^3$  sedimentary wedge offshore Isfjorden between 200 ka and 13 ka (rate:  $\sim 7.9 \times 10^6 \text{ m}^3 \text{ a}^{-1}$ ).

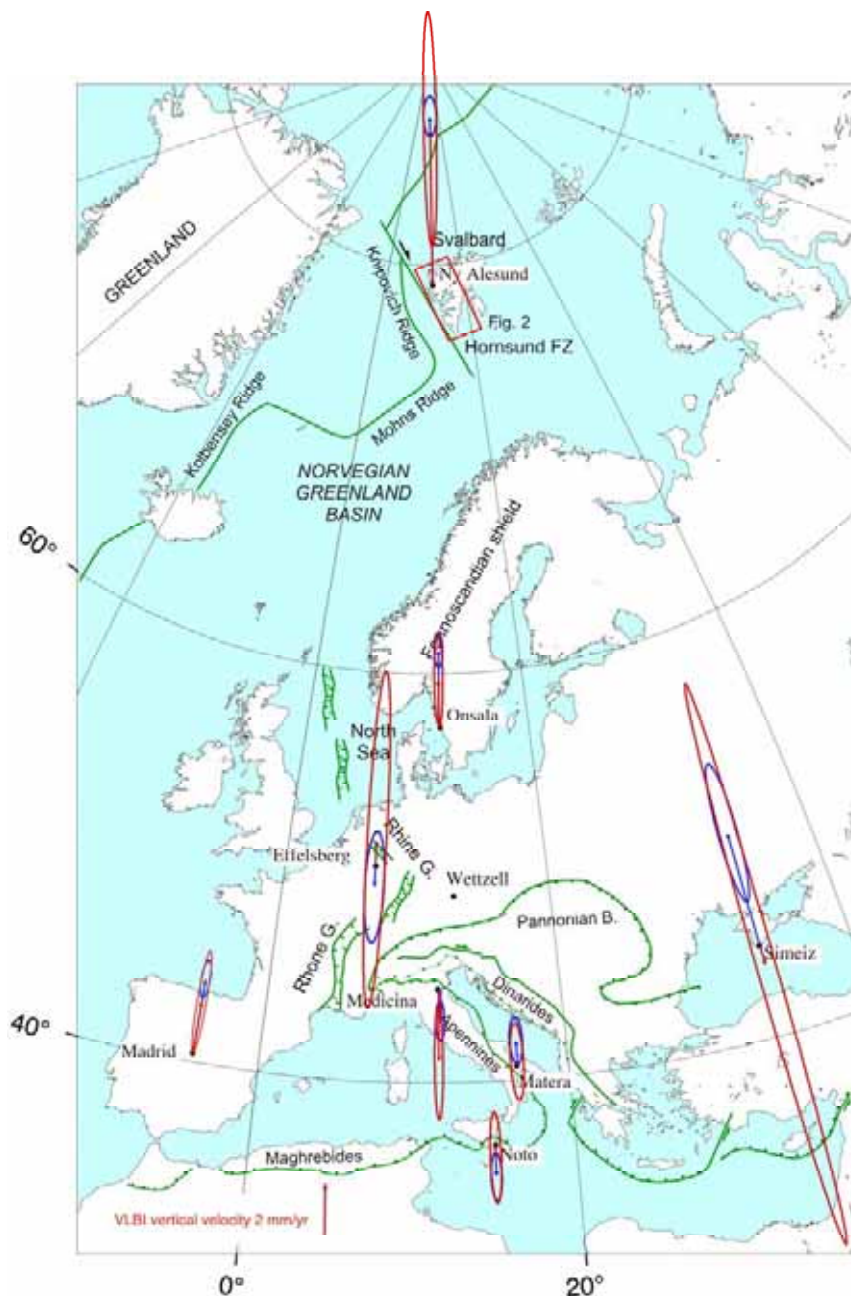


Figure 1: The European stations of the EVN and the corresponding velocities.

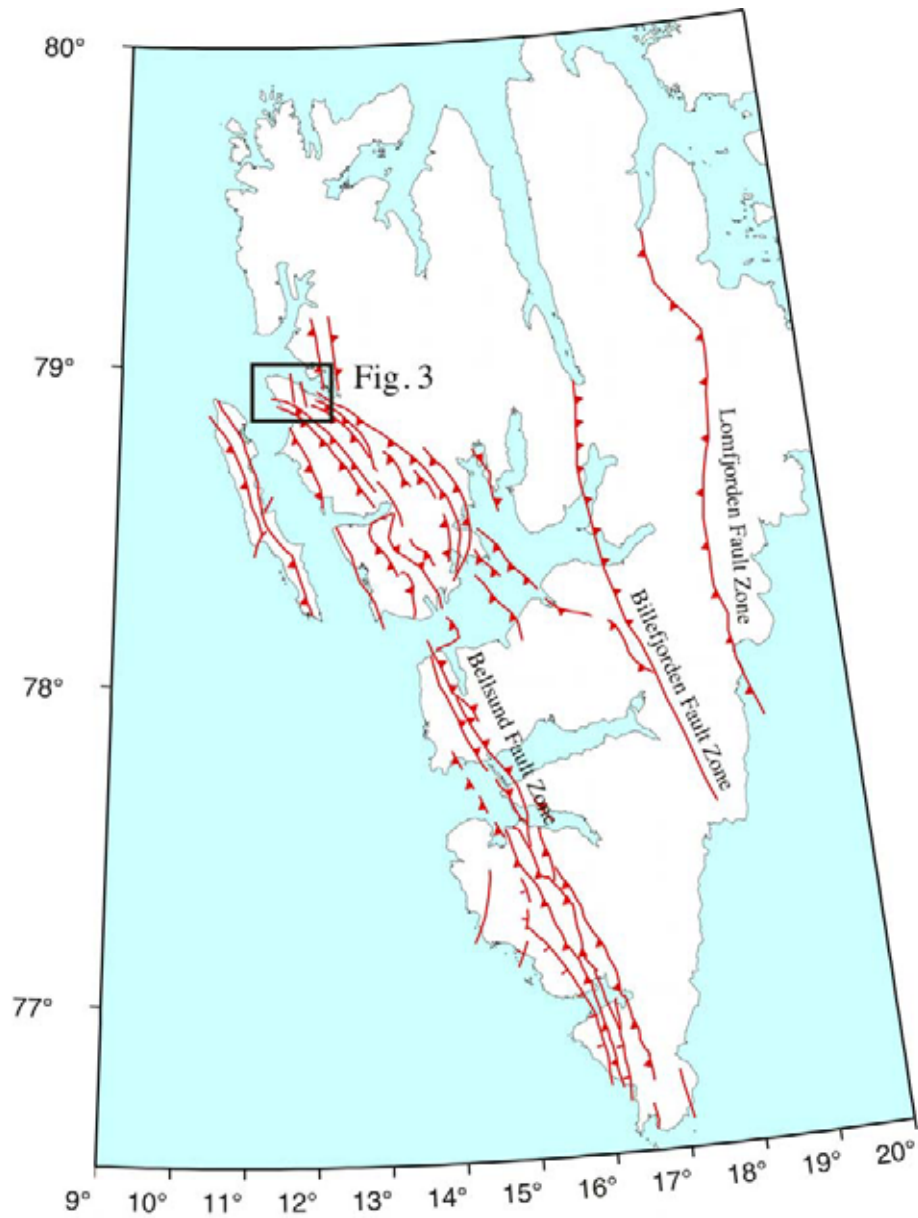


Figure 2: Map of Svalbard archipelago and major faults.

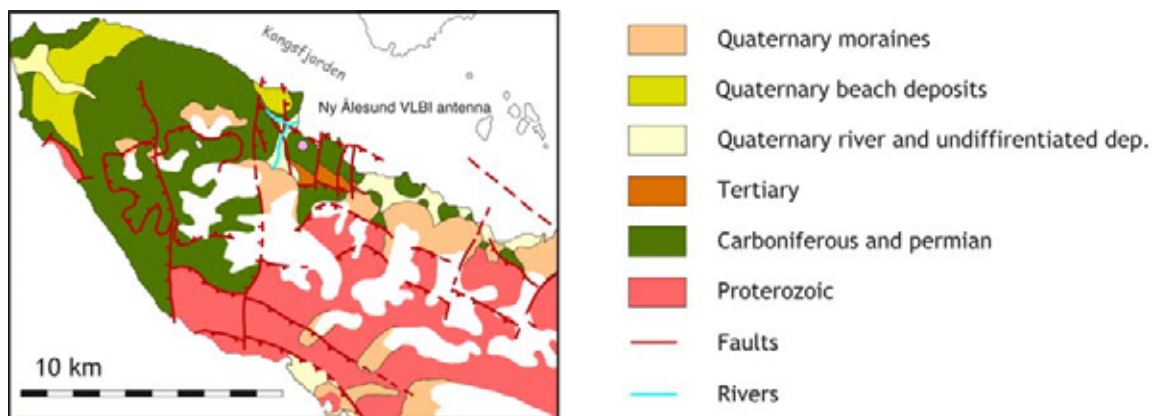


Figure 3: Map of geological characteristics in Ny Ålesund area.

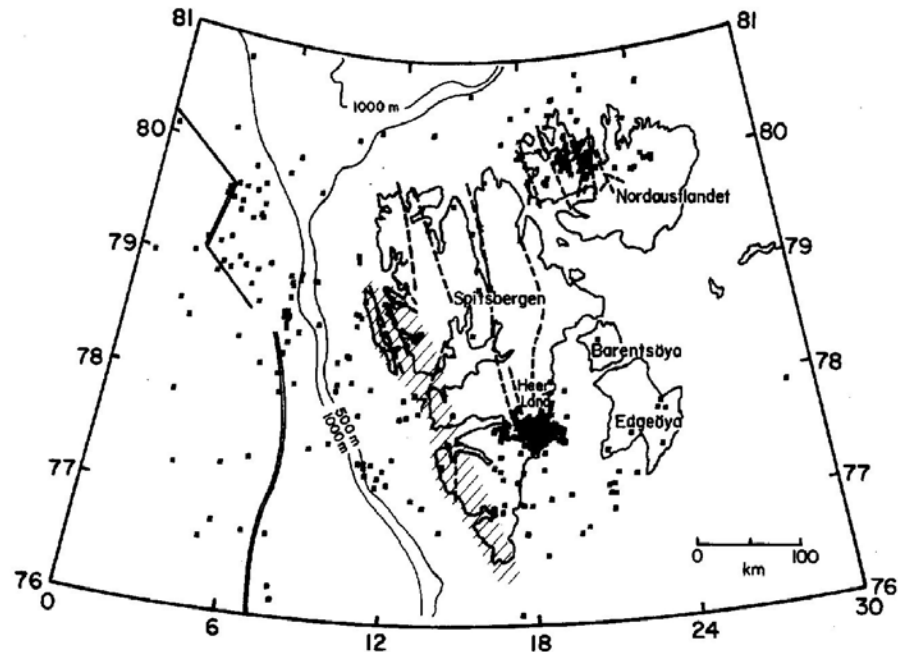


Figure 4: Seismic activity recorded in Svalbard area.

## 1.1 Space geodesy results and post glacial rebound models

The horizontal motion of Ny Ålesund relative to Wettzell is in quite good agreement with the predicted horizontal motion due to post-glacial rebound of  $1.0 \text{ mm/yr}$  with azimuth  $271.5^\circ$  with respect to Wettzell (Haas et al., 2001).

More difficult is the interpretation of the vertical movements. There is a discrepancy between geodetic results (Fig. 1) for Ny Ålesund with an uplift ranging from  $6.4 \pm 0.4 \text{ mm/yr}$  (CNR-2000) to  $5.9 \pm 1.8 \text{ mm/yr}$  (OSO-2000) and the predicted values from glacial isostatic adjustment models that range from  $+1.3 \text{ mm/yr}$  (Haas et al., 2000), to  $+1.8 \text{ mm/yr}$  according to the ICE-4G model (Soudarin et al., 1999).

This difference might be explained by both regional tectonic activity due to the vicinity of Knipovich Ridge and local geological processes. High erosion rates during and after the glaciation events might also take part to this high uplift rate, even if to a lesser degree.

In order to study the stability of the Kings Bay area, the Norwegian Mapping Authority (NMA) established in 1998 a control network roughly oriented in east-west and north-south directions approximately 50 km by 30 km (Plag et al., 2000). Up to now, three GPS campaigns have been carried out in 1998, 1999 and 2000. Unfortunately, the vertical rates determined from the campaigns still contain too large errors to be usefull and no reliable information concerning the geographical pattern of the vertical rates is available. Without this information, geophysical interpretations appears premature. These measurements may indicate that the footprint of the VLBI sites is relatively small and the measurements may be biased by very local movements.

## 1.2 Mapping and structural geology

In the first part of the work we have conducted a detailed structural survey of the area of the Ny Ålesund VLBI station with a special regard to the western part of the area where the fault bounding the tertiary basin westward, runs through a small river valley (Fig. 5). This first phase has been dedicated to

the recognition and precise mapping of the outcropping fault surfaces. We have also looked for the best outcrops located on both sides of the fault surfaces for installing geodetic markers suitable both for planimetric measurements, for high precision spirit levelling and for GPS surveys (Fig. 6). This step required identification of outcrops of true bedrock which are well oriented, allowing the most simple manipulations for the geodetic measurements in order to reach the best and most significant metric representation of the physical phenomenon. In particular, we stressed on the roughly N-S trending faults, which are the most frequently observed in the area of the VLBI antenna. According to the available bibliography, these faults should be rather old and inactive. During our survey on the southern side on the peninsula, we found some outcrops on which the Engelskbukta thrust is displaced by a roughly N-S trending fault that, according to us, might be the southern branch of the Scheteligfjellet Fault. This is a very important point and means that the N-S trending faults have a long history and have been reactivated in recent time after the late-Tertiary thrusting event.

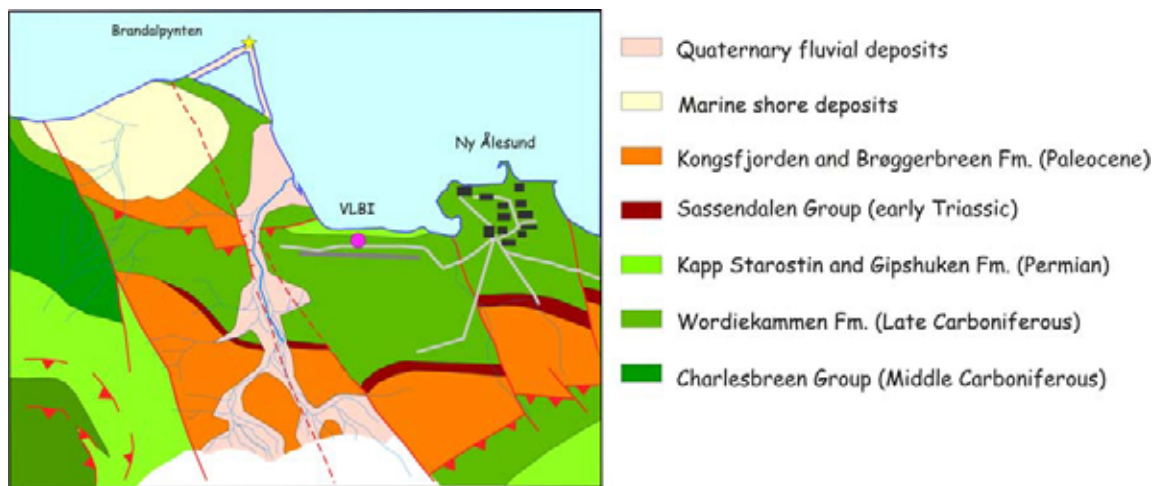


Figure 5: Detailed map of geological features around Ny Alesund geodetic observatory.

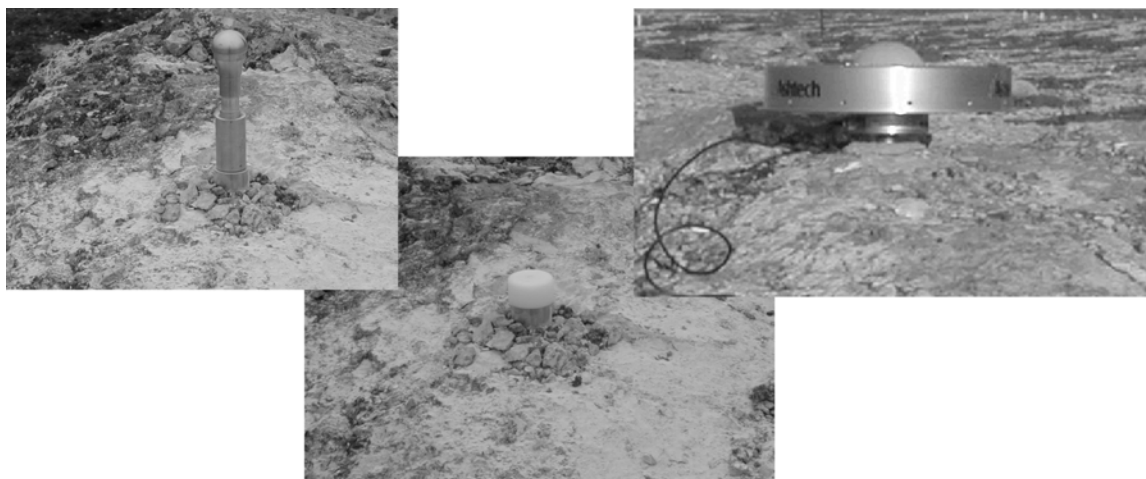


Figure 6: Benchmarks used for spirit levelling and GPS static survey.

Then, we have carried on a kinematic characterisation of the faults, based on measurement of kinematic indicators along the fault surfaces mapped at 1/1000 scale along the section running on the small cliff north of the VLBI antenna. The entire section is affected by N to NNE-trending strike-slip faults and intense fracturation that cut some earlier thrust-wedges.

During this phase we have also looked for evidence of recent tectonic activity especially in the quaternary river sediments and beach deposits along the coast of Brøggerhalvøya. In particular, we found in the area of Kjørstranda and Leinstranda (SW Brøggerhalvøya) some outcrops showing small faults that seem to offset the Quaternary beach deposits. These are preliminary results and have to be confirmed by further data analysis.

## 2 Geodetic measurements

In order to investigate local movement, an integrated network (spirit levelling and GPS) was established and measured. The existing local ground control network in Ny Ålesund has been extended mainly on the base of geological considerations obtained by a dedicated neotectonic survey (see 1.2). We have materialised four new markers on the west side of the VLBI antenna (PL01, PL02, PL03, PL04) three of which (PL02, PL03, PL04) across the small river valley where the major fault of the area has been recognized. The choice of new points was strongly influenced by a lack of rocky outcrops in the area. In Fig. 7 is reported the scheme of the extended geodetic network. Considering the great interest in a high precision vertical movements monitoring, we focused our attention in establishing vertices that are suitable both for spirit levelling benchmarks and for GPS antennas forced centring. Brass screwed bolts (supplied by Statens Kartverk with Wild 5/8" screws) have been dug in the rare suitable outcrops; a brass adaptor was realised for transforming screw bolts in spirit levelling bolts (Fig. 6).

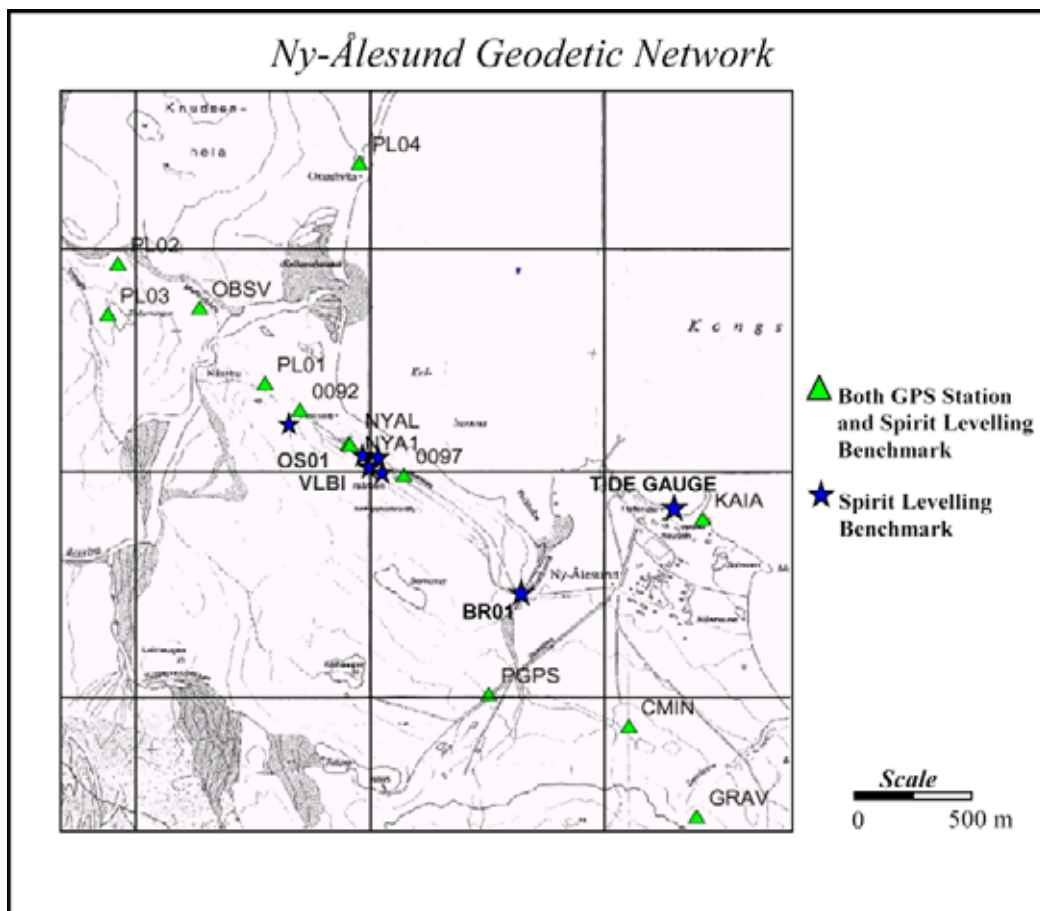


Figure 7: Local ground control network around Ny Ålesund.

Levelling measurements had been carried out using a digital DiNi 12 level from Zeiss-Trimble, coupled with INVAR coded rods.

All the existing bolts of the local network surrounding the VLBI antenna (levelling bolts on pillars 91, 92, 93, 94, 95, 96, 97, 98 and levelling bolts at the foot of the VLBI antenna VL01, VL02, VL03, VL04) were measured. Points from 91 to 98 had also been measured with terrestrial measurements in two previous surveys performed in 1999 (Tomasi et al., 2001) and 2000 (Nothnagel et al, 2001) for locating the VLBI reference point.

As origin of spirit levelling-derived heights we used the reference bolt of the Ny Ålesund tide-gauge. The height of this bolt, located near the peer, was fixed to the Statens Kartverk value of 2.7270 m. Forward and back levelling lines connected this benchmark to the whole geodetic network.

In order to have an intermediate closure check during the connection between VLBI benchmarks and the tide gauge reference bolt, an existing point (BR01) situated at the bridge on the road from Ny Ålesund to the geodetic observatory was used.

The pre-existing screwed bolts situated close to the gravimeter station east of Ny Ålesund (GRAV), KAIA close to the peer, OBSV east of the geodetic observatory were also included in present survey.

One of the main difficulties in realising these measurements originated by the particular characteristics of the upper part of the soil during the summer. Tundra presents soft strata covered by musk and lichens, where spirit levelling is very difficult to perform. In order to avoid loss of accuracy, spirit levelling that has been performed outside of marked roads has been extensively pre-planned. This approach allowed to reach good results on these critic areas too.

We have also had the possibility to extend our work thanks to the one-day availability of nine Ashtech Z-Surveyor GPS receivers (all equipped with choke-ring antennas) belonging to Statens Kartverk. We therefore performed a twelve-hour GPS static survey. Nine spirit levelled screw bolts (PL01, PL02, PL03, PL04, 92, 97, KAIA, GRAV, OBSV) were occupied by GPS. Their data have been processed together with the data of the two IGS permanent station NYAL and NYA1. This has been a key survey for obtaining a first 3-D framing of the new points in the existing network and in the ITRF.

Moreover two more points were temporarily installed and measured both with rapid static GPS and spirit levelling. The locations of these points (PGPS and CMIN) have been chosen in order to remedy a natural lack of suitable outcrops on which materialise the new bolts that causes the network to be mainly elongated towards east-west direction. The aim of these last measurements has been to recover suitable information for investigating local geoidal undulation.

## 2.1 Results of the first campaign

Levelling data have been processed using STAR\*LEV least squares adjustment software from StarPlus Software Inc.. Standard deviations of adjusted heights are at one millimetre level. GPS data were processed by means of Bernese 4.2 GPS software. In Tables 1 and 2 are reported results of levelling and GPS adjustments, respectively.

As previously stated, temporary GPS-Levelling stations have been realised in lack of natural rocky outcrops. CMIN point has been located on a reinforcement bar within a concrete platform while PGPS has been realized directly on a levelling plate.

Through a comparison between “orthometric” and GPS-derived ellipsoidal heights a preliminary local geoid model of the area has been computed (Fig. 8).

Table 1: heights derived by spirit levelling.

Station	Elevation (bolt/adaptor)	
StdDev	(m)	(m)
TIDE GAUGE	2.72700	0.00000
VL01	41.29074	0.00069
BR01	14.64414	0.00048
OS01	42.14384	0.00070
VL02	41.28456	0.00069
VL03	41.28927	0.00070
VL04	41.29201	0.00069
0098	42.05980	0.00069
0091	41.98180	0.00070
0094	42.54505	0.00070
0095	41.64538	0.00076
0096	41.33948	0.00069
0093	43.21513	0.00071
NYA1B	43.40454	0.00072
092B	38.12198	0.00076
0092	39.32139	0.00077
PL01	29.75234	0.00084
OBSV	19.36452	0.00102
PL02	40.28780	0.00108
PL03	46.17546	0.00109
GRAV	48.32682	0.00072
KAIA	7.01821	0.00022
0097	39.34592	0.00072
PGPS	29.95498	0.00073
CMIN	37.06925	0.00091

Table 2: ITRF2000 positions obtained by GPS for surveyed screwed points.

STATION NAME	PARAMETER	ADJUSTED VALUE	RMS ERROR
-----			
			-
NYAL	HEIGHT	78.4850	0.0001
	LATITUDE	78 55 46.504244	0.0001
	LONGITUDE	11 51 54.306849	0.0001
NYA1	HEIGHT	84.2167	0.0001
	LATITUDE	78 55 46.396022	0.0001
	LONGITUDE	11 51 55.109774	0.0001
PL01	HEIGHT	64.7231	0.0009
	LATITUDE	78 55 54.434028	0.0001
	LONGITUDE	11 50 52.036496	0.0001
PL02	HEIGHT	75.2766	0.0008
	LATITUDE	78 56 7.453506	0.0001
	LONGITUDE	11 49 2.625110	0.0001
PL03	HEIGHT	81.1614	0.0008
	LATITUDE	78 56 3.283673	0.0001
	LONGITUDE	11 48 56.612012	0.0001
PL04	HEIGHT	36.3052	0.0009
	LATITUDE	78 56 26.923621	0.0001
	LONGITUDE	11 51 50.604637	0.0001
0092	HEIGHT	74.3994	0.0008
	LATITUDE	78 55 50.987238	0.0001
	LONGITUDE	11 51 18.045167	0.0001
0097	HEIGHT	74.4291	0.0009
	LATITUDE	78 55 42.365436	0.0001
	LONGITUDE	11 52 35.167307	0.0001
GRAV	HEIGHT	83.2484	0.0008
	LATITUDE	78 54 55.239640	0.0001
	LONGITUDE	11 56 18.274525	0.0001
KAIA	HEIGHT	41.9511	0.0008
	LATITUDE	78 55 38.170352	0.0001
	LONGITUDE	11 56 14.317628	0.0001
OBSV	HEIGHT	54.3553	0.0008
	LATITUDE	78 56 4.860845	0.0001
	LONGITUDE	11 50 2.073156	0.0001
PGPS	HEIGHT	66.3397	0.0026
	LATITUDE	78 55 11.308363	0.0003
	LONGITUDE	11 53 44.681607	0.0002
CMIN	HEIGHT	72.9443	0.0068
	LATITUDE	78 55 7.733342	0.0004
	LONGITUDE	11 55 26.191404	0.0005

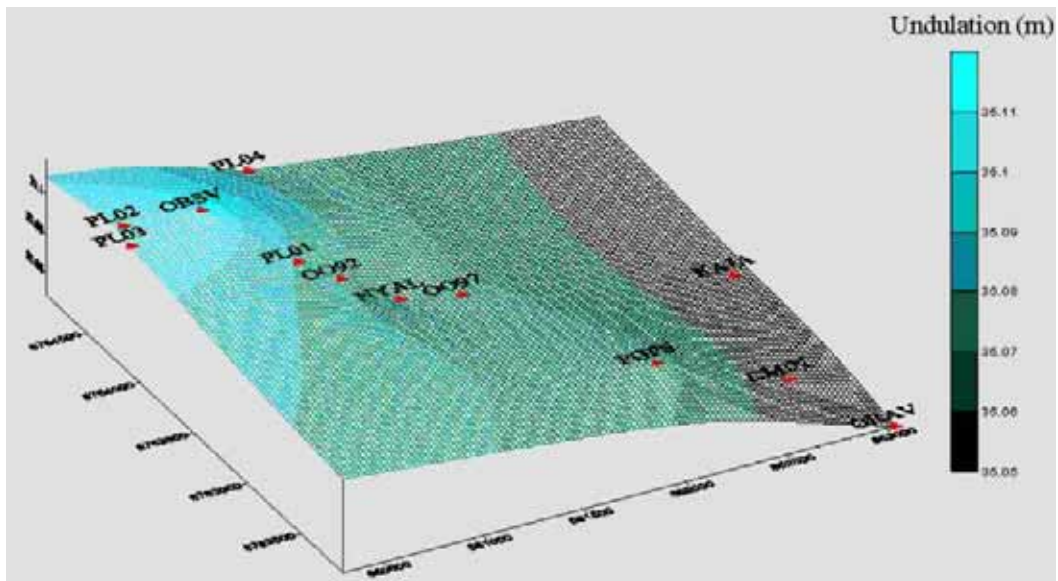


Figure 8: Local geoid undulation.

### 3 Conclusions

Local geological features of Ny Ålesund area have been used for enlarging the local ground control network. It has been measured using both spirit levelling and GPS and future surveys will provide an indication of the presence or the absence of local contribution to the general uplift trend that is determined using Space Geodesy. It will be possible to compute a mean annual uplift from spirit levelling and check the contribution of the surveyed geological structures to the local stability of the VLBI antenna.

A new awareness is now ripening within geodetic community: the use of co-located geodetic techniques (VLBI, SLR-LLR, GPS, DORIS, etc.) for obtaining the most accurate and comprehensive geodetic information is compulsory. It means that the wider amount of information at the observatory is necessary, from geological characteristics to local measurements and local ties. This implies a careful maintenance of local ground control networks.

The anomalous uplift trend of Ny Ålesund VLBI antenna underlines the importance to monitor local movements at geodetic observatories on a regular base.

An annual repetition of local measurements on ground control networks could represent an efficient way to check for local instabilities at geodetic infrastructures, and consequentially improve the significance of derived results.

### Acknowledgements

The research carried out at Ny Ålesund Geodetic Observatory, was funded by the European Community (E.C.) – Access to Research Infrastructure – Improving Human Potential Programme and Large Scale Facility Programme (LSF) under grant NMA-78/2001. We want to acknowledge the great support of the Ny Ålesund Geodetic Observatory team, and Lars Bockmann for the precious cooperation in GPS measurements.

### References

- Blythe and Kleinspehn, 1998 ; Tectonically versus climatically driven Cenozoic exhumation of the Eurasian plate margin, Svalbard: Fission track analyses. *Tectonics*, 17, 4 621-639.
- Campbell J., Nothnagel A., 2000, Comparison of European VLBI solutions from different analysis centres, In Tomasi, P., Mantovani, F. and Perez-Torres, M.-A.: Proceedings of the 14th Working Meeting on European VLBI for Geodesy and Astrometry, Castel San Pietro Terme, Sept. 8 - Sept. 9, 2000. Consiglio Nazionale Delle Ricerche, Istituto di Radioastronomia, 49-54.
- Fiedler and Faleide, 1996 Cenozoic sedimentation along the southwestern Barents Sea margin in relation to uplift and erosion of the shelf, *Glob. Planet. Change*, 12, 75-93
- Gueguen E., Tomasi P., Scherneck H-G., Haas R., Campbell J., 2001, "Recent crustal movements: Geological meaning of European Geodetic VLBI network observations" Proceedings of 15th Working Meeting on European VLBI for Geodesy and Astrometry, Barcelona, September 2001.
- Haas, R., Nothnagel, A., Campbell, J., and Gueguen, E., Recent crustal movements observed with the European geodetic VLBI network: geodetic analysis and results, IAG SRCM'01, Helsinki, August 2001.

- Hjelle, A., 1993. Geology of Svalbard. Polarhåndbok No.7, Norwegian Polar Institute, pp 162.
- Hjelle et al., 1999: Geological map of Svalbard, 1:100 000, A7G Kongsfjorden, Norwegian Polar Institute.
- Hjelstuen, B.O., Elverhøi, A., Faleide, J.I., 1996. Cenozoic erosion and sediment yield in the drainage area of the Storfjorden Fan. *Global Planet. Change* 12, 95–117.
- Hooke and Elverhøi, 1996 ; Sediment flux from a fjord during glacial periods, Isfjorden, Spitsbergen, *Glob. Planet. Change*, 12, 237-249.
- Mitchell, B.J., H. Bungum, W.W. Chan, and P.B. Mitchell , 1990, Seismicity and present-day tectonics of the Svalbard region, *Geophys. J. Int.*, 102, 139-149.
- Nothnagel, A.; Steinforth, C.; Binnenbruck, B., Bockmann L., Grimstveit L., 2001 “Results of the 2000 Ny-Ålesund Local Survey” Proceedings of 15th Working Meeting on European VLBI for Geodesy and Astrometry, Barcelona, September 2001.
- Plag, H.-P., Bockmann, L., Kierulf, H. P., Kristiansen, O., 2000: Foot-Print Study at the Space-Geodetic Observatory, Ny-Ålesund, Svalbard. In Tomasi, P., Mantovani, F. and Perez-Torres, M.-A.: Proceedings of the 14th Working Meeting on European VLBI for Geodesy and Astrometry, Castel San Pietro Terme, Sept. 8 - Sept. 9, 2000. Consiglio Nazionale Delle Ricerche, Istituto di Radioastronomia, 49-54.
- Salvigsen O. (1976) Radiocarbon dating and the extension of the Weichselian ice-sheet in Svalbard. *Norsk Polarinst. Årb.* 209-224
- Salvigsen O., Elgersma A. and Landvik J.Y. (1991) Radiocarbon dated raised beaches in northwestern Wedel Jarlsberg Land, Spitsbergen, Svalbard. *Wypr. Geogr. na Spitsbergen, UMCS, Lublin*, 9-16
- Soudarin L., Crétaux J.F., Cazenave A., 1999 Vertical crustal motions from the DORIS space-geodesy system *Geophysical Research Letters*, 26, 9
- Tomasi P., Sarti P., Rioja M.J., 2001, “The determination of the invariant point of the VLBI antenna in Ny Ålesund” *Memoirs of National Institute of Polar Research, Special Issue N.54*, pp 319-330

# The IVS-Reference Point at Onsala – High End Solution for a Real 3D-Determination –

C. Eschelbach<sup>1</sup> and R. Haas<sup>2</sup>

<sup>1</sup>*Geodetic Institute of the University of Karlsruhe, Karlsruhe, Germany*

<sup>2</sup>*Onsala Space Observatory, Chalmers University of Technology, Sweden*

**Summary:** The Onsala Space Observatory is equipped with a 20 m radio telescope used for geodetic VLBI and a permanent GPS-antenna with corresponding equipment. The two monuments are used to contribute to the International VLBI Service for Geodesy and Astronomy (IVS) and the International GPS Service (IGS), respectively. The two services IVS and IGS are important for the establishment and preservation of the International Terrestrial Reference Frame (ITRF) (Altamimi et al., 2001). To compare and combine the results of the IVS and the IGS, it is necessary to know the relative positions of their reference points with as small uncertainty as possible. Therefore, we performed a classical geodetic survey at the Onsala Space Observatory in the spring 2002 to determine the IVS-reference point clearly and to create a local tie between the IVS- and the IGS-reference points in a local reference frame. The subsequent determinations yielded the 3D-coordinates of the two reference points and their covariance matrix in ITRF and the complete detection of the telescope's axis including axes positions and axis offset. The local tie is available in the form of a Sinex-file.

## 1 Introduction

The 20 m telescope at Onsala is of azimuth-elevation type and is surrounded by an optically opaque radome which serves to protect the surface of the antenna from mechanical damage (Fig. 1). The IGS-reference point is located at a distance of about 80 m from the radome. It is a steel bolt in solid bedrock below a permanent GPS-antenna installed on a concrete pillar.



Figure 1: Radome at the Onsala Space Observatory containing the 20 m radio telescope.

All geodetic VLBI measurements refer to the reference point of the telescope which is defined for a azimuth-elevation telescope as the intersection of the azimuth axis and the elevation axis, or, if they do not intersect, as the point on the azimuth axis that is closest to the elevation axis. This definition guar-

antees an invariant position of the reference point, independent from the pointing direction of the telescope antenna. The results of VLBI-measurements are used for geodynamic investigations, for example the determination of plate tectonics and earth rotation parameters. Thus, the VLBI-data must not be affected by local displacements of the telescope. Local displacements for example could be caused by movements of the basement of the telescope or could be the result of telescope maintenance work. Determination of the coordinates of the telescope's reference point in a local reference frame on a regular basis possibly provides corrections to the VLBI series.

In a similar manner, the position of the IGS-reference point must not be affected by local displacements in order to guarantee the usefulness of the GPS-data for geodynamic investigations. Thus, also the IGS-reference point has to be monitored with respect to the local reference frame. For a combined use of VLBI- and GPS-data the local tie between the reference points is of major importance (e.g. Long and Bosworth, 2000). This local tie was established by determining the coordinates of the two reference points in a local reference frame. The results in the local reference frame were then transformed into ITRF using identical points.

## 2 Observation strategy

The observations carried out for the determination of the local tie can be summarized in four steps: first the measurement of the telescope's reference point inside the radome, which was the most time-consuming and innovative part; second and third the measurements of the IGS-reference point and of the local network, which were combined for technical reasons; and fourth the GPS-session on chosen points of the local network, to get identical points coordinated in both the local network and ITRF. All details on the classical measurements (IVS-reference point, IGS-reference point, local network) are documented in Eschelbach (2002).

### 2.1 Telescope measurements and results

Several geometric properties of the telescope structure were used to determine the invariant and immaterial reference point of the 20 m telescope. When the telescope is turned around the azimuth axis the two endpoints of the elevation axis describe two circles with the reference point as their common center. At the Onsala telescope the elevation axis is not realized as a solid metal beam but with two encoder motors at the sides of the telescope cabin. Thus, it is not possible to observe the endpoints of the elevation axis directly. Therefore, we installed four target markers near the elevation axis – two on each side of the telescope. When moving the antenna in elevation, these target markers describe four quarter circles with centers lying on the elevation axis. These four centers of the elevation circles – two of them representing two different endpoints of the elevation axis on each side – describe another four circles around the reference point when the antenna is turned around the azimuth axis. Applying a suitable analysis strategy for observing the markers when the telescope is pointed to different azimuth and elevation directions, allows to determine first the endpoints of the elevation axis and second the reference point. To achieve an accurate determination of the reference point with a reasonable number of measurements, we decided to position the telescope to 15 different azimuth positions for each telescope side, and for each azimuth position to change the elevation in 10 steps from 5° to 89°. In fact 15 azimuth positions with 10 elevation positions each for two sides, with two target markers on each side, caused app. 600 new points which had to be coordinated by measurements.

This observation procedure included horizontal direction and vertical angle measurements to each new point from pairs of two observation pillars of the local network inside the radome (four observations for a new point means redundancy). For this purpose five metal pillars distributed evenly on the radome foundation had been installed previously (see Fig. 4). A Leica T2002 (precision: 0.3 mgon) and a Leica TCR1102 (precision: 0.5 mgon) were used for the measurements. During the measurements the theodolites were orientated by measuring the horizontal direction to the furthest observation pillar. The heights of the trunnion axes of the two theodolites were determined from measurements of vertical angles to height references set up above the bottom points on the radome basement. The whole set of measurements took app. five days.

After the telescope maintenance work one month after the measurements of this first epoch a second additional epoch was carried out to try out a more time-saving observation strategy. The main idea of the new method was the installation of magnetic markers as synthetic endpoints of the elevation axis and then to move the telescope only in azimuth. In Epoch-1 the telescope antenna also had to be moved in elevation to be able to determine the indiscernible endpoints of the elevation axis. The installation of the two magnetic markers at two sides of the telescope cabin (which only has to be done once for the telescope) took one day, the measurement in different azimuth positions of the telescope antenna took another day. Fig. 2 shows three target markers (markers G and H for Epoch-1 and the later installed magnetic marker for Epoch-2) at one side of the telescope cabin.

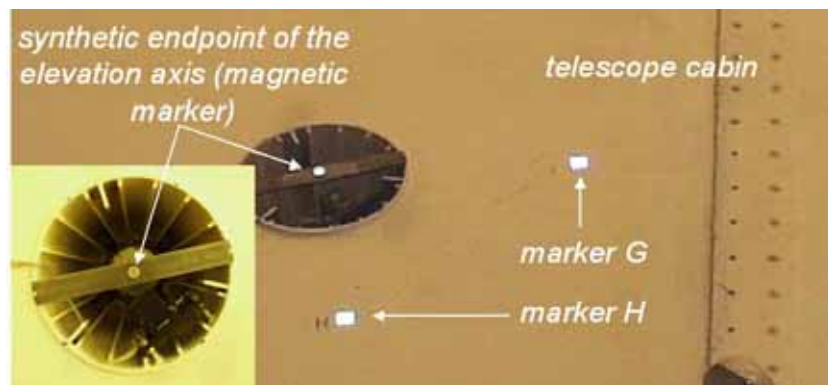


Figure 2: Two markers (G and H) at one side of the telescope cabin (Epoch-1) and the magnetic marker as the synthetic endpoint of the elevation axis at this side.

The network adjustments of the two epochs were carried out separately with Netz3D (Jäger, 1995). Netz3D achieved the coordinates of the new points and their full covariance matrix for each epoch. These matrices were necessary for the further analysis. The mean position error of the new points was below 0.2 mm.

## 2.2 The IGS-reference point

The measurement of the local network included the measurement of the IGS-reference point. Represented by the steel bolt inside the concrete GPS monument, the IGS-reference point is hardly accessible and can only be observed through two small holes at two sides of the monument. To enable observations (horizontal directions and vertical angles) to the steel bolt two new points were established in about 1m distance to the monument and included into the measurement of the local network. The horizontal position error was about 0.2 mm. The bad pointing situation for the vertical angles degraded the accuracy of the height component to 0.6 mm.

### 2.3 The local network

All measurements to the targets on the telescope cabin had to be done from inside the radome. To optimize the pointing situation for the vertical angles, five metal pillars were installed on the concrete foundation wall of the radome and were used as observation pillars for the new points at the telescope cabin. Several other bottom points connect the observation points of the IVS-reference point and the supporting points of the IGS-reference point (Fig. 3 and Fig. 4). The two windows and the main entrance door of the radome were opened during the measurements.

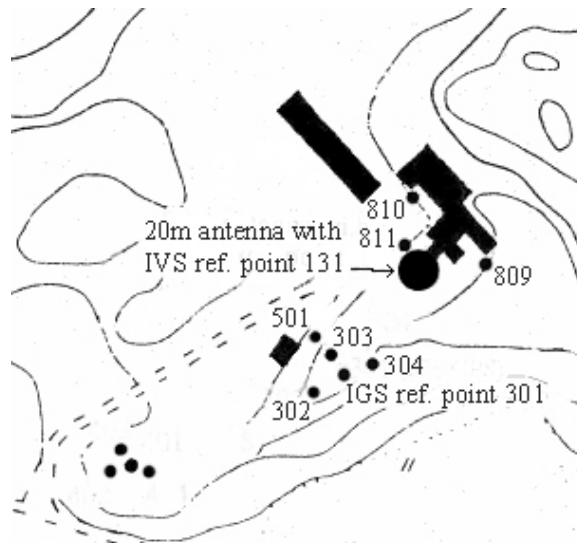


Figure 3: Map of the local network at the Onsala Space Observatory.

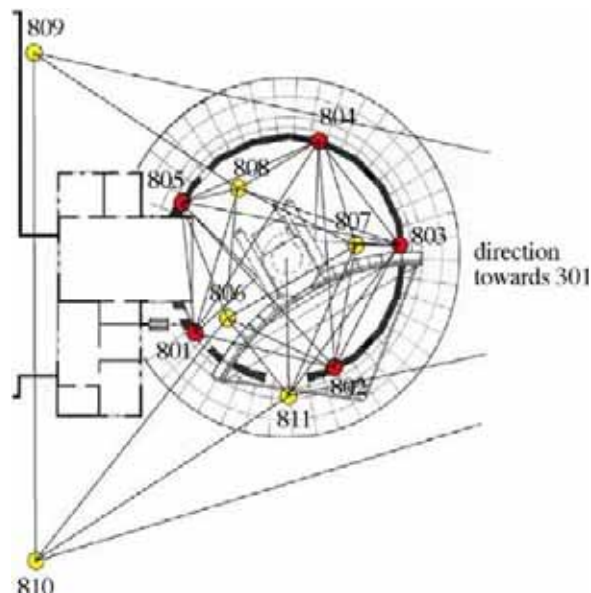


Figure 4: Schematic map of the local network near and inside the radome at Onsala Space Observatory.

The measurement of the local network was separated into horizontal direction measurements (Leica T2002) and horizontal distance measurements (Leica TCR 1102) for a 2D-network adjustment with Netz2D (Jäger et al., 1996) and digital leveling (DINI 10) for the height components. The mean horizontal

position error was 0.2 mm, the mean height error was about 0.1 mm. The current Netz2D version does not take into account centering uncertainties on an observation pillar. However, for future repetitions of the local network measurements outside the radome one should aim at including a centering uncertainty of about 0.3 mm.

## 2.4 GPS-observations in the local network

In order to be able to transform the results obtained in the local reference frame to the geocentric GPS-reference frame, we also performed GPS-observations in the local network. Points 303, 304, 809 and 810 were equipped with choke ring GPS antennas and receivers of type Ashtech and Turbo Rogue and simultaneous GPS measurements were recorded for a total duration of 55 days. Point 303 was only occupied for 10 days, while point 304, 809 and 810 were occupied for 46, 46 and 51 days, respectively. GPS data observed directly on the pillars 801-805 inside the radome unfortunately did not live up to the required data quality due to disturbing effects by the radome structure and the VLBI telescope. Thus, these data were not used for the analysis. The analysis of the 55 days of GPS observations was performed with the GPS analysis software package Bernese version 4.2 (Hugentobler, et al., 2001). The data were analyzed together with GPS data of the IGS station at Onsala and coordinates of the points 303, 304, 809 and 810 relative to the IGS site were estimated from a L1-only solution.

## 3 Computation of the IVS-reference point

After the 3D-network adjustment of the measurement of the new points at the telescope cabin the coordinates of the new points were used as data points in several 3D-circle fits (Eschelbach, 2002). The calculation models using the geometric properties of the telescope structure in principle repeat themselves. When moving the telescope in elevation the target markers at the two sides of the telescope cabin describe quarter circles which center on the elevation axis. These centers are interpreted as endpoints of the elevation axis, which on their part describe almost horizontal 3d-circles around the reference point of the telescope when the telescope antenna is moving in azimuth. Therefore, the basic algorithm of a 3D-circle fit to several data points can be used several times for the calculation of the IVS-reference point.

### 3.1 The 3D-circle fit

The adjustment of a real 3D-circle formulated in a GHM (Gauss-Helmert-Model) that minimizes the square sum of the residuals of the 3D-coordinates of all data points. The mathematical model and the stochastic model have to be designed. The mathematical model consists of a linearized system of equations. Two kinds of equations can be found for each data point, each of them describing a geometric condition:

data point  $p_i$  lies on a sphere (sphere condition):

$$f_i^1(\mathbf{x}, \tilde{\mathbf{l}}) = (\tilde{X}_i - X_0)^2 + (\tilde{Y}_i - Y_0)^2 + (\tilde{Z}_i - Z_0)^2 - R_0^2 = 0,$$

data point  $p_i$  lies in a plane (plane condition):

$$f_i^2(\mathbf{x}, \tilde{\mathbf{l}}) = A_0 \tilde{X}_i + B_0 \tilde{Y}_i + C_0 \tilde{Z}_i - l = 0.$$

Additionally, the mathematical model is completed with the restriction that the center of the sphere is part of the circle plane :

$$f^3 = A_0 X_0 + B_0 Y_0 + C_0 Z_0 - l = 0$$

with:

$(X_0, Y_0, Z_0)$  : coordinates of the center  $O$  of the sphere and the 3D-circle

$R_0$  : radius of the sphere

$(\tilde{X}_i, \tilde{Y}_i, \tilde{Z}_i)$  : true coordinates of the  $i$ -th data point

$(A_0, B_0, C_0)$  : normal vector of the plane

The stochastic model, which means the covariance matrix of the data points containing the weights of the coordinates of the data points, is extracted from the previous 3D-network adjustment.

The described mathematical model represents a one-step estimation of the unknown parameters. Another popular mathematical model consists of separating the 3D-circle fit into first a plane fit and second a 2D-circle fit (e. g. Nothnagel et al., 1999, Nothnagel and Binnenbruck, 2000; Nothnagel et al., 2001). But this two-step-solution is not a real 3D-solution, because the residuals of the two steps are rectangular to each other and the absolute residuals of the 3D-coordinates are not really minimized (Fig. 5). Therefore, the one-step solution has to be preferred to guarantee a clear and correct determination.

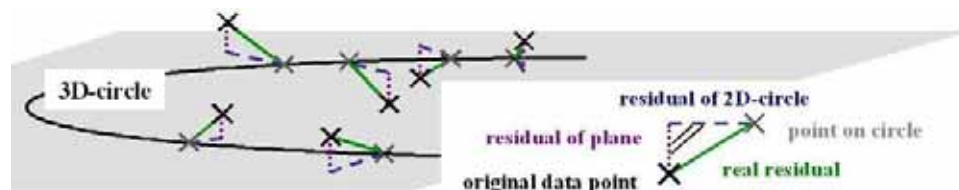


Figure 5: Dissimilarity of the residuals in a two-step circle fit and a one-step circle fit.

### 3.2 Application of the 3D-circle fit

The adjustment process of the 3D-circle fit was in principle used for both the quarter circles of the target markers created by elevation turns (elevation circles) and for the horizontal full circles which were determined (Epoch-1) respectively directly measured (Epoch-2) endpoints of the elevation axis created by azimuth turns (azimuth circles).

The two adjustment processes of the elevation (quarter) circles created by two target markers at one side of the telescope cabin were combined. The combination permitted the use of two more geometric properties. First the planes, in which the circles lie, are supposed to be parallel, thus, the components of their normal vectors have to be identical. Second, the heights of the two determined endpoints of the elevation axis at one side (two target markers create two different endpoints at each side) are supposed to have the same value. The two mentioned properties were used as restrictions for the calculation of the centers of the elevation circles. The adjustment of one double elevation circle (which consists of two quarter circles) yielded the radii of its two quarter circles, the normal vector of the two parallel planes, the coordinates of the two different endpoints of the elevation axis at one side of the telescope cabin and their covariance matrix.

In both epochs the reference point of the telescope is the common center of the 3D-circles described by the endpoints of the elevation axis. In Epoch-1 the coordinates of the endpoints of the elevation axis and their covariance matrix had to be determined by the adjustments of the double elevation circles. In Epoch-2 the synthetic endpoints of the elevation axis could be observed directly and the coordinates and their covariance matrix were determined by the 3D-network adjustment. Fig. 6 shows the error ellipses of the determined positions of one elevation axis endpoint and of the center of the fitting 3D-circle in the local reference frame.

The final step of the local tie was the transformation of the local network into ITRF. Therefore, the four points 303, 304, 809 and 810 from the GPS-session were used as identical points. The mean residual of the transformation was 0.8 mm, only two of the residuals were slightly larger than 1 mm. Tab. 1 shows the coordinates of the IGS- and the IVS-reference points and their deviation. The local tie is also available in the form of a Sinex-file.

Table 1: Coordinates of the IGS- and the IVS-reference point and their standard deviations:

Local reference frame	x [m]	Sigma [mm]	y [m]	Sigma [mm]	z [m]	Sigma [mm]
IGS 301	12.7535	±0.2	23.3877	±0.2	9.0455	±0.6
IVS 131	90.1237	±0.1	35.9493	±0.1	22.7594	±0.1
ITRF	X [m]	Sigma [mm]	Y [m]	Sigma [mm]	Z [m]	Sigma [mm]
IGS 301	3370658.5879	±0.3	711877.1097	±0.2	5349786.9288	±0.5
IVS 131	3370605.9602	±0.1	711917.5650	±0.1	5349830.8018	±0.1

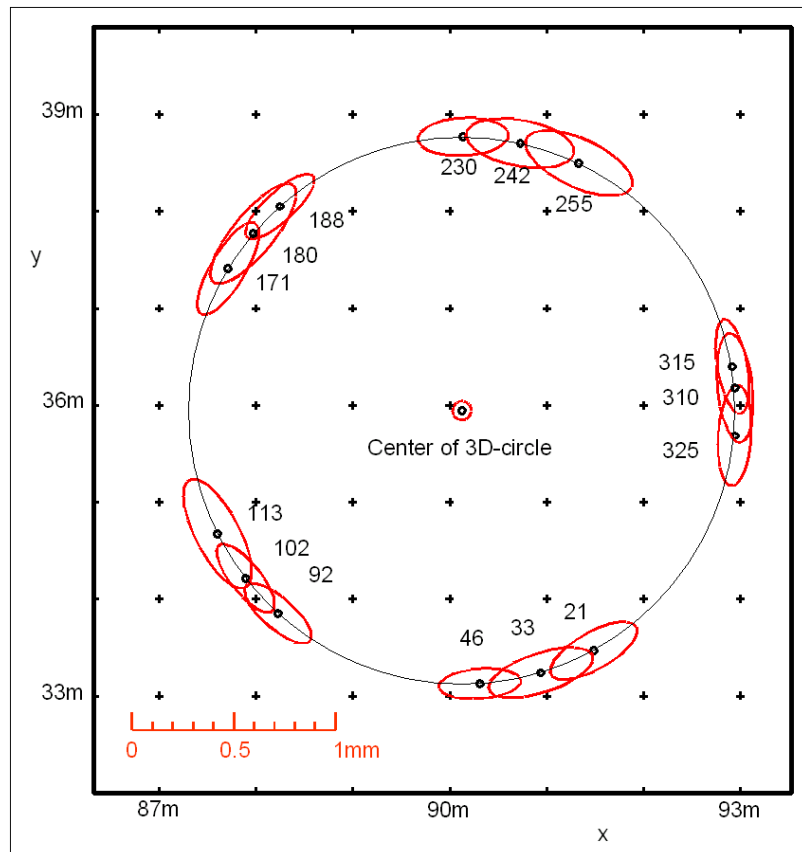


Figure 6: Error ellipses of the determined positions of one elevation axis endpoint and of the center of the fitting 3D-circle in the local reference frame (top view).

## 4 Divergences of the axes and axis offset

It was possible to extract complete information concerning the relative positions of the two axes of the telescope from the observation data of Epoch-1. Fig. 7 shows the heights of two endpoints of the elevation axis with respect to the azimuth position of the telescope antenna before and after the 3D-circle fit. The 3D-circles were developed into the plane and each of them shows one full oscillation. The divergence of the azimuth axis and the vertical is reflected in the amplitude of the oscillation and in the opposed phases of the endpoints of the elevation axis. Using the normal vectors of the 3D-circle fit of Epoch-1 the value of divergence could be determined to  $21'' (\pm 6'')$  in azimuth direction  $236^\circ$ . The effect was alleviated to  $13'' (\pm 6'')$  in Epoch-2 due to the telescope maintenance work, which included the shifting and partly replacing weights to keep the telescope in balance. The comparison of the two epochs indicates a successful realization.

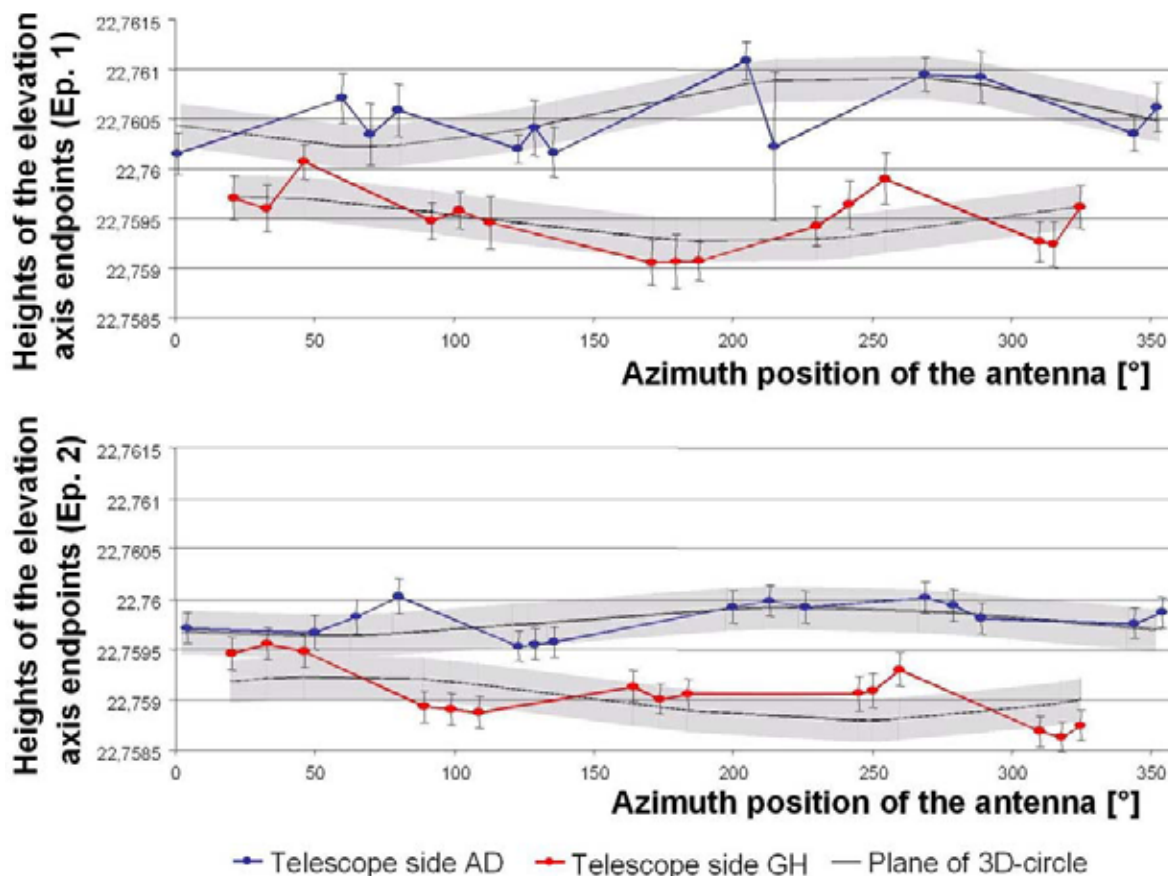


Figure 7: Heights of the determined (Epoch-1: upper plot) and the measured (Epoch-2: lower plot) endpoints of the elevation axis, their standard deviations and the run of the estimated 3D-circles.

In Epoch-1 the difference between the means of the two sides (which is identical to the height difference of the two centers of the horizontal circles) is significant for a tilted elevation axis, which means that the elevation axis is not rectangular to the azimuth axis. The deviation of the elevation axis from the orthogonal of the azimuth axis is about  $40'' (\pm 8'')$ . Epoch-2 does not contain precise height information concerning the elevation axis, because the positioning accuracy of the synthetic endpoints of the elevation axis was assumed to be too low for further interpretations.

In Epoch-2 the measured endpoints of the elevation axis allowed to determine the axis offset. Fig. 8 shows the constellation of two measured positions which enable the determination of the axis offset. In fact ten pairs of new points were measured in Epoch-2, which guarantees a high reliability. The precision of the offset mainly depends on the precision of positioning the magnetic markers at the elevation axis. The axis offset could be determined to 6 mm ( $\pm 0.4$  mm).

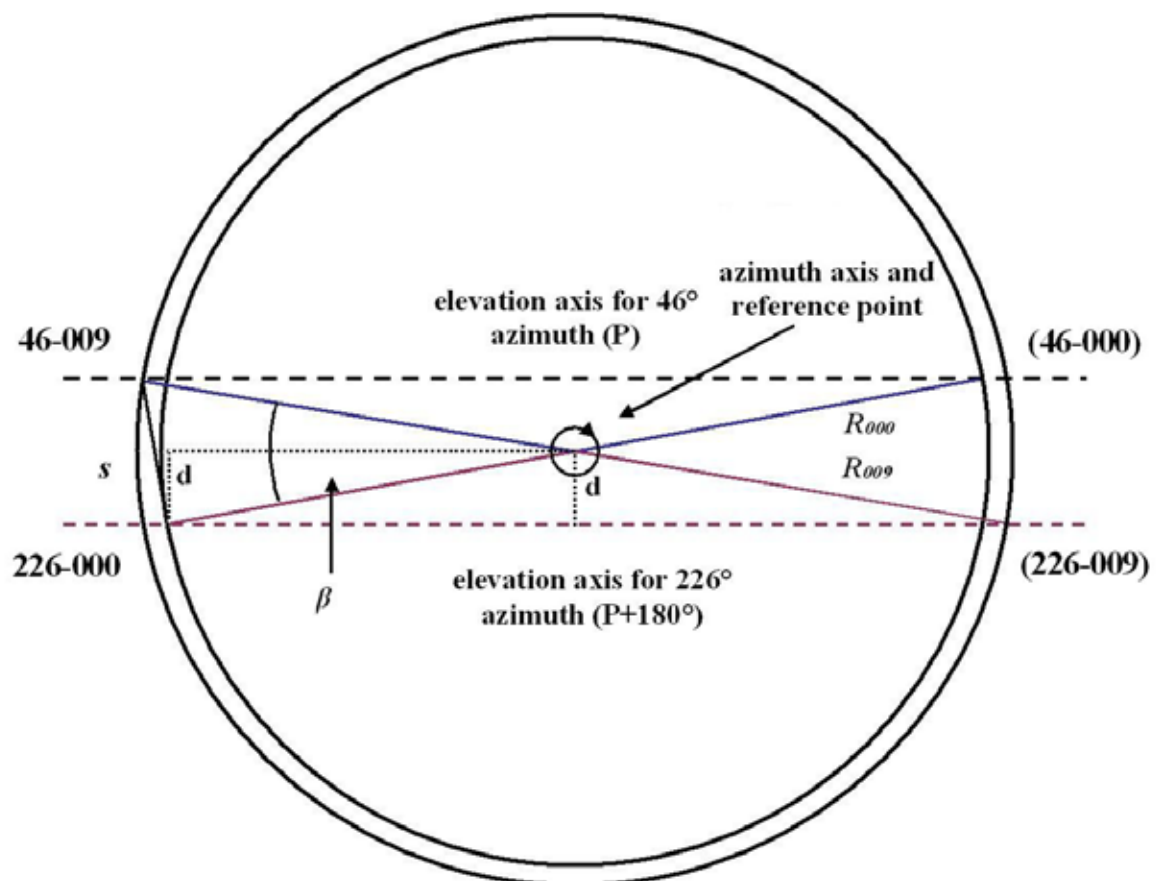


Figure 8: Position of elevation axis for different azimuth positions of the telescope antenna (P and P+180°); d is the offset of the elevation axis from the azimuth axis; only the new points 46-009 and 226-000 have been measured.

## 5 Conclusions

In the summer 2002 a local survey at the Onsala Space Observatory was carried out. The IVS-reference point of the 20 m radio telescope has been coordinated accurately in a local reference frame with a position error of about 0.25 mm and the local tie between the IVS- and the IGS-reference points has been established on the sub-mm level in a local reference frame. The determination was a real 3D-determination without separating the horizontal position and the height and was conducted by error propagation using the full covariance matrix. Using the observation data the relative position of the two telescope axes, their off-axis angle and the telescope's divergence of the vertical could be detected and the axis offset could be determined. After this first local survey further measurements of the local network inside and outside the radome will enable to control the local basement and detect local movements or displacements of the reference points.

## Acknowledgements

This project was a cooperation of the Onsala Space Observatory, Chalmers University of Technology and the Geodetic Institute of the University of Karlsruhe. We would like to thank the employees of the Geodetic Institute for their advisory support and the members of the Space Geodesy and Geodynamics Group at the Onsala Space Observatory for their active support during the measurements.

## References

- Altamimi, Z.; Angermann, D.; Argus, D.; Boucher, C.; Chao, B.; Drewes, H.; Eanes, R.; Feissel, M.; Ferland, R.; Herring, T.; Holt, B.; Johannson, J.; Larson, C.; Ma, C.; Manning, J.; Meertens, C.; Nothnagel, A.; Pavlis, E.; Petit, G.; Ray, J.; Ries, J.; Scherneck, H.-G.; Sillard, P.; Watkins, M.: The Terrestrial Reference Frame and the Dynamic Earth, EOS, Transactions, Vol. 82, No. 25, 275, 278, 2001.
- Eschelbach, C.: Determination of the IVS-reference point at the Onsala Space Observatory in a local reference frame. Geodetic Institute of the University of Karlsruhe, 2002.
- Hugentobler, U.; Schaer, S.; Fridez, P.: Bernese GPS Software Version 4.2. Astronomical Institute, University of Berne, 2001.
- Jäger, R.; Kuhn, M.; Feuchter, J.; Guhl, U.: Handbuch zu Netz2D 4.0. Geodetic Institute of the University of Karlsruhe, 1996.
- Jäger, R.: Handbuch zu Netz3D 4.0. Geodetic Institute of the University of Karlsruhe, 1995.
- Long, J.; Bosworth, J.: The Importance of Local Surveys for Tying Techniques Together. IVS 2000 General Meeting Proceedings, pages 113-117. NASA/CP-2000-209893, 2000.  
<http://ivscc.gsfc.nasa.gov/publications/gm2000/long>
- Nothnagel, A.; Wirtz, C.; Sauerbier, M.; Sobanski, M.: Local Survey at the Effelsberg Radio Telescope 1997 - Preliminary Results. In: W. Schlüter and H. Hase (Eds.): Proceedings of the 13th Working Meeting on European VLBI for Geodesy and Astrometry, Bundesamt für Kartographie und Geodäsie, Wetzell, 25-31, 1999. (available from: <http://www.wetzell.ifag.de/>)
- Nothnagel, A.; Binnenbruck, B.: Determination of the 1996 Displacement of the Medicina Radio Telescope by Local Surveys. In: P. Tomasi, F. Mantovani, M.-A. Pérez-Torrez (Eds.): Proceedings of the 14th Working Meeting on European VLBI for Geodesy and Astrometry, Castel San Pietro Terme, 61-66, 2000.
- Nothnagel, A.; Steinforth, C.; Binnenbruck, B.; Bockmann, L.; Grimstveit, L.: Results of the 2000 Ny-Ålesund Local Survey. In: A. Rius and D. Behrend (Eds.): Proceedings of the 15th Working Meeting on European VLBI for Geodesy and Astrometry, Institut d'Estudis Espacials de Catalunya, Consejo Superior de Investigaciones Científicas, Barcelona, Spain, 168-176, 2001.  
<http://www.ieec.fcr.es/hosted/15wmevga/proceedings/nothnagel2>

Session 4

# Astrometric VLBI



# Phase-reference Astrometry Investigations Using 86 GHz VLBI

R.W. Porcas<sup>1</sup> and M.J. Rioja<sup>2</sup>

<sup>1</sup>*Max-Planck-Institut für Radioastronomie, Bonn, Germany*

<sup>2</sup>*Observatorio Astronómico Nacional, Alcalá de Henares, Spain*

**Summary:** We describe the difficulties associated with phase-referenced VLBI observations at 86 GHz, and present preliminary results from a recent investigation using 7 antennas of the VLBA in dynamic scheduling mode. We present a phase-referenced map of the compact extragalactic source 1308+328, made using the nearby blazar 1308+326 as phase reference. The difference in the astrometric separation between the sources measured here, and previous measurements at other frequencies, can be explained in terms of normal jet physics.

## 1 Introduction

The VLBI *phase-reference* technique is a powerful method for imaging radio sources which are too weak for employing the *phase self-calibration* process used in standard hybrid mapping. Phase-referencing using rapid source switching (between “target” and “calibrator”) was first demonstrated by Alef (1988) and this has now become a routine procedure for radio astronomers (Beasley and Conway, 1995). A welcome by-product is that, if the target and calibration sources are sufficiently close, their relative separation can be derived to an accuracy limited by the relative phase error (Porcas and Rioja, 1996) and the precision with which reference points can be defined within the source structures.

The angular resolution of the maps and the relative astrometry can, of course, be improved by increasing either the baseline length or the observing frequency. Porcas and Rioja (2000) have demonstrated the use of space-ground baselines for relative astrometry, using the Earth-orbiting VLBI antenna on the HALCA spacecraft at 5 GHz to provide baseline lengths up to 4 times those available on the ground alone. Here we investigate the use of the phase-reference technique at 86 GHz ( $\sim 3$  mm) - a frequency which is a factor 10 higher than that of the X-band used by the geodesy community.

## 2 Difficulties with 86 GHz Phase-Referencing

Although higher frequency observations may at first sound attractive for astrometric observations (the ionospheric contribution to propagation errors becomes negligible, and wider bandwidths may be possible in principle), phase referencing at mm wavelengths is in fact much more difficult than at cm wavelengths for a number of reasons. The random fluctuations in the atmospheric paths produce much larger phase errors, resulting in much smaller temporal and spatial scales over which phase coherence can be maintained (e.g. Rogers et al. 1984). The time for switching between target and calibrator is thus much reduced, and the sources must also be much **closer** on the sky, both to reduce the effect of spatial coherence loss and because of the smaller telescope drive times available.

At the same time, the “performance” of both the observing systems and the sources are much poorer:

- Telescope gains are usually much worse, due to the greater effect of imperfections in the reflecting surface shape.
- System temperatures are much worse, due both to higher receiver noise and also to the increased noise contribution from atmospheric emission.
- Most sources which are strong at cm wavelengths have less emission at mm wavelengths.
- Due to the higher resolution, sources which are suitable as calibrators at cm wavelengths may be too resolved at mm wavelengths.

The net result of these effects is that there are far fewer sufficiently strong and compact phase-reference calibrator sources available, and the distance to the nearest calibrator from a given target is very much **increased** ! Adding to this list of problems are the facts that antenna beamwidths are much smaller, making frequent pointing scans necessary, and that the variable atmospheric absorption produces variations in amplitude calibration which are difficult to correct.

### 3 Observations

In the spirit of investigating how far one can go with the phase-referencing technique, we have made 86 GHz VLBI observations of the close pair of compact, flat-spectrum sources, 1308+326 and 1308+328, the same pair as used for our VSOP space-VLBI astrometry. The stronger source, 1308+326, is no stranger to the lists of sources observed in geodetic and astrometric programs (see the Radio Reference Frame Image Database WWW page of the US Naval Observatory (<sup>1</sup>)).

The weaker, but more compact, 1308+328 was discovered by Machalski and Engels (1994) and lies 14.3 arcmins away in PA 27°. The relative separation between these sources has been measured to sub-mas accuracy at 2.3 and 8.4 GHz with the EVN using the phase-reference technique (Rioja and Porcas, 1996; Rioja et al, 1996).

Two attempted observations using the CMVA (Coordinated mm VLBI Array; proposals CP01 observed October 1996 and CP03 observed April 1998) were unsuccessful for a number reasons, both technical and meteorological. The NRAO VLBA observations described here were proposed for “dynamic scheduling” mode (so they could wait for good tropospheric conditions) and were finally made on 19th January, 2002. The recording rate was 256 Mb/s using 4 8-MHz channels in both left- and right-hand circular polarisation modes and 2-bit sampling. Seven VLBA antennas were used (FD, KP, LA, MK, NL, OV, PT) although the data from MK had to be rejected later.

Recording was made for 14 22-minute tape passes. Before each pass a pointing observation was performed at each antenna on 3C273 at 43 GHz. Observations at 86 GHz were recorded for 2 mins each on 3C273 (~7 Jy), and 3C279 (~22 Jy), followed by 3 min scans on each of 1308+326 (~0.8 Jy) and 1308+328 (~0.4 Jy). After this followed a period of rapid switching between these 2 sources, with short scan lengths; we experimented with 10, 15 and 20 sec on different tape passes. Each pass ended with a final 3 min scan on 1308+326. A typical sequence of observations acquired from a single tape pass is shown in Table 1. The data were correlated at the VLBA correlator, with 1 s output pre-average time and 0.5 MHz frequency resolution.

<sup>1</sup><http://rorf.usno.navy.mil/rrfid.shtml>

Table 1: Sequence of source observations in a typical 22 min tape pass

Scan #	Centre time	Scan Length	Source #	Name
458	14:15:19.9	00:01:49.1	1 =	3C273
460	14:17:27.3	00:01:33.3	2 =	3C279
461	14:21:51.1	00:02:45.7	3 =	1308+326
462	14:24:44.1	00:02:56.2	4 =	1308+328
463	14:26:24.7	00:00:06.3	3	
464	14:26:36.3	00:00:12.6	4	
465	14:26:51.5	00:00:13.6	3	
466	14:27:06.7	00:00:12.6	4	
467	14:27:21.4	00:00:12.6	3	
468	14:27:36.6	00:00:13.6	4	
469	14:27:51.8	00:00:12.6	3	
470	14:28:06.4	00:00:12.6	4	
471	14:28:21.6	00:00:13.6	3	
472	14:28:36.8	00:00:12.6	4	
473	14:28:51.5	00:00:12.6	3	
474	14:29:06.2	00:00:12.6	4	
475	14:29:21.4	00:00:13.6	3	
476	14:29:36.1	00:00:11.5	4	
477	14:29:50.3	00:00:12.6	3	
478	14:30:05.5	00:00:13.6	4	
479	14:30:20.7	00:00:12.6	3	
480	14:30:35.3	00:00:12.6	4	
481	14:30:50.5	00:00:13.6	3	
482	14:31:05.7	00:00:12.6	4	
483	14:31:20.4	00:00:12.6	3	
484	14:31:35.6	00:00:13.6	4	
485	14:31:50.8	00:00:12.6	3	
486	14:32:05.5	00:00:12.6	4	
487	14:32:20.2	00:00:12.6	3	
488	14:32:35.4	00:00:13.6	4	
489	14:32:50.6	00:00:12.6	3	
490	14:33:05.3	00:00:12.6	4	
491	14:33:20.5	00:00:13.6	3	
492	14:33:35.7	00:00:12.6	4	
493	14:33:50.4	00:00:12.6	3	
494	14:34:05.6	00:00:13.6	4	
495	14:34:20.8	00:00:12.6	3	
496	14:34:35.5	00:00:12.6	4	
497	14:34:50.1	00:00:12.6	3	
498	14:35:05.3	00:00:13.6	4	
499	14:36:42.9	00:02:57.2	3	

## 4 Data Analysis

The data analysis was performed using the NRAO **AIPS** reduction package. A rough calibration of the visibility amplitudes was made by simply applying the system temperature measurements and antenna gain curves provided. The instrumental relative phases between the IF channels in both LHC and RHC polarisations were calibrated using data from the strong, compact calibration source, 3C279.

The **AIPS** fringe-fitting task, **FRING**, makes a station-based determination of the residual phases, rates and delays with respect to a reference antenna. (This is equivalent to fitting for residuals on all baselines, but forcing the constraints that the phases, rates and delays around any triangle of baselines sum to zero.) The VLBA-LA antenna was used as the reference throughout this analysis. The multi-band delay residuals resulting from initial fringe-fitting of the scans from a typical tape pass (with a delay search window of 200 ns) are shown in Figure 1 (left). Note that all the long duration scans, and most of the very short 1308+326 scans, are detected. The amplitudes and phases of the visibilities on the LA-PT baseline for this pass, averaged for 15 s after applying the residual solutions, are shown in Figure 1 (right).

The large number of detections allowed us to re-fringe-fit the data with narrower delay and rate search windows. A comparison of the results from fringe-fitting the scans of the calibrator 1308+326 with wide and narrow search windows is shown in Figure 2. All 1308+326 scans were detected in this tape pass using the narrow search window.

Figure 3 (left) shows the antenna phase solutions derived from short (15 s) scans on 1308+326 during a period of rapid source switching. The phases can be easily followed and connected between successive scans. Figure 3 (right) shows the function used for interpolating the

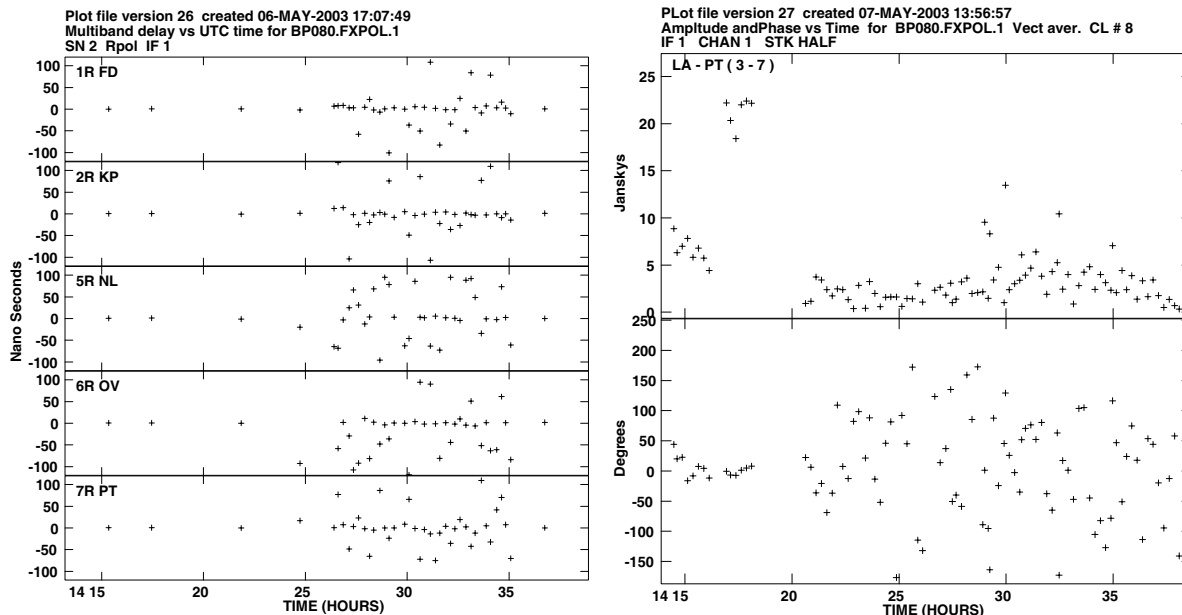


Figure 1: **Left:** Fringe-fit multiband delay solutions for all scans in a typical tape pass, using a 200 ns wide search window (using VLBA-LA as reference antenna). **Right:** Amplitude (top) and phase (bottom) every 15s for all sources in a typical tape pass on the baseline LA-PT, after application of the fringe-fit solutions. Note the high amplitude and small phase scatter for the initial observations on 3C273 and 3C279.

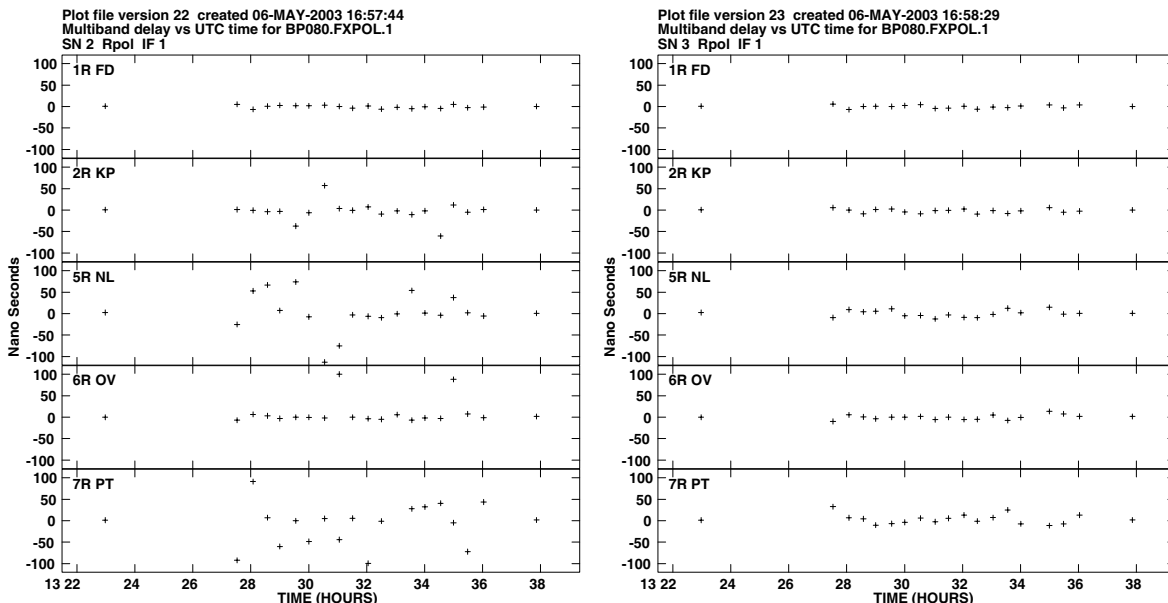


Figure 2: Fringe-fit multiband delay solutions for scans on the calibrator source 1308+326: **Left:** using a 200 ns delay search window; **Right:** using an 80 ns delay search window. Note the increase in the number of “detections” using the narrower window.

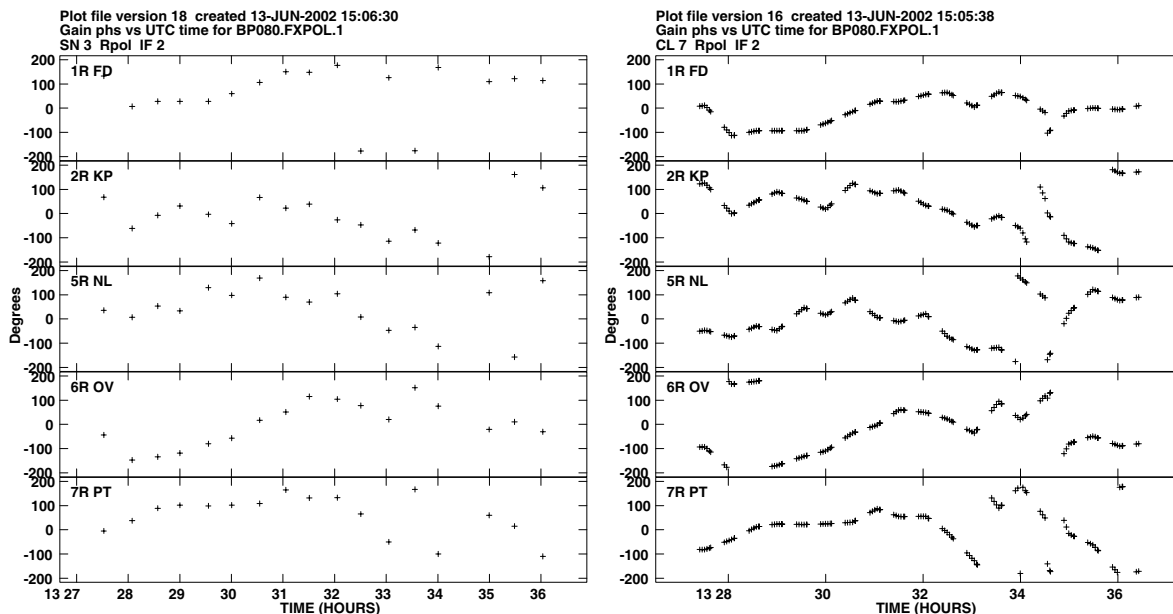


Figure 3: Antenna phases (w.r.t. VLBA-LA) for successive short 15s scans on the calibration source 1308+326. **Left:** FRINGE solutions; **Right:** Function derived for interpolating the phase to 1308+328 observations, using simple linear (nearest) phase connection

phase for the 1308+328 observations, which is a simple linear (nearest) phase connection (**AIPS** CLCAL option 'SIMP'). Interpolation in this way proved to be possible for much of the time for most antennas.

Maps of both 1308+326 and 1308+328, made from the data from the rapid switching periods only, are presented in Figure 4. For the calibrator, 1308+326 (left), the phase, delay and rate residuals derived from FRING were applied on a *per scan* basis (CLCAL option 'SELF') and

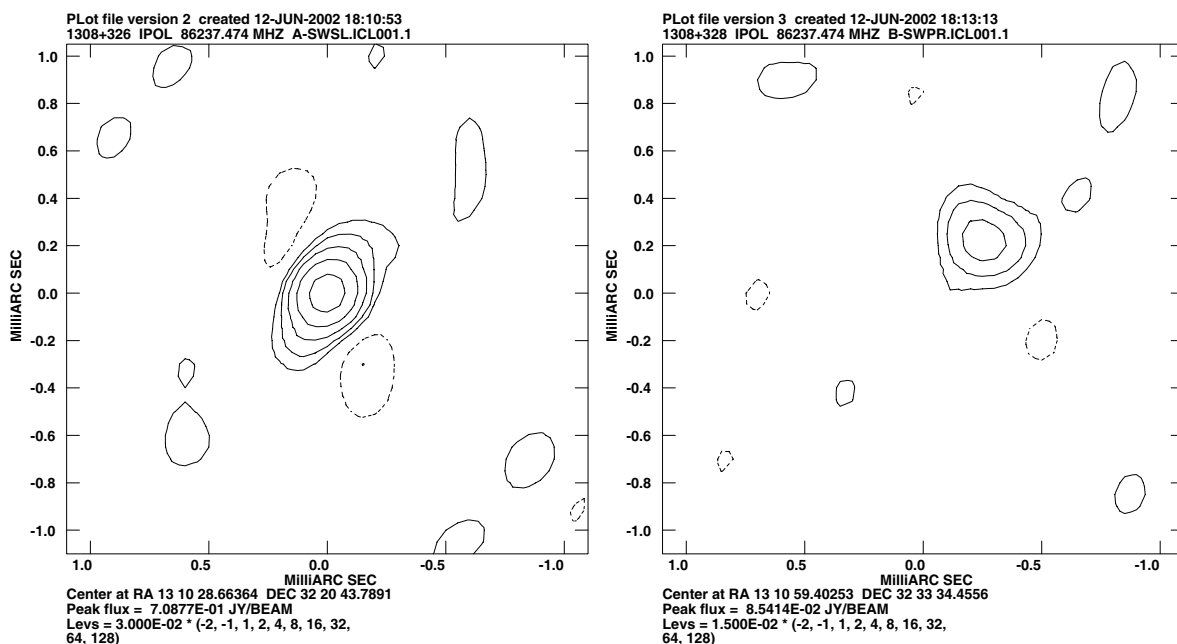


Figure 4: 86 GHz maps made with uniform weighting and CLEAN restoring beams of  $0.2 \times 0.2$  mas. **Left:** Hybrid map of 1308+326; **Right:** Phase-reference map of 1308+328.

the calibrated data were mapped and CLEANed using no further phase self-calibration. A single elliptical Gaussian fit to this map indicates that the source is slightly resolved ( $0.2$  mas in P.A.  $-39^\circ$ ).

For 1308+328 a phase-referenced map was made by applying the phase, delay and rate residuals determined by fringe-fitting the 1308+326 scans, and interpolating these to the times of the 1308+328 scans. The data were then mapped and CLEANed as for 1308+326. We believe this is the **first phase-referenced VLBI map made at 86 GHz!** The height of the peak in this map is much lower than that in maps made from self-calibrated 1308+328 data and represents a “coherence” of only 25 percent. However, this data set has not yet been fully edited and the true coherence may be rather higher. Note the offset of the peak from the centre in the phase-referenced map ( $0.34$  mas in P.A.  $-41^\circ$ ), representing a correction to the difference between the assumed positions of 1308+326 and 1308+328 used for correlation.

## 5 Comparison with other frequencies

We have now measured the relative separation between 1308+326 and 1308+328 to sub-mas accuracy on three occasions. Our “reference separation” is derived from the 8.4 GHz observations made in February 1995, with  $\sim 0.5$  mas resolution. At that epoch 1308+328 was unresolved, while 1308+326 exhibited a single component, slightly extended in P.A.  $-37^\circ$ . Our measured separation between the sources refers to the peak of this extended component.

The 5 GHz VSOP observations (June 1998) with slightly higher resolution ( $0.35$  mas) showed that 1308+328 was, again, essentially unresolved while 1308+326 was resolved into 2 components: a compact “core” component (visible on ground-space baselines), extended in P.A.  $\sim -45^\circ$ , and a more extended component (resolved out on ground-space baselines) about  $1.2$  mas away in P.A.  $\sim -80^\circ$ . The measured separation between 1308+328 and the peak of the core component in 1308+326 differs from the reference separation by  $\sim 0.12$  mas in P.A.  $-30^\circ$ ; since the

direction of this offset is similar to that of the core-jet axis of 1308+326 we attribute this to a change in the reference point used in 1308+326.

Figure 5 shows the contours of the VSOP image of 1308+326, with the map origin representing the position of the 8.4 GHz peak, assuming that the 1308+328 position does not change with time or frequency. The peak of the 5 GHz core is marked with a dot. 1308+326 is known to be highly variable, with an 8.4 GHz mas structure which varies on a timescale of months (see RRFID WWW page). It is possible that the peak measured in 1995 was a blend of the core and other jet components too close to the core at that epoch to be separately resolved, since the position lies between the 2 components seen at 5 GHz.

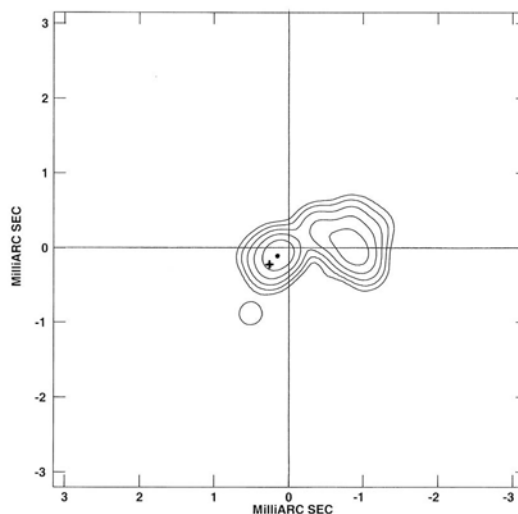


Figure 5: 5 GHz VSOP map of 1308+326 (contours) showing positions of the 5 GHz (dot) and 86 GHz (cross) peaks w.r.t the map origin at the 8.4 GHz peak (assuming that 1308+328 has an achromatic position).

At 86 GHz, with a resolution of 0.2 mas, we see a single component in 1308+326, slightly resolved in the same P.A. as in February 1995. We again assume that 1308+328 is achromatic and attribute the difference in measured separation between 1308+326 and 1308+328 to a change in reference point in 1308+326. This is plotted in Figure 5 with a cross. The change is in the sense that at 86 GHz the position of the peak is further towards the base of the jet compared to the 5 GHz peak. Although this is naturally explained as an opacity effect in the 1308+326 core, care must be taken in interpreting such results, since the position of the peak of a core may also depend on resolution (see Porcas and Rioja, 1997).

## Acknowledgements

We thank Chris Carilli and Barry Clark for advice on scheduling this project at the VLBA, and staff of the CMVA observatories who assisted in our preliminary observations. We thank Walter Alef for comments on the text. NRAO is a facility of the US National Science Foundation, operated by Associated Universities Inc.

## References

- Alef, W., 1988, in IAU Symposium 129, ed. M.J.Reid & J.M.Moran (Kluwer, Dordrecht) 523
- Beasley, A. J. & Conway, J. E., 1995 in ASP Conf. Ser. 82, Very Long Baseline Interferometry and the VLBA, eds. J. A. Zensus et al, (San Francisco: ASP), 327
- Machalski, J. and Engels, D., 1994, MNRAS, 266, L69
- Porcas, R.W and Rioja, M. J., 1996, in Proc. of the 11th Working Meeting on European VLBI for Geodesy and Astrometry, ed. G. Elgered, Goteborg, p209
- Rioja, M. J. and Porcas, R.W., 1996, in Proc. of the 11th Working Meeting on European VLBI for Geodesy and Astrometry, ed. G. Elgered, Goteborg, p219
- Porcas, R.W and Rioja, M. J., 1997, in Proc. of the 12th Working Meeting on European VLBI for Geodesy and Astrometry, ed. B. Pettersen, Honefoss, p133
- Porcas, R.W. & Rioja, M.J., 2000, in Proc. of the 14th Working Meeting of European VLBI for Geodesy and Astrometry, ed. P.Tomasi et al (IRA, Bologna) 139
- Rioja, M.J., Porcas, R.W. & Machalski, J., 1996, in Proc IAU Symposium 175, ed. R.Ekers et al, (Kluwer, Dordrecht) 122
- Rogers, A.E.E., Moffet, A.T., Backer, D.C. & Moran, J.M., 1984, Radio Science, 19, 1552

Session 5

# Geodetic VLBI Analysis and Results



# Vienna Mapping Functions

J. Boehm and H. Schuh

*Institute of Geodesy and Geophysics (IGG), TU Vienna, Austria*

**Summary:** Recently, numerical weather models NWMs have been investigated to improve mapping functions which are used for tropospheric modelling in VLBI and GPS data analyses. E.g., the Vienna mapping functions VMF are based on direct raytracing through NWMs without taking any intermediate parameters. In this study, pressure level data from ECMWF (European Centre for Medium-Range Weather Forecasts) are used. Two approaches are introduced to derive the coefficients for the continued fraction forms of the mapping functions: Whereas the 'rigorous approach' is rather time consuming, the 'fast approach' needs only one raytrace per epoch and site. Used for VLBI analyses, the VMFs improve the repeatability of baseline lengths by up to 10% compared to mapping functions without input from NWMs. Elevation angle cutoff tests with the VMFs reveal that there might be systematic effects that have not been visible with prior mapping functions.

## 1 Introduction

Raytracing through radiosonde data has often been used to develop and validate mapping functions which are used for tropospheric modelling in VLBI and GPS data analyses. E.g., the New Mapping Functions NMF (Niell, 1996), which need the station height, the station latitude and the day of the year as input parameters, were developed using radiosonde data over a wide range of latitudes.

In the past years, a lot of effort has been put into the development of mapping functions which are based on data from numerical weather models (NWMs). Niell (2001b) set up the 'isobaric' mapping functions IMF which apply as input parameters the height of the 200 mbar pressure level ('z200') and the ratio of the wet path delay along a straight line at 3.3° elevation and its zenith delay ('smfw3'). But still, the equations for the coefficients of the continued fraction form (see Eq. 1) are based on raytracing through radiosonde data.

When working on the implementation of these mapping functions with pressure level data from the ECMWF (European Centre for Medium-Range Weather Forecasts) it became evident that the NWMs could be exploited more rigorously by discarding intermediate parameters like z200 and smfw3. The main idea for the Vienna Mapping Functions VMF is to simply use the raytracing through the NWM directly instead of taking intermediate steps.

To illustrate the accuracy of NWMs and the raytracing program (see Appendix A), Figures 1a and 1b show the hydrostatic and wet mapping functions at 5° elevation derived from radiosonde data and ECMWF pressure level data at a site in Vienna ('Hohe Warte') in the year 2002. The pressure level data consist of 15 levels whereas the radiosonde data used here comprises at least 50 levels. There is a very good agreement between the time series. If multiplied by 2300 mm, the difference in the hydrostatic mapping function is  $4.1 \pm 6.5$  mm. The wet mapping functions (multiplied by 200 mm) differs by  $-0.3 \pm 4.1$  mm. It has to be mentioned that the same radiosonde data have been used to determine the ECMWF pressure levels.

Thus, the total agreement is still at the 1 cm level at 5° elevation what implies that the mapping functions can be calculated directly from raytracing through ECMWF pressure level data, at least if the pressure level data include meteorological information of sufficient accuracy at the site (e.g. from nearby radiosonde launches). This presumption is the basis for the concept of the Vienna mapping functions VMF. Tests with independent radiosonde data, i.e., that were not used for the determination of the ECMWF pressure level data would be desirable and remain to be done.

Figure 1a: Hydrostatic mapping functions at 5° elevation calculated from raytracing through radiosonde data and ECMWF pressure level data for identical epochs in 2002 for a site in Vienna ('Hohe Warte'). The seasonal variation can be clearly seen.

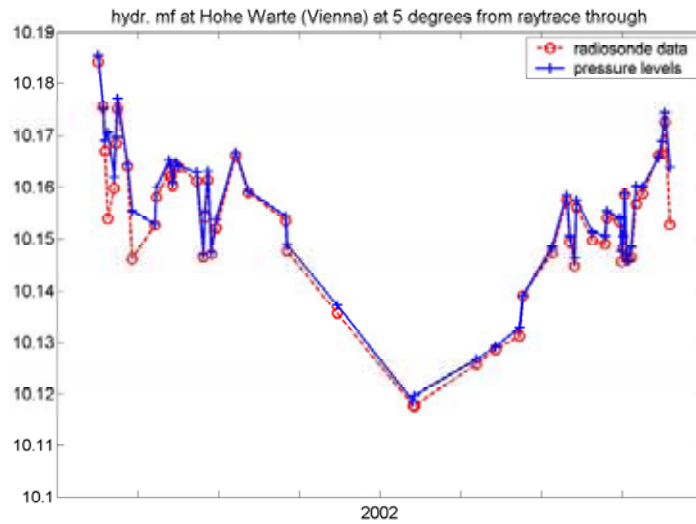
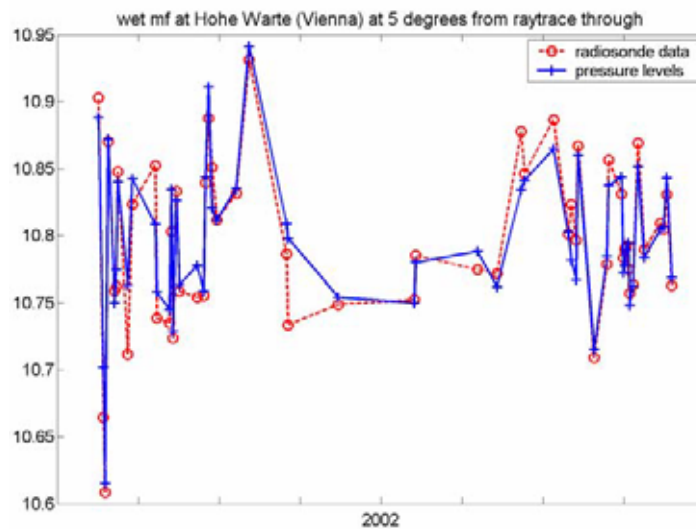


Figure 1b: Wet mapping functions at 5° elevation calculated from raytracing through radiosonde data and ECMWF pressure level data for identical epochs in 2002 for a site in Vienna ('Hohe Warte').



## 2 Determination of the Vienna Mapping Functions (VMF)

The continued fraction form which is used for the hydrostatic and wet mapping function is shown in Eq. (1). This form is also used in the NMF (Niell, 1996) and in the IMF (Niell, 2001b).

$$mf(e) = \frac{1 + \frac{a}{1 + \frac{b}{1 + c}}}{\sin e + \frac{a}{\sin e + \frac{b}{\sin e + c}}} \quad (1)$$

Table 1: Input parameters for hydrostatic and wet mapping functions.  $\varphi$  is the station latitude,  $h$  is the station height and  $doy$  is the day of the year.

	NMF	IMF	VMF
hyd.	$doy, h, \varphi$	$z200, \varphi, h$	$h, a, (b, c)$
wet	$\varphi$	$smfw3, h$	$a, (b, c)$

Three coefficients  $a$ ,  $b$  and  $c$  are sufficient to map zenith delays down to elevations of  $3^\circ$ . In the case of VMF, these coefficients have to be determined from raytracing through NWMs. The raytracing is described in Appendix A. Input parameters for the raytracing program are an initial elevation angle  $e_0$ , and values for height, temperature and water vapour pressure at 15 distinct pressure levels. The raytracing then yields the outgoing (= vacuum) elevation angle  $e$ , and the values for the hydrostatic and the wet mapping function. The hydrostatic mapping function includes the geometric bending effect.

Two ways of determining the coefficients from raytracing through ECMWF pressure levels will be presented here. The first one is the rigorous and very accurate way, whereas the second one is faster and still sufficiently accurate.

## 2.1 Rigorous determination of the coefficients

For each site (e.g. VLBI station) and each epoch when ECMWF pressure level data are available, i.e. every six hours, the hydrostatic and wet mapping functions as well as the outgoing (= vacuum) elevation angles are determined by raytracing through the pressure levels at ten different initial elevation angles ( $90^\circ$ ,  $70^\circ$ ,  $50^\circ$ ,  $30^\circ$ ,  $20^\circ$ ,  $15^\circ$ ,  $10^\circ$ ,  $7^\circ$ ,  $5^\circ$ ,  $3.3^\circ$ ). Then, the coefficients  $a$ ,  $b$  and  $c$  for the continued fraction forms (Eq. 1) for the hydrostatic and wet mapping functions are estimated in a least-squares procedure. The adjustment shows that three coefficients are enough to map down the zenith delays to  $3^\circ$  elevation. So, at each site a time series of six parameters ( $a_h$ ,  $b_h$ ,  $c_h$ ,  $a_w$ ,  $b_w$ ,  $c_w$ ) exists with a resolution of six hours. The rigorous approach is not well-suited to be used on a global grid because raytracing still takes a lot of computing time. Furthermore, it remains to be tested whether information gets lost by the spatial interpolation of the parameters  $a$ ,  $b$  and  $c$ .

## 2.2 Fast determination of the coefficient $a$

Although computers are very fast today, raytracing is still time consuming, especially if it has to be performed on a global grid, four times per day and ten times per grid point. For this reason, a fast version of the rigorous way has been developed that yields similar values for the mapping functions. Instead of determining the raytracing at ten different elevation angles, the raytracing is only calculated for one initial elevation angle of  $3.3^\circ$ . This yields one value for the hydrostatic, one for the wet mapping function and the vacuum elevation angle ( $\sim 3^\circ$ ). Then, predefined formulas are used for the  $b$  and  $c$  coefficients, and the coefficients  $a$  can be determined by simply inverting the continued fraction form (Eq. 1). For the hydrostatic mapping function the coefficients  $b_h$  and  $c_h$  are taken from the hydrostatic part of the isobaric mapping function IMF. If  $\varphi$  is the geodetic latitude, the coefficients are determined by:

$$b_h = 0.002905 \quad (2)$$

$$c_h = 0.0634 + 0.0014 \cdot \cos(2\varphi) \quad (3)$$

For the wet part the coefficients  $b_w$  and  $c_w$  are taken from NMF (valid for  $\varphi = 45^\circ$ ):

$$b_w = 0.00146 \quad (4)$$

$$c_w = 0.04391 \quad (5)$$

Contrarily to the rigorous approach, a height correction is applied for the hydrostatic part according to Niell (1996), in order to refer the hydrostatic coefficients  $a_h$  to zero height. The advantage is that the spatial interpolation yields better results when all grid points are referred to zero height. On the other hand, this height correction has to be re-applied when using the hydrostatic mapping function.

### 3 Validation of the VMF

#### 3.1 Comparison of mapping function values for CONT02

The Continuous VLBI 2002 program of the IVS (CONT02) consists of 15 consecutive 24 h VLBI experiments with the same 8 stations throughout: Algonquin, Gilmore Creek, HartRAO, Kokee Park, Ny Alesund, Wettzell, Westford, and Onsala. The sessions last from October 16 to October 30, 2002.

For this time span, the mapping function values from NMF, IMF and VMF (fast approach) are compared to those from VMF (rigorous approach). If the unit of the mapping functions is length, they refer to 2300 mm hydrostatic and 200 mm wet zenith delay. Table 2 summarizes the rms-differences for an elevation angle of 5°. If the rigorous approach was correct i.e., if the NMF was perfect, the rms-differences at 5° elevation are 1 cm, 3 cm and 5 cm for VMF (fast), IMF and NMF, respectively. Following a rule of thumb (Niell et al., 2001a), one-third of the mapping function error at the lowest elevation angle included in the analysis can be seen as station height error. So, these rms-differences would correspond to 3 mm, 1 cm and 1.7 cm station height error if the NMF was error-free.

Table 2: Rms-differences in mm of VMF (fast), IMF and NMF compared to the rigorous approach of VMF for the duration of CONT02. The total (hydrostatic plus wet) rms-differences are at about 1 cm, 3 cm and 5 cm, respectively.

Site	hydrostatic at 5° in [mm]			wet at 5° in [mm]		
	VMF (fast)	IMF	NMF	VMF (fast)	IMF	NMF
Algotpark	7	18	67	1	7	14
Gilcreek	12	18	20	1	8	15
HartRAO	4	25	19	1	7	17
Kokee	2	29	23	1	5	21
Nyales20	19	34	52	0	8	12
Wettzell	8	16	34	1	7	18
Westford	4	18	48	1	8	15
Onsala60	11	12	39	1	8	19

#### 3.2 Baseline length repeatabilities

Improved mapping functions are expected to yield improved geodetic accuracies. A good measure for the quality of geodetic results is the baseline length repeatability.

For the VLBI analysis, the classical least-squares method (Gauss-Markov model) of the OCCAM 5.1 VLBI software package (Titov et al., 2001) is used. Free network solutions are calculated for the 24 h sessions with five Earth orientation parameters being estimated (nutations, dUT1 and pole coordinates). Atmospheric loading parameters are taken from Petrov and Boy (2003), and total gradient offsets are estimated every 6 hours using the model by MacMillan (1995).

Baseline length repeatabilities are determined for CONT02, and for all IVS-R1 and IVS-R4 sessions until March, 2003. For the following investigations no baselines are used which include the station Tigo Concepcion (Chile) and the station at Gilmore Creek after the Earthquake on November 3, 2002. Figure 2 shows the baseline length repeatabilities for the IVS-R1 sessions with a cutoff angle of 5° elevation. A significant improvement of nearly 10% can be seen for the VMF (fast) as well as for the IMF when compared to NMF.

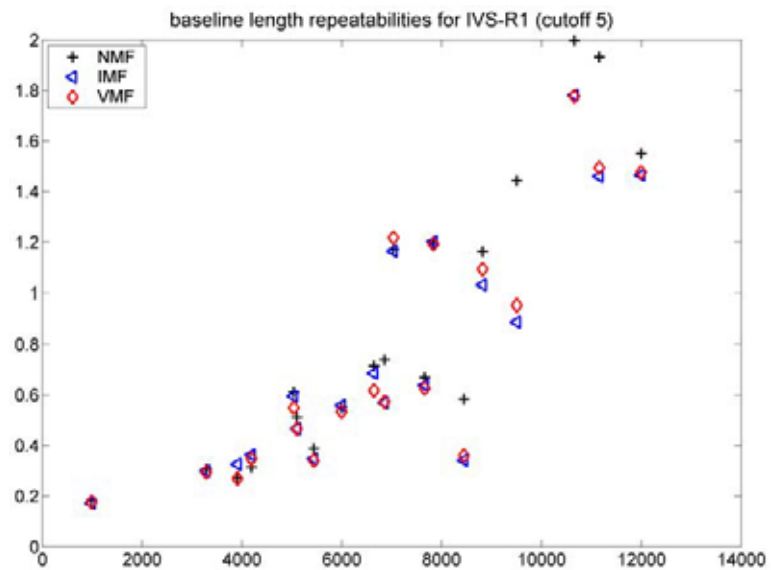


Figure 2: Baseline length repeatabilities in cm for the IVS-R1 sessions until March, 2003. A significant improvement can be seen for the VMF (fast) and the IMF i.e., the mapping functions that are based on data from NWMs when compared to the NMF.

Tables 3a and 3b provide information about the improvement of the baseline length repeatabilities of the CONT02, IVS-R1 and IVS-R4 sessions with VMF (fast) and IMF compared to NMF. Table 3a gives the percentage of improved baselines, and Table 3b provides the mean value of the relative improvement over all baselines. The cutoff elevation angle was set to 5°.

Table 3a: Baselines with better repeatabilities in %. A clear majority of the baselines is improved with the mapping functions based on NWMs.

	CONT02	IVS-R1	IVS-R4
IMF	54 %	79 %	62 %
VMF (fast)	70 %	89 %	62 %

Table 3b: Mean values of the relative improvements in %. The repeatabilities with VMF (fast) are slightly better than the repeatabilities with IMF. The improvement is largest for the IVS-R1 sessions (almost 10 %).

	CONT02	IVS-R1	IVS-R4
IMF	1.9 %	8.3 %	3.0 %
VMF (fast)	5.2 %	9.7 %	3.5 %

Figure 3 shows the station height repeatabilities for CONT02. Six out of eight (75%) of the station height repeatabilities are improved for IMF and VMF (fast) compared to NMF. The mean relative improvement is 7.2% for IMF and 10.7% for VMF (fast). For this investigation the horizontal station components were fixed to ITRF2000 and the station heights were estimated. It has to be clearly stated that the station height repeatability at one station is also effected by changes in the mapping functions at the other stations. Nevertheless, the main part of the changed repeatability is due to the mapping function used at the station itself. Figure 3 shows that only at HartRAO (South Africa) the repeatability gets slightly worse when using IMF or VMF (fast). This is likely due to the fact that the ECMWF pressure level data is lacking good input information in this area. Detailed investigations reveal that the improvement of repeatabilities for baselines lengths including HartRAO is not as big as for the other baselines.

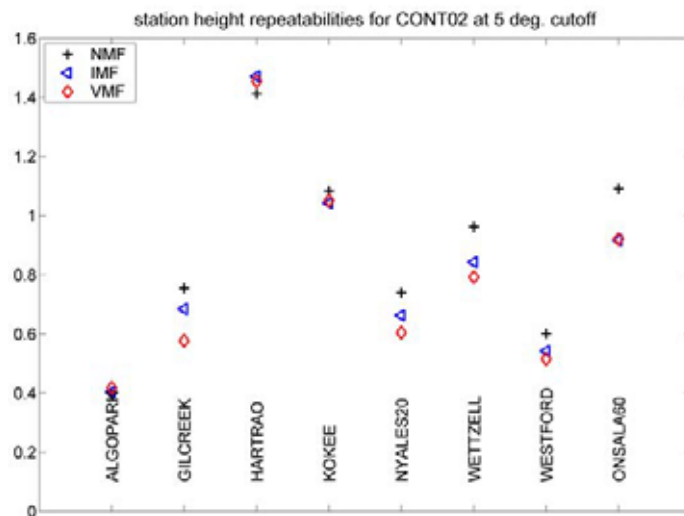


Figure 3: Station height repeatabilities in cm for CONT02. 75% of the station height repeatabilities are improved for IMF and VMF (fast) compared to NMF. The relative improvement (mean for all stations) is 7.2% for IMF and 10.7% for VMF (fast).

### 3.3 Elevation angle cutoff tests

Another measure for the quality of mapping functions can be obtained by elevation angle cutoff tests. These tests show how baseline lengths change when the cutoff elevation angle is varied. In Figures 4a, 4b and 4c the changes of the baseline lengths are plotted for the cutoff elevation angle  $5^\circ$  compared to  $7^\circ$  and  $10^\circ$  for CONT02. The plots are for NMF, IMF and VMF (fast), respectively and the changes themselves are well below the repeatabilities. The triangle in the upper right of all three plots 4a, 4b and 4c corresponds to  $10^\circ$  elevation cutoff (compared to  $5^\circ$ ) on the baseline HARTRAO to Kokee Park. Due to its length of almost one Earth diameter obviously too many observables get 'lost' when increasing the cutoff elevation angle from  $5^\circ$  to  $10^\circ$ .

In general, for the NMF (Fig. 4a) the variation of the baseline lengths is rather large for the  $10^\circ$  cutoff (between  $-0.6$  mm and  $+0.2$  mm). For the IMF (Fig. 4b) when increasing the cutoff elevation angle the scatter of the baseline lengths is getting smaller than for NMF, but a systematic effect becomes visible: The longer the baselines are, the shorter the baselines get with higher cutoff elevation angles. With VMF (fast) (Fig. 4c), this systematic effect becomes even more evident for the  $10^\circ$  cutoff solutions. For illustration a quadratic regression polynomial was fitted to the differences.

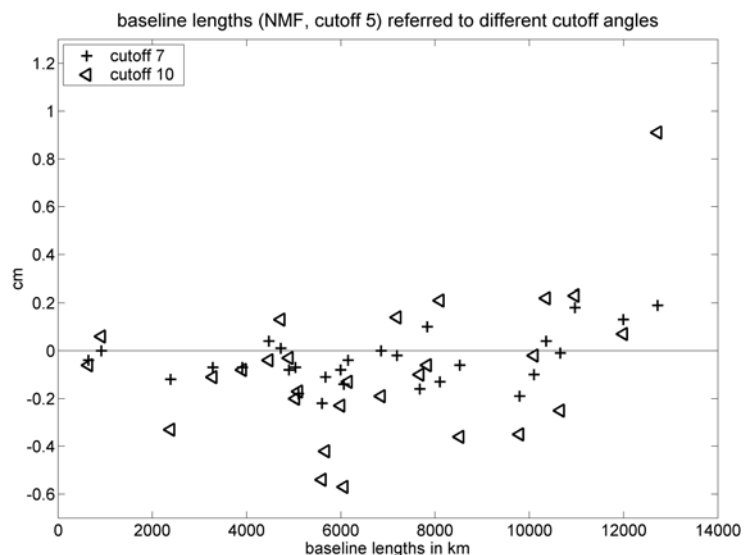


Figure 4a: Elevation angle cutoff test for CONT02 and NMF. Baseline lengths with a  $5^\circ$  cutoff elevation angle are compared to baseline lengths with a  $7^\circ$  and  $10^\circ$  cutoff elevation angle.

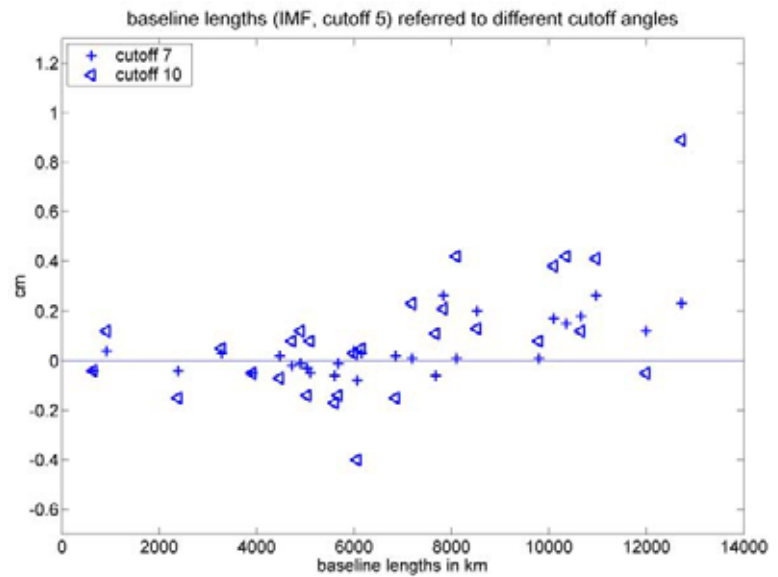


Figure 4b: Elevation angle cutoff test for CONT02 and IMF. Baseline lengths with a  $5^\circ$  cutoff elevation angle are compared to baseline lengths with a  $7^\circ$  and  $10^\circ$  cutoff elevation angle. A systematic effect might be seen for longer baselines.

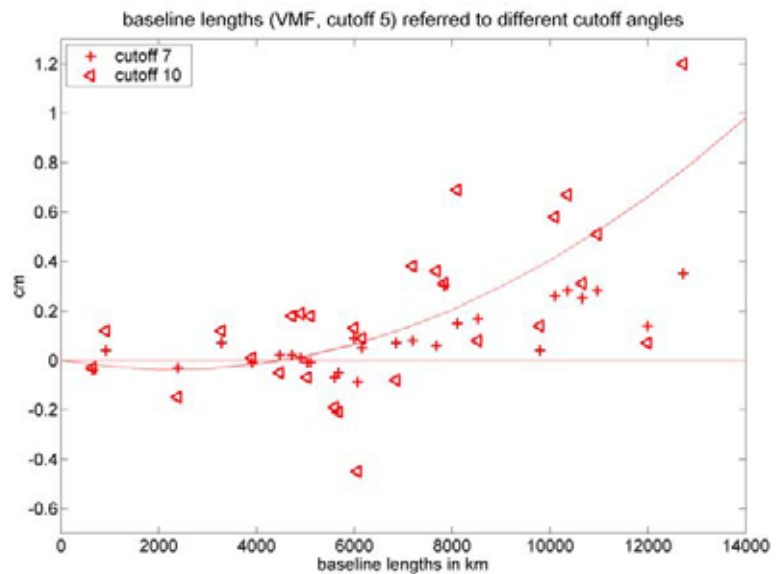


Figure 4c: Elevation angle cutoff test for CONT02 and VMF (fast). Baseline lengths with a  $5^\circ$  cutoff elevation angle are compared to baseline lengths with a  $7^\circ$  and  $10^\circ$  cutoff elevation angle. For illustration of the systematic effect a quadratic polynomial is fitted to the differences.

In spite of the reduced scatter, systematic effects could indicate problems with the mapping function. In the case of VMF (fast), a possible error source might be errors in the raytracing program. There could be other reasons as well, e.g. deficiencies in the gradient model for observations at low elevations.

Figures 5a and 5b show the cutoff elevation angle tests for IVS-R1 and IVS-R4 in the sense cutoff  $5^\circ$  minus cutoff  $10^\circ$ . Whereas IVS-R4 clearly confirms the assumption of systematic effects, it is not so evident for the IVS-R1 sessions

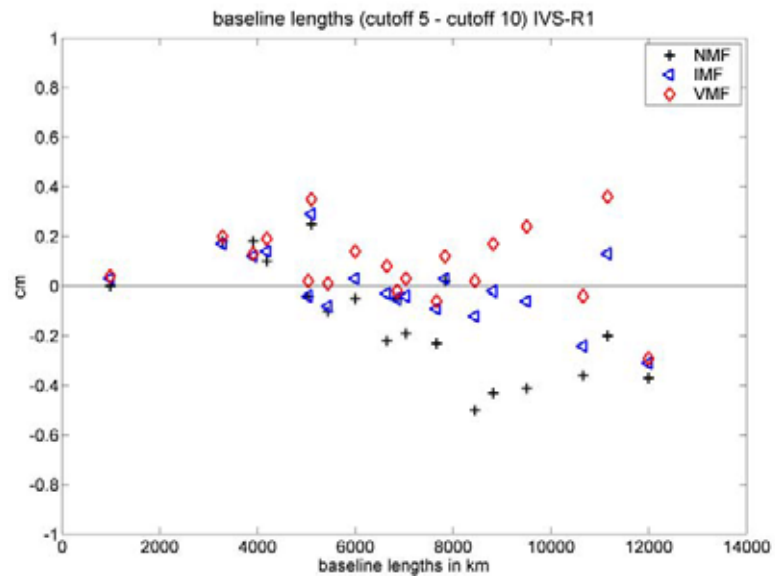


Figure 5a: Elevation angle cutoff test for IVS-R1 with NMF, IMF and VMF (fast). Baseline lengths with a 5° cutoff elevation angle are compared to baseline lengths with a 10° cutoff elevation angle.

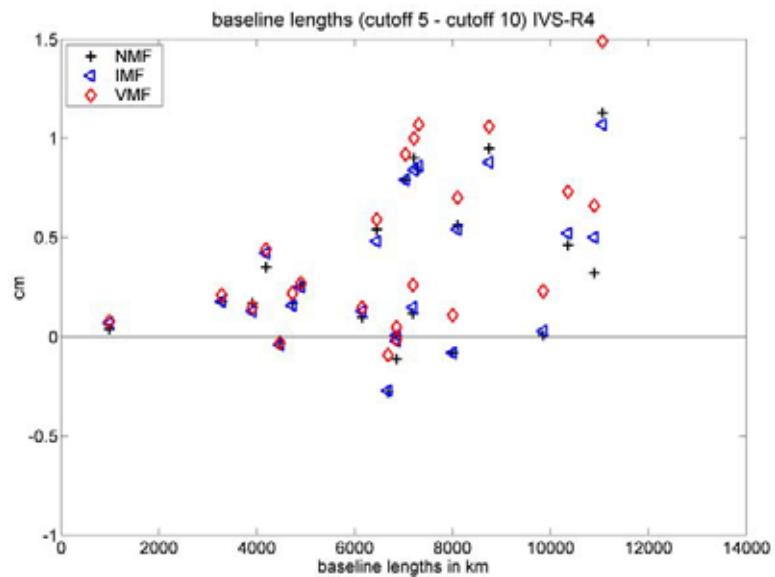


Figure 5b: Elevation angle cutoff test for IVS-R4 with NMF, IMF and VMF (fast). Baseline lengths with a 5° cutoff elevation angle are compared to baseline lengths with a 10° cutoff elevation angle.

## 4 Conclusions and recommendations

Recent mapping functions such as IMF and VMF based on data from numerical weather models like ECMWF provide better repeatabilities of baseline lengths and station heights than the NMF. However, systematic effects become visible which have to be investigated. Possibly, the modelling of tropospheric gradients has to be revised, too. Contrarily to IMF, the Vienna mapping functions VMF (especially the rigorous approach) exploit the information from NWMs completely and will be improved with every improvement in the NWM.

## Appendix A: Raytracing

Assuming azimuthal symmetry the values for the hydrostatic and wet mapping functions as well as the outgoing elevation angle can be derived rather easily from radiosonde data or NWMs. In the following description it is referred to ECMWF pressure level data, but the considerations are valid for radiosonde data as well.

### A1 Increase of the vertical resolution

ECMWF pressure level data comprise heights  $h$  in m, temperatures  $T$  in K and values for the water vapour pressure  $e$  in hPa at 15 distinct pressure level. The pressure values are [1000, 925, 850, 700, 500, 400, 300, 250, 200, 150, 100, 70, 50, 30, 10] hPa, approximately ranging from the surface of the Earth to 30 km in height. To calculate the raytracing with sufficient accuracy, the increments for the integration (distance between the pressure levels) have to be decreased and values above the 10 hPa pressure level data have to be extrapolated because the latter are significant for the light bending and the hydrostatic delay. Following Rocken (2001) height dependent increments are used (Table A1).

Table A1: Increments for the raytracing according to Rocken (2001).

Height	increment
0 km - 2 km	10 m
2 km - 6 km	20 m
6 km - 16 km	50 m
16 km - 36 km	100 m
36 km - 136 km	500 m

Linear interpolation is used for the temperature values between the 15 pressure levels. Above the 10 hPa pressure level the temperature values are taken from a standard model for the atmosphere. The values for the total pressure  $p$  and the water vapour pressure  $e$  are determined using an exponential approach.

$$p = p_0 \cdot e^{(h-h_0)/c} \quad (\text{A1})$$

$p_0$  and  $h_0$  are the pressure and the height at the adjacent pressure level below and  $c$  is a coefficient that has been determined from the adjacent pressure levels above and below. Figure A1 shows an example for the increase of the vertical resolution. There, 15 ECMWF pressure levels have been expanded to 979 levels.

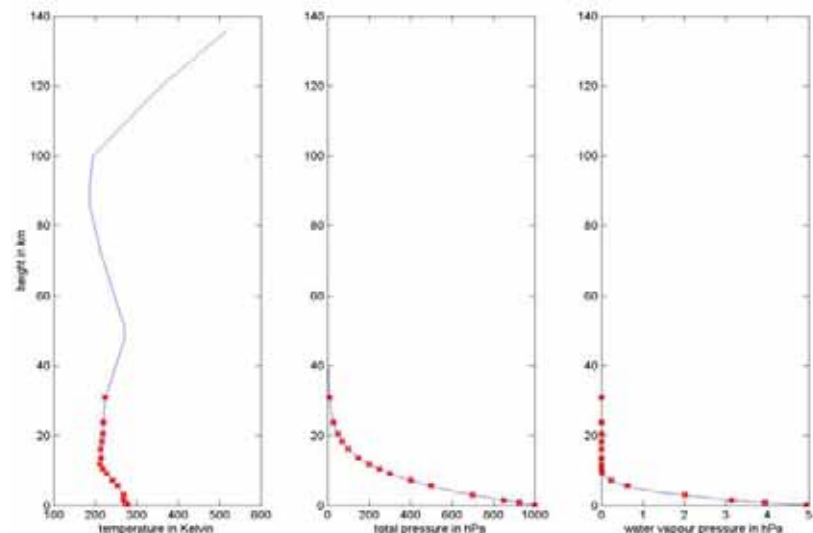


Figure A1: ECMWF pressure level data at the VLBI station Algonquin Park (Canada) on October 15, 2002 at 0:00 UT. The crosses mark the 15 pressure levels with temperature, total pressure and water vapour pressure. In between and above additional values were determined.

## A2 Refractivity

At the approximately 1000 levels, the total, hydrostatic and wet refractivities have to be determined. The first is used to calculate the bending and the latter are applied to derive the hydrostatic and wet path delays, respectively. At first, the densities of the dry part ( $\rho_d$ ) and of the wet part ( $\rho_w$ ) are determined.

$$\rho_d = (p - e) \frac{M_d}{R} \frac{1}{T} \quad (\text{A2})$$

$$\rho_w = e \frac{M_w}{R} \frac{1}{T} \quad (\text{A3})$$

R is the general gas constant, and  $M_d$  and  $M_w$  are the molar masses of dry air and water, respectively. The total density is the sum of the partial densities (A4).

$$\rho = \rho_d + \rho_w \quad (\text{A4})$$

Applying the equations above the hydrostatic and wet refractivities,  $N_h$  and  $N_w$ , at each layer can be calculated.

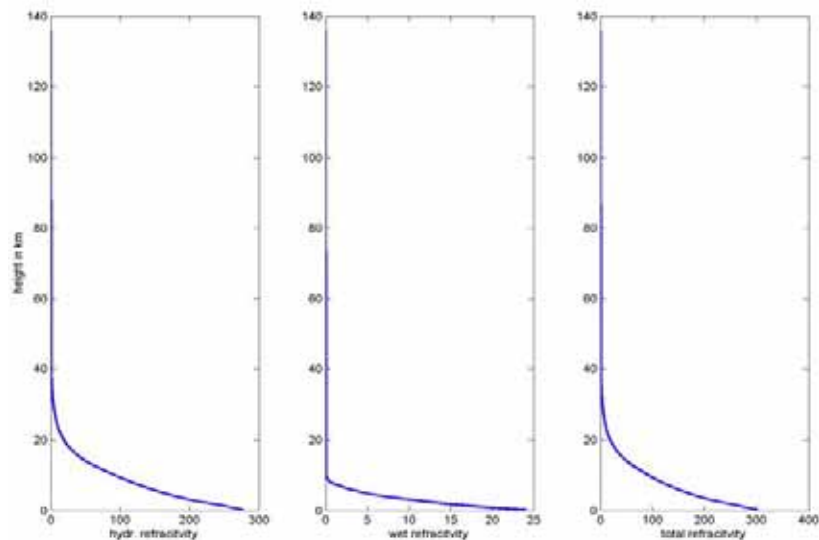
$$N_h = k_1 \frac{M_d}{R} \rho \quad (\text{A5})$$

$$N_w = k_3 \frac{e}{T^2} + k'_2 \frac{e}{T} \quad (\text{A6})$$

It has to be mentioned that the wet term in A3 does not correspond to the wet term in A6 because of the difference between the hydrostatic and the dry term. The coefficients  $k_1$ ,  $k'_2$  and  $k_3$  are empirically determined values. The total refractivity  $N$  is the sum of the hydrostatic and wet refractivity yielding the refractive index  $n$ .

$$N = (n - 1) \cdot 10^6 = N_h + N_w \quad (\text{A7})$$

Figure A2: Values for the hydrostatic, wet and total refractivities, calculated at 979 heights above the VLBI-station Algonquin Park (Canada) on October 15, 2002, at 0:00 UT. Although the refractivities are rather small above 30 km they need to be taken into account.



Finally, the levels are cut off at the actual station height, so that there are no levels apparently below the surface of the Earth contributing to the path delays.

### A3 Calculation of the raytracing

At first, it will be summarized which data are available now: At  $k$  levels ( $\sim 1000$ ) there are values for the hydrostatic and wet refractivities and for the refractive index. These are used to determine the  $(k-1)$  refractivities  $N_h$ ,  $N_w$  and  $n$  in between the levels for the respective shells (see Figure A3) by simply taking the mean. Then the distances to the geocenter are determined by adding the radius of the Earth  $r_0$  to the heights of the levels.

$$r_i = r_0 + h_i \dots \quad i = 1, \dots, k \quad (\text{A8})$$

If the initial elevation angle  $e_1$  is known, one gets for point P1 (see Figure A3)

$$\theta_1 = e_1. \quad (\text{A9})$$

Then, the distance from the first to the second point is determined with

$$s_1 = -r_1 \sin \theta_1 + \sqrt{r_2^2 - r_1^2 \cos^2 \theta_1} \quad (\text{A10})$$

and the geocentric coordinates of P1 and P2 are

$$\begin{aligned} z_1 &= r_1 & y_1 &= 0 \\ z_2 &= z_1 + s_1 \sin e_1 & y_2 &= y_1 + s_1 \cos e_1. \end{aligned} \quad (\text{A11})$$

The corresponding angles at the geocenter are

$$\begin{aligned} \eta_1 &= 0 \\ \eta_2 &= \arctan(y_2/z_2). \end{aligned} \quad (\text{A12})$$

Applying Snell's law the angles  $\theta_2$  and  $e_2$  at the point P2 can be determined.

$$\theta_2 = \arccos\left(\frac{n_1}{n_2} \cos(\theta_1 + \eta_2)\right) \quad (\text{A13})$$

$$e_2 = \theta_2 - \eta_2 \quad (\text{A14})$$

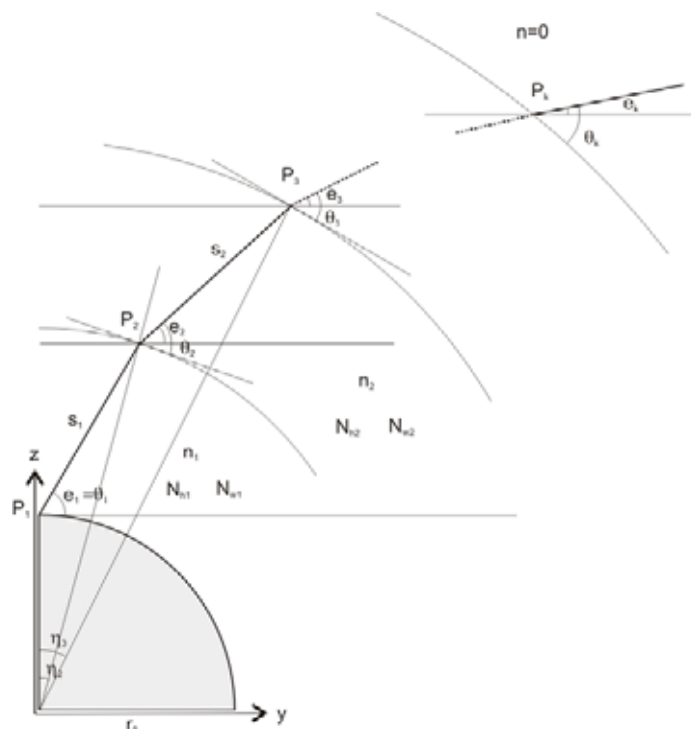


Figure A3: Raytracing.

For all other shells a loop can be set up running from 2 to (k-1).

$$s_i = -r_i \sin \theta_i + \sqrt{r_{i+1}^2 - r_i^2 \cos^2 \theta_i} \quad (\text{A15})$$

$$z_{i+1} = z_i + s_i \sin e_i \quad y_{i+1} = y_i + s_i \cos e_i \quad (\text{A16})$$

$$\eta_{i+1} = \arctan(y_{i+1}/z_{i+1}) \quad (\text{A17})$$

$$\delta_{i+1} = \eta_{i+1} - \eta_i \quad (\text{A18})$$

$$\theta_{i+1} = \arccos\left(\frac{n_i}{n_{i+1}} \cos(\theta_i + \delta_{i+1})\right) \quad (\text{A19})$$

$$e_{i+1} = \theta_{i+1} - \eta_{i+1} \quad (\text{A20})$$

Applying the equations above, all incremental distances  $s_i$  between the points and the outgoing elevation angle  $e_k$  are known. Then, the hydrostatic  $ds_h$  and the wet path delays  $ds_w$  along the bended ray can be determined by summation.

$$ds_h = \sum_{i=1}^{k-1} s_i N_{hi} \quad (\text{A21})$$

$$ds_w = \sum_{i=1}^{k-1} s_i N_{wi} \quad (\text{A22})$$

Analogously, the path delays in zenith direction are derived.

$$dz_h = \sum_{i=1}^{k-1} dh_i N_{hi} \quad (\text{A23})$$

$$dz_w = \sum_{i=1}^{k-1} dh_i N_{wi} \quad (\text{A24})$$

#### A4 Determination of the mapping functions

The path delay used with space geodetic techniques (GPS, VLBI) does not only consist of the path delay along the bended ray but also of the geometric bending effect  $d_{geo}$  itself. It can be determined by

$$d_{geo} = \sum_{i=1}^{k-1} [s_i - \cos(e_i - e_k) \cdot s_i] \quad (\text{A25})$$

This geometric effect is usually added to the hydrostatic mapping function. So, the values for the hydrostatic and wet mapping functions can be determined by

$$mf_h = (ds_h + d_{geo})/dz_h \quad (\text{A26})$$

$$mf_w = ds_w/dz_w \quad (\text{A27})$$

## Acknowledgements

We acknowledge the Zentralanstalt fuer Meteorologie und Geodynamik (ZAMG) for providing access to the ECMWF data. Also, we are also grateful to A.E. Niell for having very informative discussions about NWMs and mapping functions.

## References

- MacMillan D.S., Atmospheric gradients from very long baseline interferometry observations, *Geophys. Res. Lett.*, Vol. 22, No. 9, pages 1041-1044, 1995.
- Niell A.E., Global mapping functions for the atmosphere delay at radio wavelengths, *JGR*, Vol. 101, No. B2, pages 3227-3246, 1996.
- Niell A.E., A.J. Coster, F.S. Solheim, V.B. Mendes, P.C. Toor, R.B. Langley and C.A. Upham, Comparison of Measurements of Atmospheric Wet Delay by Radiosonde, Water Vapor Radiometer, GPS and VLBI, *Journal of Atmospheric and Oceanic Technology*, 18, 830-850, 2001a.
- Niell A.E., Preliminary evaluation of atmospheric mapping functions based on numerical weather models, *Phys. Chem. Earth*, 26, 475-480, 2001b.
- Petrov L. and J.P. Boy, Study of the atmospheric pressure loading signal in VLBI observations, submitted to *JGR*, 2003.
- Rocken C., S. Sokolovskiy, J.M. Johnson and D. Hunt, Improved Mapping of Tropospheric Delays, *Journal of Atmospheric and Oceanic Technology*, Vol. 18, pages 1205-1213, 2001.
- Titov O., V. Tesmer and J. Boehm, Occam Version 5.0 Software User Guide, Auslig Technical Report 7, 2001.



# IVS Analysis and Data Center at BKG Works in 2002/2003

G. Engelhardt, V. Thorandt, and D. Ullrich

*Bundesamt für Kartographie und Geodäsie, Leipzig, Germany*

**Summary:** The analysis activities at the International VLBI Service for Geodesy and Astrometry (IVS) Analysis Center at Bundesamt für Kartographie und Geodäsie (BKG) can be divided into routine computations of earth orientation parameter (EOP) time series and topics for applied research. At BKG an update of the EOP time series was developed and first statements about accuracy and reliability were derived. The BKG has participated in the IVS Pilot Project - Tropospheric Parameters. The automated VLBI data analysis tools at BKG were improved. A first version of a new graphics tool called REPA (Residual plotting and ambiguity resolution) was developed for the VLBI Analysis Software Solve which is independent of a specific operating system.

The BKG Data Center continued the stable operation for archiving of all VLBI related data and for providing public access for the community in connection with the other IVS Primary Data Centers.

## 1 General information

The BKG VLBI Analysis Center is responsible for the computation of EOP time series and annual solutions to be submitted to the IVS and IERS (International Earth Rotation and Reference Systems Service).

The BKG group continued the generation of calibrated databases for the sessions correlated at the Bonn Astro/Geo Mark IV Correlator (e.g. R1, T2, OHIG, EURO) and submitted them to the IVS Data Centers for distribution. The EOP time series bkg00003 computed from 24 hour VLBI sessions were replaced by the series bkg00004 with all 24 hour sessions since 1984 suitable for EOP determination. From 1984.0 to 2003.3 altogether 2756 sessions of 24 hour observing time were processed. 955 UT1 intensive sessions with about 1 hour measurement duration were analysed for the period from 1999.0 to 2003.3 (bkgint02).

A new combined global solution with a data span from January 1984 to December 2001 was computed for submission to IVS and IERS.

At BKG the Mark-IV data analysis software system CALC/SOLVE, release of December 27, 2002 (Ref.[1]) is currently used for the VLBI data processing. In addition, an independent program environment for the CALC/SOLVE software is used for the pre- and post-interactive part of the EOP series determination. At BKG the CALC/SOLVE software is installed on a HP9000/280/1 workstation with the HP-UX10.20 operating system and also on another HP workstation with the HP-UX11.00 operating system.

## 2 The BKG EOP time series bkg00004 and bkgint02

In contrast to the series bkg00003 the new series bkg00004 is characterized by no fixed Terrestrial Reference Frame (TRF) and Celestial Reference Frame (CRF). The main parameters, i.e. station coordinates and velocities, radio source positions, and EOP are estimated in one global solution. Minimal constraints for the datum definition are applied to get:

- Zero net rotation and net translation for 26 selected station positions and velocities (Ref. [2]) with respect to ITRF2000 (Ref. [3])
- Zero net rotation for 212 defining sources with respect to ICRF-Ext.1 (Ref. [4]).

The station coordinates of the stations TIGOCONC and SVETLOE are estimated as local parameters in each session. A break for the station coordinate determination of the station GILCREEK was introduced after the earthquake on Sep. 3, 2002.

The UT1 time series bkgint02 is generated with fixed TRF (ITRF2000) and CRF (ICRF-Ext.1). Estimated parameter types are only UT1, station clock, zenith troposphere.

### 3 Further development topics

The graphics tool currently used in the SOLVE software called CNPLT for interactive editing of the observations is not transferable to other non-HP operating systems, e.g. LINUX. For this reason a new graphics tool for the SOLVE software had to be developed in preparation for a portation of SOLVE to LINUX. So a first version of a new graphics software REPA was developed by the BKG VLBI group and installed in the SOLVE software in parallel to the old program CNPLT.

The automated system to manage the data flow and analysis tasks currently running at the BKG IVS Data and Analysis Center has been improved for more stability in the operational process and reduction of errors in the sub-process.

The VLBI group of BKG has joined the IVS Pilot Project -Tropospheric Parameters (Figure 1). For that a new program for the transmission of the SOLVE tropospheric results to a special defined solution independent exchange format for tropospheric estimates (SINEX-TROP) was developed. The total and wet zenith delays, the horizontal gradients and the associated standard deviations for all IVS-R1 and IVS-R4 sessions since Jan. 1, 2002, have been submitted regularly in SINEX-TROP.

* KEYWORD	GENERAL	
ELEVATION CUTOFF ANGLE		5
DOWNW. OF LOW OBSERV.		NO
TERR. REFERENCE FRAME		ITRF2000
TRF FIXED		YES
DRY MAPPING FUNCTION		NIELL 96
WET MAPPING FUNCTION		NIELL 96
* KEYWORD	ZENITH DELAYS	
SAMPLING ZENITH DELAYS		3600 SEC
APRIORI HYDROST. DELAY		SAASTAMOINEN
APRIORI WET DELAY		NONE
ZENITH DELAY MODEL	CONSTR. PIECEW. LINEAR FUNCT.	
CONSTR. ZD OFFSET		NONE
CONSTR. ZD RATE		50 PSEC/HOUR
* KEYWORD	GRADIENTS	
SAMPLING GRADIENTS		86400 SEC
APRIORI GRADIENTS		NONE
GRADIENT MODEL		OFFSETS
CONSTR. GR OFFSET		0.5 MM
CONSTR. GR RATE		0.5 MM/DAY

Figure 1: Part of SINEX-TROP file of BKG with the solution description

## 4 Comparisons and assessment of the accuracy of the BKG EOP series

The comparisons between the BKG EOP series bkg00003 and bkg00004 with IERS C04 (Ref. [5]) amount to smaller Weighted Root Mean Square (WRMS) for the new series bkg00004 (Table 1).

Table 1: WRMS of the differences of the EOP series from BKG and IERS C04 derived from a straight-line model for fitting the data from 1999.0 to 2003.0

EOP component	Units	WRMS bkg00003-C04	WRMS bkg00004-C04
UT1-UTC	msec	0.0119	0.0108
X pole	mas	0.187	0.146
Y pole	mas	0.160	0.132
dpsi	mas	0.305	0.284
deps	mas	0.114	0.114

An independent assessment of the accuracy of the BKG EOP series is possible by comparing the results of the VLBI sessions of the NEOS to the CORE program observed on the same days. Assuming that the offset between the EOP results from both series should, on average, be zero, RMS differences from pair-wise measurements ( $s_1$ ) can be estimated (Table 2). Based on these values the reliability of the formal errors ( $s_2$ ) can be checked. As a result it can be stated that the solution strategy of bkg00004 yields a better agreement with the formal standard deviations in contrast to the one of bkg00003.

Table 2: Relations between  $s_1$  and  $s_2$  for EOP components derived from 32 NEOS and 32 CORE VLBI sessions on the same day (period from 1999 to 2000.5).

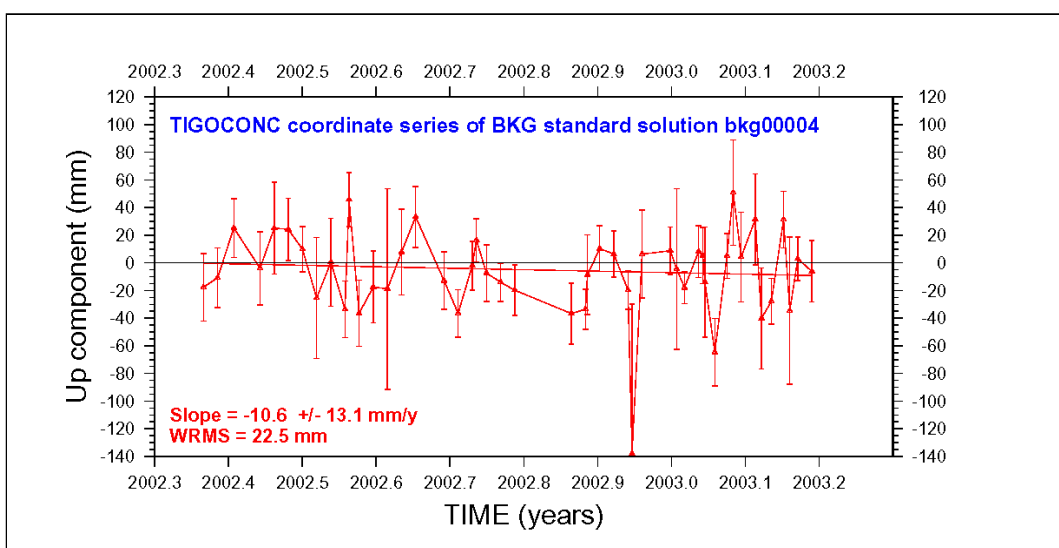
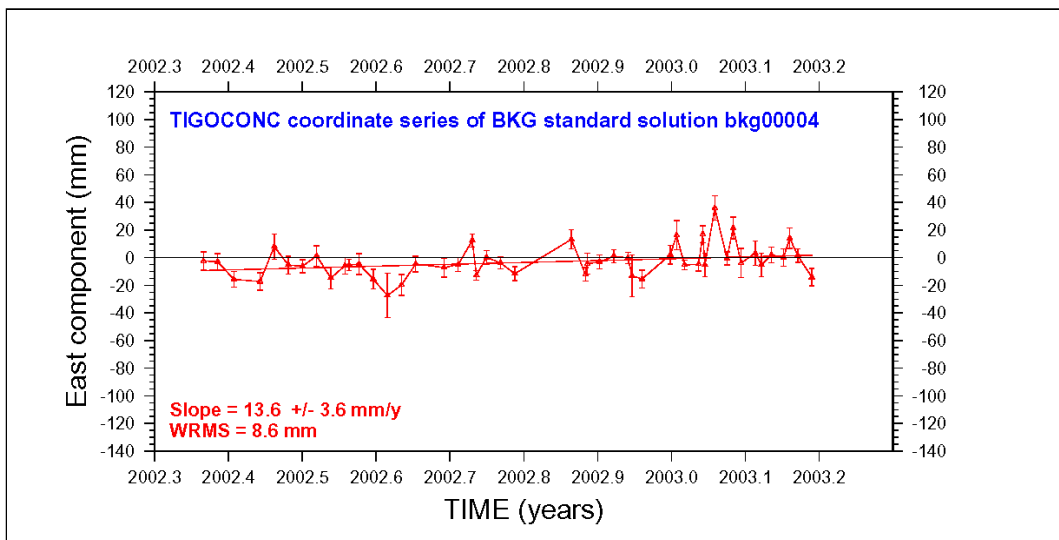
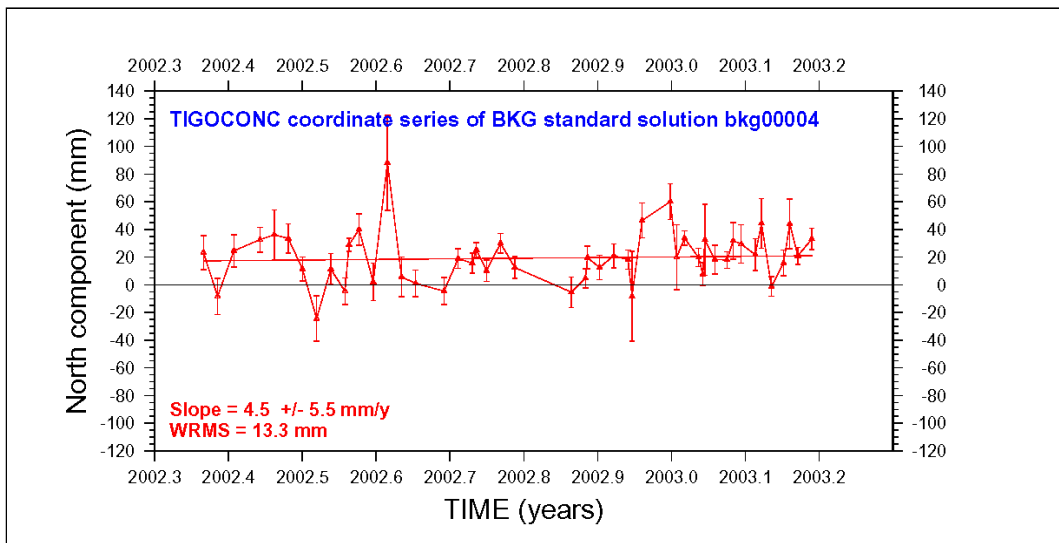
$s_1$ : standard deviation derived from pair-wise measurements (Ref. [6])

$s_2$ : mean formal standard deviation derived from the SOLVE adjustment

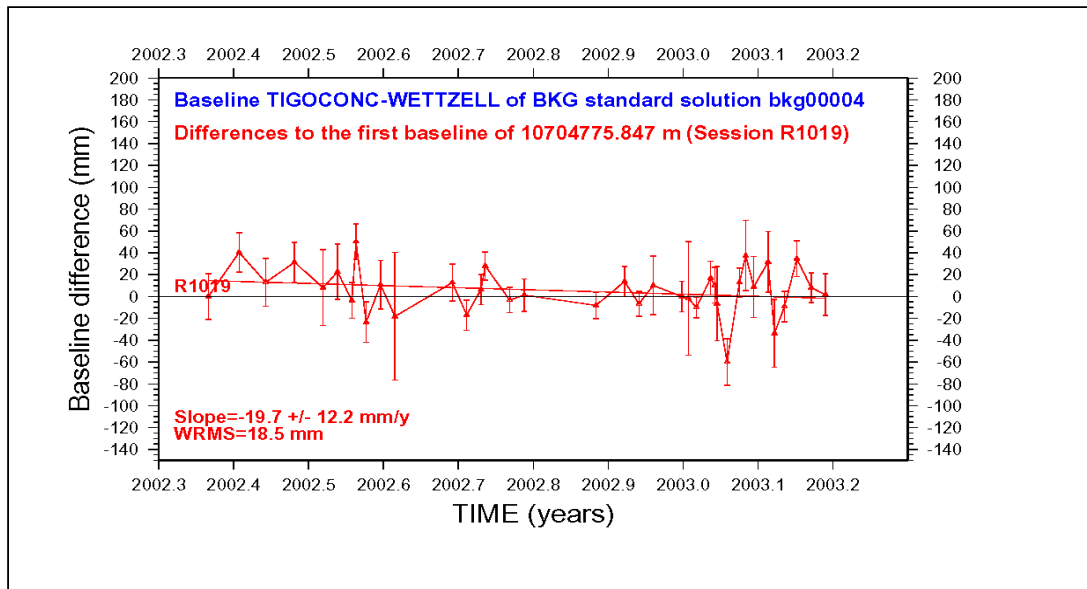
EOP component	Units	$s_1$ bkg00003	$s_1$ <sub>new</sub> bkg00004	$s_2$ bkg00003	$s_2$ <sub>new</sub> bkg00004	$s_1/s_2$ bkg00003	$s_1$ <sub>new</sub> / $s_2$ <sub>new</sub> bkg00004
UT1-UTC	msec	0.0123	0.0099	0.0064	0.0066	1.9	1.5
X pole	mas	0.276	0.266	0.163	0.166	1.7	1.6
Y pole	mas	0.157	0.157	0.135	0.138	1.2	1.1
dpsi	mas	0.335	0.337	0.189	0.234	1.8	1.4
deps	mas	0.129	0.119	0.073	0.089	1.8	1.3
mean relation						1.7	1.4

## 5 Results of the new station TIGOCONC (Chile)

By using a straight-line model for fitting the TIGOCONC coordinate series from May 13, 2002 to March 10, 2003, first velocity information about this station could be estimated (see graphics for north, east, up component of TIGOCONC). But only the velocity estimation for the east component is significant. The standard deviations for the other coordinate components north and up are larger than the estimated values. An improvement can be expected by increasing the coordinate series in future.



The accuracy (WRMS) derived from a straight line model for fitting the session-wise determined baseline lengths from each baseline with TIGOCONC, also called baseline length repeatability, is better than  $2 \times 10^{-9}$  (see an example graphic for the baseline TIGOCONC to the station WETTZELL).



## 6 Future plans

On the basis of our routine processing of new VLBI sessions further tests of the new graphic tool REPA are planned. Another important topic is the refinement of our solution strategy for the series bkg00004. That includes tests with the estimation of axis offsets, the estimation of local parameters for weakly determined sources, and the consideration of atmosphere loading models.

## References

- [1] GSFC, NASA (2002) Release of Mark-4 VLBI Analysis Software CALC/SOLVE from December 27, 2002 ([http://gemini.gsfc.nasa.gov/solve\\_root/release](http://gemini.gsfc.nasa.gov/solve_root/release)).
- [2] BKG (2003) Technical description of solution bkg00004.eops (<http://ivscc.gsfc.nasa.gov/service/bkg-products-eops.html>)
- [3] ITRF2000 (<http://lareg.ensg.ign.fr/ITRF/ITRF2000>)
- [4] ICRF-Ext.1 (<http://hpiers.obspm.fr/webiers/results/icrf/Icrf>)
- [5] IERS C04 EOP (<http://hpiers.obspm.fr/eop-pc>)
- [6] Gerald Engelhardt, Volkmar Thorandt, Dieter Ullrich (2001) The Current Status of the IVS Analysis Center at BKG. In: Dirk Behrend, Antonio Rius (ed) Proceedings of the 15<sup>th</sup> Working Meeting on European VLBI for Geodesy and Astrometry, September 7-8, 2001, Barcelona, Spain: pages 8-13



# Investigation of Atmospheric and Hydrological Loading by VLBI

G. Estermann and H. Schuh

*Institute of Geodesy and Geophysics (IGG), TU Vienna, Austria*

**Summary:** The small deformations associated with the response of the Earth to atmospheric and hydrological loading cause site-dependent vertical displacements with ranges up to  $\pm 30$ mm. Several new global and regional models of soil moisture, snow depths, and groundwater are now available and can be validated by space geodetic techniques. In this paper various atmospheric and hydrological loading models are compared with VLBI measurements. The paper mainly concentrates on vertical crustal motions on seasonal and interannual time scales. All NEOS-A sessions from 1996 to 2001 and also the CONT94 and CONT02 campaigns were used for this investigation. The correlation between VLBI station heights and sums of the various loading displacement models is still small ( $<0,3$ ) probably due to other unmodeled effects. However, the baseline length time series decrease when a priori loading corrections were applied.

## 1 Introduction

In the last decades space geodetic techniques such as VLBI (Very Long Baseline Interferometry), SLR (Satellite Laser Ranging), the GPS (Global Positioning System), and Doris (Doppler Orbitography and Radio positioning Integrated by Satellite) have proved to be very powerful for determining displacements of points on the solid Earth. These can be modeled by using various geodynamical parameters, e.g. the Love and Shida numbers in the model of the solid Earth tides and site-dependent amplitudes and phases of the ocean loading models. The temporal redistribution of oceanic, atmospheric, and hydrological masses perpetually loads and deforms the Earth's crust. Surface displacements, due to atmospheric mass circulation, are dominated by the effects of synoptic scale systems (1000 to 2000km wavelength) having periods of less than two weeks. Peak-to-peak vertical displacements of 10 to 20mm are common at mid-latitudes (Rappel and Zschau, 1985; van Dam and Wahr, 1987; Manabe et al., 1991). The effects are larger at higher latitudes due to the larger pressure variability found there. The maximum range in vertical crustal displacement due to atmospheric loading for the period 1994-1998 is plotted in Figure 1.

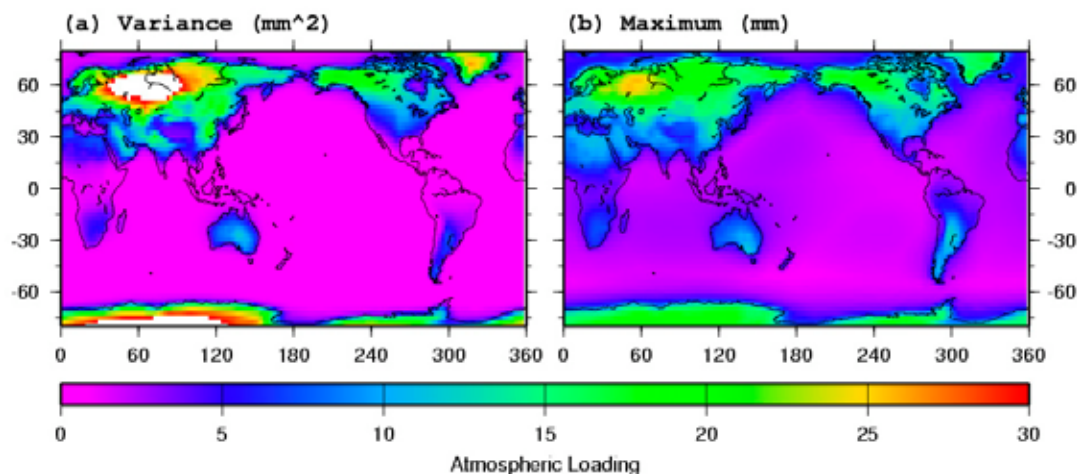


Figure 1: Maximum range and variance in vertical crustal displacement during 1994-1998 (mm) due to changes in atmospheric surface pressure (van Dam et al., 2002)

While surface displacements are largest for atmospheric pressure variations with periods of one to two weeks, annual signals are also existing having amplitudes between 0.5 and 3mm. At annual periods, variations in continental water storage become important, too.

Tidal and non-tidal motions of oceanic mass also contribute to the deformation spectrum at points on the Earth's surface. Variations in bottom pressure driven by uncompensated changes in sea surface heights can induce vertical deformations at coastal sites of up to 12mm with periods of approximately one month.

For all of these loading signals, the vertical deformations are larger than the horizontal ones by factor 3 to 10. Given the amplitude of the loading induced vertical crustal motion, it is necessary to evaluate the effects of loading on when interpreting geodetic data. Loading effects caused by the redistribution of surface masses have been observed in high-precision geodetic data for some time now (see for example, van Dam and Herring, 1994; van Dam et al., 1994; MacMillan and Gipson, 1994; Sun et al., 1995; Haas et al., 1997; Scherneck, 2000; and van Dam et al., 2001). As the results of space geodetic measurements are more and more being interpreted in terms of geodynamic processes (plate tectonics, post-glacial rebound, sea level rise, etc.) it is becoming necessary to remove loading effects from the geodetic data. In this paper, we compare various atmospheric and hydrological loading models with VLBI measurements.

## 2 Modeling loading effects of the Earth's crust

The main elements required in the computation of loading predictions include (1) an Earth model, which determines the geometry, with specific mechanical properties and if necessary, the rheology, and (2) a mathematical model for the surface load including the boundary conditions at the Earth's surface and the extension of the load. Selected parts of continuum mechanics can then be used to solve the boundary value problem to obtain the system's response to a unit load. For the problem of Earth deformation, the system's response is best described by Load Love Numbers (LLNs) which can be used to compute the Green's functions of the boundary problem.

For the actual computation of loading effects, surface load data are required for all relevant loads. These loads are then convolved with the Earth's response (either in the space or the wave number domain) to determine the loading effects (e.g. surface displacements, gravity variations, and geocenter displacements). Loading responses to non-tidal surface loads are normally computed in one of three ways:

- 1) Point loading approach in which a gridded surface mass is convolved with Green's functions to determine the load response;
- 2) Spherical harmonics approach in which the LLNs are used directly to carry out the convolution with a given surface load in the wave number domain. This approach requires the surface loads to be given as a spherical harmonic expansion;
- 3) Using a local regression coefficient determined by fitting local changes in pressure to the vertical component of observed deformation.

The point loading approach and the spherical harmonic approach can be called 'geophysical approaches' as they are both based on geophysical models. The local regression coefficient approach is an 'empirical approach'.

The approach chosen for calculating loading deformation usually depends on the proposed application. For example, if global loading corrections were desired for several years of high resolution loading data, the spherical harmonics approach would be preferred because of its computational speed. However, a potential problem arises when this approach is used for computing the effects of atmospheric pressure loading on an Earth model that includes an ocean. For simplicity an inverted barometer ocean model is usually applied. In an inverted barometer ocean, the pressure over the oceans is essentially zero. In this case, there is a discontinuity in the atmospheric pressure anomaly at all continental/ocean boundaries as the pressure goes from ambient over the continents to near zero over the oceans. This discontinuity is problematic when one tries to generate a spherical harmonics representation of the pressure. Large errors in the pressure field are introduced at coastal sites. Differences between the vertical displacement calculated using the point loading and spherical harmonics approach for an inverted barometer ocean can reach 1cm.

In the point loading approaches, the deformation at a point is determined by convolving a gridded representation of a global load of dimensions  $N \times M$  with elastic Green's function of dimensions  $N \times M$  and is thus computationally intensive.

The geophysical model approaches (point loading or spherical harmonics) for computing loading effects are based on a physical understanding of the way the pressure interacts with an elastic Earth model. The major advantage of the geophysical model approaches is that loading effects can be computed in a standardized way for any point on the Earth's surface more or less instantaneously. The geophysical model approaches currently suffer from a number of problems including the requirement of a global pressure data set, a minimum of 24 hours in time delay in the availability of the global pressure data set, limitations of the pressure data itself (low temporal and spatial resolution), uncertainties in the Green's functions, and uncertainties in the ocean response model.

In the empirical approach, site-dependent pressure loading effects are empirically computed by determining the fit of local pressure variations to the geodetic observation of the vertical crustal motion. In this case, the loading correction can be applied in quasi real-time and short-time site displacements due to rapidly changing pressure can be modeled.

A two-coefficients-approach has also been proposed (Rabbel and Zschau, 1985) which uses local barometric pressure  $p(t)$  and pressure variations in a surrounding area  $p_{2000\text{km}}$ :

$$\Delta U = -0.55(p_{2000\text{km}}(t) - p_{\text{Ref}}) - 0.35(p(t) - p_{\text{Ref}}) \quad (1)$$

A simple model using local barometric pressure  $p(t)$  and atmospheric loading coefficients  $\alpha$  for each station was proposed by Manabe et al. (1991):

$$\Delta U = \alpha \cdot (p(t) - p_{\text{Ref}}) \quad (2)$$

with  $p_{\text{Ref}}$  = reference pressure, e.g. mean of several years.

The empirical approach is likely to produce better results than the geophysical approaches for a given site but like the geophysical approaches, has a number of drawbacks as well.

- Geodetic observations have to be available for a certain period of time before a reliable regression coefficient can be determined; this period of time may be as large as several years.
- The regression coefficients cannot be extrapolated to a new site (for which no data exist);

- The regression coefficient has been observed to change with time and with observing technique;
- The regression coefficient can only be used for vertical crustal motions;
- It is uncertain that other pressure correlated geodetic signals are not being 'absorbed' into the regression coefficient determination. So while this approach would lower the scatter on a given geodetic time series the most, one would always be uncertain whether only atmospheric loading effects were being removed with the correlation coefficient.

### 3 Models used for loading computations

Here, we present various loading fields and look in detail at the computed loading effects in the vertical.

#### 3.1 Atmospheric loading

Since 1985 several studies on atmospheric loading have been carried out, e.g. by Rabbel and Zschau (1985), Rabbel and Schuh (1986), van Dam and Wahr (1987), Manabe et al. (1991), van Dam and Herring (1994), MacMillan and Gipson (1994), van Dam et al. (1994), Sun et al. (1995), Haas et al. (1997), Scherneck (2000).

Three basic methods for computing atmospheric loading corrections to geodetic data have been applied in the various references given above:

- 1) using geophysical models or simple approximations derived from these models (following schemes 1 or 2 described in section 2);
- 2) using empirical models based on site-dependent data (following scheme 3 described in section 2);
- 3) a hybrid method combining the two previous methods.

In a hybrid method (3), regression coefficients determined from a geophysical model instead of geodetic observations could be used to operationally correct observed vertical position determination from local air pressure alone. The vertical deformation caused by the change in pressure can then be given in terms of a local pressure anomaly. The regression coefficients can be determined by fitting local pressure to the vertical deformation predicted by the geophysical model. Regression coefficients determined in the manner would still suffer from both the uncertainty in the Green's functions and the quality of the air pressure data.

The data used for the atmospheric loading computations by van Dam and Crétaux - were taken from the National Center for Environmental Prediction (NCEP) reanalysis data set. This global data set is provided on a  $2.5^\circ \times 2.5^\circ$  global grid at 6 hour periods. Scherneck used the data provided by the European Centre for Medium-Range Weather Forecasts (ECMWF). The vertical displacements of the VLBI station Algonquin Park located in eastern Canada as modeled by the various authors are plotted in Figure 2.

At this site, we observe that peak-to-peak surface motions of 20mm are common. Displacements for the same period would be smaller for low altitude sites due to the smaller pressure variations found in the low to equatorial latitudes. Algonquin Park is located approximately 500km inland from the Atlantic ocean and is thus classified as a continental site (see Figure 3). Coastal sites at the same latitude would experience smaller atmospheric loading displacements due to the inverted barometer effect described in section 2.

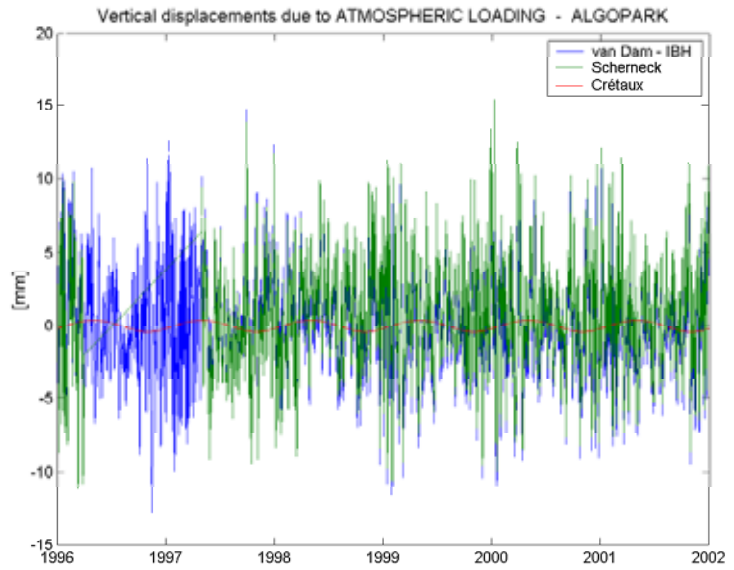


Figure 2: Vertical displacements due to atmospheric loading at Algonquin Park.

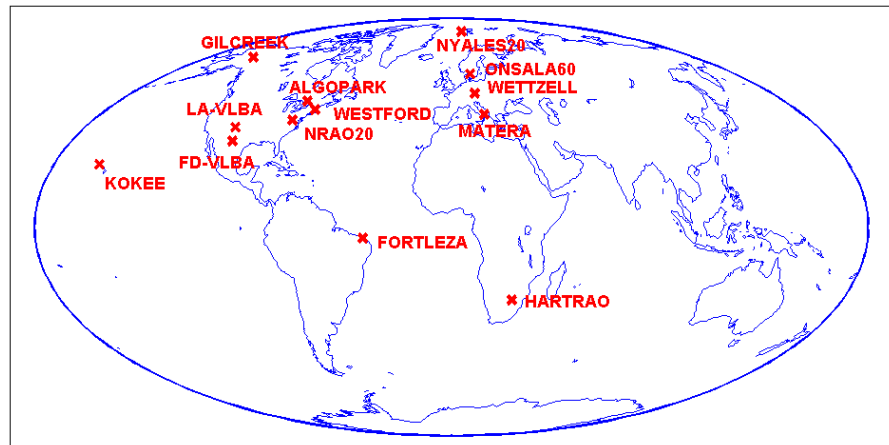


Figure 3: Global distribution of VLBI sites.

### 3.2 Hydrological loading

At annual periods, variations in continental water storage are significant. The modeled vertical displacements have ranges of up to 30mm, with root-mean-square values as large as 8mm; see Figure 4 (van Dam et al., 2002).

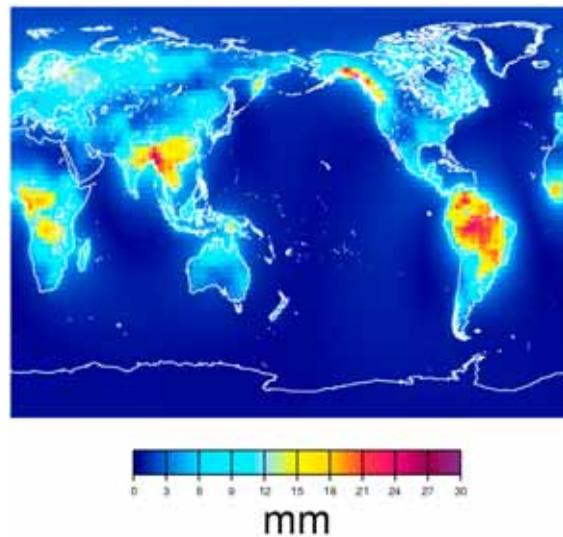


Figure 4: Maximum range in vertical crustal displacement during 1994-1998 (mm) due to changes in total continental water storage (van Dam et al., 2002)

### 3.1.1 Soil Moisture

Several new global models exist for soil moisture that were used for our study. These include

- Huang et al. (1996);
- Global Soil Wetness Project (GSWP), (Douville et al., 1999);
- Milly et al. (2002).

All models provide  $1^\circ \times 1^\circ$  gridded data of soil water in the upper layer of the ground (usually the top 2 meters) that we have interpolated to the position of the ground stations.

These models solve for a water balance equation of the form  $dw/dt = P - E - R$  (where  $w$  is soil water,  $t$  is time,  $P$  is precipitation,  $E$  is evapotranspiration, and  $R$  is runoff). In this approach, the forcing terms (precipitation and atmosphere landmass and energy fluxes) are derived from observations.

The annual displacements of Algonquin Park from each of these models are shown in Figure 5 covering a total range of 3mm. There is about a 2mm peak-to-peak difference in the annual component determined using the Huang model versus the Milly model. Current geodetic techniques can determine annual crustal motions to at least this accuracy, indicating that we may be able to use these techniques to refine the long-wavelength models of soil moisture variability.

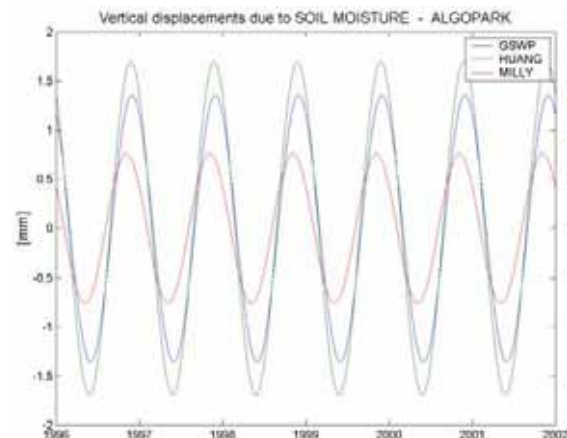


Figure 5: Vertical displacements due to soil moisture at Algonquin Park.

### 3.2.1 Snow cover

We compared vertical crustal motions predicted from the following models of snow cover:

- International Satellite Land Surface Climatology Project (ISLSCP, Meeson et al., 1995);
- Global Soil Wetness Project (GSWP, Douville et al., 1999);
- Milly et al. (2002).

The displacements were again modeled in terms of annual variations (see Figure 6) with a total range of 6mm. There is about a 2mm peak-to-peak difference in the annual component determined using the GSWP model versus the Milly model.

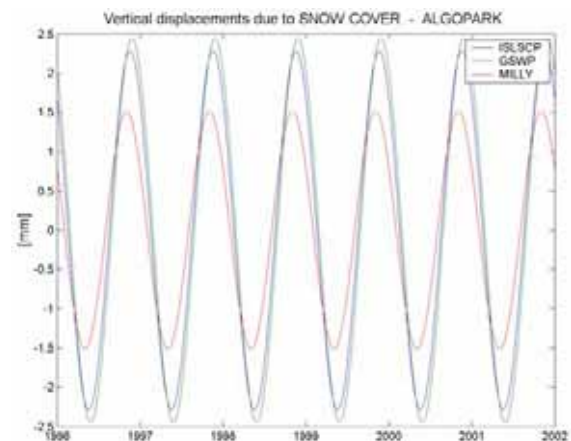


Figure 6: Vertical displacements due to snow cover at Algonquin Park.

### 3.3 Oceanic loading

Tidal and non-tidal motions of oceanic mass also contribute to the deformation spectrum at points on the Earth's surface.

#### 3.3.1 Ocean tide loading

Computation of ocean tidal loading requires two ingredients, namely ocean tidal models describing the load and Earth models, on which the load acts. For ocean tide loading the parameters provided by Scherneck et al. (2000), from his Web-based ocean loading service were used (<http://www.oso.chalmers.se/~loading>). The Green's functions are from Farrell (1972) and the Gutenberg-Bullen A Earth model was used; 11 tides were considered.

#### 3.3.2 Non-tidal oceanic loading

For non-tidal oceanic loading data were taken from TOPEX/Poseidon (T/P) and from the Parallel Ocean Climate Model (POCM, Johnson et al., 1999). From Figure 7 it can be seen that the agreement between the two models is rather poor but the effect itself is very small.

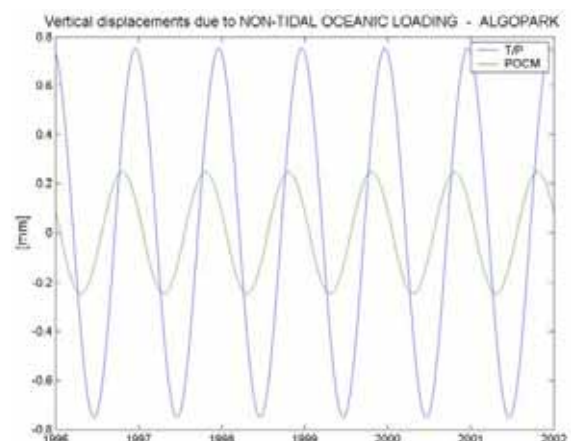


Figure 7: Vertical displacements due to non-tidal oceanic loading at Algonquin Park.

### 3.4 Special Bureau for Loading (SBL)

On 1 February 2002, the Special Bureau for Loading (SBL) was established within the Global Geophysical Fluid Center (GGFC) of the IERS (see <sup>1</sup>). The main task of the SBL is to provide loading displacements for geodetic users on an operational and regular basis.

<sup>1</sup> <http://www.sbl.statkart.no/>

## 4 Investigation of loading effects by VLBI

Considering the accuracies of a few mm that are going to be achieved by high precision global geodetic measurements, it becomes quite clear, that loading displacements have to be taken into account when analyzing space geodetic data.

### 4.1 VLBI data analysis

In the investigations reported here, all NEOS-A sessions (weekly VLBI measurements, each 24h with 5-7 stations) from January 1996 to December 2001 were analyzed and also the CONT02 session covering a continuous period of 15 days in October 2002. In a first solution following the standard procedure of VLBI analysis no a-priori loading corrections were applied. In the least-squares fit a free network solution was done for each 24h VLBI session to determine baseline lengths; then a second solution was carried out, constraining the horizontal coordinates to ITRF2000 and estimating the vertical coordinates (i.e., station heights), only. These two solutions will be called 'reference' in the following sections.

The VLBI Software package OCCAM (V 5.1) was used for the analysis of the VLBI data. It has been developed by European VLBI groups since 1983 and is applied by six IVS Analysis Centers (three of them are operational Analysis Centers). It can be applied under MS/DOS and Unix or Linux and is a very flexible VLBI program (Titov et al., 2001).

#### 4.1.1 Correlation coefficients

Various sums of the loading effects were computed for the same time epochs in which the VLBI estimates were determined considering several combinations of the different models described in section 3 (see Table 1). As an example the VLBI station heights for Algonquin Park are plotted in Figure 8. During some time intervals the agreement between model and observed station heights is quite good but there are also time intervals when the correspondence is very poor probably because the VLBI estimates are biased by other effects such as unmodeled tropospheric bending. Now, the correlation coefficient between the 'reference' and the modeled loading displacements in terms of various sums of the loading effects were calculated for all VLBI stations. For most of the stations the correlation is very weak with correlation coefficients of less than 0.3, what is probably due to insufficient models used for other effects which influence the vertical station coordinates.

Table 1: Sum of loading effects.

sum of loading effects	atmospheric loading effect	snow cover loading effect	soil moisture loading effect	non-tidal oceanic loading effect
sum 1	van Dam IBH	MILLY	MILLY	T/P
sum 2	van Dam IBH	GSWP	GSWP	T/P
sum 3	van Dam NIBH	ISLSCP	HUANG	T/P
sum 4	van Dam NIBH	ISLSCP	HUANG	POCM
sum 5	Crétaux	MILLY	MILLY	T/P
sum 6	Scherneck	MILLY	MILLY	T/P
sum 7	Scherneck	GSWP	GSWP	T/P
sum 8	Scherneck	MILLY	MILLY	POCM
sum 9	Scherneck	GSWP	GSWP	POCM

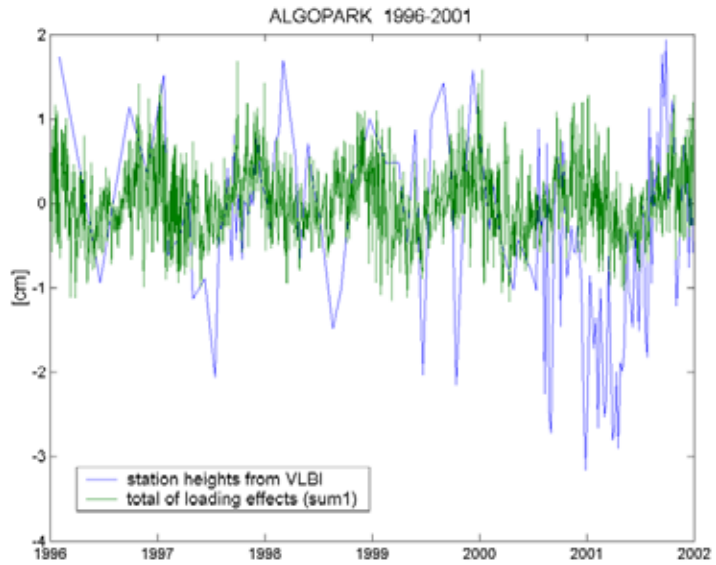


Figure 8: Station heights from VLBI and sum of loading effects at Algonquin Park.

#### 4.1.2 VLBI station heights and baseline lengths

Now, the VLBI analyses were repeated with a-priori loading corrections applied. Again all NEOS-A sessions from January 1996 to December 2001 were analyzed. The station heights and baseline lengths were determined and compared with the results of the first, uncorrected ‘reference’ solution by computing the scatter around the mean station heights and around straight-lines fitted to the baseline lengths. The histograms in Figure 9 and Figure 10 represent the number of VLBI sessions with improved repeatabilities. Improvements of the station heights and baseline lengths when correcting for loading effects were obtained in 64% of all combinations of loading models treated here. The average positive improvement is 3 to 4% never exceeding 13%. If the improvement is negative it is less than 1% on the average.

Considering all of the stations there is not one combination of the loading models that seems to be superior to the others. From this, it can be concluded that the existing mass loading models that were described in section 3 and were used for this study still have deficiencies on several regions of the globe.

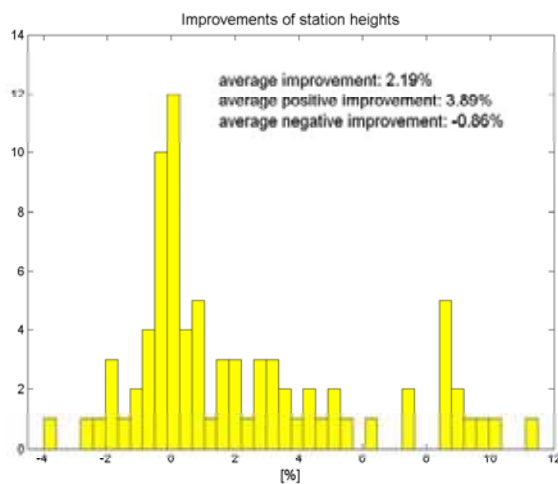


Figure 9: NEOS-A Sessions: Number of improved repeatabilities of station heights

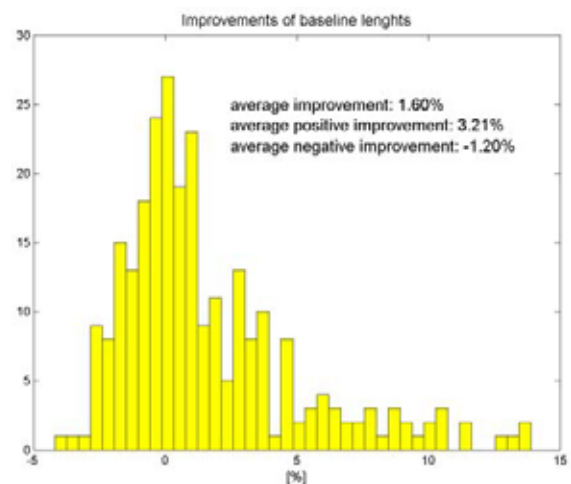


Figure 10: NEOS-A Sessions: Number of improved repeatabilities of baseline lengths.

The CONT02 campaign was a VLBI session observing 15 days continuously in October 2002. The goal of CONT02 was to acquire the best possible state of the art VLBI data over a two-week period to demonstrate the highest accuracy of which VLBI is capable.

For these sessions only displacements due to atmospheric loading computed by Scherneck were available. As for the NEOS-A sessions, the station heights and baseline lengths were determined. The results of the first “uncorrected” version were compared with the VLBI results where the atmospheric loading displacements were applied a priori. For these analyses the tropospheric mapping function NMF (Niell, 1996) was used first. Then the computations were repeated with the new tropospheric mapping function IMF (Niell, 2001) in order to test the influence of the chosen mapping function when investigating atmospheric loading.

Table 2 and Table 3 give standard deviations in [cm] representing the repeatability around a mean station height and around a straight-line fitted to the estimated baseline lengths. Each first column gives the repeatabilities of the reference solution where no loading corrections were applied. Improved repeatabilities of the station heights and baseline lengths when correcting for loading effects were obtained in about 75% of all combinations of loading models treated here. The repeatabilities improve at an average of 11% when applying the atmospheric loading displacements and using the NMF. When using the IMF the repeatabilities improve even by 17% on the average.

The results of all investigations are summarized in Table 4, which includes the statistics of the CONT94 campaign, a continuous session in January 1994. It is evident that in particular for the very precise CONT-sessions it is worth applying loading corrections to improve the quality of the geodetic results.

Table 2: CONT02 session: Repeatabilities of the station heights in [cm]; improvements are indicated by red figures.

VLBI station	NMF		IMF	
	reference	with atm. load.	reference	with atm. load.
ALGOPARK	0,51	0,40	0,52	0,40
GILCREEK	0,81	0,75	0,82	0,68
HARTRAO	1,40	1,41	1,47	1,47
KOKEE	1,08	1,08	1,04	1,04
NYALES20	0,74	0,74	0,82	0,66
ONSALA60	1,19	1,09	1,04	0,92
WESTFORD	0,74	0,60	0,65	0,54
WETTZELL	1,05	0,96	0,99	0,84

Table 3: CONT02 session: Repeatabilities of the baseline lengths in [cm]; improvements are indicated by red figures (continued on next page).

Baseline	NMF		IMF	
	reference	with atm. load.	reference	with atm. load.
ALGOPARK GILCREEK	0.54	0.54	0.58	0.57
ALGOPARK HARTRAO	1.51	1.54	1.54	1.56
ALGOPARK KOKEE	0.90	0.92	0.92	0.93
ALGOPARK NYALES20	0.66	0.66	0.59	0.60
ALGOPARK ONSALA60	0.99	0.99	0.91	0.91
ALGOPARK WESTFORD	0.22	0.23	0.22	0.23
ALGOPARK WETTZELL	0.67	0.64	0.65	0.60
GILCREEK HARTRAO	1.37	1.32	1.41	1.35
GILCREEK KOKEE	0.33	0.32	0.35	0.33
GILCREEK NYALES20	0.36	0.36	0.37	0.35
GILCREEK ONSALA60	0.82	0.80	0.79	0.75
GILCREEK WESTFORD	0.45	0.42	0.45	0.41
GILCREEK WETTZELL	0.69	0.62	0.68	0.59

Table 3 (continued)

Baseline	NMF		IMF	
	reference	with atm. load.	reference	with atm. load.
HARTRAO KOKEE	1.73	1.75	1.82	1.85
HARTRAO NYALES20	1.14	1.10	1.18	1.12
HARTRAO ONSALA60	1.03	1.00	0.99	0.94
HARTRAO WESTFORD	1.08	1.10	1.11	1.13
HARTRAO WETTZELL	0.80	0.77	0.79	0.74
KOKEE NYALES20	0.52	0.51	0.56	0.54
KOKEE ONSALA60	1.17	1.14	1.11	1.06
KOKEE WESTFORD	0.58	0.54	0.54	0.52
KOKEE WETTZELL	0.87	0.83	0.87	0.79
NYALES20 ONSALA60	0.48	0.48	0.46	0.45
NYALES20 WESTFORD	0.37	0.37	0.37	0.36
NYALES20 WETTZELL	0.35	0.32	0.33	0.29
ONSALA60 WESTFORD	0.56	0.55	0.55	0.56
ONSALA60 WETTZELL	0.35	0.34	0.34	0.33
WESTFORD WETTZELL	0.34	0.32	0.32	0.30

Table 4: Percentage of improved baseline lengths and station heights (%) and average positive improvements ( $\emptyset$ ).

	NEOS-A		CONT 94		CONT 02	
	%	$\emptyset$	%	$\emptyset$	%	$\emptyset$
<b>Baseline lengths</b>	<b>64</b>	<b>3,3</b>	<b>71</b>	<b>12</b>	<b>71 / 75</b>	<b>3,7 / 5,2</b>
<b>Station heights</b>	<b>64</b>	<b>3,9</b>	<b>43</b>	<b>25</b>	<b>75 / 75</b>	<b>10,7 / 16,8</b>

## 5 Conclusions

Non-tidal loading effects are in the range of  $\pm 10$  to 30mm and should be corrected when analyzing space geodetic data which are intended to reach an accuracy of a few mm. So far, only weak correlation ( $< 0.3$ ) between VLBI station heights and modeled radial loading displacements can be observed. When applying a-priori corrections due to loading the scatter around the mean station heights and the baseline lengths decreases for most of the stations. The improvements are the bigger the more precise the VLBI observables are and the better the tropospheric refraction is modeled. However, it is obvious, that further improvements of loading models are needed, in particular by using better global models for snow and soil moisture.

## Acknowledgements

We are grateful to T. van Dam, ECGS, J.-F. Crétau, LEGOS/GRGS/CNES, and H.-G. Scherneck, OSO, for providing their loading displacements of particular VLBI sites.

## References

Douville, H., Bazile, E., Caille, P., Giard, D., Noilhan, J., Peirone, L., and Taillefer F. (1999). Global Soil Wetness Project: Forecast and assimilation experiments performed at Météo-France. J. Meteor. Soc. Jap., Vol.77, pp.305-316.

- Farrell, W.E. (1972). Deformation of the Earth by surface loads. *Rev. Geophys. Space Phys.*, No.10, pp.761-797.
- Haas, R., Scherneck, H.-G., and Schuh, H. (1997). Atmospheric loading corrections in geodetic VLBI and determination of atmospheric loading coefficients. In: *Proceedings of the 12th Working Meeting on European VLBI for Geodesy and Astronomy*, Hønefoss, Norway, 12-13 September 1997, edited by B. R. Pettersen, pp.111-121.
- Huang, J., van den Dool, H., and Georgakakos, K.P. (1996). Analysis of Model-Calculated Soil Moisture over the United States (1931-1993) and Application to Long-Range Temperature Forecasts. *Journal of Climate*, Vol.9, No.6, pp.1350-1362.  
<http://www.cpc.ncep.noaa.gov/soilmst/paper.html>
- Johnson, T.J., Wilson, C.R., and Chao, B.F. (1999). Oceanic angular momentum variability estimated from the Parallel Ocean Climate Model, 1988-1998. *JGR*, Vol.104, pp.25183-25196.
- MacMillan, D.S. and Gipson, J. M. (1994). Atmospheric pressure loading parameters from very long baseline interferometry observations. *JGR*, Vol.99, pp.18081-18087.
- Manabe, S., Sato, T., Sakai, S., and Yokoyama, K. (1991). Atmospheric loading effect on VLBI observations. In: *Proceedings of the AGU Chapman Conference on Geodetic VLBI: Monitoring Global Change*, NOAA Tech. Rep. NOS 137 NGS 49, pp.111-122.
- Meeson, B.W., Corprew, F.E., McManus, J.M.P., Myers, D.M., Closs, J.W., Sun, K.J., Sunday, D.J., and Sellers, P.J. (1995). ISLSCP Initiative I - Global data sets for land-atmosphere models, 1987-1988, Published on CD-ROM by NASA.
- Milly, P.C.D., Shmakin, A.B., and Dunne, K.A. (2002). Global Modeling of Land Water Balances: The Land Dynamics Model (LaD). *Journal of Hydrometeorology* Vol.3, pp.283-299.
- Niell, A. E. (1996). Global mapping functions for the atmosphere delay at radio wavelengths. *JGR*, Vol. 101, No. B2, pp.3227-3246.
- Niell, A. E. (2001). Preliminary evaluation of atmospheric mapping functions based on numerical weather models. *Phys. Chem. Earth* 26, pp.475-480.
- Rabbal, W. and Schuh, H. (1986). The influence of atmospheric loading on VLBI experiments. *J. Geophys.*, Vol.59, pp.164-170.
- Rabbal, W. and Zschau, J. (1985). Static Deformations and gravity changes at the Earth's surface due to atmospheric loading. *J. Geophys.*, Vol.56, pp.81-99.
- Scherneck, H.-G. (2000). HGS Air Pressure Loading.  
<http://www.oso.chalmers.se/~hgs/apload.html>
- Scherneck, H.-G., Haas, H., and Laudati, A. (2000). Ocean Loading Tides For, In, and From VLBI. *Proc. First IVS General Meeting*, Kötzing, edited by N. Vandenberg and K. Baver, pp.257-262.
- Sun, H.P., Ducarme, B., and Dehant, V. (1995). Effect of the atmospheric pressure on surface displacements. *J. Geodesy*, Vol.70, pp.131-139.
- Titov, O., Tesmer, V., and Böhm, J. (2001). Version 5.0 of the OCCAM VLBI software. User Guide. AUSLIG Technical Reports 7, AUSLIG, Canberra.

- van Dam, T.M., Blewitt, G., and Heflin, M.B. (1994). Atmospheric Pressure Loading Effects on GPS Coordinate Determinations. *JGR*, Vol.99, pp. 23939-23950.
- van Dam, T.M. and Herring, T.A. (1994). Detection of Atmospheric Pressure Loading using Very Long Baseline Interferometry Measurements. *JGR*, Vol.99, pp.4505-4517.
- van Dam, T.M., Wahr, J.M., Milly, P.C.D., Shmakin, A.B., Blewitt, G., Lavallee, and Larson, K. (2001). Crustal displacements due to continental water loading. *Geophys. Res. Lett.*, Vol.28(4), pp.651-654.
- van Dam, T.M. and Wahr, J.M. (1987). Displacements of the Earth's Surface Due to Atmospheric Loading: Effects on Gravity and Baseline Measurements. *JGR*, Vol.92, pp.1281-1286.
- van Dam, T.M., Plag, H.-P., Francis, O., and Gegout, P. (2002). GGFC Special Bureau for Loading: Current Status and Plans. IERS Workshop, Nov. 2002, Munich.



# The K4 Intensive project 2002 for UT1 determination

D. Fischer<sup>1</sup>, A. Nothnagel<sup>1</sup>, R. Kilger<sup>2</sup>, W. Schlüter<sup>2</sup>, S. Kurihara<sup>3</sup>, and  
K. Takashima<sup>3</sup>

<sup>1</sup>*Geodetic Institute, University of Bonn, Germany*

<sup>2</sup>*Bundesamt für Kartographie und Geodäsie, Fundamentalstation Wettzell, Germany*

<sup>3</sup>*Geographic Survey Institute, Tsukuba, Japan*

**Summary:** Between July and December 2002 twenty short duration experiments have been carried out on the baseline Wettzell (Germany)-Tsukuba (Japan) using the K4 technology. The project was designed as a test series towards regular precise UT1 determinations and as an independent control of the existing Intensive observation series (Wettzell - Kokee Park (USA/Hawaii)). Numerous tests have shown a high sensitivity of short duration experiments for the geometry of schedules. Standard analyses show comparable results of both Intensive series and similar accuracy levels. Investigations have been made concerning the benefit of tropospheric path delays derived by GPS for the analysis of short duration VLBI experiments.

## 1 The project

The K4 Intensive project 2002 is a joint project of the Bundesamt für Kartographie und Geodäsie (BKG, Germany), the Geographic Survey Institute (GSI, Japan) and the Geodetic Institute of the University of Bonn (GIUB, Germany). It was established as complement and independent control of the existing Mark 4/5 Intensives by using K4 equipment on the baseline Wettzell (Germany) - Tsukuba (Japan). Schedules have been prepared at GIUB in Bonn and the correlation has been done at GSI in Tsukuba.

The baseline Wettzell - Tsukuba shows a long east-west extent but is about 1900 km shorter than the Mark 4/5 Intensive baseline Wettzell - Kokee Park. Nevertheless, it may be expected that the UT1 results of both baselines are of comparable quality.

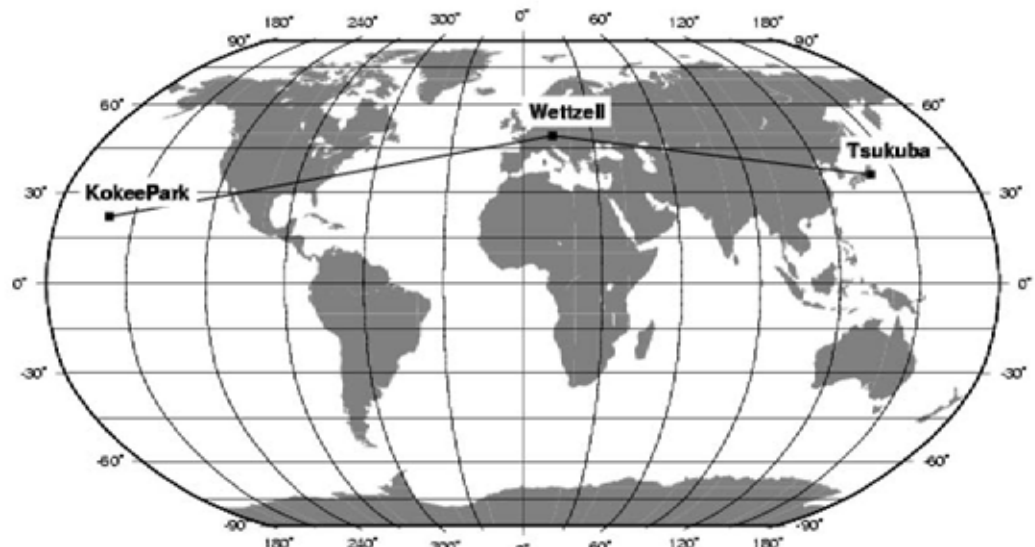


Figure 1: Both baselines of Intensive observations

Due to restricted observing times at both telescopes a quasi daily sequence of sessions has not been feasible. As a compromise one session per week was planned to end up with a more or less regular series. From July 1<sup>st</sup> to December 19<sup>th</sup> twenty experiments have been carried out, each containing 20 scans and lasting about one hour. The start time was fixed to 07:30 UT. The minimum scan duration has been set to 120 seconds and was extended if necessary for reaching the minimum SNR of 25 for X band and 20 for S band. The minimum elevation angle has been set to 10°.

## 2 Scheduling of short duration observations

The scheduling of each experiment has been done manually using the SKED program (Vandenberg, 1999). The geometry of the observations has been checked by displaying the observable sources in sky plots for each station.

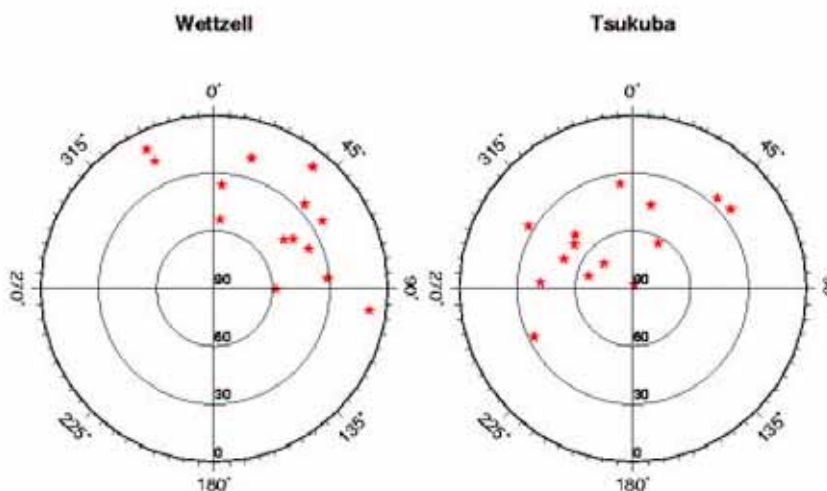


Figure 2: Simultaneously visible sources on July 1<sup>st</sup>, 2002 at the beginning of the experiment (07:30 UT)

The sky coverage of simultaneously visible sources is fairly poor and only up to one third of the full working range of each telescope is covered with observable sources (e.g. Fig. 2). It is also clearly visible that the quantity of sources with elevations below 20° is very small for Tsukuba in this example which weakens the estimation of the tropospheric path delay significantly.

A large number of test schedules has been prepared and rated by the simulated accuracies received from the normal equation matrix which can be created just from the geometry of each schedule. These tests led to a couple of conclusions which helped to generate the schedules for all twenty experiments:

- Short duration schedules with only twenty scans react very sensitive to the selection of sources. Replacing one scan in some cases changed the simulated accuracies for one or all unknown parameters significantly.
- The occurrence of scans with low elevations is absolutely necessary for the estimation of tropospheric path delays and already one single low elevation scan below 20° improves the simulated accuracy for the tropospheric delay considerably.

- The estimation of UT1-UTC itself does not seem to be influenced directly by the existence of low elevation observations.
- Sources near the equator may improve the sensitivity for UT1 and should be included in the schedule if possible. Nevertheless, experiments without any equatorial sources may still lead to reasonable UT1 results.
- To reach uniform sensitivity for all unknown parameters a well balanced sky coverage is needed and the short duration schedules have to be prepared carefully. Longer slew times should be accepted to allow relatively big changes in spatial direction from one scan to the next.

### 3 Analysis and results

The 20 experiments of 2002 were analyzed using the latest version of the Mark 4 VLBI analysis software package (SOLVE program release of 2002.12.27; revision of 2003.01.16).

Because of the low number of about twenty observations per experiment only a minimal number of parameters can be estimated. Introduced as unknowns were clock offset and rate, atmospheric path delays for both stations and UT1-UTC. Thus, five unknown parameters had to be estimated from a maximum of only twenty observations (see Tab. 1).

Table 1: Analysis procedures

	Standard	Advanced (?)
Software	Calc/Solve	Calc/Solve
Coordinates and Polar Motion	Fixed to the solution of GSFC	Fixed to the solution of GSF
Parameterization	Clock offset and rate, Atm for Ts and Wz, UT1-UTC	Clock offset and rate, - UT1-UTC
Redundancy	$20 - 5 = 15$	$20 - 3 = 17$
Dry part of tropospheric path delay	Modified Saastamoinen model ( <i>Davis et al., 1985</i> )	Modified Saastamoinen model ( <i>Davis et al., 1985</i> )
Wet part of tropospheric path delay	Estimated from observations	Fixed to wet path delay of IGS
Mapping	Niell Dry and Wet Mapping Functions	Niell Dry and Wet Mapping Functions

For visualization and evaluation, UT1-UTC values of the IERS C04 series (*IERS, 2003*) have been subtracted before plotting the results in figure 3. A quadratic interpolation has been used to calculate C04 UT1-UTC values referring to the reference epochs of the VLBI experiments.

The results of the K4 Intensives fit quite well to those observed on the Wettzell - Kokee Park baseline. On average they show similar error bars and a similar scatter. Table 2 shows a short statistical comparison of both Intensive series. For calculation of these numbers all successful experiments of both Intensive series between July 1st and December 19th were used.

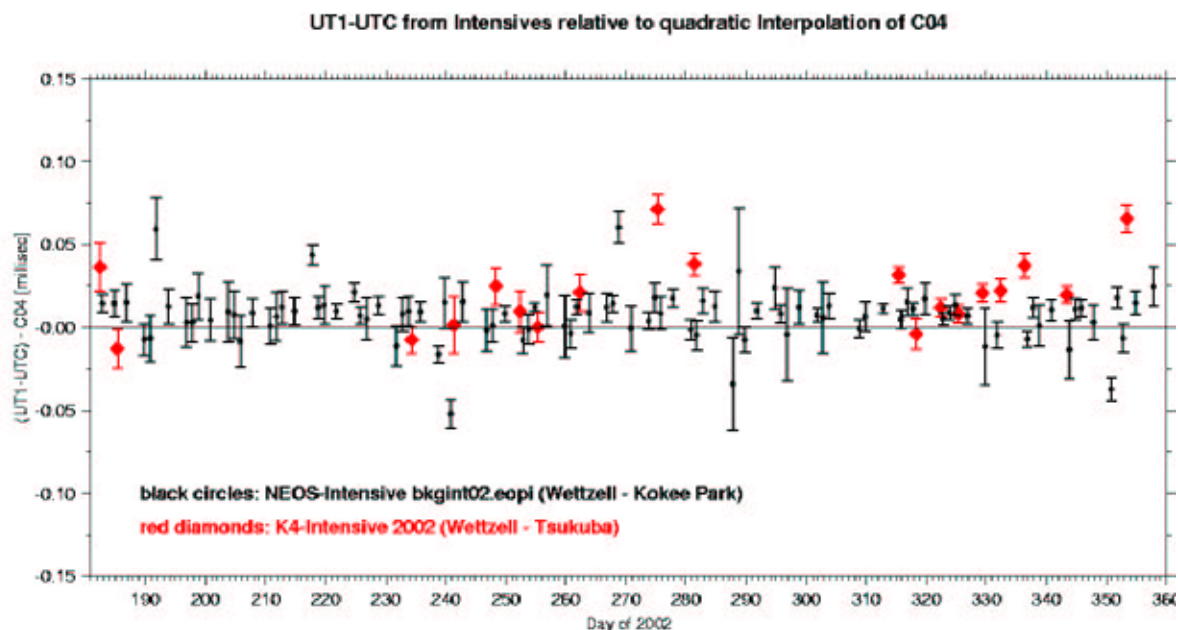


Figure 3: UT1-UTC results of both Intensive series.

Table 2: Overview of statistics.

	<b>K4-Intensives (Int2)</b> Wetzell - Tsukuba	<b>NEOS-Intensives (Int1)</b> Wetzell - Kokee Park
Number of successful experiments between 2002/07/01 and 2002/12/19	19	95
Number of successful scans per experiment in average	15 to 20 (Avg. 17.3)	14 to 20 (Avg. 17.0)
Bias relative to C04	$22.3 \mu s$	$8.1 \mu s$
WRMS of UT1-UTC after removal of bias relative to C04	$19.4 \mu s$	$11.4 \mu s$
Mean standard deviation of UT1-UTC estimates	$8.8 \mu s$	$10.0 \mu s$
Time needed for shipping and correlation	4-9 workdays	3-4 workdays

The difference in bias relative to C04 is not critical and may be induced by different station coordinates used. While the mean standard deviation is almost equal for both series, the WRMS of UT1-UTC differs quite significantly. However, this effect is possibly due to the smaller number of experiments of the K4 Intensives in 2002. Up to now the results are quite promising and a good indicator for the equality of the K4 Intensive series.

## 4 Investigations concerning the tropospheric path delay

For external determination of the tropospheric path delay one may profit from the fact that GPS signals are affected by the troposphere in the same way as VLBI observations. If the influence of troposphere is introduced from external measurements, the number of unknowns will be reduced by two in the VLBI Intensive analysis and the redundancy will increase (see Tab. 1).

In a first attempt the official IGS total zenith delay product was used and introduced as external information into the VLBI analysis. Since only the wet part is of interest, the dry part has been subtracted using air pressure and station height (cf. *Davis et al., 1985* and *Rioja and Tomasi, 1999*). The individual observations have been corrected for tropospheric

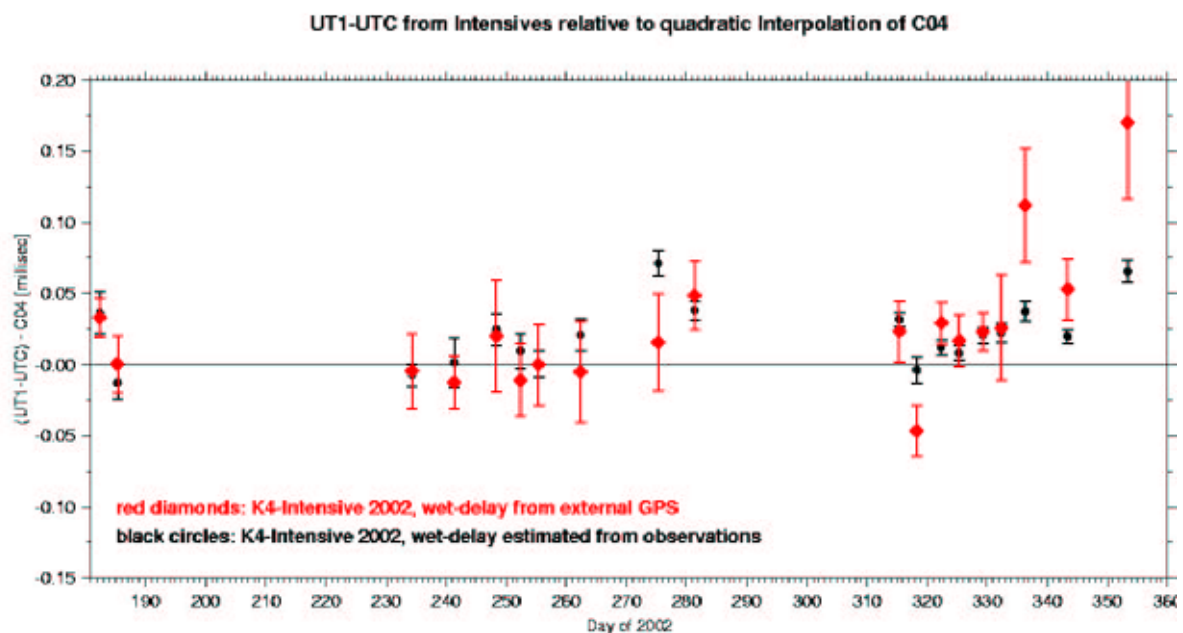


Figure 4: UT1-UTC results of standard analysis and with fixed external GPS zenith path delays.

Figure 4 shows the UT1-UTC results after fixing the wet tropospheric path delay to IGS values. Compared to the results of the standard analysis the lengths of error bars increase significantly when fixing the troposphere. This effect has not been expected and may be an indicator for a disagreement of the tropospheric delay estimated in the GPS analysis and that from VLBI. In addition the estimated tropospheric delay within the VLBI analysis covers other unmodeled influences that are not represented by the external GPS troposphere.

Nevertheless, there are some experiments (e.g. days 185, 262, 275) where the external tropospheric information improved the UT1 estimation visibly which is quite promising for the success of this approach. However there are also at least the same number of experiments (e.g. days 336, 343, 353) with the adverse effect. Further investigations are pending.

## 5 Conclusion and Outlook

The results of the K4 sessions observed in 2002 are very promising. From the good quality of the individual sessions it can be concluded that this series may perform as well as the Wettzell - Kokee Park (Mark 4/5) series if it is observed as frequently.

The continuation of the project started on April 12th, 2003 with regular experiments on Saturdays. Thus, the K4 Intensives will close the gaps of the Wettzell - Kokee Park Intensives and both series will perfectly complement each other. As soon as unattended observations are possible in Wettzell observations on Sundays will be added.

Further investigations will also be made concerning the use of GPS wet delays. Special GPS solutions for the purpose of determining the wet delay at Tsukuba and Wettzell may be a key to improved results.

## References

- Casse, J.L., "The European VLBI Network MkIV Data Processor," in *Proceedings of the 4<sup>th</sup> EVN/JIVE Symposium*, eds. M.A. Garrett, R.M. Campbell, & L.I. Gurvits, *New Astron. Rev.*, **43**, 503–508, 1999.
- Davis J., T.A. Herring, I.I. Shapiro, A.E.E. Rogers, G. Elgered (1985): *Geodesy by Radio Interferometry: Effects of atmospheric modelling errors on estimates of baseline length*. *Radio Science*, Vol. 20, 1593–1607
- IERS (2003): Data publically available under <sup>(1)</sup>.
- Niell A.E. (1996): *Global mapping functions for the atmosphere delay at radio wavelengths*. *J. of Geophys. Res.*, Vol. 101, No. B2, 3227–3246
- Nothnagel A., G. Engelhardt, H. Hase, R. Kilger, S. Ogi, K. Takashima, V. Thorandt, D. Ullrich (2000): *First Results of the 1999 Tsukuba - Wettzell UT1 Test Series*. 2000 General Meeting Proceedings, International VLBI Service for Geodesy and Astrometry, Kitzting, Febr. 21–24, 2000
- Rioja M., P. Tomasi (1999): *Integrating GPS zenith path-delay measurements into the analysis of geodetic VLBI observations from the European network*. 13th Working Meeting on European VLBI for Geodesy and Astrometry Proceedings, Viechtach/Wettzell, Febr. 12–13, 1999
- Vandenberg, N.R. (1999): *sked: Interactive/Automatic Scheduling Program*. Mark 4 Software Documentation, NASA/ Goddard Space Flight Center, Space Geodesy Program

<sup>1</sup><http://hpiers.obspm.fr/eoppc/eop/eopc04/eopc04.62-now>

# The Role of Parameter Constraints in VLBI Data Analysis

H. Kutterer

*Deutsches Geodätisches Forschungsinstitut (DGFI), Munich, Germany*

**Summary:** In VLBI parameter estimation two types of parameters are modelled. On the one hand there are the classical target parameters such as station coordinates and Earth orientation parameters. On the other hand there are additional parameters like, e.g., the coefficients of the piecewise linear functions for the troposphere and the clocks. It is common practice to add prior information on the additional parameters by means of pseudo-observations in order to stabilize the estimation. In the paper the impact of these pseudo-observations on the parameters is assessed by statistical means. Numerical results are derived from the NEOS-A sessions of 2000 and 2001.

## 1 Introduction

VLBI target parameters are typically estimated according to the least-squares (LS) principle based on the Gauss-Markov model (GMM). In its linearized form which is exclusively considered in the following the GMM reads as

$$E(\underline{\mathbf{d}}\mathbf{l}) = \mathbf{A} \mathbf{d}\mathbf{x}, \quad D(\underline{\mathbf{d}}\mathbf{l}) = \mathbf{C}_{\parallel} = \sigma_0^2 \mathbf{Q}_{\parallel} = \sigma_0^2 \mathbf{P}^{-1} \quad (1)$$

with  $E(\cdot)$  denoting the expectation operator,  $\underline{\mathbf{d}}\mathbf{l}$  the  $n$ -dimensional **random** vector of the reduced observations (observed minus computed),  $\mathbf{A}$  the column-regular configuration matrix,  $\mathbf{d}\mathbf{x}$  the update of the  $u$ -dimensional deterministic vector of the parameters  $\mathbf{x}$  with respect to some initial values  $\mathbf{x}_0$ ,  $D(\cdot)$  the dispersion operator,  $\mathbf{C}_{\parallel}$  the regular (theoretical) variance-covariance matrix (vcm) of the observations,  $\mathbf{Q}_{\parallel}$  and  $\mathbf{P}$  the corresponding cofactor matrix and weight matrix, respectively, and  $\sigma_0^2$  the (theoretical) variance factor.

The first part of the GMM is called functional model. It describes (here) the (linearized) mathematical-physical relationship between the observations and the relevant parameters; for VLBI observations see, e.g., Sovers et al. (1998). The second part of the GMM is the stochastic model; see Tesmer (2003; this volume) for more details on the stochastic VLBI model. Kutterer et al. (2003; this volume) give a description of the LS estimation. The estimated parameters ('best linear unbiased estimates', BLUE) read as

$$\mathbf{d}\hat{\mathbf{x}} = (\mathbf{A}^T \mathbf{P} \mathbf{A})^{-1} \mathbf{A}^T \mathbf{P} \mathbf{d}\mathbf{l} \quad (2)$$

with the vcm

$$\mathbf{C}_{\hat{\mathbf{x}}\hat{\mathbf{x}}} = \sigma_0^2 (\mathbf{A}^T \mathbf{P} \mathbf{A})^{-1}. \quad (3)$$

Actually, in the VLBI case the GMM consists typically of two types of observations, the VLBI travel time delay observations  $\mathbf{d}\mathbf{l}_{\tau}$  and pseudo-observations  $\mathbf{l}_{\text{constr}}$  (constraints) which are introduced in order to stabilize the estimation of some parameter types such as those referring to piecewise continuous linear functions for the clocks and for the tropospheric zenith delay.

$$\begin{bmatrix} \boldsymbol{\varepsilon} \\ \boldsymbol{\varepsilon}_{\text{constr}} \end{bmatrix} = \begin{bmatrix} \mathbf{A} \\ \mathbf{B} \end{bmatrix} \mathbf{d}\mathbf{x} - \begin{bmatrix} \mathbf{d}\mathbf{l}_{\tau} \\ \mathbf{l}_{\text{constr}} \end{bmatrix} \quad \text{with } \mathbf{B} = [\mathbf{0} \quad \mathbf{I}], \quad (4)$$

$$\mathbf{C}_{\parallel} = \begin{bmatrix} \mathbf{C}_{\tau\tau} & \mathbf{0} \\ \mathbf{0} & \mathbf{C}_{\text{constr}} \end{bmatrix} = \sigma_0^2 \begin{bmatrix} \mathbf{P}_{\tau\tau}^{-1} & \mathbf{0} \\ \mathbf{0} & \mathbf{P}_{\text{constr}}^{-1} \end{bmatrix}$$

The identity submatrix of  $\mathbf{B}$  corresponds with the constrained parameters which are (without loss of generality) located at the end of the parameter vector. Hence, the constraints are equivalent to directly observed parameters.

From an algorithmic point of view there is no distinction in the GMM between the ordinary and the pseudo-observations. From this side the benefit of the constraints is obvious. Their use allows to efficiently bridge time intervals with gaps in the data without any re-parametrization. Nevertheless, only the ordinary delays are physically observed. The pseudo-observations are subjective at least to a certain part. Optimally, the ‘observed’ values and their standard deviations are derived by a representative independent sampling. The next best basis are the skills of VLBI analysts which are founded on a lot of processing experience. And there is a possibility to use ‘arbitrary’ values which just fulfil some best-fit criterion. Hence, in neither of these cases the constraints need to be physically interpretable.

Several aspects are of interest concerning the quality and reliability of the resulting parameters. In this study, three of them are considered: the impact of the constraints on the estimated parameters (see Section 3), the actual contribution of the constraints to the LS estimation (see Section 4), and the consistency of the constraints with the observed data (see Section 5). In each of these sections the theoretical background is given as far as it is needed. The results are given exemplarily based on real data from a number of VLBI sessions (see Section 2).

## 2 Software and data

For the study, the 104 VLBI sessions of the NEOS-A program in 2000 and 2001 were considered. The observation time of each session was at least 24 hours. In most of the sessions either five or six telescopes participated. In eight sessions there were only four and in two sessions only three telescopes. The VLBI data were processed at the Deutsches Geodätisches Forschungsinstitut (DGFI) in Munich, Germany, using the software OCCAM 5.0 LSM (Titov et al., 2001). The coordinates of the VLBI antennas were fixed to the respective ITRF 2000 positions. The positions of the radio sources were taken from the ICRF Ext. 1. The nutation parameters were taken from the MHB 2000 model according to the IERS Conventions 2000 (McCarthy, 2003).

Further constraints were not introduced, neither for the two nutation parameters nor for the coordinates of the pole  $(x_{\text{pole}}, y_{\text{pole}})$  and the offset DUT1 between the rotation phase of the Earth and the atomic time UTC. For each of these five Earth orientation parameters (EOP) one value per session was estimated. Further (unconstrained) parameters are the three parameters of the clock parabola for each station (except for the one with the reference clock) and an offset per station for the tropospheric zenith delay. At DGFI, the weights for the delay observations are typically set to

$$w_i = \frac{1}{\sigma_i^2 + \sigma_{\text{const}}^2}, \quad (5)$$

with  $\sigma_i$  taken from the NGS data base and  $\sigma_{\text{const}} = 5$  mm a constant value which is added to overrule the sometimes high variation of the  $\sigma_i$ .

The standard parameter constraints are  $0 \pm 15$  mm/h for the one-hourly resolved rates of the piecewise continuous linear functions of the tropospheric zenith delays (TPWLF) per station,  $0 \pm 40$  mm/h for the one-hourly re-

solved rates of the piecewise continuous linear functions of the clocks (CPWLF) per station without the reference station, and  $0 \pm 0.3$  mm for the two offsets (GROF) of the horizontal tropospheric gradients (N-S, E-W) per station. Such values are also typical for other VLBI processing centers and software.

The considered scenarios were the same for all above-mentioned aspects of interest. For each of the sessions the standard processing was done. Afterwards, the sessions were reprocessed with solely modified standard deviations of the constraints. First, the standard deviations were decreased by a factor of ten (what corresponds with weights increased by a factor of 100) in order to tighten the constraints by one magnitude. Second, the standard deviations were increased by a factor of 10 to loosen the constraints. In the following three sections some exemplary results are presented.

### 3 Impact on the estimated EOP

The most directly visible impact of the parameter constraints is certainly on the estimated parameters themselves. In the following Figures 1-4 this is exemplarily presented for the x-coordinate of the pole and DUT1. Fig. 1 shows the reaction of  $x_{\text{pole}}$  on changes of the constraints' weights as described in the previous section. For the most part the deviations between the OCCAM standard solution and the solutions with modified weights are below 0.1 mas. However, there are individual sessions which show changes in the estimated values up to 0.3 mas, in particular for the increased weights. From Fig. 2 it obvious that not all differences between the results from different weighting are statistically significant. Analogous results for DUT1 are shown in Figures 3 and 4. Typical examples for great but non-significant parameter updates are Session No. 21 (23.05.00) and Session No. 35 (29.08.00, in particular visible in DUT1) which have some weaknesses in the configuration. In contrast, the effects in the results of Session No. 6 (08.02.00) are highly significant in  $x_{\text{pole}}$ . By taking the not-shown respective configurations into account it can be stated that the estimated values are rather stable in case of proper VLBI sessions. Otherwise there can be (significant or non-significant) changes in the parameters. However, for the assessment of significance the values of the parameters have to be contrasted to their standard deviations. The straightforward use of the parameters only may be problematic.

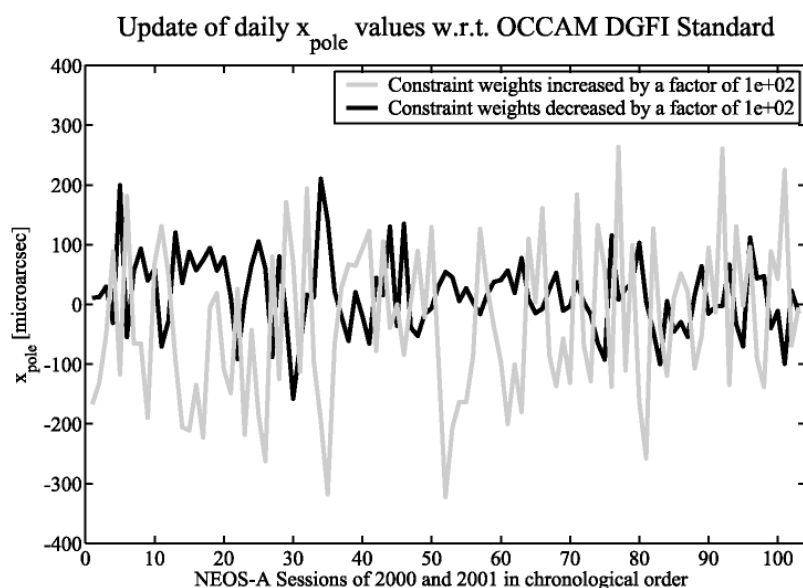


Figure 1: Reaction of the x-coordinate of the pole on changes of the constraints' weights.

Figure 2: Estimates of the x-coordinate of the pole for different constraints' weights standardized by the respective standard deviations.

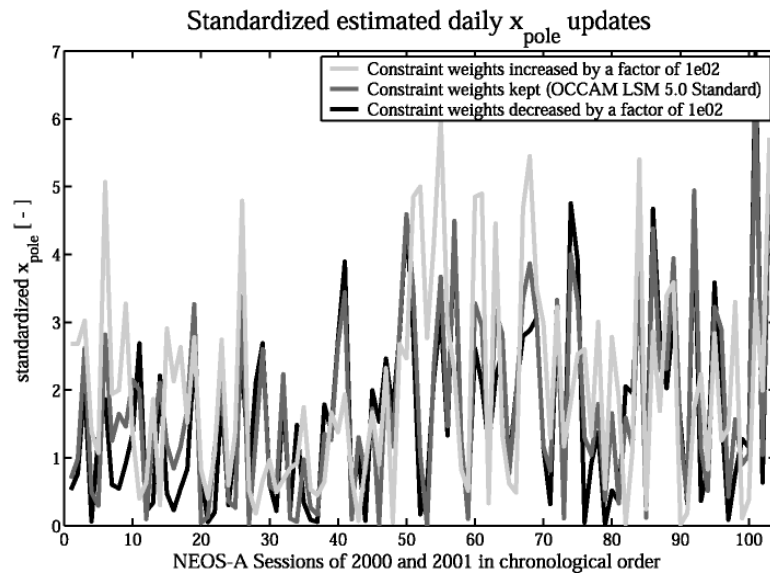


Figure 3: Reaction of DUT1 on changes of the constraints' weights.

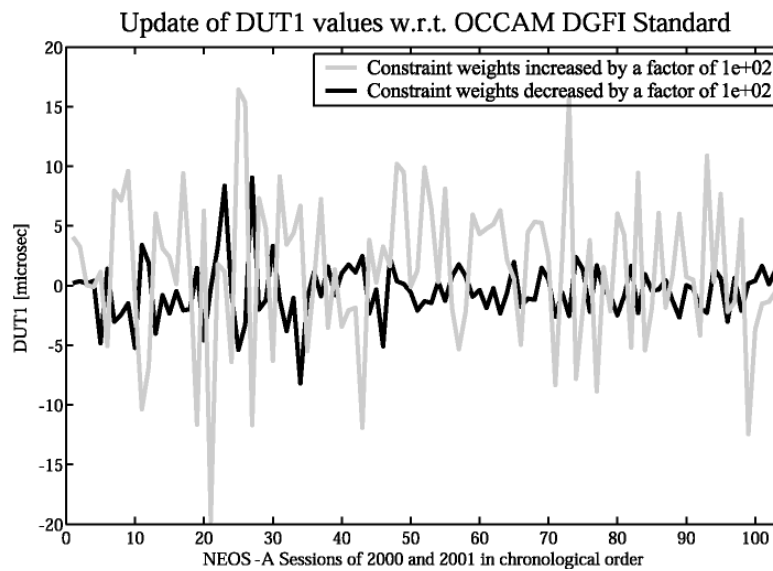
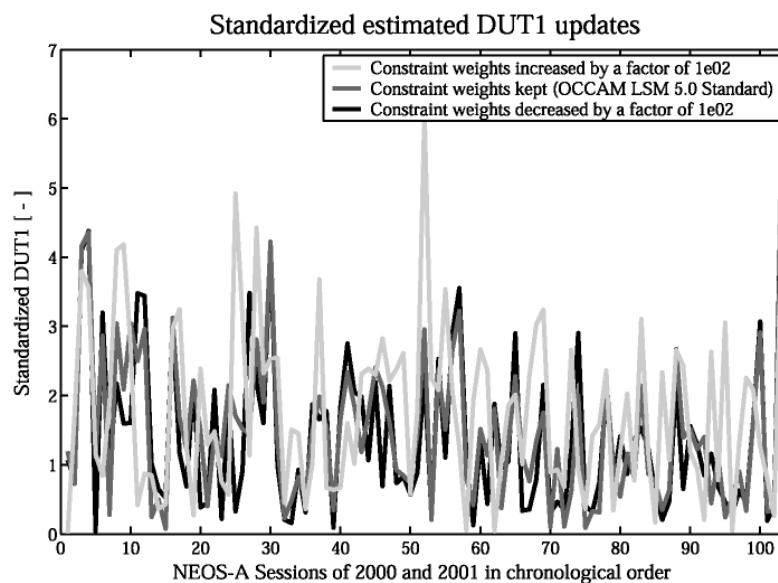


Figure 4: Estimates of DUT1 for different constraints' weights standardized by the respective standard deviations.



## 4 Contribution of the constraints to the LS estimation

A second way to assess the impact of the constraints (or prior information) on the LS estimates is given by the quantification of their particular contribution which can be measured in terms of the share  $r_{x_i}$  of the respective pseudo-observation in the finally estimated value of the associated parameter. The mathematical description is rather simple and reads as

$$r_{x_i} = \frac{\sigma_{x_i}^2}{\sigma_{x_{0,i}}^2}. \quad (6)$$

Hence, the share of prior information in the  $i$ -th parameter is the ratio of its posteriori variance to its priori variance. If the observed data do not contribute to the parameter  $x_i$  then its posteriori variance remains unchanged and the ratio equals one (maximum contribution, maximum share). If instead the observed data contribute significantly to the estimate, the posteriori variance tends to zero and so does the ratio (minimum contribution, minimum share). For details see Sneeuw (2000, p. 50).

The Figures 5, 6, and 7 show typical results which were derived for the NEOS-A session of 01.02.00. They can be seen as representative for all other considered sessions. For OCCAM standard processing there is a share of 0.1 to 0.2 of prior information in all three groups of constrained parameters (TPWLF, CPWLF, GROF). Thus, even in the case of good configurations prior information is used by the processing. For the later sessions there are exceptions due to some weaknesses in the configuration.

In case of decreased weights there is nearly no need for prior information concerning TPWLF and GROF as it is obviously not used. In case of the CPWLF parameters there is still some contribution of prior information. In addition, there are some cycles which correspond with the respective 24 CPWLF parameters of the individual stations. At the beginning and at the end of the sessions there is more need for prior information than during the other observation time. For the TPWLF there is no such characteristics.

In case of increased weights the constraints become very important for the parameter estimation. From Fig. 7 it is clear that the considered decrease and increase of the constraints' weights nearly cover the complete spectrum between no and full contribution. This is not the case for the TPWLF and the CPWLF where there is a broader range for tuning the weights.

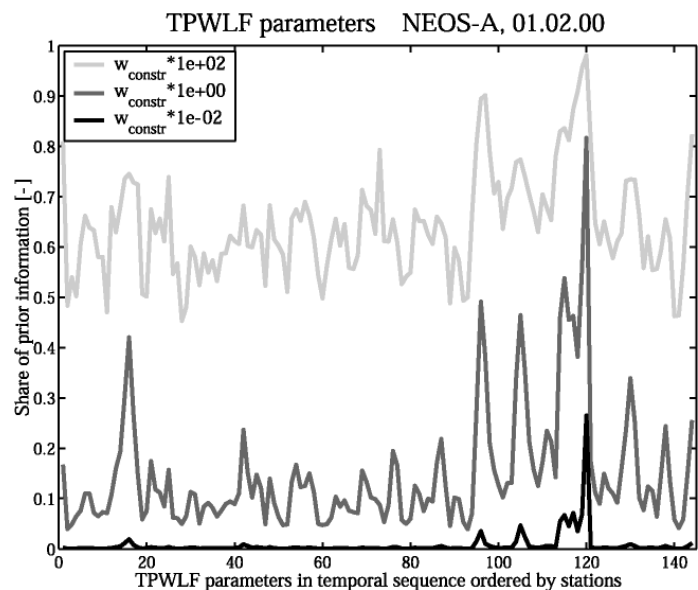


Figure 5: Importance of prior information for the estimation of the one-hourly resolved rates of the piecewise continuous linear functions of the tropospheric zenith delays (TPWLF)

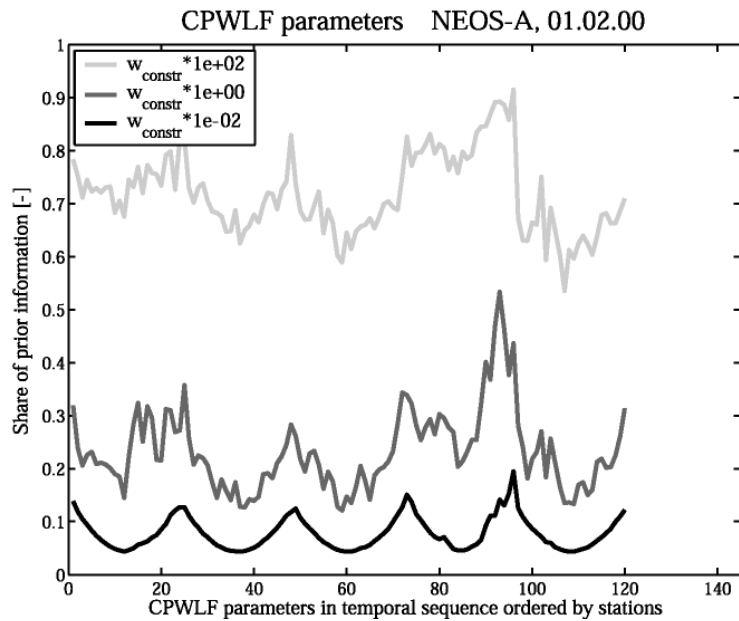


Figure 6: Importance of prior information for the estimation of the one-hourly resolved rates of the piecewise continuous linear functions of the clocks (CPWLF).

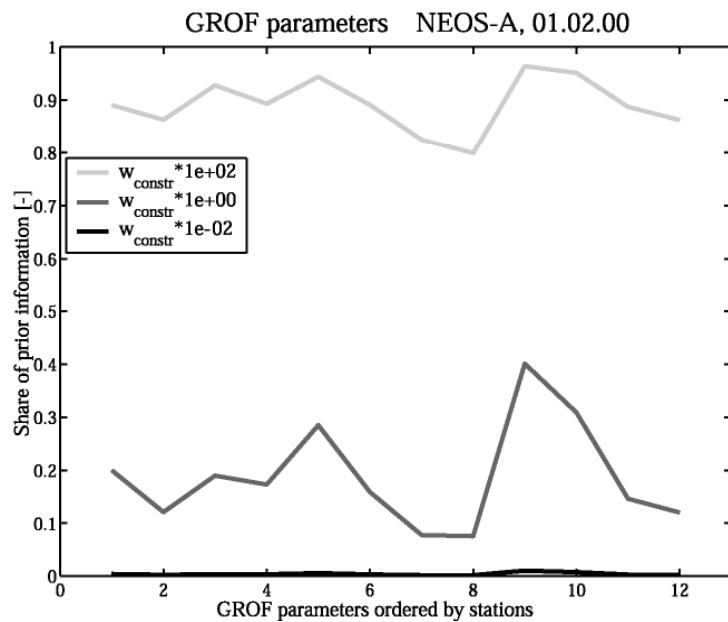


Figure 7: Importance of prior information for the estimation of the two offsets (GROF) of the horizontal tropospheric gradients (N-S, E-W).

## 5 Consistency of observed data and constraints

If sufficient originally observed data are available their consistency with the prior information formulated in terms of parameter constraints can be tested by statistical means. For the basic approach the set of all observations is divided into two subsets:  $\mathbf{dl}_1$  refers to the ordinary VLBI delays and to those pseudo-observations which are not tested, whereas  $\mathbf{dl}_2$  denotes the  $p$  pseudo-observations whose consistency with the observations  $\mathbf{dl}_1$  is tested. Let the parameters  $\mathbf{dx}_2$  correspond with  $\mathbf{dl}_2$ . Hence, the GMM according to Eq.(1) reads now

$$E \begin{pmatrix} \underline{\mathbf{dl}}_1 \\ \underline{\mathbf{dl}}_2 \end{pmatrix} = \begin{bmatrix} \mathbf{A}_1 & \mathbf{D}_1 \\ \mathbf{0} & \mathbf{D}_2 \end{bmatrix} \begin{bmatrix} \mathbf{dx}_1 \\ \mathbf{dx}_2 \end{bmatrix}, \quad D \begin{pmatrix} \underline{\mathbf{dl}}_1 \\ \underline{\mathbf{dl}}_2 \end{pmatrix} = \mathbf{C}_{ll}, \quad (7)$$

$$\mathbf{A} = \begin{bmatrix} \mathbf{A}_1 \\ \mathbf{0} \end{bmatrix}, \quad \mathbf{D} = \begin{bmatrix} \mathbf{D}_1 \\ \mathbf{D}_2 \end{bmatrix}$$

Now two hypotheses (null hypothesis  $H_0$ , alternative hypothesis  $H_a$ ) are formulated

$$H_0 : E(\underline{\mathbf{dx}}_2) = \mathbf{0}, \quad H_a : E(\underline{\mathbf{dx}}_2) \neq \mathbf{0}. \quad (8)$$

According to Koch (1999) a proper test statistic for the significance of  $H_0$  is given by

$$\underline{T} = \frac{\hat{\mathbf{y}}^T \left( \mathbf{PD}(\mathbf{D}^T \mathbf{P} \mathbf{Q}_{\hat{\mathbf{v}}\hat{\mathbf{v}}} \mathbf{PD})^{-1} \mathbf{D}^T \mathbf{P} \right) \hat{\mathbf{y}} / p}{\hat{\mathbf{y}}^T \mathbf{P} \hat{\mathbf{y}} / (n - u - p)} \quad (9)$$

with

$$\hat{\mathbf{v}} = -(\mathbf{Q}_{\hat{\mathbf{v}}\hat{\mathbf{v}}} \mathbf{P}) \mathbf{dl}, \quad \mathbf{Q}_{\hat{\mathbf{v}}\hat{\mathbf{v}}} = \mathbf{Q}_{ll} - \mathbf{A}(\mathbf{A}^T \mathbf{P} \mathbf{A})^{-1} \mathbf{A}^T \quad (10)$$

coming from the estimation of  $\mathbf{dx}_1$  only. Eq. (9) reflects the significance of the change of the squared sum of residuals induced by the additional estimation of the parameters  $\mathbf{dx}_2$ . As there is

$$\underline{T} \sim F_{p, n-u-p} \quad | H_0, \quad (11)$$

the null hypothesis  $H_0$  is rejected if for the value  $T$  of  $\underline{T}$  there is

$$T > k := F_{p, n-u-p, 1-\alpha} \quad (12)$$

with  $F_{p, n-u-p, 1-\alpha}$  the  $(1-\alpha)$  fractile value of the corresponding F-distribution.

The values of the test statistic according to Eq. (11) are shown in Fig. 8 for the TPWLF parameters, in Fig. 9 for the CPWLF parameters and in Fig. 10 for the GROF parameters. The interpretation of the figures is straightforward. As the presented values of  $\underline{T}$  are divided by the respective critical values according to Eq. (12) there is significance for all values greater than 1. Hence, in case of reduced weights there is no significance at all what means that on this level observed data and prior information are consistent.

In case of OCCAM standard weighting there is still no significance for TPWLF whereas for CPWLF the value of Session No. 21 (23.05.00) exceeds 1. This inconsistency is due to some data gaps at one of the stations which had only observed during the first three hours of the session. Obviously, the constraints which are modelled for the complete session interact with other parameters and contradict in this case the observed data. Several of the test statistic values for GROF are significant already on this level.

In case of the increased weights the TPWLF and GROF parameters are significant for (nearly) all considered sessions. A small number of sessions shows non-significant values for the CPWLF parameters. It is remarkable that the standard prior information on TPWLF and CPWLF fits quite well to the data what reflects a proper tuning. This does not hold for the GROF parameters what may be due to the inadequate assumption of a zero expectation for the pseudo-observations which is expressed through the prior information.

Figure 8: Values of the F test statistic for the TPWLF parameters for different constraints' weights divided by the respective critical value  $k$ .

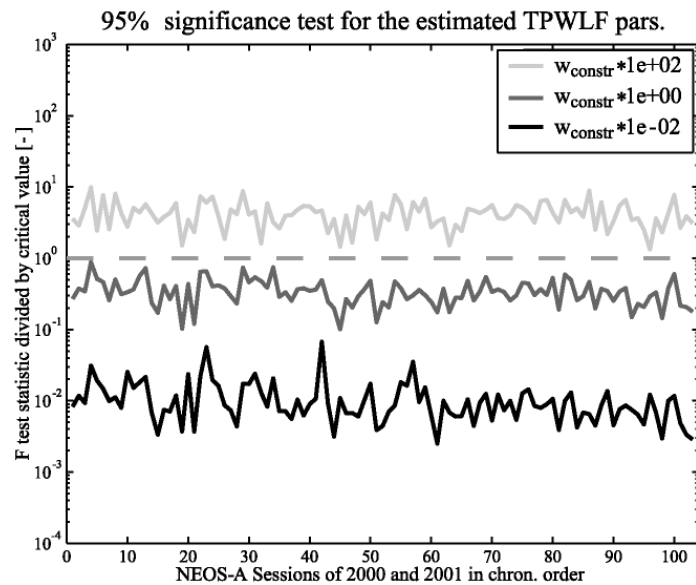


Figure 9: Values of the F test statistic for the CPWLF parameters for different constraints' weights divided by the respective critical value  $k$ .

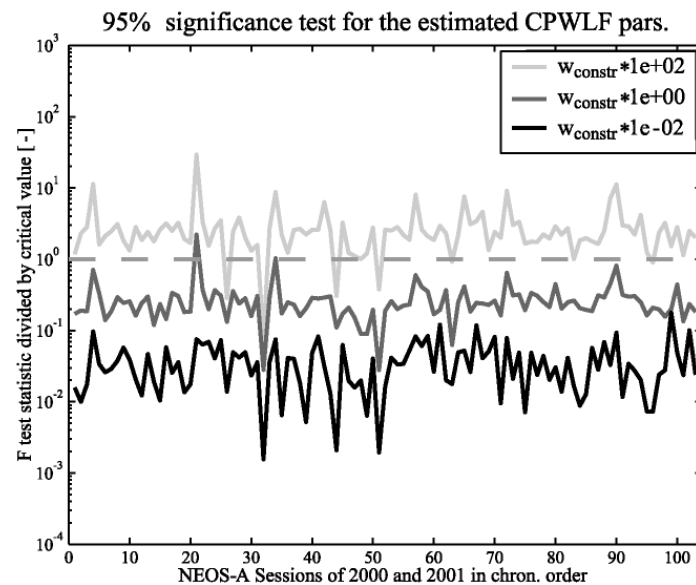
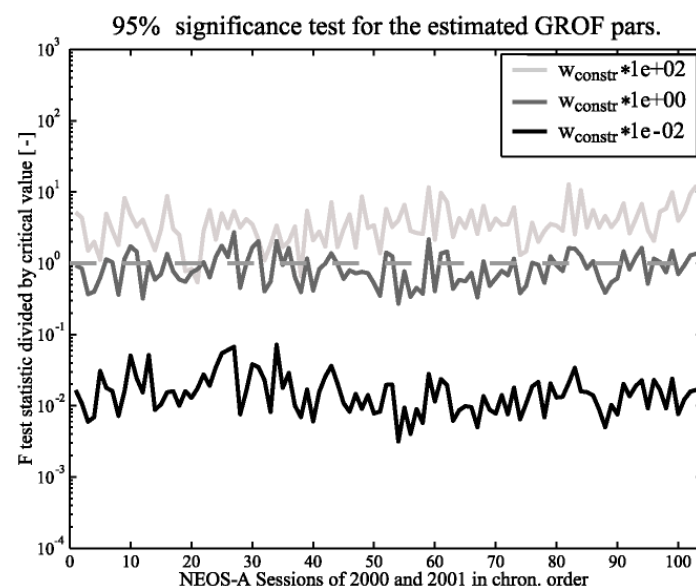


Figure 10: Values of the F test statistic for the GROF parameters for different constraints' weights divided by the respective critical value  $k$ .



## 6 Conclusions

The parameter constraints are a fundamental component of the modelling and processing of VLBI data. They show some remarkable benefit concerning a comfortable implementation of the standard parametrization into VLBI analysis software such as OCCAM LSM 5.0. In case of proper tuning reasonable parameters are obtained. However, for weak observation configurations or in case of data gaps some of the resulting parameter estimates may be artefacts.

Note that every constraint on the parameters introduces a bias. In case of the combination of different VLBI solutions to some intra-technique product or of the inter-technique integration of different space-geodetic techniques this may cause irreparable distortions of the results. For this reason it is at least necessary to document the applied constraints to make them recoverable or to set up normal equation systems which are free from prior information. The master plan for the combination and integration of space-geodetic techniques should contain dedicated studies on the identification of the optimum conditions for making parameter constraints (mostly) obsolete.

## References

- Koch, K.R.: Parameter Estimation and Hypothesis Testing in Linear Models. Springer, Berlin Heidelberg, 1999.
- Kutterer, H.; Heinkelmann, R.; Tesmer, V.: Robust outlier detection in VLBI data analysis. This volume, 2003.
- McCarthy, D.D.: IERS Conventions 2000, <http://www.iers.org>, 2003.
- Sneeuw, N.: A semi-analytical approach to gravity-field analysis from satellite observations. Deutsche Geodätische Kommission, Reihe C, 527, 2000.
- Sovers, O.J.; Fanselow, J.; Jacobs, S.: Astrometry and geodesy with radio-interferometry: experiments, models, results. Modern Physics, 70, 1393-1454, 1998.
- Tesmer, V.: Refinement of the stochastic VLBI model: first results. This volume, 2003.
- Titov, O.; Tesmer, V.; Böhm, J.: OCCAM 5.0 Users Guide. AUSLIG Technical Reports 7, AUSLIG, Canberra, 2001.



# Tropospheric Parameters From Geodetic VLBI Data Analysis

M. Negusini and P. Tomasi

*Istituto di Radioastronomia – CNR, Bologna, Italy*

**Summary:** In May 2002 a call for participation to the Pilot Project - Tropospheric Parameters, was sent by the IVS (International VLBI Service for Geodesy and Astrometry) to the IVS Analysis Centers. The Institute of Radioastronomy (IRA) joined the project with regular submission of tropospheric parameters (wet and total zenith delays, horizontal gradients) for all IVS-R1 and IVS-R4 sessions since January 1st, 2002. In order to fulfil the request of the project, we modified the CALC/SOLVE software, to produce directly the Sinex files containing the tropospheric parameters in the suitable format.

Moreover, we analyzed all the other 2001 and 2002 databases available on the IVS data centers, in order to compute the tropospheric parameters and obtain the relevant time series. Some of the tropospheric results are presented here.

We have also compared the VLBI tropospheric estimates and the GPS-derived troposphere, provided by IGS (International GPS Service), for the co-located sites. Post-processing analysis have been carried out on the time series and trends and seasonal signals are highlighted. Constant biases are found between the zenith delays derived by VLBI and GPS, although the same effects should affect both techniques.

## 1 Introduction

In May 2002 the IVS (International VLBI Service for Geodesy and Astrometry) sent a call for participation to the IVS Analysis Centers to the Pilot Project - Tropospheric Parameters. The Institute of Radioastronomy (IRA) answered positively and joined the project submitting the estimates of tropospheric parameters (wet and total zenith delays, horizontal gradients) for all IVS-R1 and IVS-R4 sessions since January 1st, 2002, on a regular basis. The IRA had a large experience of analyzing VLBI data for studying the effect of troposphere on the results (Rioja, M.J. and P. Tomasi, 2001), and for that joining the project was a natural extension of the research of the Institute.

To be ready to fulfil the request of the project, we had to modify part of the CALC/SOLVE software, in order to produce the Sinex files containing the tropospheric parameters in the suitable format.

In Figure 1 there is an example of a Sinex tropospheric file submitted by our Analysis Center to IVS. For the VLBI data analysis we used a  $5^\circ$  elevation cut-off angle and the Niell mapping functions. The solution has been computed into ITRF2000 without fixing the stations coordinates, and using a no-net-translation constraint. We compute one total and one wet zenith delay parameter per hour for all the stations involved into the experiment and only one value for both east and north gradient per station per session.

The data submitted by the different ACs are combined at the Vienna IVS center in order to obtain IVS combined products, i.e. stable and robust tropospheric parameters with 1 hour resolution and high accuracy (H. Schuh and J. Boehm, 2003). The graphs in Figure 2 and 3 show the biases and standard deviations of the solutions submitted by the different ACs participating to the project, in the case of a mean of all sites (Figure 2) and in the case of Wettzell (Figure 3). Our analysis center is named CNR and our solution is indicated by green up triangles and it is quite good with respect to the other ones and the combined solution (VLBI).

```

=>TBO 9.99 CNR 03:115:53232 CNR 03:100:66713 03:101:66625 R MIX
-FILE/REFERENCE
-DESCRIPTION          IUG Pilot Project Troposphere / CNR, Italy
-OUTPUT              Tropospheric Estimates from 24 h session
-CONTACT             Paolo Tomasi, tomasi@ira.cnr.it
-SOFTWARE             VLBI analysis system Calc/Solve, revision date 2002.06.11
-HARDWARE            HP9000/780 HP-UX B.10.20
-INPUT               VLBI experiment r4066, database $03APR10XE version 005
-FILE/REFERENCE
-TROP/STA_COORDINATES
ALFO      1 R  218024.652 -4946132.289  4561371.132  ITRF00  CNR
FURT      1 R  4985370.040 -3955020.342 -428472.215  ITRF00  CNR
GILC      1 R  -2261547.476 -1483645.155  5756399.091  ITRF00  CNR
KOKE      1 R  -5543327.694 -2054567.454  2387352.140  ITRF00  CNR
RYAL      1 R  1202462.672  252794.455  6227766.089  ITRF00  CNR
TIG0      1 R  1492054.220 -4887961.070 -3802541.406  ITRF00  CNR
WETT      1 R  4075539.790  931735.379  4801629.424  ITRF00  CNR
-TROP/STA_COORDINATES
-TROP/DESCRIPTION
SOLUTION_FIELDS_1      TROTOT TROGET  STIDEV  GRTOTM  STIDEV  GRTOIE  STIDEV
:-----
:      KEYWORD          GENERAL
ELEVATION CUT OFF ANGLE      5
DOMNO OF LOW OBSERV.        80
TERR. REFERENCE FRAME      ITRF2000
TFR FIXED                    80
DEY MAPPING FUNCTION        NIELL 96
GET MAPPING FUNCTION        NIELL 96
:      KEYWORD          ZEMITH DELAYS
SAMPLING ZEMITH DELAYS      3600 SEC
APRIORI HYDROST. DELAY     SAAS2TMO
APRIORI GET DELAY          SAAS2TMO
ZEMITH DELAY MODEL         CONSTR. PIECEW. LINEAR FUNCT.
CONSTR. ZD OFFSET          NONE
CONSTR. ZD RATE            50 PS/HR
:      KEYWORD          GRADIENTS
SAMPLING GRADIENTS         84600 SEC
APRIORI GRADIENTS         NONE
GRADIENT MODEL             OFFSETS
CONSTR. GR OFFSET          0.5 MM
CONSTR. GR RATE            2.0 MM/DAY
-TROP/DESCRIPTION
-TROP/SOLUTION
-ALGOPAK
:-----
ALFO 03:100:68400      2297.08  39.67  2.24  -0.39  0.20  0.06  0.18
ALFO 03:100:72000      2297.49  40.48  2.23
ALFO 03:100:75600      2300.12  42.80  1.84
ALFO 03:100:79200      2297.22  41.88  2.28
ALFO 03:100:82800      2298.02  42.64  2.16
ALFO 03:101:00000      2295.68  42.08  1.81
ALFO 03:101:03600      2298.62  45.26  2.08
ALFO 03:101:07200      2299.05  46.14  2.56
ALFO 03:101:10800      2297.18  44.68  2.94
ALFO 03:101:14400      2301.45  49.16  3.59
ALFO 03:101:18000      2306.22  53.98  2.77
ALFO 03:101:21600      2299.88  47.74  1.71
ALFO 03:101:25200      2299.81  47.98  1.87
ALFO 03:101:28800      2304.28  52.92  2.00
ALFO 03:101:32400      2300.34  49.85  2.00
ALFO 03:101:36000      2299.14  49.59  2.28
ALFO 03:101:39600      2296.55  47.82  2.14
ALFO 03:101:43200      2288.79  40.83  5.25
ALFO 03:101:46800      2293.25  46.65  2.61
ALFO 03:101:50400      2297.02  51.82  2.20
ALFO 03:101:54000      2299.14  45.22  2.29
ALFO 03:101:57600      2281.47  39.08  2.78
ALFO 03:101:61200      2282.60  41.59  2.27
ALFO 03:101:64800      2280.90  40.72  4.00

```

Figure 1: Sinex tropospheric file for the R4066 experiment.

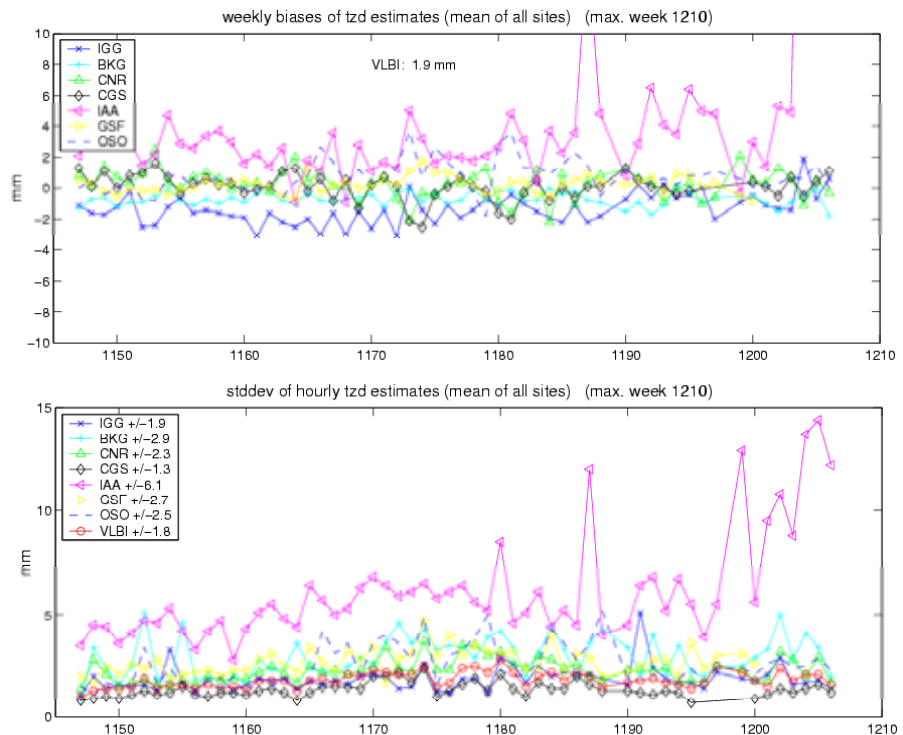


Figure 2: Weekly biases of tzd estimates (up) and standard deviations of hourly estimates (down) - mean of all sites.

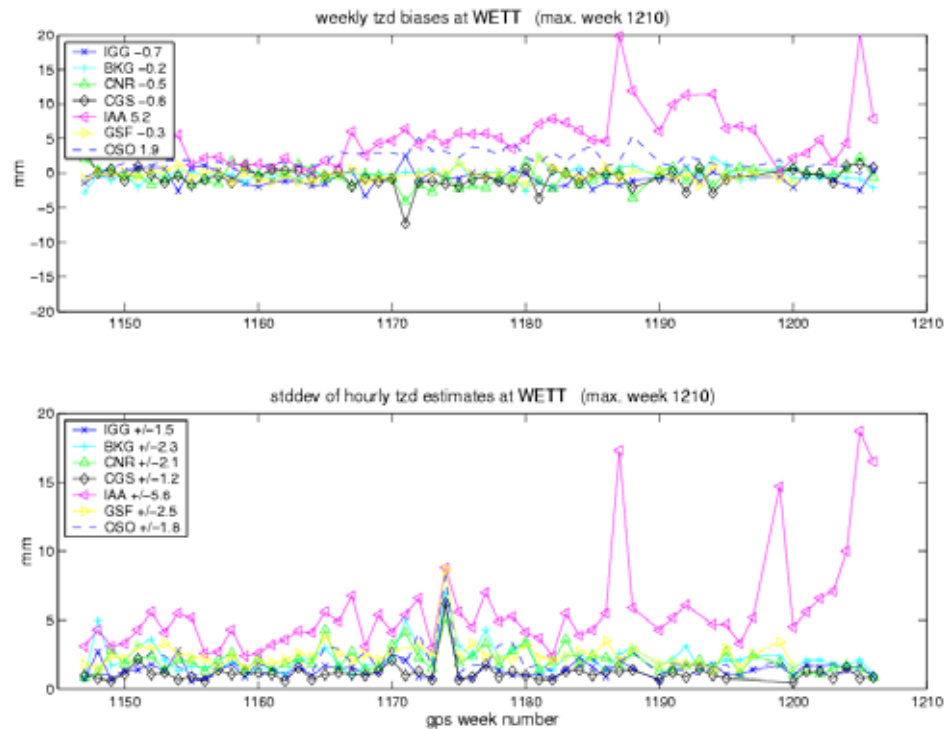


Figure 3: Weekly biases of tzd estimates (up) and standard deviations of hourly estimates (down) - Wettzell.

## 2 VLBI data analysis of all 2001-2002 databases

In order to make a deepened study of the behaviour of the troposphere, one of the parameters very important for studying the evolution of the climate and global warming, we decided to analyze all the other 2001 and 2002 databases available on the IVS Data Centers. We have used CALC/SOLVE software and a set up identical to the one described above. As a product of this analysis we obtained tropospheric parameters for each station and for every experiment available in our catalogue and the relevant time series.

In figures from 4 to 10, we show the total and wet zenith path delay time series for some of the stations involved into VLBI geodetic experiments. For Wettzell we have quite a continuous time series unlike other stations, such as Medicina or Onsala, where very sparse data are present. It should be noted that all the stations present a strong seasonal signal and a large correlation of this signal between total and wet zenith path delay. This is clearly visible in figure 11 where the dry zenith path delay for Wettzell is shown. The annual signal present in the total zenith path delay disappears when the wet delay is subtracted from the time series.

Figure 4: Total (a) and wet (b) zenith delay time series: Wetzell.

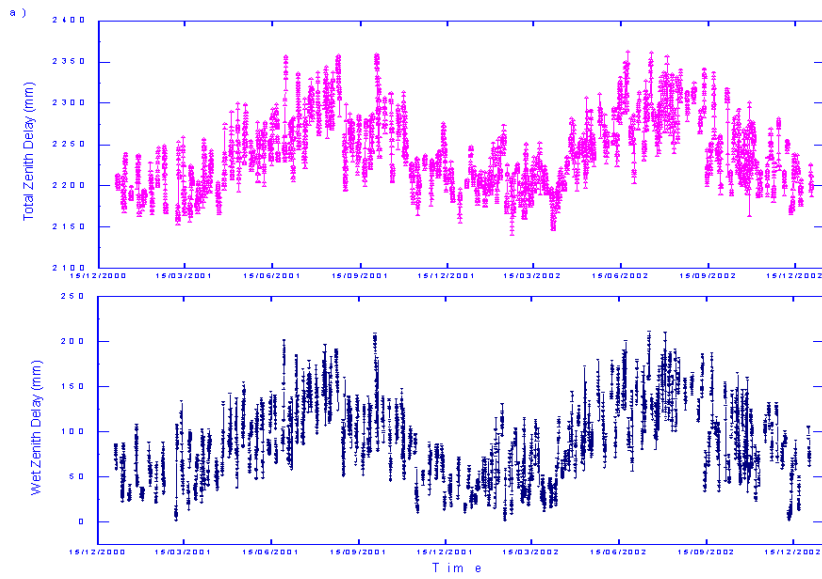


Figure 5: Total (a) and wet (b) zenith delay time series: Nyales20.

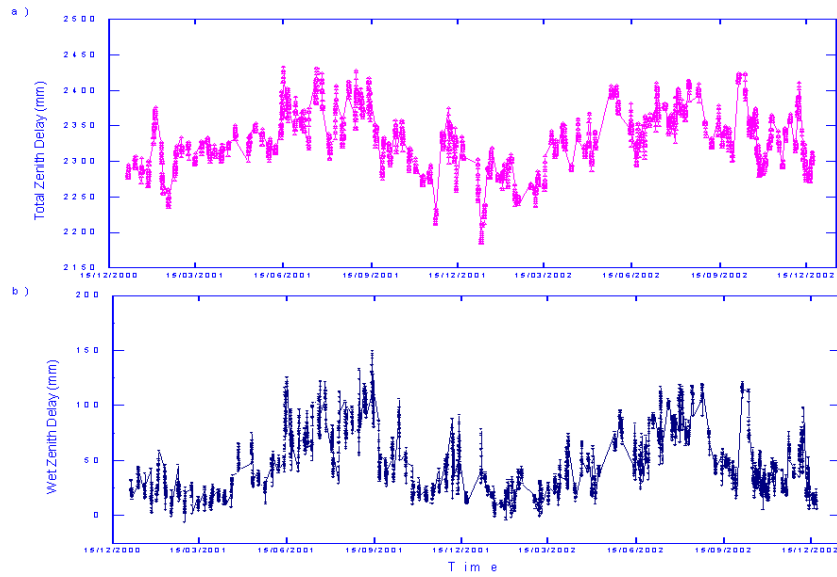
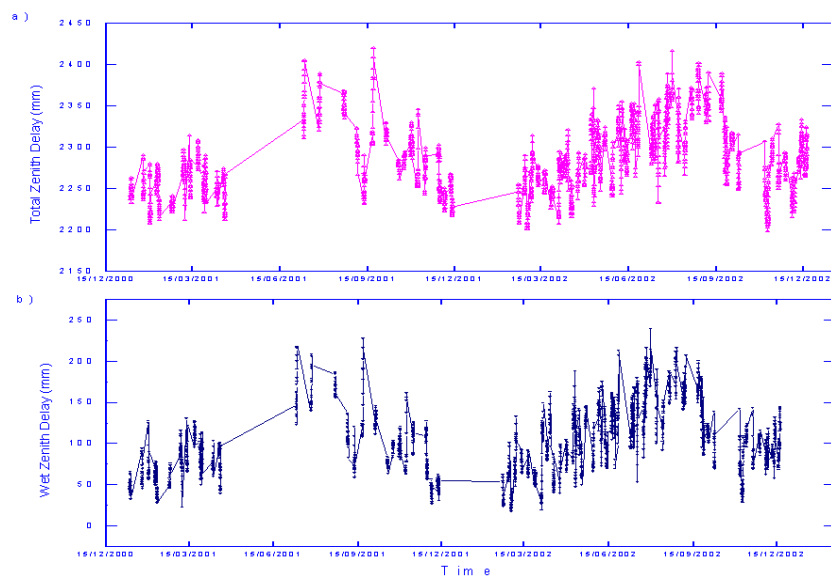


Figure 6: Total (a) and wet (b) zenith delay time series: Matera.



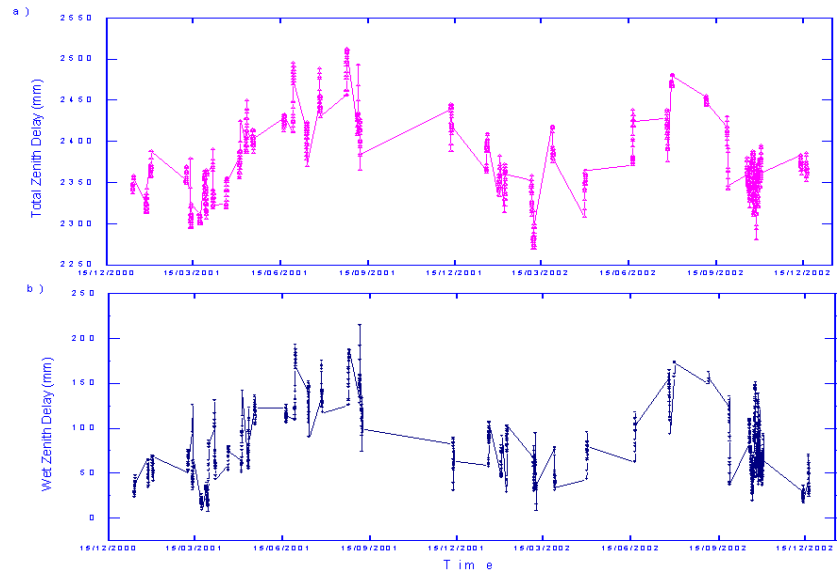


Figure 7: Total (a) and wet (b) zenith delay time series: On-sala60.

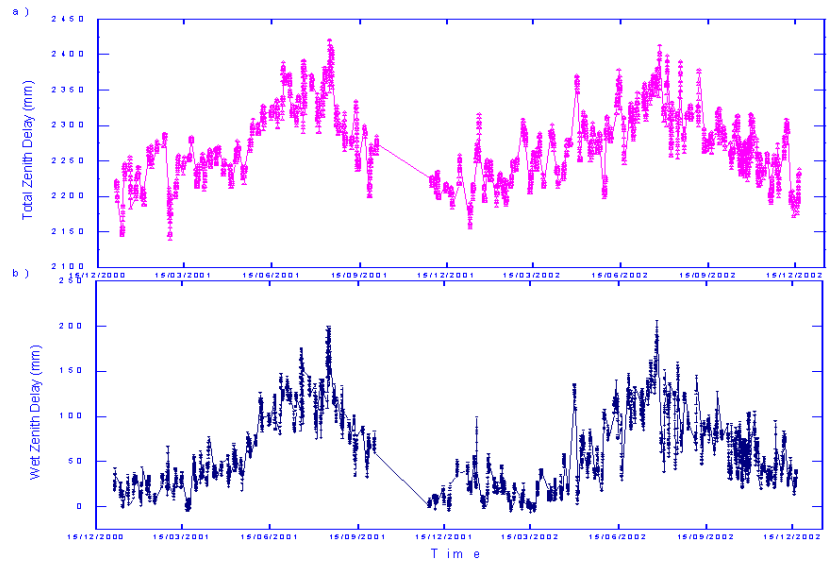


Figure 8: Total (a) and wet (b) zenith delay time series: Gil-creek.

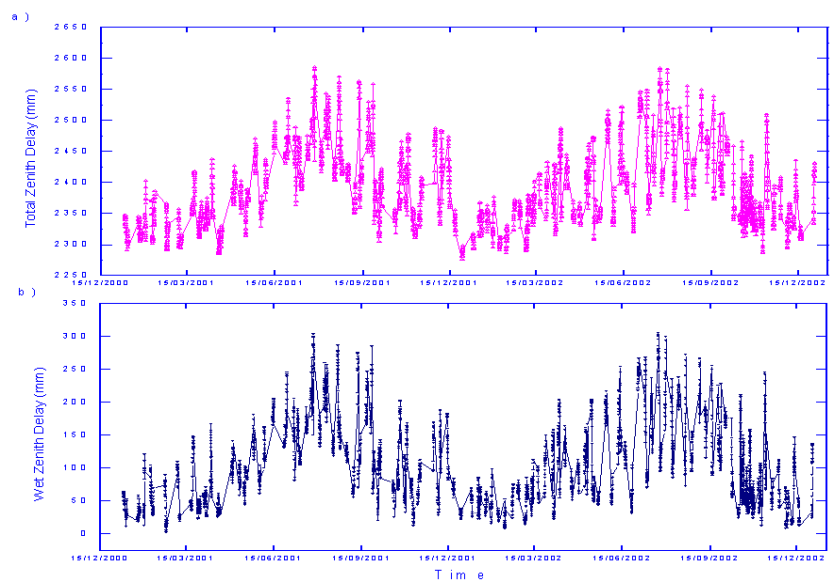


Figure 9: Total (a) and wet (b) zenith delay time series: West-ford.

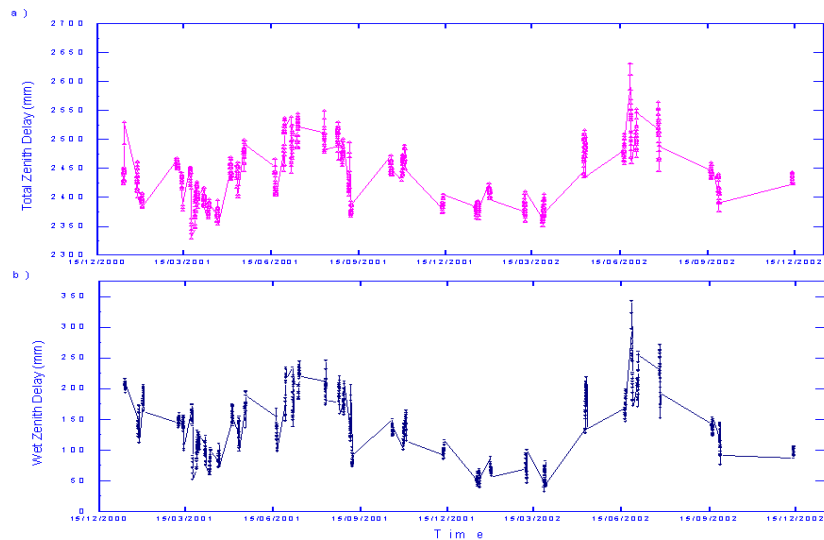


Figure 10: Total (a) and wet (b) zenith delay time series: Medicina.

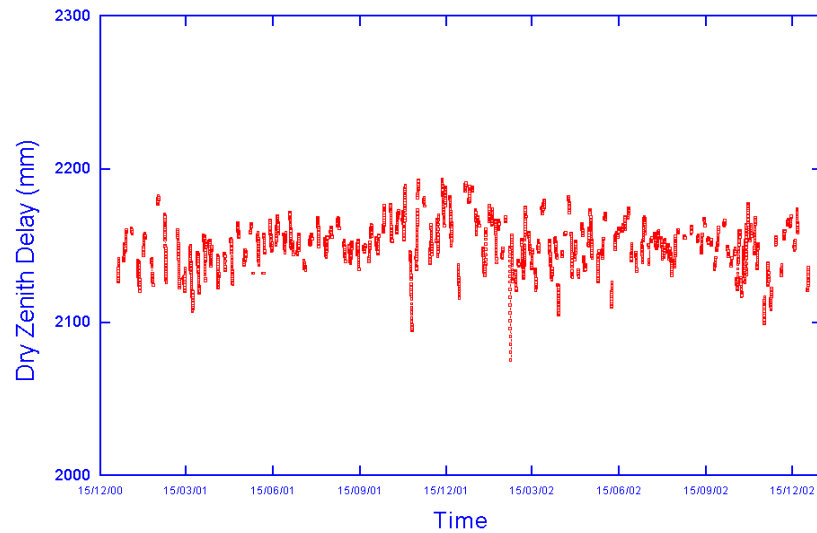


Figure 11: Dry zenith delay time series: Wettzell.

### 3 Post-processing of the time series

The annual sample of the zenith path delay for the stations present in this analysis is an interesting set of data that can be compared with the results coming from independent techniques, like GPS. For that we decided to carry out a comparison between the VLBI tropospheric estimates and the GPS-derived troposphere for the co-located sites. We used GPS data available on the web site of the CODE Analysis Center and in particular the COE EUREF daily solutions, where the troposphere parameters have 1-hour resolution and, thus, they are directly comparable with the parameters computed by our VLBI data analysis.

Post-processing analysis have been carried out on both VLBI and GPS time series, spectral analysis was performed and the results are displayed in Figures 12-15 for 4 stations. It has to be pointed out that the height of the peak of the periodogram is not directly linked to the amplitude of the signal, but it depends on the number of points of the time series. In all cases a quasi-annual period has been found. This period is identical for both techniques, for all stations but Matera. For the moment it is difficult to decide if this is a real difference in period or an artifact due to the uneven distribution of the VLBI derived tropospheric data along the two observing years.

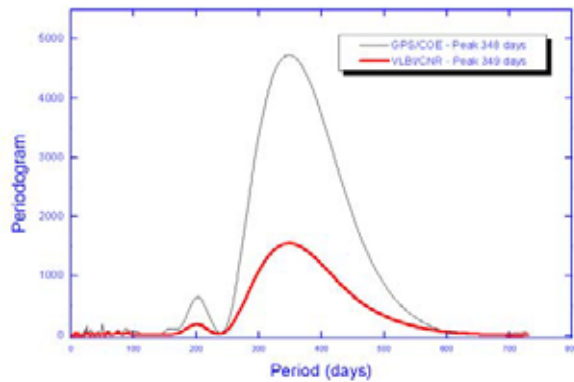


Figure 12: Spectral analysis: Wettzell.

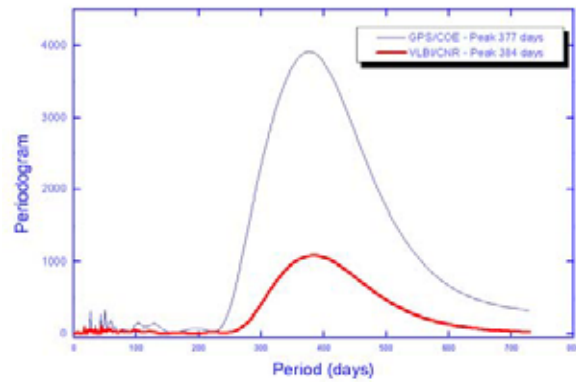


Figure 13: Spectral analysis: Ny Ålesund.

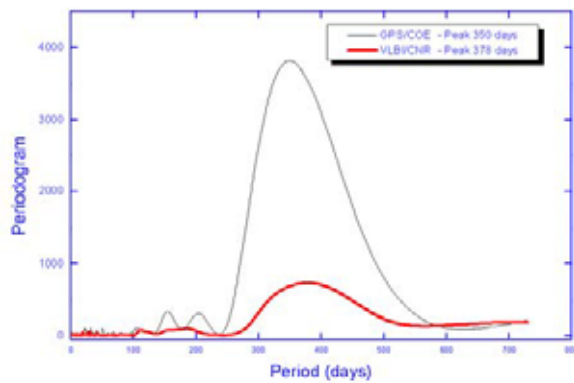


Figure 14: Spectral analysis: Matera.

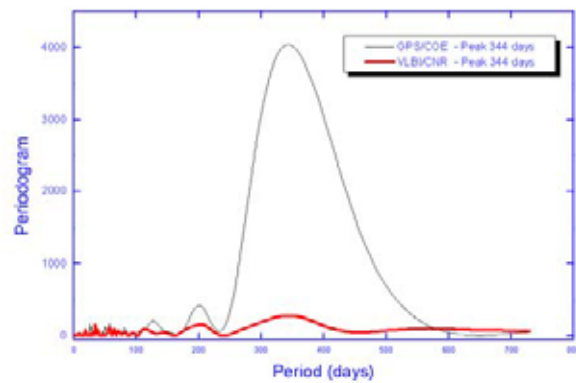


Figure 15: Spectral analysis: Onsala.

Figure 16 shows Wettzell time series, both VLBI and GPS, and the seasonal signals highlighted by means of spectral analysis. We were able to compute amplitudes and phases by means of a best-fit wave. VLBI and GPS seasonal signals have quite the same amplitudes and phases. For VLBI we found a period of  $348 \pm 6$  days and for GPS  $349 \pm 4$  days. For the amplitude we found  $46.4 \pm 1.2$  mm for VLBI and  $46.4 \pm 0.7$  mm for GPS.

For those cases where it was possible directly compare GPS and VLBI data, we computed the differences between the two time series and we obtained the relevant residuals. A positive bias is always present, as shown in Figures 17-20, and in most cases a positive trend, too, that is to be investigated in order to understand its physical meaning. In fact, both techniques are supposed to be affected by the same effects, so it is not clear what can cause this different behavior found in the residual. One known effect, that has to be taken into account, is the difference in height of the reference points of the different instruments. Thus, for a precise comparison, we have to take into account these differences in height, convert them into differences of tropospheric zenith delay and correct the residuals time series. That is quite easy for the dry component, but not for the wet component. In fact, for the first component we can assume that the delay is a fraction, proportional to the difference in height, of all the dry delay, but that assumption is not true for the wet path delay.

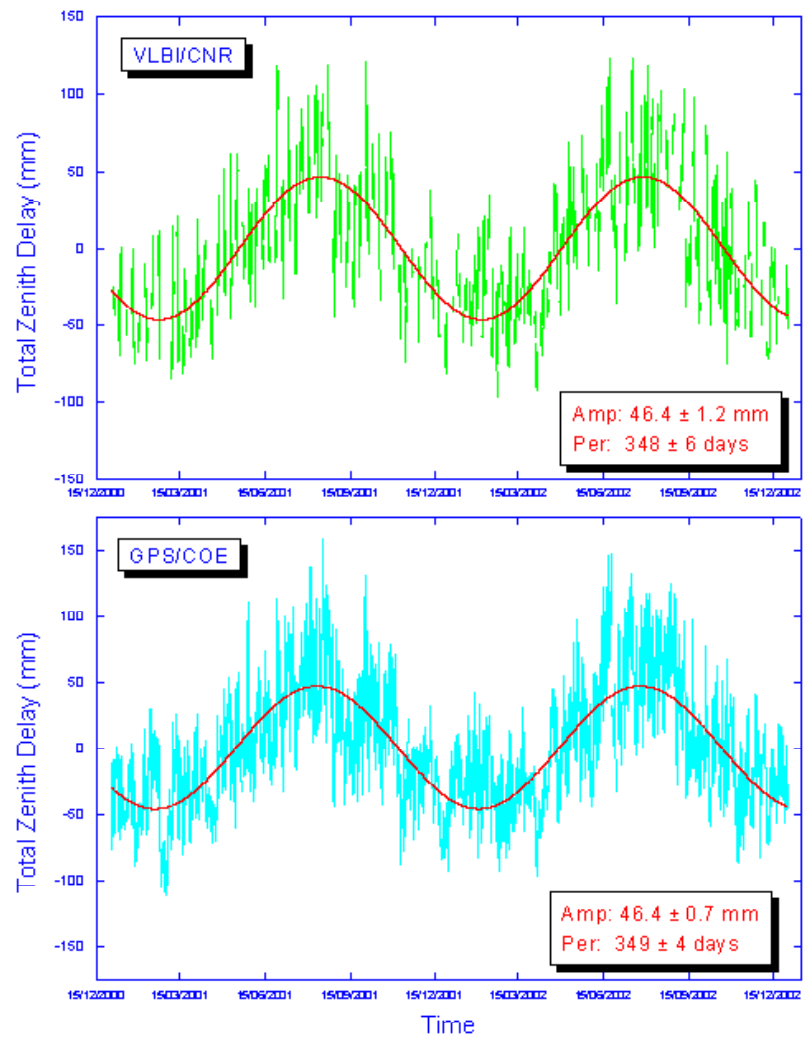


Figure 16: VLBI and GPS time series and best-fit seasonal waves: Wettzell.

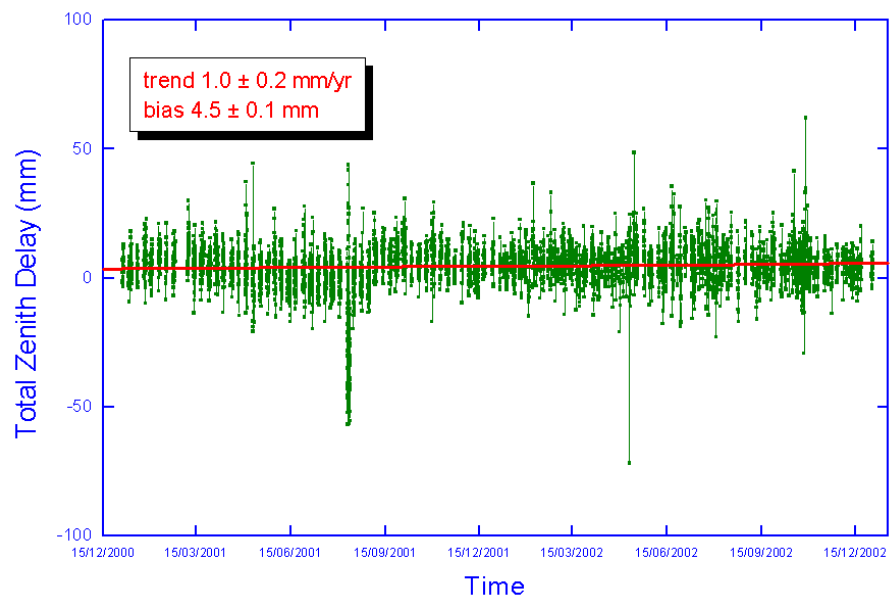


Figure 17: Difference GPS / VLBI: Wettzell.

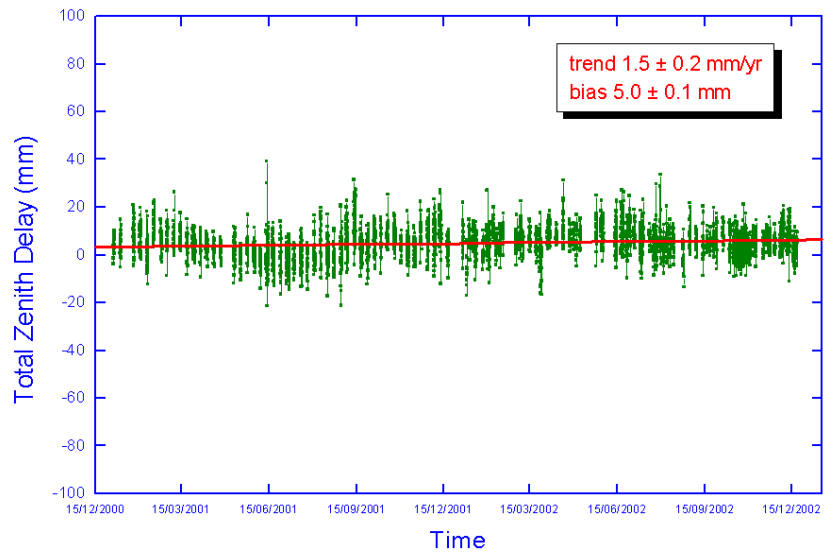


Figure 18: Difference GPS / VLBI: Ny Ålesund.

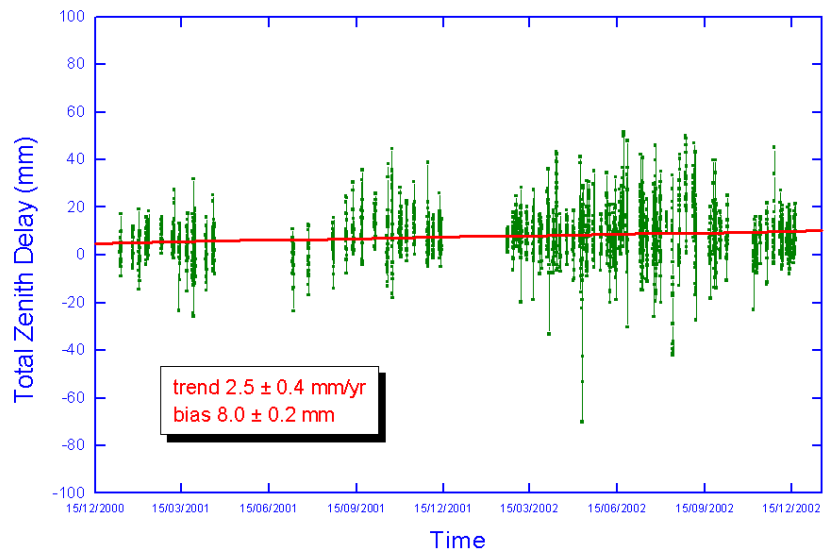


Figure 19: Difference GPS / VLBI: Matera.

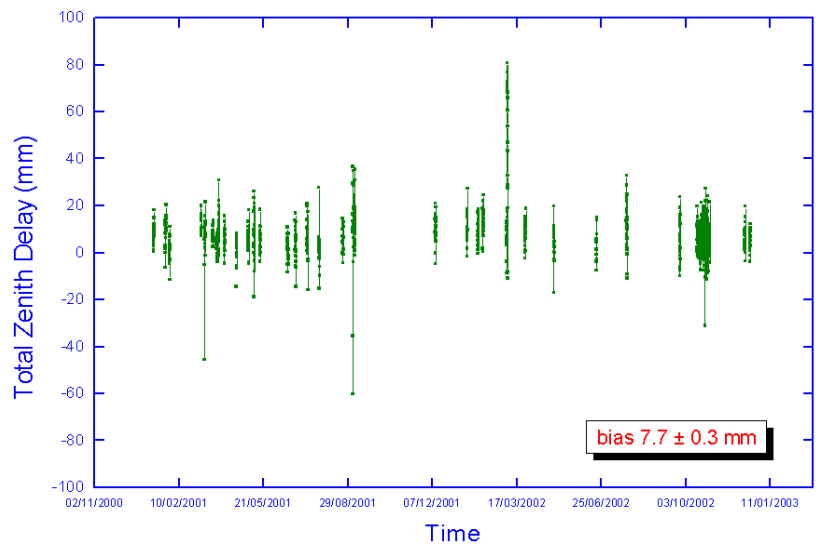


Figure 20: Difference GPS / VLBI: Onsala.

Table 1 shows the results for the 7 co-located sites. The last three rows of Table 1 present values slightly different from the others. In these cases we do not have 1-hour tropospheric parameters from GPS data. We decided to do not interpolate between 2 hours data, but we compared only rough means obtained by independent GPS and VLBI time series. This is not a rigorous method, so we are not completely confident on the results. In any case, applying this procedure we have found a negative bias for Gilcreek and Medicina, results that are meaningless. However other analysis performed in the past by our group have shown negative biases in the case of the Medicina station. We will further investigate on these topics, but it seems evident that the bias is not only due to the difference in height.

Table 1: Biases between VLBI and GPS tropospheric zenith delay before and after height corrections.

VLBI	GPS	Height diff (m)	Bias (mm)	Bias (mm) b. corr.	Bias (mm) a. corr.
Wettzell	WTZR	3,1	1,0	$4.5 \pm 0.1$	$3.5 \pm 0.1$
Nyales20	NYA1	3,1	1,1	$5.0 \pm 0.1$	$3.9 \pm 0.1$
Matera	MATE	7,7	2,5	$8.0 \pm 0.2$	$5.5 \pm 0.2$
Onsala60	ONSA	13,7	5,1	$7.7 \pm 0.3$	$2.6 \pm 0.3$
Gilcreek	FAIR	13,1	4,4	$-2.5 \pm 0.9$	$-6.9 \pm 0.9$
Westford	WES2	1,8	0,6	$4.9 \pm 1.3$	$4.3 \pm 1.3$
Medicina	MEDI	17,1	6,3	$1.1 \pm 1.6$	$-5.2 \pm 1.6$

## 4 Long-term time series

In the light of obtaining very long-term time series of tropospheric parameters, more useful for meteorological and climatologic studies, considering the fact that the time series can go back for about 15 years, we decided to analyze all the databases included in our AC catalogue, including, for the most part, experiments that contain at least three European stations. We re-analyzed all these databases in order to obtain a homogenous set of tropospheric parameters. In Figure 21 there are the results for the total zenith delay at the station of Wettzell since 1987 till 2002. In Figure 22 we have plotted the wet zenith delay and the linear trend we computed. We were very surprised to obtain a negative value that is  $-0.23 \pm 0.11$  mm/yr, but the series is very uneven and with a strong annual signal. We performed a spectral analysis in order to identify the signal, as shown in Figure 23. Then, we fitted the wet delay time series with the annual wave and we subtracted the best-fit wave from the data. On the residual series we computed the linear trend and we obtained a positive value  $0.60 \pm 0.08$  mm/yr, comparable with the one found out by another research group (Boehm et. al, 2003). We computed the linear trend of the dry zenith delay and we found out a negative value ( $-0.21 \pm 0.04$  mm/yr) as shown in figure 25. We computed the linear trend on the 2001-2002 time series for Wettzell, and we obtained positive values for wet and dry zenith delay,  $8.9 \pm 1.0$  and  $1.1 \pm 0.4$  mm/yr, respectively. We performed the same analysis also for Medicina, as shown in Figures 26-29. In this case, a positive trend is also present and its value is  $3.3 \pm 0.3$  mm/yr for the wet component.

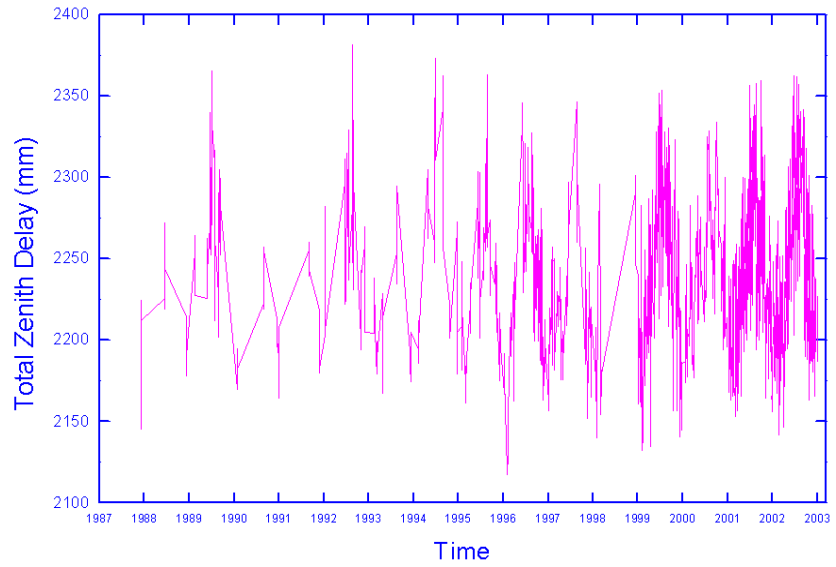


Figure 21: Total zenith delay time series: Wettzell.

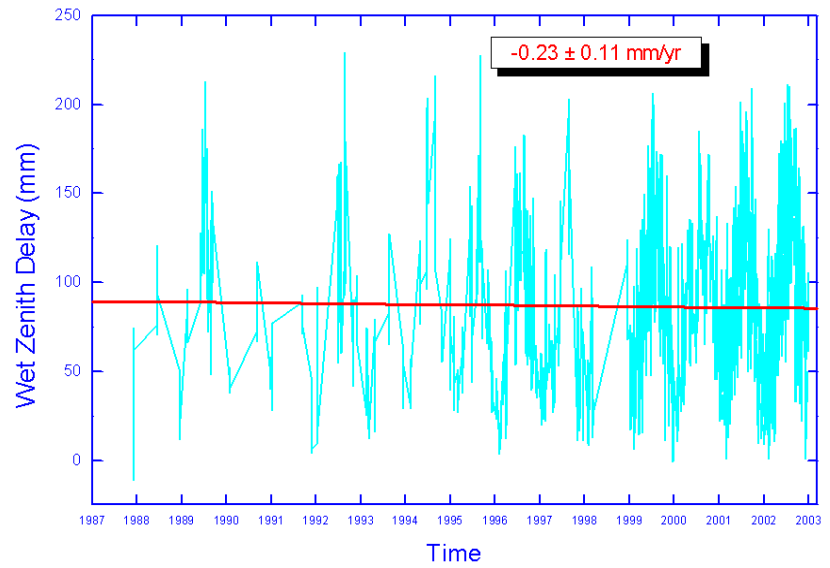


Figure 22: Wet zenith delay time series: Wettzell.

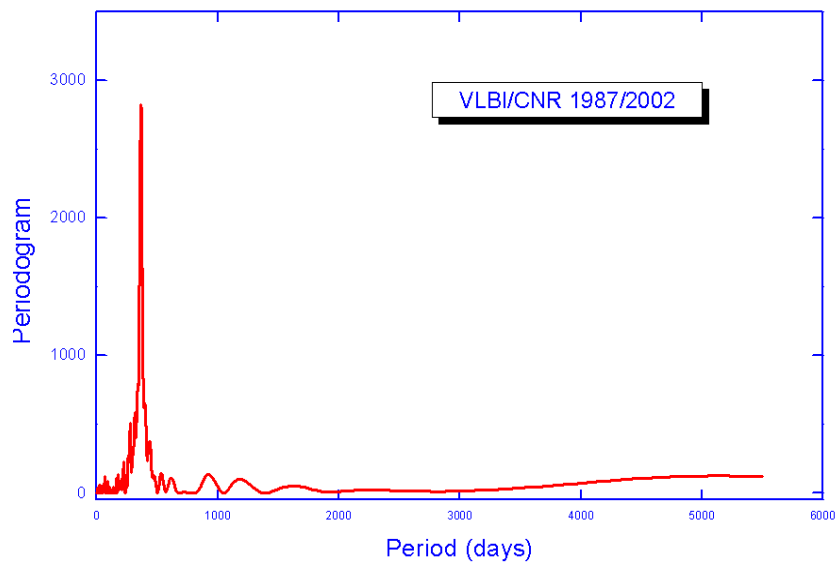


Figure 23: Spectral analysis: Wettzell.

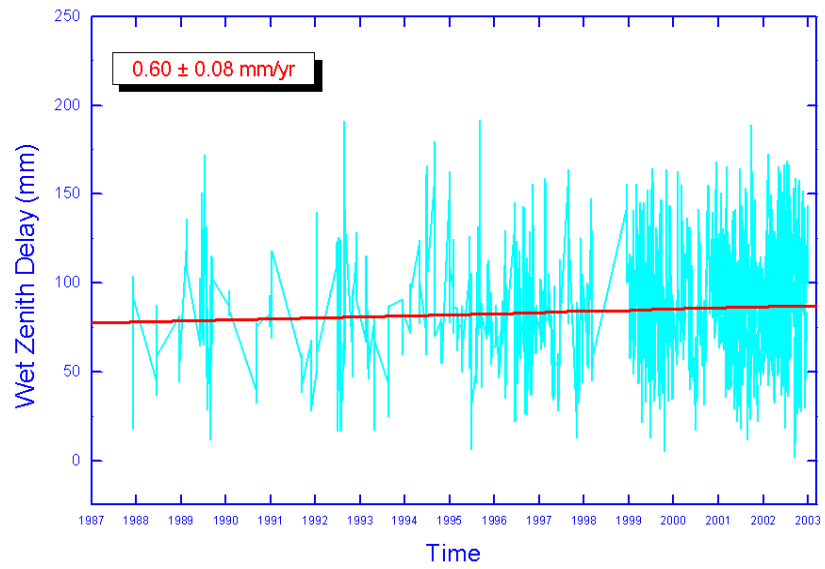


Figure 24: Wet zenith delay time series, annual signal removed: Wettzell.

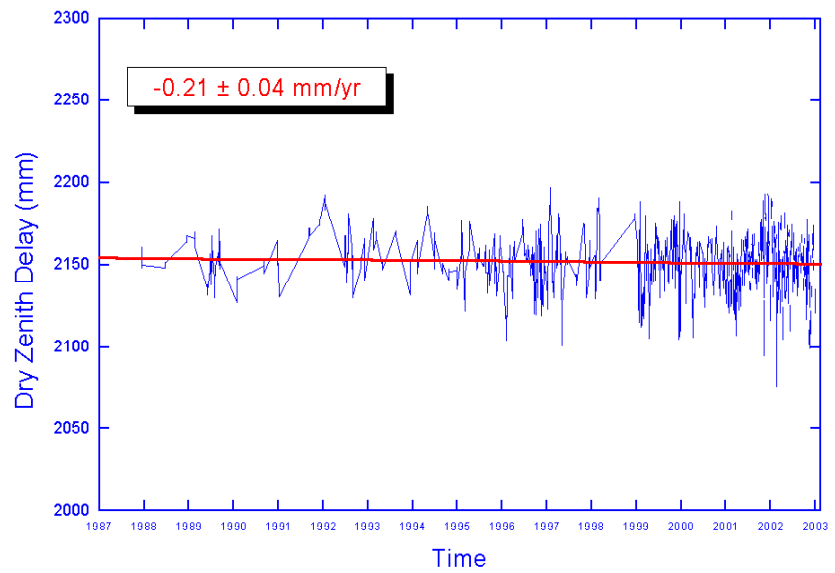


Figure 25: Dry zenith delay time series: Wettzell.

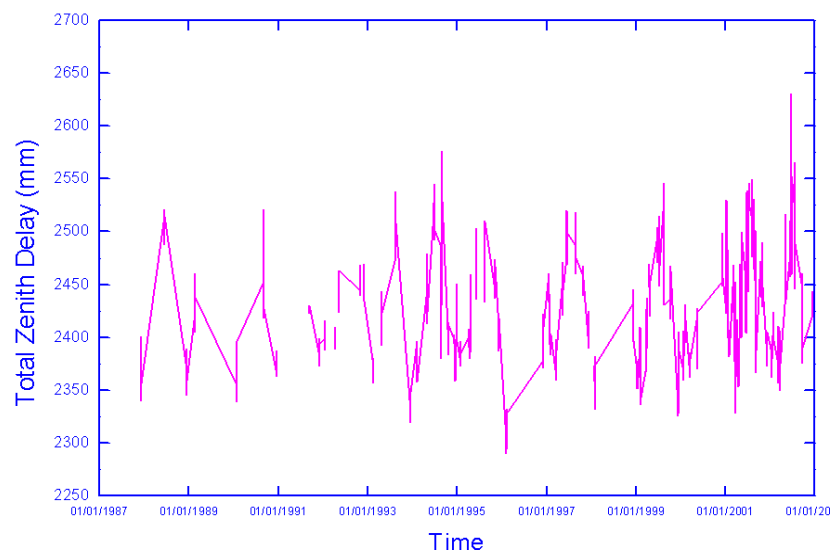


Figure 26: Total zenith delay time series: Medicina.

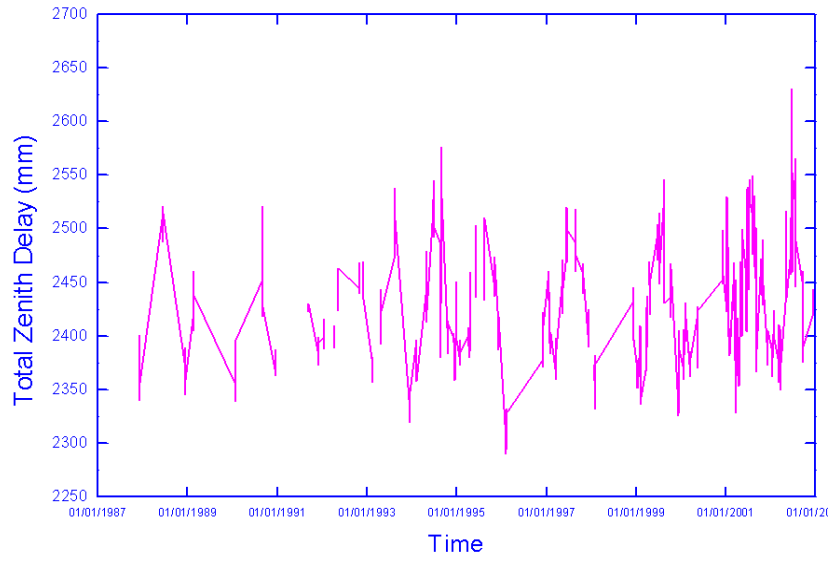


Figure 27: Wet zenith delay time series: Medicina.

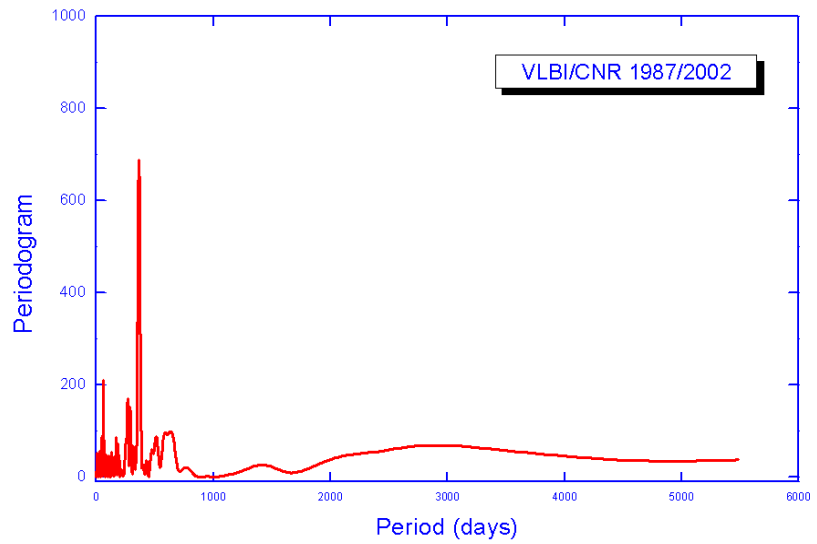


Figure 28: Spectral analysis: Medicina.

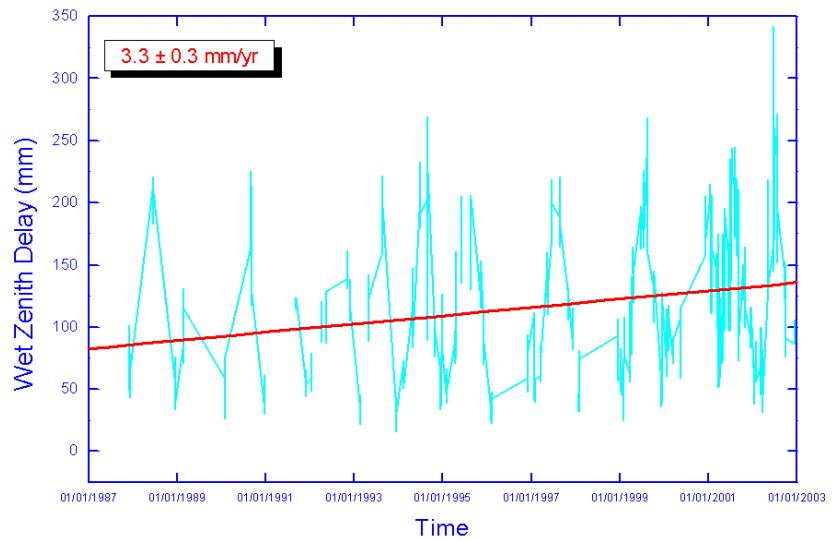


Figure 29: Wet zenith delay time series, annual signal removed: Medicina.

## 5 Conclusion and outlook

We analyzed all 2001 and 2002 databases present in the IVS data centers and, as an output, we obtained time series of tropospheric zenith delays for the stations involved into geodetic VLBI experiments. We performed spectral analysis on these series and we highlighted strong annual signals mainly due to the wet component. We compared VLBI data with GPS-derived tropospheric estimates. We found out common features and differences between the two techniques, even if they are supposed to be affected by the same effects. In particular the biases between the two techniques are confirmed and do not disappear even taking into account the height differences.

The long-term time series of tropospheric delays, confirm a positive linear trend, after the subtraction of the seasonal signal, for Wettzell and Medicina. In the case of Wettzell, for which the analysis on the shorter period has been performed, there is a strong indication of a faster increasing in time of the wet path delay. However, it should be pointed out that the period is probably too short to draw a final conclusion on a modification of the trend in global warming.

For the future we will continue the participation of our AC in the project TROP, follow-up of the PP, submitting regularly tropospheric parameters for IVS-R1 and IVS-R4 sessions. We also agreed to submit our long-term series of tropospheric parameters. We are working in order to complete our VLBI data catalogue and, at the moment, we are able to provide the project with our available data, only. But very soon we will complete the analysis also for the data bases not present, at the moment, in our catalog.

We will continue our test on comparing VLBI and GPS data and we will work on using wet zenith delay into VLBI data analysis in order to improve the repeatability of stations baselines.

## References

- Boehm, J., H. Schuh, V. Tesmer, H. Schmitz-Huebsch, 2003, Tropospheric zenith delays determined by VLBI as a contribution to climatological studies, *Oesterreichische Zeitschrift fuer Vermessung & Geoinformation (VGI)*, 1/2003, ed. by H. Schuh, F. Brunner, and H. Kahmen, pp. 21 - 28.
- Rioja, M.J. and P. Tomasi, 2001, External tropospheric calibration for VLBI observations, *Proceedings of the 15<sup>th</sup> Working Meeting on European VLBI for Geodesy and Astrometry*, pp 149-153.
- Schuh, H. and J. Boehm, 2003, Status Report of the IVS Pilot Project - Tropospheric Parameters in International VLBI Service for Geodesy and Astrometry 2002 Annual Report, edited by N. R. Vandenberg and K. D. Baver, NASA/TP-2003-211619, 13-21.

# VTRF2003: A Conventional VLBI Terrestrial Reference Frame

A. Nothnagel

*Geodetic Institute, University of Bonn, Germany*

**Summary:** A conventional terrestrial reference frame for determinations of earth orientation and tropospheric refraction parameters from VLBI observations is developed. Coordinates and velocities of a NASA Goddard Space Flight Center VLBI solution (gsf2003b) are transformed into a frame aligned to the ITRF2000 axis orientation and geocenter position. This is done on the basis of a Helmert transformation using the twelve IVS-R1 and IVS-R4 network stations as defining sites and applying the rotational and translational Helmert parameters estimated from the defining sites to transform the complete list of VLBI sites. Velocities are determined from positions of two epochs four years apart.

## 1 Introduction

The estimates of earth orientation parameters (EOP) from VLBI observations are directly dependent on the terrestrial reference frame (TRF) and the celestial reference frame (CRF) used in the solution. The choice of the CRF affects the estimates of the celestial pole parametrized by the nutation offsets. The TRF affects the polar motion estimates. UT1-UTC is dependent on the choice of both, TRF and CRF. Most recently the determination of tropospheric parameters has become another routine product from VLBI observations (Schuh and Boehm 2003) which are also affected, though probably to a lesser extent, by the choice of the TRF.

While the International Celestial Reference Frame (ICRF, Ma et al. 1996) with most of its radio source positions has been widely accepted as the most up-to-date standard for a CRF, the International Terrestrial Reference Frame in its latest realization (ITRF2000, Altamimi et al. 2002) has shown a few deficits for EOP determinations by VLBI. One of the reasons is that the ITRF2000 is based on observations until late 1999 only. Secondly, coordinates and velocities have been generated as a composite of VLBI and SLR and/or GPS results. Due to these deficits, the EOP combination of the International VLBI Service for Geodesy and Astrometry (IVS) has sometimes been degraded when IVS Analysis Centers provided EOP on the basis of fixing ITRF2000 (Steinforth, pers. communication).

Some of the VLBI analysis centers overcome this problem and determine their own realizations of a TRF and a CRF, mostly from an almost complete set of global VLBI observations. In this case, the solutions are constrained in some way to match the axis orientations and origins of the ICRF and ITRF2000. On the other hand there are groups which have to use predetermined reference frames for their purposes of analyzing VLBI observations for EOP or troposphere parameter estimation. The reason for this requirement is that not all VLBI analysis packages are able to handle the vast amount of VLBI data collected in the last 24 years to estimate station coordinates and velocities as global parameters.

The simplest way to provide an up-to-date TRF to groups requiring coordinates and velocities for their purposes would be to take over a VLBI solution from another group. However, the alignment with ITRF2000 has to be verified and possibly be corrected. The most up-to-date VLBI solution today (June 2003) in terms of data volume and state-of-the-art modeling is the gsf2003b solution of the VLBI group at NASA Goddard Space Flight Center (Ma et al. 2003). The coordinates and velocities

of this solution are used to develop a conventional VLBI terrestrial reference frame (VTRF2003) which is based on VLBI observations alone and matches the axis orientations and origin of ITRF2000 as closely as possible.

## 2 Data Analysis

Under the premises that EOP from VLBI should clearly represent the rotational relationship between the ITRF2000 and ICRF the procedure applied in generating VTRF2003 is the following: In a first step the gsf2003b station coordinates of epoch 1997.0 are transformed into station coordinates of epoch 2000.0 and 2004.0 using the velocities of this solution. The same is done with the ITRF2000 data set of VLBI sites. The next step is a least squares estimate of Helmert parameters needed to transform the gsf2003b coordinates into ITRF2000 for both epochs. The reason for using coordinates at two epochs instead of velocities is that discrepancies between the two frames become much more obvious than in the velocity domain.

The question now arises which sites to use for the determination of the Helmert parameters. The first criterion chosen is the difference of the geocentric radii between the ITRF2000 and gsf2003b solutions which should not exceed 25 mm. The site of OHIGGINS was not excluded although the difference in geocentric radius by far exceeds the threshold of 25 mm (48/66 mm). The reason is that OHIGGINS is the southernmost station at an otherwise sparsely covered area balancing the global distribution of stations. Figure 1 shows the differences of the geocentric radii for the epochs 2000.0 and 2004.0 for the 34 sites matching this criterion plus OHIGGINS. It is immediately obvious that the VLBI polyhedron is a few mm smaller than that of the ITRF2000. The discrepancy becomes even larger for the 2004.0 epoch.

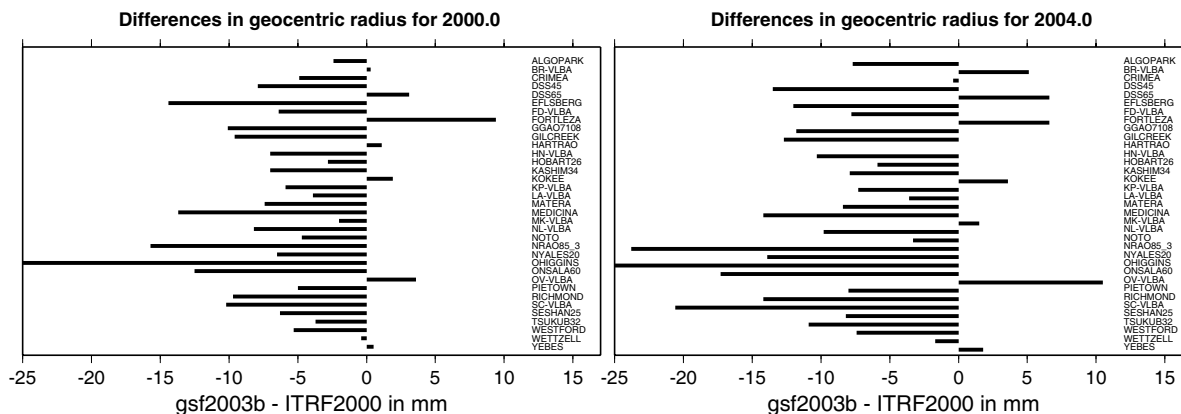


Figure 1: Differences in geocentric radii

The Helmert parameters which are estimated for transforming gsf2003b into ITRF2000 are listed in table 1. The translations and rotations are very small for both years representing a good alignment of the coordinate axes and the origins for this set of stations. However, the scale factors of 1.6 and 2.2 ppb are comparably large resulting in a displacement of about 1 cm at one earth radius. This confirms the scale difference already suggested by the differences of the geocentric radii.

At this point another aspect has to be taken into account: Only 12 of the 35 sites are regularly used in sessions for routine EOP determinations, i.e. in the weekly IVS-R1 and IVS-R4 sessions (table 2) contributing a large fraction of VLBI data observed today.

Table 1: Helmert parameters estimated using 35 sites

	2000	2004
$\alpha$	-37.5 $\pm$ 47 $\mu$ as	-43.0 $\pm$ 67 $\mu$ as
$\beta$	-36.2 $\pm$ 46 $\mu$ as	-0.1 $\pm$ 68 $\mu$ as
$\gamma$	-61.1 $\pm$ 31 $\mu$ as	-63.9 $\pm$ 45 $\mu$ as
$\Delta X$	-0.3 $\pm$ 1.1 mm	0.4 $\pm$ 1.7 mm
$\Delta Y$	0.5 $\pm$ 1.1 mm	0.3 $\pm$ 1.6 mm
$\Delta Z$	3.5 $\pm$ 1.2 mm	4.4 $\pm$ 1.8 mm
Scale	$1.6 \times 10^{-9} \pm 0.2 \times 10^{-9}$	$2.2 \times 10^{-9} \pm 0.2 \times 10^{-9}$

Table 2: List of IVS-R1 and IVS-R4 sites

ALGOPARK	FORTLEZA	GILCREEK	HARTRAO
HOBART	KOKEE	MATERA	NYALESUND
SESHAN	TSUKUBA32	WETTZELL	WESTFORD

Table 3: Helmert parameters estimated using 12 sites

	2000	2004
$\alpha$	-123.0 $\pm$ 43 $\mu$ as	-158.2 $\pm$ 70 $\mu$ as
$\beta$	-88.4 $\pm$ 42 $\mu$ as	-94.5 $\pm$ 71 $\mu$ as
$\gamma$	-27.3 $\pm$ 32 $\mu$ as	-15.3 $\pm$ 50 $\mu$ as
$\Delta X$	-2.5 $\pm$ 1.1 mm	-2.9 $\pm$ 1.8 mm
$\Delta Y$	2.6 $\pm$ 1.1 mm	3.2 $\pm$ 1.8 mm
$\Delta Z$	3.6 $\pm$ 1.2 mm	5.0 $\pm$ 1.9 mm
Scale	$0.8 \times 10^{-9} \pm 0.2 \times 10^{-9}$	$1.6 \times 10^{-9} \pm 0.3 \times 10^{-9}$

In order to evaluate the relationship between these 12 sites in gsf2003b and ITRF2000 a second Helmert adjustment has been carried out. Here, the results for the Helmert parameters look quite different (table 3) showing much larger discrepancies between the coordinate sets. The scale differences, however, are slightly smaller but still significant.

Considering the fact that these 12 stations are the predominant ground network for EOP determinations with VLBI and taking into account that the EOP should be consistent with ITRF2000 it was decided that only these 12 observatories are used as "defining" sites for the determination of the Helmert parameters.

Another item of concern is the significant difference of scale between ITRF2000 and gsf2003b. Since this is the case not only for the 12 "defining" sites but also for the 35 sites used previously, the scale difference has to be considered to be real. This is also being supported by the fact that almost all geocentric radii of the VLBI sites are larger than those of ITRF2000 (see Fig. 1)

In order to maintain the VLBI solution as such, i.e. the form and scale of the polyhedron, only the translational and rotational parameters are used to transform the gsf2003b coordinates into the ITRF2000 frame. This transformation is applied to the whole set of coordinates of 145 sites in the gsf2003b solution for the epochs 2000.0 and 2004.0.

From the two epochs the respective velocities are computed and the station coordinates are subsequently transformed to the epoch 1997.0 completing the components of VTRF2003 (Table. 4). Some of the sites are affected by earthquake induced or man-made episodic displacements. For these sites two data blocks are given, augmented with the epoch of the displacement.

The formal errors of the coordinates and velocities are computed using the error propagation law. Since the transformation parameters are estimated they have their own formal errors. In the transformation process the input formal errors of the coordinates and velocities are inflated by the contribution of the transformation parameters although the basic accuracy is not deteriorated

VTRF2003 is listed in table 4 as an appendix at end of the paper. It is also available electronically under the IVS Analysis Coordinators's Web page <sup>(1)</sup>.

### 3 Discussion

In figure 2 the differences of the input coordinate components of the 12 "defining" sites are displayed separately for the epochs 2000.0 and 2004.0. The differences of 2004.0 are generally larger than those of 2000.0 but with no obvious systematic distribution. Figure 3 then depicts the differences after a Helmert transformation using all 7 Helmert parameters. The sites of Fortaleza, Kokee Park and Tsukuba show residuals in both years which are much larger than those of the other stations. This behaviour suggests that the ITRF2000 coordinates of these sites are of a lesser quality than the others requiring a significant adjustment at the next realization of the ITRF.

The increase in scatter at 2004.0 as compared to 2000.0 suggests that the different velocities of the two systems lead to a divergence of the site positions. It can be assumed that the VLBI coordinates and velocities of gsf2003b are more up-to-date than ITRF2000 and that systematic errors in the VLBI data set are much smaller than these discrepancies. Therefore, special attention has to be paid to the velocity results at the next realization of the ITRF.

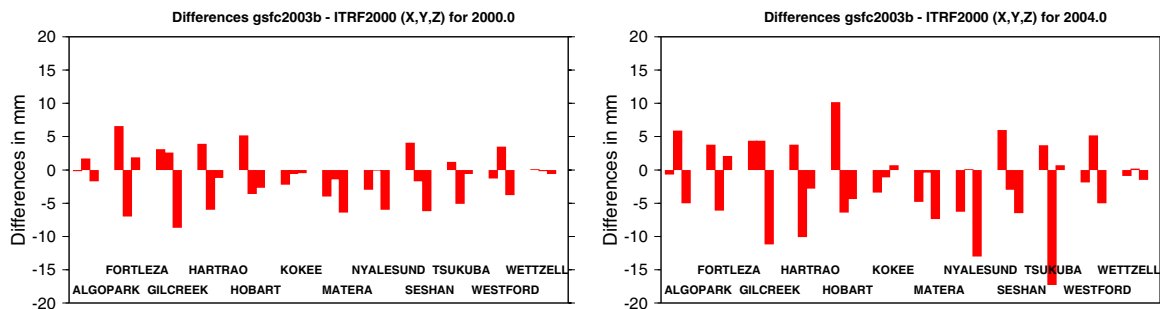


Figure 2: Differences in input coordinate components

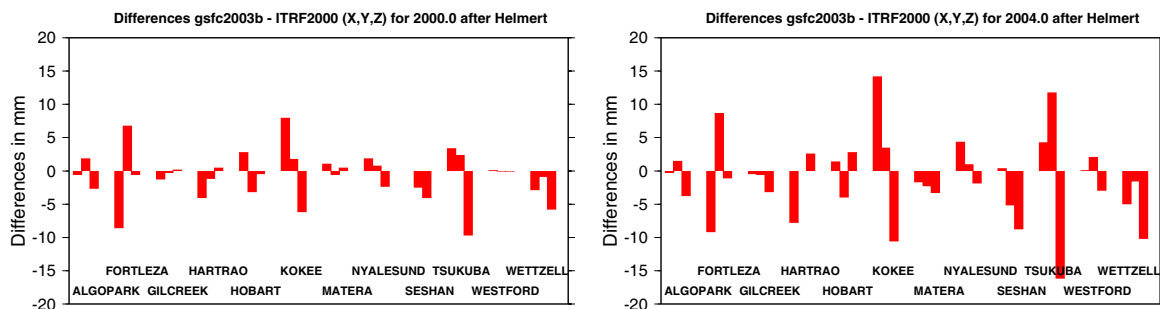


Figure 3: Differences in coordinate components after 7-parameter Helmert transformation

<sup>1</sup><http://giub.geod.uni-bonn.de/vlbi/IVS-AC>

In conclusion it can be said that the VTRF2003 has been aligned to the ITRF2000 axis orientation and to its origin as well as to its evolution in time. Keeping the scale of the gsf2003b VLBI solution guarantees that the VLBI polyhedron is not distorted. The VTRF2003 is thus well suited for the determination of earth orientation or troposphere parameters by VLBI with a fixed TRF.

## Acknowledgement

The Helmert parameter estimation program and the transformations into station coordinates of date have kindly been provided by Markus Vennebusch.

## References

- Altamimi et al. (2001): The terrestrial reference frame and the dynamic earth; *Eos Transactions, American Geophysical Union*, Vol. 82, No. 25, 273, 278-279
- Ma C., E.F. Arias, T.M. Eubanks, A.L. Fey, A.-M. Gontier, C.S. Jacobs, O.J. Sovers, B.A. Archinal, P. Charlot (1998) The International Celestial Reference Frame realized by VLBI; *Astronomy & Astrophysics*, Vol. 116, 516 - 546
- Ma C., D. MacMillan, L. Petrov, D. Gordon, K. Baver (2003): Quarterly GSFC EOP solution 2003b, NASA Goddard Space Flight Center, <http://lupus.gsfc.nasa.gov/global/glb.html>
- Schuh H. and J. Boehm (2003): Status report of the IVS Pilot Project - Tropospheric parameters; *International VLBI Service for Geodesy and Astrometry 2002 Annual Report*, N.R. Vandenberg and K. Baver (eds.) NASA/TP-2003-211619, 13 - 21

\$\$ VTRF2003, epoch 1997.0

\$\$ Sites with episodic motions have the year of the displacement

\$\$ encoded in the last two characters of their name

\$\$	X/Vx	Y/Vy	Z/Vz	Sigmas		
ALGOPARK	918034.7426	-4346132.2722	4561971.1669	0.0019	0.0018	0.0019
	-0.0164	-0.0031	0.0019	0.0003	0.0003	0.0003
FORTLEZA	4985370.0440	-3955020.3244	-428472.2856	0.0019	0.0019	0.0021
	-0.0022	-0.0041	0.0123	0.0003	0.0003	0.0004
GILCREEK	-2281547.3065	-1453645.0856	5756993.1579	0.0019	0.0019	0.0016
	-0.0220	-0.0032	-0.0095	0.0003	0.0003	0.0003
GILCRE02	-2281547.3421	-1453645.1411	5756993.1454	0.0019	0.0020	0.0017 021103
	-0.0220	-0.0032	-0.0095	0.0003	0.0003	0.0003
HARTRAO	5085442.7802	2668263.4915	-2768697.0123	0.0020	0.0019	0.0021
	-0.0013	0.0190	0.0159	0.0003	0.0003	0.0003
HOBART26	-3950236.7399	2522347.5620	-4311562.5352	0.0022	0.0021	0.0021
	-0.0387	0.0087	0.0400	0.0004	0.0003	0.0004
KOKEE	-5543837.6302	-2054567.8591	2387851.9414	0.0016	0.0018	0.0021
	-0.0099	0.0630	0.0304	0.0003	0.0003	0.0003
MATERA	4641938.7658	1393003.0160	4133325.5416	0.0018	0.0019	0.0019
	-0.0190	0.0192	0.0132	0.0003	0.0003	0.0003
NYALES20	1202462.7537	252734.3943	6237766.0394	0.0020	0.0020	0.0016
	-0.0153	0.0075	0.0076	0.0003	0.0003	0.0003
SESHAN25	-2831686.9120	4675733.6655	3275327.6899	0.0019	0.0019	0.0021
	-0.0302	-0.0115	-0.0129	0.0003	0.0003	0.0004
TSUKUB32	-3957408.7810	3310229.3938	3737494.8191	0.0024	0.0022	0.0025
	-0.0006	0.0043	-0.0078	0.0004	0.0004	0.0004
WESTFORD	1492206.5875	-4458130.5153	4296015.5379	0.0018	0.0017	0.0018
	-0.0159	-0.0009	0.0025	0.0003	0.0003	0.0003
WETZELL	4075539.8834	931735.2612	4801629.3724	0.0018	0.0019	0.0017
	-0.0160	0.0172	0.0088	0.0003	0.0003	0.0003
AIRA	-3530219.3232	4118797.5785	3344015.8725	0.0047	0.0046	0.0043
	-0.0279	-0.0089	-0.0194	0.0008	0.0007	0.0007
AUSTINTX	-737793.8412	-5459892.2834	3202990.4331	0.0330	0.0255	0.0305
	-0.0117	-0.0001	-0.0091	0.0046	0.0034	0.0043
AZORES	4552174.6197	-2186664.6916	3882779.7958	0.0155	0.0182	0.0165
	0.0004	0.0162	0.0113	0.0024	0.0029	0.0026
BERMUDA	2307209.4630	-4874215.9436	3394318.0367	0.0324	0.0426	0.0375
	-0.0126	-0.0011	0.0068	0.0045	0.0057	0.0051
BLKBUTTE	-2306307.0319	-4787914.3767	3515736.3444	0.0417	0.0843	0.0599
	-0.0160	0.0095	-0.0131	0.0058	0.0118	0.0084
BLOOMIND	302384.4070	-4941699.0731	4007908.5118	0.0408	0.0579	0.0497
	-0.0130	0.0011	-0.0014	0.0056	0.0076	0.0066
BR-VLBA	-2112064.9776	-3705356.5187	4726813.7965	0.0019	0.0018	0.0018
	-0.0143	0.0016	-0.0100	0.0003	0.0003	0.0003
BREST	4228877.0946	-333104.1821	4747181.0177	0.0245	0.0266	0.0227
	-0.0135	0.0180	0.0089	0.0034	0.0039	0.0032
CARNUSTY	3526416.3329	-171421.1960	5294098.8747	0.0254	0.0269	0.0221
	-0.0165	0.0042	0.0114	0.0036	0.0039	0.0030
CARROLGA	453520.5637	-5300506.7797	3507207.4563	0.0345	0.0436	0.0362
	-0.0143	-0.0010	0.0004	0.0048	0.0058	0.0049
CHICHI10	-4490618.4832	3483908.1712	2884899.1420	0.0053	0.0046	0.0043
	0.0223	0.0281	0.0093	0.0009	0.0008	0.0007
CHLBOLTN	4008310.0634	-100650.7471	4943794.8058	0.0427	0.0541	0.0351
	-0.0119	0.0183	0.0103	0.0057	0.0073	0.0047
CRIMEA	3785231.0621	2551207.4134	4439796.3791	0.0026	0.0022	0.0029
	-0.0197	0.0169	0.0099	0.0005	0.0004	0.0005
CTVASBAY	1091444.6699	-4351283.4943	4518706.9745	0.0202	0.0157	0.0151
	-0.0163	-0.0014	0.0028	0.0031	0.0024	0.0023
CTVASTJ	2612546.9492	-3426880.4389	4686758.3574	0.0212	0.0205	0.0176
	-0.0173	-0.0017	0.0086	0.0032	0.0030	0.0026

DEADMANL	-2336820.0032	-4732587.5038	3570330.3467	0.1296	0.2472	0.1733	
	-0.0454	-0.0550	0.0349	0.0182	0.0348	0.0244	
DSS15	-2353538.8540	-4641649.4947	3676670.0010	0.0034	0.0052	0.0055	
	-0.0188	0.0059	-0.0050	0.0005	0.0007	0.0008	
DSS15_92	-2353538.8456	-4641649.4836	3676669.9799	0.0020	0.0021	0.0023	920627
	-0.0188	0.0059	-0.0049	0.0003	0.0003	0.0004	
DSS45	-4460935.4007	2682765.7113	-3674381.1884	0.0028	0.0024	0.0027	
	-0.0359	0.0007	0.0442	0.0004	0.0004	0.0004	
DSS65	4849336.6884	-360488.7921	4114748.8390	0.0027	0.0019	0.0028	
	-0.0074	0.0191	0.0142	0.0004	0.0003	0.0005	
DSS65_97	4849336.6917	-360488.7905	4114748.8281	0.0026	0.0019	0.0028	970415
	-0.0074	0.0191	0.0142	0.0004	0.0003	0.0005	
EFLSBERG	4033947.4617	486990.5107	4900430.8017	0.0030	0.0020	0.0033	
	-0.0145	0.0176	0.0084	0.0005	0.0003	0.0005	
EFLSBE96	4033947.4786	486990.5144	4900430.8212	0.0028	0.0020	0.0031	961001
	-0.0145	0.0177	0.0084	0.0004	0.0003	0.0005	
ELY	-2077236.4066	-4486712.7098	4018753.6833	0.0239	0.0513	0.0424	
	-0.0182	0.0033	-0.0113	0.0034	0.0073	0.0060	
FD-VLBA	-1324009.1284	-5332181.9656	3231962.4686	0.0018	0.0016	0.0020	
	-0.0127	0.0004	-0.0062	0.0003	0.0003	0.0003	
FLAGSTAF	-1923992.7774	-4850854.6341	3658589.3170	0.0223	0.0534	0.0415	
	-0.0185	-0.0084	-0.0033	0.0031	0.0075	0.0059	
FORT_ORD	-2697026.9718	-4354393.0744	3788077.8293	0.0307	0.0492	0.0424	
	-0.0307	0.0287	0.0221	0.0043	0.0069	0.0059	
FORTORDS	-2699840.4701	-4359126.8629	3781051.1899	0.0259	0.0415	0.0355	
	-0.0307	0.0287	0.0221	0.0037	0.0059	0.0051	
FORTOR89	-2699840.4448	-4359126.8377	3781051.2296	0.0222	0.0355	0.0306	891001
	-0.0307	0.0287	0.0221	0.0033	0.0052	0.0045	
FTD_7900	-1324228.1352	-5332062.8366	3232023.2669	0.0266	0.0199	0.0244	
	-0.0002	0.0000	0.0001	0.0035	0.0026	0.0032	
GBT-VLBA	882589.6547	-4924872.4031	3943729.4192	0.0023	0.0039	0.0033	
	-0.0145	-0.0022	0.0029	0.0004	0.0005	0.0005	
GGA07108	1130794.7591	-4831233.8071	3994217.0386	0.0020	0.0028	0.0027	
	-0.0153	-0.0003	0.0004	0.0003	0.0005	0.0005	
GIFU3	-3787518.2176	3564247.1748	3679797.1929	0.0134	0.0130	0.0144	
	-0.0110	-0.0065	-0.0045	0.0021	0.0021	0.0023	
GOLDVENU	-2351129.1861	-4655477.0323	3660956.8788	0.0057	0.0097	0.0092	
	-0.0143	0.0081	-0.0078	0.0008	0.0014	0.0013	
GORF7102	1130686.5083	-4831353.0320	3994110.9308	0.0026	0.0061	0.0051	
	-0.0153	-0.0003	0.0004	0.0004	0.0009	0.0007	
GRASSE	4581697.6438	556125.7549	4389351.4603	0.0224	0.0265	0.0229	
	-0.0132	0.0189	0.0104	0.0032	0.0039	0.0032	
HALEAKAL	-5465998.5481	-2404408.0223	2242228.7595	0.0148	0.0074	0.0074	
	-0.0100	0.0649	0.0313	0.0019	0.0010	0.0010	
HATCREEK	-2523970.0452	-4123506.3267	4147752.5550	0.0043	0.0065	0.0062	
	-0.0196	0.0063	-0.0074	0.0006	0.0009	0.0009	
HAYSTACK	1492404.7397	-4457266.5274	4296881.7819	0.0022	0.0032	0.0035	
	-0.0147	-0.0020	0.0041	0.0003	0.0005	0.0005	
HN-VLBA	1446375.1125	-4447939.6569	4322306.1184	0.0019	0.0018	0.0019	
	-0.0154	-0.0013	0.0030	0.0003	0.0003	0.0003	
HOFN	2679650.2578	-727916.4424	5722807.2552	0.0184	0.0186	0.0187	
	-0.0065	0.0146	0.0130	0.0029	0.0030	0.0026	
HOHENFRG	3778214.7103	698644.6263	5074053.6988	0.0227	0.0270	0.0178	
	-0.0336	-0.0031	0.0196	0.0033	0.0039	0.0026	
HOHNBERG	4213687.2409	820422.9601	4702784.2484	0.0194	0.0189	0.0194	
	-0.0100	0.0192	0.0061	0.0029	0.0030	0.0028	
HRAS_085	-1324210.9895	-5332023.1252	3232118.3411	0.0022	0.0041	0.0034	
	-0.0117	0.0034	-0.0088	0.0003	0.0006	0.0005	
JPL_MV1	-2493306.2168	-4655197.4756	3565519.4529	0.0289	0.0526	0.0394	
	-0.0324	0.0179	0.0084	0.0040	0.0073	0.0055	

KANOZAN	-3991747.4430	3355061.7986	3661225.3479	0.0165	0.0161	0.0164	
	-0.0001	0.0061	-0.0106	0.0025	0.0026	0.0026	
KARLBURG	3653204.3446	884427.6138	5135732.0775	0.0214	0.0190	0.0239	
	0.0063	0.0236	-0.0100	0.0031	0.0030	0.0033	
KASHIM11	-3997505.6724	3276878.4045	3724240.7130	0.0023	0.0022	0.0024	
	0.0013	0.0040	-0.0088	0.0004	0.0003	0.0004	
KASHIM34	-3997649.2202	3276690.7470	3724278.8345	0.0028	0.0026	0.0027	
	0.0013	0.0040	-0.0088	0.0004	0.0004	0.0004	
KASHIMA	-3997892.2678	3276581.2771	3724118.2371	0.0021	0.0020	0.0022	
	-0.0011	0.0061	-0.0095	0.0003	0.0003	0.0004	
KAUAI	-5543846.0631	-2054563.6353	2387814.1167	0.0026	0.0021	0.0026	
	-0.0100	0.0649	0.0313	0.0004	0.0003	0.0004	
KIRSBERG	3879830.8653	987963.3080	4948713.2774	0.0193	0.0186	0.0196	
	0.0175	0.0122	-0.0178	0.0029	0.0030	0.0028	
KODIAK	-3026940.3008	-1575911.7815	5370362.4979	0.0346	0.0223	0.0591	
	-0.0208	0.0029	-0.0010	0.0049	0.0032	0.0084	
KOGANEI	-3941937.4418	3368150.9024	3702235.3019	0.0028	0.0026	0.0028	
	-0.0010	0.0026	-0.0049	0.0005	0.0004	0.0005	
KOGANEI3	-3942077.3723	3368332.1040	3701904.8344	0.0110	0.0109	0.0102	
	-0.0010	0.0026	-0.0049	0.0015	0.0014	0.0014	
KP-VLBA	-1995678.6288	-5037317.7144	3357328.1263	0.0018	0.0017	0.0020	
	-0.0134	0.0011	-0.0083	0.0003	0.0003	0.0003	
KWAJAL26	-6143536.3253	1363997.8063	1034707.6775	0.0585	0.0170	0.0236	
	0.0191	0.0714	0.0267	0.0081	0.0024	0.0033	
LA-VLBA	-1449752.3610	-4975298.5898	3709123.9236	0.0018	0.0016	0.0019	
	-0.0142	0.0014	-0.0069	0.0003	0.0003	0.0003	
LEONRDOK	-522231.6283	-5145676.8797	3720152.3480	0.0328	0.0288	0.0299	
	-0.0125	0.0017	-0.0043	0.0046	0.0039	0.0041	
MAMMOTHL	-2448246.8070	-4426738.1336	3875435.7697	0.0975	0.1730	0.1424	
	-0.0136	0.0219	-0.0159	0.0134	0.0238	0.0196	
MARCUS	-5227446.4549	2551379.6651	2607604.9887	0.0295	0.0187	0.0201	
	0.0511	0.0526	0.0205	0.0048	0.0031	0.0033	
MARPOINT	1106629.2935	-4882907.1811	3938086.9734	0.0053	0.0159	0.0131	
	-0.0157	0.0014	-0.0005	0.0008	0.0022	0.0019	
MCD_7850	-1330008.1910	-5328391.5890	3236502.7099	0.0287	0.0199	0.0261	
	-0.0126	-0.0001	-0.0064	0.0041	0.0028	0.0037	
MEDICINA	4461369.9765	919596.8216	4449559.1976	0.0019	0.0019	0.0020	
	-0.0189	0.0193	0.0091	0.0003	0.0003	0.0003	
MEDICI96	4461369.9837	919596.8199	4449559.2070	0.0019	0.0019	0.0020	960601
	-0.0189	0.0193	0.0091	0.0003	0.0003	0.0003	
METSHOVI	2890652.7526	1310295.3372	5513958.7455	0.0292	0.0275	0.0281	
	-0.0160	0.0149	0.0092	0.0041	0.0040	0.0038	
MIAMI20	961255.3291	-5674092.5958	2740533.7931	0.0020	0.0031	0.0025	
	-0.0096	-0.0003	0.0007	0.0003	0.0005	0.0004	
MILESMON	-1204439.0667	-4239211.1053	4596266.0198	0.0320	0.0417	0.0407	
	-0.0141	-0.0005	-0.0072	0.0045	0.0056	0.0054	
MIURA	-3976129.9629	3377927.8818	3656753.8476	0.0032	0.0029	0.0031	
	0.0120	0.0027	0.0037	0.0006	0.0005	0.0005	
MIURA_00	-3976129.9628	3377927.8668	3656753.8547	0.0040	0.0036	0.0038	000701
	0.0120	0.0027	0.0037	0.0006	0.0006	0.0006	
MIYAZAKI	-3582768.0630	4052033.9555	3369020.5386	0.1063	0.0717	0.1093	
	-0.0221	-0.0087	-0.0123	0.0139	0.0094	0.0143	
MIZNAO10	-3857236.1032	3108803.2087	4003883.0747	0.0071	0.0059	0.0068	
	0.0035	0.0024	-0.0065	0.0012	0.0010	0.0012	
MIZUSGSI	-3862411.8942	3105015.0177	4001944.8655	0.0106	0.0087	0.0104	
	0.0035	0.0024	-0.0065	0.0016	0.0013	0.0016	
MK-VLBA	-5464074.9627	-2495249.1156	2148296.8452	0.0017	0.0018	0.0021	
	-0.0144	0.0627	0.0299	0.0003	0.0003	0.0004	
MOJ_7288	-2356494.1721	-4646607.6470	3668426.6063	0.0061	0.0113	0.0085	
	-0.0149	0.0075	-0.0065	0.0008	0.0015	0.0011	

MOJAVE12	-2356171.0534	-4646755.8473	3668470.5864	0.0020	0.0023	0.0026	
	-0.0149	0.0075	-0.0065	0.0003	0.0004	0.0004	
MOJAVE92	-2356171.0760	-4646755.8536	3668470.5792	0.0023	0.0030	0.0032	920627
	-0.0149	0.0075	-0.0064	0.0004	0.0004	0.0005	
MON_PEAK	-2386289.6280	-4802346.3159	3444884.0693	0.0136	0.0277	0.0199	
	-0.0324	0.0315	0.0068	0.0019	0.0039	0.0028	
MV2ONSLA	3370641.9532	711866.1152	5349796.1723	0.0081	0.0037	0.0128	
	-0.0144	0.0148	0.0090	0.0011	0.0005	0.0017	
NL-VLBA	-130872.2563	-4762317.1166	4226851.0347	0.0019	0.0017	0.0019	
	-0.0155	0.0015	-0.0036	0.0003	0.0003	0.0003	
NOBEY_6M	-3871168.2933	3428273.9971	3723697.5992	0.0215	0.0217	0.0209	
	-0.0043	0.0072	-0.0107	0.0031	0.0031	0.0030	
NOME	-2658150.6223	-693821.9911	5737236.6014	0.0331	0.0140	0.0633	
	-0.0279	-0.0084	-0.0033	0.0047	0.0020	0.0089	
NOTO	4934563.1178	1321201.2594	3806484.4938	0.0023	0.0019	0.0022	
	-0.0174	0.0178	0.0142	0.0004	0.0003	0.0004	
NRAO_140	882879.8840	-4924482.3067	3944130.6868	0.0019	0.0027	0.0026	
	-0.0149	0.0000	-0.0001	0.0003	0.0004	0.0004	
NRAO20	883772.7463	-4924385.5943	3944042.4911	0.0019	0.0018	0.0020	
	-0.0145	-0.0022	0.0029	0.0003	0.0003	0.0003	
NRAO85_1	883555.5460	-4924490.8854	3943961.9597	0.0022	0.0049	0.0043	
	-0.0149	0.0000	0.0000	0.0003	0.0007	0.0006	
NRAO85_3	882325.5577	-4925137.9909	3943397.6792	0.0019	0.0020	0.0021	
	-0.0155	0.0007	-0.0005	0.0003	0.0003	0.0004	
OCOTILLO	-2335601.3858	-4832244.0010	3434392.8051	0.0450	0.0540	0.0484	
	-0.0297	0.0252	0.0155	0.0061	0.0071	0.0065	
OHIGGINS	1525833.0138	-2432463.6474	-5676174.4785	0.0032	0.0037	0.0057	
	0.0177	-0.0006	-0.0002	0.0006	0.0006	0.0010	
ONSALA60	3370606.0250	711917.4829	5349830.7408	0.0019	0.0019	0.0018	
	-0.0144	0.0148	0.0090	0.0003	0.0003	0.0003	
ONSALA85	3370966.1237	711465.9552	5349664.0288	0.0111	0.0039	0.0175	
	-0.0144	0.0148	0.0090	0.0015	0.0005	0.0023	
OV-VLBA	-2409150.1142	-4478573.2312	3838617.3965	0.0018	0.0017	0.0019	
	-0.0182	0.0074	-0.0058	0.0003	0.0003	0.0003	
OVR_7853	-2410421.3065	-4477800.3592	3838690.2952	0.0066	0.0117	0.0096	
	-0.0168	0.0084	-0.0068	0.0009	0.0016	0.0013	
OVRO_130	-2409600.8383	-4478349.5150	3838603.2038	0.0045	0.0085	0.0073	
	-0.0168	0.0084	-0.0067	0.0006	0.0012	0.0010	
PARKES	-4554232.0113	2816758.9717	-3454035.8428	0.0187	0.0122	0.0149	
	-0.0351	-0.0032	0.0470	0.0032	0.0021	0.0026	
PBLOSSOM	-2464071.0000	-4649425.3836	3593905.6645	0.0405	0.0745	0.0557	
	-0.0168	0.0300	-0.0072	0.0056	0.0103	0.0077	
PENTICTN	-2058840.5478	-3621286.5380	4814420.8486	0.0329	0.0530	0.0689	
	-0.0225	-0.0141	0.0079	0.0047	0.0076	0.0099	
PIETOWN	-1640953.7131	-5014816.0253	3575411.8760	0.0018	0.0016	0.0020	
	-0.0154	0.0001	-0.0088	0.0003	0.0003	0.0003	
PINFLATS	-2369636.0959	-4761324.7966	3511116.2114	0.0242	0.0466	0.0353	
	-0.0245	0.0161	0.0040	0.0034	0.0065	0.0049	
PLATTVIL	-1240708.2190	-4720454.4020	4094481.6334	0.0104	0.0309	0.0262	
	-0.0169	-0.0033	-0.0057	0.0015	0.0044	0.0037	
PRESIDIO	-2707704.9867	-4257609.3815	3888374.2348	0.0294	0.0459	0.0405	
	-0.0205	0.0275	0.0029	0.0041	0.0064	0.0057	
PRESID89	-2707704.9759	-4257609.3746	3888374.2177	0.0218	0.0339	0.0303	891001
	-0.0205	0.0275	0.0029	0.0032	0.0050	0.0045	
PT_REYES	-2732333.2956	-4217634.7393	3914491.2917	0.0213	0.0319	0.0301	
	-0.0290	0.0203	0.0238	0.0031	0.0046	0.0043	
PVERDES	-2525452.9640	-4670035.3899	3522886.8436	0.0366	0.0654	0.0496	
	-0.0258	0.0355	0.0049	0.0052	0.0094	0.0071	
QUINCY	-2517230.9988	-4198595.1563	4076531.2278	0.0164	0.0266	0.0250	
	-0.0196	0.0100	-0.0091	0.0023	0.0038	0.0035	

RICHMOND	961258.0539	-5674090.0529	2740533.8056	0.0020	0.0027	0.0024	
	-0.0096	-0.0003	0.0007	0.0003	0.0004	0.0004	
ROBLED32	4849245.2304	-360278.1612	4114884.6069	0.0529	0.0110	0.0444	
	-0.0074	0.0191	0.0142	0.0069	0.0014	0.0058	
SAGARA	-3913437.8276	3501122.8098	3608593.5369	0.0206	0.0188	0.0207	
	-0.0117	0.0011	-0.0132	0.0030	0.0029	0.0031	
SANPAULA	-2554476.9179	-4608627.2348	3582138.4526	0.0353	0.0626	0.0475	
	-0.0354	0.0194	0.0135	0.0050	0.0089	0.0068	
SANTIA12	1769693.1154	-5044504.5277	-3468434.9656	0.0033	0.0049	0.0043	
	0.0242	-0.0069	0.0095	0.0006	0.0009	0.0008	
SC-VLBA	2607848.5187	-5488069.6866	1932739.5348	0.0018	0.0019	0.0021	
	0.0074	0.0094	0.0109	0.0003	0.0003	0.0004	
SEATTLE1	-2295347.9947	-3638029.3635	4693408.4970	0.0691	0.4438	0.4433	
	-0.0076	0.0153	-0.0268	0.0102	0.0663	0.0662	
SEST	1838237.8852	-5258699.2655	-3100588.7474	0.0251	0.0222	0.0235	
	-0.0003	-0.0046	0.0081	0.0037	0.0031	0.0034	
SINTOTU	-3642141.9139	2861496.5661	4370361.6485	0.0151	0.0124	0.0161	
	-0.0086	0.0024	-0.0100	0.0021	0.0017	0.0023	
SINTOTU3	-3642142.0819	2861496.6704	4370361.8351	0.0066	0.0055	0.0072	
	-0.0086	0.0024	-0.0099	0.0011	0.0009	0.0012	
SNDPOINT	-3425462.0255	-1214669.1176	5223858.1691	0.0407	0.0255	0.0617	
	-0.0210	0.0033	-0.0109	0.0059	0.0037	0.0089	
SOURDOGH	-2419993.6781	-1664228.7276	5643538.0903	0.0461	0.0357	0.1061	
	-0.0272	0.0031	-0.0207	0.0064	0.0049	0.0147	
SOURD087	-2419993.6625	-1664228.7480	5643538.1356	0.0347	0.0270	0.0796	871201
	-0.0273	0.0032	-0.0207	0.0050	0.0039	0.0115	
SUWON	-3062023.9952	4055453.8006	3841809.9765	0.0183	0.0178	0.0176	
	-0.0287	-0.0073	-0.0096	0.0028	0.0027	0.0027	
SVETLOE	2730173.9640	1562442.5798	5529969.0371	0.0213	0.0226	0.0132	
	-0.0182	0.0139	0.0054	0.0032	0.0034	0.0019	
SYOWA	1766194.0922	1460410.9375	-5932273.3026	0.0272	0.0227	0.0450	
	0.0101	-0.0032	-0.0013	0.0046	0.0038	0.0076	
TATEYAMA	-4000983.4132	3375275.9607	3632213.1935	0.0034	0.0031	0.0033	
	0.0140	-0.0007	0.0078	0.0006	0.0005	0.0006	
TATEYA00	-4000983.4132	3375275.9228	3632213.2100	0.0044	0.0038	0.0041	000701
	0.0140	-0.0007	0.0078	0.0007	0.0006	0.0007	
TIGOCONC	1492054.0095	-4887960.9555	-3803541.4364	0.0152	0.0118	0.0149	
	0.0266	-0.0044	0.0116	0.0023	0.0018	0.0023	
TIGOWTZL	4075572.6788	931755.1203	4801584.3651	0.0025	0.0020	0.0027	
	-0.0160	0.0172	0.0089	0.0004	0.0003	0.0004	
TITIJIMA	-4489356.6037	3482989.6692	2887931.2731	0.0483	0.0414	0.0439	
	0.0155	0.0166	0.0047	0.0064	0.0056	0.0059	
TOULOUSE	4627949.9790	119843.6717	4372863.0183	0.0213	0.0193	0.0210	
	-0.0135	0.0187	0.0091	0.0030	0.0031	0.0030	
TROMSONO	2102904.0356	721602.5936	5958201.3426	0.0179	0.0116	0.0419	
	-0.0204	0.0213	0.0068	0.0028	0.0018	0.0064	
TRYSILNO	2988029.1762	655957.0698	5578669.1749	0.0323	0.0108	0.0587	
	-0.0065	0.0094	0.0219	0.0051	0.0017	0.0093	
TSUKU3	-3957184.4848	3310224.7896	3737709.1317	0.0098	0.0088	0.0092	
	-0.0006	0.0043	-0.0078	0.0013	0.0012	0.0012	
TSUKUBA	-3957172.9296	3310237.9569	3737708.9505	0.0222	0.0188	0.0217	
	-0.0028	0.0064	-0.0077	0.0032	0.0027	0.0032	
URUMQI	228310.7257	4631922.8877	4367064.0743	0.0027	0.0045	0.0047	
	-0.0330	-0.0063	0.0016	0.0005	0.0008	0.0008	
USUDA64	-3855355.4189	3427427.6141	3740971.2934	0.0449	0.0413	0.0473	
	-0.0043	0.0048	-0.0046	0.0060	0.0056	0.0063	
VERNAL	-1631473.3755	-4589129.0042	4106759.8880	0.0240	0.0607	0.0521	
	-0.0162	-0.0083	-0.0021	0.0034	0.0087	0.0075	
VICTORIA	-2341310.1392	-3539083.8922	4745768.3210	0.0248	0.0260	0.0266	
	-0.0106	-0.0014	-0.0062	0.0036	0.0037	0.0037	

VNDNBERG	-2678094.9481	-4525450.5755	3597410.3407	0.0049	0.0072	0.0065	
	-0.0307	0.0305	0.0191	0.0007	0.0010	0.0009	
WHTHORSE	-2215213.2711	-2209261.1577	5540291.6511	0.1067	0.0981	0.2342	
	0.0227	0.0431	-0.0853	0.0148	0.0136	0.0325	
WHTHOR87	-2215213.3948	-2209261.2755	5540291.8459	0.0826	0.0764	0.1822	871201
	0.0227	0.0431	-0.0853	0.0119	0.0110	0.0263	
YAKATAGA	-2529744.3628	-1942091.1236	5505028.2257	0.0515	0.0419	0.1060	
	-0.0224	0.0228	0.0253	0.0072	0.0058	0.0148	
YAKATA87	-2529744.3936	-1942091.0834	5505028.1096	0.0402	0.0328	0.0829	871201
	-0.0224	0.0228	0.0253	0.0058	0.0048	0.0120	
YEBES	4848780.2980	-261702.0782	4123035.7511	0.0051	0.0022	0.0046	
	-0.0101	0.0193	0.0113	0.0009	0.0004	0.0008	
YELLOWKN	-1224124.6447	-2689530.6711	5633555.3205	0.0058	0.0118	0.0238	
	-0.0212	-0.0041	-0.0010	0.0008	0.0015	0.0031	
YLOW7296	-1224399.5716	-2689273.2612	5633620.2640	0.0020	0.0021	0.0022	
	-0.0212	-0.0041	-0.0010	0.0003	0.0003	0.0004	
YUMA	-2196778.0150	-4887337.1664	3448425.2516	0.0271	0.0593	0.0418	
	-0.0176	-0.0085	-0.0031	0.0038	0.0083	0.0059	



# Refinement of the Stochastic VLBI Model: First Results

V. Tesmer

*Deutsches Geodätisches Forschungsinstitut (DGFI), Munich, Germany*

**Summary:** Previous improvements of parameter estimations using the observations of "Very Long Baseline Interferometry (VLBI)" were mainly achieved by refining the functional representation of the geometric-physical properties of the observations. Further progress in this field mostly implicates big efforts and is not possible with any precision. The stochastic properties of the observations (due to functionally not ascertainable influences) have in contrast not been handled with much care so far. Therefore, this paper deals with a qualitative description of deficits of VLBI observations' stochastic model as well as the quantification of these deficits by means of estimation of variance- and covariance components. The largest shortcomings of the stochastic VLBI model (derived during the correlation process) were found to be mainly station and elevation dependent. In this work, it is additionally demonstrated that standard VLBI solutions can be improved using a refined stochastic model for the observations.

## 1 Introduction

VLBI lead the way in many fields of geodesy, geophysics and astronomy since the seventies of the 20th century (RYAN AND MA 1998, CAMPBELL 2000). Although the stochastic model is an important part of the VLBI observation equations, only few relevant published investigations exist, like QIAN (1985), SCHUH AND WILKIN (1989) and SCHUH AND TESMER (2000). The refinement of the stochastic VLBI model presented in this paper is based on the two following basic ideas: (1) Discrepancies between the functional model and the observations can be conceived at least approximately as variances of the observations. (2) Deficits of the functional model which affect several observations quasi-systematically, might be interpreted as covariances (correlations) between observations.

## 2 Refined stochastic model of VLBI observations

### 2.1 Gauss-Markoff Model

The Gauss-Markoff Model can be written as

$$\mathbf{X}\boldsymbol{\beta} = \mathbf{y} + \mathbf{e} \quad \text{with} \quad \mathbf{D}(\mathbf{e}) = \mathbf{D}(\mathbf{y}) = \boldsymbol{\Sigma}_{yy} = \sigma_0^2 \mathbf{P}^{-1} = \sigma_0^2 \mathbf{Q} \quad .$$

The functional model consists of  $\mathbf{y} = y_1, y_2, \dots, y_n$ , the vector of  $n$  observations,  $\boldsymbol{\beta} = \beta_1, \beta_2, \dots, \beta_u$ , the vector of  $u$  unknowns as well as the vector of the "random" errors  $\mathbf{e}$  of the observations and the matrix of partial derivatives  $\mathbf{X}$  with  $X_{ij} = \partial y_i / \partial \beta_j$  ( $i = 1, 2, \dots, n$  and  $j = 1, 2, \dots, u$ ). The stochastic properties of the observations are described in the stochastic model, respectively the matrix of the variances and covariances  $\boldsymbol{\Sigma}_{yy}$  of the observations derived from the weight matrix  $\mathbf{P}$  of the observations or their cofactor matrix  $\mathbf{Q}$  and  $\sigma_0^2$ , a factor to describe the variance level of the observations.

The estimated parameters  $\hat{\boldsymbol{\beta}}$  and the estimated level of variance  $\hat{\sigma}_0^2$  of the observations (and therefore of the parameters, derived using the error propagation law) are computed as follows:

$$\hat{\boldsymbol{\beta}} = (\mathbf{X}'\mathbf{P}\mathbf{X})^{-1} \mathbf{X}'\mathbf{P}\mathbf{y} \quad (I-1)$$

$$\text{and} \quad \hat{\sigma}_0^2 = \frac{\hat{\mathbf{e}}'\mathbf{P}\hat{\mathbf{e}}}{n - u} \quad (\text{with } \hat{\mathbf{e}} = \mathbf{X}\hat{\boldsymbol{\beta}} - \mathbf{y}) \quad (I-2).$$

## 2.2 Cofactor matrix $\mathbf{Q}$ used for standard VLBI parameter estimations

The cofactor matrix  $\mathbf{Q}$  describes the ratios of the variances and covariances of the observations:

$$\mathbf{Q} = \begin{bmatrix} \sigma_1^2 + \sigma_{\text{const}}^2 & 0 & \cdots & 0 \\ 0 & \sigma_2^2 + \sigma_{\text{const}}^2 & & \cdots \\ \cdots & & & \\ 0 & \cdots & & \sigma_n^2 + \sigma_{\text{const}}^2 \end{bmatrix} \quad (I-3)$$

$$= \text{diag}(\sigma_1^2, \sigma_2^2, \dots, \sigma_n^2) + \sigma_{\text{const}}^2 \mathbf{I}$$

Usually it is a main diagonal matrix only, which consists of the variances  $\sigma_i^2$  of the  $n$  observations ( $i=1,2,\dots,n$ ), derived from their formal errors  $\sigma_i$ . A constant part  $\sigma_{\text{const}}^2$  is often added to consider quasi-random deficiencies in the functional model. The formal errors  $\sigma_i$ , derived during the correlation process can be approximated with the following formula (e.g. SCHUH AND CAMPBELL 1994):

$$\sigma_\tau = \frac{1}{2\pi \cdot \text{SNR} \cdot B_{\text{eff}}} \quad \text{with} \quad \text{SNR} = \frac{\eta S}{2k} \cdot \frac{\sqrt{A_1 \cdot A_2}}{\sqrt{T_{S1} \cdot T_{S2}}} \cdot \sqrt{2 B_{\text{eff}} T}$$

Parameters are the loss factor  $\eta$  due to digitization and filtering, the flux density  $S$  of the source, Boltzmann's constant  $k$ , the geometric mean of the antenna apertures  $A_1$  and  $A_2$  as well as the geometric mean of the system temperatures of the receivers  $T_{S1}$  and  $T_{S2}$ , the effective bandwidth  $B_{\text{eff}}$  of the recorded signal and the integration time  $T$  of the observation.

## 2.3 Refined stochastic model

The refinement of the stochastic model can be expressed in a very simple way: The "traditional" approach which consists of one stochastic property only, the level of the variances of the observations  $\sigma_0^2$  is expanded to a more differentiating representation with  $k$  stochastic properties  $\boldsymbol{\theta} = \theta_1, \theta_2, \dots, \theta_k$ :

Traditional stochastic model:

$$D(\mathbf{y}) = \sigma_0^2 \mathbf{Q} \quad (I-4)$$

Refined stochastic model ( $m = 1, 2, \dots, k$ )

$$D(\mathbf{y}) = \theta_1 \mathbf{V}_1 + \theta_2 \mathbf{V}_2 + \dots + \theta_k \mathbf{V}_k = \sum_{m=1}^k \theta_m \mathbf{V}_m \quad (I-5)$$

The matrices  $\mathbf{V}_m$  in the refined case have the same function as the cofactor Matrix  $\mathbf{Q}$  in the usual case, they define the ratios of the variances or covariances of the single observations for each stochastic property. In this work, they are filled with the variances derived during the correlation process, if the corresponding observations are expected to have one certain stochastic property. If not, the corresponding elements are zero. In the usual case, the "level of the variances of all observations"  $\sigma_0^2$  is estimated as  $\hat{\sigma}_0^2$  according to (I-2), in the refined case, the "levels of different stochastic properties"  $\boldsymbol{\theta} = \theta_1, \theta_2, \dots, \theta_k$  can be estimated as variance and covariance components  $\hat{\boldsymbol{\theta}} = \hat{\theta}_1, \hat{\theta}_2, \dots, \hat{\theta}_k$  with a Minimum Norm Quadratic Unbiased Estimation (MINQUE) as described in RAO (1973, p. 303f), KOCH (1997, p. 246f) or GRAFAREND AND D'HONE (1978).

### 3 Deficits of the stochastic model of VLBI observations in data analysis

Deficits of the stochastic model can be caused by discrepancies between the observations and the functional model, which either affect single observations quasi-randomly (see variances, 3.1) or several observations systematically (see correlations, 3.2).

#### 3.1 Variances of VLBI observations

- Common level of variance of all observations  
This is the simplest stochastic property of observations and is usually determined in the context of parameter estimation (equal to  $\sigma_0^2$  estimated as  $\hat{\sigma}_0^2$ ). It describes the common level of variance of the observations and the pseudo observations (constraints) which are often used to stabilise auxiliary parameters weakly determined from the real observations due to observing geometry etc.
- Additive variance  
In many VLBI solutions, it is common to add a  $\sigma_{\text{const}}^2$  to the variances of the observations (not the pseudo observations) derived during the correlation process (see (1-3)). It can be interpreted as generalisation of the variances' refinement. The added value is usually chosen empirically (SCHUH 1987, p. 83 or NOTHNAGEL 1991, p. 21).
- Source dependent variances  
The coordinates of some sources used for geodetic VLBI can not be specified precisely enough as positions constant in time. Some efforts were made to correct the positions using source structure corrections (e.g. SOVERS et al. 2002), which were not as successful as expected. Therefore, it might be possible to describe the influence of instabilities of sources at least partially as a variance component valid for the observations of certain sources with similar stability characteristics.
- Station dependent variances  
Possible reasons for station dependent variances are technological as well as physical properties of the telescopes which are not included in the functional model. Additionally, poorly predicted station dependent effects like ocean loading, atmospheric loading and thermal deformations have to be considered. Note that for the description of the variance of a (baseline-) observation the two station dependent variance components of the corresponding baseline always have to be added.
- Elevation dependent variances  
The lower elevations of observations are, the longer is the ray trace through the troposphere and an increasing part of the atmosphere of non-uniform density (especially of the wet part of the troposphere) complicates the tropospheric delay cumulatively. Therefore, simple mapping functions will describe its influence on observations increasingly worse with descending elevation. For VLBI solutions, observations with low elevations are important to define estimates of the zenith path delay as well as azimuthal gradients and to separate the tropospheric parameters from other estimated parameters (e.g. MACMILLAN AND MA 1994). That is why uncertainties in the functional description of observations of all elevations are attempted to be described with suitable variance components. Alike the station dependent variance components, only the couple of elevation angles of both observing telescopes represent the variance of a (baseline-) observation.

### 3.2 Correlations between VLBI observations

- Deficits of the tropospheric modelling  
The functional description of the tropospheric effect on VLBI observations has deficiencies in the prediction (e.g. because the wet part of the troposphere can not be well described with simple topocentric functions), as well as in the estimation of remnant influences (e.g. time- and space-dependent irregularities can not be estimated in enough detail because VLBI's observing geometry does not allow a reasonable resolution without heavily solution-deforming stabilisation with constraints). For these reasons, observations with the same ray trace through the troposphere may be falsified by a similar value. Especially observations taken from the same baseline with a short time lag and in similar topocentric directions have ray traces through the similar part of the troposphere. The maximum systematic falsification is to be expected for observations which contribute to the same rate of a piece-wise linear function for the estimation of the zenith path delay.
- Deficits of the modelling of the station coordinates  
The largest uncertainty of the station position related part of the functional model is the ocean loading correction (e.g. SCHERNECK et al. 2000). Possible errors can falsify certain groups of observations systematically, taken from the same telescope with a short time lag. The same effect is to be expected from (maybe local) uncertainties of the Love and Shida numbers. A height component of a telescope's coordinates (for which the maximum effect is to be expected), falsified by  $\Delta h$ , influences the delay  $\tau$  of a baseline by the value  $\Delta\tau = -\Delta h \cdot \sin\varepsilon$ , dependent on the elevation  $\varepsilon$  of the falsified telescope. The largest correlations are to be expected between observations of the same baseline under similar elevation angles with a short time lag. Accordingly, the largest correlations are to be expected between observations of the same baseline under similar elevation angles with a short time lag.
- Correlations caused by the correlation process  
If  $n$  VLBI telescopes recorded the same microwave signal from the same radio source, usually all  $n(n-1)/2$  possible combinations for baseline delays (the "real" observation in geodetic VLBI) are derived in the correlation process (WHITNEY 2000 or TAKAHASHI et al. 2000, p. 70ff). As the number of delays is larger than the number of originally recorded signals, the delays can not contain completely independent information. Different from differencing of GPS observations, VLBI observations are not derived rigorously mathematically but with a process that can not be reproduced with arbitrary precision and the number of used delays does not have to be reduced to  $n-1$  baselines. Nevertheless, the correlation process itself as well as functionally poorly acquired effects on a recorded signal influence delays systematically that are derived from that signal. Such delays must be considered as not being independent. For a formulation of possible correlations between corresponding delay observations, care must be taken of the "direction" of the delay, respectively the sign of the correlation coefficient.
- Radiophysical correlations  
As not modelled (apparent) variations of the coordinates of radio sources could falsify all observations of that source systematically, correlations between such observations can be assumed. The correlations would be independent from the observing baseline and topocentric observing directions, its value should decrease with time.

## 4 Refinement of the stochastic model of the VLBI observations

The MINQUE is a method for determining stochastic properties of observations often used in the context of geodetic research (e.g. TIBERIUS AND KENSELAAR 2000, SATIRAPOD et al. 2002). As the applications mostly use simplified algorithms and the problems which are to be solved usually are not very complex, a short report on the experiences made in this work is given:

- quite complex structures of stochastic properties can be estimated, which however need a careful choice of the formulation of the properties (like e.g. the choice of categories for the elevation dependent variances). It must be differentiating enough, but at the same time as representative for as many VLBI observations as possible.
- Most stochastic properties can only be solved robustly if the necessary information is accumulated analogically to the accumulation of normal equations for parameter estimation.
- Even after some minor simplifications and great efforts avoiding unnecessary operations, MINQUE is even with today's computing capacities very time consuming (one iteration step estimating the 58 components shown in table 4-1 and figure 4-1 for the ~ two million observations of 2124 sessions takes more than two days).
- Usually, no more than eight iterations are necessary to reach convergence.

### 4.1 Components not used for the refinement of the stochastic model

Eight different correlations due to deficits of the tropospheric modelling were estimated. One criterion was the difference between the "observing directions"  $\Delta\omega$  of the observations:

$$\Delta\omega = [\text{acos}(\cos(\Delta\varepsilon_A) \cos(\Delta\alpha_A)) + \text{acos}(\cos(\Delta\varepsilon_B) \cos(\Delta\alpha_B))]/2$$

(with the differences between the topocentric observing directions of both telescopes A and B of the same baseline in elevation  $\Delta\varepsilon_A, \Delta\varepsilon_B \in [0^\circ, 90^\circ]$  and in azimuth  $\Delta\alpha_A, \Delta\alpha_B \in [0^\circ, 360^\circ]$ ). The second criterion was the time lag between the observations  $\Delta t$ . The estimated values were 0.14, 0.13, 0.11 and 0.09 for  $0 < \Delta t \leq 15$  minutes and  $0^\circ \leq \Delta\omega < 5^\circ$ ,  $5^\circ \leq \Delta\omega < 10^\circ$ ,  $10^\circ \leq \Delta\omega < 15^\circ$  and  $15^\circ \leq \Delta\omega < 20^\circ$ . For  $15 < \Delta t \leq 30$  minutes the respective values were 0.10, 0.07, 0.05 and 0.05. All of them were assessed to be negligible in standard VLBI solutions as well as the correlations due to the correlation process, which were estimated with the value 0.21.

It was also decided not to use source dependent variance components for the refinement of the stochastic model of VLBI observations, although it was possible to estimate them well. Two different kinds of source dependent variance components were determined:

- four components from which three represent the defining, candidate and other sources of ICRF-Ext1 (e.g. MA AND FEISSEL 1997), as well as one component for the sources not included in ICRF,
- five components from which four represent the four stability classes according to FEISSEL-VERNIER (2003), and again one for sources not contained in this classification.

With none of both classification schemes, large differences between estimated components could be detected (compared to the station and elevation dependent variance components), wherefore stochastic properties of corresponding observations are not "refined" very much using such components.

Correlations (respectively covariances) caused by deficits of the modelling of the station coordinates were estimated with values not significantly deviant from zero. The radiophysical correlations did not converge. For both, no definite conclusion can be given if the components' formulation was bad or the assumed physical causes were wrong.

## 4.2 Components of the refined stochastic model

The stochastic model  $\Sigma_{yy}$  of the observations  $y$  used for VLBI parameter estimations is refined with the following variance components: the common level of variance  $\hat{\sigma}^{2\text{niveau}} = \hat{\theta}^{\text{niveau}}$  of all observations including the pseudo observations, the additive variance  $\hat{\sigma}^{2\text{add}} = \hat{\theta}^{\text{add}}$ , 47 station dependent variance components  $\hat{\sigma}^{2\text{telescope}^j} = \hat{\theta}^{\text{telescope}^j}$  and 9 elevation dependent variance components  $\hat{\sigma}^{2\text{elev}^\varepsilon} = \hat{\theta}^{\text{elev}^\varepsilon}$  (valid for  $\varepsilon = 0^\circ\text{-}5^\circ, 5^\circ\text{-}8^\circ, 8^\circ\text{-}11^\circ, 11^\circ\text{-}15^\circ, 15^\circ\text{-}20^\circ, 20^\circ\text{-}30^\circ, 30^\circ\text{-}45^\circ, 45^\circ\text{-}65^\circ$ , the component for  $\varepsilon = 65^\circ\text{-}90^\circ$  was not estimated to avoid singularities). According to (I-5), the refined stochastic model reads:

$$\begin{aligned} \Sigma_{yy} = & \hat{\sigma}^{2\text{niveau}} \mathbf{V}^{\text{niveau}} + \hat{\sigma}^{2\text{add}} \mathbf{V}^{\text{add}} \\ & + \sum_{j=1}^{47} \hat{\sigma}^{2\text{telescope}^j} \mathbf{V}^{\text{telescope}^j} + \sum_{j=1}^{47} \hat{\sigma}^{2\text{telescope}^B j} \mathbf{V}^{\text{telescope}^B j} \\ & + \sum_{m=1}^9 \hat{\sigma}^{2\text{elev}^A m} \mathbf{V}^{\text{elev}^A m} + \sum_{m=1}^9 \hat{\sigma}^{2\text{elev}^B m} \mathbf{V}^{\text{elev}^B m} \end{aligned} \quad (4-1)$$

The  $\mathbf{V}$ -matrices for the station and elevation dependent variance components, as well as for the component representing the common level of variance of all observations and pseudo observations are constructed with the variances of the usually used stochastic model (derived during the correlation process). For the additive component, the respective elements of the matrices  $\mathbf{V}$  have the value one.

In the following, the corresponding 58 components are illustrated together with their formal errors from MINQUE, both in table form and graphically. It is emphasised that the two negative values for FD-VLBA and OV-VLBA are not erroneous. In (4-1), it can easily be recognised that the variances of the observations consist of several "parts" which are to be added. Although their sum must not be zero or negative for any observation, single components can have arbitrary values.

To use the components, the following experiences made during their estimation can be of interest:

- The components represent almost all observations of the 2230 VLBI sessions between 1984 and the end of 2001, which are used at DGFI. Doubtful are only the ones representing observations up to an elevation of  $5^\circ$  as well as the observations of the VLBA, YEBES and EFLSBERG, because not all of the corresponding observations (sessions) were used for the component estimation.
- The components can be used for all VLBI solutions set up with standard parameterisations.
- The components should not be used partially, because some of them have distinct dependencies with other components.

Table 4-1: 58 components for the refined stochastic model of VLBI observations.

type	estimated value
Niveau	0.391 ± 0.0011
Add	0.086 ± 0.0016
WESTFORD	0.203 ± 0.0036
HRAS 085	0.512 ± 0.0085
MOJAVE12	0.225 ± 0.0052
RICHMOND	0.331 ± 0.0056
WETTZELL	0.123 ± 0.0035
ONSALA60	0.189 ± 0.0057
KASHIMA	0.344 ± 0.0091
HATCREEK	0.489 ± 0.0226
OVRO 130	0.317 ± 0.0252
HAYSTACK	0.438 ± 0.0183
KAUAI	0.334 ± 0.0068
GILCREEK	0.144 ± 0.0034
KWAJAL26	0.306 ± 0.0252
ALGOPARK	0.148 ± 0.0053
HARTRAO	0.241 ± 0.0086
MEDICINA	0.067 ± 0.0067
SESHAN25	0.352 ± 0.0140
DSS65	0.223 ± 0.0113

PIETOWN	0.206 ± 0.0103
NRAO 140	0.400 ± 0.0462
DSS45	0.191 ± 0.0170
NRAO85 3	0.309 ± 0.0059
NOTO	0.257 ± 0.0115
HOBART26	0.338 ± 0.0137
KASHIM34	0.420 ± 0.0226
MATERA	0.168 ± 0.0057
LA-VLBA	0.135 ± 0.0087
EFLSBERG	0.245 ± 0.0277
FD-VLBA	-0.119 ± 0.0079
SANTIA12	0.362 ± 0.0196
KP-VLBA	0.140 ± 0.0153
NL-VLBA	0.155 ± 0.0127
HN-VLBA	0.216 ± 0.0208
OHIGGINS	0.416 ± 0.0435
BR-VLBA	0.084 ± 0.0109
DSS15	0.110 ± 0.0160
KOKEE	0.155 ± 0.0042
SC-VLBA	0.354 ± 0.0184

FORTLEZA	0.161 ± 0.0050
MK-VLBA	0.086 ± 0.0137
OV-VLBA	-0.047 ± 0.0130
CRIMEA	0.421 ± 0.0198
NYALES20	0.214 ± 0.0050
NRAO20	0.112 ± 0.0048
YEBES	0.277 ± 0.0280
URUMQI	0.031 ± 0.0169
TSUKUB32	0.027 ± 0.0105
ε = 0°-5°	3.498 ± 0.0857
ε = 5°-8°	1.170 ± 0.0117
ε = 8°-11°	0.748 ± 0.0078
ε = 11°-15°	0.545 ± 0.0059
ε = 15°-20°	0.387 ± 0.0048
ε = 20°-30°	0.247 ± 0.0034
ε = 30°-45°	0.106 ± 0.0028
ε = 45°-65°	0.036 ± 0.0027
ε = 65°-90°	( 0 ) ( ± 0 )

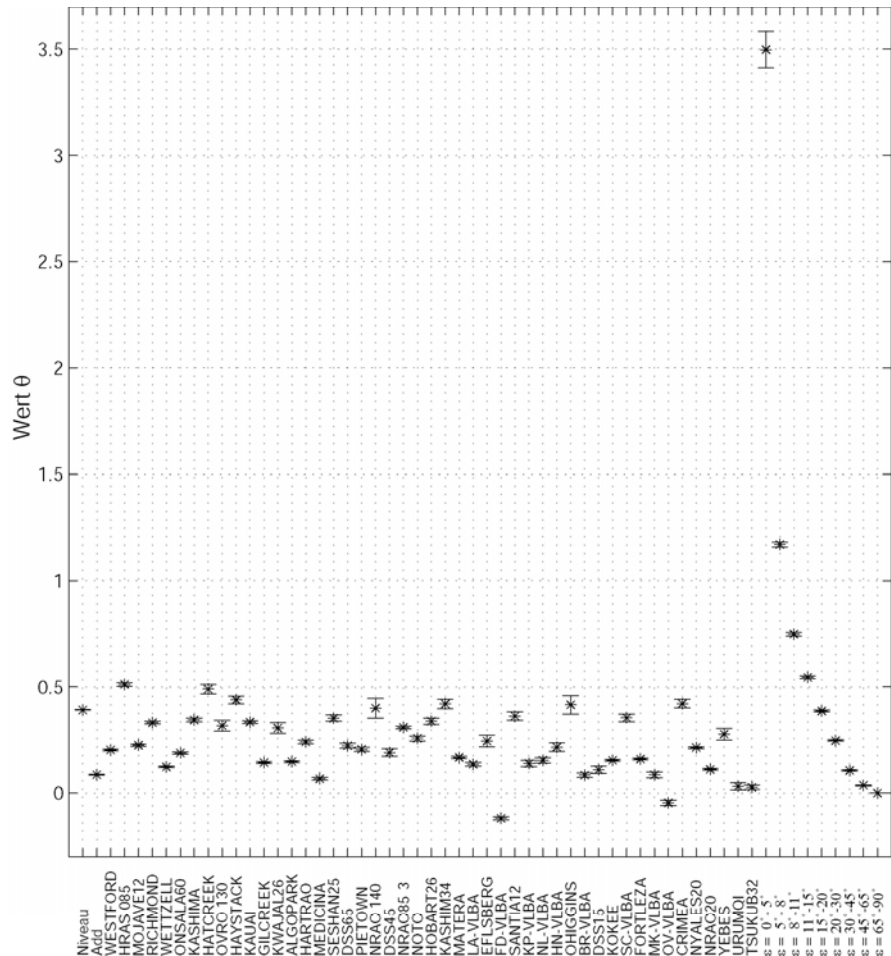


Figure 4-1: 58 components for the refined stochastic model of VLBI observations.

## 5 Influence of the refined stochastic VLBI model on parameter estimations

### 5.1 Indirect influence of the refined stochastic model on parameter estimations

Besides influencing the parameter estimations directly (see chapter 5.2), the refinement of the stochastic model has some indirect attendant influences (especially problematic are possible interactions between the indirect influences):

- Influence of observations under very low elevations  
For usual VLBI solutions at DGFI, observations below 8° elevation are downweighted by 100000, which in fact has the same effect as deleting them from the equation system. With the refined stochastic model in principle all observations are used. Observations under very low elevations have considerable influence on the sensitive estimates of the tropospheric azimuthal gradients and the zenith path delay. If the behaviour of such observations can really be described sufficiently well by a stochastic property (as found out in this work with a higher variance), remains unclear. Latest VLBI solutions do not use observations under 5° elevation.
- Outliers and common level of variance  $\hat{\sigma}_0^2$  of all observations  
In OCCAM, all observations of each single session are subject to a simple test for outliers during every computation of a solution: The residuals  $\hat{e}$  of a first solution are compared to their formal error. Observations with residuals three times larger than their formal errors remain in the equation system, but are downweighted by 100000 for the computation of a final, second solution (more sophisticated outlier tests will be implemented soon). Changes in the stochastic model of the observations (like its refinement) affect the residuals as well as their formal errors, which will again change the observations marked as outliers and therefore the estimated level of variance  $\hat{\sigma}_0^2$ .
- Influence of the constraints on the parameter solution  
Constraints are pseudo observations of parameters that are artificially added to the equation system to stabilise weak auxiliary parameters. Due to a lack of reliable knowledge about such parameters, the corresponding parameter value is usually zero. The influence of these pseudo observations is dependent on their (pseudo-) variance, expressed in the stochastic model as well as the variance and the number of real observations contributing information to the corresponding parameter. Moreover, it depends on how well the configuration of the real observations (similar to the observing geometry) already “defines” such a parameter. Prior investigations showed that MINQUE-determined (pseudo-) variances of such pseudo observations do not improve parameter estimations. As they are an indispensable part of VLBI equation systems, they can not be neglected realising variance component estimations with VLBI observations. Hence in this work, their (pseudo-) variance level was estimated together with the component representing the common variance level of all observations. Impacts on estimated parameters are not clear and can only barely be quantified.

## 5.2 Repeatability of station coordinates

For each of the 2230 VLBI sessions between 1984 and 2001 used at DGFI, solutions were computed for epoch coordinates of the respective telescopes. The rotational and translational degrees of freedom of the station coordinates were removed respectively by no-net-rotation and no-net-translation conditions with respect to the coordinates of the VLBI solution DGFI02R02 computed at DGFI.

The estimations were done with three stochastic models, (1) with the usually used, “traditional” one, (2) with the refined stochastic model and (3) with an approach with all observations being equally weighted with the variance  $1.9302 \text{ cm}^2$ , neglecting the formal errors derived in the correlation process (this value consists of  $1.6802 \text{ cm}^2$ , the median of the median variances of all sessions, plus an added variance  $0.25 \text{ cm}^2$ , according to the usual weighting procedure for VLBI solutions at DGFI). The impact of the choice of the stochastic model on estimated parameters is illustrated in table 5-1. It displays the RMS-values (root mean square) and the WRMS-values (weighted root mean square) for the estimated corrections to the station coordinates in latitude, longitude and the radial component. The values in table 5-2 are relative repeatabilities with respect to the ones derived with the traditional stochastic model (a value smaller than 100 % expresses that the repeatability is better, compared to the traditional approach).

Table 5-1: Repeatability of epoch coordinates, estimated with three different stochastic models.

	RMS [cm]			WRMS [cm]		
	refined stoch. model	traditional stoch. model	all observations equally weighted	refined stoch. model	traditional stoch. Model	all observations equally weighted
lat.	0.506	0.521	0.568	0.291	0.296	0.340
long.	0.495	0.503	0.552	0.285	0.293	0.334
radial	1.085	1.099	1.205	0.350	0.322	0.367

Table 5-2: Relative repeatability of epoch coordinates, estimated with three different stochastic models.

	repeatability refined / traditional stoch. model [%]		repeatability all obs. same weight / trad. stoch. model [%]	
	RMS	WRMS	RMS	WRMS
lat.	97.11 %	98.33 %	108.90 %	114.91 %
long.	98.48 %	97.43 %	109.72 %	114.06 %
radial	98.67 %	108.61 %	109.66 %	114.01 %

Obviously, the assumption that all observations are equally precise is a very bad approximation. The variances derived during the correlation process (the stochastic model usually used for VLBI parameter estimation) also have deficits. However, gross errors of the variances (e.g. due to hardware problems during the observation or the correlation process) can be avoided with the traditional stochastic model.

Using the refined model (see table 4-1 and figure 4-1 respectively), quite robust improvements can be achieved in VLBI solutions, even if its influence is not exclusively positive: Although the RMS-values of station coordinates decrease, the WRMS-values partly even get larger. This indicates that the estimated parameters themselves improve, whereas their formal errors do not become more realistic (especially for the station heights, which even become less realistic). This might be due to the indirect influences of the refined stochastic model on parameter estimations as mentioned in the previous paragraph 5.1. All three indirect influences mentioned there are possible reasons for too optimistic formal errors of the station heights. As they interact and none of them can be easily excluded from solutions, this must be subject to further investigations.

### 5.3 EOP-differences from simultaneously observing NEOS-A and CORE-A networks

The analysis of EOP, determined from simultaneous NEOS-A and CORE-A VLBI sessions between 1997 and middle of 2000 was published before several times (e.g. MACMILLAN et al. 1999 or TESMER AND SCHUH 2000). Originally, the aim of these simultaneous sessions was to get an insight in network-dependent systematics of EOP estimations. Part of the VLBI sessions stored at DGF1 were 67 pairs of independently observed 24-h NEOS-A and CORE-A sessions, whose observations began and ended diverging less than 15 minutes. This restriction supposed the EOP, estimated from both networks, to represent exactly the same average angles. The positions of the telescopes were fixed to the corresponding coordinates given by DGF102R02 and ICRF-Ext1, respectively.

For each session, two solutions were computed, one with the traditional stochastic model of the observations and another using the refined stochastic VLBI-model. The WRMS and RMS values of the differences between the EOP, estimated from the two simultaneously observing networks are summarised in the following table 5-3.

Table 5-3: RMS and WRMS of the differences between EOP from 67 parallel VLBI sessions.

	RMS			WRMS		
	refined stoch. model	traditional stoch. model	refined / traditional stoch. model [%]	refined stoch. model	traditional stoch. model	refined / traditional stoch. model [%]
$X_p$ [ $\mu$ as]	230.29	232.51	99.02 %	207.92	210.28	98.88 %
$Y_p$ [ $\mu$ as]	194.61	197.87	98.35 %	183.94	187.06	98.33 %
$\Delta UT1$ [ $\mu$ s]	10.050	10.232	98.22 %	9.584	9.731	98.49 %
$\Delta\psi$ [ $\mu$ as]	381.25	410.47	92.88 %	347.39	364.95	95.19 %
$\Delta\epsilon$ [ $\mu$ as]	143.15	140.71	101.73 %	130.91	131.29	99.71 %

Alike in the last section, a small but apparently noticeable advancement of the estimates can clearly be recognised, although such a conclusion can not be considered as absolutely reliable due to the small number of data points. As the EOP are almost only dependent on the horizontal components of the station coordinates and not the vertical one, the RMS as well as the WRMS improve.

## 6 Conclusions and outlook

The refinements of the stochastic VLBI model help to describe the properties of VLBI observations in context of a parameter estimation more realistically. The repeatability of station coordinates improves when using refined variances of the observations. Besides, the differences between EOP, determined from observations of two independent, simultaneously observing VLBI-networks are getting smaller. However, the potential of the refinement of the stochastic model of the VLBI observations is not yet exhausted. The following continuative investigations might implicate further advancements:

- Single variance components are doubtful (the ones representing observations up to an elevation of  $5^\circ$  as well as the observations of the VLBA, YEBES and EFLSBERG), because they were determined with few observations only and therefore are not representative. 106 of the 2230 sessions stored at DGF1 were not used for the estimation of the stochastic model, and the unreliable components can be easily stabilised by adding further sessions. As some of the 106 sessions contain up to ten thousand observa-

tions, this will multiply the computing time and further optimisations of the corresponding algorithms could be necessary.

- Further improvements could also be achieved using more differentiating formulations for the stochastic properties, especially the elevation dependent variances, e.g. for seasonal or station dependent fractions. The elevation dependent variances might also have fractions that are dependent on the latitude of the corresponding telescopes. Another idea for a further refinement would be to estimate one variance component per observed source (~700). This could only be done with simplified algorithms, that would be forced to many restrictions compared to the full MINQUE.
- Another important step forward could be done if the indirect influences of the refinement of the stochastic model on parameter estimates could be controlled better. If observations, taken under very low elevation can not be well described with either functional and/or (quasi-) stochastic modelling, they should eventually be eliminated from solutions. The chosen (quasi-) variances of the constraints (pseudo observations that are artificially added to the equation system to stabilise weak auxiliary parameters) and their influence on parameter estimates, respectively should at least be re-adapted heuristically.

## Acknowledgements

It is gratefully acknowledged that this work was supported by the German research association “Deutsche Forschungsgemeinschaft (DFG)” by funding the author (contract DR 143/11-1). The author also thanks the GSFC (Goddard Space Flight Center) and the IVS (International VLBI Service for Geodesy and Astrometry) for kindly providing the observation data.

## References

- CAMPBELL, J.: From Quasars to Benchmarks: VLBI Links Heaven and Earth. In: Vandenberg, N., K. Baver (eds): IVS 2000 General Meeting Proc., NASA/CP-2000-209893, 20-34, 2000.
- FEISSEL-VERNIER, M.: Selecting Stable Extragalactic Compact Radio Sources from the Permanent Astrogeodetic VLBI Program. *Astronomy & Astrophysics* manuscript no. MS3523, accepted and to be published, 2003
- GRAFAREND, E., A. D'HONE: Gewichtsschätzung in geodätischen Netzen. DGK Reihe A, Heft 88, Verlag der Bayerischen Akademie der Wissenschaften, München, 1978
- KOCH, K.-R.: Parameterschätzung und Hypothesentests. Dümmlers Verlag, Bonn, 1997
- MA, C., M. FEISSEL (eds): Definition and Realisation of the International Celestial Reference System by Astrometry of Extragalactic Objects. IERS Technical Note 23, Paris, 1997
- MACMILLAN, D., C. MA: Evaluation of Very Long Baseline Interferometry Atmospheric Modelling Improvements. *J. of Geoph. Res.*, 99 B1, 637-651, 1994
- MACMILLAN, D., W. HIMWICH, C. THOMAS, N., VANDENBERG, J. BOSWORTH, B. CHAO, T. CLARK, C. MA: CORE: Continuous, High-Accuracy Earth Orientation Measurements. In: Proc. of the 13<sup>th</sup> Working Meeting on European VLBI for Geodesy and Astrometry, Viechtach, 166-171, 1999

- NOTHNAGEL, A.: Radiointerferometrische Beobachtungen zur Bestimmung der Polbewegung unter Benutzung langer Nord-Süd-Basislinien. DGK Reihe C, Heft 368, Verlag des Instituts für Angewandte Geodäsie, Frankfurt am Main, 1991
- QIAN, ZHI-HAN: The Correlations on VLBI Observations and its Effects for the Determinations of ERP. In: I. Mueller (ed): Proc. of the Int. Conference on Earth Rotation and the Terrestrial Reference Frame, Vol. 1, Columbus, Ohio, 360-365, 1985
- RAO, C.: Linear Statistical Inference and its Applications. Verlag John Wiley & Sons, New York, London, 1973
- RYAN, J., C. MA: NASA-GSFC's Geodetic VLBI Program: a Twenty-year Retrospective. Phys. Chem. Earth, 23 No. 9-10, 1041-1052, 1998
- SCHUH, H.: Die Radiointerferometrie auf langen Basen zur Bestimmung von Punktverschiebungen und Erdrotationsparametern. Verlag der Bayerischen Akademie der Wissenschaften, Reihe C, München, 1987
- SCHUH, H., A. WILKIN: Determination of Correlation Coefficients between VLBI-Observables. In: A. Rius (ed): Proc. of the 7<sup>th</sup> Working Meeting on European VLBI, Madrid, Spain, CSIC, 79-91, 1989
- SATIRAPOD, C., J. WANG, C. RIZOS: A Simplified Minque Procedure for the Estimation of Variance-Covariance Components of GPS-Observables. Survey Review, 36(286), 582-590, 2002
- SCHUH, H., J. CAMPBELL: VLBI in Geodynamical Investigations. Acta Geod. Geophys. Hung., Vol. 29 (3-4), 397-420, 1994
- SCHUH, H., V. TESMER: Considering a-priori Correlations in VLBI Data Analysis. In: Vandenberg, N., K. Baver (eds): IVS 2000 General Meeting Proc., NASA/CP-2000-209893, 237-242, 2000
- SOVERS, O.J., P. CHARLOT, A.L. FEY, D. GORDON: Structure Corrections in Modeling VLBI Delays for RDV Data. In: Vandenberg, N., K. Baver (eds): IVS 2002 General Meeting Proc., NASA/CP-2002-210002, 243-247, 2002
- SCHERNECK, H.-G., R. HAAS, A. LAUDATI: Ocean Loading Tides for, in, and from VLBI. In: Vandenberg, N., K. Baver (eds): IVS 2000 General Meeting Proc., NASA/CP-2000-209893, 257-262, 2000
- TAKAHASHI, F., T. KONDO, Y. TAKAHASHI, Y. KOYAMA: Very Long Baseline Interferometer. Ohmsha Ltd./IOS Press, 2000
- TESMER, V., H. SCHUH: Comparison of the Results Obtained by Different VLBI Networks. In: Tomasi, P., F. Mantovani, M. Perez Torres (eds): Proc. of the 14<sup>th</sup> Working Meeting on European VLBI for Geodesy and Astrometry, Instituto di Radioastronomia, Bologna, 7-12, 2000
- TIBERIUS, C., F. KENSELAAR: Estimation of the Stochastic Model for GPS Code and Phase Observables. Survey Review, 35(277), 441-454, 2000
- WHITNEY, A.: How do VLBI Correlators Work? In: Vandenberg, N., K. Baver (eds): IVS 2000 General Meeting Proc., NASA/CP-2000-209893, 187-205, 2000

# Investigations on European Baseline Rates

M. Vennebusch

*Geodetic Institute, University of Bonn, Germany*

**Summary:** For about twelve years European VLBI-sessions have been performed in order to determine coordinates and velocities of the participating stations and to control the stability of the European land mass. At first only five stations participated, while nowadays up to nine stations are part of a so-called EUROPE-network. The north-south extension of this network is up to 5000 km, reaching from subtropical Mediterranean areas (Noto) to polar regions (Ny-Ålesund).

Among the results are baseline lengths and the changes of these baseline lengths, so-called baseline rates. Two methods for the determination of baseline rates are described. Their results, computed with different atmosphere-parametrisations, are being discussed.

## 1 EUROPE-sessions

For about twelve years European VLBI sessions have been performed in order to determine coordinates and velocities of the participating stations (Haas et al., 2002). Within 67 sessions (May 2003) at first only five stations participated, while nowadays up to nine stations are part of a so-called EUROPE-network. The north-south extension of these networks is up to 5000 km, reaching from subtropical Mediterranean areas (Noto) to polar regions (Ny-Alesund).

## 2 Determination of baseline rates

The main intention of the EUROPE sessions is the determination of coordinates and velocities of the participating stations (Haas et al., 2000); further results are baseline lengths and the changes of these baseline lengths with time, so-called baseline rates (Nothnagel and Campbell, 1993, Malkin et al., 2001).

There are two different possibilities for the determination of baseline rates:

### 1. Arc solution:

This method is based on analysing each VLBI session separately and determining one baseline length within one session. After a few sessions a computation of an adjusting straight line can be performed and the slope of this adjusting straight line represents the baseline rate between two stations. Due to repairs of a radio telescope it may be necessary to estimate offsets within the adjusting straight line, while keeping one joint slope for the whole period of VLBI sessions used for the determination of a baseline rate.

Thus the results of an ARC solution are the baseline rate, its accuracy and -as a measure of the scatter of the baseline lengths around their adjusting straight line- the WRMS. The WRMS is used because of its independence from the number of sessions used for the determination of baseline rates.

### 2. Vector solution:

The second method for the determination of baseline rates is based on the accumulation of normal equations of different sessions (Ma et al., 1990). The primary results of these so-called vector solutions

are coordinates and velocities of the participating stations and the accuracies of these parameters.

The computation of a baseline rate from a vector solution is possible by using the directional derivative:

$$\partial_a f(x) = \overbrace{\text{grad } f(x)}^{\vec{v}} \cdot \vec{a} = \sum_{i=1}^3 f_{x_i}(x) a_i$$

By subtracting the absolute values of these products for both stations the baseline rate is obtained:

$$\text{baseline rate} = |\vec{v}_A \cdot \vec{a}| - |\vec{v}_B \cdot \vec{a}|$$

where  $\vec{v}$  denotes the vector of velocity of a station and  $\vec{a}$  denotes the (unit-)vector between two stations. Baseline rates can be computed by

$$\text{rate} = \frac{1}{\sqrt{r}} \cdot \left[ \begin{aligned} &(X_B - X_A) \cdot (\dot{X}_B - \dot{X}_A) + \\ &(Y_B - Y_A) \cdot (\dot{Y}_B - \dot{Y}_A) + \\ &(Z_B - Z_A) \cdot (\dot{Z}_B - \dot{Z}_A) \end{aligned} \right]$$

$$\text{with } \sqrt{r} = \sqrt{(X_B - X_A)^2 + (Y_B - Y_A)^2 + (Z_B - Z_A)^2}$$

After the computation of baseline rates by using the formula above one is able to compare the results of arc and vector solutions.

### 3 Atmosphere parametrisations and WRMS

An important issue for the following investigations is the impact of atmosphere parametrisations on the determination of baseline rates (MacMillan and Ray, 1991, Ray and Corey, 1991). Usually one piece-wise linear atmosphere-parameter is estimated for every sixty minutes, depending on the person analysing the VLBI-data.

The impact of different atmosphere parametrisations on baseline rates can be seen in figure 1 (arc solution): There are three different baselines (Wettzell-Noto, Onsala-Noto and Ny-Alesund-Noto) parametrised in two different ways. In the upper row one atmosphere parameter is estimated for every twelve hours, while in the lower row one atmosphere-parameter is estimated for every sixty minutes.

It can be seen quite clearly that the scatter decreases with an increasing number of atmosphere parameters.

As mentioned above the number of atmosphere-parameters affects the repeatability (WRMS) and therefore the accuracy of the determination of baseline rates.

Now the impact of different atmosphere-parametrisations on baseline rates will be investigated. Due to software restrictions in the following investigations all stations are parameterised in the same way.

A selection of twenty-three European baseline rates and their formal errors can be seen in Table 1. These baseline rates agree well with the results of Haas and Tomasi, 2002, but are based on a longer time span.

In figure 2 the WRMS of 36 European baselines parameterised with at least four different atmosphere-parametrisations is shown. These baselines are sorted by their length and the number of sessions used for the determination of baseline rates is displayed below. Numbers smaller than twenty are put in brackets, because baselines with less than twenty sessions should be neglected in this analysis.

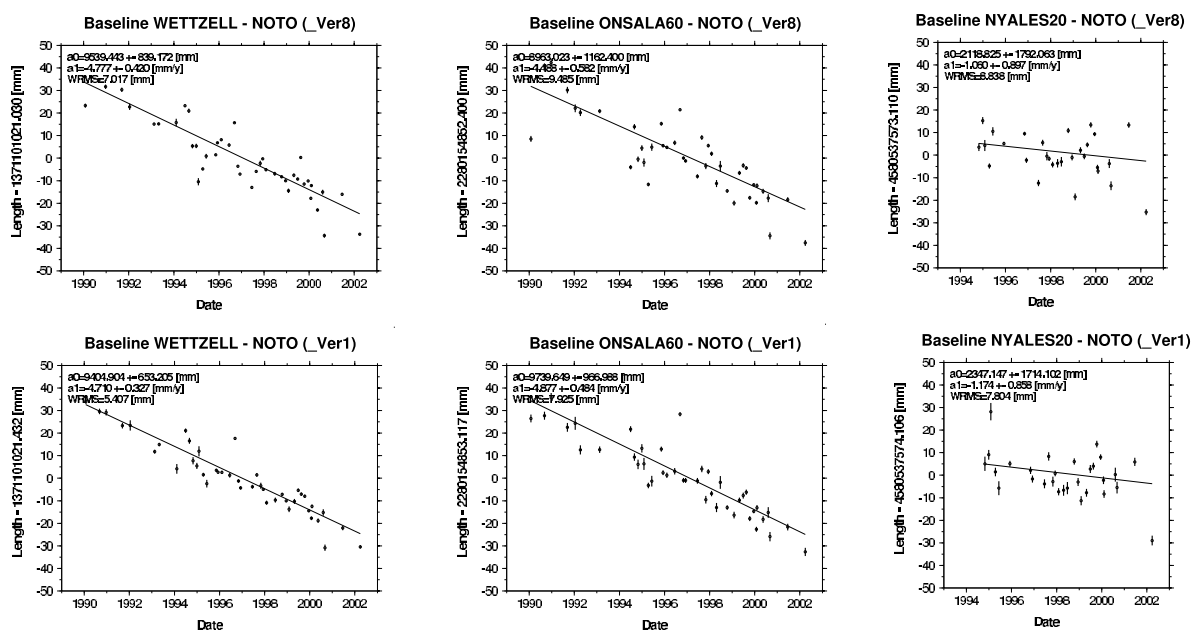


Figure 1: Impact of atmosphere-parametrisations on baseline rates

Table 1: Rates of selected European baselines in mm/y, computed with four different atmosphere-parametrisations (Data from 1990 to June 2002), AT1-AT4=One atmosphere-parameter for every 30, 60, 120 and 180 minutes.

Baseline	Ses- sions	AT1		AT2		AT3		AT4	
		Rate	±	Rate	±	Rate	±	Rate	±
MATERA-NOTO	39	0.48	0.23	0.48	0.24	0.43	0.24	0.27	0.27
EFLSBERG-WETTZELL	14	-1.57	0.91	-1.28	0.94	-0.84	0.86	-0.11	0.93
MEDICINA-WETTZELL	50	-2.82	0.32	-2.87	0.34	-2.96	0.36	-2.83	0.39
MATERA-MEDICINA	47	-2.98	0.30	-2.78	0.31	-2.51	0.42	-2.81	0.38
MEDICINA-NOTO	39	-3.51	0.40	-3.17	0.49	-3.10	0.54	-3.50	0.54
ONSALA60-WETTZELL	55	-0.47	0.18	-0.53	0.19	-0.42	0.22	-0.58	0.20
MATERA-WETTZELL	50	-3.93	0.19	-3.88	0.18	-3.91	0.23	-4.03	0.21
NOTO-WETTZELL	43	-4.71	0.32	-4.60	0.35	-4.72	0.38	-4.81	0.43
DSS65-MEDICINA	40	3.33	0.47	2.78	0.47	2.32	0.62	2.25	0.57
MEDICINA-ONSALA60	49	-3.08	0.45	-3.39	0.50	-3.28	0.55	-3.41	0.53
DSS65-WETTZELL	44	0.64	0.39	0.55	0.48	0.50	0.43	0.59	0.43
CRIMEA-WETTZELL	20	0.29	0.73	0.93	0.81	1.00	0.90	0.15	0.93
DSS65-NOTO	34	-1.54	0.49	-1.76	0.53	-1.14	0.65	-1.63	0.65
DSS65-MATERA	39	2.39	0.46	2.20	0.45	2.38	0.66	2.16	0.54
MATERA-ONSALA60	48	-4.38	0.32	-4.22	0.33	-4.35	0.41	-4.51	0.39
DSS65-ONSALA60	43	1.31	0.65	0.89	0.74	0.49	0.73	0.59	0.69
NOTO-ONSALA60	42	-4.87	0.48	-4.81	0.53	-4.78	0.60	-4.95	0.57
NYALES20-ONSALA60	35	2.04	0.47	2.24	0.45	1.89	0.44	1.83	0.44
NYALES20-WETTZELL	35	1.64	0.48	1.82	0.52	1.75	0.49	1.76	0.44
NYALES20-MEDICINA	30	-0.21	0.95	-0.75	1.08	-1.18	1.00	-0.61	0.85
NYALES20-MATERA	29	-1.86	0.78	-1.45	0.78	-1.73	0.73	-2.19	0.67
NYALES20-DSS65	24	2.37	1.80	1.30	1.75	0.72	1.74	1.64	1.83
NYALES20-NOTO	29	-1.17	0.85	-0.39	1.02	-0.47	1.05	-0.02	0.99

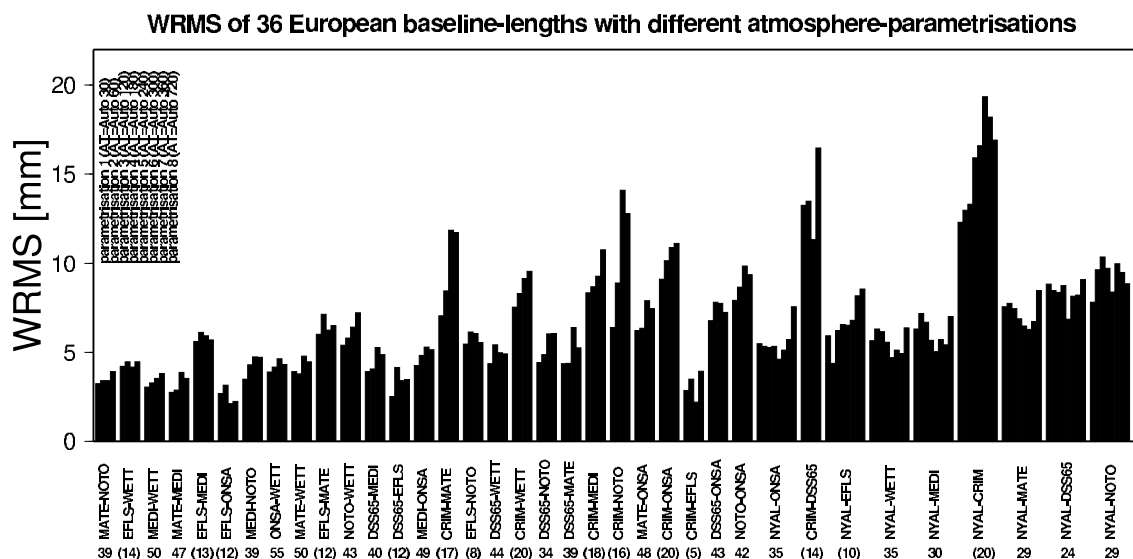


Figure 2: WRMS of 36 European baselines

Most of the WRMS-values of the first twenty-seven baselines (baselines without Ny-Alesund) show an upward trend, this confirms again that the WRMS increases with decreasing number of atmosphere parameters. This was expected, because a higher number of parameters usually leads to a smaller WRMS. Thus for a small network an atmosphere-parametrisation with a fairly high number of atmosphere-parameters is convenient.

Looking at the longer baselines (with Ny-Alesund) the opposite occurs: first a downward trend and then an upward trend can be seen. A minimal WRMS can be achieved by parameterising all stations with parameterisation 5 (i.e. one atmosphere parameter for every 240 minutes).

The reasons for these anomalies are being investigated below.

## 4 Comparison of arc and vector solutions

Provided that there are enough sessions available, baseline rates determined within arc and vector solutions are very similar (see figure 3 for an example for one baseline). The differences of all 36 European baseline rates are usually much less than 0.5 mm/y.

Figure 4 shows these differences for the second parameterisation (one atmosphere-parameter for every sixty minutes). Dark bars indicate differences of baseline rates determined within more than twenty sessions. In most cases where differences exceed 0.5 mm/y so-called episodic motions occurred due to telescope repairs or episodic tectonic movements. These motions occurred at stations Effelsberg, Madrid (DSS65) and Medicina and weaken the determination of these baseline rates.

A comparison of the accuracies of the two methods is difficult, since the formal errors of arc and vector baseline rates are determined in completely different ways: The formal error of a baseline rate of an arc solution denotes the accuracy of the slope of an adjusting straight line determined by at most 60 observations (which are the baseline lengths).

The formal error of a baseline rate determined within a vector solution is a result of the analysis of many thousands of observations, which are the original VLBI-delays. Furthermore the formal error of a vector baseline rate is computed by applying the error propagation law on the formal errors of the velocities of two stations.

### Baseline NOTO-WETTZELL

baseline rate and accuracy of baseline rate (with four different atmosphere-parametrisations)

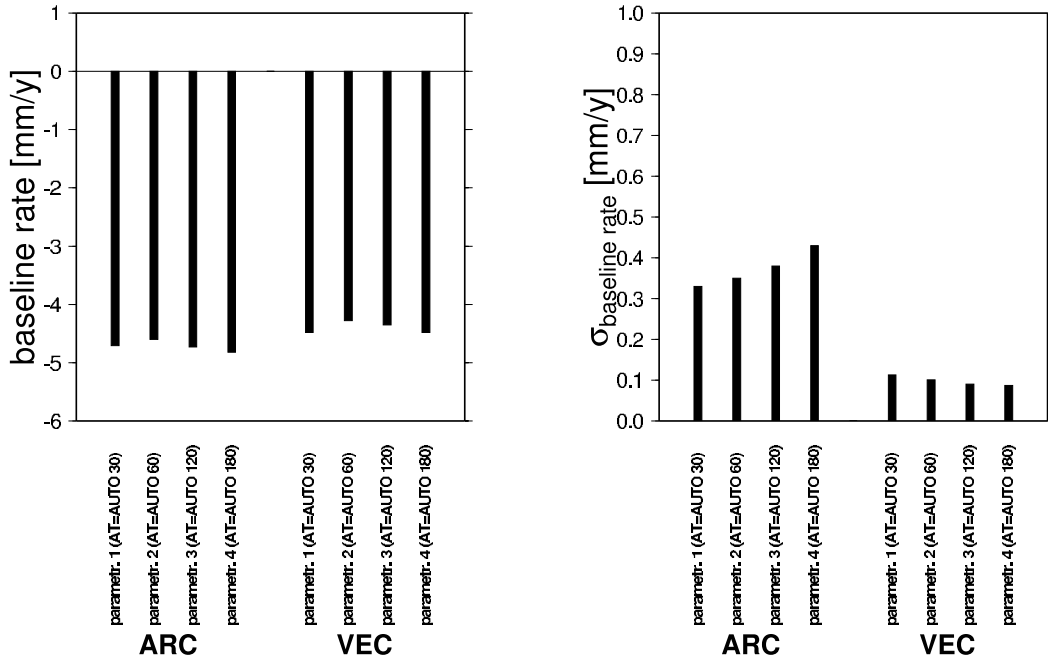


Figure 3: Baseline rate and accuracy of baseline Noto-Wettzell

### Differences between arc- and vector-baseline rates (only parametrisation 2 (AT=AUTO 60))

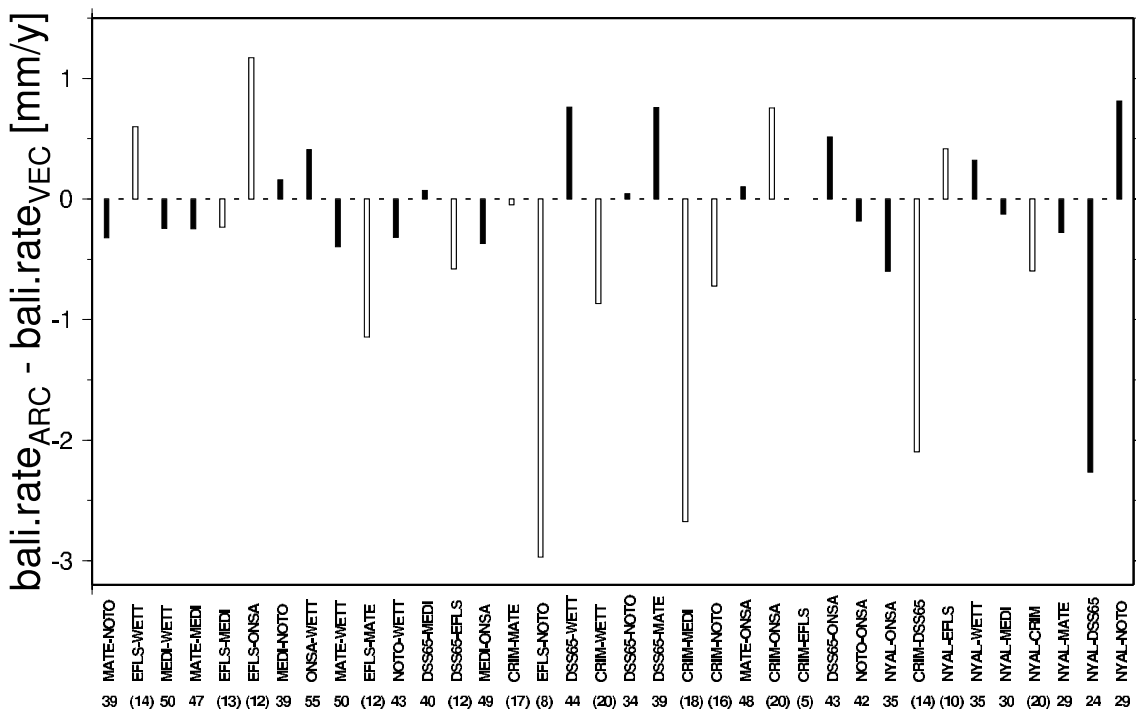


Figure 4: Differences between arc- and vector-baseline rates

## 5 Consideration of the anomalies at Ny-Alesund

According to the results in figure 2 a recommended atmosphere-parametrisation for the best determination of baseline rates with Ny-Alesund involved is one atmosphere-parameter for every 240 minutes (for all stations).

One of the reasons for this could be a weak source-distribution, an example can be seen in figure 5. This is an example for only one session, but the source-distributions of other sessions look very similar.

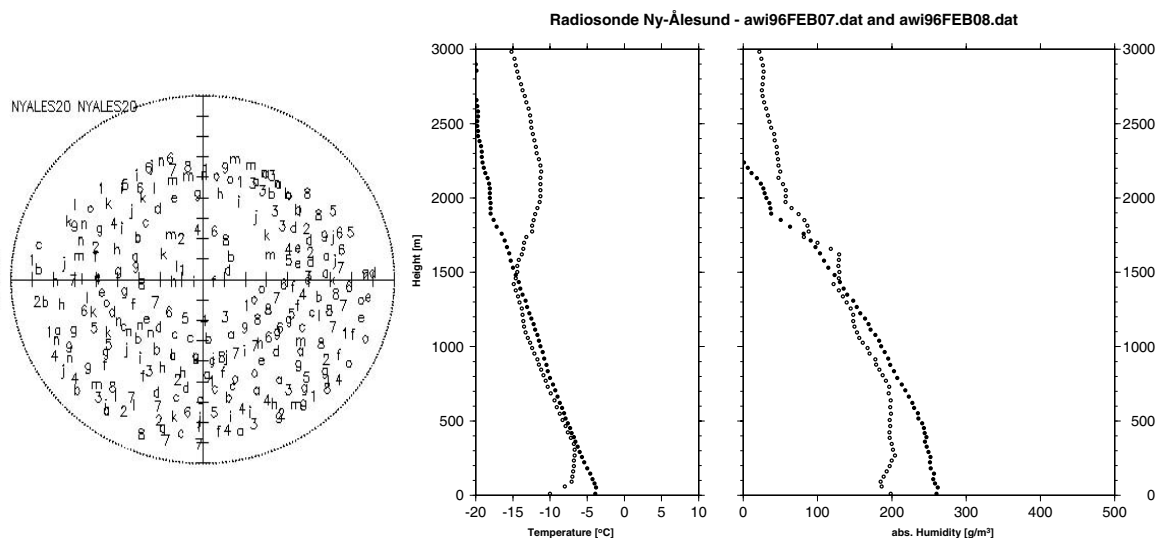


Figure 5: Source-distribution and profiles of temperature and humidity at Ny-Alesund

There are no sources at all in the northern part of the hemisphere above Ny-Alesund in a sector from  $-85$  till  $+85$  degree in azimuth and up to an elevation angle of 30 degrees which could cause an imperfect modeling of the zenith path delay and therefore an inaccurate determination of baseline lengths and baseline rates.

Another reason for the behaviour of the WRMS could be an extraordinary condition of the atmosphere at station Ny-Alesund.

Therefore a closer look at the atmospheric situation at Ny-Alesund is appropriate. Next to the VLBI-antenna at Ny-Alesund a stratospheric observatory is located, run by the Alfred-Wegener-Institute for Polar and Marine Research. A radiosonde for the determination of air temperature, humidity and pressure is launched every day and its data can be used to find correlations between the condition of the atmosphere and the accuracy of VLBI-data.

For a VLBI-session of 24 hours two profiles of temperature and humidity can be used to compare the condition of the atmosphere with the accuracy of the coordinates of station Ny-Alesund and with the accuracy of the respective baseline rates (see figure 5) (Davis et al., 1991).

A comparison of the radiosonde data and the accuracy of coordinates and baseline rates can be performed by looking at the similarity of two profiles for air temperature or air humidity. A large difference between two profiles shows a significant change in weather conditions close to the VLBI-antenna and may cause a noticeable inaccuracy of baseline components.

Comparison of the radiosonde data and the formal errors of coordinates and baseline rates shows no correlation, so a likely reason for the unexplained behaviour of the WRMS could be the weak source distribution. Further studies are necessary to add proof to this assumption.

## 6 Conclusions

Provided that there are enough sessions available and no episodic movements of the antenna occurred in the time span considered here, both methods yield the same baseline rates. The differences between European baseline rates determined with arc and vector solutions are usually less than 0.5 mm/y. This holds true for all kinds of atmosphere-parametrisations used in these investigations.

Since the accuracies of the determined baseline rates can not be compared directly an assessment of the two methods may be carried out by considering practical aspects:

An advantage of the determination of baseline rates by means of an arc solution is the possibility to detect outliers within baseline lengths. A disadvantage is the fact that there are only as many "observations" as number of sessions where that particular baseline was observed (presently at most 67 sessions), and their degree of temporal correlation is unknown.

An advantage of the determination of baseline rates within a vector solution is the statistically correct consideration of correlations between the parameters (coordinates). A disadvantage is that outliers might not be identified.

Concerning the parametrisation of the atmosphere it is necessary to find a compromise depending on the size of the network: usually the WRMS decreases and therefore the accuracy of an arc baseline rate increases with the number of atmosphere parameters estimated. Therefore many analysts use an atmosphere parametrisation with one parameter for every sixty minutes or even less.

Based on the investigations above this kind of atmosphere parametrisation can also be recommended for small European VLBI-networks, i.e. sessions without station Ny-Alesund. Networks with larger extension, in this case sessions with station Ny-Alesund participating, have to be parameterised in a different way. In order to improve the accuracy of longer baseline rates an atmosphere parametrisation with one parameter for every 240 minutes appears to be convenient.

For the determination of baseline rates a compromise has to be found, so that one atmosphere-parameter for every 60 till 240 minutes should be estimated, depending on the size of the network. A convenient atmosphere parametrisation can be found iteratively.

Further investigations need to be done, e.g. using different atmosphere-parametrisations for particular stations. However due to software restrictions it is not possible at present to parameterize different stations in different ways, so all stations have to be parameterised in the same way.

## References

- Davis, J.L., T.A. Herring, and I.I. Shapiro, *Effects of atmospheric modeling errors on determination of baseline vectors from VLBI*, J. Geophys. Res., 96(B1), p.643-650, 1991.
- Haas, R. and P. Tomasi: *Results of the Geodetic VLBI Observing Program*, Measurements of Vertical Crustal Motion in Europe by VLBI, TMR Network Report, p. 98-106, 2002.
- Haas, R. et al.: *Crustal motion results derived from observations in the European geodetic VLBI network*, Earth Planets Space, 52, p. 759-764, 2000.
- Ma, C. et al.: *Measurement of Horizontal Motions in Alaska Using Very Long Baseline Interferometry*, Journal of Geophysical Research, Vol. 95, No. B13, p. 21991-22011, 1990.

- MacMillan, D.S. and J.R. Ray, *Current Precision of VLBI Vertical Determinations*, Proceedings of the AGU Chapman Conference on Geodetic VLBI: Monitoring Global Change, NOAA Technical Report NOS 137 NGS 49, p. 428-436, 1991.
- Malkin, Z. et al.: *Length Variations of Europeans Baselines Derived from VLBI and GPS Observations*, In: D. Behrend and A. Rius (Eds.): Proceedings of the 15th Working Meeting on European VLBI for Geodesy and Astrometry, p. 116-123, Barcelona, Spain, 2001.
- Nothnagel, A., Campbell, J.: *European Baseline Rate Determination with VLBI*, In: J. Campbell and A. Nothnagel (Eds.): Proceedings of the 9th Working Meeting on European VLBI for Geodesy and Astrometry, p. 56-59, Bonn, 1993.
- Ray, J.R., B.E. Corey: *Current Precision of VLBI Multi-Band Delay Observables*, Proceedings of the AGU Chapman Conference on Geodetic VLBI: Monitoring Global Change, NOAA Technical Report NOS 137 NGS 49, p. 123-134, 1991.

# Preliminary Analysis of the Free Core Nutation From VLBI Data

Z. Malkin<sup>1</sup> and D. Terentev<sup>1,2</sup>

<sup>1</sup>*Institute of Applied Astronomy (RAS), St. Petersburg, Russia*

<sup>2</sup>*Sobolev Astronomical Institute, St. Petersburg State University, Russia*

**Summary:** Several VLBI EOP series were investigated with goal of determination of parameters of the Free Core Nutation (FCN). Both the amplitude and period of the FCN were studied. Our preliminary analysis reveals a variability of both the amplitude (known also from other investigations) and period of the FCN nutation term. The FCN amplitude varies in the range about 0.1–0.3 mas, and the FCN period — in the range about 415–490 solar days.

## 1 Introduction

In this paper we investigate variability of the FCN parameters. Whereas variations of the FCN amplitude was already investigated (see e.g. *Herring et al., 2002; Shirai and Fukushima, 2001*), variations of the FCN period is not been studied yet.

Modern theory of nutation predicts the steady FCN period of 431.2 sidereal days (*Dehant and Defraigne, 1997*). The FCN period also have been estimated from VLBI observations, and found to be about 430–431 sidereal days or about 429–430 solar days (see, e.g. Table 4 in *Shirai01 and Fukushima, 2001*).

In this paper we analyze four VLBI nutation series available in the IVS data base, sufficiently long and dense to obtain reliable estimates. We consider the differences between observed values of nutation angles and IAU2000A model (which is equivalent to MHB2000 model without FCN contribution). For our purpose, we interpret the unpredicted part of observed nutation series in the FCN frequency band as the FCN contribution.

## 2 Data used in analysis

The series used in our analysis are BKG00003, GSF2002C, IAAO0201, USN2002B. We analyzed both raw (i.e. given on original epochs) and smoothed (equally spaced by 0.05 year) series. For smoothed series we also computed weighted mean one. The parameter of smoothing was chosen in such a way to suppress oscillations with periods less then 1 month. Common time span for all series is 1984.0–2002.8. Figure 1 shows smoothed series used in our analysis.

## 3 Analysis and results

### 3.1 Spectral analysis

For estimation of the power spectral density from both raw (unequally spaced) and smoothed (equally spaced) nutation series we used the Ferraz-Mello's method (*Ferraz-Mello, 1981*) which allows us to process both types of data. For supplement testing, we also compute the power spectral density using the Burg's method (*Marple, 1987*). Figures 2–4 show the normalized results of spectral estimation, and Table 1 presents the estimates of the FCN period.

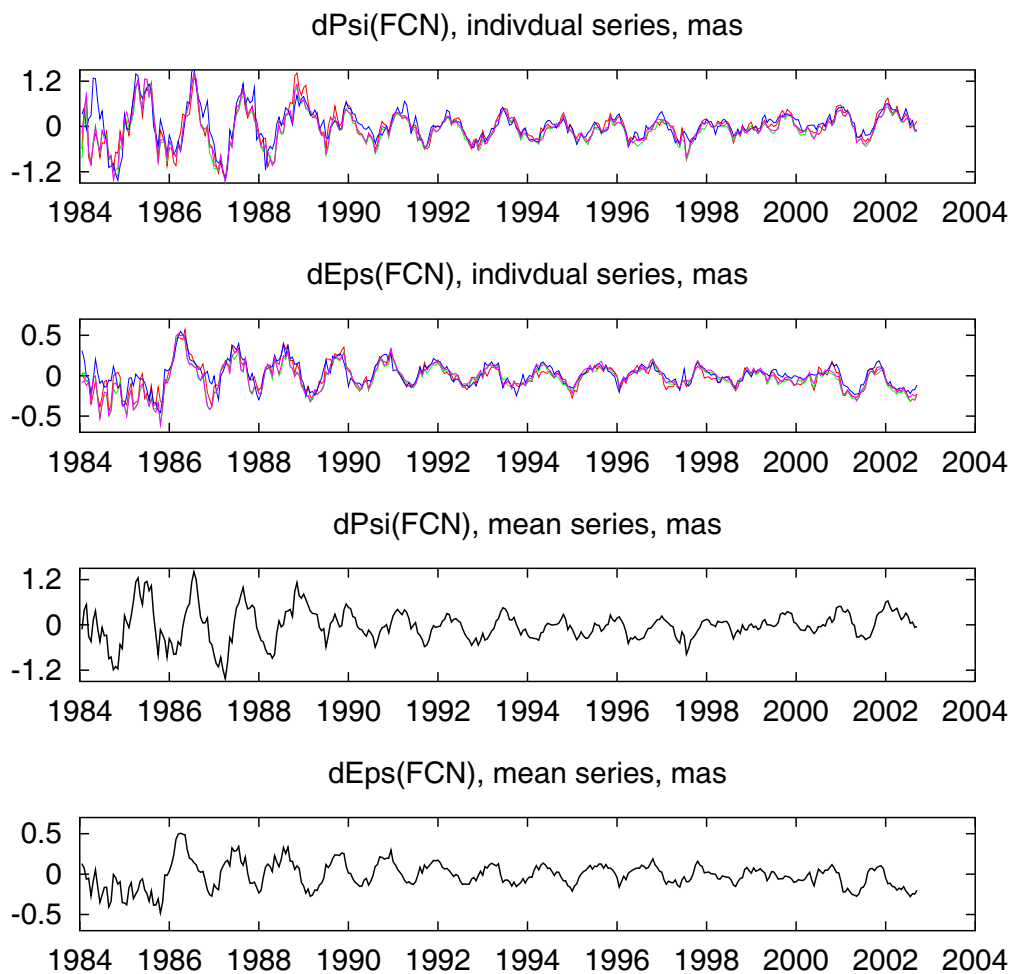


Figure 1: FCN contribution in the individual and mean series.

The average estimated value of the FCN period is of about 434 solar days (about 435 sidereal days). This value is substantially greater than one found in *Shirai and Fukushima (2001)* ( $431.0 \pm 0.6$  sidereal days). However, when we used for spectral analysis only nutation series cut at the epoch 2000.2 which corresponds to the data span used in *Shirai and Fukushima (2001)*, we obtain the FCN period of about 432 sidereal days which is close to found in *Shirai and Fukushima (2001)* (see the last line in each section of Table 1).

### 3.2 Wavelet analysis

At the next step we applied wavelet analysis to all the nutation series. For this analysis we used program WWZ, developed by the American Association of Variable Star Observers and available at <sup>(1)</sup>. Theoretical background of this method can be found in *Foster (1996)*.

Results of wavelet analysis are presented in Figures 5–9. Figures 5–7 show the skeletons (a period at which the wavelet is maximum). In all these figures the results for the first and the last 2-year periods are not shown since they are affected by the edge effect. All the periods in the figures are given in solar days, and all amplitudes computed from the smoothed values are to be multiplied by 1.01 to recover the smoothing effect.

<sup>1</sup><http://www.aavso.org/cdata/wwz.shtml>

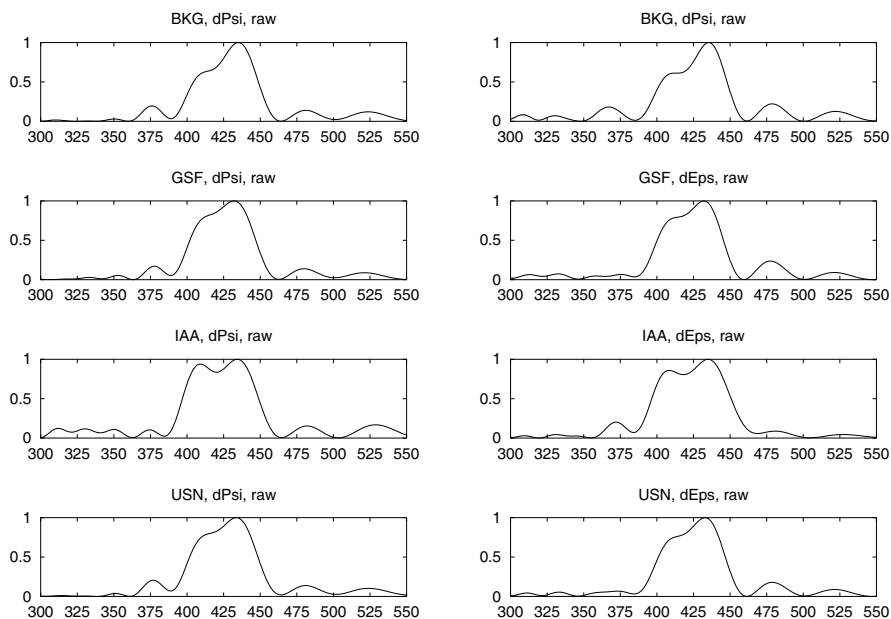


Figure 2: Spectra of raw data, Ferraz-Mello's method, solar days.

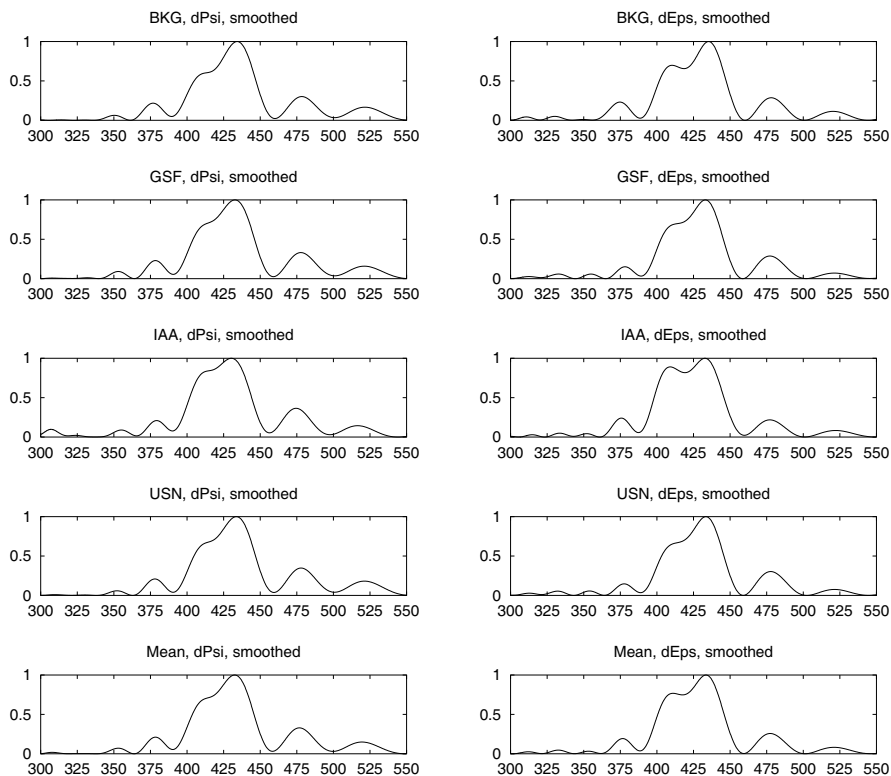


Figure 3: Spectra of smoothed data, Ferraz-Mello's method, solar days.

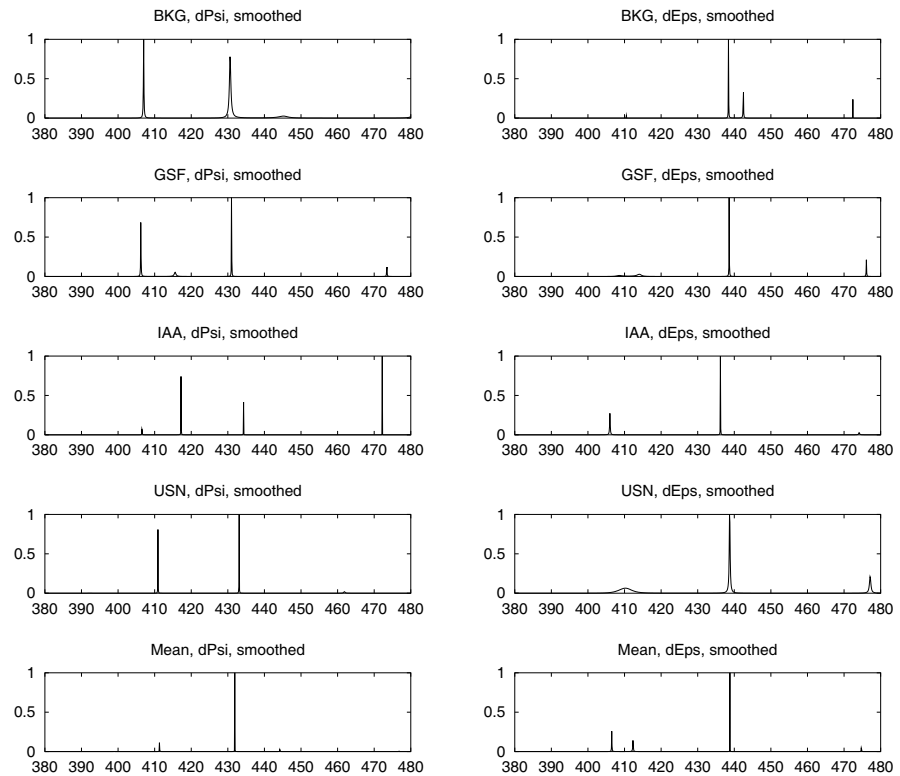


Figure 4: Spectra of smoothed data, Burg's method, solar days.

Table 1: Periods of the FCN contribution, solar days.

Series	Method	BKG	GSF	IAA	USN	Mean
<b>dPsi</b>						
Raw	Ferraz-Mello	435.0	432.2	434.4	433.7	—
Smoothed	Ferraz-Mello	434.2	432.7	430.3	433.7	432.5
Smoothed	Burg	430.6	431.0	434.3	433.1	431.9
Smoothed	Burg (-2000.2)	433.4	430.0	428.5	433.4	431.9
<b>dEps</b>						
Raw	Ferraz-Mello	435.4	432.2	435.0	432.9	—
Smoothed	Ferraz-Mello	435.4	433.1	432.9	433.5	433.5
Smoothed	Burg	438.4	438.6	436.2	438.7	438.8
Smoothed	Burg (-2000.2)	431.7	428.5	429.5	430.1	429.9
<b>Mean of dPsi and dEps</b>						
Raw	Ferraz-Mello	435.2	432.2	434.7	433.3	—
Smoothed	Ferraz-Mello	434.8	432.9	431.6	433.6	433.0
Smoothed	Burg	434.5	434.8	435.2	435.9	435.4
Smoothed	Burg (-2000.2)	432.6	429.2	429.0	431.8	430.9

Figure 9 presents the final results of the present investigation. It should be mentioned that based on comparison of FCN amplitudes found here and previous investigations (*Malkin, 2002*), we consider the results obtained before 1990 as not very reliable.

Of course, an important question arising from the obtained result is whether the variations of the period found from our analysis is an actual geophysical signal or an artifact caused by inadequate computational procedures. One can see that large increasing of the FCN period after  $\approx 1998$  corresponds to relatively low amplitude of the FCN oscillation. We have performed some tests to estimate how result of wavelet analysis depend on variable amplitude of input signal. Our conclusion is that found variations of the FCN period cannot be explained by computational errors. Besides, results of spectral analysis made for different subset of data also corroborate our conclusion.

## 4 Discussion and conclusions

The results of our investigations allow us to make some preliminary conclusions.

The FCN period most likely varies with time. Probably, change in the period is physically connected with change in amplitude. On the other hand, one can see that the variations of the FCN period show clear periodicity with a period about 5 years, whereas variations of the FCN amplitude does not show such an effect.

Another reason of the observed behavior of the FCN period maybe a jump(s) in the FCN phase. Analogous effect was found also at the Chandler frequency (*Vondrak, 1988*), for which dependence of the period on amplitude, and the phase jump occurred during the period of the lowest amplitude were also found.

It is interesting, that the Chandler wobble period also decreased in  $\approx 1986-1988$ , and increased in  $\approx 1989-1996$  (see *Höpfner, 2003, Schuh et al., 2001*). Unfortunately, Polar Motion series studied in those papers are much shorter than one analyzed here to perform a reliable comparison.

Variations of FCN amplitudes show several possible epochs of the excitation of the FCN, most of them are close to ones detected in *Shirai and Fukushima (2001)*.

Some tests we performed allow us to make a conclusion that investigated nutation series really contain such a signal with variable amplitude and period, however it's not clear if this corresponds to a known geophysical process(es). As stated above, we interpret the differences between observed nutation and the IAU2000A model as FCN contribution, which may be too strong assumption.

We plan to continue our analysis to detect and investigate more carefully the complex observed signal and possible geophysical interpretation.

## Acknowledgments

Authors are grateful to V. Vityazev for useful discussion of methods and results of spectral and wavelet analysis.

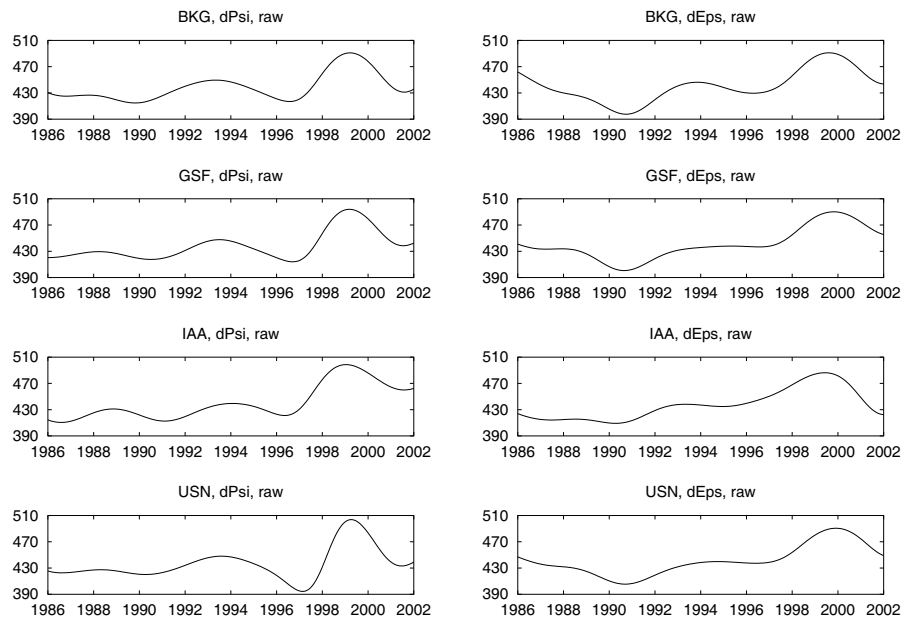


Figure 5: Variations of the FCN period with time, raw data, solar days.

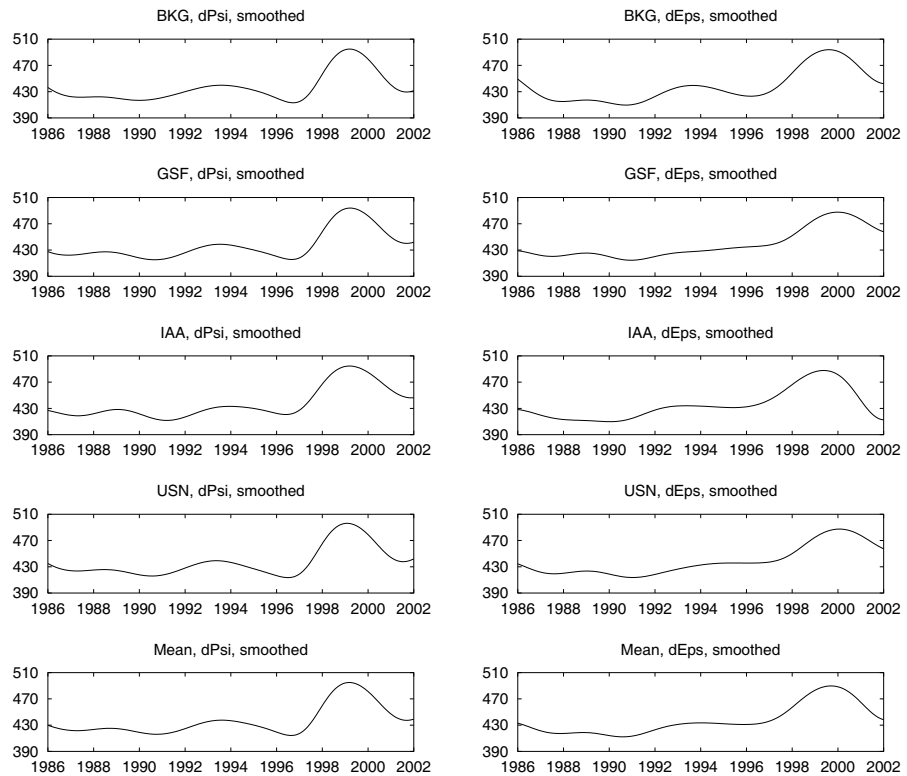


Figure 6: Variations of the FCN period with time, smoothed data, solar days.

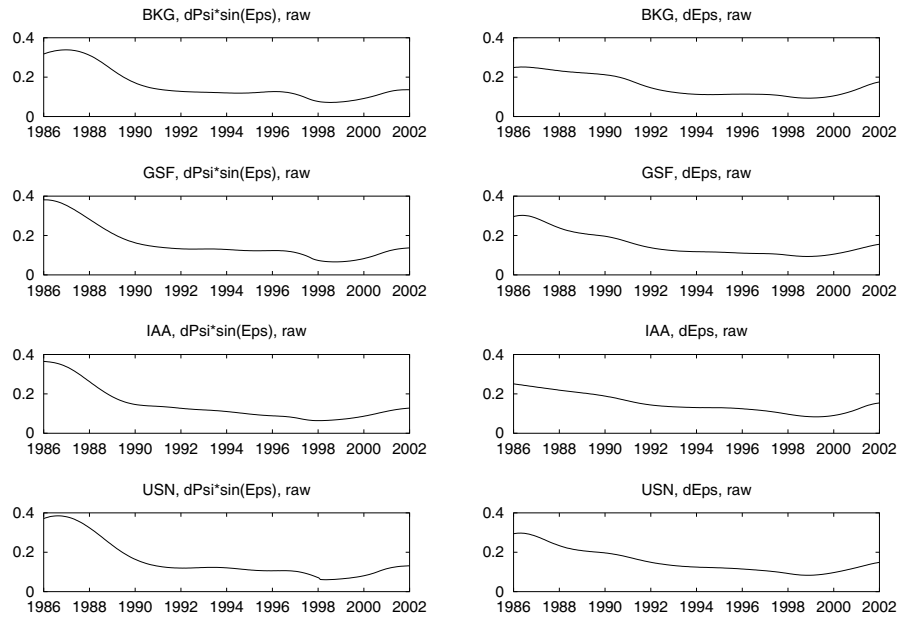


Figure 7: Variations of the FCN amplitude with time, raw data.

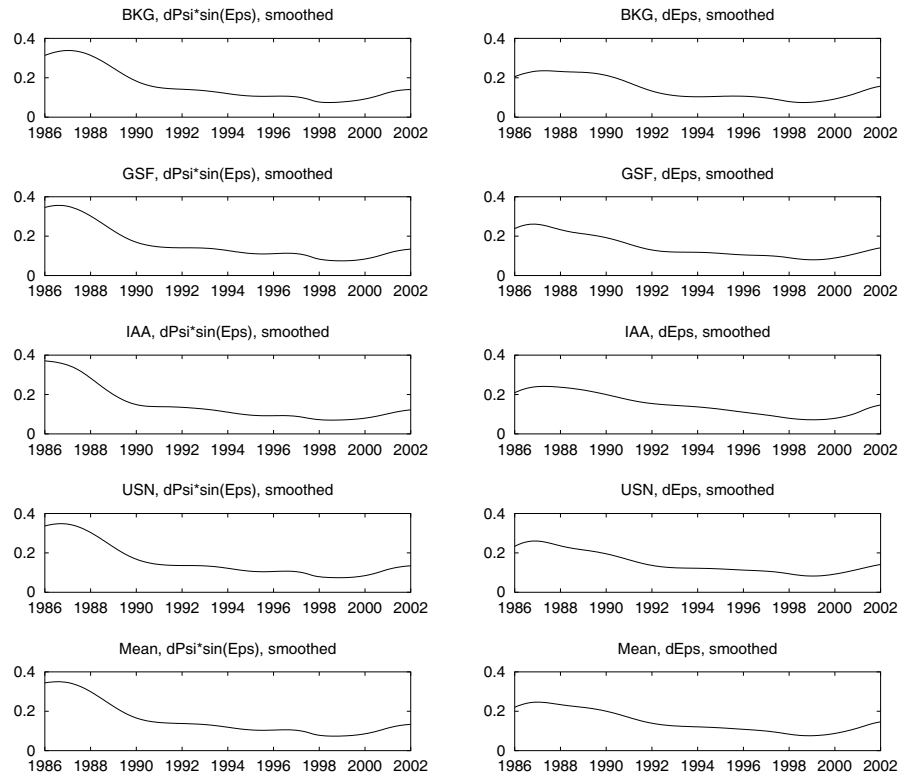


Figure 8: Variations of the FCN amplitude with time, smoothed data.

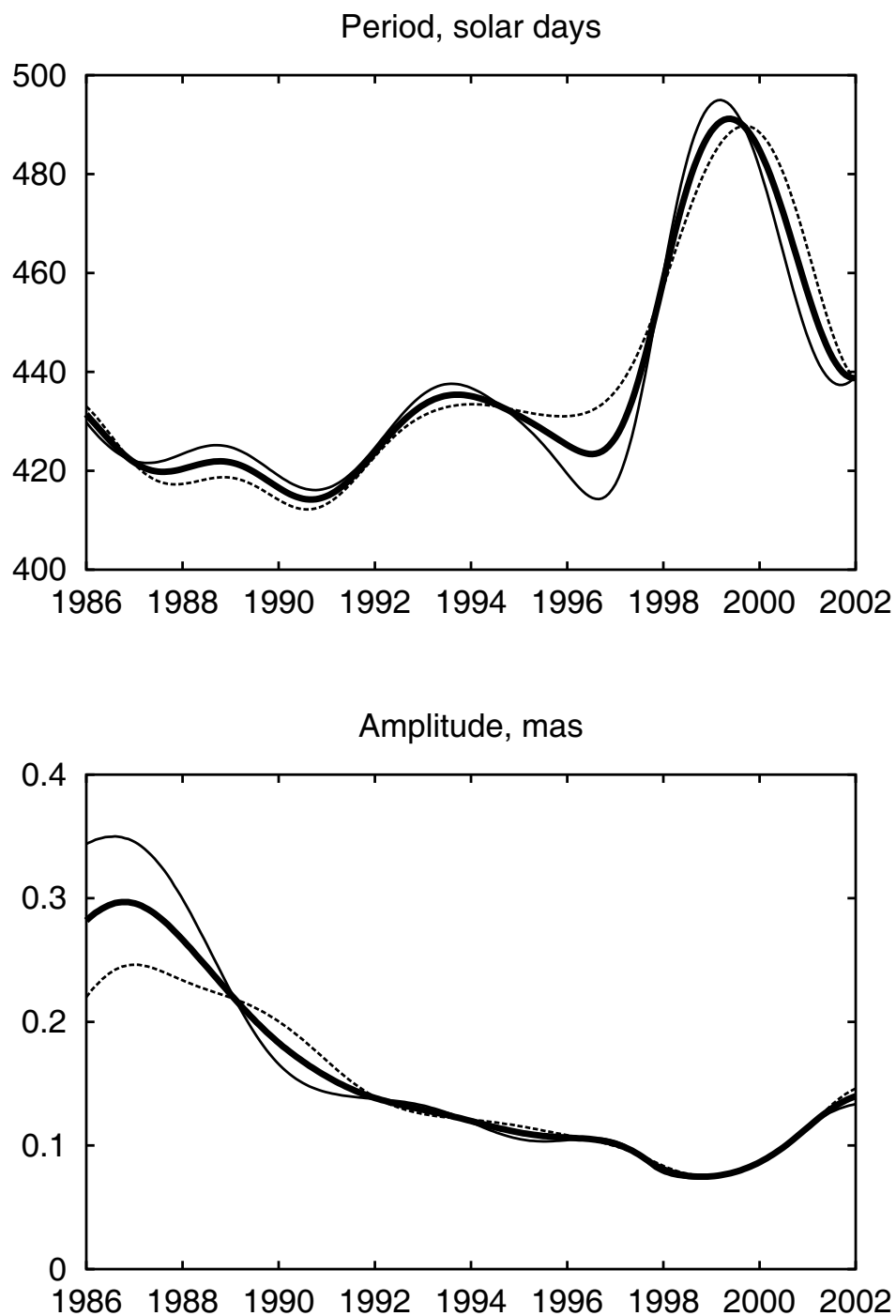


Figure 9: Variations of the FCN period and amplitude with time;  $\Delta\psi * \sin(\varepsilon)$  (solid line),  $\Delta\varepsilon$  (dashed line), and mean of  $\Delta\psi$  and  $\Delta\varepsilon$  (bold line).

## References

- Herring, T. A., Mathews, P. M., Buffet, B. A.: Modelling of Nutation-Precession: Very long baseline interferometry results. *J. Geophys. Res.*, 2002, JB000165.
- Shirai, T., T. Fukushima: Did Huge Earthquake Excite Free Core Nutation. *J. Geodetic Soc. Japan*, 2001, **47**, No 1, 198–203.
- Dehant, V., P. Defraigne: New Transfer Functions for Nutation of a Nonrigid Earth. *J. Geophys. Res.*, 1997, **102**, 27659–27687.
- Shirai, T., T. Fukushima: Construction of a New Forced Nutation Theory of the Nonrigid Earth. *Astron. J.*, 2001, **121**, 3270–3283.
- Ferraz-Mello, S.: Estimation of periods from unequally spaced observations. *Astron. J.*, 1981, **86**, No 4, 619–624.
- Marple, S. L., Jr.: *Digital Spectral Analysis with Applications*. Prentice-Hall, Inc., Englewood Cliffs, N. J., 1987.
- Foster, G.: Wavelets for period analysis of unevenly sampled time series. *Astron. J.*, 1996, **112**, No 4, 1709–1729.
- Malkin, Z.: A Comparison of the VLBI Nutation Series with IAU2000 Model. In: *IVS 2002 General Meeting Proceedings*, eds. N. R. Vandenberg, K. D. Baver, NASA/CP-2002-210002, 2002, 335–339.
- Vondrak J.: Is Chandler frequency constant? In: A. K. Babcock, G. A. Willis (eds.), *The Earth's Rotation and Reference Frames for Geodesy and Geodynamics*, Proc. IAA Symp. 128, 1988, 359–364.
- Höpfner, J.: Low-frequency variations, Chandler and annual wobbles of polar motion as observed over one century. Scientific Technical Report STR03/01, GeoForschungsZentrum Potsdam, Germany.
- Schuh H., S. Nagel, T. Seitz. Linear drift and periodic variations observed in long time series in polar motion. *J. Geod.*, 2001, **74**, No 10, 701–710.



# Tropospheric Zenith Delays Determined by VLBI as a Contribution to Climatological Studies

J. Boehm<sup>1</sup>, H. Schuh<sup>1</sup>, V. Tesmer<sup>2</sup>, and H. Schmitz-Huebsch<sup>2</sup>

<sup>1</sup> Institute of Geodesy and Geophysics (IGG), TU Vienna, Austria

<sup>2</sup> Deutsches Geodätisches Forschungsinstitut (DGFI), Munich, Germany

**Summary:** As consistent VLBI observations at various stations over the whole globe have been carried out since 1984, it is possible to determine long time series not only of baseline vectors and Earth orientation parameters, but also of tropospheric parameters. Time series of wet zenith delays provide information about trends and periodic variations of the amount of water vapour in the troposphere. At Wettzell (Germany) there is a trend of  $\sim +0.7$  mm/year in the wet zenith delay which corresponds to  $\sim +0.1$  mm/year precipitable water vapour. Additionally, periodic variations in the time series are revealed by Fourier and wavelet analyses, and information about the precipitable water provided by the ECMWF (European Centre for Medium-Range Weather Forecasts) is used to evaluate the VLBI estimates.

## 1 Introduction

The total path delay for an observation at the elevation angle  $\varepsilon$  consists of the hydrostatic and the wet part. Each of these parts is the product of the delay in zenith direction and the corresponding mapping function. Assuming azimuthal symmetry at a VLBI station, the total path delay in the neutral atmosphere  $\Delta L(\varepsilon)$  can therefore be modelled as:

$$\Delta L(\varepsilon) = \text{HZD} \cdot \text{mf}_h(\varepsilon) + \text{WZD} \cdot \text{mf}_w(\varepsilon) \quad (1)$$

HZD	hydrostatic zenith delay
WZD	wet zenith delay
$\text{mf}_h(\varepsilon)$	hydrostatic mapping function
$\text{mf}_w(\varepsilon)$	wet mapping function

In standard VLBI analyses, the wet zenith delay (WZD) is estimated, while the other three parameters (HZD,  $\text{mf}_h$ ,  $\text{mf}_w$ ) are assumed to be known. Since consistent VLBI observations have been carried out for about 20 years, long time series of the wet zenith delays at various stations can be determined and used for climatological studies. Table 1 gives an overview of the VLBI stations that have been used for these investigations. On the average, 24 h geodetic VLBI sessions have been performed every 4th to 5th day, which yields a temporal coverage between 19% and 25%.

Table 1: Overview of selected VLBI stations, their latitudes, temporal coverage by VLBI sessions and the year of the first observation that was included in the analyses.

Station	latitude	temporal coverage	1st observation in the year
Wettzell, Germany	49°	25%	1984
Fortaleza, Brazil	-4°	20%	1993
Westford, Mass., U.S.A.	43°	19%	1984
Kokee Park, Hawaii, U.S.A.	22°	24%	1993
Gilcreek, Alaska, U.S.A.	65°	21%	1984

In VLBI analysis, wet zenith delays are estimated in the least-squares fit for each station of the observing session with a temporal resolution of 1 or 2 hours. The accuracy level of the absolute values is at about  $\pm 5$  mm (Niell, 2001, or Schuh et al., 2003b). Meteorological parameters are recorded at all VLBI stations, which is very valuable if we want to separate the hydrostatic and wet delays.

The contribution of GPS-derived wet zenith delays to climatology derived from nearly continuous GPS observations since 1994 has been reported recently (Eyer, 1999, Gradinarsky et al., 2002). Since the spatial coverage of these observations is much denser than that of VLBI, it allows also regional studies. However, GPS-derived wet zenith delays can suffer from antenna phase center variations, multipath effects and the replacement of antennas or radomes. Thus, a comparison with wet zenith delays determined by VLBI at selected stations seems advisable, in particular because a better long-term stability of the latter can be assumed due to the higher stability of the celestial and terrestrial reference frames used in VLBI. First results of trends detected in time series of tropospheric parameters at selected VLBI stations were reported by Schuh et al. (2003a) and Niell (2003).

## 2 Accuracy of the terrestrial reference frame

In order to detect significant trends in the wet zenith delays, the terrestrial reference frame has to be sufficiently accurate. This requirement is above all due to the high correlation of about -0.4 between station heights and zenith path delays, i.e. if a station height is wrong by +10 mm, the zenith path delay at this site will be shifted by about -4 mm (see Figure 1). If one assumes that the station coordinates of station A are error-free, that both stations are fixed in the analysis and that the observation in station B is taken in zenith direction, an error of the station height coordinate of B (vertical arrow) will be fully transferred (with opposite sign) into an error of its wet zenith delay. As in typical VLBI sessions the observations are taken at elevations down to  $\sim 5^\circ$ , the correlation decreases from -1 to about -0.4.

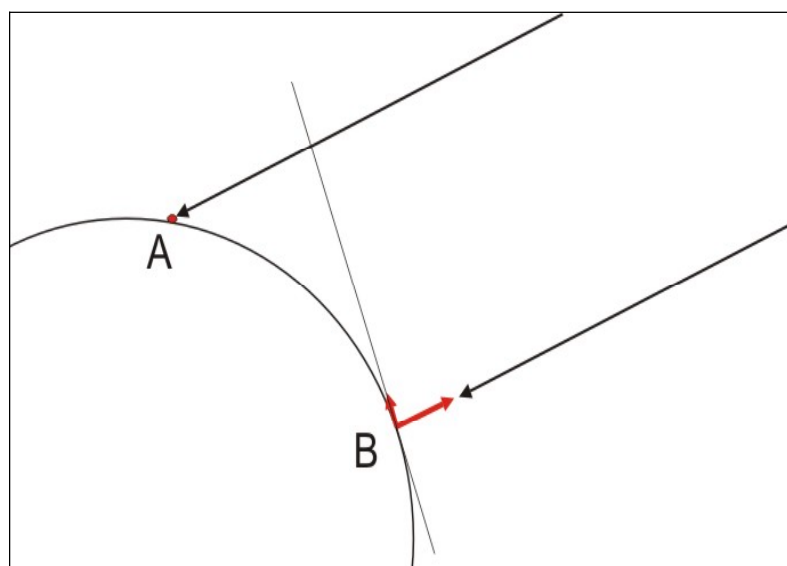


Figure 1: Geometry of a VLBI observation. The arrows at station B mark horizontal and vertical errors in the station coordinates (see text).

As this paper focuses on linear trends and periodic variations of the wet zenith delays rather than on absolute values, the station velocities and their standard deviations are of primary importance in this context. Two different terrestrial reference frames were applied to check the impact of their differences on the trends observed in wet zenith delays. In addition to the ITRF2000, which is a combined solution of VLBI, GPS, SLR, and DORIS measurements, a terrestrial reference frame purely determined by VLBI (DGFI02R02) was used for the analyses of the VLBI sessions. While the imprecision of the DGFI02R02 velocities is about  $\pm 0.1$  mm/year and that of the ITRF2000 is about  $\pm 0.5$  mm/year, the differences in station height velocities between both realizations do not exceed 0.8 mm/year for the subset of stations treated here (Table 2). Thus,  $\pm 0.8$  mm/year can be considered as a rough estimate of the inaccuracy of the terrestrial reference frame. Comparisons with the terrestrial reference frame for VLBI called VTRF2003 (Nothnagel, 2003, personal communications) confirm the statements above. The latter is similar to the DGFI02R02 terrestrial reference because it has also been made up by VLBI observations only.

Table 2: Differences in station height velocities between ITRF2000 and DGFI02R02 in mm/year (ITRF2000 minus DGFI02R02).

Gilcreek	Kokee Park	Westford	Fortaleza	Wetzell
0.5	-0.5	0.8	0.8	0.1

The maximum deviation of 0.8 mm/year in station height velocity corresponds to about -0.3 mm/year in the wet zenith delay. Thus, if the linear trend in WZD exceeds  $\sim 0.3$  mm/year, it can be assumed as significant as far as the accuracy of the reference frame is concerned. To check this statement, different analysis strategies were compared: Fixing the coordinates to ITRF2000 and DGFI02R02 and calculating free network solutions with respect to both terrestrial reference frames yields similar trends for the wet zenith delays which will be presented in the following section.

### 3 Analysis and results

For this investigation, all 24 h geodetic VLBI sessions were analyzed that have been carried out since 1984. The VLBI software package OCCAM V 5.1 (Titov et al., 2001) was applied using the Gauss-Markov model for the least-squares adjustment. The wet zenith delays were estimated as 1 h piecewise linear functions, the elevation angle cutoff was set to  $8^\circ$ , and the ITRF2000 was fixed. The mapping functions by Niell (1996) were used throughout.

#### 3.1 Linear long-term trends in wet zenith delays

Six-hour values of the wet zenith delays were extracted by interpolating between the two closest hourly estimates (Figure 2a) to allow comparison with meteorological data from numerical weather models (Figure 4a,b). In these data, e.g. at Wetzell (Germany) a big seasonal variation can be seen ranging from 0 mm (on some winter days) to 200 mm (on some summer days) and by an unweighted least-squares fit the linear trend was estimated to 0.83 mm/year. Then mean seasonal values were determined. On the basis of these seasonal values, the overall rate of the wet zenith delays was estimated to  $+0.7$  mm/year at Wetzell (Figure 2b). It is slightly different from the trend of the original time series, due to the different averaging processes within the computation of the seasonal values. The trend at Gilcreek (Alaska) for the time period 1989 - 2001 was determined to  $+0.3$  mm/year (Figure 2d). Fol-

lowing the conclusion of section 2, the trend at Wettzell is significant, i.e. above the possible influence of the chosen reference frame whereas for Gilcreek another few years of VLBI observations are needed. Multiplication of the observed rate by the length of the time series yields an increase of the wet zenith delays of approximately 13 mm in 18 years. For the other VLBI stations the determination of reliable linear trends was not possible because either the time series were too short (Fortaleza, Kokee Park) or the seasonal wet zenith delays were too noisy (Westford). Figure 2c shows the averaged winter WZD values at Wettzell with a linear trend of 0.74 mm/year. The lowest average WZD were obtained for winter 1983/84 and 1995/96. Meteorological records at Wettzell station confirm that these winters were extraordinarily cold and dry.

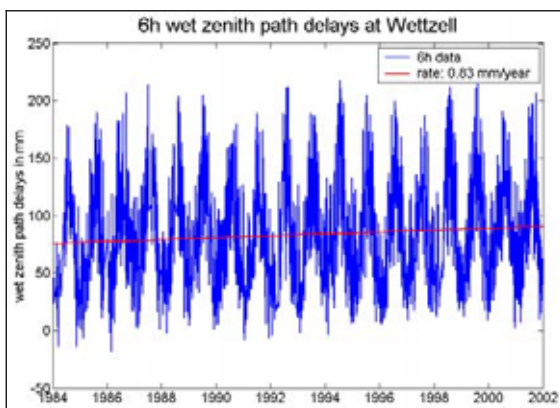


Figure 2a: 6 h wet zenith delays at Wettzell since 1984.

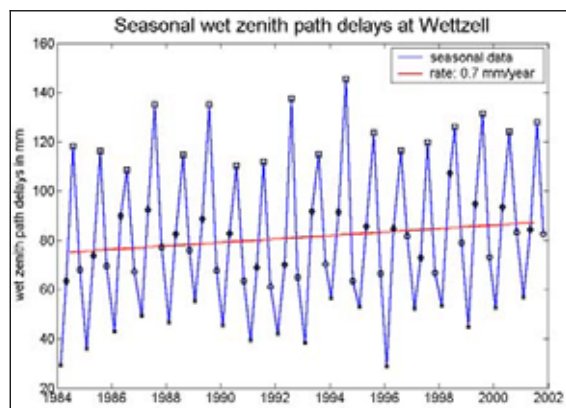


Figure 2b: Mean seasonal values of the wet zenith delays at Wettzell. The linear trend is estimated to 0.7 mm/year. Different markers are used for the seasons ( $\diamond$  spring,  $\square$  summer,  $\circ$  autumn,  $\times$  winter).



Figure 2c: Wet zenith delays at Wettzell in winter. The linear trend is estimated to 0.74 mm/year. In 1983/84 and 1995/96 the winters were extraordinarily dry (= cold).

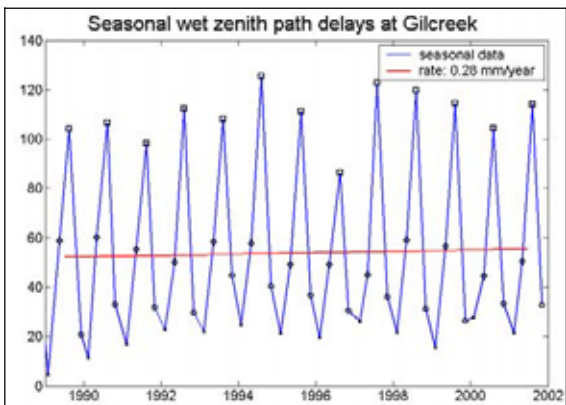


Figure 2d: Mean seasonal values of the wet zenith delays at Gilcreek. The linear trend is estimated to 0.3 mm/year. Different markers are used for the seasons ( $\diamond$  spring,  $\square$  summer,  $\circ$  autumn,  $\times$  winter).

### 3.2 Climatological interpretation of trends in the wet zenith delays

Although wet zenith delays cannot be directly derived from meteorological data recorded at a site, there are equations that yield approximate values, e.g. by Moran et al. (2001):

$$\text{WZD} \approx \frac{e}{T^2} \quad [\text{m}], \quad (2)$$

where  $e$  is the water vapour pressure in hPa and  $T$  is the temperature in K. The VLBI databases comprise information about the temperatures and the relative humidities recorded close to each radiotelescope. At Wettzell, since 1984 the relative humidity has been rather constant at about 80% whereas the temperature has increased by about 0.13 K/year. The relative humidity  $f$  is defined by

$$f = \frac{e}{E(T)}. \quad (3)$$

As the saturated water vapour pressure  $E(T)$  is increasing with rising temperature, the water vapour pressure  $e$  is increasing with rising temperature, too, if  $f$  is kept constant. Although (2) implies that the wet zenith delays are decreasing with increasing temperature, the influence of the increase in  $e$  (see (3)) is dominating over this effect. Using a mean temperature of 15 °C and a mean relative humidity of 80%, (3) and (2), applied for an increase in the temperature of 0.13 K per year, yield an increase in the wet zenith delay of 0.9 mm/year, what is close to the results from VLBI (0.7 mm/year to 0.8 mm/year).

Table 3: Change in the WZD after one year, when the temperature is rising by 0.13 K and the relative humidity is assumed to be constant at 80 %.

t in °C	e in hPa (see (3))	T <sup>2</sup> in K <sup>2</sup>	WZD in mm (see (2))
15.00	13.635	83030	124.8
15.13	13.750	83105	125.7

### 3.3 Periodic variations in the wet zenith delays

Classical Fourier analyses and wavelet transformations of the six-hour time series were performed to find periodic variations of the wet zenith delays. The Fourier spectra show wide peaks at the annual periods for tropical stations (Fortaleza, Kokee Park) (Figure 3b, plots at left side) and sharp peaks for stations in mid-latitudes (Wettzell, Westford). This is due to the fact that there are no pronounced differences between the seasons in the tropics, while the large seasonal differences of the temperatures for continental stations are mirrored in the strong annual variations of the wet zenith delays.

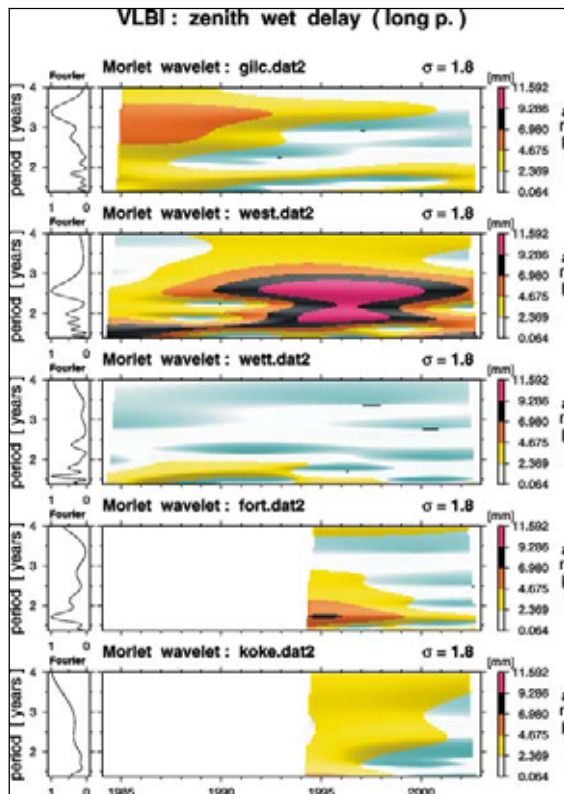


Figure 3a: Fourier and Morlet wavelet spectra for periods between 500 and 1460 days for the VLBI stations Gilcreek (gilc.dat2), Westford (west.dat2), Wettzell (wett.dat2), Fortaleza (fort.dat2) and Kokee Park (koke.dat2).

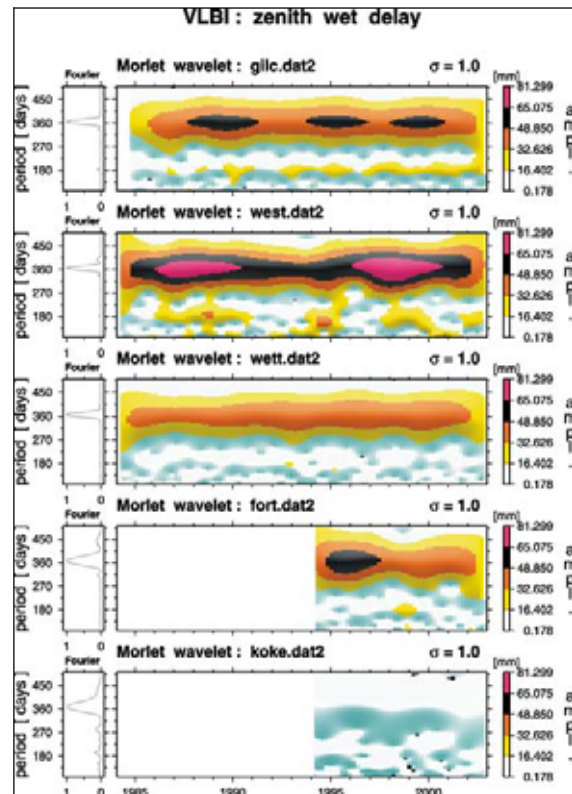


Figure 3b: Fourier and Morlet wavelet spectra for periods between 100 and 500 days for the VLBI stations Gilcreek (gilc.dat2), Westford (west.dat2), Wettzell (wett.dat2), Fortaleza (fort.dat2) and Kokee Park (koke.dat2).

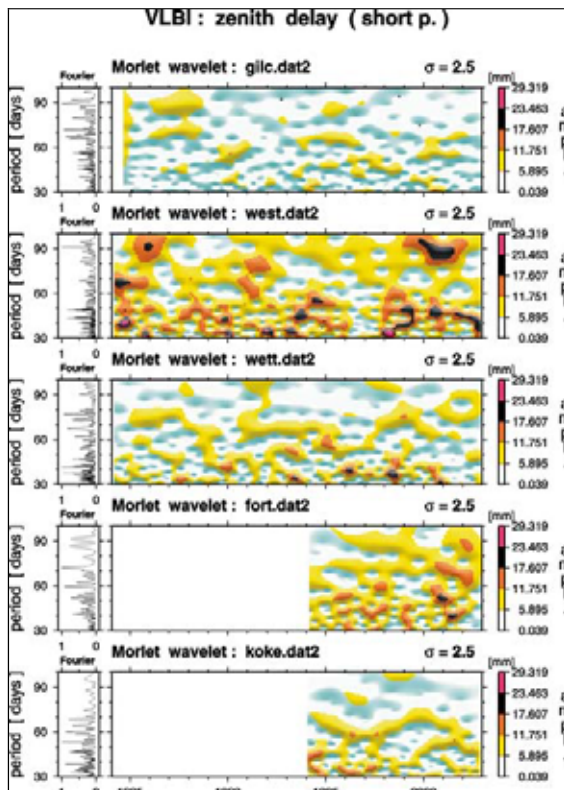


Figure 3c: Fourier and Morlet wavelet spectra for periods between 30 and 100 days for the VLBI stations Gilcreek (gilc.dat2), Westford (west.dat2), Wettzell (wett.dat2), Fortaleza (fort.dat2) and Kokee Park (koke.dat2).

The wavelet analyses do not only provide information about the main periods of the wet zenith delays but also about the temporal variations of periods and amplitudes. The most remarkable results are:

- strong annual periods at all stations with variable amplitudes (Figure 3b),
- irregular variations at 1.6 - 1.7 years (Figures 3a),
- irregular variations with periods between 30 and 90 days (Figure 3c); the strongest of these variations occurred at Westford, in particular with periods shorter than 50 days.

## 4 Comparison with ECMWF data

The European Centre for Medium-Range Weather Forecasts (Reading, UK) provides meteorological data at six-hour intervals. The precipitable water is the parameter that is comparable to the wet zenith delay WZD. Firstly, the wet zenith delay has to be transformed into the integrated water vapour IWV (units kg/m<sup>2</sup>):

$$IWV = WZD \cdot \Pi \quad (4)$$

The parameter  $\Pi$  is as follows:

$$\Pi = \frac{10^6 \cdot M_w}{\left(k_2' + \frac{k_3}{T_m}\right) \cdot R} \quad (5)$$

where

$$M_w = 18.0152 \frac{\text{kg}}{\text{kmol}},$$

$$k_2' = 17 \pm 10 \frac{\text{K}}{\text{hPa}},$$

$$k_3 = 373900 \pm 1200 \frac{\text{K}^2}{\text{hPa}},$$

$$R = 8314.34 \frac{\text{J}}{\text{kmol} \cdot \text{K}}.$$

$M_w$  is the molar mass of water,  $k_2'$  and  $k_3$  are empirically determined coefficients,  $T_m$  is the mean temperature above the station, and  $R$  is the general gas constant. With the density of liquid water  $\rho_w$ , the precipitable water PW (units: m) can be determined:

$$PW = IWV / \rho_w . \quad (6)$$

The precipitable water can be approximated by the formula

$$PW \approx 0.15 \cdot WZD . \quad (7)$$

The comparison between precipitable water from VLBI and ECMWF, which is available since 1994, shows a very good agreement at the level of  $\pm 1.85$  mm corresponding to a zenith delay of  $\sim \pm 12$  mm (Figures 4a,b). Compared to the standard deviation of  $\pm 1.85$  mm (precipitable water) the bias between the time series is very small (0.44 mm PW or 3 mm WZD).

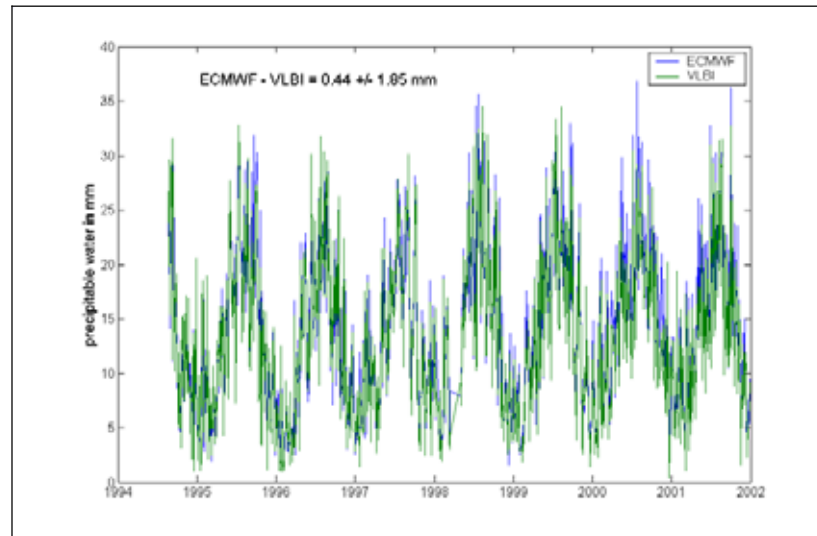


Figure 4a: Precipitable water from ECMWF and VLBI at Wettzell (1994 - 2002).

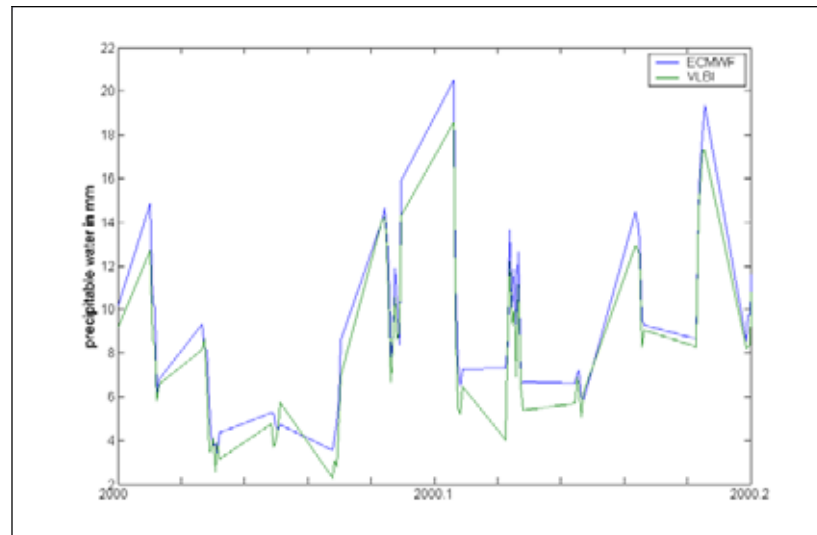


Figure 4b: Precipitable water from ECMWF and VLBI at Wettzell (2000.0 - 2000.2). ECMWF values are plotted only when VLBI values are available.

## 5 Conclusions and outlook

The investigations presented here reveal a systematic increase of the wet zenith delays at Wettzell in the past two decades. This trend is significantly above the potential influence of the chosen terrestrial reference frame. Thus, the results obtained from VLBI might be useful for climatological studies. A closer look remains to be taken at the other VLBI sites to possibly detect similar features in the time series of the tropospheric parameters. Similarly to the comparison with data from ECMWF, the tropospheric zenith delays can be compared with those provided by IGS as shown by Schuh and Boehm (2003b). Moreover, GPS-derived zenith delays can be used to fill the gaps between the results of VLBI and to finally obtain a robust combined time series.

## Acknowledgements

We would like to thank the Zentralanstalt für Meteorologie und Geodynamik (ZAMG), Austria, for giving us access to the ECMWF data and to Burghard Richter (DGFI, Munich) for giving valuable hints to this publication.

## References

- Eyer M., Der Einsatz des GPS zur Wasserdampfmodellierung in der Klimatologie, Satelliten-Beobachtungsstation Zimmerwald, Bericht Nr. 28, 1999.
- Gradinarsky L.P., J.M. Johansson, H.R. Bouma, H.-G. Scherneck, G. Elgered, Climate Monitoring using GPS, *Physics and Chemistry of the Earth*, 27, pages 335 - 340, 2002.
- Niell, A.E., Global mapping functions for the atmosphere delay at radio wavelengths, *J. of Geophys. Res.*, Vol. 101, No. B2, 3227-3246, 1996.
- Niell, A.E., A.J. Coster, F.S. Solheim, V.B. Mendes, P.C. Toor, R.B. Langley, C.A. Upham, Comparison of Measurements of Atmospheric Wet Delay by Radiosonde, Water Vapor Radiometer, GPS and VLBI, *Journal of Atmospheric and Oceanic Technology*, 18, pages 830 - 850, 2001.
- Niell, A.E., A Role for VLBI in Climate Studies, *IVS Newsletter*, issue 5, 5, 2003.
- Schuh H., J. Boehm, Determination of tropospheric parameters by VLBI as a contribution to climatological studies, In: *Proceedings of the Weikko A. Heiskanen Symposium in Geodesy (Oct. 2002)*, edited by C. Jekeli, Ohio State University, 2003a.
- Schuh H., J. Boehm, Status Report of the IVS Pilot Project - Tropospheric Parameters, in *International VLBI Service for Geodesy and Astrometry 2002 Annual Report*, edited by N. R. Vandenberg and K. D. Baver, NASA/TP-2003-211619, 2003b.
- Thompson, A.R., J.M. Moran, G.W. Swenson jr., *Interferometry and Synthesis in Radio Astronomy*, John Wiley and Sons, 2001.
- Titov O., V. Tesmer, J. Boehm, OCCAM Version 5.0 Software User Guide, AUSLIG Technical Report 7, 2001.



# Robust Outlier Detection in VLBI Data Analysis

H. Kutterer, R. Heinkelmann, and V. Tesmer

*Deutsches Geodätisches Forschungsinstitut (DGFI), Munich, Germany*

**Summary:** The detection and elimination of outliers in VLBI observations is an important pre-processing step for VLBI parameter estimation. A common technique to handle this problem is based on a so-called 3-sigma rejection criterion. It starts with an initial least-squares adjustment. Afterwards, all observations are eliminated from the data whose residuals exceed their respective standard deviations (sigma) by a factor greater than three. The final parameters are estimated in a second step. This technique which is also implemented in the VLBI processing software OCCAM LSM 5.0 is compared in this study with several robust estimators which are less restrictive regarding data elimination. From a methodological point of view all considered techniques are least-squares estimations using iterative reweighting. Data from more than 2000 VLBI sessions over a time span of 20 years were used for performance tests. The following results can be given: The 3-sigma criterion is rather fast but usually too simplistic since it tends to wrongly eliminate correct observations. Among the robust estimators the BIBER by Wicki performed best. It proved to be both efficient and reliable.

## 1 Introduction

The use of the Gauss-Markov model (GMM) is common practice in VLBI data analysis. It reads as

$$\mathbf{v} = \mathbf{A} \mathbf{d}\mathbf{x} - \mathbf{d}\mathbf{l}, \quad \mathbf{C}_{\parallel} = \sigma_0^2 \mathbf{Q}_{\parallel} = \sigma_0^2 \mathbf{P}^{-1} \quad (1)$$

with  $\mathbf{v}$  denoting the observation residuals,  $\mathbf{d}\mathbf{x}$  the update of the parameters  $\mathbf{x}$  with respect to some initial values  $\mathbf{x}_0$ ,  $\mathbf{d}\mathbf{l}$  the reduced observations (observed minus computed),  $\mathbf{A}$  the column-regular configuration matrix,  $\mathbf{C}_{\parallel}$  the regular (theoretical) variance-covariance matrix (vcm) of the observations,  $\mathbf{Q}_{\parallel}$  and  $\mathbf{P}$  the corresponding cofactor matrix and weight matrix, respectively, and  $\sigma_0^2$  the (theoretical) variance factor. The first part of the GMM is called ‘functional model’, the second part with the vcm is called ‘stochastic model’. A comprehensive summary of the functional VLBI model is given by, e.g., Sovers et al. (1998). For the refinement of the stochastic VLBI model see Tesmer (2003; this volume).

The least-squares (LS) principle reads as

$$\hat{\mathbf{v}}^T \mathbf{P} \hat{\mathbf{v}} = \min_{\mathbf{d}\mathbf{x} \in \mathbb{R}^n} \left[ (\mathbf{A} \mathbf{d}\mathbf{x} - \mathbf{d}\mathbf{l})^T \mathbf{P} (\mathbf{A} \mathbf{d}\mathbf{x} - \mathbf{d}\mathbf{l}) \right], \quad (2)$$

i.e. those parameters  $\mathbf{d}\hat{\mathbf{x}}$  are derived which minimize the squared sum of residuals. The hat symbol (‘^’) indicates estimated quantities. The corresponding normal equations systems is

$$\mathbf{A}^T \mathbf{P} \mathbf{A} \mathbf{d}\hat{\mathbf{x}} = \mathbf{A}^T \mathbf{P} \mathbf{d}\mathbf{l} \quad (3)$$

and consequently the estimated parameters (‘best linear unbiased estimates’, BLUE) read as

$$\mathbf{d}\hat{\mathbf{x}} = (\mathbf{A}^T \mathbf{P} \mathbf{A})^{-1} \mathbf{A}^T \mathbf{P} \mathbf{d}\mathbf{l} \quad (4)$$

and the residuals as

$$\hat{\mathbf{v}} = -\left( \mathbf{I} - \mathbf{A} (\mathbf{A}^T \mathbf{P} \mathbf{A})^{-1} \mathbf{A}^T \mathbf{P} \right) \mathbf{d}\mathbf{l} \quad (5)$$

with the associated vcms

$$\mathbf{C}_{\hat{\mathbf{x}}\hat{\mathbf{x}}} = \sigma_0^2 (\mathbf{A}^T \mathbf{P} \mathbf{A})^{-1} \quad (6)$$

and

$$\mathbf{C}_{\hat{\mathbf{v}}\hat{\mathbf{v}}} = \sigma_0^2 \left( \mathbf{Q}_{\mathbf{11}} - \mathbf{A} (\mathbf{A}^T \mathbf{P} \mathbf{A})^{-1} \mathbf{A}^T \right) \quad (7)$$

Instead of the theoretical value  $\sigma_0^2$ , the unbiasedly estimated value

$$\hat{\sigma}_0^2 = \frac{\hat{\mathbf{v}}^T \mathbf{P} \hat{\mathbf{v}}}{n - u} = \frac{\hat{\mathbf{v}}^T \mathbf{P} \hat{\mathbf{v}}}{r} \quad (8)$$

could be used with  $n$  denoting the number of observations,  $u$  the number of unknown parameters and  $r$  the redundancy of the estimation problem.

For the above-mentioned unbiasedness of the given estimators it is necessary that the deviations between model and data which are reflected by  $\mathbf{dl}$  are purely random with zero expectation. This does not hold in any case due to several reasons such as outliers in the data or systematic errors. The latter are not subject of this study. Incorrect observations (outliers) must either be identified and eliminated from the data or estimators must be used such as the robust techniques which minimize the bias on the estimated parameters. See Koch (1999) as a reference for both least-squares estimation in the GMM and for an overview of robust estimation. The robust estimators which are considered in this paper are explained in the following section. They all share the main idea that the observations with significant residuals are downweighted in an iterative procedure in order to reduce their influence on the estimates. The various robust estimators differ in the respective downweighting scheme. Note that in practice there is some ambiguity in the outlier detection procedures as two contributors are relevant. Either the observation is actually an outlier and does not fit to the model or the standard deviation of the observation is incorrect which is the basis for the comparison and final decision (see Section 2).

## 2 Considered outlier detection techniques

### 2.1 General reweighting scheme

The initial solution for the robust estimation is coming from a LS estimation as described in the previous section. The matrix  $\mathbf{P}$  is used as initial weight matrix  $\mathbf{W}^{(0)}$ :

$$\mathbf{v} = \mathbf{A} \mathbf{dx} - \mathbf{dl}, \quad \mathbf{W}^{(0)} = \mathbf{P} \Rightarrow \mathbf{A}^T \mathbf{W}^{(0)} \mathbf{A} \mathbf{d}\hat{\mathbf{x}}^{(0)} = \mathbf{A}^T \mathbf{W}^{(0)} \mathbf{dl} \quad (9)$$

The corresponding residuals

$$\hat{\mathbf{v}}^{(0)} = - \left( \mathbf{I} - \mathbf{A} (\mathbf{A}^T \mathbf{W}^{(0)} \mathbf{A})^{-1} \mathbf{A}^T \mathbf{W}^{(0)} \right) \mathbf{dl} \quad (10)$$

yield the new weights according to

$$w_i^{(m+1)} = \begin{cases} w_i^{(m)}, & \text{if } |\hat{v}_i^{(m)}| \leq k\sigma \\ " < w_i^{(m)} ", & \text{if } |\hat{v}_i^{(m)}| > k\sigma \end{cases}, \quad (11)$$

where  $\sigma$  is a standard deviation which refers to a particular estimator. Some examples are given below in Section 2.2. Hence, if an estimated residual is an element of a proper interval, the weight of the corresponding observation remains unchanged ( $w_i^{(m+1)} = w_i^{(m)}$ ). If not, it is reduced ( $w_i^{(m+1)} < w_i^{(m)}$ ) following the particular estimation rules. The new weight matrix is again diagonal and reads as

$$\mathbf{W}^{(m+1)} = \text{diag} \left( w_i^{(m+1)} \right)_{i=1, \dots, n} \quad (12)$$

Now the estimation step is repeated as long as either the update of the weights or of the estimated parameters is numerically non-significant.

$$\begin{aligned} \mathbf{v}^{(m+1)} &= \mathbf{A} \mathbf{d}\mathbf{x}^{(m+1)} - \mathbf{d}\mathbf{l}, \quad \mathbf{W}^{(m+1)} \\ \Rightarrow \mathbf{A}^T \mathbf{W}^{(m+1)} \mathbf{A} \mathbf{d}\mathbf{x}^{(m+1)} &= \mathbf{A}^T \mathbf{W}^{(m+1)} \mathbf{d}\mathbf{l} \Rightarrow \hat{\mathbf{v}}^{(m+1)} \end{aligned} \quad (13)$$

Typically, only a small number of iterations is needed until convergence. Note that the initial cofactor matrix and weight matrix of the observations are interpretable as precision measures based on the theory of stochastics. In general, this does not hold for the corresponding final matrices resulting from the iteration procedure because the reduced weights may no longer correspond with a realistic standard deviation.

## 2.2 Different techniques

In the following it is assumed that the initial weight matrix is the  $n$ -dimensional identity matrix what can easily be achieved by means of a simple transformation of the original matrix. The so-called '3 sigma' rejection is a commonly used reweighting technique for the elimination of outliers in the observations. It is standard in VLBI data processing using the OCCAM LSM 5.0 software (Titov et al., 2001). The main idea is to compare each residual with its standard deviation based on a critical value  $k$  (typically  $k=3$ ). In case of significance (residual greater than its standard deviation), the weight of the corresponding observation is reduced by a factor of 100000. Otherwise, it is kept. The downweighting practically nulls the impact of the observation on the estimated parameters. Eq. (14) shows two possibilities to compute the standard deviations. In the first line the theoretical factor  $\sigma_0$  is used what corresponds with a normal distribution whereas the factor  $\hat{\sigma}_0$  which is used in the last line points to a  $t$ -distribution

$$w_i = \begin{cases} 1, & \text{if } |\hat{v}_i| \leq k \sigma_{v_i} \\ 1/100.000, & \text{if } |\hat{v}_i| > k \sigma_{v_i} \end{cases}, \quad (14)$$

$$\text{with } \sigma_{v_i} = \begin{cases} \sigma_0 \sqrt{q_{v_i v_i}} \\ \text{or} \\ \sqrt{\frac{\mathbf{v}^T \mathbf{P} \mathbf{v} - v_i^2 / q_{v_i v_i}}{n - u - 1}} \sqrt{q_{v_i v_i}} \end{cases}$$

It is obvious that the decision pro or con an outlier is binary. An observation is either used for the estimation or not.

A less restrictive and hence more moderate reweighting is given by the Huber estimator (Huber, 1981)

$$w_i^{(m+1)} = \begin{cases} 1, & \text{if } |\hat{v}_i^{(m)}| \leq k\sigma_{l_i} \\ \frac{k\sigma_{l_i}}{|\hat{v}_i^{(m)}|}, & \text{if } |\hat{v}_i^{(m)}| > k\sigma_{l_i} \end{cases}, \quad i = 1, \dots, n. \quad (15)$$

Here, the theoretical standard deviations  $\sigma_{l_i}$  of the observations are used for the comparison. The downweighting is inversely proportional to the relation of the absolute values of the residuals and  $\sigma_{l_i}$ . Hence, the more significant the residual, the less is the new observation weight. Note that in case of non-significant residuals the same estimated values are obtained as for standard LS estimation.

The so-called modified Huber estimator was developed as a refinement of the Huber estimator in order to overcome the so-called leverage point problem. Leverage points can be characterized as having strong impact on the parameter estimation without being effectively controlled themselves.

$$w_i^{(m+1)} = \begin{cases} \sqrt{q_{v_i v_i}}, & \text{if } |\hat{v}_i^{(m)}| \leq k\sigma\sqrt{q_{v_i v_i}} \\ \frac{k\sigma\sqrt{q_{v_i v_i}}}{|\hat{v}_i^{(m)}|}, & \text{if } |\hat{v}_i^{(m)}| > k\sigma\sqrt{q_{v_i v_i}} \end{cases}, \quad i = 1, \dots, n \quad (16)$$

For further reading see, e.g., Huber (1981) or Rousseuw and Leroy (1987).

The BIBER estimator was developed by Wicki (1998). It comprises the step-by-step reduction of single observation weights in contrast to the other robust estimators which modify all relevant observation weights in a particular iteration step. The algorithm is elaborated both in a weight reduction formulation which reads as

$$w_i^{(m+1)} = \begin{cases} \frac{k\sigma\sqrt{q_{v_i v_i}}}{|\hat{v}_i^{(m)}|}, & \text{if } |\hat{v}_i^{(m)}| = \max_{j=1, \dots, n} [|\hat{v}_j^{(m)}|] > k\sigma\sqrt{q_{v_i v_i}} \\ 1, & \text{else} \end{cases} \quad (17)$$

and equivalently based on observation modification. The corresponding weight matrix is derived after convergence. The modification of the observations is significantly more efficient than explicit reweighting regarding computer run-time since the normal equations matrix is inverted only once.

### 3 Assessment of the techniques

#### 3.1 Used VLBI software and data

For the study, 2230 VLBI sessions between 1984 and 2001, each with at least 24 hours of observation time, were considered in total. The criteria for the selection of the sessions were the same as for the VLBI solution DGFI01R01 (Tesmer, 2002). For example, restrictions regarding a minimum number of telescopes and observations were taken into account. The VLBI data were processed at the Deutsches Geodätisches Forschungsinstitut (DGFI) in Munich, Germany, using the software OCCAM 5.0 LSM (Titov et al., 2001). The coordinates of the VLBI antennas were referred to the ITRF 2000 by means of No-Net-Translation (NNT) and No-Net-Rotation (NNR) constraints. The positions of the radio sources were taken from the ICRF Ext. 1.

### 3.2 Computer run-time and general reweighting results

The techniques which were described in the previous section were assessed regarding their practical applicability to routine VLBI data processing. Hence, they were studied concerning the number of iterations and corresponding computer run-time until convergence. The 3-sigma rejection (in the following denoted by *ksr*) and the BIBER estimator based on observation modification (*mbi*) are both very efficient. The Huber (*hub*) and the modified Huber (*mhu*) estimator needed in general more iterations and more run-time. In case of huge amounts of data as for global VLBI solutions (see Section 3.4) these two techniques turned out to be rather slow and hence inefficient.

In addition, the resulting weights were checked. The Figures 1a-d show the final weights resulting from the four techniques which were applied to VLBI data of the CORE-A session at 25.01.2000. The residuals of ten representatively selected observations, their standard deviations (see Eqs. (5) and (7)) and the corresponding standardized residuals are given in Table 1.

The observations a and b are likely to be outliers. The observation e is just above the  $3\sigma$  level. For this reason these three observations are eliminated by the standard OCCAM 5.0 outlier handling technique (*ksr*). The outliers a and b are detected by all other techniques as well. They are down-weighted according to the values of the standardized residuals. The weight of observation e is changed marginally. The disadvantage of the modified Huber estimator (Fig. 1c) is obvious. In order to overcome the problem of leverage points which can mislead the outlier detection it actually down-weights all observations what is hard to interpret practically.

Table 1: Absolute values of residuals, standard deviations and standardized residuals of 10 selected observations of the CORE-A session at 25.01.2000. The standardized residuals of the observations a and b clearly exceed the critical value  $k=3$  and the respective value of observation e is slightly greater than 3. All other observations are not significant. The physical unit of the residuals and their standard deviations is cm.

	$ \hat{v}_i^{(0)} $	$\sigma_{v_i}^{(0)}$	$ \hat{v}_i^{(0)} /\sigma_{v_i}^{(0)}$
a	3,97	0,97	4,08
b	3,35	0,62	5,38
c	2,79	0,97	2,87
d	2,75	0,98	2,82
e	2,63	0,87	3,02
f	0,09	0,41	0,22
g	0,10	0,47	0,21
h	0,65	0,52	1,26
i	0,84	0,55	1,52
k	1,38	0,63	2,19

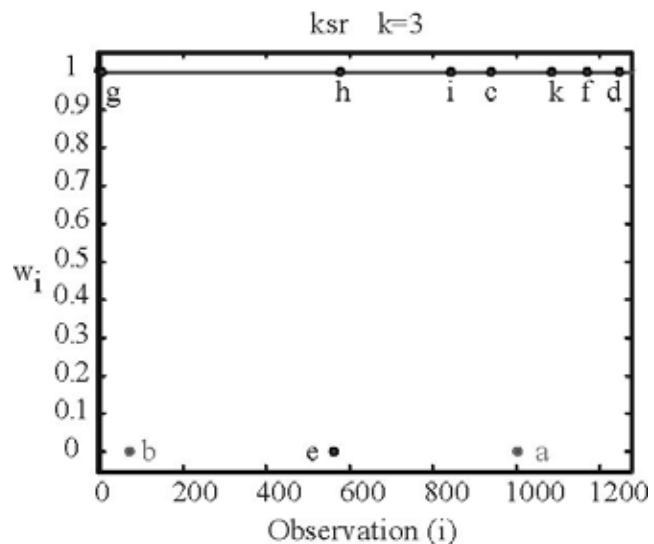


Figure 1a: The 3-sigma rejection strategy (*ksr*) classifies the observations a, b and e as outliers and eliminates them from the observation data (final weights practically equal zero).

Figure 1b: The Huber estimator (*hub*) reduces the weights of a, b, and e according to the values of the corresponding residuals. The observations are kept but with reduced weights.

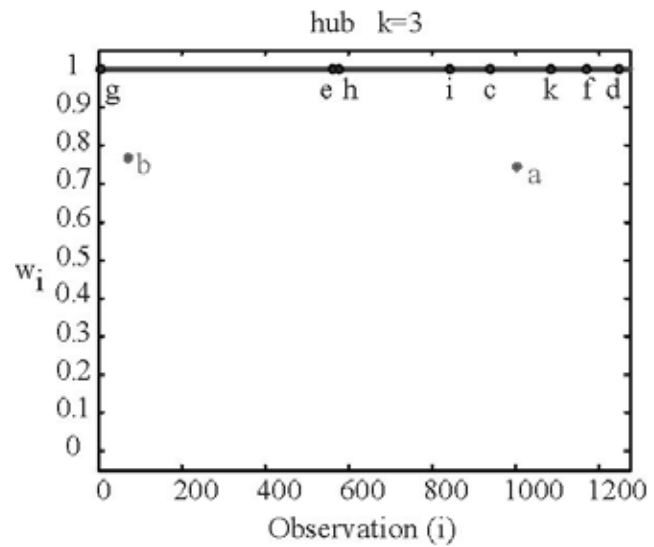


Figure 1c: The modified Huber estimator (*mhu*) reduces the weights of most of the observations in order to compensate the impact of leverage points. Here, the reweighting can not be interpreted in terms of outlier identification. Nevertheless, the parameters are estimated in a robust way.

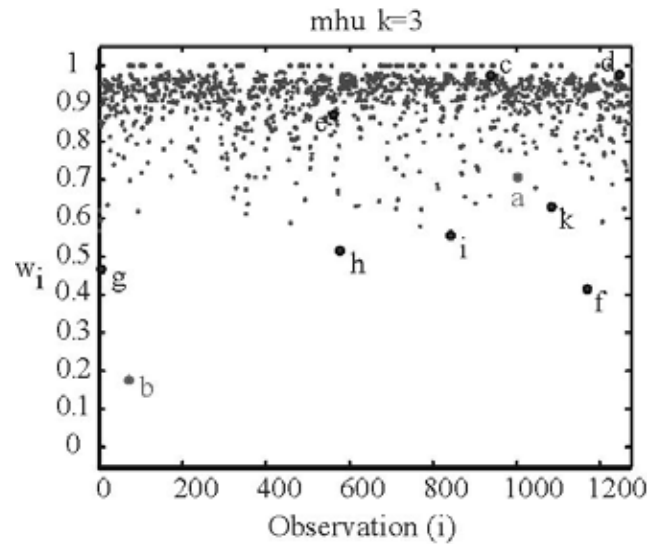
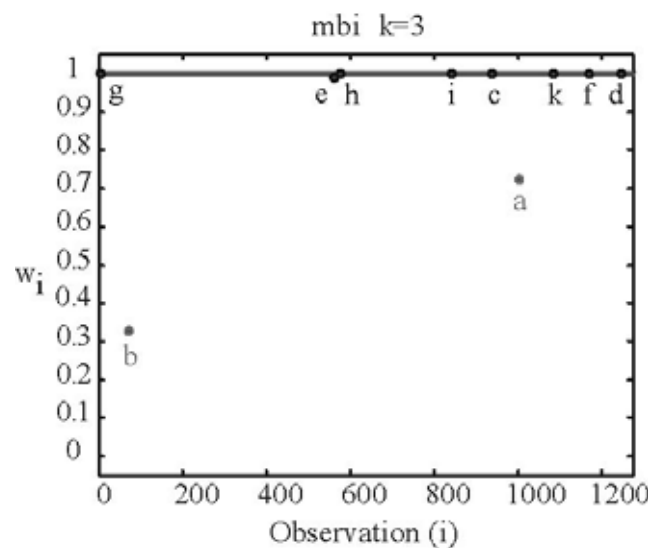


Figure 1d: The BIBER estimator (*mbi*) reduces the weights of a, b and e according to the values of the standardized residuals. All observations are kept in the data.



### 3.3 Tests with faked outliers

Several faked outliers were introduced to the data of the CONT session of 23.01.94 in order to check the performance of several robust estimators. The selected session was considered as 'save' because it did not show any problems in standard processing. The specifics of the four different test scenarios are given in Table 2. The values for the magnitudes of the small errors were taken directly from the minimum detectable bias (MDB) in the respective observations based on single outlier hypothesis tests (Koch, 1999) with the probability of a Type I error of 1 % and of a Type II error of 20 %. For the medium errors the respective MDB values were increased by a factor of 8. Hence, the small errors can be considered as merely detectable whereas the medium errors should be indicated in any case.

Figure 2 gives an overview of the results of the respective techniques on the different scenarios. For the hub and mhu  $k=2$  and  $k=3$  were considered. Obviously, the observations with medium errors are clearly identified by each technique. In case of small errors there are some differences. Just about half of them are indicated by the different techniques. The best rate is achieved by *mhu* and  $k=2$ , the worst rate by *hub* and  $k=3$ . Note that in case of *mhu* all weights are modified. Observations with final weights less than 0.5 were considered as outliers.

An additional problem has to be mentioned. All techniques indicate more or less observations as outliers whose values were not faked. This is in particular obvious for the *ksr* and for the *hub* with  $k=2$ . On the other hand, the *mhu* and the *mbi* do not tend to eliminate 'good data'. In case of *hub* and  $k=2$  there is a high sensitivity since a lot of small errors are detected correctly but even more good observations are mis-indicated. In case of *hub* and  $k=3$  the sensitivity is significantly reduced because only the medium errors are handled properly. Hence, it is clear that the various techniques have to be tuned properly to guarantee a sure indication only of actual outliers.

Table 2: Different scenarios for the introduction of faked outliers to the CONT session data of 23.01.94.

Outlier scenario	Number of		Error rate
	small errors	medium errors	
a	0	0	0,0 %
b	5	5	0,3 %
c	10	10	0,7 %
d	20	20	1,3 %

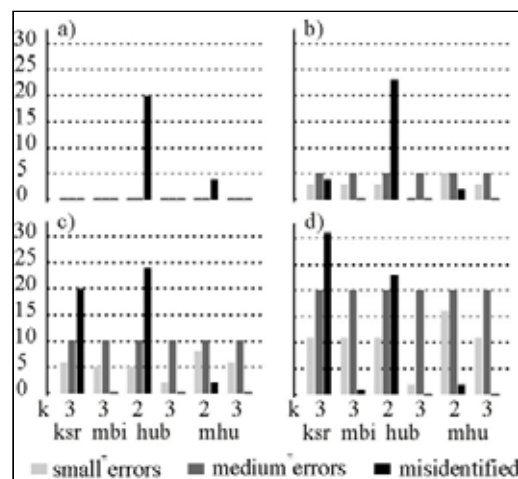


Figure 2: Statistics of the performance (number of observations indicated as an outlier) of the various outlier detection techniques regarding the different test scenarios.

### 3.4 Tests with real data

In a last test the impact of the *ksr* and the *mbi* on VLBI session solutions for station positions was studied. The restriction to these two techniques was due to the reduced efficiency of the other techniques in case of huge amounts of data. All VLBI sessions mentioned in Section 4.1 were processed. Regarding some global measures such as the resulting weighted root mean square error (WRMS) of the station positions with respect to a linear site motion model there are no significant differences between the two techniques.

However, as indicated in Table 3, for some sessions there are significant differences between the *ksr* and the *mbi*. Two results should be emphasized. First, the *ksr* tends to reject more observations than the *mbi*, for particular sessions even more than 4 %. Second, the estimated values  $\hat{\sigma}_0^2$  for the variance factor are greater in case of *mbi*. Both reflects the different philosophies behind the two techniques. In case of *ksr* an outlier is seen as incompatible with the functional model due to some error sources. In case of robust estimators and hence especially for *mbi*, the misfit of observation and model is to some extent considered as caused by improperly modelled observation noise. Nevertheless, for weak observation configurations it is mandatory to keep as many data as possible.

Table 3: Rates for the acceptance of observations in case of *ksr* and *mbi* for some sessions.

Sessionname	<i>ksr</i>		<i>mbi</i>	
	1- $\epsilon$	$\hat{\sigma}_0^2$	1- $\epsilon$	$\hat{\sigma}_0^2$
EUROPE, 02.02.98	95,3 %	0,99	99,9 %	1,03
IRIS-S, 19.07.99	96,1 %	0,86	99,6 %	1,12
IRIS-A, 13.11.89	95,1 %	1,00	97,7 %	1,43
VLBA, 09.02.98	91,5 %	0,79	94,0 %	1,09
IRIS-A, 06.07.89	96,0 %	1,15	98,4 %	1,56
IRIS-S, 03.05.99	97,4 %	0,84	99,7 %	1,01
IRIS-A, 26.07.89	96,8 %	1,23	98,8 %	1,40
NEOS-A, 11.05.93	95,9 %	0,89	97,9 %	1,18
IRIS-S, 02.03.95	93,1 %	1,03	95,0 %	1,40
VLBA, 19.05.97	92,8 %	1,10	94,7 %	1,47

## 4 Conclusions

Several techniques for the identification of outliers in the observations were studied in the context of VLBI data processing with the software OCCAM LSM 5.0. The techniques were assessed using some illustrative criteria such as algorithmic efficiency, interpretability of the results in the context of the Gauss Markov model and high sensitivity only concerning actual outliers in the observations. Correct observations must not be wrongly indicated as outliers. Regarding the complete set of requirements the BIBER estimator performed best as it is both fast and reliable. Hence it has to be recommended as the optimum choice. The 3-sigma rejection which is used as standard in OCCAM is also very fast but it tends to eliminate more observations than necessary what can be problematic in case of few data or weak observation configurations. In addition, it yields rather small estimates of the variance factor which are hard to interpret as the ‘outlier-free’ observations may be not fully representative.

## References

- Huber, P.J.: Robust Statistics. Wiley, New York, 1981.
- Koch, K.R.: Parameter Estimation and Hypothesis Testing in Linear Models. Springer, Berlin Heidelberg, 1999.
- Rousseuw, P.J.; Leroy, A.M.: Robust regression and outlier detection. Wiley, New York, 1987.
- Sovers, O.J.; Fanselow, J.; Jacobs, S.: Astrometry and geodesy with radio-interferometry: experiments, models, results. *Modern Physics*, 70, 1393-1454, 1998.
- Tesmer, V.: VLBI solution DGF101R01 based on least-squares estimation using OCCAM 5.0 and DOGS-CS. In: Vandenberg, N.R.; Bayer, K.D.: Proceedings of the 2<sup>nd</sup> IVS General Meeting, Tsukuba, Japan, NASA/CP-2002-210002, 2002.
- Tesmer, V.: Refinement of the stochastic VLBI model: first results. This volume, 2003.
- Titov, O.; Tesmer, V.; Böhm, J.: OCCAM 5.0 Users Guide. AUSLIG Technical Reports 7, AUSLIG, Canberra, 2001.
- Wicki, F.: Robuste Schätzverfahren für die Parameterschätzung in geodätischen Netzen. Mitteilungen Nr. 67, Institute of Geodesy and Photogrammetry, ETH Zürich, Switzerland, 1998.



# Determination of Tropospheric Parameters Within the new IVS Pilot Project

H. Schuh and J. Böhm

*Institute of Geodesy and Geophysics (IGG), TU Vienna, Austria*

**Summary:** In April 2002 the IVS (International VLBI Service for Geodesy and Astrometry) set up the Pilot Project - Tropospheric Parameters, and the Institute of Geodesy and Geophysics (IGG), Vienna, was put in charge of coordinating the project. Seven IVS Analysis Centers have joined the project until now and submitted their estimates of tropospheric parameters (wet and total zenith delays, horizontal gradients) for all IVS-R1 and IVS-R4 sessions since January 1st, 2002, on a regular basis. The individual submissions are combined by a two-step procedure to stable, robust and highly accurate tropospheric parameters with 1 h resolution. The zenith delays derived by VLBI (Very Long Baseline Interferometry) are compared with those provided by the International GPS Service (IGS). At collocated sites (VLBI and GPS antennas at the same station), almost constant biases are found between the GPS (Global Positioning System) and VLBI derived zenith delays, although the signals recorded by both techniques are subject to the same tropospheric delays. Possible reasons for these biases are discussed.

## 1 Introduction

In the last few years, the collaboration between geodesy and meteorology/climatology has become more and more intensive. GPS (Global Positioning System) has proved to be very important for meteorology, and because of the short delay between the GPS observations and the availability of tropospheric results, these can even be used for weather-forecasts. Tropospheric parameters determined by VLBI (Very Long Baseline Interferometry) are mainly useful for climatological studies. Since there is a long history of consistent VLBI sessions since 1984, they comprise accurate information about the long-term development of precipitable water above the VLBI sites. Furthermore, due to their high accuracy, the parameters derived by VLBI are of interest for the validation and calibration of parameters determined by GPS, WVR (water vapour radiometer) and other techniques.

In VLBI data analysis, tropospheric modelling is one of the major error sources. Therefore, a comparison of tropospheric parameters was part of the 2nd IVS (International VLBI Service for Geodesy and Astrometry) Analysis Pilot Project in 2001. Ten time series submitted by nine Analysis Centers (ACs) were compared by the IVS Associate Analysis Center at the Institute of Geodesy and Geophysics (IGG) of the University of Technology, Vienna. The investigations showed that the series submitted by IVS ACs are consistent and of high quality (Boehm et al., 2002b, [2]). At the 7th IVS Directing Board meeting in Tsukuba (Feb. 2002) it was decided to set up an IVS Pilot Project on Tropospheric Parameters coordinated by IGG. This Pilot Project (PP) is a research and study project with a structure similar to the IVS Working Groups. After the call for participation by the IVS Analysis Coordinator in May 2002, six IVS ACs agreed to take part in the PP. In January 2003, the IVS AC at Onsala Space Observatory, Sweden, joined the project as the seventh AC. A Pilot Project Group (PPG) has been set up to coordinate all activities within the PP and to discuss all steps that should finally lead to operational products.

	IVS Analysis Center
BKG	Federal Agency for Cartography and Geodesy, Germany
CGS	Centro di Geodesia Spaziale, Italy
CNR	Istituto di Radioastronomia, Italy
GSF	NASA Goddard Space Flight Center, U.S.A.
IAA	Institute of Applied Astronomy, Russia
IGG	Institute of Geodesy and Geophysics, Austria
OSO	Onsala Space Observatory, Sweden

Table 1: . IVS ACs taking part in the PP - Tropospheric Parameters.

## 2 Submissions by the ACs

Most of the ACs have provided their tropospheric parameters beginning with January 2002. That allows the generation of a combined series since the start of the IVS-R1 and IVS-R4 sessions. Total and wet zenith delays as well as gradients are submitted by all ACs. GSF and IGG even apply a priori gradients calculated from numerical weather models. Most of the ACs use the CALC/SOLVE software package, only IAA and IGG apply the QUASAR and OCCAM software, respectively. About half of the ACs fix the ITRF2000, and all ACs use cutoff elevation angles at or below 5°. The Niell mapping functions (Niell, 1996, [5]) are used throughout - only IGG applies the isobaric mapping function of the hydrostatic part (Niell, 2001, [6]). Meteorological parameters can be extracted from the databases.

AC	a priori gradients	ITRF2000 fixed	software
BKG	no	yes	CALC/SOLVE
CGS	no	no	CALC/SOLVE
CNR	no	no	CALC/SOLVE
GSF	yes	no	CALC/SOLVE
IAA	no	yes	QUASAR
IGG	yes	yes	OCCAM
OSO	no	yes	CALC/SOLVE

Table 2: Features of the submissions. Two ACs use a priori gradients; four ACs fix ITRF2000.

The tropospheric parameters should be provided for every full hour, i.e. in equidistant time intervals of 60 minutes, starting at the first integer hour of the session. If other time intervals are used for the computation (e.g., longer time intervals for the gradients), all parameters have to be referred to the same hourly instants. More details about the Pilot Project - Tropospheric Parameters, the Pilot Project Group and the submissions of the ACs are described in Schuh et al. (2003, [8]).

## 3 Combination strategy for the total and wet zenith delays

Each AC that is taking part in the IVS Pilot Project - Tropospheric Parameters submits two files per week, namely one for the IVS-R1 and one for the IVS-R4 session. They are combined to weekly files in order to be comparable with results provided by the IGS, although most VLBI sites take part in one 24 h session per week only.

GPS week	IVS-R1 session	IVS-R4 session
1147	---	IVS-R4 001
1148	IVS-R1 001	IVS-R4 002
1149	IVS-R1 002	IVS-R4 003
1150	IVS-R1 003	IVS-R4 004
...	...	...

Table 3: The IVS-R1 and IVS-R4 sessions are combined to weekly files.

Before the combination, the data submitted by the ACs are edited using a limit of 30 mm for the formal errors. Estimates with larger formal errors are discarded. No interpolation has to be carried out to get the tropospheric parameters at the same time instants because the ACs were asked to provide their estimates at integer hours (see section 2). The combination itself is a two-step procedure which is carried out site by site, week by week and parameter by parameter (see Figure 1).

In the first step preliminary VLBI time series of the total and wet zenith delays are produced. This combination comprises the removal of biases and the calculation of mean values at each time without any outlier elimination. Then the mean standard deviations between the preliminary VLBI time series and the time series of the ACs (shifted to the common mean) are computed for each week and each station. If a standard deviation is larger than 20 mm at a certain station, data from this AC will not contribute to the second step of the combination. Furthermore, a mean value of the standard deviations for all VLBI sites is determined for each AC. These mean standard deviations are used for assigning weights to the individual AC solutions in the final (second) combination.

In the second step the biases between the weekly time series are removed at each station using a limit of  $1.5 \sigma$  ( $\sigma$  .. standard deviation). Then the VLBI values of the tropospheric parameters at each time are calculated as weighted means. Again, outliers are removed that exceed a limit of  $2.5 \sigma$ .

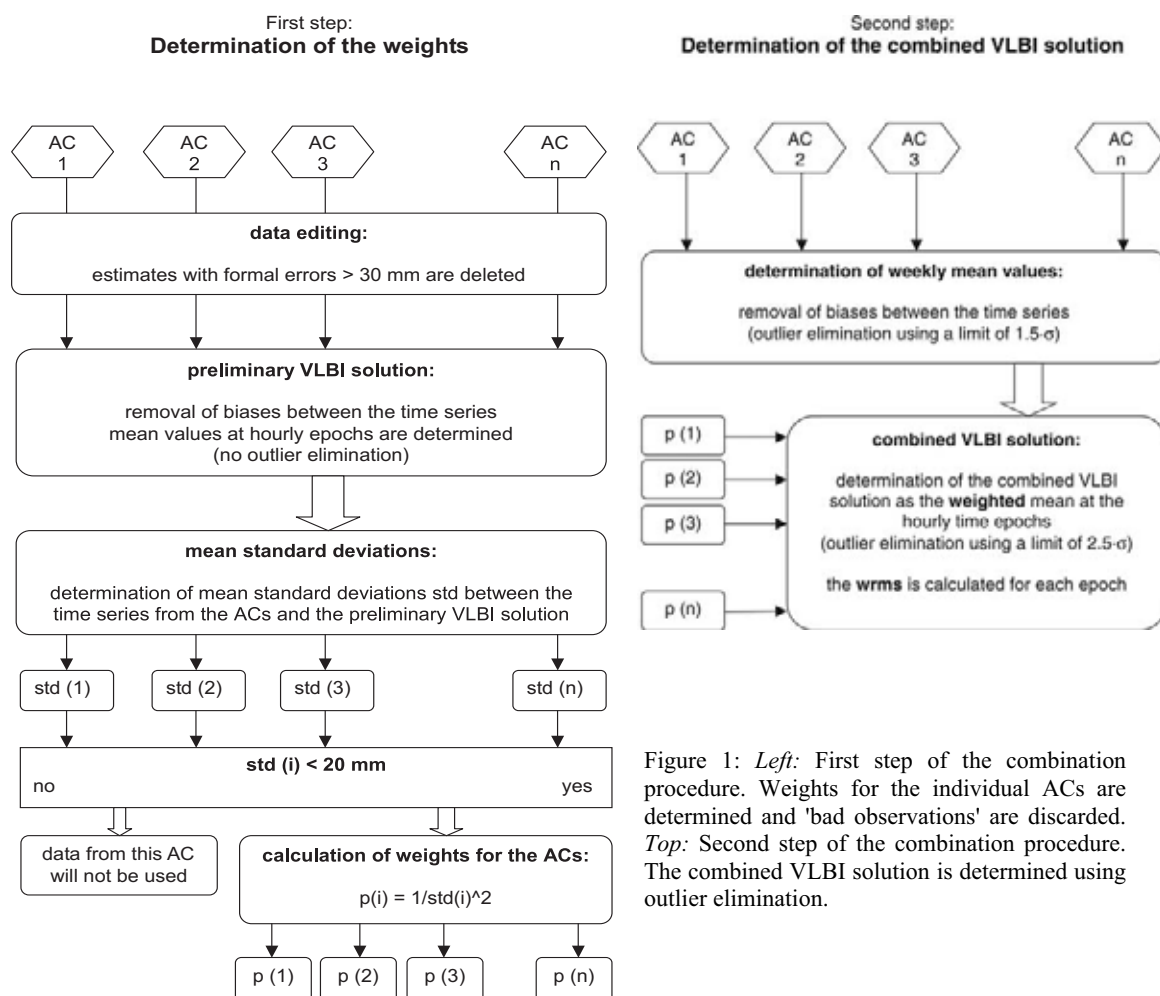


Figure 1: *Left:* First step of the combination procedure. Weights for the individual ACs are determined and 'bad observations' are discarded. *Top:* Second step of the combination procedure. The combined VLBI solution is determined using outlier elimination.

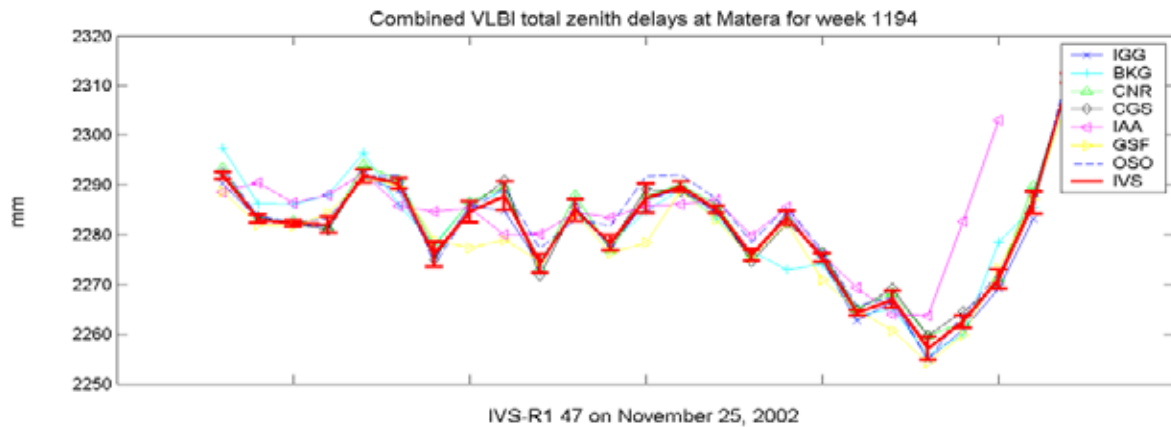


Figure 2: Submissions for the wet zenith delays at Matera by the various Analysis Centers (GPS week number 1194) and the combined VLBI solutions (red bold line with error bars). A rather good agreement between the time series can be seen. The mean of the standard deviations of the combined hourly results is  $\pm 1.5$  mm.

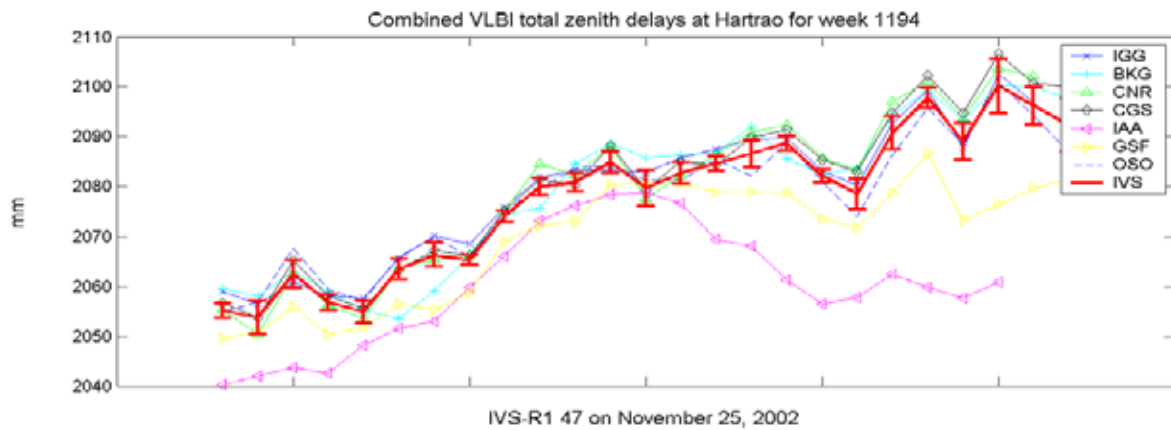


Figure 3: Submissions for the wet zenith delays at Hartrao by the various Analysis Centers (GPS week number 1194) and the combined VLBI solutions (red bold line with error bars). The mean of the standard deviations of the combined hourly results is  $\pm 2.5$  mm.

With the approach described above, one VLBI time series is determined for the total and one for the wet zenith delays. Two examples with the wet zenith delays as submitted by the ACs and the combined solution can be seen in Figures 2 and 3. While Figure 2 (Matera) shows a rather good agreement between the ACs ( $\pm 1.5$  mm), the mean of the standard deviations of the combined hourly results in Figure 3 (Hartrao) is larger ( $\pm 2.5$  mm). Anyway, the combined series is usually much smoother and thus probably more stable and robust than the individual submissions of the ACs. On the other side, short period variations of the zenith delays as for instance at Matera (Figure 2) seem to be reproduced by the combined values. In some sessions there were gaps in the observations at certain stations that have not been recognized by the ACs. For instance, if there were no observations in the middle of a 24 h session, the ACs might not be aware of this fact because they are using piecewise linear functions with constraints for the rates of the zenith delays. Another critical case occurs when no pressure data is available for a station and the ACs use adopted mean values for the pressure. Then the estimated wet delays are not used for the final product. To avoid these problems, IGG discards all combined estimates if there are no pressure data available in the database within one hour around the combination time.

Furthermore, so far a combined solution is only computed if there are at least data from three ACs contributing. Finally for cross checking, meteorological data are taken from the databases to compute the hydrostatic zenith delays at each station by the formula of Saastamoinen (1973, [7]). If the difference between the total and the hydrostatic plus wet delay of the combined solution is larger than 3 mm, the combined value at this time epoch is discarded.

## 4 Accuracy of the combined zenith delays

There are two kinds of accuracies that can be investigated. On the one hand, there is the accuracy of the absolute values. Apart from systematic errors due to the VLBI technique that might be inherent in the zenith delays submitted by all ACs, the weekly biases between the ACs should be a good criterion to evaluate the (remaining) absolute accuracy. Possible reasons for systematic biases in the VLBI estimates might be:

- errors of the terrestrial reference frame (at least for those solutions where the ITRF2000 is fixed),
- errors of the mapping functions,
- unmodelled effects (atmospheric loading, antenna deformation, ..)

On the other hand, relative accuracies can be determined after removing the weekly biases between the time series when the standard deviations at the hourly instants are evaluated.

### 4.1 Absolute accuracies

As can be seen in Figure 4, the weekly biases of the total (and wet) zenith delays are within  $\pm 2$  mm for most of the ACs. This indicates that - apart from systematic effects as described above - the accuracy of the absolute values of the zenith delays is at the 2 mm level, which is a mean value for all VLBI sites.

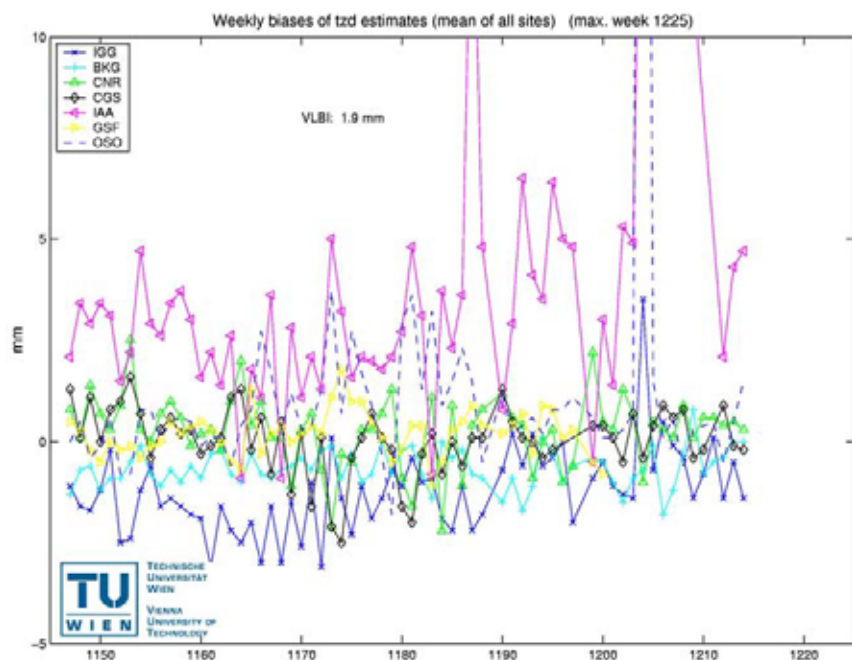


Figure 4: Weekly biases of the total zenith delays since 2002.0 . The biases are within  $\pm 2$  mm for most of the ACs.

## 4.2 Relative accuracies

Relative accuracies can be calculated as the mean standard deviations at the hourly epochs after removing the weekly biases. Figure 5 shows the mean values (averaged per week) of the hourly standard deviations of the combined VLBI solution (red solid line) of the total zenith delays (mean of all sites). Additionally, the mean standard deviations of the hourly estimates of the individual time series against the combined VLBI solution are shown. Thus, the relative accuracy of the combined VLBI zenith delays is  $\sim \pm 1.8$  mm.

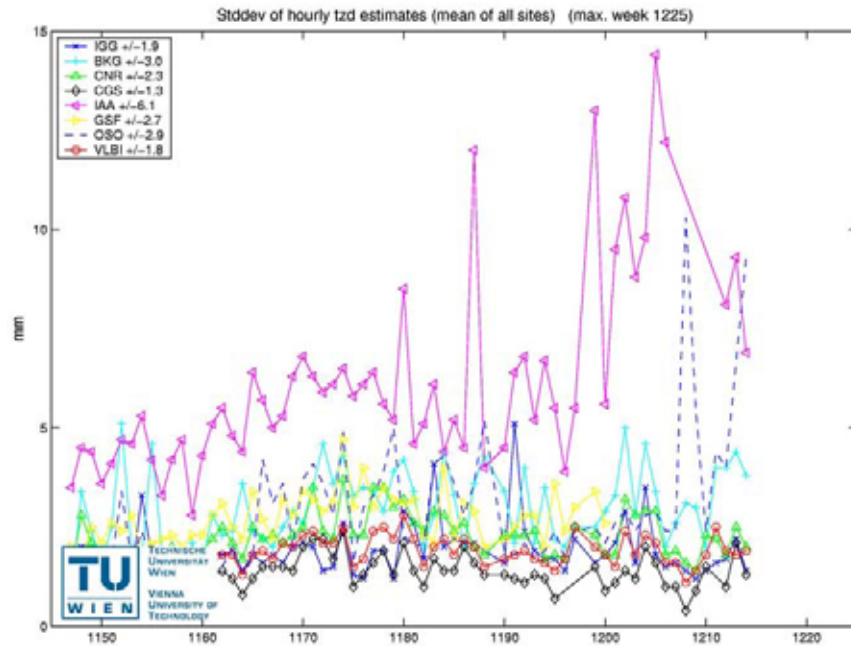


Figure 5: Mean values averaged per week of the standard deviations of the combined hourly zenith delays since 2002.0. Additionally, the mean values of the standard deviations for all stations are shown that were achieved by the individual ACs.

## 5 Comparison with tropospheric parameters determined by IGS

The IGS has produced tropospheric parameters for 150 IGS sites since 1997 (Gendt, 1996, [4]). This allows to compare at collocated sites (stations with VLBI and GPS antennas nearby) the combined total zenith delays derived by VLBI within the IVS-PP with those published by the IGS.

Table 4: Collocated sites with VLBI and GPS antennas. The 4-letter IGS acronyms are given as well as the height differences (VLBI - GPS) between the antennas. The fourth and fifth columns show mean values of the hourly standard deviations for the combined IVS and IGS time series for identical epochs. The last two columns show the biases (IGS - IVS) and the standard deviation between the time series. Although the height difference between the antennas is taken into account all biases are positive.

site	IGS acronym	height diff. [m]	std. IVS [mm]	std. IGS [mm]	bias [mm]	std. (IGS-IVS) [mm]
Algotpark	algo	23.0	$\pm 1.6$	$\pm 2.2$	7.1	$\pm 4.8$
Fortleza	fort	3.3	$\pm 2.6$	$\pm 4.4$	13.5	$\pm 9.6$
Gilcreek	fair	14.2	$\pm 1.5$	$\pm 2.2$	4.2	$\pm 3.7$
Hartrao	hrao	2.3	$\pm 2.4$	$\pm 3.1$	5.2	$\pm 8.1$
Hobart26	hob2	24.9	$\pm 2.4$	$\pm 2.6$	3.2	$\pm 7.4$
Matera	mate	8.7	$\pm 1.8$	$\pm 3.9$	3.9	$\pm 6.8$
Medicina	medi	18.1	$\pm 1.1$	$\pm 1.3$	1.4	$\pm 4.6$
Nyales20	nyal	6.5	$\pm 1.4$	$\pm 1.6$	4.1	$\pm 3.8$
Seshan25	shao	8.2	$\pm 1.8$	$\pm 4.4$	1.5	$\pm 6.0$
Wettzell	wtzt	4.1	$\pm 1.5$	$\pm 1.8$	2.4	$\pm 4.3$
Onsala60	onsa	13.8	$\pm 1.0$	$\pm 1.8$	4.8	$\pm 4.5$

Because both services, IGS and IVS, use very similar combination strategies, a comparison of the mean values of the hourly standard deviations is possible. Table 4 shows these values for identical times at collocated sites. As mentioned before, the relative accuracy of the VLBI derived total zenith delays is at the  $\pm 2$  mm level, and for most of the stations treated here it is slightly better than that from GPS.

In a second step, the biases and standard deviations between the IGS and IVS time series of the total zenith delays are determined. The height differences between the VLBI and GPS stations are accounted for by means of meteorological data recorded at the VLBI stations for the calculation of the differential hydrostatic and wet delays. Table 4 shows the mean biases between the time series and the standard deviations after removing these biases. Although the standard deviations between the IVS and VLBI time series are at the  $\pm 5$  mm level or even worse, it is noticeable that all mean values of the total zenith delays derived by GPS are larger than those derived by VLBI. The positive biases are between +1.4 mm (Medicina) and +13.5 mm (Fortaleza). This confirms first results reported by Boehm et al. (2002a, [1]). Apart from the systematic effects for VLBI described above, there might be some problems with GPS observations as well:

- higher cutoff elevation angles applied in GPS (larger than 10 degrees),
- multipath effects,
- phase center variations of the antennas,
- errors of satellite ephemerides,
- same mapping function for the hydrostatic and wet delays instead of using different mapping functions  $m_h$  and  $m_w$ .

## 6 Conclusions and future outlook

VLBI is capable of determining very accurate tropospheric zenith delays. Apart from systematic errors that might be inherent in the VLBI technique, the accuracy of the combined hourly VLBI results is at the 2-4 mm level. The first year of the Pilot Project clearly showed that comparing and combining the results of several ACs which use different VLBI software or apply different analysis strategies allows

- to give feedback to the individual AC in case of any problems,
- to determine stable, robust and highly accurate final IVS products with standard deviations that are usually significantly smaller than those of the individual submissions.

Zenith delays derived by VLBI can be compared to those derived by GPS and WVR. The always positive and almost constant biases between the GPS and VLBI time series at collocated sites need to be investigated in more detail.

The other field of application for zenith delays derived by VLBI is the contribution to climatological studies, at least when the time series cover a longer time interval. First results are reported by Boehm et al. (2003, this issue, [3]).

As this Pilot Project proved to be very successful, it was decided at the 9th IVS Directing Board meeting in Paris (April 2003) that the tropospheric parameters would become operational IVS products. Again, the IGG was asked to coordinate the project called IVS-TROP.

## Acknowledgements

The authors would like to thank all IVS Analysis Centers who contributed to the Pilot Project and to all members of the Pilot Project Group.

## References

- [1] Boehm, J., H. Schuh and R. Weber: Influence of tropospheric zenith delays obtained by GPS and VLBI on station heights. In: Proceedings of the IAG Symposium on Vertical Reference Systems, Cartagena, Colombia, Feb. 2001, edited by H. Drewes, A. Dodson, L. Fortez, L. Sanchez, P. Sandoval, Springer Verlag Berlin-Heidelberg, 2002a.
- [2] Boehm, J., E. Messerer and H. Schuh: Comparison of Tropospheric Parameters Submitted to the 2nd IVS Analysis Pilot Project. In: IVS 2002 General Meeting Proceedings, edited by N. R. Vandenberg and K. D. Baver, NASA/CP-2002-210002, 340-344, 2002b.
- [3] Boehm, J., H. Schuh, V. Tesmer and H. Schmitz-Hübsch: Determination of tropospheric parameters by VLBI as a contribution to climatological studies, this issue, 2003.
- [4] Gendt, G.: Comparisons of IGS tropospheric estimates. Proceedings IGS Analysis Center Workshop, 19-21 March 1996 Silver Spring, Maryland USA, Eds. R. E. Neilan, P. A. Van Scoy, J. F. Zumberge, 151-164, 1996.
- [5] Niell, A.E.: Global mapping functions for the atmosphere delay at radio wavelengths, *J. Geophys. Res.*, 101 (B2), 3227-3246, 1996.
- [6] Niell, A.E.: Preliminary evaluation of atmospheric mapping functions based on numerical weather models, *Phys. Chem. Earth*, 26, 475-480, 2001.
- [7] Saastamoinen, J.: Contributions to the Theory of Atmospheric Refraction, Part II, *Bulletin Geodesique*, Vol. 107, 13-34, 1973.
- [8] Schuh, H. and J. Boehm: Status Report of the IVS Pilot Project - Tropospheric Parameters in International VLBI Service for Geodesy and Astrometry 2002 Annual Report, edited by N. R. Vandenberg and K. D. Baver, NASA/TP-2003-211619, 2003.

Session 6

# Combination of VLBI and other Space Geodetic Techniques



# European Vertical Site Motions by VLBI and GPS An Update

J. Campbell

*Geodetic Institute, University of Bonn, Germany*

**Summary:** Horizontal and vertical motions of the VLBI sites in Europe have been routinely determined by VLBI and GPS. The data spans have reached ten years or more and provide an excellent basis for detailed time series analysis and comparisons between techniques. In recent solutions the accuracy of the velocities for the best stations is at the level of  $\pm 0.1$  mm/y for the horizontal and  $\pm 0.3$  mm/y for the vertical component, with a wrms of daily solution at  $\pm 0.3$  mm/y horizontally and  $\pm 0.9$  mm/y in the vertical. In this paper, we will specifically address the vertical component, because it is most sensitive to systematic errors from different origin. We will look at the degree of consistency between the VLBI and GPS results and discuss systematic effects in the time series.

## 1 Introduction

Space geodetic data have been routinely providing results for site positions and motions over time spans of a decade and more. Solutions from different analysis centers and groups and combinations of solutions are available, e.g. in the form of successive realisations of the International Terrestrial Reference Frame (ITRF). If we wish to study tectonic motions of parts of the Earth's crust, an assessment of the level of significance of the site velocities derived from the solutions has to be made. In this paper, the attention is focussed on site motions in Europe, in the frame of the ongoing studies of European crustal motion. Special interest has been drawn to the vertical component, in view of its importance for the studies of Postglacial Rebound and Mean Sea Level Change (Campbell et al. 2002). Here, we will deal with aspects of vertical accuracy in time series from space geodetic measurements

## 2 Accuracy of vertical component from VLBI and GPS

Solutions from individual observing sessions, usually done by least squares estimation, provide statistical information on the accuracy level achieved. This information is based on the quality of the modeling and on the noise of the data. The errors of the parameters estimated in these solutions are usually called 'formal errors', as opposed to 'true errors' or 'realistic errors' because individual observing sessions constitute only a small sample of the total stochastic process under consideration.

If we repeat the observing sessions with individual errors  $\sigma_r$  at regular intervals  $\Delta t$  and estimate a linear trend over the total time span  $T$  of the series, we may use the well known error formula for the accuracy  $\sigma_v$  of the slope of the straight line fit to the data (e.g. Coates et al. 1985, Zhang et al. 1997, equ. 21):

$$\sigma_v = \frac{\sigma_r}{T} \sqrt{\frac{12T / \Delta t}{(1 + T / \Delta t)(2 + T / \Delta t)}} \quad (1)$$

This formula is true only for random (white) noise in the data, which is certainly not the case in reality. Still, it gives a good indication of the way in which results for site velocity estimates behave if we compare time series of different density and length. Fig.1 shows the effects of length of data span on the velocity error for a good time series of daily GPS vertical estimates with a wrms ( $\sigma_r$ ) of  $\pm 8$  mm.

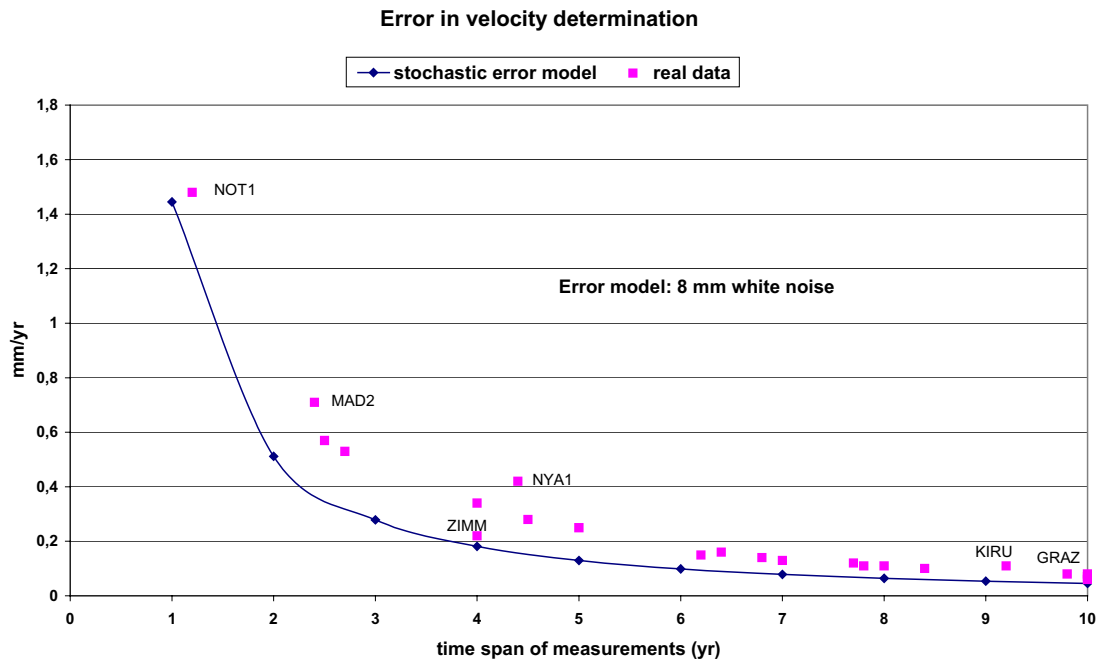


Figure 1: Error of slope of straight line fit to time series as a function of data span and data interval

Table 1: Vertical velocities of European permanent GPS stations (from JPL FLINN Analysis), including stochastic and systematic error parameters. Note that velocities in this table refer to the JPL global GPS solution and not to WTZR.

Station	velocity mm/yr	T (yr)	sigma veloc mm/yr	wrms mm	jumps (no. of)	amplitude ann. Period	wrms due to ann. Period
NYA1	5,59	4,4	0,42	9,7		8	5,7
TROM	2,57	10,0	0,08	9,7		4	2,8
KIRU	6,44	9,2	0,11	14,6		11	7,8
METS	4,56	10,0	0,07	9,6		6	4,3
ONSA	2,94	7,0	0,13	8,1	1	4,5	3,2
KOSG	0,13	10,0	0,06	7,4		3	2,1
BRUS	1,98	8,4	0,1	8,2		3	2,1
POTS	0,80	7,8	0,11	8,6		4	2,8
WTZR	0,37	6,8	0,14	8,1		3	2,1
WETT	1,50	4,5	0,28	10		4	2,8
ZIMM	0,91	4,0	0,22	8,8	1	5	3,6
GRAZ	-0,39	9,8	0,08	9,1		4	2,8
MEDI	-3,15	6,4	0,16	9		5	3,6
MATE	0,35	6,2	0,15	9,1	2	8	5,7
NOTO	0,56	2,7	0,53	10	1	8	5,7
NOT1	-1,66	1,2	1,48	7,5		10	7,1
MADR	-0,53	5,0	0,25	11,4	8	5	3,6
VILL	-1,15	7,7	0,12	8,7	1	6	4,3
SFER	0,97	4,0	0,34	8,3	2	6	4,3
WTZT	0,97	2,5	0,57	7,9	1	3	2,1
MAS1	1,63	8,0	0,11	9,8		9	6,4
MAD2	4,66	2,4	0,71	11,3	8	8	5,7

The actual accuracy of daily solutions can be taken from time series results of the different analysis centers around the world, e.g. from the JPL FLINN Analysis, a contribution to the IGS global network of permanent GPS stations (Heflin 1992). The compilation includes time series of different lengths and quality and the corresponding plots show both the wrms of the daily results and the error of the velocity estimates. If we superimpose the actual velocity errors from different European IGS-sites (Tab.1, 4<sup>th</sup> column) on the plot of the formal error in Fig.1, we obtain a good visual impression of the quality of these sites.

In the following paragraphs, we will consider the most important of systematic effects that interfere with normal statistical behaviour of the space geodetic measurements.

## 2.1 Periodicities

Upon visual inspection of the time series, in most cases a clear periodic behaviour, usually with annual period, can be seen (Zhang et al. 1997). Many different causes concur in producing these variations. The main contributions come from seasonal effects, which act on the observations themselves, e.g. by mismodeling of the atmospheric path delay corrections, and on the local site motion due to ground water changes, loading effects etc (Zerbini et al. 2001). Very prominent periodic variations can be seen at stations in snow-bound areas like the Alps and Scandinavia. This effect is not only seen in the vertical component (Jaldehyag et al. 1996), but frequently also or even more pronounced in one or both of the horizontal components (see e.g. the EUREF station of HFLK, a site in the Alps at 2000 m altitude). The thickness of the snowcover near the antenna increases steadily in autumn and through the winter and shrinks rapidly in spring, when melting begins (Fig. 2). The main part of this effect is probably generated by the corresponding change in the multipath geometry.

The effect of periodic variations on the velocity estimation can be visualised by plotting the slope estimates as a function of length of data span. In the first year, the full amplitude of the variation stands out, and with increasing length this effect is mitigated until it drops to near insignificance. Fig. 3 shows an example for an annual variation buried in relatively high noise (Campbell 1990). The series represents early VLBI baseline measurements between Wettzell (Germany) and Westford (Eastern USA) and demonstrates that annual variation is not limited to GPS alone. One needs at least 3.5 years of data to obtain a reduction in the effect of the annual period on the linear fit to below 10% of the amplitude (Blewitt et al. 2002).

The amplitude  $a_1$  of a sinusoid with annual period adds to the wrms by the root of the sum of squared values of  $a_1 \cdot \sin\omega(t_i - t_0)$ , which results in  $a_1 \cdot \sqrt{\sum \sin^2\omega(t_i - t_0)/(N-1)} = a_1 \cdot 0.71$  for  $N=365$ . This rule-of-thumb factor is useful to show the relation between the total wrms and the contribution of the periodic term. In Table 1 and the associated diagram (Fig. 4) we show the amplitudes of annual terms in the data sets of European permanent GPS sites considered here. Obviously, the sites in central Europe display the lowest level of contamination with annual effects (only 2mm in a total noise level of around 8 mm). KIRU is a typical site for the effects of snow cover on and near the antenna, while the short series of NOT1 displays a section of a pure sinusoid and little other noise.

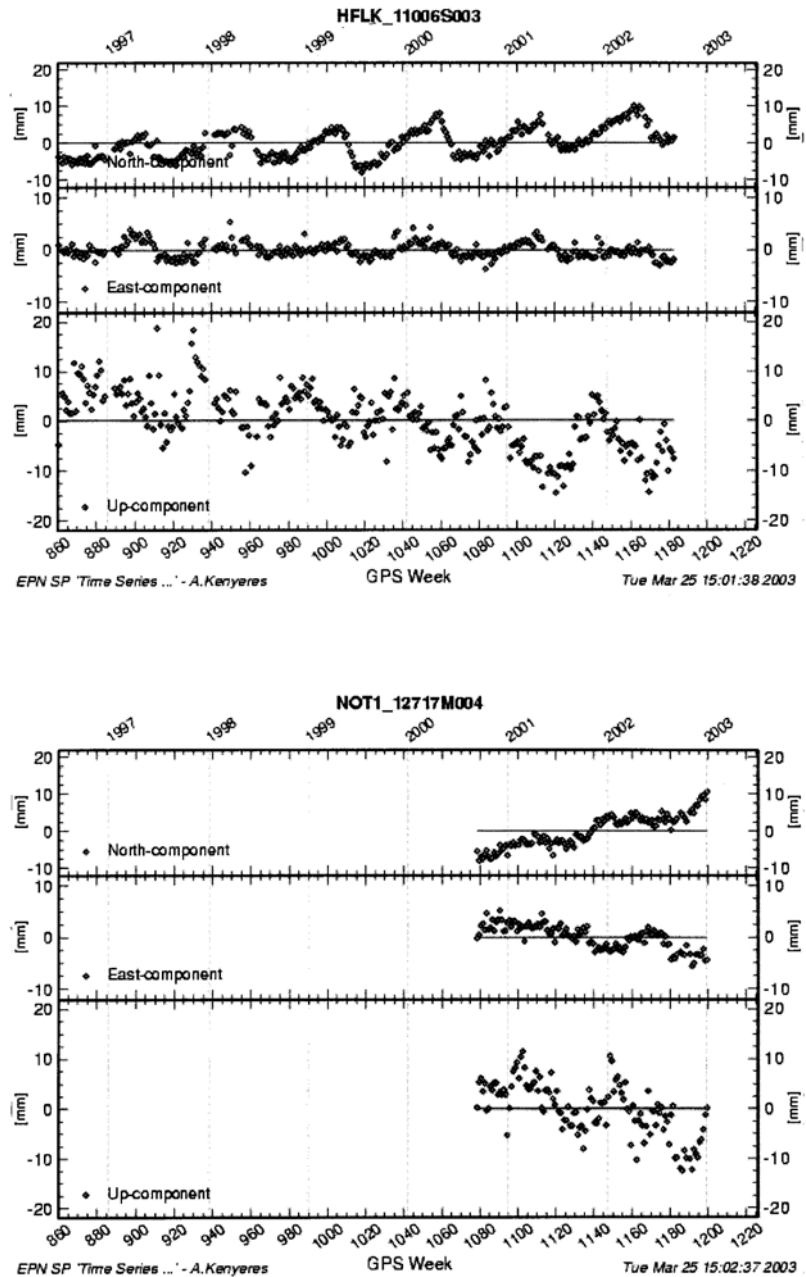


Figure 2: Examples of annual terms in GPS time series. Above: Station Hafelekar (near Innsbruck, Austria) at 2300m altitude, effect of snow cover on north component. Note that vertical component has period with different shape and phase! Below: Station Noto on Sicily, Italy with prominent annual period in vertical component. Note the striking similarity with vertical signal at Hafelekar.

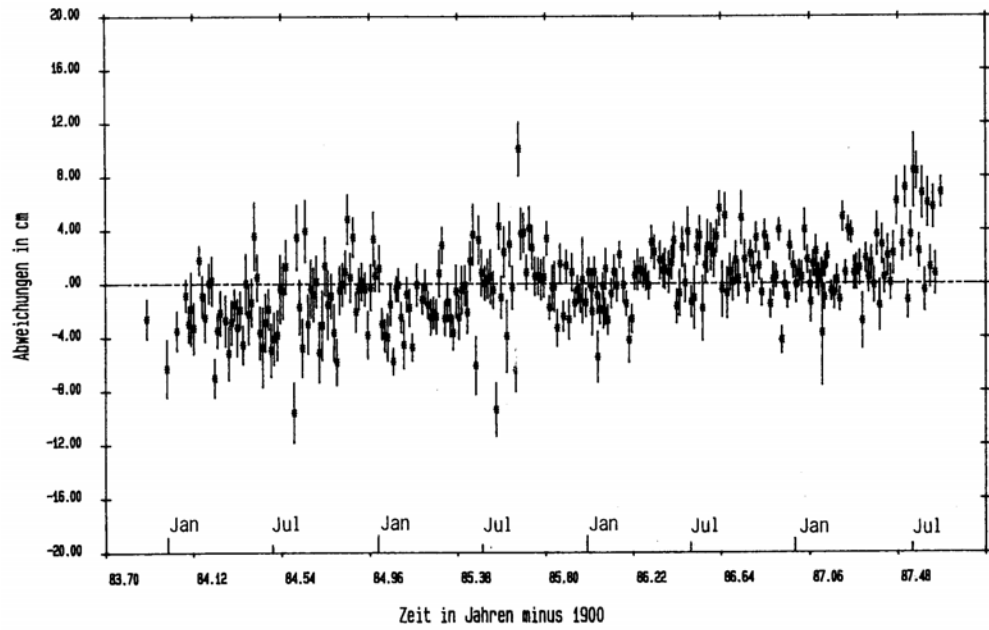


Abb. 4.2.5: Entwicklung der Basislänge Wettzell-Westford.

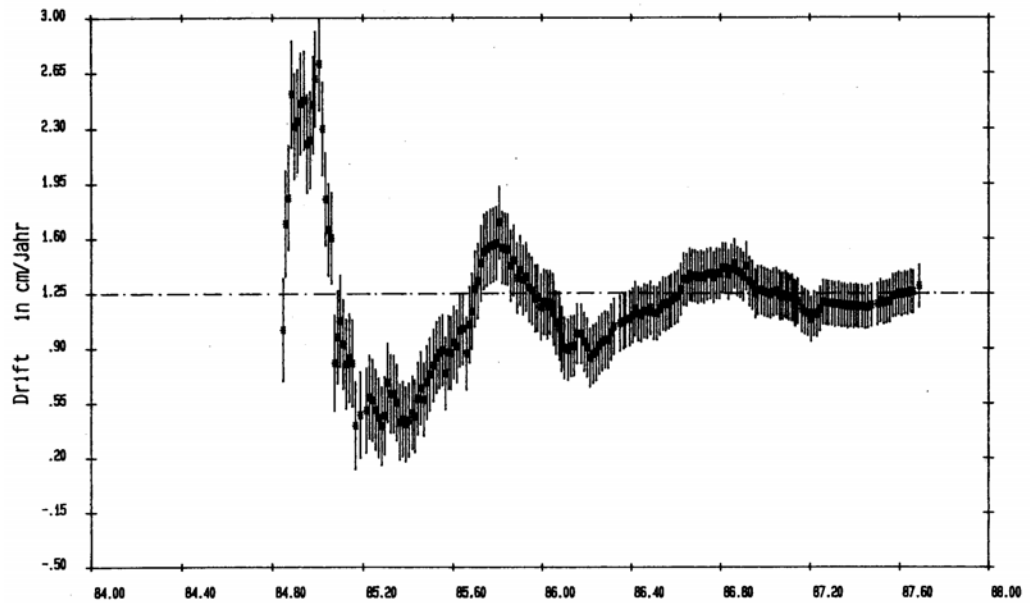


Abb. 4.2.6: Entwicklung der Längenänderung der Basis Wettzell-Westford.

Figure 3: Effect of annual term on the estimates of baseline length change (‘baseline velocity’) from time series of VLBI baseline measurements between Wettzell (Germany) and Westford (Eastern US). The data span is 3.5 yr from 1984.0 to 1987.5. Data spacing is 5 days (Campbell 1990).

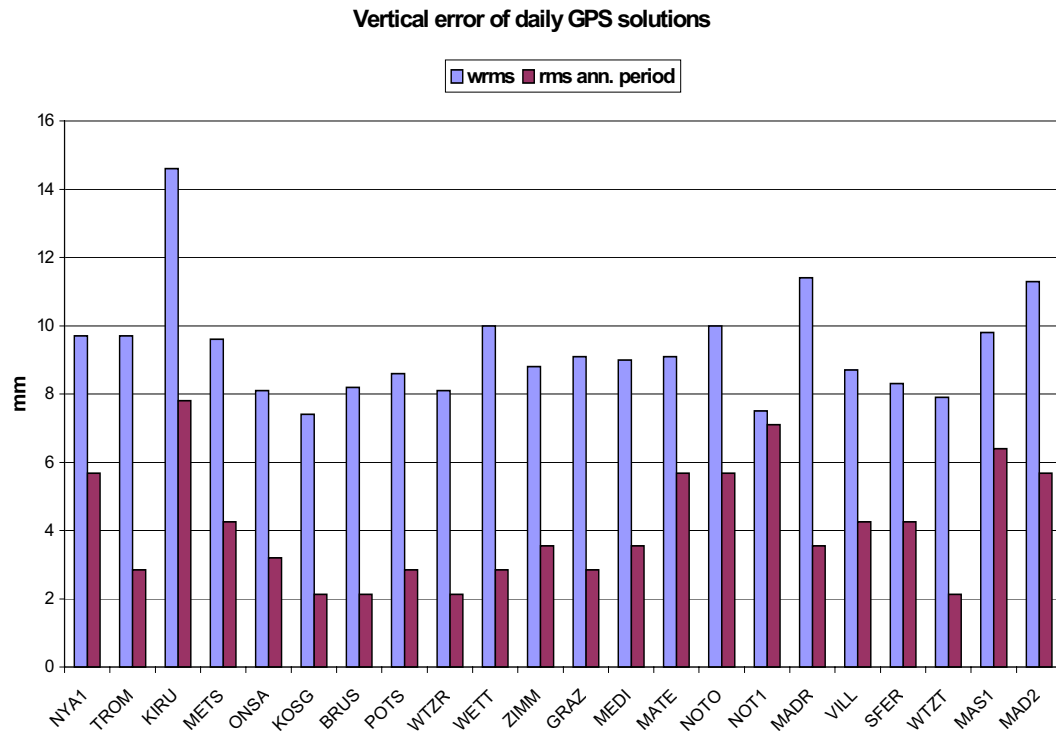


Figure 4: RMS amplitudes of annual signal in the time series of European Permanent GPS Stations compared to total WRMS

## 2.2 Breaks, jumps and offsets

Unfortunately, a large part of the the GPS sites have experienced discontinuities in the operations at the stations causing breaks, jumps or offsets in the time series. The treatment of these discontinuities varies between analysis centers and may also be subject to changes in successive solutions by the same analysis center. Usually, at the epoch of discontinuity an offset parameter is introduced while keeping the slope parameter unchanged. This is done to absorb the effect of the unknown offset. However, the effect on the accuracy of the slope of the straight line fit is negative: depending on where the break occurred, the data span is cut into shorter pieces and offers much less stability. A case in point: at Matera, the time series is interrupted in 1996.5 (approximately) and has been cut from a total of 9 years into two portions of 4.5 years (Fig. 5). Expression (1) for the accuracy of the velocity shows that cutting in half of a series causes the error to be doubled (the fact that we have two of the shorter series produces a factor  $\sqrt{2}$ , but this still leaves us with a loss in accuracy of  $\sqrt{2}$ ). An even more serious disadvantage is that shorter time series are much more vulnerable to systematic (or non-stochastic) variations in the series.

A way to look at the effects of the treatment (or non-treatment) of discontinuities on the velocity determinations from time series is to follow the evolution of solutions from the analysis centers over the years. In Fig.6 we present successive solutions from the JPL FLINN analysis as they were recorded during the GPS/VLBI comparison studies in the European VLBI project. While some of the stations considered here show a stable behaviour, several other stations stand out with prominent changes. At Onsala for instance, we know that a change of the radome on the GPS antenna has produced a vertical offset of 9 mm. The way this discontinuity has been dealt with in the JPL analysis can be inferred from the step in the value of the ONSA vertical velocity of

2 mm/yr between the dates of 14.03.01 and 31.01.02. An even more drastic change can be seen at Noto, where the transition from the old site NOTO to the new site NOT1 has caused a change in the velocity value from -3 mm/yr to +0,5 mm/yr in the global analysis. Additionally, there is a rather prominent jump of 1-2 mm/yr in the velocity at most of the stations between the dates of 14.03.01 and 06.11.01, which may be attributed to major changes in the global analysis at JPL.

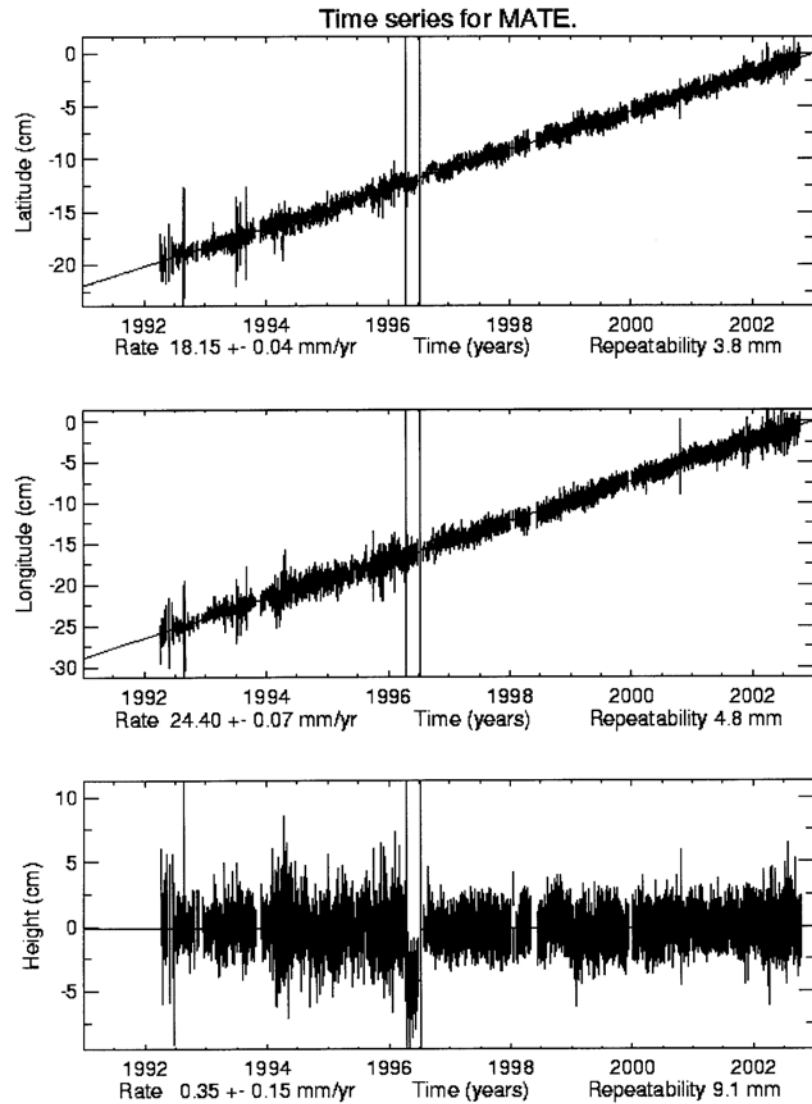


Figure 5: Example of a time series with breaks (station Matera, Italy). JPL-FLINN Analysis of permanent GPS data in the frame of the global IGS network.

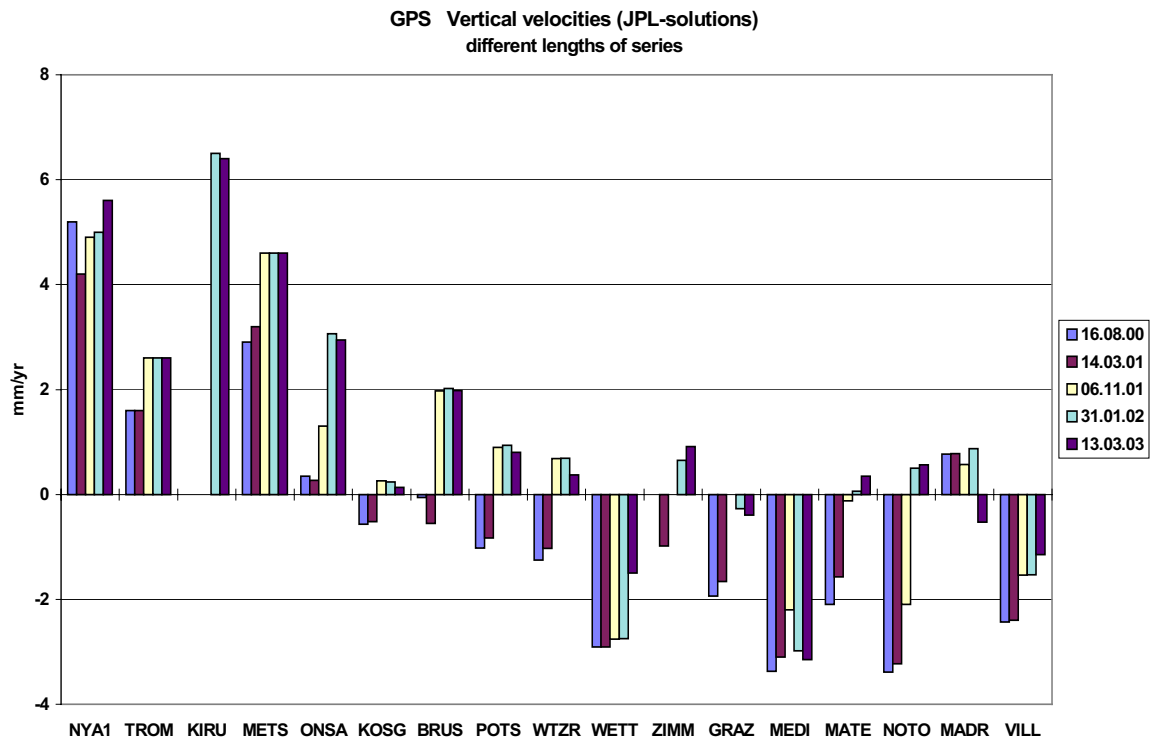


Figure 6: Effect of different length of series on the velocity estimates (example for the JPL-FLINN global analysis). The aberrant result at WETT refers to the old receiver at Wettzell, which was replaced by WTZR from 1995 onwards. Note that velocities in this diagram are referred to the global JPL solution and not to WTZR.

### 3 Comparisons between different analysis centers for GPS and VLBI

For those sites where both GPS and VLBI are available, the results of the velocity determinations can be readily compared without having to resort to the local excentricities. In the report on the European Geodetic VLBI Network (Campbell et al. 2002) extensive comparisons between different GPS and VLBI solutions have been presented, some of which are taken up here and are supplemented with more recent data.

Discontinuities in GPS time series are quite common, but VLBI, too, has been subject to changes in the offsets of the telescope reference points, chiefly due to the repair work at those instruments equipped with wheel-and-track mounts (Nothnagel et al. in Campbell et al. 2002, p. 62ff). Vertical offsets had to be introduced in the analysis of the stations of Madrid, Medicina and Effelsberg (Haas and Tomasi in Campbell et al. 2002, p. 98ff). In recent years, the offsets have been determined by special surveys and these values will be used in the coming solutions after some more testing has been carried out (Nothnagel et al. in Campbell et al. 2002, p. 62ff, Tomasi et al., these proceedings).

In the case of GPS one has to keep in mind that any changes at the GPS antenna (new antenna, new support, new location etc.) will have an effect on the multipath environment, which means that even if the offsets are measured with greatest care, there will be a remaining unseen offset due to the change in the multipath pattern. This is different for VLBI because there is no multipath when directional antennas are used.

The level of agreement between the results of different analyses can be visualised in form of diagrams (Fig. 7). Four different VLBI solutions are considered here, three (OSO, CNR and BKG) computed with the GSFC CALC/SOLVE software and one (DFGI) with OCCAM (Tesmer 2002). The OSO solution uses only the EUROPE sessions, while the others include part or all of the global VLBI data. The spread (or jitter) of the velocity values between solutions is small compared to the velocities themselves, which allows us to accept these values as highly significant and confirms the scenario of vertical motions in Europe described and discussed in Campbell et al. 2002.

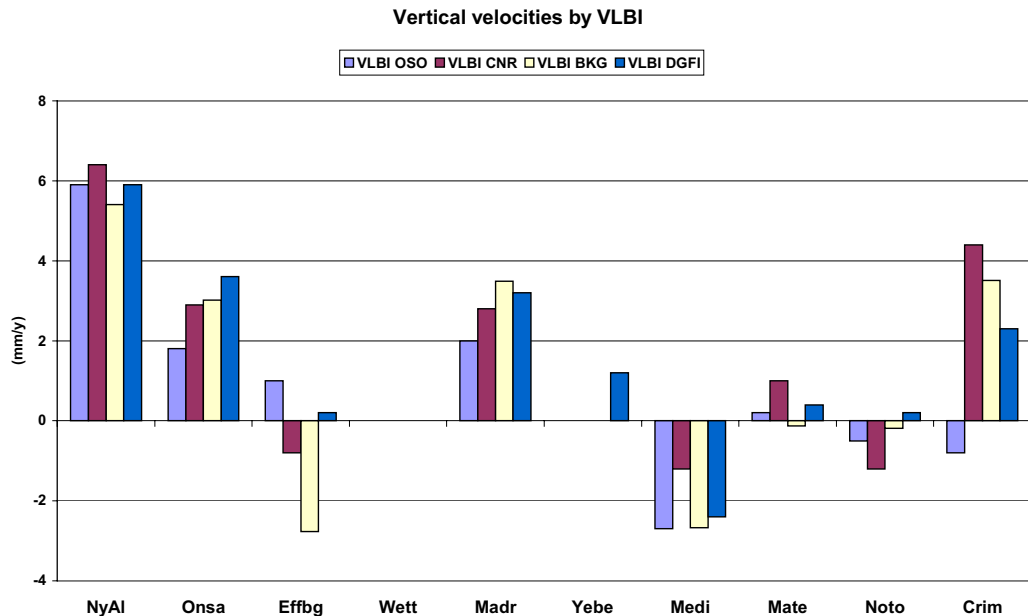


Figure 7: Vertical velocities from different VLBI solutions (OSO=Onsala Space Observatory, CNR=Consiglio Nazionale delle Ricerche, Bologna, BKG=Bundesamt für Kartographie und Geodäsie, Leipzig, DFGI=Deutsches Geodätisches Forschungsinstitut, München) (Wett=WTZR)

A similar agreement is seen for the results of different GPS analyses, if we exclude certain special cases discussed earlier (Fig. 8). The larger number of permanent GPS stations in Europe allows the formation of a central European velocity platform which has small motions (smaller than 1 mm/yr) with respect to Wettzell. The representation in the diagram of fig. 8 confirms the vertical motion pattern seen by VLBI in a more refined way: central Europe (KOSG, POTS, WTZR, GRAZ and ZIMM) show little relative motion, and MATE as well as NOTO are apparently in a similarly stable condition vertically. Medicina is under the influence of subsidence in the Po-plain (probably anthropogenic). Madrid is uncertain due to problems with GPS but may be in an uplift zone, if the VLBI results are confirmed. The Scandinavian stations are clearly subject to postglacial uplift, although Ny Alesund on Spitsbergen shows more (about twice as much) uplift than theory permits.

Looking at a comparison between the simple means taken among the different VLBI and GPS solutions (Fig. 9), we find that the agreement between techniques is good only at the level of around 1 mm/yr. It is quite clear that efforts have to be made to improve these results before they can be of value for geologists and geophysicists. Outside the very active areas, long term tectonic vertical motions are usually much smaller than 1 mm/yr.

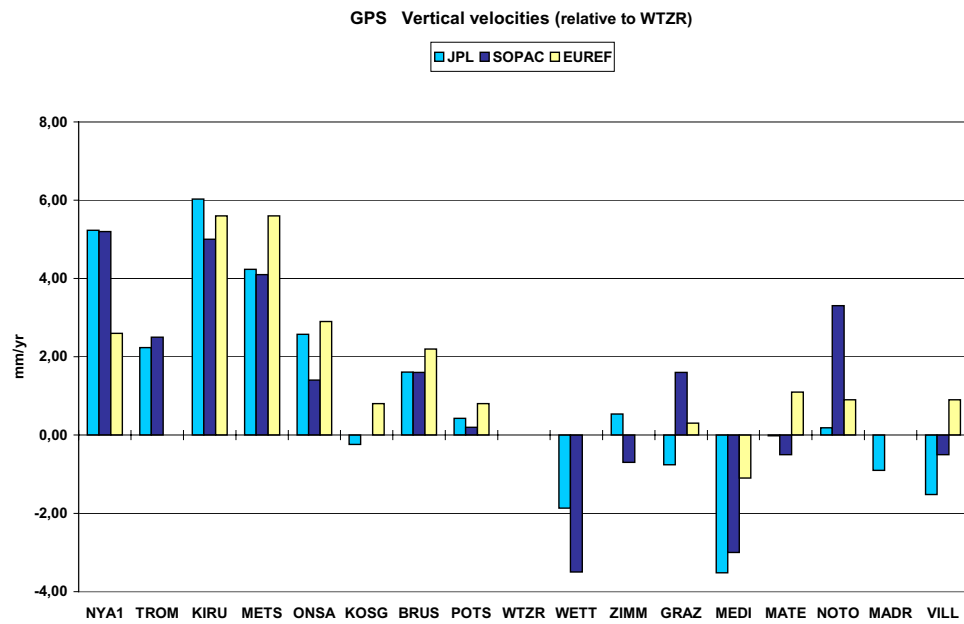


Figure 8: Comparison of vertical velocities from different GPS analysis centers (JPL=Jet Propulsion Laboratory, USA, SOPAC=SCRIPPS Orbit and Permanent Array Center, USA, EUREF=EUREF Permanent GPS-Network, Brussels, Belgium)

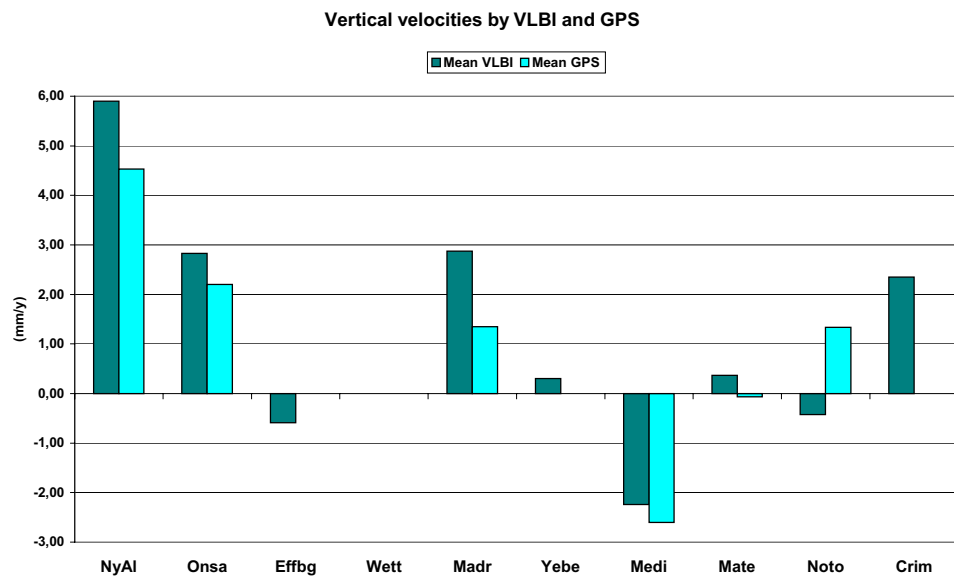


Figure 9: Comparison of mean results for VLBI and GPS at the collocated sites of the European VLBI network. (Wett=WTZR)

## 4 Conclusions

The error analysis of the vertical motions by GPS and VLBI in the European region shown here is converging to a set of reliable estimates of accuracy and precision which hold true for both techniques and suggest (or confirm) that the major part of the errors present in the time series of both techniques originates from the same sources. Even if statistical theory cannot be rigorously applied to the data in the face of numerous systematic errors of different character, classical standard deviations, if interpreted in the correct context, may be used as excellent indicators of the quality and reliability of the results.

The empirical evaluation of the data used here, shows that essentially healthy time series from GPS and VLBI should have wrms daily repeatabilities in the vertical component of around 8 mm/yr or better, and a total uninterrupted time span of data covering 6 years or more, in order to achieve velocity accuracies of around 0.1 mm/yr. In contrast to these formal errors (or error predictions), the true errors are revealed by comparisons of different solutions from different techniques and indicate uncertainties on the order of 1 mm/yr. These tenfold higher errors are always associated with severe problems in the time series, such as for example undetected breaks. The importance of a correct handling of breaks (discontinuities) in the time series is presently still being underestimated. Changes at the stations do happen, but if timely measures are taken to record and document the changes as well as to take them into account in the analysis, there will be much less negative effect on the accuracy of the final results.

## 5 References

- Blewitt, G., D. Lavallée: Effect of annual signals on geodetic velocity. *JGR*, Vol. 107, No. B7, 2002
- Campbell, J.: Basislängenänderungen – abgeleitet aus VLBI-Beobachtungen im Projekt IRIS. In: *Satellitengeodäsie*, M. Schneider ed., DFG Sonderforschungsbereiche. VCH Verlagsgesellschaft Weinheim 1990, p. 269-289
- Campbell, J., R. Haas, A. Nothnagel: Measurement of vertical crustal motion in Europe by VLBI. European Commission, TMR Networks publication No. KI-NA-20-084-ENC, ISBN 92-894-0763-8, Geodetic Institute, University of Bonn, 2002
- Coates, R.J., H. Frey, G.D. Mead, J. Bosworth: Space-Age Geodesy: The NASA Crustal Dynamics Project. *IEEE Transactions on Geoscience and Remote Sensing*, Vol. GE-23, No.4, p. 360-368, 1985
- Heflin, M.B. et al.: Global Geodesy using GPS without fiducial sites. *Geophys. Res. Lett.*, Vol. 19, p. 131-134, 1992
- Jaldehyag, R.T.K., J.M. Johansson, J.L. Davis and P. Elósegui: Geodesy using the Swedish permanent GPS network: Effects of snow accumulation on estimates of site positions. *Geophys. Res. Letters*, Vol. 23, p. 1601-1604, 1996
- Tesmer, V.: VLBI Solution DGF101R01 Based on Least-Squares Estimation Using OCCAM 5.0 and DOGS-CS. Proceedings of the IVS 2002 General Meeting, Feb. 4-7, 2002 in Tsukuba, Japan, NASA/CP-2002-210002, p. 295-299, 2002
- Tomasi, P., P. Sarti, L. Vittuari, M. Negusini: 2002 local geodetic survey of VLBI and GPS reference points and excentre at Medicina. These Proceedings
- Zerbini, S., B. Richter, M. Negusini, C. Romagnoli, D. Simon, F. Domenichini, W. Schwahn: Height and Gravity variations by continuous GPS, gravity and environmental parameter observations in the southern Po Plain, near Bologna, Italy. *Earth and Planetary Science Letters* 5949, p. 1-13, 2001
- Zhang, J., Y. Bock, H. Johnson, P. Fang, S. Williams, J. Genrich, S. Wdonski, and J. Behr: Southern California Permanent GPS Geodetic Array: Error analysis of daily position estimates and site velocities. *JGR*, Vol. 102, B8, P. 18,035-18,055, 1997



# Assessing Long Term Trends in the Atmospheric Water Vapor Content by Combining Data From VLBI, GPS, Radiosondes and Microwave Radiometry

R. Haas, G. Elgered, L. Gradinarsky, and J. Johansson

*Onsala Space Observatory, Chalmers University of Technology, Sweden*

**Summary:** Consistent time series of integrated precipitable water vapor (IPWV) are important when estimating long term trends associated with climate change. Space geodetic and remote sensing techniques offer different advantages in terms of a long observation history, instrumental stability, and measurement uncertainty. We use four different techniques at the Onsala Space Observatory on the Swedish west coast namely geodetic VLBI, ground-based GPS, microwave radiometry, and radiosondes. The individual advantages and disadvantages are exploited to assess the long-term trend in the IPWV. A combined linear trend for the IPWV and the time period 1980-2002 is estimated to  $+0.17 \pm 0.01$  mm/yr.

## 1 Introduction

Water vapor in the atmosphere is one of the most effective so-called "greenhouse gases". Thus, consistent time series of integrated precipitable water vapor (IPWV) are an important data product for meteorology and climate research. Since changes in the atmospheric water vapor might be related to climate change scenarios originating to some extent from antropogenic influences, the monitoring of possible changes of IPWV is of major interest to society.

Different remote sensing and space geodetic techniques are sensitive to atmospheric water vapor and thus can contribute to this task. For example, trends in the IWPV have been derived from radiosonde data covering more than a decade of observations (Gaffen *et al.*, 1992). Also microwave radiometry observations covering more than 15 years have been used to derive long-term trends in the IWPV (Elgered and Jarlemark, 1998). Recently, many years of observations with the Global Positioning System (GPS) have been used to derive trends in the atmospheric water vapor content (Gradinarsky *et al.*, 2001). The possible importance of VLBI results for climate studies has also been pointed out (Niell *et al.*, 2001).

However, each of the above mentioned techniques has its specific advantages and disadvantages in terms of instrumental stability, long observation history, measurement uncertainty, temporal and spatial sampling. Therefore, a combination of results from complementing techniques promises to be a robust approach for the assessment of possible long term trends in the atmospheric water vapor content. For this purpose we use data obtained with several different techniques at the Onsala Space Observatory at the Swedish west coast. The observatory hosts collocated equipment for space geodetic and remote sensing techniques, i.e. for geodetic VLBI, the Global Positioning System (GPS) and microwave radiometry. Furthermore, radiosonde launches are performed at the Gothenburg-Landvetter Airport at about 37 km distance from the observatory. Thus, results for IPWV from these four techniques will be compared and combined.

Sections 2-5 of this paper describe the four different techniques, their specialities, advantages and disadvantages. They present the individual data analysis and the results derived for long term trends in IPWV from the individual techniques. In Section 6 we compare the results of the individual techniques and address the question of data sampling and complementing

data sets. Section 7 deals with the combination of the results obtained with the four techniques. Finally, Section 8 briefly discusses the combination results and draws some conclusions.

## 2 Geodetic VLBI observations at the Onsala Space Observatory

The first successful Mark III geodetic VLBI observations were performed at the Onsala Space Observatory in 1980. Since then the observatory participates regularly in geodetic VLBI sessions and usually 20 to 30 individual VLBI sessions per year are observed. During the years the observatory also participated in a number of continuous campaigns, e.g. Cont94, Cont95, Cont96, Cont01 and Cont02. Nevertheless, the observation sessions unfortunately were not, and are not, on regular intervals. This is definitely a disadvantage of the technique and causes a sampling problem for the monitoring of the IPWV. Besides the temporal sampling, also the spatial sampling of VLBI is one of the techniques disadvantages. There are less than 150 telescopes world-wide that have been and are used for geodetic VLBI and 90% of them are located on the northern hemisphere. The number of telescopes that have been used for observations over a total time span of more than 10 years is less than 30. On the other hand, the VLBI technique has the advantage of high long term stability due to its stable instrumentation. Another advantage is that the relatively small amount of available VLBI data easily can be reprocessed for specific purposes using consistent assumptions and models.

The VLBI data used for this study were analysed using the Calc/Solve analysis software package (Ma *et al.*, 1990). Zenith wet delays (ZWD) were estimated every 1 hour, horizontal delay gradients (HDG) were estimated every 3 hours. The Niell mapping functions (Niell, 1996) were applied. The ZWD results were converted into IPWV results using a conversion formula based on the season and latitude of the station (Emardson *et al.*, 1998). Figure 1 shows the IPWV results obtained from VLBI, the upper plot the total values and the lower plot the corresponding formal errors. It is clearly visible that the measurement uncertainty decreased over the years. This is mainly due to increased number of observations per observation session and improved and optimised observation geometry.

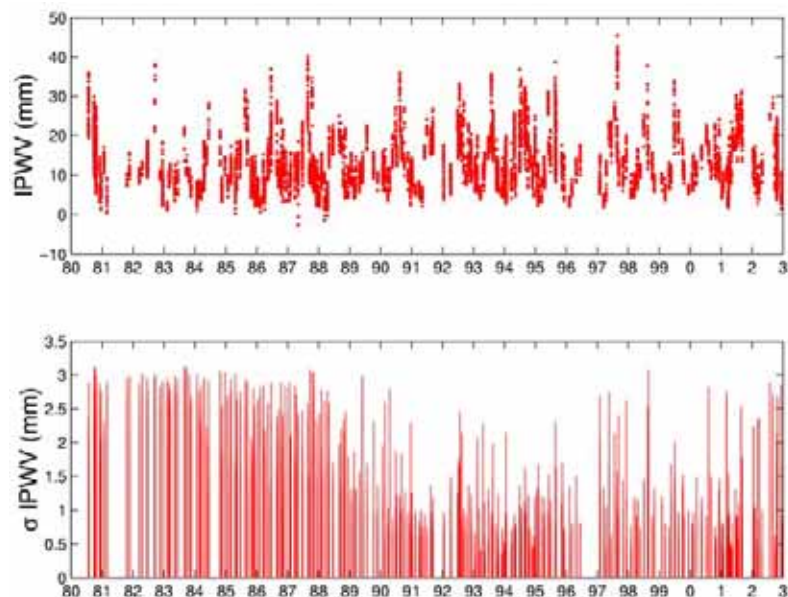


Figure 1: IPWV results derived from VLBI observations at the Onsala Space Observatory between 1980 and 2003.

### 3 Microwave Radiometry at the Onsala Space Observatory

Microwave radiometry measurements are performed at the Onsala Space Observatory with the water vapor radiometer (WVR) ASTRID since 1980 (Elgered *et al.*, 1991). The instrument is equipped with 2 channels with center frequencies at 21.0 and 31.4 GHz. It has two horn antennas with full width half power beams of 6 degrees. During the 1980ies the instrument was mainly operated during VLBI sessions only. Since 1993 the instrument is used almost continuously in a so-called "sky-mapping mode". In 1991/1992 the instrument was upgraded and mechanical parts and calibration loads were improved. Recently (Elgered and Haas, 2003, this volume), the instrument was upgraded again in terms of an improved data acquisition software. A disadvantage of the technique is that a long term stable calibration is rather difficult to achieve, as is the case for most instruments performing emission measurements. The data quality of the derived atmospheric parameters depends on the accuracy of the retrieval algorithms that are applied. The spatial sampling of ground based microwave radiometers is rather poor and many instruments in use are unique instruments. An advantage of the technique is that it gives direct and instantaneous measurements of atmospheric properties in any direction and the temporal sampling can be quite high.

The data acquired with the WVR Astrid at Onsala were analysed using the RadGrad software and zenith wet delays and gradients were estimated and averaged with a time resolution of 30 minutes. The ZWD were converted to IPWV as described before. Figure 2 shows the IPWV values derived from the WVR (upper plot) and their corresponding uncertainties (lower plot). These are assumed to be 5% of the total value, reflecting mainly uncertainties in the absolute calibration using the tip-curve method and the retrieval algorithms.

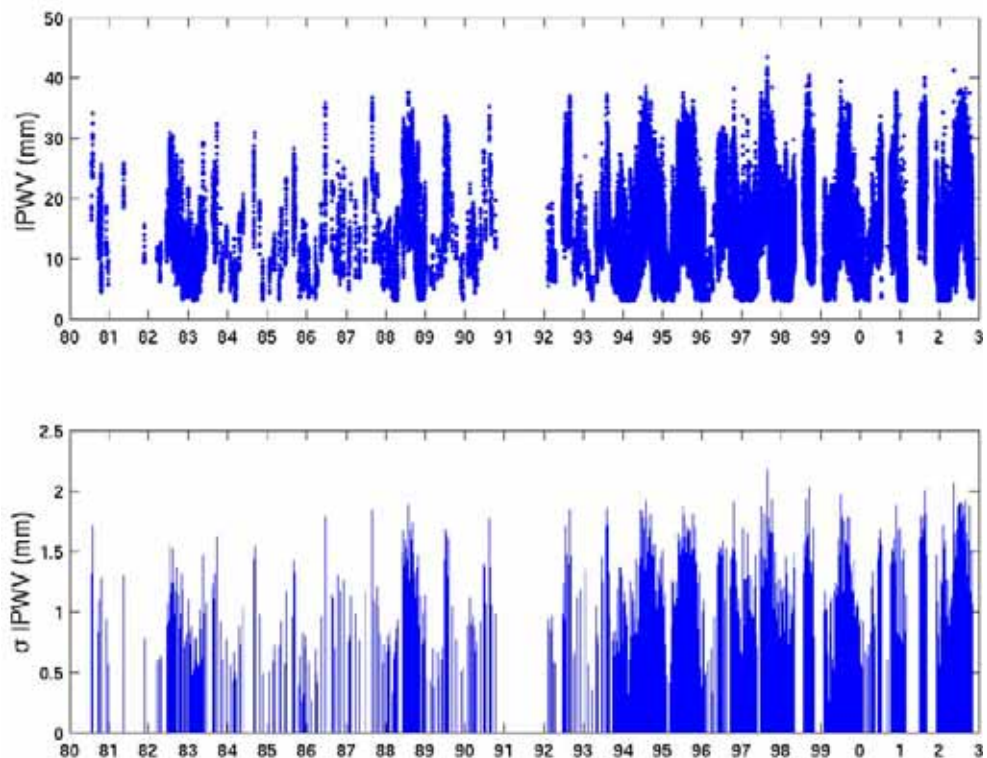


Figure 2: IPWV results derived from microwave radiometry at the Onsala Space Observatory with the water vapor radiometer (WVR) Astrid.

## 4 Global Positioning System observations at the Onsala Space Observatory

The first GPS-observations at Onsala were acquired during campaigns in the mid 1980ies. The site became a continuous site in the CIGNET network in late 1987 and later an IGS site. During the first years of operation a number of instrumental changes have occurred at the site, e.g. change of receivers and antenna foundation, which are a disadvantage of the technique. Since 1993 the site is part of the Swedish SWEPOS network performing continuous GPS observations. Here we will use the GPS data from the start of SWEPOS in August 1993. After this time, only one major change has occurred, a new hemispherical radome was installed on February 1, 1999. The GPS technique has the advantage to deliver continuous and almost uninterrupted time-series of atmospheric parameters during all types of weather. Besides the temporal sampling, GPS networks offer also a high spatial sampling since there are a large number of continuous GPS stations in national GPS networks almost worldwide.

Figure 3 shows results for IPWV obtained from GPS-observations at the Onsala Space Observatory. The data have been analysed using the Gipsy/Oasis II GPS analysis software (Webb and Zumberge, 1993) in the so-called "precise-point-positioning" (PPP) technique (Zumberge *et al.*, 1997). The resulting total zenith delays (TZD) obtained for 5 minute intervals were first converted to ZWD by subtracting the zenith hydrostatic delay (ZHD) based on pressure data observed at the site and then converted to IPWV as described before. Figure 3 shows the IPWV values (upper panel) and their corresponding formal errors from the Gipsy output (lower panel). The uncertainties do not show any systematic behaviour.

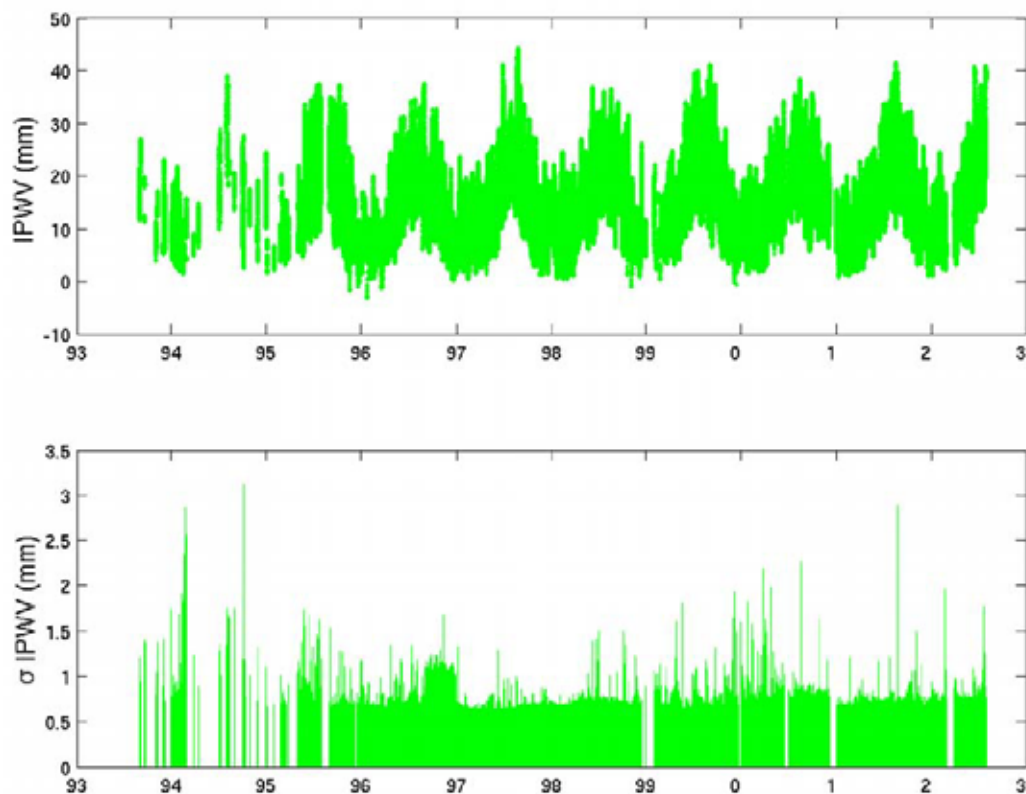


Figure 3: IPWV results derived from GPS observations at the Onsala Space Observatory.

## 5 Radiosonde observations at Landvetter airport

Radiosondes (RS) are a traditional measurement device for upper air observations in meteorology. The Swedish Meteorological and Hydrological Institute (SMHI) launches radiosondes at Landvetter airport at about 37 km distance from the Onsala Space Observatory every 6 to 12 hours. (The launching interval has varied over the years.) These radiosondes measurements have a long and continuous observation history. However, the type of radiosondes used has changed over the years. Before March 1986 the radiosonde type Vaisala RS18 was in use and since December 1985 the radiosonde type Vaisala RS80 is in use. During the four months December 1985 to March 1986 both types were used in parallel. The low but regular temporal sampling of 6-12 hours is not critical for long term monitoring since the time scales of air mass changes is typically a few days. The spatial sampling of radiosonde observations is however a limitation since the launches are expensive and often only performed at larger airports. The observations are available in form of atmospheric profiles of pressure, temperature, and humidity and thus give information on the vertical structure.

The data taken at Landvetter have been analysed using the in house developed CalcRS software. Figure 1 shows IPWV results from radiosonde launches at Landvetter for 1980 to 2003. The upper plot shows the IPWV results and the lower plot the corresponding accuracies. The accuracies are assumed to be 5% of the absolute value, based on measurement accuracies of the sensors used in the radiosondes (England *et al.*, 1993).

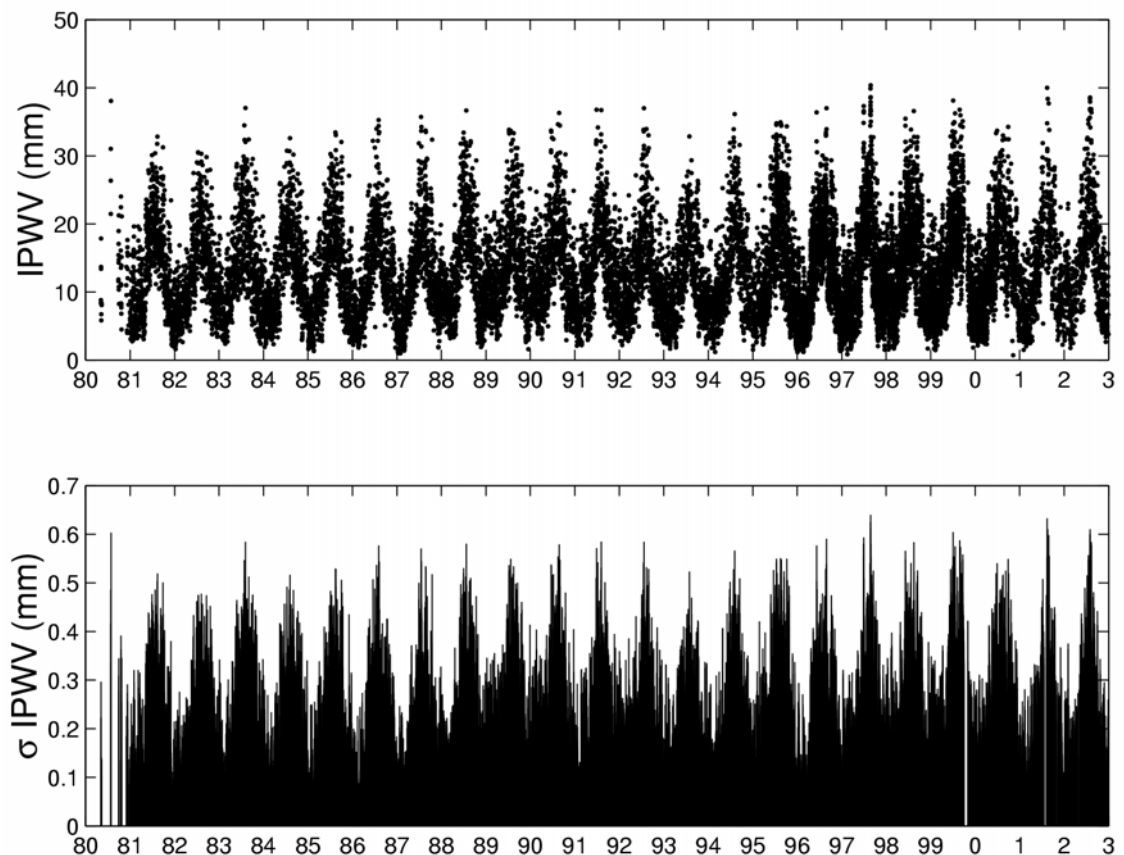


Figure 4: IPWV results derived from radiosondes (RS) launched at Landvetter airport

## 6 Comparing the four techniques

As a first approach the IPWV time series of each technique can be analysed individually. A simple first-order mathematical model is to estimate four parameters from a time series. These parameters are an offset ( $a_1$ ), a rate ( $a_2$ ), and a sine amplitude ( $a_3$ ) and cosine amplitude ( $a_4$ ) to describe an annual variation of the IWPV while fixing the period to be 365.25 days. For the estimation process the weighting of the data points is of importance. As seen in Figures 2 and 4, the WVR and the RS results have uncertainties on the order of 5 % of the total values. If these uncertainties were used as input for the weighting of the data points, this would lead to a systematic down-weighting of the winter periods since the IPWV values during winter are smaller than during summer. Figure 1 shows that the formal errors of the earlier VLBI observations are larger compared to the more recent ones. Thus, taking the formal errors into account for the weighting of the data points would down-weight the VLBI results obtained from observations performed in the 1980ies. Only the standard deviations of the GPS results do not show any systematic behaviour and could be used without having any systematic impact on the results.

Instead of using standard deviations for the weighting, it appears to be more appropriate to use the same weighting for all data points and to force the reduced chi-square to unity. Using this approach, the following results are obtained for the IPWV trend parameter ( $a_2$ ):

Table 1: IPWV trends from four different space geodetic and remote sensing techniques.

Technique	Data period	Number of data points	IPWV trend ( $a_2$ )
VLBI	1980-2002	8477	+0.03 ± 0.01 mm/yr
WVR	1980-2002	212260	+0.13 ± 0.01 mm/yr
GPS	1993-2002	693127	+0.24 ± 0.01 mm/yr
RS	1980-2002	18597	+0.04 ± 0.01 mm/yr

The derived IPWV trends are statistically significant and positive for all techniques. However, VLBI and RS give only a slight increase, while WVR and GPS show significantly larger values. To understand this discrepancy it has to be noted that the individual input time series cover different time periods and have different temporal sampling. The VLBI time series is the most sparse one with only 20-30 observation sessions of 24 hours per year and a couple of continuous observation sessions of several days length. This is a clear undersampling of the IPWV variations during one year. For the first half of the time series the WVR was operated mainly only during VLBI session, but in the second half the instrument was operated nearly continuously. The GPS time series has the most regular sampling and almost continuous data. The RS time series is also quite regular, however the sampling is less frequent, than that of the other techniques, with one data point every 6 to 12 hours only. In the following it will be shown that the different sampling of the four techniques causes the significant differences in the derived IPWV trend parameters.

The question of the impact of the sampling on the trend results is closely related to the question of complementing time series. Here the question is, whether it is possible and reasonable to fill up gaps in the IWPV time series of one technique with values obtained by another technique. In this case the techniques would complement each other and the combined time series would give more robust and reliable results than each of the individual time series on its own. To address this question, it is useful to compare the four techniques pairwise and to use only data from epochs where both techniques

have IPWV results. We therefore formed six datasets including pairwise results of two techniques each that were sampled at the same or close time epochs. We then used the simple mathematical model as described before and determined trend parameters for each of the two techniques involved in this pairwise comparison. The definition of what the same or close sampling means depends on the sampling frequency of the original individual time series. We required that the sampling epochs agreed within the shortest sampling interval length of the two techniques to be compared. Table 2 shows the results for IPWV trends derived from pairwise time series with synchronised sampling and the corresponding rms-differences.

Table 2: Pairwise comparison of the four different techniques using synchronized sampling epochs.

Comparison pair	Number of common data points	IPWV trend from (a) (mm/yr)	IPWV trend from (b) (mm/yr)	Bias (a)–(b) (mm)	RMS-diff. (mm)
VLBI (a), WVR (b)	1925	+0.19 ± 0.01	+0.13 ± 0.01	+0.43 ± 0.04	1.6
VLBI (a), GPS (b)	2045	−0.07 ± 0.01	−0.05 ± 0.01	−0.33 ± 0.03	1.3
VLBI (a), RS (b)	753	+0.05 ± 0.01	+0.03 ± 0.01	+0.60 ± 0.08	2.1
WVR (a), GPS (b)	128978	+0.31 ± 0.01	+0.31 ± 0.01	−0.57 ± 0.01	1.6
WVR (a), RS (b)	1755	+0.11 ± 0.01	+0.12 ± 0.01	+0.29 ± 0.05	1.7
GPS (a), RS (b)	7120	+0.25 ± 0.01	+0.20 ± 0.01	+0.96 ± 0.02	2.0

The pairwise comparison proves that the sampling is an important factor when deriving trends from the IPWV time series. The largest deviation seen is 0.06 mm/yr and the mean deviation is 0.03 mm/yr. We see that when the time series of two techniques have synchronised sampling epochs, the derived IPWV trends agree reasonably well. This becomes especially apparent in the comparison between VLBI and GPS. From each of the techniques itself a positive, but different IPWV trend was derived, see Table 1. The difference is more than 0.2 mm/yr. But using synchronised sampling epochs, both IPWV trends become negative and agree within 0.02 mm/yr. Thus, the two techniques VLBI and GPS appear to sense the same physical signal.

Regarding the pairwise differences between the techniques, there are only small systematic variations left, the biases between the techniques are less than 1 mm and the rms-differences are on the level of 1.3 to 2.1 mm. The conclusion from these comparisons is that it indeed appears to be reasonable to use the four techniques as complementing techniques for a combination approach.

## 7 Combining the four techniques

A nine parameter model was used for the combination of the complementing IPWV results of the four techniques. The model consisted of four individual offset parameters ( $b_1, b_2, b_3, b_4$ ), one for each technique, a common rate parameter ( $b_5$ ) for all techniques, a sine amplitude ( $b_6$ ) and a cosine amplitude ( $b_7$ ) to describe the annual variation for the three techniques collocated at the Onsala Space Observatory, and a sine amplitude ( $b_8$ ) and a cosine amplitude ( $b_9$ ) for the radiosondes at Landvetter airport. All data points got identical weighting and the chi-square per degree of freedom was forced to unity. The numerical results are shown in Table 3.

The results show that the four techniques have individual offset values that differ within a total range of 0.5 mm. The pairwise differences between these

offsets (biases) confirm the findings of Section 6. The tendencies (positive or negative bias) are the same while the absolute values are slightly different. The estimated annual signals for Onsala and Landvetter differ slightly. The total amplitude of the annual signal is larger for the three collocated techniques at Onsala ( $6.68 \pm 0.01$  mm) than for the radiosondes at Landvetter airport ( $6.43 \pm 0.02$  mm). The phase of the annual signal expressed in day of the year (doy) is earlier by three days for the three collocated techniques at Onsala (doy  $240.1 \pm 0.1$ ) as compared to Landvetter (doy  $243.1 \pm 0.2$ ). The common trend in IPWV was estimated to  $+0.17 \pm 0.01$  mm/yr. Figure 5 shows the combined solution.

Table 3: Estimated parameters of the nine parameter model: Four offset parameters (VLBI –  $b_1$ , WVR –  $b_2$ , GPS –  $b_3$ , RS –  $b_4$ ) one common trend parameter ( $b_5$ ), sine amplitude ( $b_6$ ) and cosine amplitude ( $b_7$ ) for the annual variation of the collocated techniques at Onsala (VLBI, WVR, GPS), and sine amplitude ( $b_8$ ) and cosine amplitude ( $b_9$ ) for the radiosondes at Landvetter airport.

$b_1$ (mm)	$b_2$ (mm)	$b_3$ (mm)	$b_4$ (mm)	$b_5$ (mm/yr)	$b_6$ (mm)	$b_7$ (mm)	$b_8$ (mm)	$b_9$ (mm)
11.22 $\pm 0.02$	10.79 $\pm 0.02$	11.29 $\pm 0.02$	10.97 $\pm 0.02$	0.17 $\pm 0.01$	-3.67 $\pm 0.01$	-5.59 $\pm 0.01$	-3.25 $\pm 0.02$	-5.55 $\pm 0.02$

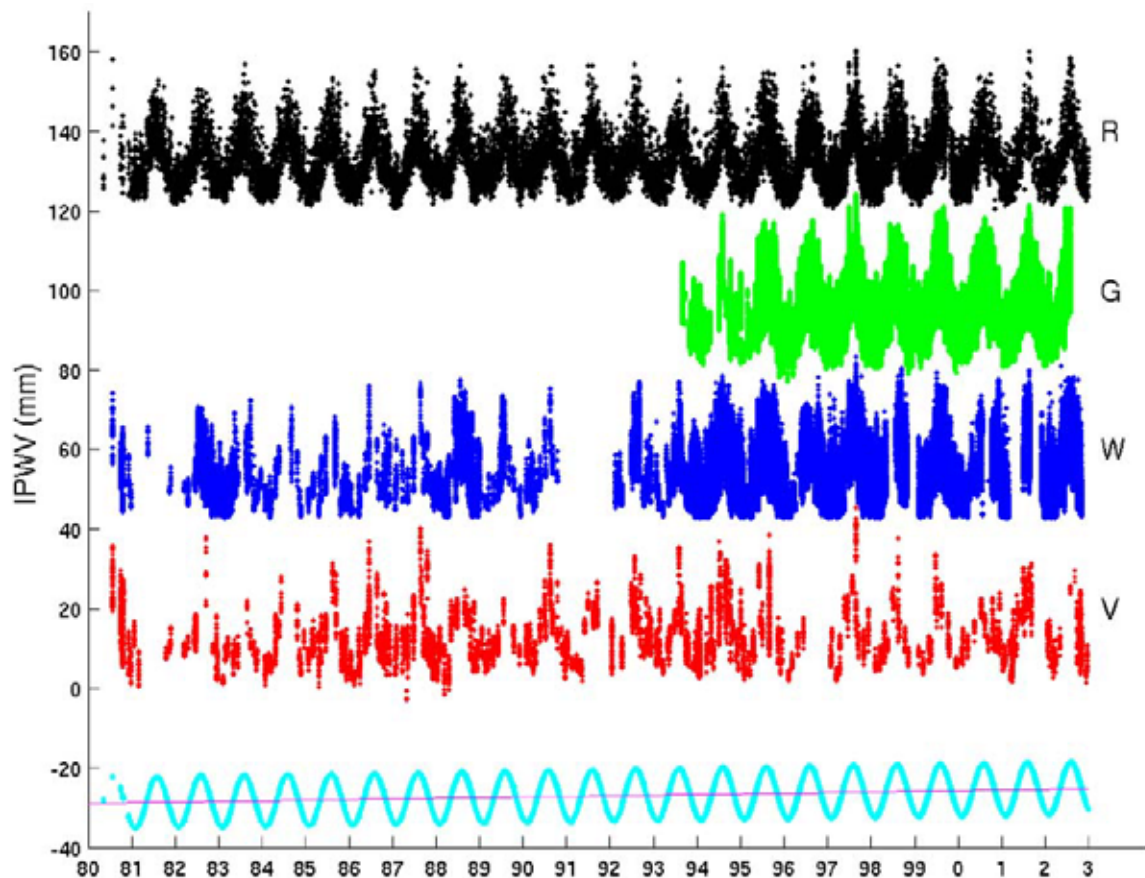


Figure 5: Combined time series of IPWV from four different techniques over 23 years. Shown are the original data sets, i.e. VLBI (V) without offset, WVR (W) offset by +40 mm, GPS (G) offset by +80 mm, RS (R) offset by +120 mm, together with the sinusoidal mean annual variation and the common linear trend (offset by -40 mm). The common trend in IPWV is  $+0.17 \pm 0.01$  mm/yr.

## 8 Discussion and conclusion

Time series of IPWV derived from different space geodetic and remote-sensing techniques can be used to derive long term trends of the IPWV. Different techniques have their individual advantages and disadvantages in terms of long observation history, instrumental stability, temporal sampling and measurement accuracy and also give different results due to different sampling epochs. However, the comparison of IPWV results from different collocated space geodetic and remote sensing techniques at the Onsala Space Observatory shows that the techniques give similar results for synchronised sampling epochs. The agreement for IPWV trends is on the level of 0.05 mm/yr, the biases between the absolute IPWV values of the different techniques are less than 1 mm, and the rms differences are on the level of 1.3 to 2.1 mm when the absolute IPWV values are compared. The best agreement in terms of rms-differences is found between VLBI and GPS.

This investigation indicates that a combination of results from different complementing techniques is a useful and promising approach to derive long term trends in the atmospheric water vapor. Using the collocated techniques at the Onsala Space Observatory we derive an IPWV trend of  $+0.17 \pm 0.01$  mm/yr.

These results have been derived using very simple mathematical models. Future investigations will apply more advanced mathematical models that address the individual advantages and disadvantages of the individual techniques in more detail. This will for example include studying possible effects due to instrumental changes at the microwave radiometer. Robust estimates for long term trends in atmospheric water vapor will be derived.

## Acknowledgements

We thank the VLBI group at the Bundesamt für Kartographie und Geodäsie Leipzig for allowing access to their computer system and their archive of global VLBI data.

## References

- Elgered, G., and Haas, R.: The Geodetic VLBI Network Station at the Onsala Space Observatory: Activities during 2002. In: Proceedings of the 16<sup>th</sup> Working Meeting on European VLBI for Geodesy and Astrometry, held at Leipzig, May 9-10, 2003, edited by W. Schwegmann and V. Thorandt, Bundesamt für Kartographie und Geodäsie, 61-66, (this volume), Frankfurt/Leipzig, 2003.
- Elgered, G., and Jarlemark, P. O. J.: Ground-based microwave radiometry and long-term observations of atmospheric water vapor. *Radio Science*, **33(3)**, 707-717, 1998.
- Emardson, T. R., Elgered, G., and Johansson, J. M.: Three months of continuous monitoring of atmospheric water vapor with a network of Global Positioning System receivers. *Journal of Geophysical Research*, **103**, 1807-1820, 1998.
- England, M. N, Schmidlin, F. J., and Johansson, J. M.: Atmospheric Moisture Measurements: A Microwave Radiometer – Radiosonde Comparison. *IEEE Transactions of Geoscience and Remote Sensing*, **31(2)**, 389-398, 1993.

- Gaffen, D. J., Elliott, W. P., and Robock, A.: relationships between troposphere water vapor and surface temperature as observed by radiosondes. *Geophysical Research Letters*, **19**, 1839-1842, 1992.
- Gradinarsky, L. P., Johansson, J. M., Bouma, H. R., Scherneck, H.-G., and Elgered, G.: Climate monitoring using GPS. *Physics and Chemistry of the Earth*, **27**, 225-340, 2002.
- Ma, C., Sauber, J. M., Bell, J. L., Clark, T. A., Gordon, D., and Himwich, W. E.: Measurement of horizontal motions in Alaska using very long baseline interferometry. *Journal of Geophysical Research*, **95(B13)**, 21991-22011, 1990.
- Niell, A., Global mapping functions for the atmosphere delay at radio wavelength. *Journal of Geophysical Research*, **101(B8)**, 3227-3246, 1996.
- Niell, A. E., Coster, A. J., Solheim, F. S., Mendes, V. B., Toor, P. C., Langley, R. B., and Upham, C. A.: Comparison of measurements of atmospheric wet delay by radiosonde, water vapor radiometer, GPS, and VLBI. *Journal of Atmospheric and Oceanic Technology*, **18(6)**, 830-850, 2001.
- Webb, F. H., and Zumberge, J. F.: An introduction to GIPSY/OASIS II. *JPL Publication D-11088*, Jet Propulsion Laboratory, Pasadena, CA, 1993.
- Zumberge, J. F., Heflin, M. B., Jefferson, D. C., Watkins, M. M., and Webb, F. H.: Precise point positioning for the efficient and robust analysis of GPS data from large networks. *Journal of Geophysical Research*, **102(B3)**, 5005-5017, 1997.

Session 7

## Future Perspectives of VLBI



# The Project “VLBIonos” – How VLBI Contributes to Ionospheric Research

T. Hobiger, J. Boehm, S. Todorova, and H. Schuh

*Institute of Geodesy and Geophysics (IGG), Vienna University of Technology, Austria*

**Summary:** In geodetic Very Long Baseline Interferometry (VLBI) the observations are performed at two distinct frequencies (2.3 and 8.4 GHz) in order to determine ionospheric delay corrections. This allows information to be obtained from the VLBI observables about the sum of electrons (total electron content - TEC) along the ray path through the ionosphere. Due to the fact that VLBI is a differential technique, only the differences in the behavior of the propagation media over the stations determine the values of the observed ionospheric delays. However, in a first simple approach, an instrumental delay offset per baseline shifts the TEC measurements by a constant value. This offset is independent of the azimuth and elevation of the observed radio source and allows separation of the ionospheric parameters for each station from the instrumental delay offsets per baseline in a least-squares adjustment. In first tests of this method Fourier coefficients up to the 4th order plus a constant value and a linear trend were estimated to represent the vertical TEC (VTEC). Slant TEC (STEC) values are converted into VTEC values by a mapping function. A disadvantage of this approach is the assumption that these values are assigned to the station coordinates but not to the geographical coordinates of the intersection point of the ray path and the infinitely thin ionospheric layer. The precision of the estimated values is about  $\pm 5$  to  $\pm 7$  TEC units (TECU). The results obtained from VLBI agree with a standard deviation of  $\pm 10$  TECU with other techniques like GPS, and rarely exceed 20 TECU. A second approach, developed at the TU Vienna, using piece-wise linear functions (VTM – Vienna TEC model) was also tested.

## 1 The Earth’s ionosphere

The Earth’s ionosphere is defined as that part of the upper atmosphere where free electrons occur in sufficient density to influence the propagation of electromagnetic radio frequency waves (Hargreaves, 1992, [1]). The ionization depends primarily on the Sun and its activity. Ionospheric structures vary strongly with time corresponding to the sunspot cycle and seasonal and diurnal cycles and with geographical location (polar, auroral, mid-latitude and equatorial regions). Certain further ionospheric disturbances can be related to the Sun. The major part of the ionization is produced by solar X-ray and ultraviolet radiation and by corpuscular radiation from the Sun. The most noticeable effect is seen as the Earth rotates with respect to the Sun. Ionization increases in the sunlit hemisphere and decreases on the shadowed side. Although the Sun is the largest contributor to the ionization, cosmic rays are the source of a small contribution, too.

The ionosphere is a dynamic system depending on many parameters, including acoustic motions of the atmosphere, electromagnetic emissions, and variations of the geomagnetic field. Any atmospheric disturbance affects the distribution of the ionization, and, because of its extreme sensitivity to atmospheric changes, the ionosphere can be used as a sensor of atmospheric events. A description of the structure of the ionosphere, in terms of its vertical profile, its main geographic regions and its temporal variations is given by Hobiger et al. (2003, [2]).

## 2 Impact on space geodetic techniques

One of the problems for all space geodetic techniques operating with electromagnetic waves is the determination of the propagation velocity of the signals. If these waves propagated in vacuum, the traveled distance would be just the product of the propagation time between emitter and receiver and the speed of light in vacuum. When signals travel through the ionosphere, the interaction between the electromagnetic field and the free electrons influences both the speed and the propagation direction of the signal, an effect known as ionospheric refraction (Hartmann and Leitinger, 1984, [3]). The ratio between the propagation speed of a wave in vacuum  $C$  and the propagation speed in a given medium  $V_{ph}$  is known as the refractive index  $n$

$$n = \frac{C}{V_{ph}} \quad (1.1)$$

The Appleton-Hartree theory (Hartmann and Leitinger, 1984, [3]) allows the calculation of the refractive index for a single wave which propagates through a plasma (= ionized medium). By neglecting higher order terms we obtain an approximation for  $n$  (see Hobiger et al., 2003 [2]).

$$n \approx 1 - \frac{40.28 N_e}{f^2} \quad (1.2)$$

where  $f$  is the carrier frequency expressed in Hz and  $N_e$  is the free electron density in the medium. Using this result the group refractive index  $n_g$  can be determined by

$$n_g \approx 1 + \frac{40.28 N_e}{f^2} \quad (1.3)$$

Now we can calculate the carrier phase delay,  $d_{ph}$ , to obtain the influence of the ionized medium on the propagation delay, expressed in SI units (meters)

$$d_{ph} = \int_S (n_{ph} - 1) dS = -\frac{40.28}{f^2} \int_S N_e dS = -\frac{40.28 \cdot 10^{16}}{f^2} STEC \quad (1.4)$$

The integral of the electron density along the signal path  $S$  is usually called **STEC** (Slant Total Electron Content). This quantity can be interpreted as the total amount of free electrons in a cylinder with a cross section of  $1 \text{ m}^2$  of which the axis is the slant signal path. **STEC** is measured in Total Electron Content Units (TECU), which is equivalent to  $10^{16} \text{ electrons} \cdot \text{m}^{-2}$ . The effect of the ionized medium on group propagation can be expressed by

$$d_g = \int_S (n_g - 1) dS = \frac{40.28}{f^2} \int_S N_e dS = \frac{40.28 \cdot 10^{16}}{f^2} STEC \quad (1.5)$$

The last two expressions show how the electron content in the ionosphere can influence measurements ranging from outer space to Earth-based stations. If the behavior of the ionosphere is known, these effects can be computed and can be used to correct measurements on radio frequencies. If ionospheric parameters are not available, observing at two different radio frequencies allows the elimination of ionospheric influences.

### 3 A new field of research - ionospheric investigations by geodetic VLBI

The project 'VLBlonos', supported by the Austrian Science Fund (FWF), started on March 1<sup>st</sup>, 2003, and aims at the investigation of the ionosphere using geodetic VLBI. VLBI observations are performed at two different frequencies (2.3 and 8.4 GHz, S- and X-band) in order to determine the ionospheric delay. As shown by Kondo (1991, [4]) this information can be used to model the ionosphere above each station. It has to be mentioned that only the differences in the ionospheric delay between the two stations are measured. Instrumental offsets at each station bias these measurements, which leads us to

$$\tau_{model}(t) = \tau_{ion,1}(t) - \tau_{ion,2}(t) + \tau_{offset,1} - \tau_{offset,2} \quad (2.1)$$

The ionospheric delay  $\tau_{ion}(t)$  at X-band ( $f_x$ ) over station  $i$  can be modeled as

$$\tau_{ion,i}(t) = \frac{1.34 \cdot 10^{-7}}{f_x^2} \cdot S(E_i) \cdot VTEC_i(t) \quad , \quad (2.2)$$

where

$$S(E_i) = \frac{1}{\cos\left\{\arcsin\left[\frac{R \cos E_i}{R+h}\right]\right\}} \quad (2.3)$$

and  $VTEC_i(t)$  represents the vertical TEC value at the intersection point of the ray path with the infinitesimally thin ionospheric layer assumed to be at the height  $h$ . The radius of the (spherical) Earth is abbreviated with  $R$ . Under the assumption that horizontal gradients in the ionosphere can be neglected within a range of about 300 kilometers,  $VTEC_i(t)$  can be assigned to the geographical coordinates of the VLBI station. In our first investigation we concentrate on modeling the behavior of the ionosphere over the stations by two different approaches.

- Model proposed by Kondo (1991, [4])

In this model  $VTEC_{Kondo}(t)$  for station  $i$  and time  $t$  is calculated as suggested by Kondo [4] using a constant offset, sine and cosine functions, and a daily rate

$$VTEC_{Kondo,i}(t) = a_{i0} + \sum_{k=1}^4 \left[ a_{ik} \cos\left(\frac{kt\pi}{12}\right) + b_{ik} \sin\left(\frac{kt\pi}{12}\right) \right] + c_i t \quad (2.4)$$

- Vienna TEC Model (VTM)

In this model  $VTEC_{VIENNA}(t)$  is calculated as a piece-wise linear function

$$VTEC_{VIENNA,i}(t) = offset_i + rate_{i1}(t_1 - t_0) + rate_{i2}(t_2 - t_1) + \dots + rate_{in}(t_n - t) \quad (2.5)$$

and  $t \leq t_n$ .

After calculating the partial derivatives

$$\left( \frac{\partial \text{VTEC}_{\text{Kondo},i}}{\partial a_{ij}}, \frac{\partial \text{VTEC}_{\text{Kondo},i}}{\partial b_{ij}}, \frac{\partial \text{VTEC}_{\text{Kondo},i}}{\partial c_i} \right)$$

or

$$\left( \frac{\partial \text{VTEC}_{\text{VIENNA},i}}{\partial \text{offset}_i}, \frac{\partial \text{VTEC}_{\text{VIENNA},i}}{\partial \text{rate}_{ij}} \right)$$

a least-squares adjustment allows separation of the VTEC values from the constant instrumental offset  $\tau_{\text{offset},i}$ . This is possible because observations are performed at different elevation angles which prevents the design matrix from becoming singular. The VTM approach also includes constraints on the VTEC rate of about  $\pm 30$  TECU per hour for the following two reasons: to get physically reasonable values and to get a non-singular design matrix even if there are gaps in the data.

## 4 Results

### 4.1 Ionospheric values and maps derived by GPS

Data relevant to this work stored in IONospheric Exchange format (IONEX) (see Schaer et al., [5]) on the IGS web server are provided by the following analysis centers:

- Center for Orbit Determination in Europe (CODE), University of Berne, Switzerland,
- Geodetic Survey Division of Natural Resources Canada – formerly Energy, Mines and Resources Canada (EMR), Ontario, Canada,
- European Space Operations Centre (ESOC) at the European Space Agency (ESA), Darmstadt, Germany,
- Jet Propulsion Laboratory (JPL), Pasadena, U.S.A.,
- Group of Astronomy and Geomatics, Universidad Politecnica de Catalunya (gAGE/UPC), Barcelona, Spain.

So far (summer 2003), a combined series of these GPS analysis centers does not exist. Additionally, regional ionospheric models were derived in this study (i.e. at the Institute of Geodesy and Geophysics (IGG) of TU Vienna) from GPS data using BERNESE software. For this purpose data from five to ten uniformly distributed stations around the ‘center station’ were taken to calculate a model represented by spherical harmonics. If the VLBI station is close to the center of the area covered by the GPS sites a better agreement between the two techniques would be expected than with IONEX because no interpolation of gridded data is necessary. In section 4.3 these regional GPS solutions will be referenced as GPS-IGG/BERNESE.

### 4.2 TEC values derived from VLBI NEOS-A sessions

Figure 1 shows VTEC values determined by VLBI from the NEOS-A session on January 16<sup>th</sup>, 2001 over the station Fortaleza (solid lines) compared to TEC numbers derived by GPS (dashed lines). Fortaleza is located close to the equator and shows high maxima and a strong variability of the TEC numbers during 24 hours. The results of both VLBI approaches (Kondo approach and VTM approach) agree quite well between each other and also with the solutions of the different IGS analysis centers. Sometimes the differences between the individual GPS solutions are even bigger than the differences from VLBI results what might depend on the various models chosen and the constraints set in the GPS analyses. In figure 2 the amplitudes

$$A_{ik} = \sqrt{a_{ik}^2 + b_{ik}^2} \quad (4.1)$$

of the harmonic terms are plotted i.e., for periods of 24h, 12h, 8h, and 6h, for all stations involved in this experiment according to the Kondo approach. The error bars show the precision of each amplitude  $A_{ik}$  and the x-axis corresponds to the geographical latitudes of the VLBI stations. It is obvious that stations which are closer to the equator show larger amplitudes for the diurnal period. This correlation between amplitude and pole distance ( $90^\circ$  minus absolute latitude) cannot be seen for the sub-diurnal periods. From the error bars of the amplitudes we estimate the overall precision of the VLBI TEC values to  $\pm 5$  to  $\pm 7$  TECU.

Figure 1: VTEC over the station Fortaleza, Brasil, comparison between VLBI (Vienna TEC Model and Kondo approach) and individual GPS solutions.

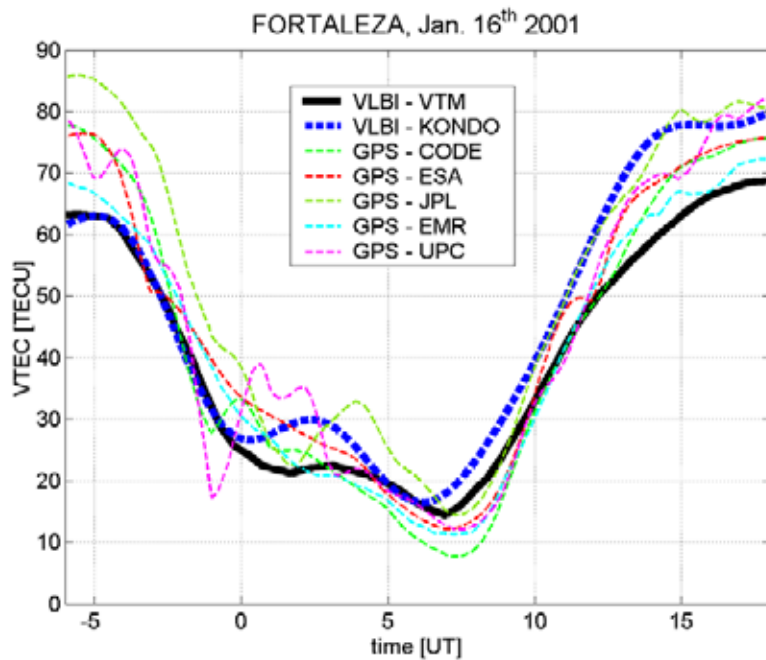
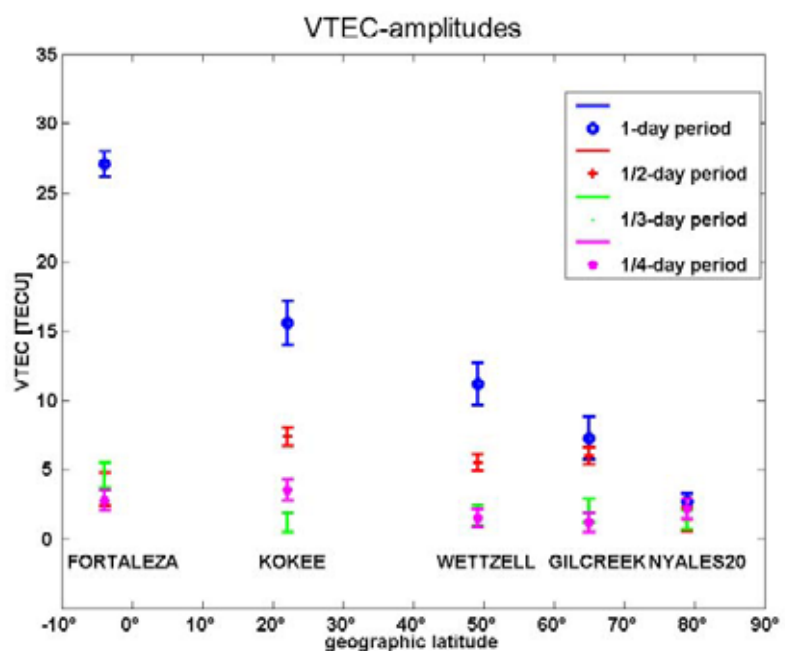


Figure 2: Amplitudes  $A_{ik}$  and their precision from the NEOS-A session on January 16<sup>th</sup>, 2001 (Kondo approach).



The same session as before was used for deriving TEC numbers for station Gilcreek (figure 3) which were compared to the GPS computations. In spite of the generally good agreement between the various GPS solutions and the two VLBI approaches, the residual discrepancies should be subject to a detailed investigation.

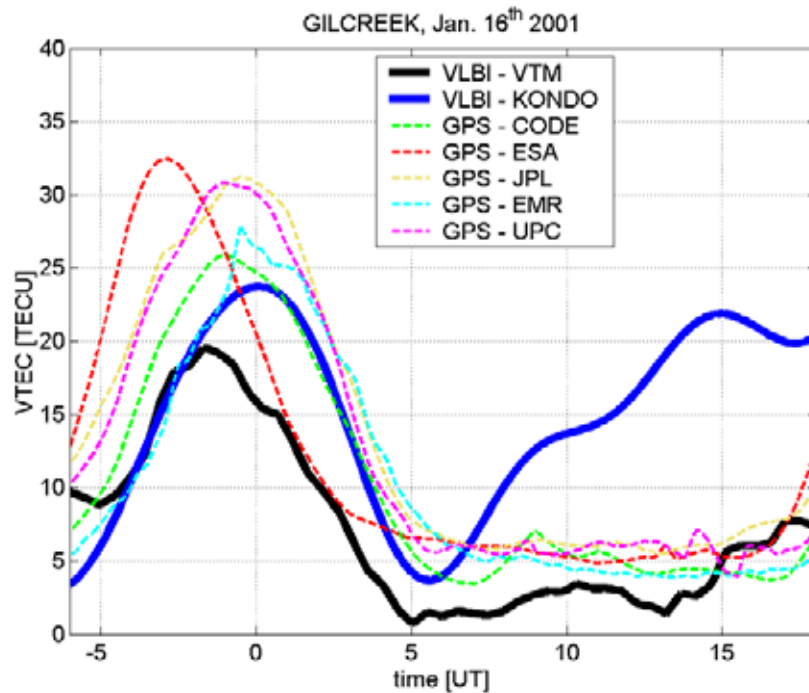


Figure 3: VTEC over the station Gilcreek, Alaska, U.S.A., comparison between VLBI (Vienna TEC model and Kondo approach) and individual GPS solutions.

#### 4.3 Analyzing the CONT02 session with the VTM approach

CONT02 was a VLBI session observing 15 days continuously in October 2002. The goal of the CONT02 campaign was to acquire the best possible state of the art VLBI data over a two-week period to demonstrate the highest accuracy of which VLBI is capable. The solutions of all IGS IONEX analysis centers for station Wettzell are plotted in figure 4 as dashed lines and compared with the VTM result (thick line). Figure 5 is an amplified part showing the results for station Wettzell for a period of 24 hours starting on 25th of October, 00:00 UT, 2002 in comparison with the solution derived at IGG by BERNESE software. In section 4.1 it was mentioned that so far no combined IONEX solution exists. Thus, the VLBI results could only be compared with the individual GPS solutions. For all stations in the CONT02 network the differences between the VLBI and GPS solutions were calculated every 0.1 hour and plotted in one histogram (figure 6). This should give a first idea about the accuracy of the VTM approach. Further statistical analyses will follow.

The histogram shows a mean difference ('bias') between VTEC values derived by GPS and VLBI of about +7 TECU. This constant effect has to be subject to further investigations.

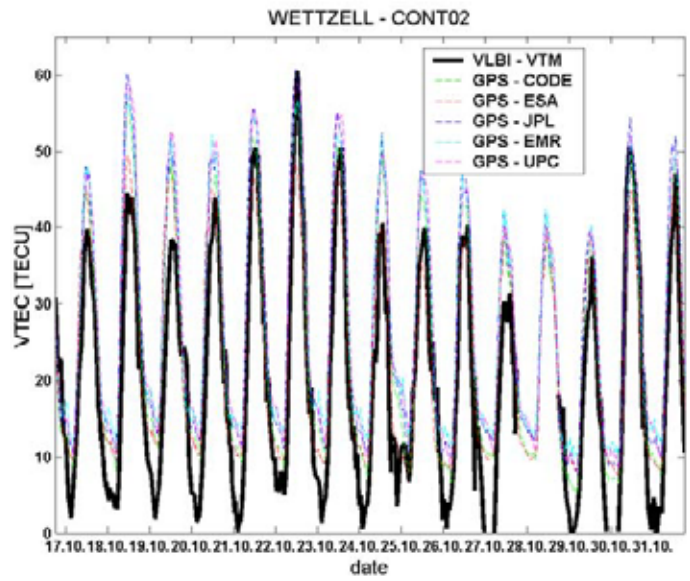


Figure 4: VTEC over station Wetzzell; comparison between VLBI (VTM approach) and GPS solutions of all IONEX analysis centers of the IGS.

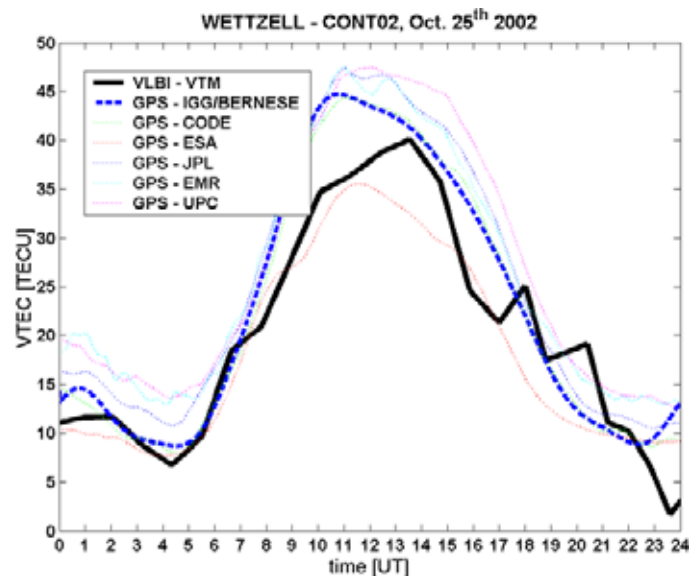


Figure 5: VTEC over station Wetzzell, comparison between VLBI (VTM approach), GPS solutions of all IONEX analysis centers and a local TEC model derived at IGG by BERNESE GPS software.

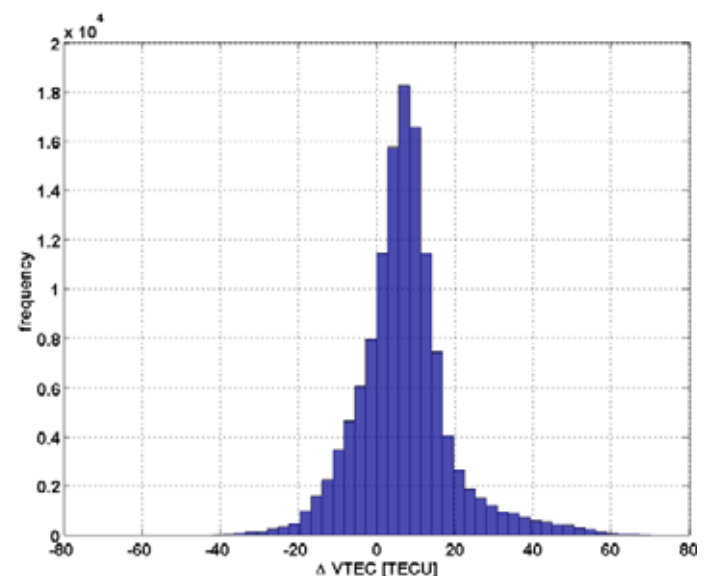


Figure 6: Histogram of the differences between all GPS and VLBI solutions for CONT02.

## 5 Outlook

First investigations have shown that VLBI is able to deliver information about the spatial distribution and temporal variation of the ionosphere. Further research should deal with the problem that the calculated TEC values are not vertically located above the station. Concerning the GPS results combined TEC series have not been published by IGS till summer 2003. However, it was decided at the last IGS governing board meeting to develop a solid procedure for combining the results of the various analysis centers. If these combined series will exist they can be used for a thorough comparison with the results obtained by VLBI.

## Acknowledgements

The research project P161366-N06 "Investigation of the ionosphere by geodetic VLBI" (VLBIonos) is funded by the Austrian Science Fund (FWF).

## References

- [1] Hargreaves, J.K., The solar-terrestrial environment, Cambridge atmospheric and space science series, Cambridge University Press, 1992
- [2] Hobiger T., Boehm J., Schuh H., VLBIonos – Probing the ionosphere by means of Very Long Baseline Interferometry, Oesterreichische Zeitschrift fuer Vermessung & Geoinformation (VGI), 1/2003, ed. by H. Schuh, F. Brunner, and H. Kahmen, 29-37, 2003
- [3] Hartmann, G.K., Leitinger, R., Range Errors Due to Ionospheric and Tropospheric Effects for Signals above 100 MHz, Bulletin Géodésique, Nr. 58, 109-136, 1984
- [4] Kondo T., Application of VLBI data to measurements of ionospheric total electron content, Journal of the Communications Research Laboratory, Vol .38, No. 3, 613-622, Tokyo, Japan, 1991
- [5] Schaer, S., Gurtner, W., Feltens, J., IONEX: The Ionosphere Map Exchange Format Version 1, Proceedings of the IGS AC Workshop, Darmstadt, Germany, 9.-11. Februar, 1998,  
<ftp://igscb.jpl.nasa.gov/igscb/data/format/ionex1.pdf>

Annex  
List of Participants  
Programme



## Participants of the 16<sup>th</sup> European VLBI Meeting

Name	Institution	Country	E-mail
Alef, Walter	MPIfR, Bonn	Germany	walef@mpifr-bonn.mpg.de
Andersen, Per Helge	FFI	Norway	per-helge.andersen@ffi.no
Bertarini, Alessandra	GIB, Univ of Bonn	Germany	abertari@mpifr-bonn.mpg.de
Böhm, Johannes	IGG, TU Vienna	Austria	jboehm@luna.tuwien.ac.at
Campbell, Bob	JIVE, Dwingeloo	Netherlands	campbell@jive.nl
Campbell, James	GIB, Univ of Bonn	Germany	campbell@uni-bonn.de
Elgered, Gunnar	OSO, Onsala	Sweden	kge@oso.chalmers.se
Engelhardt, Gerald	BKG, Leipzig	Germany	engelhardt@bkg.bund.de
Eschelbach, Cornelia	GIK, TU Karlsruhe	Germany	eschelbach@gik.uni-karlsruhe.de
Estermann, Gisela	IGG, TU Vienna	Austria	gisela@luna.tuwien.ac.at
Fischer, Dorothee	GIB, Univ of Bonn	Germany	dorothee.fischer@uni-bonn.de
Grünreich, Dietmar	BKG, Frankfurt	Germany	dietmar.gruenreich@bkg.bund.de
Haas, Rüdiger	OSO, Onsala	Sweden	haas@oso.chalmers.se
Hase, Hayo	BKG Project TIGO	Chile	hayo.hase@bkg.bund.de
Hobiger, Thomas	IGG, TU Vienna	Austria	thobiger@luna.tuwien.ac.at
Kutterer, Hansjörg	DGFI, Munich	Germany	kutterer@dgfi.badw.de
Lanotte, Roberto	CGS, Matera	Italy	lanotte@asi.it
Müskens, Arno	GIB, Univ of Bonn	Germany	mueskens@mpifr-bonn.mpg.de
Negusini, Monia	IRA-CNR, Matera	Italy	negusini@ira.cnr.it
Nothnagel, Axel	GIB, Univ of Bonn	Germany	nothnagel@uni-bonn.de
Paunonen, Matti	FGI, Masala	Finland	Matti.Paunonen@fgi.fi
Porcas, Richard	MPIfR, Bonn	Germany	porcas@mpifr-bonn.mpg.de
Reinhold, Andreas	BKG, Leipzig	Germany	ar@leipzig.ifag.de
Richter, Bernd	BKG, Frankfurt	Germany	bernd.richter@bkg.bund.de
Rottmann, Izabela	GIB, Univ of Bonn	Germany	owsianik@mpifr-bonn.mpg.de
Roy, Alan	MPIfR, Bonn	Germany	aroy@mpifr-bonn.mpg.de
Schlüter, Wolfgang	BKG, FS Wettzell	Germany	wolfgang.schlueter@bkg.bund.de
Schuh, Harald	IGG, TU Vienna	Austria	hschuh@luna.tuwien.ac.at
Schwegmann, Wolfgang	BKG, Frankfurt	Germany	wolfgang.schwegmann@bkg.bund.de
Sohn, Bong Won	MPIfR, Bonn	Germany	bwsohn@mpifr-bonn.mpg.de
Steinforth, Christoph	GIB, Univ of Bonn	Germany	steinforth@uni-bonn.de
Tesmer, Volker	DGFI, Munich	Germany	tesmer@dgfi.badw.de
Thorandt, Volkmar	BKG, Leipzig	Germany	vt@leipzig.ifag.de
Todorova, Sonya	IGG, TU Vienna	Austria	stodo@luna.tuwien.ac.at
Tomasi, Paolo	IRA-CNR, Matera	Italy	tomasi@itis.mt.cnr.it
Ullrich, Dieter	BKG, Leipzig	Germany	dieter.ullrich@bkg.bund.de
Vennebusch, Markus	GIB, Univ of Bonn	Germany	Vennebusch@uni-bonn.de
Whitney, Alan	MIT Haystack Obs	USA	awhitney@haystack.mit.edu
Zeitlhöfler, Reinhard	FESG, TU Munich, FS Wettzell	Germany	zeitlhoefler@wettzell.ifag.de



# Programme of the 16<sup>th</sup> European VLBI Meeting

## Thursday, 8<sup>th</sup> May 2003

- 19:00-22:00 Icebreaker Party at BKG  
20:00-20:30 Slide Show (A. Reinhold: „Crossing Greenland 2002”)

## Friday, 9<sup>th</sup> May 2003

- 08:30-09:00 Registration  
09:00-09:30 Introduction  
Grünreich, D. (President of BKG)  
Campbell, J.  
Schlüter, W.  
09:30-09:40 Organizational Remarks (Richter, B.)

### Session 1: Station Activities

Chair: Schuh, H., Schluter, W.

- 09:40-10:00 Schlüter, W. International VLBI Service for Geodesy and Astrometry (IVS)  
- Status and Perspective -  
10:00-10:20 Alef, W. MPIfR-BKG MK IV Correlator report  
10:20-10:40 Rottmann, I. Geodetic experiments at the Bonn Correlator  
10:40-11:10 Coffe Break  
11:11-11:30 Campbell, R.M. The EVN MkIV Data Processor at JIVE  
11:30-11:50 Roy, A. Tropospheric Delay Measurements at Effelsberg  
with Water-Vapour Radiometry  
11:50-12:00 Hase, H. First Results of the TIGO Borehole Tiltmeters  
in Concepción

### Session 2: Technical Developments

Chair: Schluter, W., Kutterer, H.

- 12:00-12:20 Elgered, G. The Geodetic VLBI Network Station at the Onsala  
Space Observatory - Activities During 2002 -  
12:20-12:30 Thorandt, V. Residual Plotting and Ambiguity Resolution (REPA)  
12:30-13:30 Lunch  
13:30-14:00 Poster Session (posters are displayed permanently)  
14:00-14:20 Withney, A. Mark 5 VLBI Data System Update

### Session 3: Local Ties

Chair: Kutterer, H.

- 14:20-14:40 Steinforth, Ch. Stability of Space Geodetic Reference Points  
at Ny Ålesund and their Excentricity Vectors  
14:40-15:00 Tomasi, P. 2002 Local Geodetic Survey of VLBI and GPS Reference  
Points and Eccentricity at Medicina (Italy)  
15:00-15:20 Tomasi, P. Neotectonic Geological Study and Classical Geodesy  
Methods Applied to Active Fault Monitoring in  
Ny Ålesund (Western Svalbard)

#### **Session 4: Astrometric VLBI**

**Chair: Kutterer, H.**

15:20-15:40 Porcas, R. Phase-reference Astrometry Investigations using 86 GHz VLBI

15:40-16:10 Coffee Break

#### **Session 5: Geodetic VLBI Analysis and Results**

**Chair: Campbell, J.**

16:10-16:30 Böhm, J. Vienna Mapping Functions

16:30-16:50 Engelhardt, G. IVS Analysis and Data Center at BKG - Works in 2002/2003

16:50-17:10 Estermann, G. Investigations of atmospheric and hydrological loading by VLBI

17:10-17:30 Fischer, D. The K4 Intensive project 2002 for UT1 determination

18:15-19:00 Guided city tour (centre)

19:00 Dinner at „Auerbachs Keller“

### **Saturday, 10<sup>th</sup> May 2003**

#### **Session 5: Geodetic VLBI Analysis and Results**

**Chair: Tomasi, P.**

09:00-09:20 Kutterer, H. The role of parameter constraints in VLBI data analysis

09:20-09:40 Negusini, M. Tropospheric parameters from geodetic VLBI data analysis

09:40-10:00 Nothnagel, A. VTRF2003: A Conventional VLBI Terrestrial Reference Frame

10:00-10:20 Tesmer, V. Refinement of the stochastic VLBI model: first results

10:20-10:40 Vennebusch, M. Investigations on European baseline rates

10:40-11:10 Coffee Break

#### **Session 6: Combination of VLBI and other Space Geodetic Techniques**

**Chair: Nothnagel, A.**

11:10-11:30 Campbell, J. European Vertical Site motions by VLBI and GPS - An Update

11:30-11:50 Haas, R. Assessing Long Term Trends in the Atmospheric Water Vapor Content by Combining Data From VLBI, GPS, Radiosondes and Microwave Radiometry

#### **Session 7: Future Perspectives of VLBI**

**Chair: Nothnagel, A.**

11:50-12:10 Hobiger, Th. The project „VLBIonos“ - how VLBI contributes to ionospheric research

12:10-12:40 Proceedings, date and location of next meeting, closing remarks